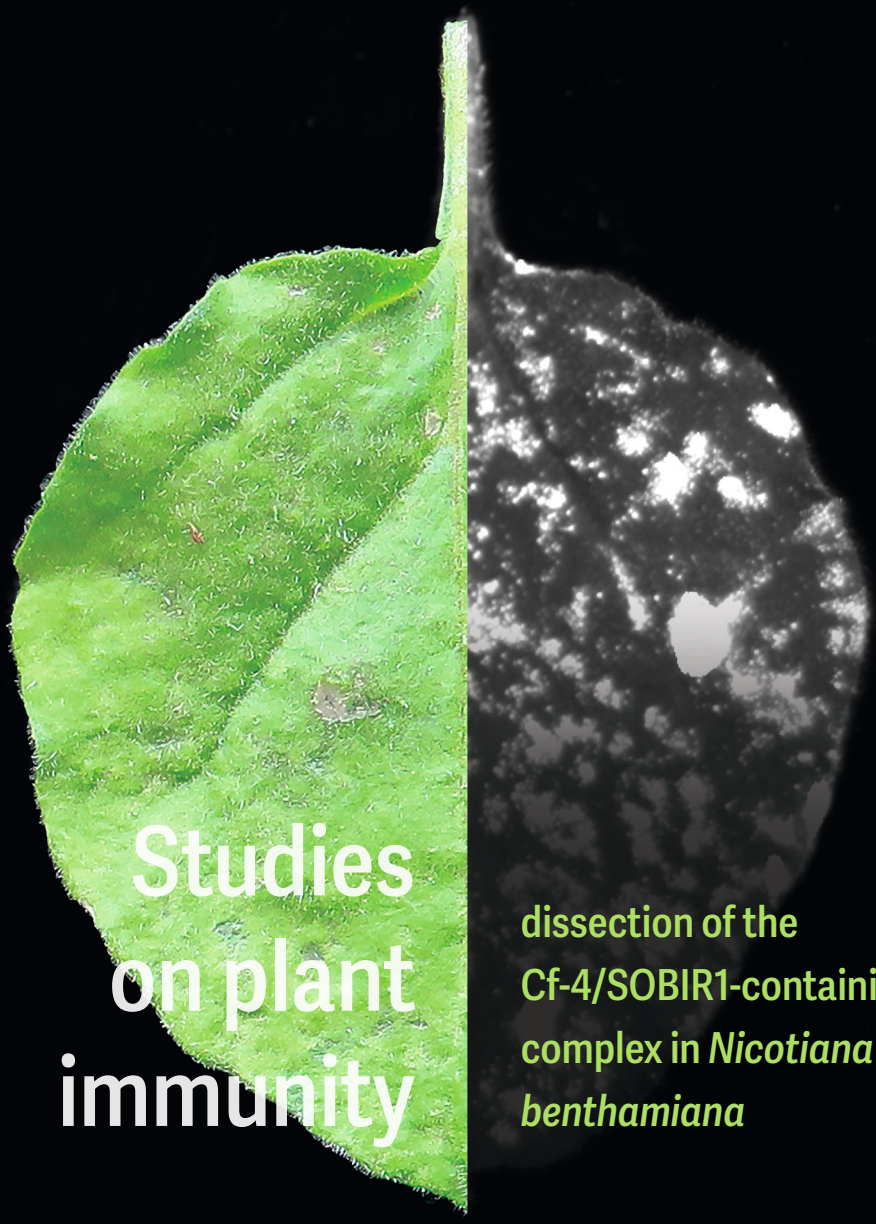

Studies on plant immunity

dissection of the Cf-4/SOBIR1-containing complex in *Nicotiana benthamiana*

Sergio Landeo Villanueva

Propositions

1. Red light imaging provides a more reliable and standardised measurement of plant cell death than traditional staining techniques. (this thesis)

2. Deployment of proximity-dependent labelling followed by mass spectrometry provides a unique snapshot of the molecular environment of plant cell-surface receptors. (this thesis)

3. Viruses should be regarded as life forms in biology textbooks.

4. Delaying the adoption of regulations for proper deployment of GMOs in agriculture is an expensive mistake.

5. Considering visa challenges when choosing international conference sites will promote the diversity of perspectives in scientific discourse.

6. The goals of the Paris Agreement are no longer realistic.

Propositions belonging to the thesis, entitled:

Studies on plant immunity: dissection of the Cf-4/SOBIR1-containing complex in *Nicotiana benthamiana*

Sergio Landeo Villanueva
Wageningen, 31 October 2023

Studies on plant immunity: dissection of the Cf-4/SOBIR1-containing complex in *Nicotiana benthamiana*

Sergio Landeo Villanueva

Thesis committee

Promotors

Dr Matthieu H.A.J. Joosten
Associate professor, Laboratory of Phytopathology
Wageningen University & Research

Prof. Dr Gert H.J. Kema
Professor of Phytopathology
Wageningen University & Research

Other members

Prof. Dr Dolf Weijers, Wageningen University & Research
Dr Aska Goverse, Wageningen University & Research
Prof. Dr Jonathan Jones, University of East Anglia, UK
Dr Birgit Kemmerling, University of Tuebingen, Germany

This research was conducted under the auspices of the Graduate School
Experimental Plant Sciences

Studies on plant immunity: dissection of the Cf-4/SOBIR1-containing complex in *Nicotiana benthamiana*

Sergio Landeo Villanueva

Thesis

submitted in fulfilment of the requirements for the degree of doctor
at Wageningen University
by the authority of the Rector Magnificus,
Prof. Dr A.P.J. Mol,
in the presence of the
Thesis Committee appointed by the Academic Board
to be defended in public
on Tuesday 31 October 2023
at 4 p.m. in the Omnia Auditorium.

Sergio Landeo Villanueva
Studies on plant immunity: dissection of the Cf-4/SOBIR1-containing complex in *Nicotiana benthamiana*, 355 pages
PhD thesis, Wageningen University, Wageningen, the Netherlands (2023)
With references, with summary in English

ISBN: 978-94-6447-885-3
DOI: https://doi.org/10.18174/638708

TABLE OF CONTENTS

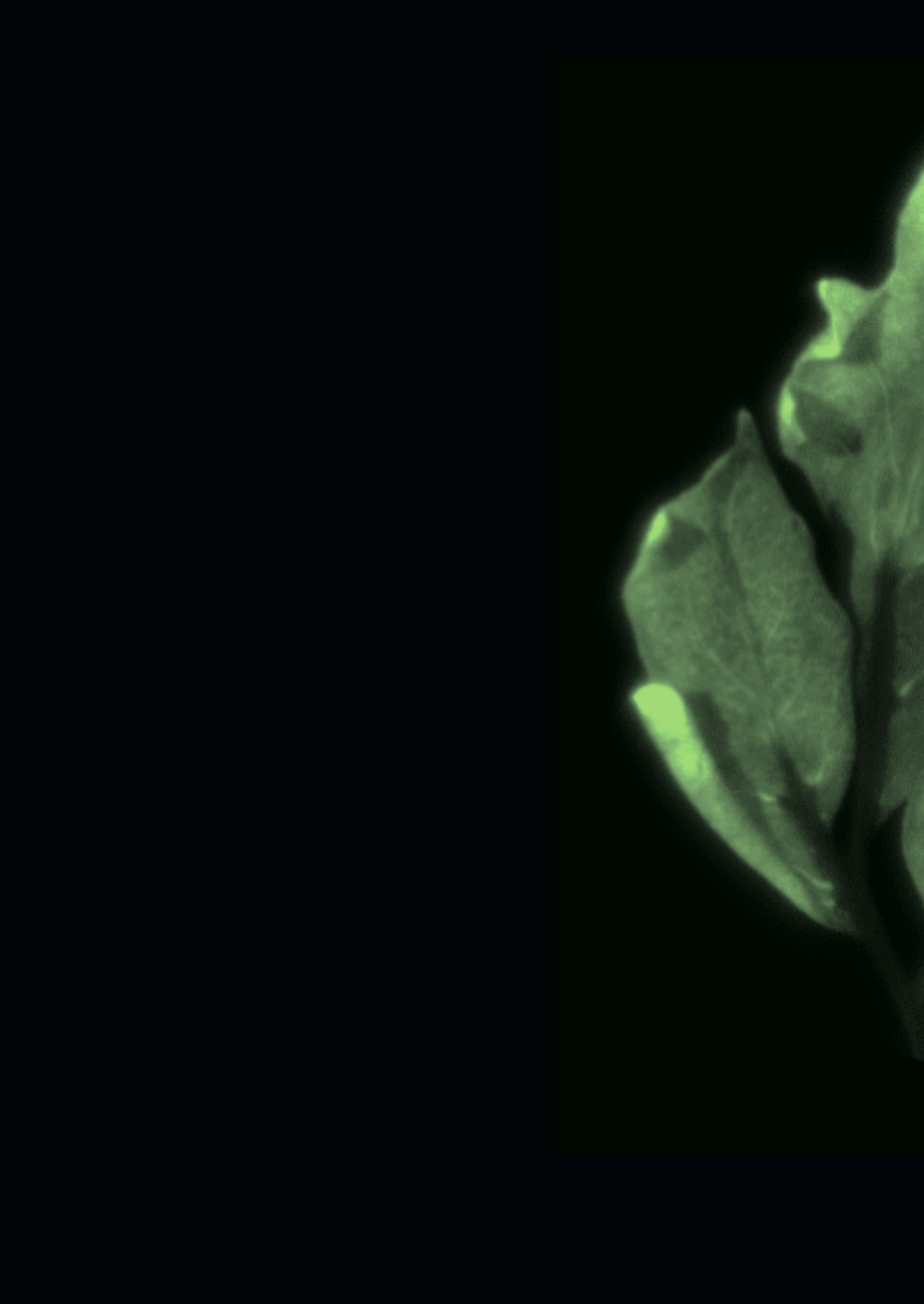

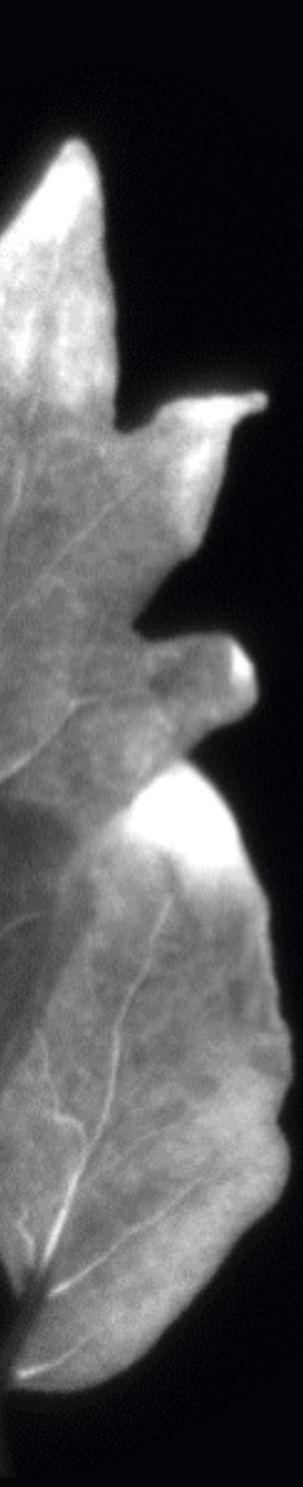

CHAPTER 1

Introduction

Plants provide the oxygen we breathe, the food we eat, as well as the materials that we use to protect ourselves and to transform our environment to more favourable conditions. The need to sustain the ever-growing human population, without increasing the agricultural frontier in such a way that we seriously harm the robustness of our climate, represents a serious challenge to our agricultural practices. Plants, like all organisms, are constantly challenged by pathogens that threaten agricultural production. The global losses of food crops, because of the damage caused by pests and pathogens, are estimated to be around 20-30% [1]. This infestation occurs despite an intensive use of pesticides, with unintended consequences for the environment and human health [2,3]. In this context, it is clear that a detailed knowledge of the molecular mechanisms by which resistant plants can prevent pathogen infection, is instrumental for the improvement of our crops through modern biotechnology.

Plants have evolved a series of defence mechanisms that allows to protect themselves against diseases. Once in contact with the plant, the first layers of defence that a pathogen has to overcome comprise passive defences. These include anatomical barriers, such as the cuticle, which is a waxy protective shield covering the aerial surfaces of plants [4]. These passive defences also include preformed antimicrobial compounds referred to as phytoanticipins, like α-tomatine, that accumulate at relatively high levels in leaves, flowers and green fruits of tomato (*Solanum lycopersicum, Sl*) plants [5]. The next layers of defence are provided by the plant's immune system. Plants lack mobile defender cells and rely on an innate immune system in which each cell is able to perceive danger signals and can appropriately respond to combat pathogen infections [6,7]. This level of immunity is achieved by the concerted action of receptors that perceive immunogenic patterns (IPs) at the cell-surface and in the cytoplasm of the plant cells (Figure 1) [8–10]. IPs can be conserved structural components of the pathogen, known as microbe-associated molecular patterns (MAMPs), such as bacterial flagellin and fungal chitin [11–13]. They can also be endogenous molecules released from the plant because of pathogen invasion, known as damage-associated molecular patterns (DAMPs), like cell wall fragments [14], that

normally do not occur in healthy plants. IPs can also be compounds secreted by the pathogen, with the purpose of enhancing virulence, known as effectors [15]. The mechanisms of action of these effectors are diverse. Effectors can suppress plant immune responses, enhance the access to nutrients, and might also manipulate the host microbiome to benefit the pathogen [15–17]. However, when the pathogen's effectors are perceived by an appropriate immune receptor of the host plant, they activate the plant defence responses, resulting in host resistance and pathogen avirulence. Thus, in this case the recognised effectors become a liability for the pathogen and are referred to as avirulence (Avr) factors [18,19]. The perception of effector proteins by resistant plants is not always the result of a direct interaction with the immune receptors. Often, plant immune receptors act by guarding the virulence target of the pathogen's effectors [20–22]. In this way, mutations in the effector gene are less likely to circumvent the activation of the immune responses, without affecting its virulence function, as the pathogen will have to stop manipulating the virulence target [23].

Most characterized cell-surface receptors perceive either MAMPs or DAMPs, and therefore they are frequently described as pattern recognition receptors (PRRs), triggering MAMP-triggered immunity (MTI). Conversely, inside the plant cells, all the cytoplasmic immune receptors characterized so far perceive effector proteins, and the immune responses that they activate are collectively referred to as effector-triggered immunity (ETI) [6,20]. However, the distinction between MAMPs and effectors, and therefore between MTI and ETI, is not always clear [24]. Hence, these two outputs of the plant immune system can therefore be better defined based on the location where the IPs are perceived [18]. Extracellular immunogenic patterns (ExIPs) are perceived by cell-surface receptors and intracellular immunogenic patterns (InIPs) are perceived by cytoplasmic immune receptors, thereby resulting in extracellularly-triggered immunity (ExTI) and intracellularly-triggered immunity (InTI), respectively [18].

Plant immune receptors

The first set of immune receptors that a plant pathogen encounters once in contact with the host is located at the surface of the cell. These cell-surface receptors are either receptor-like kinases (RLKs) or receptor-like proteins (RLPs) (Figure 1). RLKs possess an extracellular domain to recognise ExIPs, a single-pass transmembrane (TM) domain, and an intracellular kinase domain for downstream signalling. RLPs have a similar structure, but lack the cytoplasmic kinase domain [25]. Further distinctions between cell-surface receptors can be made based on their extracellular

domains. Different extracellular domains involved in the perception of ExIPs include: a lysin motif (LysM), a lectin (Lec) domain, an epidermal growth factor (EGF)-like domain, and leucine-rich repeats (LRRs) [20]. Cell-surface receptors with a LysM-containing extracellular domain recognise fragments of the fungal cell wall and bacterial peptidoglycan [26,27], whereas lectin receptor-like kinases (LecRKs) activate ExTI upon recognition of several molecules, including extracellular ATP [28], bacterial lipopolysaccharides [29], effector proteins [30], and sphingolipids [31]. RLKs with EGF-like repeats in their extracellular domain bind to pectin present in the plant cell walls and are referred to as cell wall-associated kinases (WAKs). WAKs regulate cell expansion by their interaction with cross-linked pectin at the cell wall, and also activate immune responses upon binding to pectin fragments that are released due to the action of invading pathogens [32,33]. RLKs and RLPs with LRRs in their extracellular domain form the largest group of cell-surface receptors [34,35]. LRR-RLKs and LRR-RLPs activate immune responses upon perception of a large set of ExIPs, including MAMPs [36,37], DAMPs [38,39] and effector proteins [40,41].

InIPs are perceived by a second set of immune receptors. These cytoplasmic immune receptors comprise proteins with a variable N-terminal domain, a conserved nucleotide-binding and oligomerization domain (NOD), and a C-terminal LRR domain. According to the composition of their N-terminal domain, these nucleotide-binding, LRR-containing proteins (NLRs) can be broadly categorised into three groups: Toll/INTERLEUKIN RECEPTOR-LIKE (IL1) resistance proteins (TIR)-type NLRs (TNLs), coiled-coil (CC)-type NLRs (CC-NLRs or CNLs), and RESISTANCE TO POWDERY MILDEW 8 (RPW8)-type CNLs (CC_R-NLRs or RNLs) (Figure 1) [42]. From a functional point of view, NLRs can be divided into "sensor NLRs" that perceive InIPs and "helper NLRs" that act downstream of sensor NLRs [43]. Activation of both cell-surface receptors and NLRs leads to defence-related responses, such as MITOGEN-ACTIVATED PROTEIN KINASE (MAPK) phosphorylation, a burst of reactive oxygen species (ROS), a Ca^{2+} influx into the cytoplasm, massive transcriptional reprogramming, and the production of defence-related hormones such as salicylic acid (SA). However, in contrast to the recognition of MAMPs and DAMPs, the perception of effectors by cell-surface receptors and NLRs usually triggers more intense and prolonged responses, including a form of programmed cell death, referred to as the hypersensitive response (HR) [18,44].

Activation of cell-surface receptor complexes

At the level of the plasma membrane (PM), the activity of cell-surface receptors is regulated by their dynamic interaction with co-receptors and regulatory RLKs (Figure 1) [25]. As mentioned earlier, most of the characterised cell-surface receptors have extracellular domains with LRRs [20], and one of the best characterised LRR-RLKs mediating immune responses is the widely conserved cell-surface receptor FLAGELLIN-SENSING 2 (FLS2) [45–49]. Extensively studied in the model Brassicaceous plant, *Arabidopsis thaliana* (hereafter referred to as *Arabidopsis*), FLS2 was found to detect flagellin, which is a MAMP derived from the bacterial flagellum [36,50]. Upon recognition of the flagellin epitope, flg22, FLS2 associates with its co-receptor, the LRR-RLK BRASSINOSTEROID-INSENSITIVE 1 (BRI1)-ASSOCIATED KINASE (BAK1), also known as SOMATIC EMBRYOGENESIS RECEPTOR KINASE 3 (SERK3), further referred to as BAK1 [51,52]. The extracellular domain of both BAK1 and FLS2 physically interacts with flg22, which promotes the heterodimerization of the receptor complex [53]. The recruitment of BAK1 triggers a series of phosphorylation events between the cytoplasmic kinase domains of BAK1 and FLS2, resulting in the activation of the FLS2/BAK1 complex [54]. This mechanism also holds for the activation of LRR-RLKs recognising DAMPs, such as plant elicitor peptides (PEPs). The LRR-RLK PEP1 RECEPTOR 1 (PEPR1) and PEPR2 perceive the MAMP- and wound-induced endogenous peptides Pep1 and its paralogs to further amplify the immune responses [38,39,55,56]. Although BAK1 has a predominant role in the activation of receptor complexes present at the cell surface, FLS2 and PEPR1/2 also form ligand-induced complexes with close paralogs of BAK1, such as BAK1-LIKE1/SERK4 (BKK1/SERK4, further referred to as BKK1) and other members of the SERK family. [57]. This family consists of five members in *Arabidopsis* and their recruitment is required for the activation of a large set of LRR-RLKs and LRR-RLPs [58–60].

Without a cytoplasmic kinase domain for downstream signalling, RLPs have to associate with adaptor kinases and thereby form bimolecular receptors that can both perceive signals from the apoplast and activate downstream cytoplasmic signalling cascades [61]. This phenomenon was first observed for an RLP regulating developmental processes. The Arabidopsis LRR-RLP CLAVATA2 (CLV2) interacts with the PM-associated protein kinase CORYNE (CRN) to regulate the meristem size in response to perception of the endogenous CLV3 peptide [62,63]. Later, such a ligand-induced interaction with an RLK was also observed for the CHITIN ELICITOR BINDING PROTEIN (CEBiP), which is a LysM-RLP from rice (*Oryza sativa, Os*) that

recognises chitin oligosaccharides [64]. Perception of these oligosaccharides in rice induces the formation of a hetero-oligomeric complex, including CEBiP and the LysM-RLK CHITIN RECEPTOR KINASE 1 (OsCERK1), resulting in the activation of downstream signalling for mounting various immune responses [65].

The adaptor kinase for plant LRR-RLPs mediating immune responses was discovered while studying the tomato immune receptors Cf-4 and Ve1 [18,61,66]. Cf-4 is an LRR-RLP that confers resistance to strains of the hemibiotrophic fungal pathogen *Cladosporium fulvum* (syn. *Fulvia fulva*), expressing the effector protein Avr4 [40,67,68]. This pathogen colonises the apoplastic space between the cells of the mesophyll of the tomato leaves [69]. There, the Avr4 protein, which contains a chitin-binding domain, is secreted by the invading fungus and binds to the chitin present in the fungal cell wall. In this way, this effector promotes the virulence of the pathogen by protecting the fungal hyphae from hydrolysis by host chitinases that are secreted into the apoplast as a response to the fungal invasion [70–73]. The immune receptor Ve1 is an LRR-RLP that confers resistance to the vascular fungal pathogens *Verticillium dahliae*, *V. albo-atrum* and *Fusarium oxysporum f. sp. lycopersici*, expressing the effector protein Ave1 [74,75]. Ave1 displays antimicrobial activity, and promotes pathogen virulence through the manipulation of the host microbiome by suppressing the proliferation of microbial antagonists [17]. Affinity purification of Cf-4 and Ve1, both fused to GREEN FLUORESCENT PROTEIN (GFP), followed by mass spectrometry analysis of the co-purifying proteins, resulted in the discovery of two tomato homologs of SUPPRESSOR OF BAK1-INTERACTING RLK-1 (BIR1)-1 (SOBIR1) as the adaptor RLKs that are required for the accumulation and the functionality of both LRR-RLPs [66]. Further research showed that the Cf-4/SOBIR1 bi-molecular receptor also recruits BAK1 and related SERK family members, such as SERK1, upon perception of Avr4 [76]. Similar to the activation mechanism of LRR-RLKs such as FLS2, the recruitment of BAK1 is proposed to trigger a series of phosphorylation events between the kinase domains of BAK1 and SOBIR1, leading to the activation of the LRR-RLP-containing receptor complex [77].

The requirement of SOBIR1 and SERK family members, such as BAK1, is a general feature of LRR-RLPs mediating immune responses against pathogens. For instance, in tomato, the homologs of both SOBIR1 and BAK1 are required for the activity of the immune receptor Ve1 [66,78,79]. Furthermore, in the Solanaceous research model plant *Nicotiana benthamiana* and in the wild potato species *Solanum microdon-*

tum, these LRR-RLKs are required for the activity of the LRR-RLPs RESPONSIVE TO ELICITINS (REL) and ELICITIN RESPONSE protein (ELR), respectively. Both REL and ELR contribute to resistance to oomycetes belonging the *Phytophthora* genus by perceiving elicitins, including INFESTIN 1 (INF1) from *Phytophthora infestans* [80–83]. Also in *N. benthamiana*, these LRR-RLKs are required for the activity of the LRR-RLP RESPONSE TO XEG1 (RXEG1), which recognises several glycoside hydrolase family 12 proteins, including XYLOGLUCAN-SPECIFIC ENDOGLUCANASE (XEG1) from *Phytophthora sojae* [84,85]. In *Arabidopsis*, SOBIR1 and SERK family members are required for the activity of LRR-RLPs, such as RLP23, RLP30 and RLP42. RLP23 activates defence responses against infection by bacterial, oomycetes and fungal pathogens producing NECROSIS- AND ETHYLENE-INDUCING PROTEIN 1 (NEP1)-like proteins (NLPs) [86–89], whereas RLP30 contributes to resistance against the necrotrophic fungi *Sclerotinia sclerotiorum* and *Botrytis cinerea* by perceiving SCLEROTINIA CULTURE FILTRATE ELICITOR 1 (SCFE1) [90]. RLP42 triggers plant defence upon perception of fungal endo-polygalacturonases, such as *B. cinerea* ENDOPOLYGALACTURONASE 3 (BcPG3) [91,92].

The activation of LRR-RLKs and LRR-RLPs is negatively regulated by the dynamic interaction of BAK1 and related SERKs with members of the BAK1-INTERACTING RECEPTOR-LIKE KINASE (BIR) family of LRR-RLKs [93–97]. *Arabidopsis* possesses four *BIR* genes (*BIR1* to *BIR4*) of which three, *BIR1* to *BIR3,* are known to negatively regulate BAK1 complex formation with cell-surface receptors. In the resting state, BIR2 for example constitutively interacts with BAK1, thereby preventing BAK1 complex formation with LRR-RLKs perceiving IPs, such as FLS2 and PEPR1 [94]. Consequently, *Arabidopsis bir2* mutants display typical features of constitutive defence activation, including elevated levels of SA and transcriptional up-regulation of the SA-responsive gene *PATHOGENESIS RELATED 1* (*PR1*) [94]. Unlike BIR2, BIR3 not only interacts with BAK1 but also targets ligand-binding LRR-RLKs themselves, including FLS2, to regulate their recruitment of BAK1 [96]. BIR3 also modulates developmental processes by its interactions with BAK1 and the LRR-RLK BRASSINOSTEROID-INSENSITIVE 1 (BRI1) [96]. BRI1 is the major receptor for brassinosteroids (BRs), which are growth-promoting steroid hormones in plants [98,99]. Hence, *Arabidopsis bir3* mutants display enhanced immune responses upon perception of flg22, and BIR3-over-expressing plants are insensitive to flg22 and have a dwarf phenotype [96]. Among the BIR family members, only BIR1 possesses an active cytoplasmic kinase domain [93,94,96]. BIR1 interacts constitutively with BAK1, but not with FLS2 or BRI1. BIR1 seems to have no

role in regulating the perception of flagellin or BRs [93,100]. *Arabidopsis bir1* knockout mutants have a seedling lethality phenotype, because of the constitutive activation of at least two parallel pathways that mediate signalling for the activation of defence responses. One of these pathways requires the activity of PHYTOALEXIN DEFICIENT 4 (PAD4) and ENHANCED DISEASE SUSCEPTIBILITY 1 (EDS1), as the activation of cell death and defence responses in *bir1* mutants partially depends on *PAD4* and *EDS1* [93]. This suggests a role for a yet unidentified TNL in the signalling cascade (see next section). The other pathway signals trough SOBIR1 and BAK1, as knockout mutants of *SOBIR1* suppress the cell death and defence responses of *bir1* mutants, and knockout mutants of *BAK1* show a partial suppression of the *bir1* phenotype [93,100]. Evidence suggests that BIR1 is a negative regulator of the activation of LRR-RLP/SOBIR1 receptor complexes by BAK1, as SOBIR1 only co-immunoprecipitates with BAK1 when the accumulation of BIR1 is compromised by virus-induced gene silencing (VIGS) [100]. The role of the various BIR family members in regulating the activity of cell-surface receptors seems to be conserved, at least in Solanaceous plants. The tomato homolog of *Arabidopsis* BIR3 appears to have conserved its role in regulating the perception of flg22 and BRs [101], and VIGS of *BIR1* homologs in *N. benthamiana* also results in a lethal phenotype [102].

Activation of cytoplasmic immune receptors

Many pathogens translocate their effectors into the host cell, aiming to perturb the physiology of the host and suppress defence responses to promote infection. In response, plants have evolved a diverse set of NLRs as intracellular immune receptors to recognise these effectors as InIPs (Figure 1) [18,103]. The LRRs of the NLRs are involved in the specific perception of the InIPs, whereas the NOD domain typically mediates the activation of the NLR protein by exchanging ADP for ATP in its nucleotide binding pocket. The N-terminal domains, TIR, CC, CC_R and CC_{G10}, are the components that execute downstream immune signalling upon perception of the InIPs.

NLRs can recognise their ligands directly. For example, the TNLs RECOGNITION OF PERONOSPORA PARASITICA 1 (RPP1) from *Arabidopsis* and RECOGNITION OF XOPQ (ROQ1) from *N. benthamiana* interact directly with their matching InIPs [104,105]. RPP1 confers resistance to the foliar oomycete pathogen *Hyaloperonospora arabidopsidis* expressing the effector protein ARABIDOPSIS THALIANA RECOGNISED 1 (ATR1) [106,107]. ROQ1 confers resistance to bacterial pathogens of the genus *Xanthomonas*, expressing the effector protein XANTHOMONAS OUTER PROTEIN Q

(XopQ) [108]. Both TNLs recognise their ligand by their LRRs, in combination with a conserved LRR-adjacent, C-terminal "jelly roll" and Ig-like (C-JID) domain, which forms a horseshoe-shaped scaffold that curls around the InIP, recognising multiple regions of the substrate [104,105]. Direct interaction between an NLR and matching InIP has also been reported for the wheat (*Triticum monococcum*) CNL STEM RUST 35 (Sr35) resistance protein [109]. Sr35 confers resistance to wheat stem rust caused by the fungus *Puccinia graminis* f. sp. *Tritici*, expressing the effector AvrSr35 [110,111].

However, recognition of effector proteins by plant immune receptors in most cases is an indirect process. Rather than interacting directly with the InIPs, the NLRs perceive the modification of another plant protein that is induced by the pathogen's effector [22,23]. For instance, the *Arabidopsis* CNL HOPZ-ACTIVATED RESISTANCE 1 (ZAR1) acts by guarding plant receptor-like cytoplasmic kinases (RLCKs). RLCKs are key players in the signalling cascade downstream of cell-surface receptors [112,113], and therefore these protein kinases are frequent targets of pathogen's effectors [114–117]. ZAR1 confers resistance of *Arabidopsis to Xanthomonas campestris* pv. *campestris* expressing the effector protein AvrAC [118]. This effector protein uridylylates several RLCKs in order to inhibit the immune signalling cascade [116]. In the resting state, ZAR1 forms a complex with the RLCK RESISTANCE-RELATED KINASE 1 (RKS1). Upon infection, AvrAC uridylylates the RLCK AVRPPHB SUSCEPTIBLE 1 (PBS1)-LIKE PROTEIN 2 (PBL2). The modified PBL2 ($PBL2^{UMP}$) associates with RKS1 in the preformed ZAR1/RKS1 complex, activating immune responses [118]. NLRs can also perceive InIPs through their interaction with integrated sensor domains. These integrated domains evolved by duplication of the effector's virulence target, followed by a translational fusion to the NLR [119,120]. This is, for example, the case for the genetically linked TNLs (called paired TNLs) RESISTANCE TO RALSTONIA SOLANACEARUM 1 (RRS1) and RESISTANCE TO PSEUDOMONAS SYRINGAE 4 (RPS4). RRS1 and RPS4 cooperate in providing resistance to different pathogens, including the root-infecting bacterium *Ralstonia solanacearum* expressing the effector PopP2 and the leaf-infecting bacterium *Pseudomonas syringae*, expressing the effector AvrRps4 [121,122]. Interestingly, RRS1 possesses an LRR-adjacent C-terminal WRKY transcription factor domain [123]. WRKY transcription factors are among the largest family of transcriptional regulators in plants and play important roles in defence responses to several pathogens [124]. The effectors PopP2 and AvrRps4 both interact with the WRKY domain of RRS1, causing a chain of domain reconfigurations that derepress the activity of the executor TNL RPS4 [125].

Recognition of InIPs results in the oligomerization of plant NLRs and the formation of large wheel-like complexes, referred to as resistosomes (Figure 1) [126]. The first resistosome described in plants is a pentameric structure, containing the CNL ZAR1 [127]. The association of ZAR1/RSK1 with PBL2^{UMP}, as described above, induces a conformational change in ZAR1, resulting in the oligomerization of the activated ZAR1/RSK1/PBL2 ^{UMP} complex. When present in the resistosome, the N-terminal α helix of the CC domain of ZAR1 is exposed, forming a funnel-shaped structure. This structure then inserts into the PM, forming a calcium ion (Ca^{2+}) channel, triggering Ca^{2+} influx, disruption of the chloroplasts, production of ROS and a subsequent HR [128]. The assembly of CNLs into pentameric resistosomes triggering Ca^{2+} influx seems to be a conserved feature. The activation of the wheat CNL Sr35, for example, results in a similar structure, which also acts as a Ca^{2+} channel [109,129]. Different from CNLs, the activation of TNLs results in tetrameric resistosomes that display nicotinamide adenine dinucleotide nucleosidase (NADase) activity and produce signalling molecules. The recognition of ATR1 by RPP1 in *Arabidopsis*, and the recognition of XopQ by ROQ1 in *N. benthamiana* results in the formation of highly conserved tetrameric structures [104,105]. For both resistosome complexes, RPP1/ATR1 and ROQ1/XopQ, the TIR domains bind to each other, creating active sites for NAD^+ hydrolysis. The resulting holoenzymes possess multiple enzymatic activities, resulting in the production of molecules that function as second messengers, including 2′-(5′′-phosphoribosyl)-5′-adenosine diphosphate/monophosphate (pRib-ADP/AMP) and ADP-ribosylated adenosine triphosphate/ADPr-ADPR (ADPr-ATP/di-ADPR) [130–133].

The CNLs ZAR1 and Sr35 are examples of singleton NLRs, because they perceive the InIPs themselves and subsequently execute immune signalling, likely through their pore-forming activity in the PM [127,128,134]. Many NLRs, like the paired TNLs RRS1 and RPS4, have specialised into either sensing the InIPs (sensor NLRs) or executing immune signalling (helper NLRs) [121,122,125]. This functional specialisation is also observed in CNLs, such as the rice PYRICULARIA ORYZAE RESISTANCE K-1 (Pik-1) and Pik-2 proteins. These paired CNLs confer resistance to the fungal pathogen *Magnaporthe oryzae* [135]. The sensor CNL Pik-1 perceives the fungal InIP AVR-Pik by its interaction with an integrated Heavy-Metal Associated (HMA) sensor domain, which is located between the CC and the NOD domains of the CNL [136]. Perception of AVR-Pik triggers the formation of a tri-partite complex with Pik-1 and Pik-2, which forms likely the activated state of this pair of receptors [137].

Besides the one-to-one relation between sensor and helper NLRs, several helper NLRs also function as signalling components for multiple NLRs [134]. An example of this is the NB-LRR-REQUIRED FOR CELL DEATH (NRC) network in solanaceous plants. In this network, a small set of CNLs, referred to as NRCs, function as redundant helpers for multiple sensor CNLs, while also having distinct specificities towards different sensor CNLs [43,138]. For instance, all three NRCs present in *N. benthamiana* (NRC2, NRC3, and NRC4) are redundantly required for the activity of the sensor CNL Rx, which confers resistance to potato virus X (PVX) [43,139]. In contrast, the CNL Rpi-blb2 specifically requires the activity of the helper CNL NRC4 to confer resistance to *P. infestans* [43,140]. Another example of helper NLRs acting downstream of several sensor NLRs are N REQUIRMENT GENE 1 (NRG1) and ACTIVATED DISEASE RESISTANCE 1 (ADR1), which form two lineages of RNLs that are conserved in dicot plants [141]. These helper RNLs are required for the activity of TNLs. *Arabidopsis* possesses five full-length RNLs, which are two NRG1 paralogs (NRG1.1 and NRG1.2) and three ADR1 paralogs (ADR1, ADR1-L1 and ADR1-L2) [42]. In Brassicaceae, NRG1s and ADR1s tend to be unequally redundant [142,143]. For example, downstream of the paired TNLs RPS4 and RRS1, ADR1s have a prominent role in restricting bacterial growth, but are dispensable for the HR when NRG1s are active [144,145]. In *N. benthamiana*, which possesses only one copy of ADR1 and one copy of NRG1, TNLs signal primarily through NRG1 [142,145–147]. The signal transduction from the sensor TNLs to the helper RNLs is mediated by a small family of lipase-like proteins, comprising ENHANCED DISEASE SUSCEPTIBILITY 1 (EDS1), SENESCENCE-ASSOCIATED GENE 101 (SAG101), and PHYTOALEXIN-DEFICIENT 4 (PAD4). EDS1 forms mutually exclusive heterodimers with SAG101 or PAD4, which are required for activation of NRG1s and ADR1s, respectively [148–150]. EDS1/SAG101 and EDS1/PAD4 heterodimers act as receptors for the signalling molecules that are produced upon activation of TNLs. The dimer EDS1/SAG101 is a receptor for pRib-ADP/AMP, resulting in the activation of the RNL NRG1 [132], whereas the dimer EDS1/PAD4 is a receptor for ADPr-ATP/di-ADPR, resulting in the activation of the RNL ADR1 [133]. The activation of both sensor CNLs and TNLs, results in homo-oligomerization of the helper NRCs and RNLs, which results in a pore-forming activity, similar to the one produced by the activation of the singleton CNL ZAR1 [151–153].

Downstream signalling from cell-surface receptors

Upon their activation, all cell-surface receptors that have up till now been characterised signal through RLCKs (Figure 1) [25,112,154].

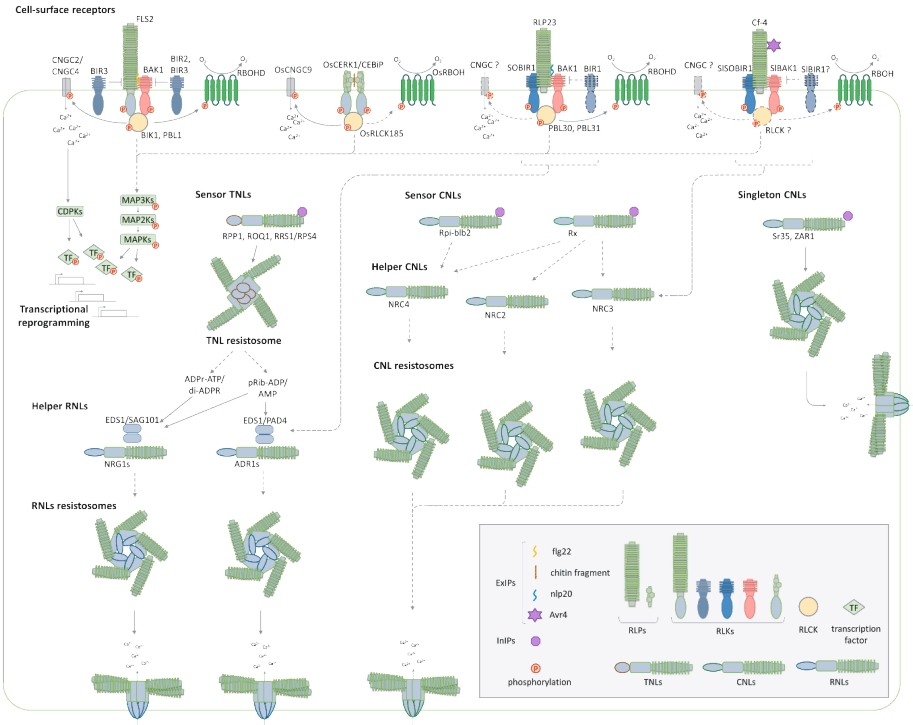

Figure 1. Molecular mechanisms involved in the activation of a selection of cell-surface receptors and cytoplasmic immune receptors (NLRs), and the downstream responses that they trigger. The perception of ExIPs by cell-surface receptors triggers a series of responses that include the generation of ROS in the apoplast, the activation of MAPK cascades, an influx of Ca^{2+}, and the transcriptional reprogramming of the responding host cells. The perception of InIPs by NLRs results in the potentiation of host defence responses, leading to programmed cell death of the responding host cells (the hypersensitive response; HR).

In ***Arabidopsis,*** perception of flg22 by FLS2 and its co-receptor BAK1 results in the phosphorylation of the RLCK-VII members BIK1 and PBL1. The activation of these RLCKs is required for the generation of ROS by RBOHD, and for the influx of Ca^{2+} through channels formed by CYCLIC NUCLEOTIDE-GATED CHANNEL 2 (CNGC2) and CNGC4.

In rice, the perception of chitin fragments is mediated by a receptor complex formed by the LysM-RLP CEBiP and the LysM-RLK CERK1. Upon perception of chitin, the RLCK-VII member OsRLCK185 associates with, and is phosphorylated by CERK1, mediating downstream signalling processes, such as the activation of MAPK cascades and an influx of calcium, mediated by OsCNGC9.

The perception of nlp20, which is the epitope of NLPs, by RLP23/SOBIR1, also triggers the recruitment of BAK1 and the phosphorylation of RLCK-VII members. The RLCKs PBL30 and PBL31 are required for the generation of ROS upon perception of nlp20. The EDS1/PAD4/ADR1 node is required for proper activation of RLP23-triggered defence responses.

In tomato, perception of the fungal effector Avr4 by the constitutive Cf-4/SOBIR1 complex triggers the recruitment of BAK1, followed by activation of the receptor complex by phosphorylation. Unlike RLP23/SOBIR1, the activation of Cf-4/SOBIR1 results in an HR that largely depends on the helper CNL NRC3.

In the cytoplasm, activation of TNLs, such as *N. benthamiana* ROQ1 and *Arabidopsis* RPP1 and RRS1/RPS4, results in the formation of a tetrameric resistosome with multiple enzymatic activities. These TNL resistosomes produce signalling molecules, including ADPr-ATP/di-ADPR and pRib-ADP/AMP. A dimer composed of EDS1 and SAG01 acts as a receptor for ADPr-ATP/di-ADPR, thereby activating the helper RNL NRG1, while a dimer composed of EDS1 and SAG101 is the preferential receptor complex for pRib-ADP/AMP, which activates the helper RNL NRG1.

The potato CNLs Rpi-blb2 and Rx require the activity of helper CNLs to activate defence responses. When expressed in *N. benthamiana*, Rpi-blb2 requires the helper CNL NRC4, while Rx has a redundant requirement of the three NRCs present in *N. benthamiana*.

Singleton CNLs, such as *Arabidopsis* ZAR1 and wheat Sr35, do not require helper NRCs to oligomerize in a pentameric structure with pore-forming activity in the PM, inducing a Ca^{2+} influx and an HR. Helper RNLs and NRCs are proposed to form Ca^{2+} channels with an activity comparable to the one of ZAR1.

Solid lines indicate validated molecular mechanisms, and dashed lines indicate hypothetical models and pathways requiring more experimental validation. The sections of the figure depicting the molecular mechanisms of NLRs are modified from Kourelis and Adachi (2022) [169].

These RLCKs are a large family of cytoplasmic protein kinases. For example, there are close to 160 members in *Arabidopsis*, many of which associate with the PM through N-acylation [155,156]. RLCKs are divided into 17 groups, and members of the particular group RLCK-VII have prominent roles in immune signalling [113]. For instance, the RLCK-VII members BOTRYTIS-INDUCED KINASE 1 (BIK1) and its close paralog PBS1-LIKE 1 (PBL1), are required for mounting the immune responses that are initiated by LRR-RLKs, including FLS2, PEPR1 and PEPR2. BIK1 and PBL1 constitutively interact with these LRR-RLKs and become phosphorylated, and thereby activated, upon perception of the corresponding ExIPs and subsequent recruitment of BAK1 [115,157,158]. Activated BIK1 and PBL1 then dissociate from the receptor complexes and activate the PM-localised RESPIRATORY BURST OXIDASE HOMOLOG D (RBOHD) by phosphorylation, resulting in a fast production of ROS in the apoplast [159] (Figure 1). The activation of RLCKs downstream of cell-surface receptors, such as FLS2, also results in the activation of MAPK cascades and cyclic nucleotide-gated channels (CNGCs). The phosphorylation of CNGCs results in a rise of the concentration of cytosolic Ca^{2+}, which in turn activates CALCIUM-DEPENDENT PROTEIN KINASES (CDPKs). Together, these processes act as signal transducers, resulting in transcriptional reprogramming for defence responses [25,160,161].

Recent reports have shed some more light on the signalling mechanisms of LRR-RLPs mediating immune responses and have established a connection of LRR-RLP signalling with the signalling processes mediated by NLRs. In *Arabidopsis*, the RLCK-VII members PBL31 and its close paralog PBL30 are required for the ROS burst triggered upon activation of the LRR-RLP RPL23 [162]. Additionally, the EDS1/PAD4/ADR1 node is required for a subset of the immune responses that are triggered by the LRR-RLPs RPL23 and RPL42, while having a less prominent role downstream of the LRR-RLK FLS2 [162,163]. In the solanaceous plants tomato and *N. benthamiana*, the RLCK-VII member AVR9/CF-9-INDUCED KINASE 1 (ACIK1) is required for full Cf-mediated immune responses, including the HR [164]. However, its exact role in the signalling cascade remains undiscovered. Intriguingly, while the signalling cascade downstream of the tomato LRR-RLP Ve1 requires EDS1, evidencing a link with the signalling cascades downstream of TNLs, the HR triggered by the LRR-RLP Cf-4 in *N. benthamiana* is largely mediated by the helper CNL NRC3 [165]. Considering that all the LRR-RLPs characterised so far signal through the adaptor RLK SOBIR1 and the regulatory RLK BAK1 (and related SERKs), it is puzzling that different LRR-RLPs require different downstream signalling partners and trigger immune responses with different intensities. For instance, in *Arabidopsis*, the recognition of fungal endopolygalacturonases (PGs) by RLP42 triggers an HR [91], while the recognition of necrosis and ethylene-inducing peptide 1-like proteins (NLPs) by RLP23 does not trigger an HR [89]. In tomato, although the recognition of Avr4 by Cf-4 and Avr9 by Cf-9 produces a strong HR, the activation of Cf-4 and Cf-9 results in macroscopically distinct necrotic patterns [166]. Furthermore, the HR triggered by Cf-2 and Cf-5 is much slower and less intense that the HR triggered by Cf-4 and Cf-9.

Historically, the signalling cascades downstream of cell-surface receptors and NLRs were regarded as separate pathways [6,19]. Currently, emerging evidence shows that immune signalling by cell-surface receptors and NLRs mutually potentiates each other by inducing the upregulation of their core signalling components [9,10]. For instance, in the absence of cell-surface immune signalling, the activation of NLRs, such as the paired TNLs RRS1 and RPS4, does not result in an HR [9]. Thus, our current view of the mechanisms mediating plant defence responses, describes cell-surface receptors and cytoplasmic NLRs as a united front against invasion by detrimental pathogens [8,167,168].

OUTLINE OF THIS THESIS

The LRR-RLP Cf-4 is a cell-surface receptor that triggers an HR upon perception of the effector protein Avr4 of the fungal pathogen *Cladosporium fulvum* (Syn. *Fulvia fulva*). Cf-4 and Avr4 represent an example of the blurred distinction between MAMPs and effectors, and between PTI and ETI [24]. The receptor Cf-4 interacts constitutively with the adaptor RLK SOBIR1, forming a bimolecular receptor that recruits the RLK BAK1 upon perception of Avr4 [66,76]. The formation of the Cf-4/SOBIR1/BAK1 complex is proposed to trigger a series of phosphorylation events between the kinase domains of SOBIR1 and BAK1 and downstream signalling partners that eventually activate downstream signalling cascades required for the activation of defence responses [77]. From this point, little is known about the additional components regulating this receptor complex and for example the identity of the immediate downstream signalling components is largely unknown. The studies described in this thesis are aimed at gaining more knowledge into the molecular mechanism of Cf-4-mediated immune signalling.

The first challenge when studying the regulation of a receptor complex triggering an HR, is to have a proper read-out to use as a proxy for the intensity of the cell death processes happening within the plant tissue upon immune activation. In **Chapter 2**, a new method is presented for the visualisation and quantification of the intensity of the HR. It is shown that red light fluorescence detection by a multipurpose imaging system allows for an objective quantification of the intensity of the cell death responses within a plant tissue. The utility and flexibility of the method by imaging the HR triggered by an LRR-RLP, a TNL, a CNL, and the cell death caused by the cytolytic activity of a protein that forms pores in the plasma membrane is shown. Additionally, the non-destructive nature of this approach allows to monitor the development of cell death responses over a time course of an inoculation assay.

In **Chapter 3**, we aim to transfer relevant biological information from the model plant *Arabidopsis* to the solanaceous research model plant *N. benthamiana*. We performed a gene expression network analysis on a large set of publicly available microarray data from *Arabidopsis* and found that genes encoding components of the SOBIR1 complex belong to a transcriptional cluster that is enriched in genes associated with plant immune responses. Several genes in this cluster, involved in immune responses mediated by SOBIR1 in *Arabidopsis*, were assessed for their role

in transgenic *N. benthamiana* expressing the RLP Cf-4. We combined the application of virus-induced gene silencing, phenotypic analysis, such as ROS burst measurements and red light imaging assays, and protein interaction analysis, to gain novel insights into the regulation of the downstream signalling events that are activated upon perception of Avr4 by the Cf-4/SOBIR1 complex in *N. benthamiana*.

Chapter 4 addresses the challenges associated with identifying transient and weak protein-protein interactions involving membrane-associated proteins. To overcome these limitations, we implemented proximity-dependent labelling (PL), using the TurboID biotin ligase. The chapter outlines the adaptation of a PL protocol and the validation of TurboID-tagged bait proteins, enabling the selective biotinylation of proteins that are present in close proximity to the baits.

With the TurboID-tagged versions of the Cf-4 and SOBIR1 baits that were generated, in **Chapter 5** we explore the molecular environment of the Cf-4/SOBIR1 complex by performing PL, followed by mass spectrometry analysis of the biotinylated proteins. This approach resulted in the consistent identification of a set of proteins that was found to be in close-proximity to the Cf-4/SOBIR1 complex across multiple experiments. This proximal proteome includes proteins that are known to be functionally related to the receptor complex, as well as multiple candidates for further laboratory evaluation.

Finally, **Chapter 6** explores the primary pathways of programmed cell death in the context of the interactions of plants with their microbial pathogens. It presents the main findings that are described in this thesis in relation to the signalling cascade that is activated upon perception of Avr4 by the Cf-4/SOBIR1 complex in *N. benthamiana*.

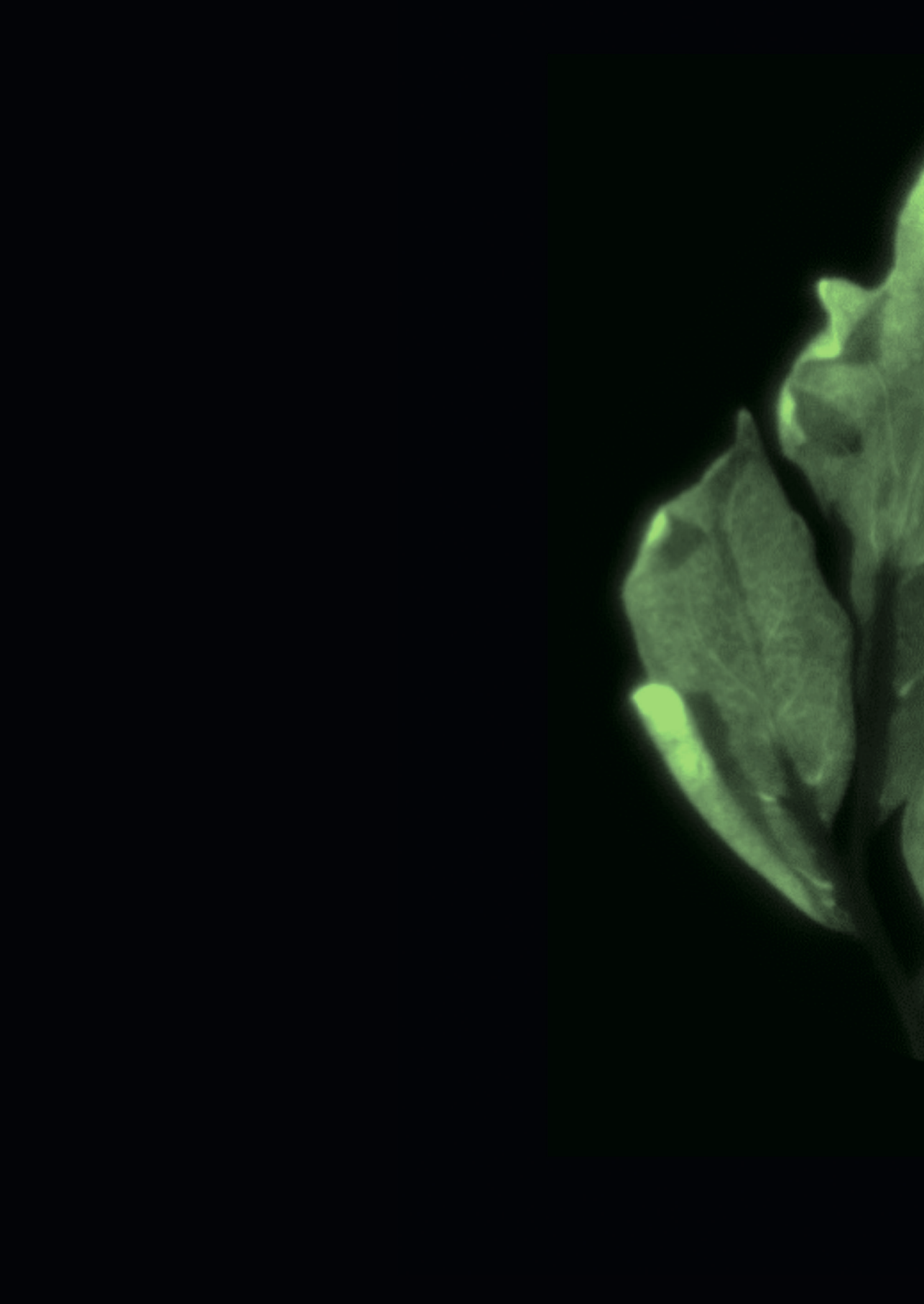

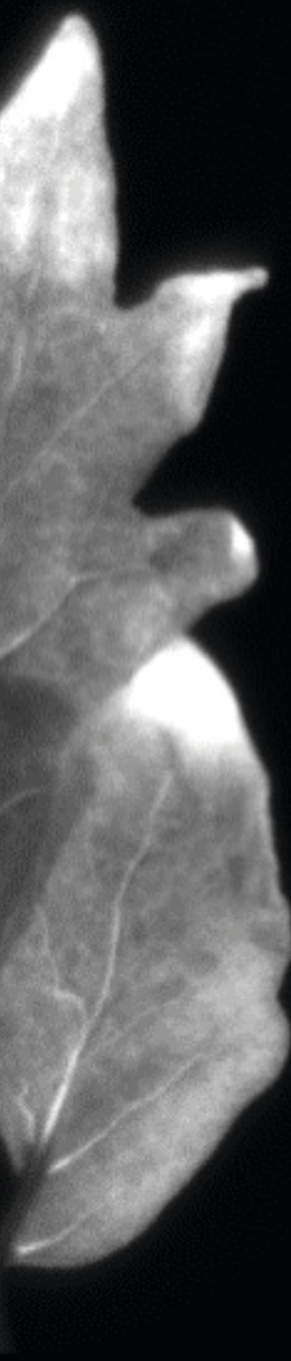

CHAPTER 2

Red light imaging for programmed cell death visualisation and quantification in plant–pathogen interactions

Sergio Landeo Villanueva[a#], Michele C. Malvestiti[a#], Wim van Ieperen[b], Matthieu H.A.J. Joosten[a], Jan A.L. van Kan[a]

[a] Laboratory of Phytopathology, Wageningen University & Research, Droevendaalsesteeg 1, 6708 PB Wageningen, The Netherlands

[b] Horticulture and Product Physiology, Wageningen University & Research, Droevendaalsesteeg 1, 6708 PB Wageningen, The Netherlands

[#] These authors contributed equally

A slightly modified version has been published in: Mol. Plant Pathol. **22**, *361–372 (2021).*

ABSTRACT

Studies on plant–pathogen interactions often involve monitoring disease symptoms or responses of the host plant to pathogen-derived immunogenic patterns, either visually or by staining the plant tissue. Both these methods have limitations regarding resolution, reproducibility, and the ability to quantify the results. In this study, we show that red light detection by the red fluorescent protein (RFP) channel of a multipurpose fluorescence imaging system that is probably available in many laboratories can be used to visualise plant tissue undergoing cell death. Red light emission results from chlorophyll fluorescence on thylakoid membrane disassembly during the development of a programmed cell death process. The activation of programmed cell death can occur during either a hypersensitive response to a biotrophic pathogen or an apoptotic cell death triggered by a necrotrophic pathogen. Quantifying the intensity of the red light signal enables the magnitude of programmed cell death to be evaluated and provides a readout of the plant immune response in a faster, safer, and non-destructive manner when compared to previously developed chemical staining methodologies. This application can be implemented to screen for differences in symptom severity in plant–pathogen interactions, and to visualise and quantify in a more sensitive and objective manner the intensity of the plant response on perception of a given immunological pattern. We illustrate the utility and versatility of the method using diverse immunogenic patterns and pathogens.

INTRODUCTION

In natural environments as well as in agricultural systems, plants are constantly threatened by pathogens, including nematodes, oomycetes, fungi, bacteria, and viruses. In order to invade, colonise, and obtain nutrients from their host, these pathogens must deal with plant defence mechanisms, and therefore they have evolved different lifestyles and strategies to overcome the plant immune system and cause disease. Given their sessile nature, plants rely in the first line of their defence on anatomical barriers and preformed phytochemical compounds to prevent pathogen invasion. However, when pathogens can overcome these first passive defence layers, recognition of the invaders by the plant can take place within the host tissue. To perceive danger, plants have evolved a wide range of receptors and their function consists of the recognition of so-called immunogenic patterns (IPs), in both the apoplast and the cytoplasm [18,170]. Triggers of plant immunity include damage-associated molecular patterns (DAMPs) [48], structural components of the invaders (microbe-associated molecular patterns, MAMPs), and pathogen-secreted compounds known as effectors that serve to perturb plant defence responses and promote virulence [171]. Apoplastic triggers of immunity are referred to as extracellular immunogenic patterns (ExIPs) [18]. These are perceived by cell-surface receptors, which have been grouped into receptor-like kinases (RLKs, containing a cytoplasmic kinase domain) and receptor-like proteins (RLPs, which lack such a domain) [171]. By contrast, cytoplasmic danger signals are referred to as intracellular immunogenic patterns (InIPs) and are recognised by the activity of cytoplasmic receptors, usually from the category of nucleotide-binding leucine-rich repeat receptors (NLRs) [18]. Extra- and intracellular receptors possess highly variable LRR domains that confer specific binding capacity to a wide array of ExIPs and InIPs [18]. On perception of immunogenic patterns, cell-surface receptors and NLRs activate downstream signalling pathways, leading to the induction of immune responses to block the invader.

Plant immune responses comprise multiple cellular processes, among others, alkalisation of the extracellular space [172,173], cell wall reinforcement via callose deposition [174,175], accumulation of reactive oxygen and nitrogen species [176], an increase in intracellular calcium [177], biosynthesis of pathogenesis-related (PR) proteins [178] and phytoalexins [179], and the release of small RNAs to interfere with the transcriptional machinery of the invading pathogen [180]. In an attempt to stop pathogen invasion and disease development, the affected plant cells can commit suicide by undergoing

programmed cell death (PCD). Even though it represents a decisive and seemingly altruistic response of an individual plant cell to pathogen invasion, PCD can lead to either resistance or to disease development, depending on the lifestyle of the pathogen. In incompatible interactions with biotrophic pathogens, PCD is referred to as the hypersensitive response (HR) and manifests itself as an effective resistance response of the plant upon pathogen recognition. The HR represents a form of autophagic PCD, preventing the spread of biotrophic microbes [181,182]. For example, race 5 of the biotrophic fungus *Cladosporium fulvum*, which causes leaf mould of tomato following a typical gene-for-gene interaction, cannot cause disease on tomato carrying the gene encoding the RLP Cf-4 [40,68]. This cell-surface receptor recognises the Avr4 effector protein that is secreted by *C. fulvum* race 5 and mediates the activation of the HR, leading to leaf mould resistance [68]. On the other hand, in interactions with necrotrophs, PCD occurs after induction of apoptosis of the affected host cells and becomes visible as a necrotic lesion [183,184]. In this situation, PCD shows specific apoptosis hallmarks, which include cell shrinkage and membrane blebbing with retention of plasma membrane integrity, loss of mitochondrial membrane potential and release of cytochrome c into the cytoplasm, protease activation, chromatin condensation and nucleosome cleavage, decrease in ATP, and increase in reactive oxygen species (ROS) [185]. Necrotrophic pathogens, such as fungi of the genus *Botrytis*, exploit the plant PCD pathway by actively triggering apoptosis in host cells through the activity of an array of effector compounds, allowing the pathogen to acquire nutrients from the dead plant cells and to colonise the plant tissue [186].

To determine the level of resistance or susceptibility of a given plant genotype, assessment of disease symptoms in an infection assay is a key step to evaluate the outcome of an interaction between host and pathogen. Thus, visualisation and quantification of PCD over a given period of time are essential to understand how the plant responds upon contact with the pathogen. Furthermore, a visual assessment is often performed to study the effect of individual pathogen IPs (including effectors) on the host, which is done by applying such molecules to a plant tissue by either agroinfiltration or IP injection. This approach allows plant genotypes to be compared for their responses to pathogens or specific IPs and for disease development or the establishment of resistance responses to be monitored over time.

At present, the most widely used and commonly accepted method to visualise plant cell death is the trypan blue staining (TBS) technique, which is a cell viability test

based on the principle that live cells, possessing intact and functional cell membranes, exclude trypan blue dye whereas dead cells do not. This staining method was first described by Ehrlich [187] in a study in which trypan blue dye was injected into animal tissue and he observed that the brain tissue showed less staining. Subsequent research showed that when trypan blue was injected directly into the central nervous system instead, the brain tissue would stain equally well, but the stain would not travel to the rest of the body, showing a compartmentalization between the cerebrospinal fluid and the vasculature in the rest of the body [187,188]. In the course of the 20th century and until current times, TBS has been successfully implemented in plant biology and phytopathological studies because it was found that TBS allows plant vascular tissue [189], dead *Arabidopsis thaliana* cells because of HR induced by *Pseudomonas syringae* effectors [190], or cell death responses in *Brassica rapa* cotyledons to oomycete elicitin [191] to be visualised. TBS consequently became useful to assess the extent of plant tissue colonisation by microbial pathogens and, for example, for detecting (micro-)lesions in plant–microbe interactions [192]. Nevertheless, TBS has four major drawbacks. First, it is not understood how trypan blue dye can pass membranes of dead cells and of hyphae of live fungi and oomycetes, whereas the dye is specifically excluded from live plant cells with an intact plasma membrane. Second, the method requires the use of toxic chemicals, such as the dye itself, phenol, and chloral hydrate. Third, TBS represents a destructive assay that does not allow disease progression and/or the occurrence of plant cell death responses to be followed in the same sample over time, nor does it allow the tissue to be sampled for RNA, protein, or metabolite analyses after it is stained. Finally, the method provides a qualitative test of cell viability, but it does not easily allow PCD to be quantified in a standardised way

We here report a non-destructive, nontoxic, and reproducible method to visualise and quantify cell death in green plant tissues. This method can be implemented to study different pathosystems and allows the development of PCD to be followed over time. The protocol is based on the detection of light signals emitted by plant cells undergoing cell death. With the aid of a fluorescence imaging system, we observed red light emission by leaf tissue upon infiltration with known PCD-inducing compounds, agroinfiltration, or infection by a pathogen. We provide evidence that the red light signal originates from the increase in chlorophyll fluorescence due to the dismantling of chloroplast thylakoid membranes in cells undergoing PCD. We provide several illustrations that this method can be used as a versatile tool for

quantitative and non-destructive evaluation of plant responses to microbial pathogens or their IPs.

RESULTS

This study was initiated after the observation that on exposure to a green light source, leaf tissue undergoing a typical HR emits light that could be detected using the red light filters of a fluorescence imaging system. Our initial experiments indicated that the intensity of the emitted light positively correlated with the severity of visual signs of cell death. We set out to explore whether this method would be suitable for the development of an alternative, fast, simple, and safe non-destructive tool to visualise cell death in plant tissue. This tool should allow users to quantify PCD in a standardised and reproducible manner and to follow the development of PCD over a given time course. Therefore, we first tested whether the areas yielding a light signal that was detected with red light imaging originated from the affected tissue that in PCD tests is normally stained with trypan blue. *Nicotiana benthamiana:Cf-4* leaves were infiltrated with pure Avr4 protein from *C. fulvum* and we compared the visible HR symptoms with the classic TBS and the red light signal on the same leaves (Figure 1).

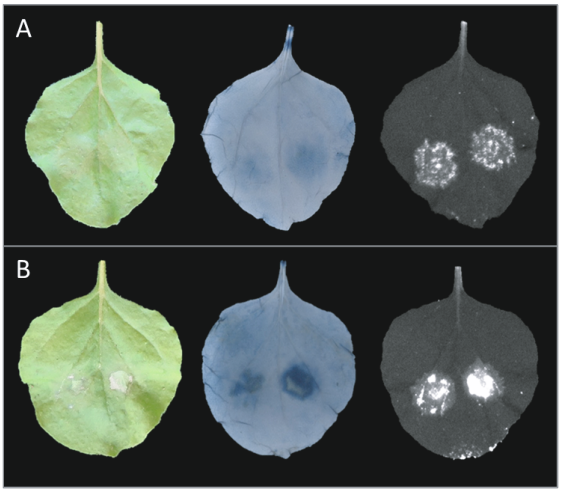

Figure 1. Cell death symptoms caused by Avr4 infiltration (A: 1 µM; B: 5 µM) in leaves of ***N. benthamiana:Cf-4*** plants, visualised at 3 days after infiltration with visible light (left column), trypan blue staining (middle column), and red light imaging system (right column)

At 3 days after infiltration (dai), HR symptoms were observed on leaves infiltrated with 5 µM of Avr4 but not 1 µM (Figure 1, left column). Comparing TBS (Figure 1, middle column) to the red light signal (Figure 1, right column), it can be noticed that the areas stained with trypan blue exactly match with the areas from which the red light signal is detected by the imaging system. The signal intensity was clearly stronger at higher Avr4 concentration and showed a punctate pattern, with the most intense red light emission from areas that displayed the most obvious signs of cell death.

Recently, several studies have used UV transillumination to monitor cell death responses [137,193]. We compared the use of UV light as a source of excitation for imaging of tissue undergoing PCD to the imaging based on green light excitation described above (Figure S1). When the leaves were excited with UV light, a much stronger background signal was detected in the healthy tissue and in the leaf veins. Such a background signal interferes with the red light signal that derives from tissue undergoing PCD, thereby rendering the UV imaging system less sensitive for areas yielding lower signal intensities.

Having shown that the necrotic areas exactly match with the areas from which the red light signal originates, we infiltrated different IPs into leaves of *N. benthamiana* to test whether the intensity of the red light signal correlates with the severity of the visible PCD symptoms (Figures 2-4). On infiltration of flg22, at 3 dai no cell death symptoms were observed on the leaves, and also no red light signal was detected (Figure 2A). On the other hand, a clear red light signal was detected on Avr4 infiltration in leaves of *N. benthamiana* stably expressing Cf-4, but, apart from some chlorosis, no cell death symptoms were observed (Figure 2B). In contrast, BcNEP1 infiltration caused the swift development of a clearly visible area of dry necrotic tissue that matched with the area yielding a strong red light signal (Figure 2C). In a ROS burst assay, the incubation of leaf disks of *N. benthamiana* in a solution containing either flg22, Avr4, or BcNEP1 triggered a strong ROS burst (Figure 2, lower panel).

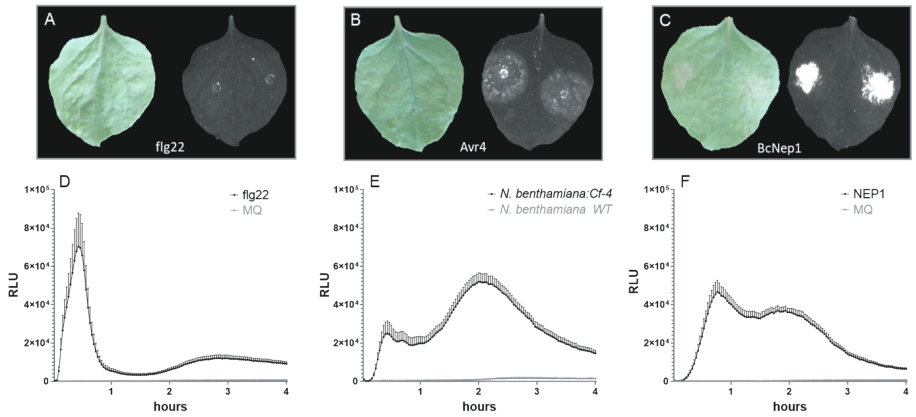

Figure 2. Visible cell death symptoms (left) and detected red light signal (right) on infiltration of 0.1 µM flg22 (A), 0.01 µM Avr4 (B), and 0.004 µM BcNEP1 (C) at 3 days after infiltration in leaves of ***N. benthamiana:Cf-4***. Reactive oxygen species burst triggered by 0.1 µM flg22 and the Milli-Q water (MQ) control in ***N. benthamiana*** wild-type (WT) (D), 0.01 µM Avr4 in ***N. benthamiana:Cf-4*** and the ***N. benthamiana*** WT control plant (E), and 0.004 µM BcNEP1 and the MQ control in ***N. benthamiana*** WT (F). n = 8, error bars show the SE.

To test whether this method can also be used in combination with *Agrobacterium* transient transformation assays (ATTA; agroinfiltration), genes encoding IPs and their corresponding immune receptors were transiently expressed in *N. benthamiana* leaves and the development of HR was monitored. Expression of Avr4 or Cf-4 alone caused no symptoms of HR and no red light signal was detected outside the area of wounding caused by the syringe during the infiltration. Transient expression of both Avr4 and Cf-4 in the same leaf area caused symptoms of HR and a clear red light signal was detected (Figure 3A). Similarly, transient expression of the protein Avr4BS4 from *Xanthomonas campestris* pv. *vesicatoria* and its matching tomato immune receptor, the NLR BS4, triggered symptoms of HR and a red light signal only when infiltrated in combination (Figure 3B) [194]. Moreover, the elicitor-independent HR triggered by NRC1^{D481V} was also tested, which is a constitutively active mutant of the tomato NLR NRC1. In the agroinfiltrated areas, HR symptoms were observed together with a strong emission of a red light signal. In contrast, expression of NRC1^{K191R}, which is an inactive mutant of NRC1, caused no HR and no red light signal was detected (Figure 3C) [195]. Furthermore, quantification of HR upon agroinfiltration was assessed by transiently expressing Avr4 in *N. benthamiana:Cf-4* after virus-induced silencing of the gene encoding the immune receptor Cf-4. A significant decrease in the signal intensity was observed when Cf-4 was silenced (Figure 3D).

To explore whether the imaging system also functions for plants other than *N. benthamiana*, we infiltrated a different IP, namely the *Botrytis cinerea* polygalacturonase 3 (BcPG3) protein, in detached leaves of wild-type (WT) *Arabidopsis* Col-0 plants and in an *Atsobir1 Arabidopsis* mutant [91]. As depicted in Figure S2, necrotic tissue in combination with a clear red light signal was observed only in leaves of the WT plants, whereas neither necrotic spots nor a red light signal were detected on BcPG3 infiltration in the *Atsobir1* mutant. In addition, a specific red light signal was detected in leaves of transgenic tomato seedlings systemically expressing both the *C. fulvum* Avr4 and the Cf-4 resistance protein [40], even before symptoms of necrosis were observed (Figure S3).

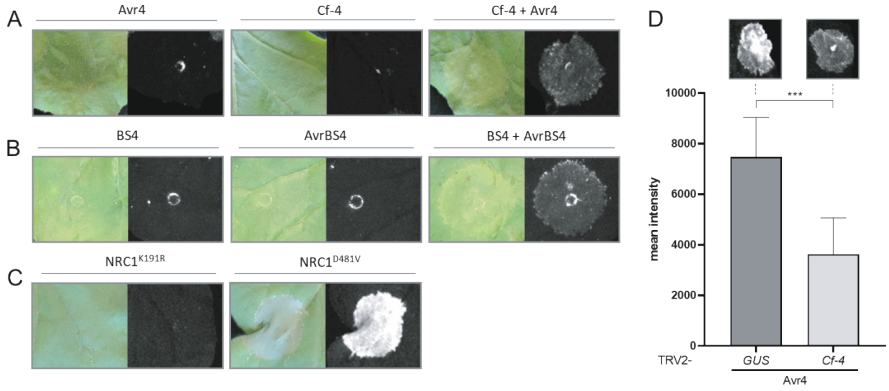

Figure 3. Cell death symptoms on agroinfiltration of Avr4/Cf-4 (A), AvrBS4/BS4 (B), NRC1^{K191R} and NRC1^{D481V} (C) in ***N. benthamiana*** leaves at 3 days after infiltration (dai), visualized under visible light and with the red light imaging system. (D) Red light signal intensity measured upon agroinfiltration of Avr4 after virus-induced gene silencing of ***Cf-4*** in ***N. benthamiana:Cf-4*** at 3 dai, n = 8. Bars represent SD. ***Significant difference using a t test, $p < 0.001$

Besides the qualitative visualisation of PCD in different plant species, this methodology should also allow the quantification of the magnitude of PCD by measuring the intensity of the red light signal. To test this application, we infiltrated leaves of *N. benthamiana:Cf-4* with different concentrations of Avr4 protein from *C. fulvum* and BcNEP1 protein from *B. cinerea* (Figure 4). While even the highest concentration (1 µM) of Avr4 protein barely induced any sign of PCD as observed with the naked eye (Figure 4D), the imaging system detected increasing red light signal intensities emitted by the infiltrated tissue on infiltration of higher Avr4 concentrations (Figure 4D,E). By contrast, no red light signal was detected in the mock-infiltrated

areas, except at sites where the syringe was applied and pressed on the leaf to infiltrate the Milli-Q water (MQ), thereby causing some wounding (Figure 4D, MQ). On the other hand, BcNEP1 infiltration caused visible necrotic spots even at the lowest concentrations used (Figure 4A), whereby the red light signal intensity measured on BcNEP1 infiltration was up to 25-fold higher than in Avr4 infiltrated leaves (Figure 4E,F). In addition, it can be noticed that when BcNEP1 was infiltrated at higher concentrations no clear differences in the necrotic tissues could be observed (Figure 4B,C). However, when quantified with the imaging system, increasing red light signal intensities were recorded in leaves infiltrated with increasing BcNEP1 concentrations (Figure 4F).

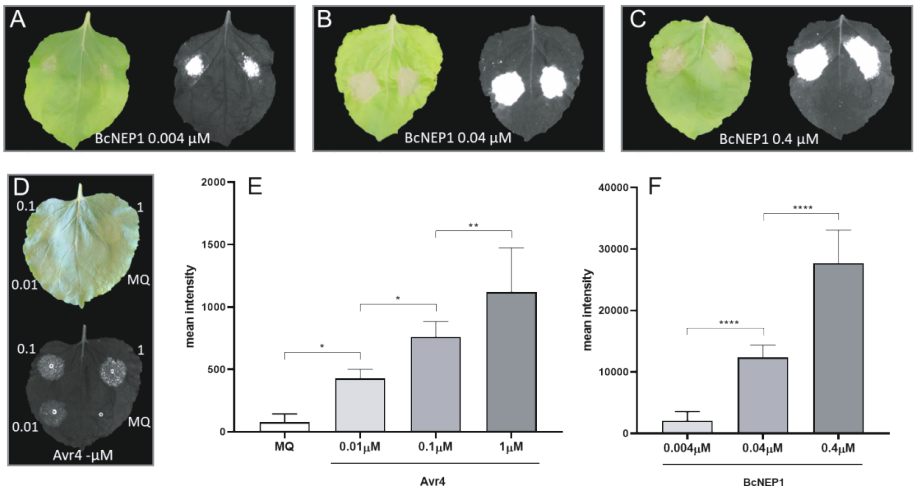

Figure 4. Dose-dependent cell death symptoms caused by BcNEP1 (A, B, C) and Avr4 (D) protein infiltration in *N. benthamiana:Cf-4* at 3 days after infiltration, as visualized under visible light and with the red light imaging system. Quantification of red light signal intensities emitted by *N. benthamiana:Cf-4* leaves infiltrated with 0.01, 0.1, and 1 µM Avr4 protein and Milli-Q water (MQ) as a control (E), and with 0.004, 0.04, and 0.4 µM BcNEP1 protein (F). Bars represent averages ± SD (n = 8). Significant difference using analysis of variance followed by Tukey's test, *p < 0.05, **p < 0.01, ****p < 0.0001.

Furthermore, to monitor the development of PCD over a given time course of infection, leaves of *N. benthamiana* and *Arabidopsis* Col-0 were inoculated with a conidial suspension of *B. cinerea*. In both cases, development of necrotic lesions was observed from 2 days post inoculation (dpi) and the imaging system detected

a clear red light signal at the site of the lesion (Figure 5A,B). For *N. benthamiana*, pictures of the same detached leaves were taken at 2, 3, and 4 dpi. This was not possible for *Arabidopsis* leaves because they were too fragile after detachment, and therefore symptom development was followed on detaching different leaves at 2 and 3 dpi. Following incubation, we observed that the lesions expanded and that the red light signal was sometimes detected in irregular shapes, outside of the circular necrotic spot caused by the fungus. The latter light-emitting zones were not visible to the naked eye (Figure 5A,B, yellow arrows). Moreover, the imaging system detected a red light signal for both *Arabidopsis* and *N. benthamiana*, which was visible as concentric rings of different intensities at the location where the necrotic lesions developed (Figure 5A,B, red arrows). Besides leaves, the red light imaging system was also tested to detect disease symptoms on stem tissue. When *B. cinerea* conidia were inoculated onto *N. benthamiana* intact and cut stems, red light emission was observed in stem tissue showing visible disease symptoms (Figure S4).

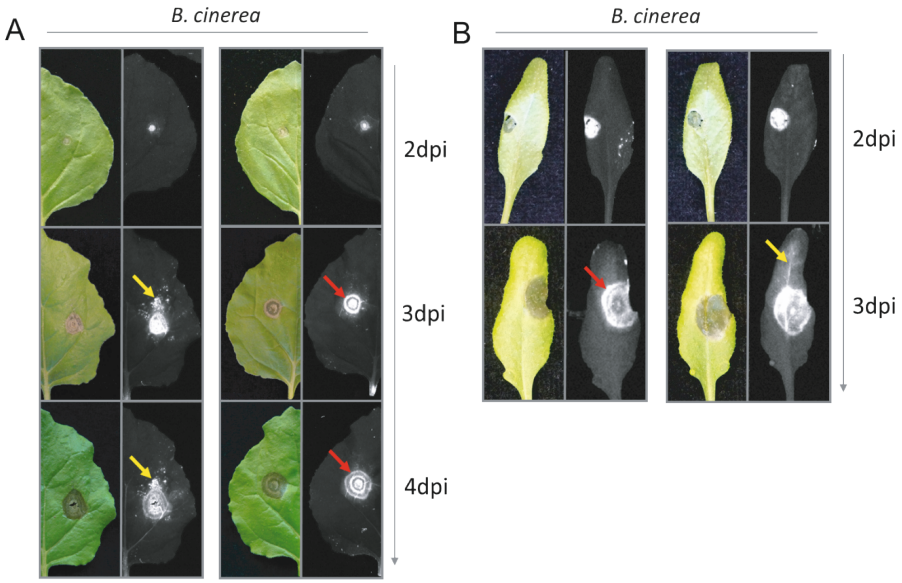

Figure 5. Necrotic lesions developing after *Botrytis cinerea* inoculation on leaves of (A) *N. benthamiana* and (B) *Arabidopsis*, visualized with visible light (left) and with the red light imaging system (right). Yellow arrows indicate the red light signal detected in tissue outside the necrotic lesions; red arrows indicate distinct concentric rings with different red light signal intensities within the lesion. dpi, days post inoculation.

We also followed the development of necrotic lesions on two lily cultivars inoculated with two different *Botrytis elliptica* isolates. Figure 6 shows the necrotic lesions that were observed at 3 and 4 dpi. In all cases, the lesions expanded during the incubation. With both isolates, distinct areas were observed emitting a light signal of different intensities, with a fairly abrupt transition between them (Figure 6B). The outer area showed a lower red light intensity (Figure 6B) and this was not visible as necrotic tissue when the picture was taken with visible light. Moreover, for the most aggressive isolate (Be9401) in both cultivars the imaging system detected a much weaker red light signal in the centre of the lesion compared to the concentric rings around the inoculation site and the red light signal was also detected in leaf veins. In contrast, for the less aggressive isolate (Be9732), the signal remained intense at the inoculation site, while the lesions were still expanding and no red light signal was detected in the leaf veins. To illustrate the differences in symptom severity and to compare isolate virulence and cultivar susceptibility, the signal intensities over the lesion areas were quantified, and the values were plotted on a bar chart (Figure S5).

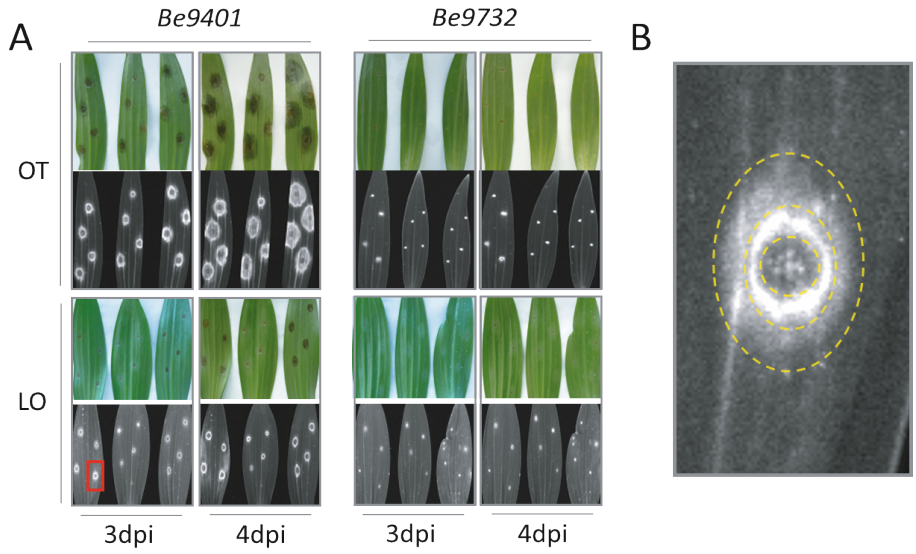

Figure 6. (A) Necrotic lesions developed after inoculation of ***Botrytis elliptica*** isolates ***Be9401*** and ***Be9732*** on leaves of lily genotypes OT and LO, visualized with visible light (upper) and with the red light imaging system (bottom), at 3 and 4 days post inoculation (dpi). For each time point and cultivar, three representative leaves are shown. (B) Magnification of a necrotic lesion observed at 3 dpi on genotype LO, highlighted by a red rectangle in (A), showing an area with different light signal intensities. Yellow dashed lines indicate the borders between these areas.

To explain the origin and nature of the observed red light signal in tissue undergoing PCD, we hypothesized that the signal might derive from the disassembly of thylakoid membranes of the chloroplasts. To test this hypothesis, chloroplasts were isolated from *N. benthamiana* leaves and treated with different concentrations of the membrane-disrupting surfactants Nonidet P-40 and sodium dodecyl sulphate (SDS), and the surfactant solutions were also directly infiltrated in detached *N. benthamiana* leaves (Figures S6 and S7). As shown in Figure 7A,C, red light emission was detected in the chloroplast suspension after treatment with both surfactants, whereas no red light was emitted by the untreated chloroplast suspension and the pure surfactant solutions.

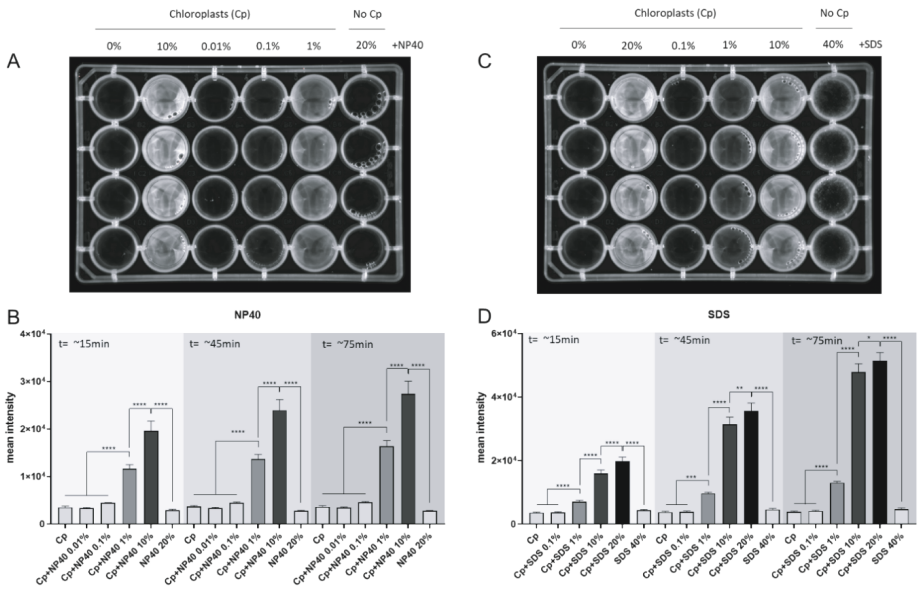

Figure 7. Red light emission in a 24-well plate containing a chloroplast suspension obtained from *N. benthamiana* leaves after treatment with Nonidet P-40 (NP40) (A, B) or sodium dodecyl sulphate (SDS) (C, D) at different concentrations. Red light signal intensities, determined at three time points after the indicated treatments, were quantified and bars represent averages ± SD (n = 4). Significant difference using analysis of variance followed by Tukey's test, *p < 0.05, ***p < 0.001, ****p < 0.0001

The graphs in Figure 7B,D show that the red light intensities increased when the chloroplasts were treated with a higher concentration of the surfactant, as well as with a longer incubation time with 10% Nonidet P-40, and with 10% and 20%

SDS. On direct leaf infiltration with the surfactant solutions, the tissue collapsed in a dose-dependent manner and eventually showed a brownish colouration that resembled the necrotic tissue observed upon infiltration of various IPs and in the inoculation assays (Figures S3-S5).

DISCUSSION

Advantages and applications of red light imaging for studies in plant pathology

Various imaging systems have been developed to investigate plant defence responses. These include quantification methods for ion flux changes and ROS accumulation [196], nitric oxide generation [197], and biophoton generation [198]. Despite focusing on plant defence responses, none of these methods allows PCD to be investigated as a determinant of the outcome of the interaction in a given pathosystem, which usually requires a destructive staining method, TBS. In this study, we describe a simple methodology to visualise and quantify PCD in green plant tissues using the red light filter of a fluorescence–luminescence imaging system, which was originally purchased for imaging DNA or protein gels and western blots. We show that the system can also be applied for imaging plant cell death during interactions with pathogens or their IPs.

Compared to classical TBS, the red light imaging method has several advantages. First of all, it is safer because it does not require the use of toxic chemicals for preparing the staining and destaining solutions, and it generates no chemical waste. The method is fast and simple because it is solely based on the detection of a light signal that is automatically processed by the imaging system. This allows the analysis of a large number of samples in a short time, which makes it useful for large-scale screenings, with up to hundreds of leaves per day. Importantly, in contrast to TBS, this method is non-destructive and the same samples can be analysed at different time points to monitor the progression of PCD or the imaging may assist in selecting different regions in the sample for extraction of RNA, proteins, or metabolites. Both in the case of leaf infiltration with different IPs and in inoculation assays with pathogens, the method allows the plant response to be observed at different time points, enabling the development of symptoms to be followed during the interaction over a given time span (Figures 5 and 6). The red light imaging system allows

PCD to be visualised and quantified in a standardised manner. Different parameters, such as the exposure time and the focus on particular sites of the sample, can be set in advance and with the aid of software, the red light intensities can be quantified for comparison among different samples. On the other hand, for lesion size measurements, it is possible to quantify the area of the tissue in which the red light signal exceeds the background levels. In contrast, in TBS, the staining intensity may depend on how long the tissue is treated with the staining and destaining solutions, thereby only permitting a qualitative visualisation of PCD, hampering a quantitative comparison across multiple samples. It is important to note that the imaging system requires placing the samples on a flat surface, therefore it is not possible to acquire images from three-dimensional objects such as whole plants because in that case the device is unable to bring the complete area to be studied into focus. More specialised and expensive equipment would be needed for such purposes.

This simple and non-destructive method allows new research aimed at studying the role of PCD in plant–pathogen interactions to be pursued. PCD symptoms can be detected before becoming visible to the naked eye and different stages of PCD might be distinguished depending on light intensities. In necrotic lesions caused by *Botrytis* spp., distinct concentric areas were observed showing a red light signal of different intensity. The absence of a red light signal at the centre of the lesion (Figure 6B) indicates that, at that location, the light signal emitting compounds have been completely degraded. In some cases, when moving distally from the centre of the lesion, the first area surrounding the inoculation site showed a higher signal intensity as compared to the lesion periphery, resulting in the formation of a concentric ring (Figure 6B). This observation might indicate that PCD is more advanced in the brighter region and is only just induced in the peripheral area. It remains to be established whether higher signal intensities correlate with more advanced stages of PCD. Moreover, by inoculating plant tissue with transgenic pathogen strains expressing green fluorescent protein (GFP), it should be possible to investigate whether host tissue colonisation has already occurred in the areas displaying low-intensity red light signals, or whether PCD has been induced by effector compounds that are secreted by the pathogen and have moved into the surrounding host tissue.

We tested the versatility of the methodology for investigating PCD development by infiltration of different IPs. Upon flg22 infiltration, we observed neither a red light signal nor development of a necrotic lesion, despite the fact that flg22 recogni-

tion took place in the leaf tissue and triggered a ROS burst, as previously reported (Figure 2) [199]. This observation confirms that PCD activation requires specific signalling mechanisms to be induced and that not all IPs equally trigger PCD [18]. There was a dose- and time-dependent cell death response on infiltration of various IPs at different concentrations (Figures 1 and 4). Because the symptoms are not always clearly visible, the red light filter of the imaging system provides a more reliable and objective tool to quantitatively determine the contribution of given IPs to PCD induction in the host tissue. Finally, this method will help to investigate the function of pathogen-secreted effectors. For example, by labelling pathogen-secreted effectors with fluorescent tags, it will be possible to study their mobility in the tissue and localisation over time during host infection, in conjunction with the host response to these effectors. Additionally, by identifying areas that are in an early stage of PCD, showing low-intensity red light signals, it should be possible to specifically dissect and process tissue areas to isolate proteins or RNAs at the appropriate time and location. Possibly, in this way also specific effector targets in the host cells and PCD signalling components can be identified via co-immunoprecipitation assays, as the appropriate tissue can be collected using the imaging system.

PCD, chlorophyll fluorescence, and the red light signal

This study shows that tissue undergoing PCD emits red light that can be detected by means of the imaging system. We hypothesised that the red light signal derives from increased chlorophyll fluorescence, as a consequence of the disassembly of the thylakoid membranes in the chloroplasts. This hypothesis was tested by treating isolated chloroplasts with membrane-disrupting surfactants (Figure 7) and by leaf infiltration with such surfactants (Figures S6 and S7). The membrane-disrupting properties of the surfactants caused a concentration-dependent emission of the red light signal from isolated chloroplasts and infiltrated leaves. From a photochemical point of view, this phenomenon can be explained by the abortion of photochemical activity due to the dismantling of the chloroplast thylakoid membranes in cells undergoing PCD, resulting in an increase in chlorophyll fluorescence. In photochemically active plant cells, chlorophyll molecules are tightly packed together in light-harvesting complexes (LHCs) that are located at the thylakoid membranes of the chloroplasts. Chlorophyll fluorescence is quenched by photochemical activity when LHC-photosystem II (PSII) complexes are assembled in thylakoids. Chlorophylls have two distinct absorption wavelength peaks in the visible light spectrum: the highest is found in the blue spectrum at c.450 nm and the lowest at 650 nm in the red spectrum.

Moreover, chlorophylls possess a fluorescence emission peak in the red spectrum at c.680 nm. During PCD or on perturbation of thylakoid membrane stability, LHC-PSII super-complexes are disassembled from chloroplast thylakoid membranes. This causes cessation of the electron flow required for photochemical activity because the connection between PSII and photosystem I via plastoquinone, cytochrome-b6f, and plastocyanin is lost. As a consequence, light-excited chlorophyll molecules will dissipate photon energy through heat and fluorescence [200].

CONCLUSION

In this study, we show that red light fluorescence detection by a multipurpose imaging system can be used to visualise plant tissue undergoing cell death. Quantifying the intensity of the red light signal enables the magnitude of cell death to be evaluated and thereby provides a readout of the plant immune response in a faster, safer, and non-destructive manner when compared to previously developed chemical staining methodologies. This application can be implemented to screen for differences in symptom severity in plant–pathogen interactions, and to visualise and quantify in a more sensitive and objective manner the intensity of the plant response on perception of a given immunogenic pattern.

MATERIALS AND METHODS

Plant material and growth conditions

Transgenic *N. benthamiana* plants stably expressing Cf-4 (*N. benthamiana:Cf-4*) [201] and WT *N. benthamiana* plants were grown under 16 hr light at 24 °C and 8 hr darkness at 22 °C and RH of 75%.

Arabidopsis ecotype Col-0 and the *Atsobir1* mutant line in the Col-0 background [93], were grown under 12 hr light at 21 °C and 12 hr darkness at 19 °C at an RH of 75%.

Lilium genotypes from the hybrid types OT (Oriental × Trumpet) and LO (Longiflorum × Oriental) were planted as bulbs and grown in the greenhouse under natural day/night light regime and temperatures. Mature leaves of 2-month-old plants were used for the inoculation assays.

Red light imaging and signal quantification

Treated plant material was placed in a ChemiDoc MP imaging system, model Universal Hood III (Bio-Rad), and images were acquired on excitation by a light source in the green visible spectrum (Green LED Module kit no. 1708284) or in the UV spectrum (UV-B Transillumination no. 1001361), with filters capturing the light emitted in the red visible spectrum (filter 605/50). The exposure time was adjusted to avoid image saturation. For comparison purposes, the images shown were auto-scaled according to the treatment that yielded the lowest signal intensity.

For the IP infiltration assays, the mean signal intensity was calculated using Image Lab v. 6.0.1 software by manually selecting the treated areas and subtracting the background signal intensity value. For the disease assay in *Lilium*, the spots yielding a light signal were manually highlighted, and the signal was calculated as the intensity over the selected area among 12 inoculations sites on three leaves per plant cultivar and per *B. elliptica* isolate at 2, 3, and 4 dpi.

Statistical analysis

GraphPad Prism v. 8.4.0 was used to perform an analysis of variance (ANOVA) with a post hoc Tukey's test on the IP infiltration experiments, chloroplast treatment with surfactants, and the *Botrytis* disease assays in *Lilium*.

Immunogenic pattern-triggered cell death assays

NEP1 protein from *B. cinerea* (BcNEP1) was produced in *Pichia pastoris* [202] and dissolved in 10 mM phosphate buffer, pH 5.5. The peptide flg22 (EZBiolab) and the protein Avr4 (produced in *P. pastoris*) [203] from *C. fulvum* were dissolved in water. Protein infiltration was carried out in the first fully expanded leaf of 5- to 6-week-old *N. benthamiana:Cf-4* and WT plants, and the cell death response was scored at 3 dai. The infiltrated areas were photographed and the average red light signal intensities were calculated.

B. cinerea polygalacturonase 3 (BcPG3) protein produced in *P. pastoris* [91] was dissolved in 10 mM sodium acetate buffer pH 4.2 and infiltrated at a concentration of 1.5 µM in fully expanded rosette leaves of 6- to 7-week-old *Arabidopsis* plants. The necrotic areas were photographed and analysed by red light imaging at 8 dai.

Tomato (*Solanum lycopersicum*) seedlings stably expressing both Avr4 and Cf-4 were generated by crossing transgenic tomato cv. Moneymaker (MM) expressing *C. fulvum* effector Avr4 to MM-Cf-4 plants [204,205]. After sowing, plants were grown for 4 weeks at 33 °C and 100% RH to suppress systemic PCD. Synchronised systemic PCD was eventually induced by transferring the seedlings to 20 °C and 70% RH. The first fully developed tomato leaves were harvested 4 hr after transfer and were photographed.

Agrobacterium-mediated transient transformation and virus-induced gene silencing in *N. benthamiana*

Agrobacterium-mediated transient transformation (agroinfiltrations) were performed as previously described [206]. The constructs pMOG800-Cf-4, pGWB20-BS4, pVsF-AvrBS4, pBINKS-NRC1D481V, and pBINKS-NRC1K191R-GFP were infiltrated with *Agrobacterium tumefaciens* cultures at OD600 = 1. The construct pMOG800-Avr4 was infiltrated with *A. tumefaciens* cultures at OD600 = 0.03. Symptoms were evaluated at 3 dai.

Virus-induced gene silencing (VIGS) using tobacco rattle virus (TRV)-based vectors was performed in *N. benthamiana:Cf-4* as previously described [207].

Trypan blue staining

N. benthamiana leaves infiltrated with BcNEP1 protein were harvested at 3 dai and boiled for 2–5 min in staining solution, consisting of 16.6% (wt/vol) of trypan blue in an ethanol/lactic acid/phenol/water (3:1:1:1) mixture. After this, the leaves were destained with chloral hydrate and photographed.

ROS burst measurements

For each treatment, we used eight leaf discs (5 mm) punched from the first fully expanded leaf of 5- to 6-week-old *N. benthamiana:Cf-4* plants. The discs were floated on 50 µl of Milli-Q water (MQ) in a 96-well plate and kept in the dark at room temperature for 5 hr. The MQ was then removed using tissue paper, replaced by 50 µl of MQ, and kept in the dark for 1 hr at room temperature. After this, 50 µl of solution containing the IPs, 50 µM luminol L-012 (FUJIFILM), and 10 µg horseradish peroxidase were added to each well. The luminescence values were measured using a CLARIOstar plate reader (BMG LABTECH) over a period of 4 hr.

Disease assays with *Botrytis* spp.

Leaves, intact and cut stems of *N. benthamiana* plants, and leaves of WT *Arabidopsis* Col-0 were inoculated with conidia of *B. cinerea* B05.10. The fungus was grown on malt extract agar (50 g/L; Oxoid) and sporulation was induced by illumination with UV-A lamps. After harvesting, the concentration of the conidia was adjusted to 106/ml using potato dextrose broth (PDB; Oxoid) at 24 g/L PDB, and inoculated in 2-µl droplets on the adaxial side of the leaves. Mock inoculation was carried out by applying 2-µl droplets of PDB solution. Inoculated plants were then incubated in moist plastic boxes and were kept under the same light conditions under which the plants were grown before. Inoculated leaves were detached at 2 dpi, photographed, and analysed by red light imaging. The leaves were then stuck into wet floral foam and returned to the plastic boxes to allow disease progression to take place. This procedure was repeated at 3 and 4 dpi to visualize symptom development. Given the fragility of inoculated *A. thaliana* leaves, it was only possible to record symptom development for *N. benthamiana* leaves. Symptom development on inoculated *N. benthamiana* stems was evaluated at 4 dpi.

Detached leaves from two different cultivars of *Lilium* spp. (OT and LO) were abaxially inoculated with 2-µl droplets of *B. elliptica* conidia from isolates Be9401 and Be9732, respectively (105 conidia/ml in 12g/L PDB). Mock inoculation was carried out with 2-µl droplets of PDB. Inoculated leaves were incubated in moist plastic boxes and pictures of red light imaging were taken at 3 and 4 dpi, with 2 s exposure. The signal intensities were analysed in a manually drawn area, encompassing the necrotic lesion for all the cultivar × pathogen combinations. An area of variable size was selected in each control leaf for subtraction of the background signal of healthy tissue.

Thylakoid disassembly test

Intact chloroplasts were isolated from *N. benthamiana* by stirring cut leaf pieces and following the protocol as described by Ho and Theg [208]. After ultracentrifugation, the Percoll layer containing the chloroplasts was transferred to a 24-well plate with 150 µl aliquots per well. Two surfactants with membranolytic activity were added to each well to perturb thylakoid membrane stability. The surfactants were used at final concentrations of 0.01%, 0.1%, 1%, and 10% for Nonidet P-40 (wt/vol = g/100 ml) and 0.1%, 1%, 10%, and 20% for SDS (wt/vol = g/100 ml). One hundred and fifty microlitres of the respective surfactant at the different concentrations was added to the wells containing the chloroplast suspension. Untreated chloroplast suspen-

sion and pure surfactants at the highest concentration were used as controls. After gently mixing and 20 min of incubation in the dark, the microtiter plates were placed in the imaging system to detect the light signal using red light imaging, at an exposure time of 10 s.

ACKNOWLEDGEMENTS

The research of S.L.V. is funded by the Peruvian Council for Science, Technology and Technological Innovation (CONCYTEC) and its executive unit FONDECYT, PhD scholarship contract 119-2017-FONDECYT. The research of M.C.M. is funded by the Dutch NWO-Science domain (NWO-ENW), project GSGT.GSGT.2018.008.

SUPPLEMENTARY DATA

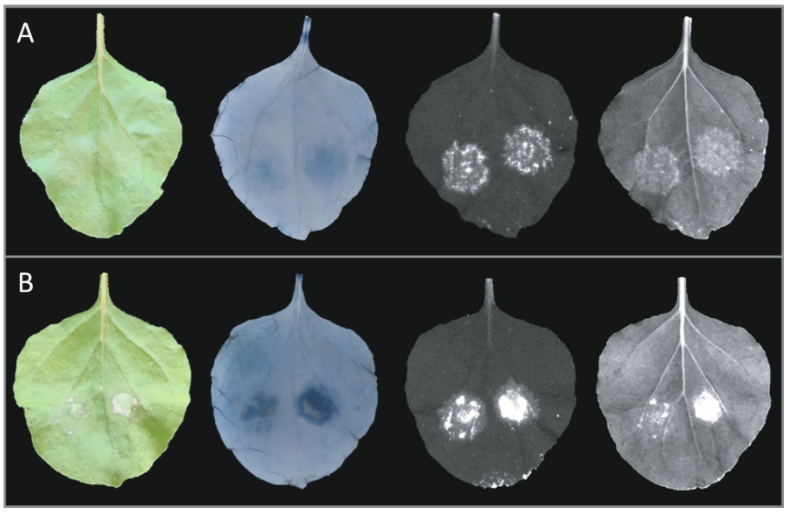

Figure S1. Cell death symptoms caused by Avr4 infiltration for (A) 1 µM and (B) 5 µM) in leaves of *N. benthamiana:Cf-4* plants, visualised at 3 days post inoculation with visible light (left column), trypan blue staining (middle-left column), and red light imaging using green (middle-right column) and UV light (right column) as excitation wave lengths.

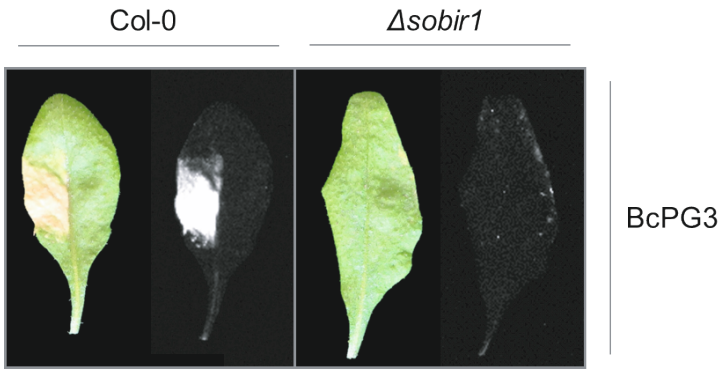

Figure S2. Cell death symptoms monitored at 8 days post inoculation caused by BcPG3 protein infiltration in an *Arabidopsis* wild-type Col-0 plant (left panels) and in a *Atsobir1* deletion mutant (right panels). Each leaf was visualized under visible light with visible light (left) and red light imaging (right).

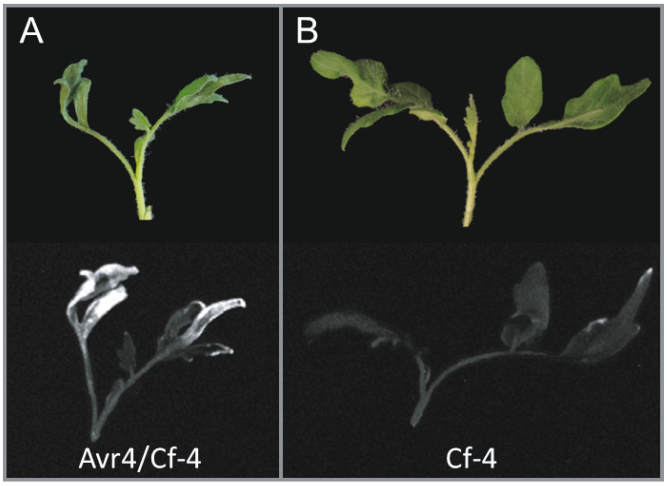

Figure S3. Red light signal detected in leaves of Avr4/Cf-4 tomato seedlings (A) and in control leaves of only Cf-4-expressing tomato seedlings (B) harvested 4 hr after changing growth conditions to a permissive temperature (see Experimental Procedures).

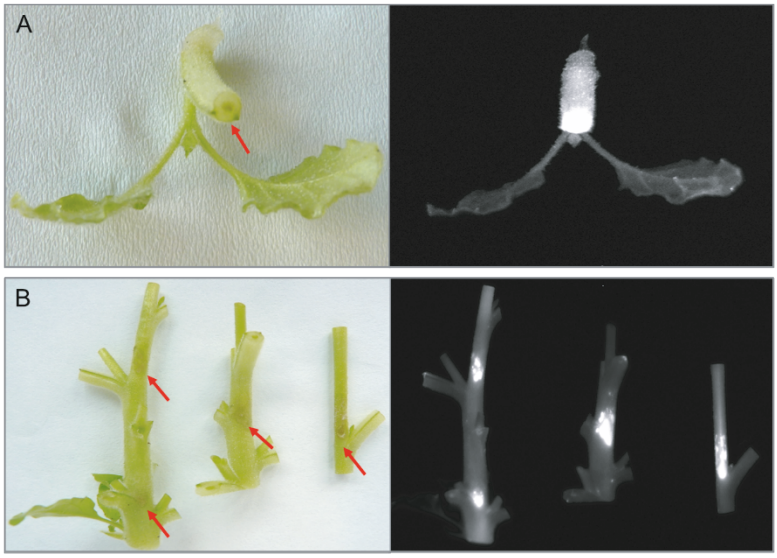

Figure S4. Necrotic lesions developing upon *Botrytis cinerea* inoculation of cut stems (A) and intact stems (B) of *N. benthamiana* at 4 days post inoculation, visualised with visible light (left) and red light imaging (right). Red arrows indicate the inoculation sites on the stem.

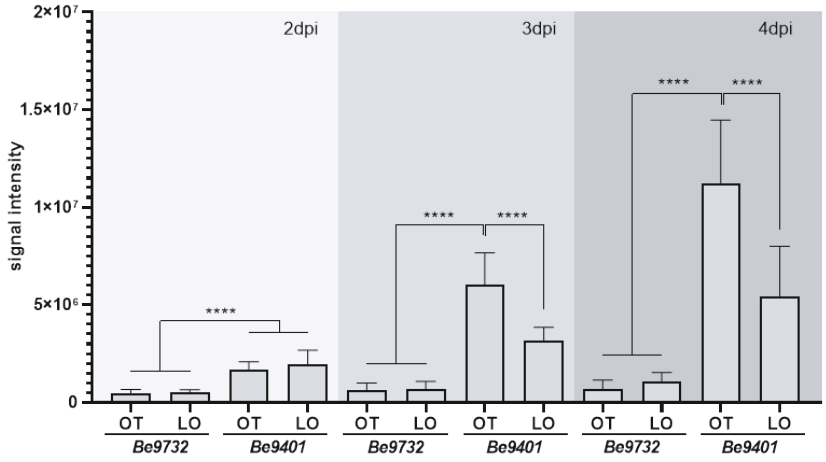

Figure S5. Red light signal intensity over the lesion areas measured at 2, 3, and 4 days post inoculation from necrotic lesions developed on lily OT and LO, inoculated with *Be9401* and *Be9732*. Bars represent averages ± SD (n = 12). Asterisks indicate significant differences using analysis of variance followed by Tukey's test.

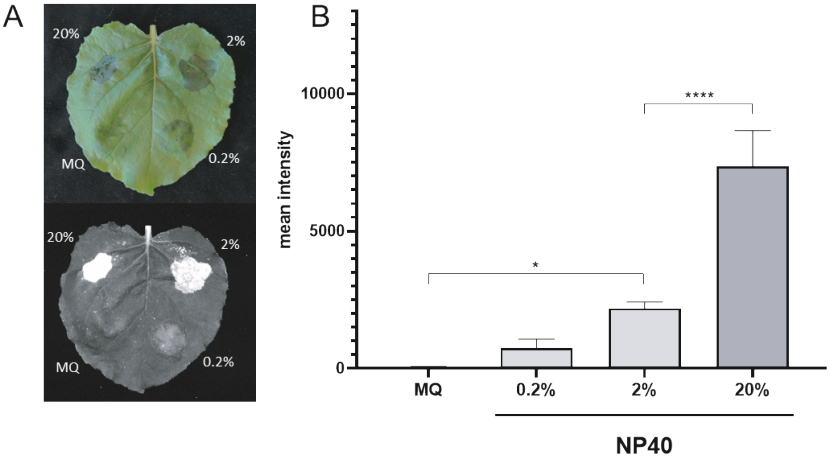

Figure S6. (A) Leaf response of *N. benthamiana* infiltrated with NP40 at the indicated concentrations, visualized under visible light (upper panel) and with red light imaging (lower panel) at 20 min after infiltration of the surfactant. (B) Red light signal intensity values measured at 20 min after infiltration with NP40 at the indicated concentrations. Bars represent averages ± SD (n = 3). Asterisks indicate significant differences using analysis of variance followed by a Tukey test.

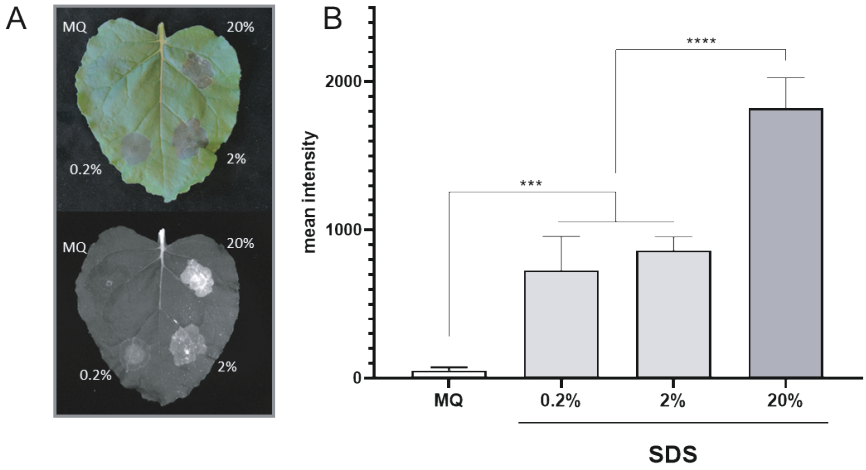

Figure S7. (A) Leaf response of *N. benthamiana* infiltrated with sodium dodecyl sulphate (SDS) at the indicated concentrations, visualized under visible light (upper panel) and with red light imaging (lower panel) at 20 min after infiltration of the surfactant. (B) Red light signal intensity values measured at 20 min after infiltration with SDS at the indicated concentrations. Bars represent averages ± SD (n = 4). Asterisks indicate significant differences using analysis of variance followed by a Tukey test.

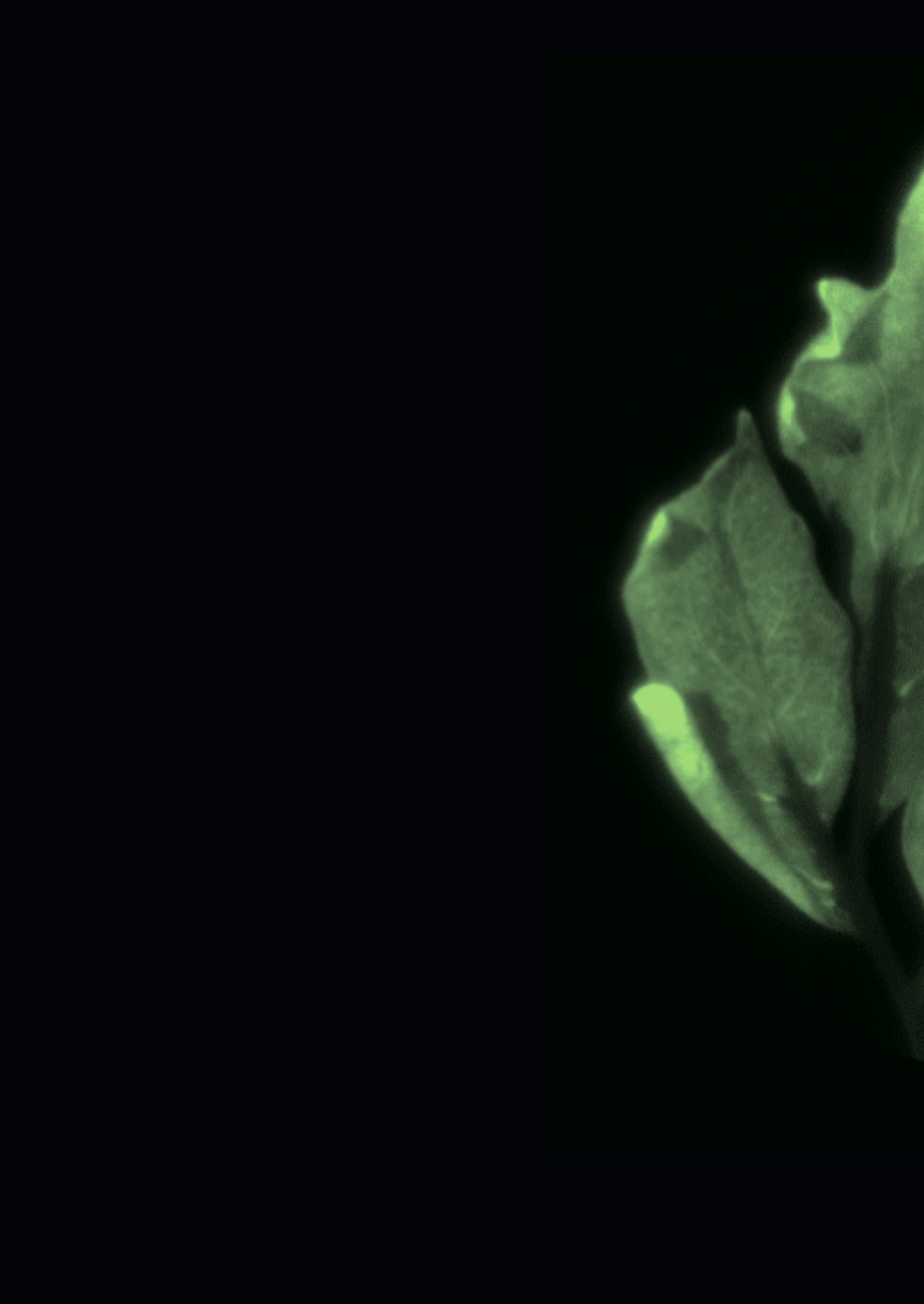

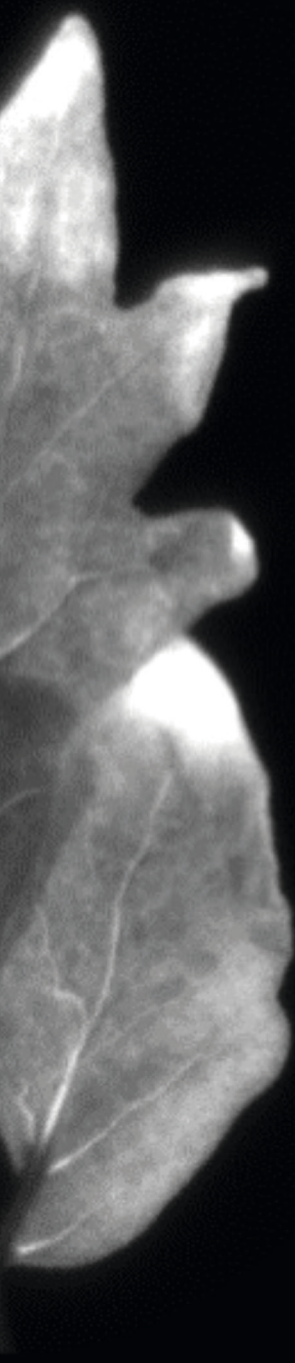

CHAPTER 3

The SOBIR1-complex from *Arabidopsis* to *Nicotiana benthamiana*: studying the signalling cascade downstream of a cell-surface receptor complex

Sergio Landeo Villanueva[a], Nick Pelzers[a], Maikel Zerdoner[a], Sam van Zwoll[a], Laurens Deurhof[a], Wen R.H. Huang[a], Michael F. Seidl[b], Matthieu H.A.J. Joosten[a]

[a] Laboratory of Phytopathology, Wageningen University & Research, Droevendaalsesteeg 1, 6708 PB Wageningen, The Netherlands

[b] Theoretical Biology & Bioinformatics Group, Department of Biology, Utrecht University, 3584 CH Utrecht, The Netherlands

ABSTRACT

Plants rely on an innate immune system to recognise and respond to pathogens. The first layer of this immune system is composed of immune receptors that are present at the cell membrane. These immune receptors can be classified as receptor-like kinases (RLKs) and receptor-like proteins (RLPs), according to the presence or absence, respectively, of an intracellular kinase domain for downstream signalling. RLPs interact constitutively with the RLK SOBIR1, providing the intracellular kinase domain for signal transduction. Regulation and signal initiation and transduction mechanisms of RLP/SOBIR1 complexes are far from being understood, and this study aims to acquire fundamental knowledge on the molecular mechanisms regulating the signalling cascade downstream of SOBIR1-containing immune complexes in Solanaceae. Based on the assumption that essential components of SOBIR1-containing immune complexes will tend to be conserved, we sought to transfer relevant biological information from the well-studied model plant *Arabidopsis thaliana* (*Arabidopsis*) to the solanaceous research model plant *Nicotiana benthamiana*. We explored publicly available *Arabidopsis* microarray data and found that genes encoding components of the SOBIR1 complex are co-expressed under various conditions of biotic stress and belong to a transcriptional cluster that is enriched in genes related to immune responses. Several genes that are included in this cluster, and are involved in immune responses triggered by the SOBIR1 complex in *Arabidopsis*, were evaluated to play a role in transgenic *N. benthamiana* expressing the RLP Cf-4. We show that the respiratory burst enzyme NbRBOHB produces a biphasic ROS burst upon activation of Cf-4 by the matching effector Avr4 of the fungal tomato pathogen *Cladosporium fulvum*, and that this process is dispensable for the onset of the hypersensitive response (HR). Also, we show that between *N. benthamiana* and *Arabidopsis*, signalling cascades are not strictly conserved: A heterodimer formed by the lipase-like proteins EDS1 and PAD4 is required for immune responses downstream of SOBIR1 in *Arabidopsis*, but we do not detect a measurable role in *N. benthamiana*. We also evaluated the relevance of heterotrimeric G-proteins in immune signalling and found that different extra-large G-proteins (XLGs) have opposing roles in regulation of the activity of the SOBIR1 complex. Finally, we provide evidence suggesting a role for the copine protein NbBON1A as a negative regulator of a guarding mechanism based on a TNL resistance protein, acting on the SOBIR1 complex.

INTRODUCTION

Plants are continuously challenged by pathogenic microbes, and when crops get diseased, the economic losses are enormous. The first layer of defence, which is activated upon the first contact of the plant with a pathogen, is provided by immune receptors localised at the plasma membrane (PM). These cell-surface receptors detect immunogenic patterns (IPs), which can be structural compounds of the pathogen, such as chitin and lipo-polysaccharides, or specific virulence factors of the pathogen (so-called effectors) of which the encoding genes are *in planta*-induced to promote disease, and which accumulate in the intercellular spaces [6,25].

Cell-surface receptors can be subdivided into receptor-like kinases (RLK) and receptor-like proteins (RLPs), of which the latter lack an intracellular kinase domain that can directly initiate cytoplasmic signalling. The extracellular domain is responsible for recognition of extracellular signals and different kinds of extracellular domains can recognise different types of signals. A typical extracellular domain of cell-surface receptors is the leucine-rich repeat (LRR) domain that generally plays a role in protein-protein interactions, and LRR-RLKs and LRR-RLPs are known to recognise a plethora of proteins and peptides that are derived from pathogens [20]. For this reason, they play a very important role in the resistance of our crop plants to diseases.

Defence signalling by LRR-RLKs is well-studied, particularly in the model plant *Arabidopsis thaliana* (*Arabidopsis*). An example of an elucidated signalling pathway that is triggered by such an LRR-RLK is the cascade of molecular and biochemical events that is initiated by the LRR-RLK FLAGELLIN-SENSING 2 (FLS2), and which eventually leads to plant resistance. FLS2 is a widely conserved immune receptor that recognises the bacterial peptide flg22, which is derived from the bacterial flagellum [36]. Upon recognition of flg22, FLS2 associates with the co-receptor BRASSINOSTEROID-INSENSITIVE 1 (BRI1)-ASSOCIATED KINASE (BAK1) [51,209]. Subsequently, a series of transphosphorylation events between the kinase domains of both RLKs results in the release of the receptor-like cytoplasmic kinase (RLCK) BOTRYTIS-INDUCED KINASE 1 (BIK1) from the complex [157]. Once activated, BIK1 phosphorylates the NADPH oxidase RESPIRATORY BURST OXIDASE HOMOLOG PROTEIN D (RBOHD), and this activated enzyme then produces the burst of flg22-induced reactive oxygen species (ROS) [210,211].

Although the defence signalling pathway triggered by LRR-RLKs like FLS2 is known in quite some detail, much less is known about the molecular mechanisms underlying the immune responses mediated by LRR-RLPs. The first LRR-RLP that was identified as an immune receptor is the tomato (*Solanum lycopersicum*) Cf-9 protein [212]. This protein confers resistance of tomato to infection by strains of the tomato pathogen *Cladosporium fulvum* carrying the matching effector, which is the avirulence protein Avr9. The activation of this immune receptor triggers a response that includes the swift accumulation of ROS and a type of programmed cell death that is observed as a hypersensitive response (HR) [213]. The recent discovery that tomato LRR-RLPs constitutively interact with the LRR-RLK SUPPRESSOR OF BIR1-1 (SOBIR1) provided an explanation of how these membrane-bound immune receptors do trigger downstream signalling, while lacking a cytoplasmic domain themselves [66]. Further research showed that the formation of bimolecular receptor kinases by the interaction with SOBIR1-type of adaptors is a general and conserved feature of LRR-RLPs [61,82,85,88,90,91,214–217]. Upon ligand recognition, the LRR-RLP/SOBIR1 complex also recruits the regulatory LRR-RLK BAK1 [76], and similar to FLS2 signalling a series of transphosphorylation events are proposed to initiate further downstream signalling [77]. From this point, very little is known about the next downstream components in the signalling cascade leading to the HR. It is known that the tomato RLCK AVR9/CF-9-INDUCED KINASE 1 (ACIK1) is required for Cf-mediated immune responses, including the development of an HR [164], although its exact role in the signalling cascade is yet to be discovered. More recently, the intracellular nucleotide-binding domain leucine-rich repeat-containing receptor (NLR or NB-LRR) NB-LRR REQUIRED FOR HR-ASSOCIATED CELL DEATH-3 (NRC3) was shown to be required for the actual HR upon activation of another tomato Cf protein, which is the LRR-RLP Cf-4 that recognises the avirulence protein Avr4 of *C. fulvum* [165]. More insight into the downstream signalling events triggered by LRR-RLP/SOBIR1 immune complexes came from research on the *Arabidopsis* LRR-RLPs RLP42 and RLP23. RPL42 perceives the fungal polygalacturonase PG3 [91], whereas RLP23 recognises a conserved peptide (nlp20) that is found in a family of effector proteins produced by bacteria, fungi and oomycetes; the NECROSIS AND ETHYLENE-INDUCING PEPTIDE 1 (NEP1)-like proteins (NLPs) [87]. The immune responses triggered by these LRR-RLPs were recently shown to be mediated by the RLCKs AVRPPHB SUSCEPTIBLE 1 (PBS1)-LIKE 30 (PBL30) and PBL31, as well as by the signalling module composed by the lipase-like proteins PHYTOALEXIN-DEFICIENT 4 (PAD4) and ENHANCED DISEASE SUSCEPTIBILITY 1 (EDS1), which is also required for downstream signalling by intracellular NLRs [162].

While PBL30 and PBL31 are also required downstream of LRR-RLKs like FLS2, the PAD4-EDS1 signalling module plays only a limited role downstream of FLS2. In addition to this, the RLCK BIK1 was found to have opposing roles when regulating LRR-RLKs and LRR-RLPs, as *bik1* knock-out mutants show stronger immune responses upon treatment with PG3 and nlp20, which are the ligands of RLP42 and RLP23, respectively, whereas the FLS2-triggered response to flg22 is compromised [218].

Plant defence responses need to be tightly regulated, as there is a fitness cost related to the relocation of resources from growth to defence [219]. At the membrane level, BAK1-mediated immune responses are negatively regulated by the dynamic interaction of BAK1 with additional LRR-RLKs belonging to the BAK1 INTERACTING RECEPTOR KINASES (BIR) family. Arabidopsis possesses four *BIR* genes (*BIR1* to *BIR4*), and of which the first one, *BIR1*, was described in 2009, together with its suppressor mutation sobir1-1 [93]. BIR1 interacts with BAK1, thereby preventing its interaction with SOBIR1, and the *bir1* knock-out mutant phenotype shows spontaneous activation of cell death and constitutive defence responses, which are partially dependent on SOBIR1 and BAK1 [100]. Unlike *BIR1*, the second and the third Arabidopsis *BIR* genes, *BIR2* and *BIR3*, code for inactive kinases. These two members of the BIR family negatively regulate BAK1 complex formation with LRR-RLKs other than SOBIR1, including the RLK FLS2. BIR2 functions by interacting only with BAK1 [94], while BIR3 regulates BAK1/FLS2 complex formation by interacting with FLS2 as well [96]. BIR3 also regulates developmental processes by controlling the interaction of BAK1 with the LRR-RLK BRASSINOSTEROID-INSENSITIVE 1 (BRI1), which is the major *Arabidopsis* brassinosteroid (BR) receptor [96]. Additionally, the tomato ortholog of BIR3, SlBIR3, has conserved its roles in regulating the perception of flg22 and of brassinosteroid hormones [101]. The biological role of the last member of the BIR family, BIR4, remains to be uncovered.

The identification of interacting partners is a critical step in understanding how immune receptor complexes are constituted, how their activity is regulated and what downstream signalling components are recruited upon their activation. Nowadays, *in-silico* methodologies have the potential to identify promising candidates, which can be further validated by wet-lab experiments. It has for example been shown that protein pairs encoded by co-expressed genes interact significantly more frequently than random protein pairs [220], whereas correlation coefficients between gene expression patterns are generally higher between protein interaction partners, as com-

pared to pairs of proteins that are not known to interact directly [221]. Therefore, the correlation between expression profiles from genome-wide gene expression data, for example derived from microarrays or RNA sequencing, can be used to establish a network that connects co-expressed genes and subsequently to infer biological functions [222].

A network can be described in terms of graph theory, as nodes connected by edges [221,223]. The number of edges for each node is referred as its "degree". There are two theoretical network models that are relevant to this work: a random network [224] and a scale-free network [225]. In a random network, the edges are randomly distributed, and the number of edges per node, the degree distribution, follows a Poisson distribution, indicating that most nodes have approximately the same number of edges, close to the average. Scale-free networks on the other hand are characterized by a degree distribution that follows a power of law, observed as a straight line when plotting the degree distribution with both X- and Y-axes in a logarithmic scale. In these networks, most nodes have few edges, and very few highly connected nodes, called "hubs", hold the network together. Interestingly, this signature is shared by many social [226–228], technological (world-wide web) [229,230] and cellular networks, such as metabolic networks [231], in which nodes are metabolites and links are enzyme-catalysed reactions, or genetic regulatory networks [232], where nodes are individual genes and the edges represent expression correlations, and protein-protein interaction networks [233,234] that describe direct physical interactions among proteins in one organism.

The regulation and signal transduction partners of LRR-RLPs are far from being understood. For instance, no RLCK has yet been shown to act as the first downstream signalling component required for HR induction by LRR-RLPs. This study aims to identify novel components of LRR-RLP/SOBIR1-containing receptor complexes. Based on the hypothesis that protein-protein interaction partners tend to be co-expressed [221], a network is established from publicly available microarray expression data of *Arabidopsis*. By focusing on genes that are co-regulated with known members of the complex, we here identify a cluster containing several genes coding for proteins already known to be involved in the regulation of SOBIR1-containing complexes. To substantiate the use of this network as a tool to prioritize genes for laboratory validation in solanaceous plants, selected candidates were evaluated for their role in immune signalling in stable transgenic *N. benthamiana:Cf-4* plants. Such plants were subjected to virus-induced gene silencing (VIGS) of the candidate

genes and we subsequently made use of the red-light imaging method [235] to quantify the HR, and also optimized a luminol-based essay for ROS burst measurements, in order to quantify the intensity of the immune outputs upon challenge with Avr4.

RESULTS

Interaction partners of SOBIR1-containing complexes belong to a cluster of co-expressed genes in *Arabidopsis*

To build a gene expression network from available transcription data, the input must cover the variation of gene expression in comparable *Arabidopsis* accessions along a large set of different treatments. We retrieved the microarray expression data from 29 experiments, covering the variation of gene expression along different developmental stages, under various types of abiotic stress, upon exposure to different hormones or a range of immunogenic patterns, and after challenge with various pathogens. Across all the data used, the number of replicates was between 2 and 3 per treatment, with an average of 2.5 and a total amount of measurements of 763 (see Table S1 for an overview of the experiments used, as well as their accession number and the number of treatments and number of measurements). Except for four treatments using *Arabidopsis* ecotype Ler-0 (one in E-GEOD-5687 and three in E-GEOD-5701), all other treatments were using the same *Arabidopsis* ecotype (Col-0). Thus, in summary, the data used to build the network were derived from 29 experiments, covering 249 different treatments of wild type *Arabidopsis* plants.

We assessed the co-expression to infer potential protein interaction partners by calculating correlation coefficients of the expression levels of their encoding genes, and an initial cut-off threshold level for this correlation coefficient was used as a start point for subsequent co-expression analysis. After normalization of the microarray data, the Pearson's correlation coefficient was calculated for all pairs of genes (the "probes"), along all 249 treatments, yielding 260,136,645 correlation values. From here, the probes will be referred as "nodes" and the correlation values as "edges" connecting these nodes. This initial network is extremely large as all nodes are connected with each other, yet the vast majority of the edges has correlation coefficients of around zero, and therefore do not point to biologically relevant connections between the genes. To identify biologically relevant connections, it is necessary to assess an initial correlation coefficient cut-off. When plotting the expression patterns of known

interactors along pathogen inoculation-related treatments, a high similarity in the obtained profiles is observed (Figure 1A), which supports the approach of building a network based on the correlation coefficient of the expression level of the genes encoding the interacting proteins. Then, in order to increase the significance of the coefficients, the correlations along all 249 treatments were plotted, pointing out the correlations of the gene expression levels of the known interactors SOBIR1-BAK1 (0.543), BIR1-BAK1 (0.693) and BIR2-BAK1 (0.791) (Figure 1B). Therefore, an initial cut-off for the correlations of ≥0.5 was established to obtain a more significant subset of the data (Figure 1B, in red).

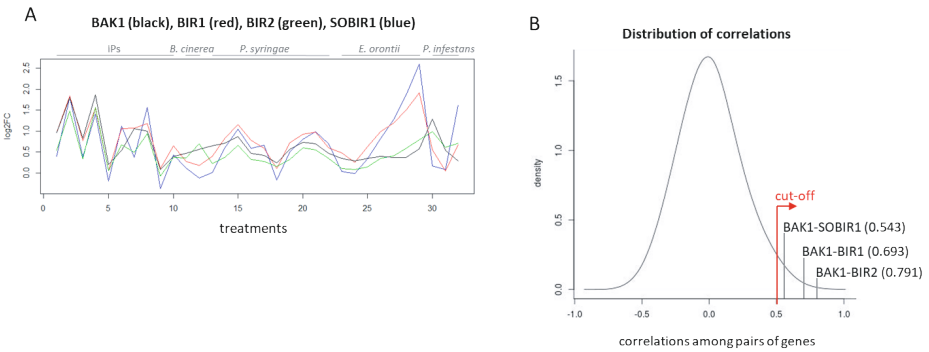

Figure 1. Distribution of correlations and expression profiles of selected genes. (A) Expression profile of *BAK1*, *BIR1*, *BIR2* and *SOBIR1* across the 32 treatments with various pathogens and IPs (Table S1). IPs that were used for the experiments of which the gene expression levels are included in the profile: Harpin HrpZ, GST-necrosis-inducing *Phytophthora* protein (NPP1), the bacterial flagellin-derived peptide flg22 and cell wall-derived lipopolysaccharide (LPS). (B) Density distribution of the expression correlations among all nodes, calculated across all 249 treatments. The selected initial cut-off is shown in red. The p-values for the three correlations that are indicated: BAK1-SOBIR1, BAK1-BIR1 and BAK1-BIR2 are all below $2.2 * 10^{-16}$.

To predict possible interactors of SOBIR1-containing receptor complexes, it is necessary to build a scale-free network, containing known interactors of the complex [223,236]. The network used for the analysis was built by merging three groups of co-expressed genes (Figure 2A-B). Each group was generated using a known member of SOBIR1-containing complexes as a "guide", which were either SOBIR1 itself, BIR1 or BAK1. Each group consisted of all the nodes of which the expression was correlated with its guide and included all the correlations among the various members of each group (correlation cut-off ≥0.5) (Figure 2A).

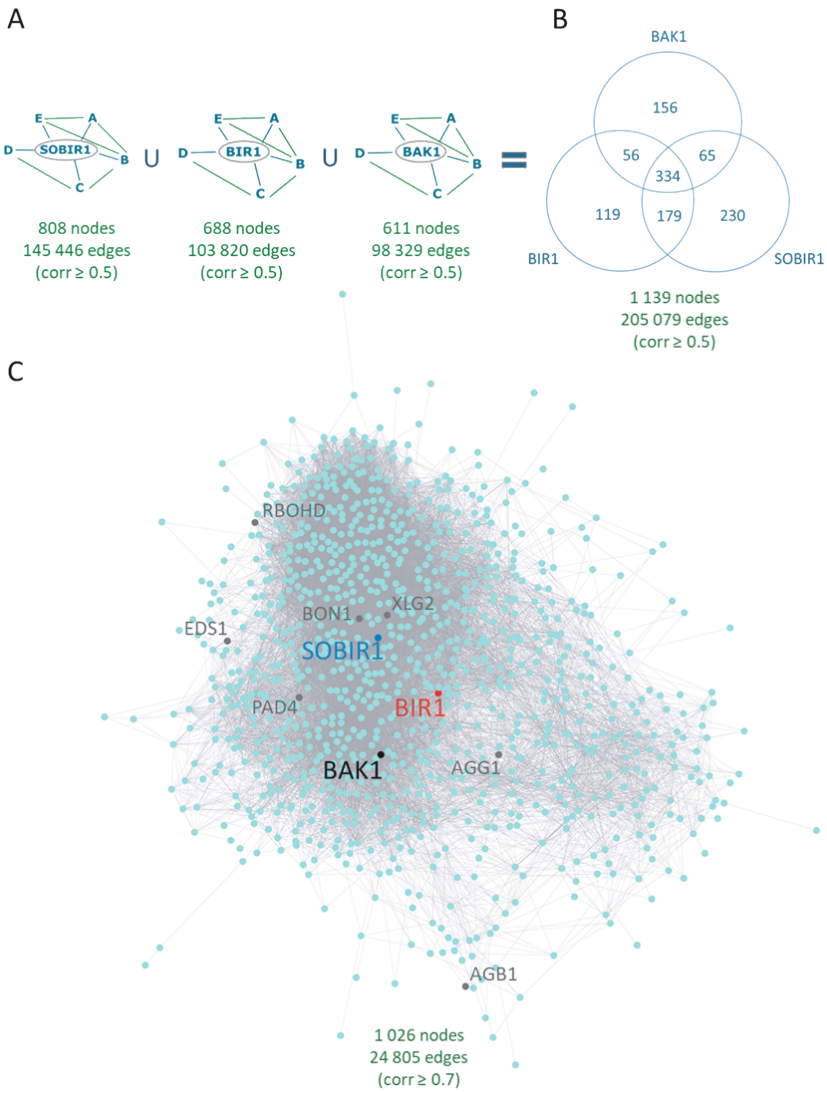

Figure 2. Construction of a scale-free network around known interactors of SOBIR1-containing complexes. (A) The three groups of co-expressed genes extracted from the list of correlations, indicating the number of nodes and edges in each group, are shown. (B) Venn diagram showing the results of merging the three groups. The numbers in the diagram indicate the number of nodes in each group. (C) Scale-free network representation using the yFiles Organic Layout algorithm in Cytoscape [241]. SOBIR1 is indicated in blue, BAK1 in black, and BIR1 in red. Several proteins known to be functionally related to SOBIR1-containing immune-related complexes are indicated in grey. The genes that are represented in the cluster are ranked by their number of connections (degree), as shown in Table S2.

Comparison between these groups revealed 1,139 nodes, connected by 205,079 edges, and 29.3% of the nodes are shared by the three groups, and 55.7% of the nodes are shared by two of them (Figure 2B). After merging of the three groups, the resulting topology is very compact, and any two nodes can be connected by three edges (diameter), and the probability of any two random nodes being connected is 0.316 (density). The node degree distribution of the generated network was found to be similar to what can be expected from a random network, and therefore does not have a scale-free topology (Figure S1A). This observation suggests that increasing the correlation cut-off is required to generate a scale-free topology. Upon stepwise increasing the correlation cut-off, a scale-free topology was obtained at a correlation cut-off of ≥0.7 (Figure S1A-D). The resulting scale-free network consists of 1,026 nodes, connected by 24,805 edges, and possesses a diameter of 8 edges and a density of 0.047 (Figure 2C).

This network was characterized by a gene ontology (GO) terms enrichment analysis. In the Cellular Components category, we found enrichment of GO terms related to components of the plasma membrane (PM), with the highest enrichment corresponding to "extrinsic component of cytoplasmic side of PM" (GO:0031234, 16.44-fold enriched, p-value: 2.13E-03) (Table S3). In the Biological Process category, we found enrichment of several GO terms related to immune responses, including "phospholipid translocation" (GO:0045332, 8.43-fold enriched, p-value: 2.52E-03) and "response to external biotic stimulus" (GO:0043207, 5.24-fold enriched, p-value: 4.83E-06) (Table S4). For the case of Molecular Function, the highest enrichment corresponds to "calmodulin binding" (GO:0005516, 7.42-fold enriched, p-value: 1.62E-07), "calcium binding" (GO:0005509, 4.37-fold enriched, p-value: 1.11E-04), and "protein kinase activity" (GO:0004672, 2.73-fold enriched, p-value: 1.79E-08). Thus, the GO terms enrichment analysis describes a network that is enriched in genes involved in the regulation of immune responses triggered by cell-surface receptors. Interestingly, several proteins that are functionally related to SOBIR1-containing complexes are present in this network (Figure 2C). For instance, this network includes the respiratory burst oxidase homolog RBOHD, which is responsible for the apoplastic ROS burst produced upon immune activation [237], and BONZAI 1 (BON1), which is a calcium-dependent phospholipid-binding protein that is a negative regulator of immune responses and which interacts with BIR1 and BAK1 [238]. Furthermore, several suppressors of the activation of constitutive immune responses that were earlier reported in *Arabidopsis bir1* mutants, including PAD4, EDS1, and the sub-

units of heterotrimeric G proteins EXTRA-LARGE GTP-BINDING PROTEIN 2 (XLG2), ARABIDOPSIS GTP BINDING PROTEIN BETA (AGB1) and ARABIDOPSIS G PROTEIN GAMMA-SUBUNIT 1 (AGG1) [93,239,240], were also found. These observations corroborate the network as a framework to identify novel candidate genes encoding proteins playing a role in the functioning of SOBIR1-containing receptor complexes.

To identify highly connected nodes (hubs) and possible novel interactors of the SOBIR1-containing complex, the network was further analysed using centrality metrics: closeness centrality and betweenness centrality [242]. Both metrics are based on the concept of the shortest path between two nodes in a graph, defined as the path that connects two nodes, while going through the minimum number of edges. The closeness centrality identifies hubs based on their distance, in numbers of edges, to all other nodes in the network. It is expressed as the reciprocal of the sum of the shortest paths connecting a particular node with the rest of the nodes in the network. The betweenness centrality, on the other hand, focuses on how important a hub is in connecting different components of the network. It is expressed as the proportion of all the shortest paths in a network that pass through a particular node. When plotting these centrality metrics, we observed that no clear cut-off could be defined to subdivide the data, without excluding known functional components of SOBIR1-containing complexes (Figure 3 A and B).

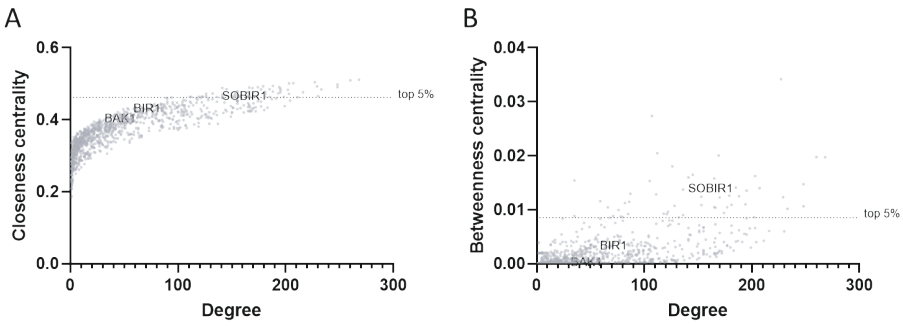

Figure 3. Centrality analysis of the scale-free network around known interactors of SOBIR1-containing complexes. (A) Closeness centrality (CC) vs node degree and (B) betweenness centrality (BC) vs node degree. In both plots, the dotted line indicates the cut-off value to retrieve the top 5% of the nodes (CC ≥ 0.463 and BC ≥0.00855). Centrality values: SOBIR1, CC=0.4632 and BC=0.014; BAK1, CC=0.4 and BC=6.469*10-5; BIR1, CC=0.429 and BC=0.0031.

For instance, arbitrary cut-off values chosen to select the top 5% of the central nodes for each centrality parameter would exclude BAK1 and BIR1, thereby keeping only SOBIR1 in the list of candidates from the expression analysis. Any other threshold selected to keep SOBIR1, BIR1, as well as BAK1 in the list, would retain at least 29% of the nodes for the case of closeness centrality and 49% of the nodes for the case of betweenness centrality. For this reason, we decided not to further subdivide the data.

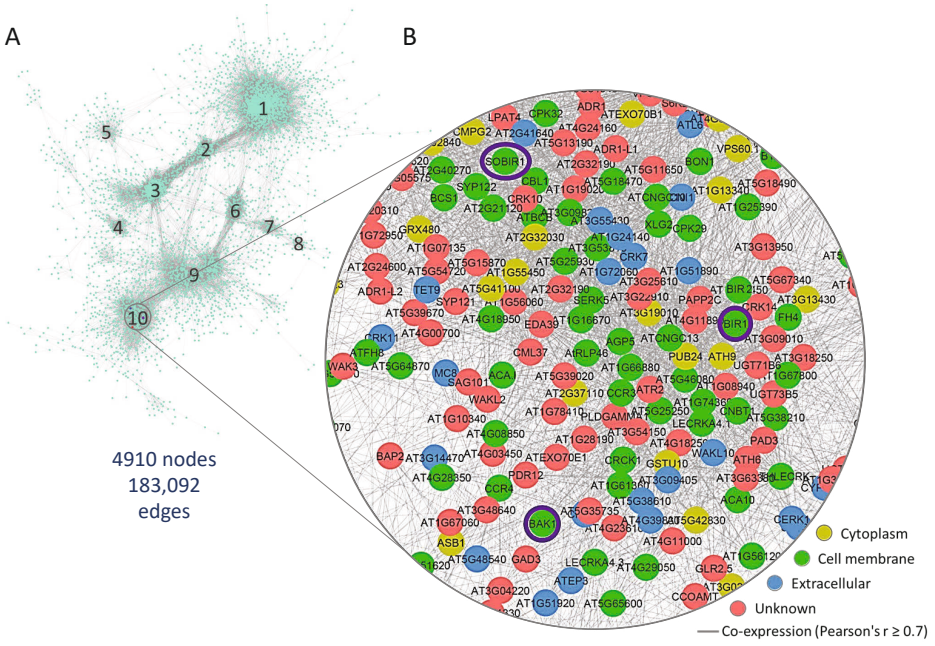

Figure 4. Co-expression landscape of the proteins of *Arabidopsis*, after filtering out proteins predicted to be located in the nucleus, chloroplasts, mitochondria and Golgi bodies. (A) Co-expression network built by compiling publicly available microarray data of 29 experiments (249 treatments), performed with *Arabidopsis*. The edges represent Pearson Correlation Coefficients with a cut-off of 0.7. Visualisation was done in Cytoscape, using the unweighted Prefuse Force-Directed Layout [241]. The blue, red and purple dots in group 10 show the positions of SOBIR1, BAK1 and BIR1, respectively. GO term enrichment analysis of the clusters is shown in Figure S2. (B) Zoom in of the SOBIR1-containing area of group 10. The colours depict the predicted subcellular localisation (from www.arabidopsis.org). The purple circles highlight the positions of SOBIR1, BAK1 and BIR1.

Considering the compactness of the scale-free network that was built around known interactors of SOBIR1-containing complexes (Figure 2C), we decided to explore whether this network corresponds to a particular cluster in the context of the gene co-expression landscape of *Arabidopsis*. We used our previously compiled set of correlations to build a network comprising the part of the genome of *Arabidopsis* that is covered by the microarray expression datasets. Because we are searching for novel interactors of a protein complex located at the PM, this time we filtered out all the proteins predicted to be located in the nucleus, chloroplasts, mitochondria and Golgi bodies [243]. After applying the correlation cut-off that was previously estimated to produce a scale-free network around known interactors of the complex, we obtained a scale-free network representing 4,910 nodes and 183,092 edges, with a diameter of 20 edges and a density of 0.015. We visualized the network by using a Prefuse Force-Directed Layout [241], and we observed roughly ten groups of highly interconnected nodes (Figure 4A), in which known components of the system, like SOBIR1 itself, BIR1 and BAK1 are in close proximity inside a single group (Figure 4B).

Network validation and transfer of the biologically relevant information from *Arabidopsis* to *N. benthamiana*

To validate the results of the network analysis as a source of candidate genes for further experimental evaluation, and also to transfer biologically relevant information from *Arabidopsis* to the solanaceous model plant *N. benthamiana*, for further evaluation we selected proteins that belong to the scale-free network closely around known interactors of SOBIR1-containing complexes (Figure 2C), and that are involved in immune responses triggered by the SOBIR1 complex in *Arabidopsis*. Proteins that were eventually selected are the *N. benthamiana* homologs of RBOHD, which is responsible for the apoplastic ROS burst generated upon IP perception at the cell membrane [237], the PAD4-EDS1 module that is required for the cell death phenotype of *bir1* mutants [93], the Gα subunit of heterotrimeric GTP-binding proteins (G-proteins) that modulate immune responses by their association with RLKs [244,245] and BON1, which is a calcium-dependent phospholipid-binding protein that interacts with BIR1 and BAK1 to modulate plant growth and cell death [238].

NbRBOHB produces a biphasic ROS burst upon perception of Avr4 by *N. benthamiana:Cf-4*

The production of ROS by the respiratory burst oxidase homologs RBOHD and, to a lesser extent by RBOHF, is one of the first read-outs that can be obtained after immune activation in plants [237]. When measuring the production of apoplastic ROS in *N. benthamiana* by means of a luminol-based chemiluminescence assay using leaf discs, we observed that perception of flg22 or Avr4 triggers clearly distinguishable ROS burst profiles. The perception of the flg22 peptide by the RLK FLS2 triggers a ROS burst profile that reaches its peak after about 20 minutes and goes down to background level within 1 hour. In contrast, the recognition of Avr4 by Cf-4 triggers a typical biphasic ROS-burst, having a first peak at about 40 minutes and a second peak at about 2.5 hours after elicitation (Figure 5A).

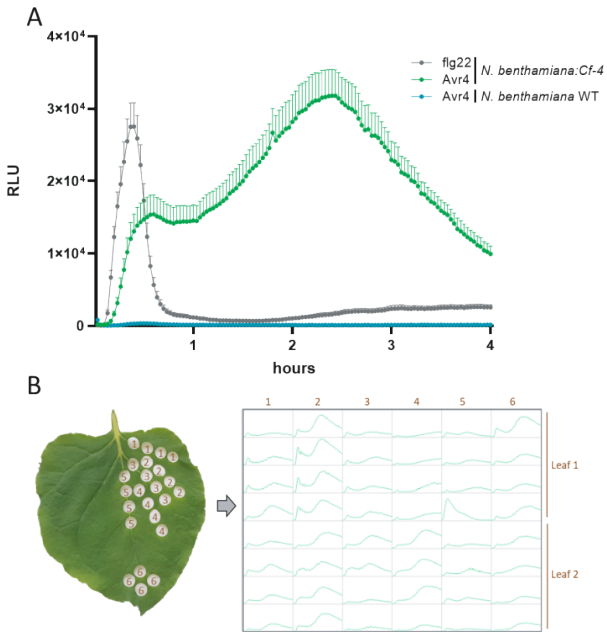

Figure 5. Apoplastic ROS profiles obtained upon elicitation of *N. benthamiana*. (A) ROS burst triggered by elicitation with flg22 or Avr4 of *N. benthamiana*. Leaf discs taken from *N. benthamiana:Cf-4* were treated with either the flg22 peptide (0.1µM) or with the Avr4 protein (0.1µM). As a control, leaf discs taken from *N. benthamiana* wild type (WT) plants were treated with Avr4 protein (0.1µM). ROS was measured by a luminol-based bioassay over a period of 4 hours. The values are given in relative light units (RLU). Bars show the standard error, n=12. (B) Variation in the ROS burst profiles triggered by Avr4 (0.1µM) in leaf discs taken from different parts of leaves of *N. benthamiana:Cf-4*.

Interestingly, although always being biphasic, we observed a considerable variation in the ROS burst profiles between leaf discs taken from different parts of the leaves (Figure 5B). This observation allowed us to reduce the variation in our ROS burst measurements by always taking leaf discs from the same area of the leaves (sector 2 in Figure 5B).

We then set out to explore the source of the biphasic ROS burst that is produced upon perception of Avr4 by the RLP Cf-4. For this, we employed virus-induced gene silencing (VIGS) to knock-down the expression levels of *N. benthamiana NbRBOHB* and *NbRBOHA*, which are the homologs of *Arabidopsis RBOHD* and *RBOHF*, respectively (Figure S3). As a control, we targeted the *N. benthamiana* homologs of *BAK1* for silencing, as they are required for the flg22-triggered ROS production and the Avr4-triggered HR [52,76]. We also targeted the *N. benthamiana* homeologs of *Arabidopsis RBOHE* (*NbRBOHE*) for VIGS, an enzyme which is involved in tapetal programmed cell death and pollen development [246] (Figure S3). Three weeks after agroinfiltration, when silencing of the various *BAK1* homologs resulted in the characteristic stunted phenotype, we observed a clear reduction in the size of the *NbRBOHE*-silenced plants, whereas no clear phenotypes upon silencing of *NbRBOHA* and *NbRBOHB* were observed (Figure 6A). We then measured the apoplastic ROS burst produced upon flg22 and Avr4 perception by the silenced plants and detected that silencing of *NbRBOHB* almost completely abolished the flg22- and the Avr4-triggered ROS burst (Figure 6B and C). Unexpectedly, we detected no reduction of the Avr4-triggered ROS burst upon silencing of the *N. benthamiana* homologs of *BAK1*, even though the flg22-triggered ROS burst was significantly reduced (Figure 6C). These results suggest that both the first and the second peak of the Avr4-triggered ROS burst are the result of activation of NbRBOHB.

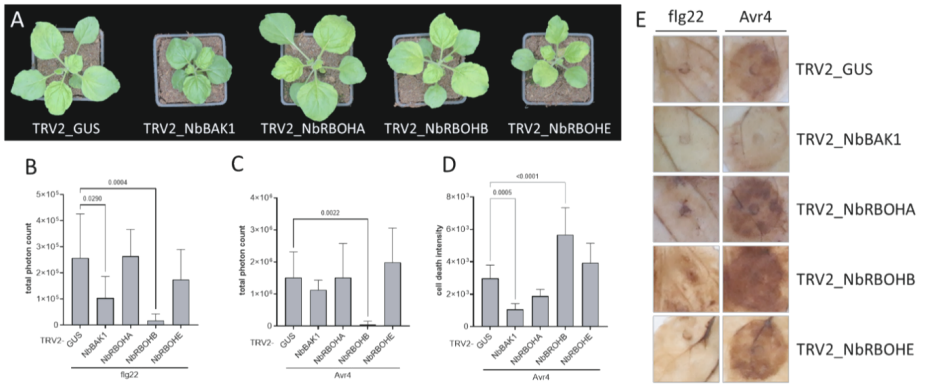

Figure 6. NbRBOHB is responsible for the apoplastic ROS burst detected upon perception of flg22 and the Avr4 protein by *N. benthamiana:Cf-4*. (A) Phenotypes of *N. benthamiana:Cf-4* agroinfiltrated with the indicated TRV2 constructs triggering virus-induced gene silencing (VIGS) of the target genes. Pictures were taken three weeks after agroinfiltration for VIGS. (B) Total photon count, reflecting the intensity of the flg22-triggered apoplastic ROS burst, determined using leaf discs taken from *N. benthamiana:Cf-4* plants, subjected to VIGS of the various target genes. Leaf discs were exposed to 0.1 µM of flg22 and ROS was measured over a period of 1 hour. Error bars show the standard deviation (SD), n=8. P-values are indicated when they are below 0.05 (ANOVA, Dunnett's test) (C) Total photon count, reflecting the intensity of the Avr4-triggered apoplastic ROS burst determined using leaf discs taken from *N. benthamiana:Cf-4* plants, subjected to VIGS of the various target genes. Leaf discs were exposed to 0.1 µM of Avr4 protein and ROS was measured over a period of 5 hours. n=8, error bars show the SD. P-values are indicated when ≤0.05 (ANOVA, Dunnett's test). (D) Quantification of the HR by means of red-light imaging in *N. benthamiana:Cf-4* upon perception of Avr4. Measurements were done three days after infiltration of a 10 µM solution of the Avr4 protein in leaves of plants subjected to VIGS of the various target genes. n=10, error bars show the SD. P-values are indicated when they are below 0.05 (ANOVA, Dunnett's test). (E) 3,3'-Diaminobenzidine (DAB) staining of *N. benthamiana:Cf-4* leaves subjected to VIGS of the various target genes. The staining procedure was performed three hours after infiltration of 10 µM solutions of flg22 and Avr4 protein into *N. benthamiana:Cf-4* leaves. Note that only targeting *BAK1* and its homologues by VIGS results in a clearly reduced staining of the leaf tissue.

We also evaluated the relation between the ROS burst and the Avr4-triggered HR in *N. benthamiana:Cf-4*. For this, we infiltrated pure Avr4 protein into the leaves of the various silenced plants and we quantified the intensity of the resulting HR by red-light imaging [235]. Silencing of the *BAK1* homologs resulted in the expected reduction in HR intensity, when compared to the control [76]. Remarkably, when quantifying the HR intensity shown by the different *RBOHs*-silenced plants, we observed an

increased response upon silencing of *NbRBOHB* (Figure 6D). This showed that the apoplastic ROS burst is not required for the onset of the Avr4-triggered HR.

The development of the HR also involves the generation of ROS from intracellular sources, like the chloroplasts and the mitochondria [247–252]. To determine whether also in these plants intracellular ROS production might be affected, we infiltrated flg22 and Avr4 protein into the leaves of the various silenced plants and performed a 3,3'-Diaminobenzidine (DAB) staining at three hours after infiltration. This time point corresponds with the second, and higher peak of the NbRBOHB-generated apoplastic ROS burst (Figure 5A). Infiltration of flg22 did not result in the deposition of a brown precipitate in the tissue upon DAB staining, indicating no detection of intracellular ROS. Infiltration with the Avr4 protein, on the other hand, did result in the deposition of a brown precipitate in the tissue upon DAB staining, and of which the intensity correlated with the intensity of the HR measured at three days after Avr4 infiltration (Figure 6D and 6E). When compared to the controls, there was a clear reduction in the amount of intracellular ROS detected by DAB staining after silencing the homologs of *BAK1* (Figure 6E). This observation is in clear contrast with the unaffected Avr4-triggered apoplastic ROS burst observed after silencing of the *BAK1* homologs in *N. benthamiana:Cf-4* (Figure 6C). Strikingly, DAB staining of the leaves of the *RBOHs*-silenced *N. benthamiana:Cf-4* plants detected amounts of ROS that more or less correlated with the intensity of the HR that was triggered in these plants upon infiltration of the Avr4 protein (Figure 6E). Interestingly, upon silencing of Nb*RBOHB*, the apoplastic ROS is more or less absent (Figure 6C), whereas the HR is increased (Figure 6D) and the ROS detected by DAB also (Figure 6E), when compared to the control and the other treatments. These results suggest that the DAB staining indeed detects ROS originating from a source that is different from the PM-bound NbRBOHB.

The PAD4-EDS1 module is not required for downstream signalling by the activated Cf-4/SOBIR1 complex in *N. benthamiana*

In *Arabidopsis*, the seedling lethality and the constitutive activation of immune responses upon loss of the negative regulator BIR1, is dependent on SOBIR1, BAK1, EDS1 and PAD4 [93,100]. To explore the conservation of the requirement of these proteins for the same process in *N. benthamiana*, we performed VIGS targeting of both homeologs of *BIR1* in different *N. benthamiana* genotypes, including wild-type (WT) plants and knockout mutants in *sobir1(-like)*, *bak1*, *pad4* and *eds1* [253–255]

(Figure 7A). We observed that the lethal phenotype produced by silencing *NbBIR1* was suppressed in *N. benthamiana:Cf-4 sobir1(-like)*, although these plants were still smaller than the controls. This observation is reminiscent of the finding of Gao and co-workers [93], who showed that a knockout of *SOBIR1* in *Arabidopsis* partly suppresses the *bir1-1* seedling lethality phenotype, hence its name, *SUPPRESSOR OF BIR1-1*. Silencing of *NbBIR1* in *N. benthamiana bak1* mutants also resulted in plants that were still viable at three weeks after agroinfiltration of the recombinant TRV2-NbBIR1 construct to initiate VIGS. It should be noted that the silenced *bak1* mutants were smaller than the silenced *sobir1(-like)* knockout mutants. When assessing the outcome of silencing *NbBIR1* in the knockout mutants of the *PAD4* and *EDS1* homologs, we observed no requirement of this signalling module for obtaining the lethal phenotype that is associated with knocking down the *BIR1* homologs in *N. benthamiana*, as these plants showed WT lethality. This observation is in clear contrast with what was observed in *Arabidopsis*, as, similar to a knockout mutation in *SOBIR1*, a knockout of *PAD4* or *EDS1* clearly suppressed the *bir1-1* lethal phenotype [93].

Recent evidence shows that in *Arabidopsis*, the PAD4-EDS1 module is not only required for constitutive immune activation as described above, but also for many aspects of the immune responses mediated by an RLP/SOBIR1 complex, including the apoplastic ROS burst triggered upon perception of nlp20 by RLP23/SOBIR1 [162,163]. We tested whether this requirement also holds for the Cf-4/SOBIR1-mediated immune responses in *N. benthamiana*. For this purpose, we expressed by agroinfiltration the RLP Cf-4 in *N. benthamiana* WT and in the knockout mutant lines *sobir1(-like), bak1*, *pad4* and *eds1* (Figures 7B and S5), and subsequently quantified the apoplastic ROS burst triggered after treating leaf discs with pure Avr4 protein. As a control for the ROS produced due to *Agrobacterium* recognition in the plant tissue, we also expressed by agroinfiltration β-Glucuronidase (GUS) in *N. benthamiana* WT plants. Measurement of the apoplastic ROS burst produced after expression of GUS in *N. benthamiana* WT and subsequent treatment with Avr4, suggests that perception of *Agrobacterium* primes the tissue, causing a basal generation of ROS (Figures 7B & S4). In contrast, the expression of Cf-4 in *N. benthamiana* WT resulted in the characteristic biphasic Avr4-triggered ROS burst profile (Figure S4). When comparing the total amount of Avr4-triggered ROS, as a total photon count, after expression of Cf-4 in the different *N. benthamiana* genotypes, we observed, as expected, a significant reduction of the ROS burst in the *sobir1(-like)* and *bak1* mutant lines.

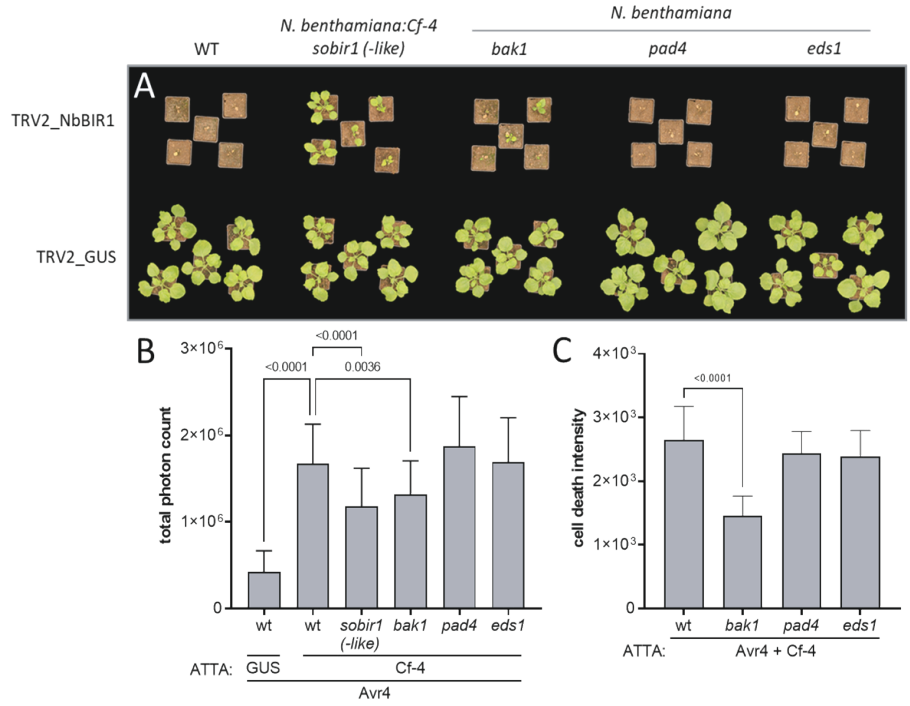

Figure 7. The homologs of *EDS1* and *PAD4* are not required for downstream signalling by SOBIR1 in *N. benthamiana*. (A) Phenotype produced after VIGS of *NbBIR1* in different *N. benthamiana* genotypes. Images were taken three weeks after agroinfiltration of the indicated recombinant TRV2 constructs. (B) Luminol-based measurement of the ROS generated over a period of five hours after treating *N. benthamiana* leaf discs with 0.1 µM of Avr4 protein. Measurements were performed at three days after agroinfiltration for the expression of Cf-4 or GUS in the indicated *N. benthamiana* genotypes. The error bars show the SD, n= 48. P-values are indicated when ≤0.05 (ANOVA, Dunnett's test). One outlier was removed from the results of the *sobir1(-like)* genotype (as determined by the ROUT method). Note that the total photon count for this genotype is relatively high, although the ROS burst profile does not show a biphasic pattern (Figure S4) (C) Quantification of the HR at three days after agroinfiltration for the expression of Avr4 and Cf-4 in the indicated *N. benthamiana* genotypes. Cf-4 was agroinfiltrated at OD=1 and Avr4 was agroinfiltrated at OD=0.03. Error bars show the SD, n=10. P-values are indicated when ≤0.05 (ANOVA, Dunnett's test).

However, the *N. benthamiana* knockout mutants in the homologs of *PAD4* and *EDS1* showed an Avr4-triggered ROS burst that was not different from the ROS burst observed in wild-type plants (Figure 7B). We also evaluated the requirement of the PAD4-EDS1 module for mounting the Avr4-triggered HR. For this purpose, we expressed Avr4 and Cf-4 in *N. benthamiana* WT and in the knockout mutant lines: *bak1*,

pad4 and *eds1* (Figure 7C). While the *bak1* mutants showed a reduced HR upon expression of Avr4 and Cf-4 when compared to the WT plants, the *pad4* and the *eds1* mutant lines again showed no reduction in the intensity of the HR (Figure 7C). Together, these results indicate that the requirement of the PAD4-EDS1 module for downstream signalling by SOBIR1 in *Arabidopsis*, is not conserved in *N. benthamiana*.

The different Gα subunits of heterotrimeric G-proteins have opposing roles in regulating the activity of the SOBIR1 complex in *N. benthamiana*

Heterotrimeric GTP-binding proteins (G-proteins) are signal transduction complexes consisting of three subunits: Gα, Gβ, and Gγ, in which the Gβ and Gγ subunits form a non-dissociable Gβγ dimer [256]. We decided to explore a possible role of G-proteins in the regulation of the Avr4-triggered immune responses in *N. benthamiana*. For this purpose, we performed VIGS targeting the genes encoding the Gα and Gβ subunits of G-proteins (Figure S5). We developed TRV2-recombinant constructs targeting the *N. benthamiana* homologs of the canonical *GPA1* (TRV2-NbGPA1) and *AGB1* (TRV2-AGB1) genes, as well as targeting the homologs of the non-canonical *XLG1* (TRV2-NbXLG1), *XLG2* (TRV2-NbXLG2), and *XLG3* (TRV2-NbXLG3) genes. We also targeted two homeologs of the extra-large G-protein NbXLG4 that are not present in *Arabidopsis*, using the construct TRV2-NbXLG4 (Figure S5). As controls, we silenced the gene encoding Cf-4 (TRV2-Cf-4), the homologs of *BAK1* (TRV2-BAK1), and the homologs of *SOBIR1* (TRV2-NbSOBIR1). Three weeks after agroinfiltration, we observed that silencing of the homologs of *BAK1*, *XLG3*, *XLG4* and *GPA1* in *N. benthamiana:Cf-4* plants resulted in a clear reduction of the size of the plants (Figure 8A). We then measured the apoplastic ROS burst triggered upon treatment with Avr4, and we observed that, while silencing of *Cf-4* itself caused a reduction of the apoplastic ROS burst, there was no significant reduction of the Avr4-triggered ROS burst upon targeting any of the Gα subunits in *N. benthamiana:Cf-4*. In contrast, silencing of the *AGB1* homologs did result in a reduction of the Avr4-triggered ROS burst (Figure 8B). We explored the possibility of this lack of phenotype being due to functional redundancy of the various Gα subunits by performing agroinfiltration of tandem TRV2-constructs targeting several genes encoding Gα subunits at the same time (Figure S6A-C). Agroinfiltration of none of these tandem constructs resulted in a reduction of the Avr4-triggered apoplastic ROS burst (Figure S6B). Since the *Arabidopsis* XLGs have been shown to be redundantly required for the ROS burst triggered upon challenge with flg22 [239,257], we also tested the flg22-triggered ROS burst in the Gα- and Gβ-agroinfiltrated *N. benthamiana:Cf-4* plants (Figure S6C).

Silencing of *AGB1* homologs resulted in a reduction of the flg22-trigered ROS burst. However, when evaluating the requirement of the Gα subunits, we only observed a reduction of the flg22-triggered ROS burst upon targeting all of the *XLGs* in *N. benthamiana* at the same time, by agroinfiltration with the construct TRV2-NbXLG1234. These results point to a difference in the regulation of the flg22- and Avr4-triggered ROS burst, which is in fact produced by the same NbRBOHB. While we did detect a requirement of the XLGs in the case of the ROS burst produced upon treatment with flg22, indicating proper silencing of the target genes, we obtained no evidence for a role of the Gα subunits of heterotrimeric G-proteins in regulation of the Avr4-triggered apoplastic ROS burst. Additionally, these results suggest that the Gβ subunit of G-proteins modulates the Avr4-triggered ROS burst by a mechanism that is independent of its participation in a heterotrimeric G-protein complex.

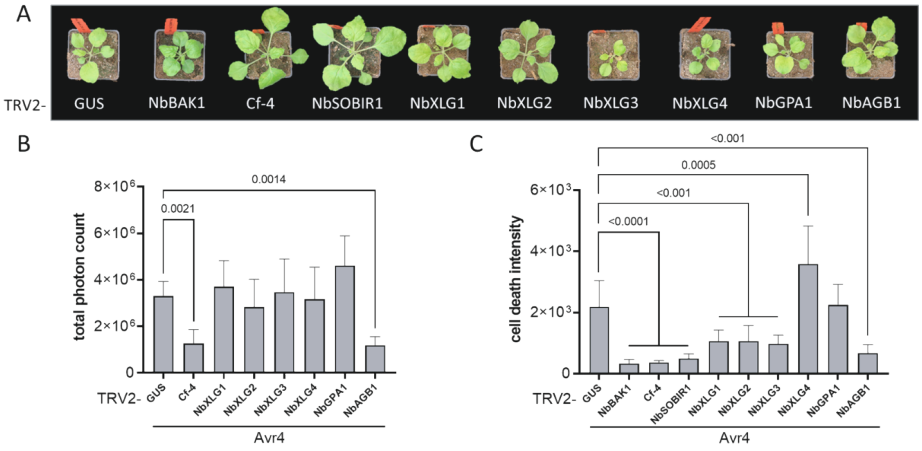

Figure 8. Extra-large G proteins regulate the Avr4-triggered HR in *N. benthamiana:Cf-4*. (A) Phenotypes of *N. benthamiana:Cf-4* agroinfiltrated with the indicated TRV2 constructs for VIGS. Pictures were taken three weeks after agroinfiltration. (B) Total amount of Avr4-triggered apoplastic ROS burst detected from leaf discs from *N. benthamiana:Cf-4* plants subjected to VIGS using the indicated constructs. Leaf discs were exposed to 0.1 μM of Avr4 and ROS was measured over a period of 5 hours. Error bars show the SD, n=8. P-values are indicated when ≤0.05 (ANOVA, Dunnett's test). (C) Quantification of the Avr4-triggered HR in *N. benthamiana:Cf-4*. Measurements were done at three days after infiltration of 10 μM of Avr4 protein in leaves of plants subjected to VIGS using the indicated constructs. Error bars show the SD, n=8. P-values are indicated when ≤0.05 (ANOVA, Dunnett's test).

In order to explore a possible role of G-proteins in the regulation of the Avr4-triggered HR, we infiltrated pure Avr4 protein in the *N. benthamiana:Cf-4* plants subjected to VIGS and analyzed the intensity of the response by red-light imaging [235]. We observed a reduction of the intensity of the HR when silencing the *N. benthamiana* homologs of *XLG1*, *XLG2* and *XLG3* and *AGB1* (Figure 8C and S6D). Unexpectedly, silencing of *NbXLG4* resulted in an increased HR. These results suggest that in *N. benthamiana* all the XLGs and the Gβ subunit are involved in regulation of the Avr4-triggered HR. While some Gα subunits, like NbXLG1, NbXLG2 and NbXLG3 seem to have a positive regulatory role, the extra-large Gα NbXLG4 subunit seems to play a negative regulatory role. We also quantified the intensity of the Avr4-triggered HR upon agroinfiltration of tandem TRV2-constructs targeting all the *N. benthamiana XLG* subunits at the same time (Figure S6D). The results suggest that the effect of silencing *NbXLG1*, *NbXLG2* and *NbXLG3* at the same time masks the effect of silencing *NbXLG4*, as the result was an overall reduction in the intensity of the HR.

Considering the dynamic interaction that has been reported for the Gα subunits XLG2 and XLG3 to take place with the RLK FLS2 and the RLCK BIK1 in *Arabidopsis* [245], we decided to test for a possible interaction between the tomato homologs of Gα and SOBIR1. However, after cloning of the tomato homologs of *XLG1*, *XLG2*, *XLG4* and *GPA1* (Figure S5), we could not obtain evidence for an interaction between these Gα subunits and tomato SOBIR1, by co-immunoprecipitation (co-IP) (data not shown).

Overall, these results show that *N. benthamiana* XLG-Gβγ complexes play a role in regulation of the Avr4-triggered immune responses, with different XLG subunits having opposing roles in the regulation of the HR. Our ROS burst measurements revealed a difference in regulation of the flg22- and Avr4-triggered ROS burst, mediated by the respiratory burst oxidase homolog NbRBOHB. While we detected a requirement of XLGs for the ROS burst produced upon flg22 perception, we found no evidence of a role of XLGs in regulation of the Avr4-triggered apoplastic ROS burst. Furthermore, the results suggest a possible heterotrimer-independent role for the Gβ homologs in the regulation of the Avr4-triggered ROS burst in *N. benthamiana:Cf-4*, as silencing of the *Gβ* homologs reduced the Avr4-triggered ROS burst.

BON1 interacts with components of the SOBIR1 complex

BON1 is a copine-like, calcium-dependent, phospholipid-binding protein. It is a negative regulator of plant defence responses that interact with BIR1 and BAK1,

in modulation of the cell death response [238,258]. To evaluate its relevance for the regulation of the activity of the SOBIR1 complex in *N. benthamiana*, we first set out to identify the functional orthologs of BON1. From a phylogenetic analysis of the copine-like proteins in *Arabidopsis*, tomato, and *N. benthamiana*, we identified two pairs of homeologs as candidates to be the functional orthologs of *Arabidopsis* BON1 in *N. benthamiana*. We designated them NbBON1A and NbBON1B, and designed a TRV2-recombinant construct targeting their encoding genes for VIGS (Figure S7). Three weeks after agroinfiltration of the silencing constructs in *N. benthamiana:Cf-4*, the *NbBON1A*-silenced plants were either dead or severely stunted (Figure 9A). This phenotype, that resembles the "bonzai" phenotype of *Arabidopsis* knockout mutants in *BON1* [259], prevented further analysis of the Avr4-triggered ROS burst and HR in these plants. In contrast, the *NbBON1B*-silenced plants showed a phenotype comparable to the control plants that had been agroinfiltrated with TRV2-GUS (Figure 9A). In these *NbBON1B*-silenced plants, the intensity of the Avr4-triggered apoplastic ROS burst, as well as the intensity of the HR triggered by the expression of Avr4, were comparable to the control plants agroinfiltrated with TRV2-GUS (Figure S8A and B).

Considering the resemblance of the phenotype observed when silencing *NbBON1A* in *N. benthamiana:Cf-4* with the "bonzai" phenotype of *BON1* mutants in *Arabidopsis*, we decided to clone the tomato homolog *SlBON1A* (Figure S7), with the aim to test its possible interaction with the tomato homologs of BAK1 and the BIR proteins. For this, C-terminally Myc-tagged SlBON1A was transiently co-expressed in *N. benthamiana:Cf-4* with C-terminally GFP-tagged SlBIR1, SlBIR2B or SlBAK1. As a control for interaction specificity, SlBON1A was also co-expressed with GFP-tagged beta-glucuronidase (GUS). At 2 dpi, leaves were infiltrated with either a 1 µM solution of pure Avr4 protein or with Milli-Q water, and leaves were harvested 30 minutes later. The GFP-tagged proteins were subsequently immunoprecipitated using GFP-trap beads, and the immunopurified proteins were detected by Western blot. This co-IP experiment revealed that SlBON1A-Myc co-purifies with SlBAK1-GFP, SlBIR1-GFP and SlBIR2B-GFP (Figure 9B). When evaluating a potential change in the detected protein-protein interactions as a consequence of the perception of the Avr4 protein, repeated experiments produced inconsistent results. Therefore, we cannot conclude whether the detected interaction of SlBON1A with the different components of the SOBIR1 complex is dynamic.

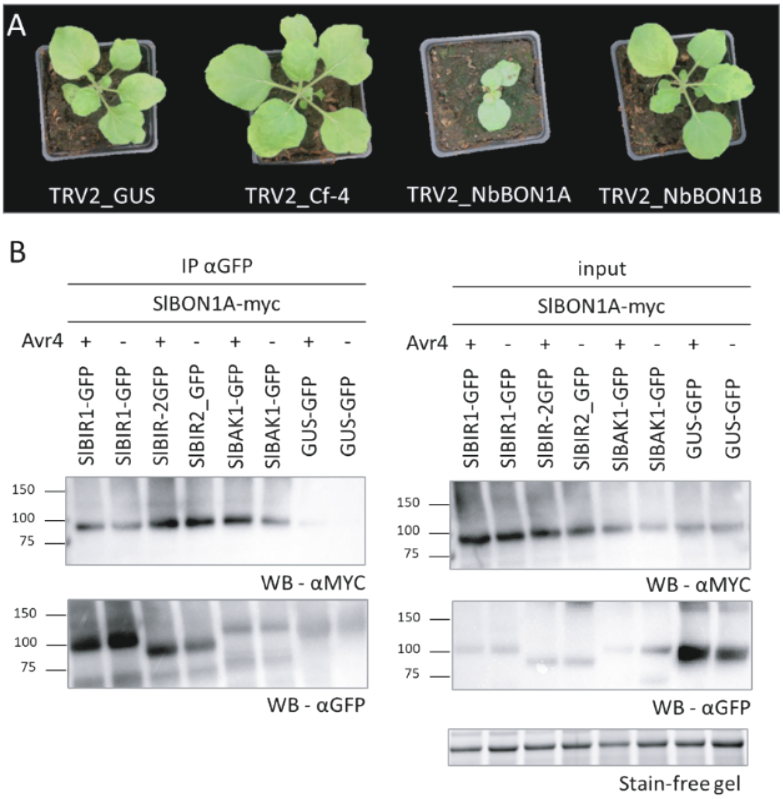

Figure 9. The interaction of BON1 with components of SOBIR1-containing complexes is conserved in Solanaceae. A) Representative images of *N. benthamiana:Cf-4* plants agroinfiltrated with the indicated TRV2 constructs for VIGS. Pictures were taken three weeks after agroinfiltration. (B) Tomato SlBON1A interacts with SlBAK1, SlBIR1 and SlBIR2. The OD_{600} used for agroinfiltration was 1.0 per construct. At 2 dpi, leaves were infiltrated with either Avr4 at 1 μM (+) or Milli-Q (-), and they were harvested after 30 minutes. Total protein extracts (input, right) were subjected to immunoprecipitation using GFP-trap beads (left), followed by Western blot analysis. The Rubisco band in the input samples (Stain-free gel) indicates equal loading. The experiment was repeated twice, and representative blots are shown.

The reduction in growth and constitutive activation of defence responses in Arabidopsis *bon1* mutants can be suppressed by mutations in *PAD4* and *EDS1* [260]. In addition to this, although *Arabidopsis* mutants in *BON2*, which is a closely related paralog of *BON1* (Figure S7), show no abnormal growth, the double *bon1 bon2* mutant shows a stronger phenotype than the *bon1* mutant, causing seedling lethality [261]. To our surprise, when evaluating the phenotypes three weeks after agroinfiltration,

we observed that the stunted/lethal phenotype caused by silencing *NbBON1A* in *N. benthamiana:Cf-4*, was not apparent in *N. benthamiana* WT (Figure 10 and S9), as if the presence of the *Cf-4* transgene causes this stunted/lethal phenotype upon silencing of *NbBON1A*. In line with this observation, we observed that the knockout of SOBIR1(-like) in *N. benthamiana:Cf-4*, which causes loss of Cf-4 functionality [66,253], has rescued the lethal phenotype resulting from silencing *NbBON1A* in *N. benthamiana:Cf-4*. Additionally, among the other *N. benthamiana* knockout mutant lines that were evaluated, only the *bak1* mutant line showed a reduction in size upon VIGS of *NbBON1A*, when compared to the controls (Figure 10 and S9). Strikingly, the *pad4* and *eds1* mutants showed no reduction in size, which corresponds with the observation that in *Arabidopsis* dwarfing caused by a knockout of *BON1* is suppressed by mutations in *PAD4* and *EDS1* [260]. This role of PAD4 and EDS1 in lethality caused by a knock-down of the negative regulator *BON1* contrasts with the absence of a role of PAD4/EDS1 in lethality caused by VIGS of the negative regulator *BIR1* (Figure 7A), whereas the role of SOBIR1 appears to be similar in both cases (Figure 7A and 10).

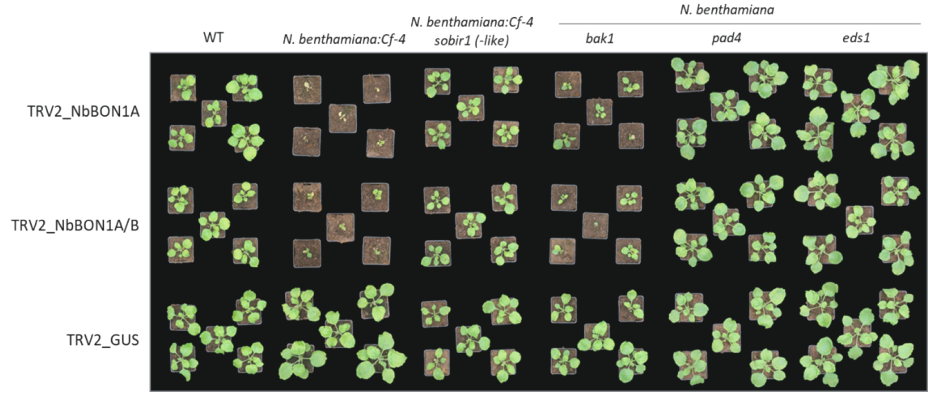

Figure 10. Genetic interaction of *N. benthamiana* homologs of BON1 with components of the SOBIR1-containing complex. Images of the different *N. benthamiana* genotypes upon silencing of *BON1* homologs and the *GUS* control, are shown. Note that, in contrast to the lethality caused by VIGS of *NbBIR1* in the *pad4* and *eds1* mutants, PAD4 and EDS1 do play a role in the lethal response of the plant to VIGS of the *BON1* homologs, whereas SOBIR1, albeit less prominent, appears to play a role in both types of lethality (Figure 7A). Pictures were taken at three weeks after agroinfiltration of the indicated recombinant TRV2 constructs.

Taken together, these results provide evidence for the interaction of BON1 homologs with components of the Cf-4/SOBIR1 receptor complex. At a genetic level, this inter-

action is manifested as a lethal/stunted phenotype observed when silencing these *BON1* homologs in *N. benthamiana bak1* mutants and in transgenic *N. benthamiana:Cf-4*. Additionally, this interaction is also manifested by a conserved interaction between the homologs of BON1 and the BIR proteins.

DISCUSSION

"Guilt-by-association" - components of the SOBIR1 complex are co-expressed in *Arabidopsis*

In this study, a network of co-regulated genes was generated for *Arabidopsis* by combining multiple time course microarray datasets originating from different conditions, with the aim to identify new components of the SOBIR1 receptor complex. By calculating Pearson correlations and focusing on known components of the complex, we generated a scale-free network, representing 1,026 genes. This network was enriched for genes related to plant immune responses (Tables S3-S5). Considering that centrality metrics have been shown to be good predictors of biological relevance in gene co-expression networks [242,262–265], we analysed the network in an attempt to further reduce the amount to candidate genes. However, for any of the metrics of centrality used (degree, closeness centrality and betweenness centrality), no clear cut-off could be identified to further subset the data, while conserving the known interactors of the complex: SOBIR1, BAK1 and BIR1 (Figure 3). So, we decided to not to narrow down the list of candidates represented in the network.

To assess the significance of the list of candidates, we used the previously estimated Pearson correlation cut-off to produce a network covering all the genes represented in the microarray. After filtering by predicted subcellular localisation, we observed that the known members of the protein complex belong to one of roughly ten groups of highly interconnected nodes. Each one of these groups is enriched in genes related to different biological functions, such as translation, pollen exine formation, pollen tube growth, cell wall organization, synthesis of suberin, and immune responses (Figure S2). This shows that the network built around known interactors of the complex also represents a group of highly interconnected nodes, or co-expressed genes, in the context of the co-expression landscape of *Arabidopsis*.

A limitation of the current approach is the lack of precision in the prediction of interactors. The resulting list of genes is larger than what can be efficiently screened, following an unbiased approach using laboratory techniques like VIGS. Since co-regulation does not necessarily imply that genes are functionally related, it is necessary to increase the selection of functionally relevant edges, resulting in only those edges that indeed reflect the connection of genes that share a function. This could be achieved by generating an equivalent network from another plant species and keeping only the edges that connect orthologous genes in both networks [266]. Another, and more direct approach, would be to use the current list of genes as a criterion to prioritize candidates obtained from experimental methods to screen for protein-protein interactions, like yeast two-hybrid [267], or mass spectrometry-based methods using affinity purification or proximity-dependent labelling of SOBIR1, BAK1 and BIR1 [268,269].

A considerable portion of what is known regarding downstream signalling by plant cell-surface immune receptors was discovered in *Arabidopsis* [25], as this is the most widely studied plant in modern biology [270]. However, the immune receptor whose signalling we aim to decipher, which is the LRR-RLP Cf-4, is a tomato protein [68]. Considering that the SOBIR1 receptor complex is widely conserved throughout the Plant Kingdom [271], it is expected that there is some level of conservation in the signalling cascade downstream of SOBIR1 leading to the HR. Because of the difficulties of performing VIGS and agroinfiltration in tomato, we validated the network using a close relative of tomato, which is the research model plant, *N. benthamiana* [272,273].

The Avr4-triggered ROS burst, and the HR are read-outs of different branches of the immune signalling cascade downstream of the Cf-4/SOBIR1 complex

A key aspect to consider when studying a signalling cascade downstream of an immune receptor is to have reliable read-outs for quantification of the plant immune responses upon elicitor perception. The production of ROS, such as superoxide O_2, and its dismutation product H_2O_2, is one of the most rapid defence reactions in plants [249], and we have now optimized its quantification using a luminol-based assay on leaf discs. Our measurements of the apoplastic ROS burst in *N. benthamiana* showed that, while the perception of flg22 by the RLK FLS2 produced a monophasic ROS burst, perception of Avr4 by the RLP Cf-4 resulted in a biphasic ROS burst (Figure 5A). A similar ROS burst, in terms of timing and profile, has been described in transgenic Cf-9-expressing tobacco suspension cultures that were elicited with

the Avr9 protein [274], whereas biphasic ROS bursts have also been observed in incompatible interactions of tobacco and soybean with different pathovars of *P. syringae* [275,276], and also in potato leaves inoculated with spore suspensions of *Phytophthora infestans* [277]. In all these cases, the first phase of the ROS burst is non-specific, while the second burst is observed only in incompatible interactions. These observations are consistent with our observations, as recognition of flg22 by FLS2 does not trigger the HR, which does take place when the Avr4 protein is recognised by Cf-4 [235].

Our silencing experiments showed that, although with different profiles, the apoplastic flg22- and Avr4-triggered ROS burst in *N. benthamiana* is produced by the same enzyme, NbRBOHB, which is the ortholog of *Arabidopsis* RBOHD (Figure 6B & C, Figure S3). In *Arabidopsis*, RBOHD and, to a lesser extent, RBOHF, are key sources of the apoplastic ROS produced after pathogen perception [237]. In *N. benthamiana*, their orthologs NbRBOHB and NbRBOHA, respectively, were described ~20 years ago to be the major source of the ROS produced in response to *Phytophthora* infection [278]. A possible explanation for the regulation of the Avr4-triggered ROS burst came from the studies on the perception of the *Phytophthora infestans* INF1 elicitin. This protein is perceived in *N. benthamiana* by an as yet unknown receptor that requires SOBIR1 and BAK1, and is therefore most likely to be a LRR-RLP [81,82]. Besides this, as is the case for Avr4 perception, recognition of INF1 also triggers an HR and a biphasic ROS burst. It was shown that the second phase of the ROS burst requires transcriptional activation of *NbRBOHB* via a MAPK-WRKY pathway, while the first phase is also performed by NbRBOHB, but is independent of this signalling module [279]. Considering these observations, it is likely that the first phase of the ROS burst triggered by the perception of Avr4 is also activated through phosphorylation of NbRBOHB, likely by an RLCK, following a similar mechanism as is the case for signalling downstream of flg22 perception [210,211]. Possibly, the second phase of the Avr4-triggered ROS burst also requires a MAPK-WRKY pathway. Interestingly, the ROS burst triggered by flg22 in *N. benthamiana* is not only independent of MAPK activation, but even seems to be negatively regulated by MAPK activation, as silencing of the two major defence-associated *MAPK* genes, *NbSIPK* and *NbWIPK*, increases the flg22-triggered ROS burst [280]. The resulting ROS burst profile is similar to the flg22-triggered ROS burst in *N. benthamiana sobir1* mutants, which produce a biphasic ROS burst [253]. These observations suggest that the proposed inhibitory activity of the RLP/SOBIR1 signal transduction pathway on the immune signalling route employed by FLS2 [253] happens via a MAPK signalling cascade.

There are several sources of ROS associated with the immune responses of plants, as in addition to the extracellular ROS produced by cell wall-associated peroxidases and RBOHs, there are also intracellular sources of ROS, like the chloroplasts, the mitochondria, and the peroxisomes [247–252,281]. Inside the cells, the chloroplasts are a major source of ROS associated with the development of an HR . It has been proposed that the apoplastic ROS signal is transduced to the chloroplasts, which then act as amplifiers of the signal that is received from the apoplast, thereby transmitting the signal to the nucleus, and resulting in the transcriptional reprogramming associated with the HR [251]. We explored this possibility by performing DAB staining of leaves of *N. benthamiana:Cf-4* and quantifying the intensity of the HR upon silencing of *NbRBOHB*, followed by treatment with either flg22 or Avr4. The DAB staining procedure, although qualitative, allows detection of ROS from intracellular sources [247,282], whereas the red light imaging method allows a sensitive quantification of the intensity of the cell death response [235]. Our results showed that upon Avr4 perception, the signal that triggers the ROS detected by DAB staining is independent of the generation of the apoplastic ROS burst by NbRBOHB (Figure 6E). The development of the HR is not only also independent of the apoplastic ROS burst, but even seems to be negatively regulated by the apoplastic ROS, as the intensity of the HR increased upon silencing of *NbRBOHB*. This raises many questions regarding the exact role of the apoplastic ROS burst triggered upon elicitor perception. For instance, if it has signalling purposes, what is the mechanism by which this signal is transduced towards the cytoplasm and chloroplasts? Overall, our results are consistent with previous observations in tobacco (*Nicotiana tabacum*), showing that activation of MAPK signalling triggers a light-dependent ROS burst from the chloroplasts and initiates a subsequent HR-like cell death [247]. The reported damage to the chloroplasts that is associated with the accumulation of ROS [247,248] could explain why the red light imaging method is so sensitive, as it is detecting the increase in chlorophyll fluorescence because of thylakoid membrane disassembly [235]. It then becomes relevant to know whether the production of the chloroplastic ROS and its associated damage to the chloroplasts define the onset of the cell death process, as this damage is what the new technique is measuring as a proxy for the intensity of the cell death response of the plant tissue.

EDS1 and PAD4 - immune signalling pathways across different plant families appear to differ

The list of genes represented in the scale-free network build around known interactors of the SOBIR1 complex (Figure 2C, Table S2) contains not only genes associated with the signalling of receptor complexes at the PM, like the components of the SOBIR1 complex itself (Figure 2C). It also contains several cytoplasmic immune receptors, including the NLRs HOPZ-ACTIVATED RESISTANCE 1 (ZAR1), RESISTANCE TO P. SYRINGAE PV MACULICOLA 1 (RPM1), RESISTANCE TO PSEUDOMONAS SYRINGAE2 (RPS2), RPS6, and RPS4 . The list also includes the lipase-like proteins EDS1, PAD4, and SENESCENCE ASSOCIATED GENE101 (SAG101). EDS1 forms mutually exclusive heterodimers with PAD4 or SAG101, forming two signalling modules which are required downstream of several NLRs, particularly for the subset of NLRs that contains an N-terminal Toll-interleukin 1 receptor (TIR) domain (TIR-NLRs or TNLs) [149,283]. This group of co-expressed genes seems to represent a sort of "tool kit" that is activated upon pathogen perception, either by membrane-bound receptors, or by intracellular immune receptors. In line with this, recent reports show that the immune responses triggered by cytoplasmic and intracellular receptors cross-potentiate each other in achieving pathogen resistance [9,10].

The RLK SOBIR1 was initially described in *Arabidopsis* as a suppressor of the lethal activation of immune responses in *bir1* mutants [93]. In that same report, it was shown that the constitutive activation of cell death and defence responses in *bir1-1* also depends on PAD4 and EDS1. This led the authors to hypothesize that the signal triggering this lethal phenotype is transmitted via two parallel pathways. The first pathway requires SOBIR1, whereas the second one, is mediated by one or more TNLs that depend on the PAD4-EDS1 module to trigger cell death and immune responses [93]. Further research provided evidence for a role of both proposed pathways. It was later discovered that *BAK1* is also a suppressor of cell death and defence responses in *bir1-1*, and that silencing of *BIR1* causes BAK1 to associate with SOBIR1 in *Arabidopsis* [100]. Furthermore, recent reports provide evidence for the requirement of the PAD4-EDS1 signalling module downstream of a SOBIR1-containing immune complex in *Arabidopsis* [162,163], and we tested if this requirement for PAD4 and EDS1 downstream of the SOBIR1 complex is also conserved in *N. benthamiana*. VIGS of *BIR1* in *N. benthamiana* produces a lethal phenotype, consistent with the reported phenotype of *bir1-1* mutants in *Arabidopsis* [102,219]. By performing VIGS in different genotypes of *N. benthamiana*, we found that, as expected, the lethal phenotype

resulting from silencing *BIR1* homologs, was suppressed in the *sobir1(-sobir1-like)* mutant line (Figure 7A). The resulting plants were still smaller than the controls, suggesting that indeed there is an additional SOBIR1-independent immune signalling pathway that is activated upon silencing of *BIR1* homologs. We also observed that silencing *BIR1* homologs in a *N. benthamiana bak1* mutant resulted in plants that were just alive, although severely stunted (Figure 7A). The difference in plant size between the *sobir1(-sobir1-like)* and the *bak1* mutant lines upon VIGS of *BIR1* homologs is consistent with previous reports on the role of NbSERK1, which is a paralog of NbBAK1, in the activation of SOBIR1-containing immune complexes [76,79]. When silencing *BIR1* homologs in *N. benthamiana* knockout mutants in *PAD4* or in *EDS1*, we observed that none of the plants survived the silencing experiment, indicating that neither PAD4 nor EDS1 play a role in establishing the lethal phenotype (Figure 7A). We also evaluated the Avr4-triggered ROS burst and HR in the different *N. benthamiana* genotypes and found no evidence for a role of the PAD4-EDS1 module downstream of the SOBIR1 complex (Figure 7B & C). This observation highlights the risk of transferring biological information from *Arabidopsis* to solanaceous plants, as their evolutionary distance implies that there can be differences in the signalling cascades downstream of membrane-bound immune receptors.

Intriguingly, when measuring the Avr4-triggered ROS burst, we actually observed no significant difference between the total amount of ROS produced in the *bak1* and in the *sobir1(-sobir1-like)* mutant lines (Figure 7B). While the *N. benthamiana bak1* mutant line is expected to show only a reduced response to Avr4, because of functional redundancy of additional *NbBAK1* paralogs such as *NbSERK1* [76], the knockout of *SOBIR1* and *SOBIR1-like* in *N. benthamiana* is expected to completely abolish the functionality of transiently expressed Cf-4 [253]. The difference in the ROS burst profiles of these two treatments explains this observation (Figure S4). While the ROS burst profile generated in the *bak1* mutant line is still biphasic, the ROS burst profile of the *sobir1(-like)* mutant is not biphasic anymore but remains at a certain plateau. This observation suggests that this ROS burst is more likely to be background noise due to the agroinfiltration for the expression of Cf-4, than a real read-out that is the consequence of the Avr4-triggered activation of Cf-4-mediated downstream signalling.

G-proteins have multiple roles in regulation of the SOBIR1 complex

Highly connected nodes (hubs) inside a particular cluster in a co-expression network are more likely to be of biological relevance than nodes that only have a few connections [242,262–265]. If we consider the centrality of a node as a criterion to infer its biological relevance, the gene *XLG2*, coding for one of the extra-large Gα subunits of plant heterotrimeric G-proteins, is an interesting candidate for further laboratory validation. This gene is one of the most central genes in the network built around known interactors of the SOBIR1 complex (Fig. 2C, Table S2). Interestingly, this network also contains *AGB1,* coding for the Gβ subunit, and *AGG1*, coding for one of the Gγ subunits in *Arabidopsis* (Figure 2C, Table S2). So, genes encoding all three subunits of heterotrimeric G-protein complexes are co-expressed with genes encoding known components of the SOBIR1 complex. G-protein complexes are key components of many signal transduction pathways and are conserved in most eukaryotes [256]. In plants, these complexes modulate immune responses by their association with RLKs [244,284–286]. Upon activation of the complex, the Gα subunit dissociates from the Gβγ dimer and both the Gα subunit and the Gβγ dimer subsequently regulate different downstream targets [256]. In animals, these complexes are activated by an exchange of GDP for GTP on the Gα subunit. However, in plants their activation mechanism is still an open question. It has been proposed that plant heterotrimeric G-proteins are regulated by their interaction with RLKs, implying a phosphorylation/dephosphorylation-based mechanism, which is different from the way they are activated and de-activated in animals [245,287].

Plants possess canonical G-proteins, represented in *Arabidopsis* by GPA1 (Gα), AGB1 (Gβ) and AGG1/AGG2 (Gγ), and non-canonical G-proteins like *Arabidopsis* AGG3 (Gγ). Besides this, plants also possess extra-large (XLG) Gα subunits, which are represented in *Arabidopsis* by XLG1, XLG2 and XLG3 [287]. We included all the genes encoding Gα subunits of *N. benthamiana* in our silencing experiments, because of the evidence of redundancy in their function. For instance, *Arabidopsis* XLG1, XLG2 and XLG3 are redundantly required for regulating root morphogenesis [288], in addition to the flg22-induced ROS burst [257]. However, the role of XLG1 in modulating the flg22-induced ROS burst is unclear, as there is evidence suggesting that only XLG2 and XLG3 are part of the XLG-Gβγ complexes that regulate signalling by the receptor FLS2 [239,240]. Our silencing experiments showed that the requirement of XLG-Gβγ complexes for the ROS burst produced upon flg22 perception, is conserved in *N. benthamiana* (Figure S6C), as employing a TRV2-construct targeting

all *XLG*s at the same time, resulted in a reduction of the flg22-triggered ROS burst that is comparable to the reduction observed when silencing *AGB1* homologs. In contrast to this, we detected no requirement of the Gα subunits of G-proteins for the ROS burst produced upon perception of Avr4 (Figure 8B and S6B). This indicates that there is a difference in the regulation of NbRBOHB activity upon perception of either flg22 or Avr4. Intriguingly, despite the results regarding the Gα subunits, silencing of *AGB1* homologs did result in a reduction of the Avr4-triggered apoplastic ROS burst (Figure 8B). Possibly, the lack of a growth phenotype when targeting all genes encoding Gα subunits for silencing, is the result of insufficient silencing of the individual genes, although the reduction of the flg22-triggered ROS burst and of the Avr4-triggered HR in these plants, suggest otherwise (Figures S6C and 8C). It is possible that the AGB1 homologs in *N. benthamiana* regulate the Avr4-triggered apoplastic ROS burst produced by NbRBOHB through a yet unknown heterotrimer-independent mechanism. The possibility of such a mechanism was proposed earlier, in consideration of the predominant phenotypes of *agb1*, suggesting that it plays multiple roles in different physiological processes, when compared to the phenotypes of null alleles of the Gα subunits [289].

The knockout mutants *xlg2*, and *agb1*, as well as the double knockout mutant *agg1 agg2*, suppress the cell death phenotype of the *bir1* mutant in *Arabidopsis* [239,240]. Taking this into consideration, we measured the intensity of the Avr4-triggered HR upon VIGS of genes encoding different G-protein subunits in *N. benthamiana:Cf-4*. We observed that *N. benthamiana* homologs of *XLG1*, *XLG2*, *XLG3* and *AGB1* are required for proper induction of the HR upon perception of Avr4 (Figure 8C). However, to our surprise, one of the XLGs that is absent in *Arabidopsis*, designated NbXLG4, showed to be a negative regulator of the SOBIR1 complex, as in this case the Avr4-triggered HR increased upon silencing of its encoding gene. These results provide evidence that different XLGs have opposite roles in the regulation of the HR in *N. benthamiana*. In Arabidopsis, XLG2/3-Gβγ complexes regulate signalling by FLS2 by attenuating the proteasome-mediated degradation of the RLCK BIK1 [245]. Hence, it is possible that NbXLG1/2/3-Gβγ complexes are stabilizing one or more signalling components of the SOBIR1 complex in *N. benthamiana*. Considering the results of our ROS burst measurements, this stabilization appears to be dispensable for activation of the Avr4-triggered apoplastic ROS burst, but seems to be required for the activation of the flg22-triggered ROS burst. Regarding the observed negative regulatory role of NbXLG4, we do not have enough data to speculate about its un-

derlying mechanism. It could be that NbXLG4 is exerting this role after dissociating from an XLG-Gβγ complex. It is also possible that NbXLG4 negatively regulates the SOBIR1 complex by its participation in an NbXLG4-Gβγ complex that has a different regulatory role than the G-protein complex composed of NbXLG1/2/3-Gβγ. For both options, silencing of the genes encoding the components of the NbXLG1/2/3-Gβγ seems to have an epistatic effect on the phenotype produced upon silencing of *NbXLG4*, as the use of a tandem construct targeting all *XLGs* present in *N. benthamiana* resulted in the same outcome as silencing of the Gβ subunit only, which was a reduction in the intensity of the HR (Figure S6D).

We detected no involvement of *N. benthamiana* homologs of *GPA1* in the immune output upon treatment with flg22 or Avr4. This is consistent with previous reports on *Arabidopsis* showing that *GPA1* is neither involved in the development of an HR, nor in the ROS burst triggered by flg22 [240,290]. These results illustrate how complexes composed by XLG-Gβγ and GPA1-Gβγ have evolved different signalling specificities [289]. While XLG-Gβγ complexes regulate immune responses mediated by mesophyll cells [245,291], GPA1-Gβγ complexes play a positive role in defence by mediating stomatal closure [292–294].

BON1 – could this copine protein be part of a guarding mechanism?

The last protein that we selected for laboratory validation is BON1, which is also referred to as COPINE1 (CPN1). Its encoding gene is present in the network built around known interactors of the SOBIR1 complex among the top 5% of central nodes, based on closeness centrality (Figure 2C, Table S2). BON1 belongs to the copine protein family, which was originally identified in a protozoan and was found to be conserved in nematodes, mammals and plants [295]. This group of proteins was named with the French feminine noun *copine,* which means friend, to reflect their association with lipid membranes, as "companions". Copines are typically composed of two C2 domains at their N-terminal half, followed by a von Willebrand factor A (vWA) domain in their C-terminal half [295]. The C2 domains are Ca^{2+}-dependent phospholipid binding domains, mostly found in proteins with functions related to signal transduction or membrane trafficking [296]. The vWA domain is frequently found in proteins that function in multi-protein complexes [297]. In *Arabidopsis*, *bon1* mutants show a temperature-dependent growth arrest and enhanced defence responses [259,298]. This phenotype depends on several TNLs, of which *SNC1* being the major contributor [258,260,261]. Interestingly, BON1 interacts with BIR1 and BAK1 *in planta,* and

overexpression of *BON1* and *BIR1* can partially complement the mutant phenotypes of *bir1* and *bon1*, respectively [238]. Hence, it is likely that BON1 has an important function in regulating SOBIR1-containing complexes.

From our phylogenetic analysis of copine proteins in *N. benthamiana,* we identified two pairs of homeologs as potential candidates to be the functional orthologs of *Arabidopsis BON1* and we designated them *NbBON1A* and *NbBON1B* (Figure S7). While silencing of *NbBON1A* in *N. benthamiana:Cf-4* produced plants that were dead or severely stunted, silencing of *NbBON1B* resulted in plants that were comparable with the control plants in size (Figure 9A), and also in the intensities of the Avr4-triggered ROS burst and HR (Figure S8). We cloned the tomato ortholog of *NbBON1A* based on the observed phenotype, because of its resemblance to the dwarf phenotype of *Arabidopsis bon1* mutants and observed by co-immunoprecipitations that the interactions between BON1 and the RLKs BIR1 and BAK1 are conserved in *N. benthamiana* (Figure 9).

We performed VIGS experiments to evaluate the genetic interactions between *NbBON1A* and genes coding for components of the SOBIR1 complex. To our surprise, the dwarf/lethal phenotype observed upon silencing *NbBON1A* in *N. benthamiana:Cf-4* was absent in *N. benthamiana* WT. Similarly, this phenotype was also absent in *N. benthamiana:Cf-4 sobir1(-like)* (Figures 10 and S9A). As SOBIR1 is required for the accumulation and functionality of the receptor Cf-4 [66,253], these results suggest that the presence of Cf-4 in *N. benthamiana* causes the dwarf/lethal phenotype observed upon silencing *NbBON1A.* The stunted phenotype of *Arabidopsis bon1* mutants is a consequence of TNL activation and these observations in *N. benthamiana* could be explained by *NbBON1A* having a negative regulatory role on a TNL-based guarding mechanism that is acting on the SOBIR1 complex. Such a guarding hypothesis has been proposed before as an explanation for particular observations in *Arabidopsis*, as in this plant *bak1* mutant plants develop a spreading necrosis upon pathogen infection [299], and the double knockouts *bak1* and *bak1-like (bkk1)* suffer from seedling lethality and constitutive activation of defence responses [300]. In our silencing experiments, the *N. benthamiana bak1* mutants were also severely stunted upon silencing of *NbBON1A* (Figure 10). Activation of this hypothesized guarding mechanism by introducing the tomato receptor Cf-4 in *N. benthamiana* could explain why *N. benthamiana:Cf-4* plants are smaller than WT

plants (data not shown), as the activation of immune responses has a fitness cost because of relocation of resources from growth to defence [219].

As mentioned above, the stunted phenotype of *Arabidopsis* knockout mutants in *BON1* is a consequence of TNL activation and depends on the PAD4-EDS1 module [258,260,261]. In *N. benthamiana*, PAD4 homologs seem to be dispensable for these signalling processes, and TNL-mediated immune responses require EDS1 complexes, incorporating homologs of SENESCENCE ASSOCIATED GENE101 (SAG101) [301]. Because of our initial observation of the lethal/stunted phenotype upon silencing *NbBON1A* in *N. benthamiana:Cf-4*, we included the knock-out lines *pad4* and *eds1* in our silencing experiments. Indeed, we observed that *N. benthamiana eds1* knockout plants were much bigger than the WT plants upon silencing of *NbBON1A* (Figure S9B and S9C). Intriguingly, this was also the case for the *pad4* knockout line, suggesting a role for *PAD4* homologs in the signalling process regulated by NbBON1A. However, we cannot exclude the possibility of this observation being an artifact of the silencing process itself, as agroinfiltration of the TRV2-GUS recombinant construct has a similar effect, particularly with the *eds1* knockout line (Figure S9D). An experiment to test this hypothesized guarding mechanism would be to cross the *N. benthamiana:Cf-4* plants with the knockout lines *eds1* and *pad4*. Absence of the stunted/lethal phenotype upon silencing *NbBON1A* in *N. benthamiana:Cf-4 eds1* plants would support our working hypothesis, and the phenotype of *N. benthamiana:Cf-4 pad4* lines upon silencing *NbBON1A* would shed some light on the role of PAD4 homologs in *N. benthamiana*.

CONCLUSIONS

We here made use of the solanaceous model plant *N. benthamiana* as a stepping-stone to acquire knowledge on the signalling processes triggered by SOBIR1-containing immune complexes from tomato. We followed the assumption that structural components of the immune receptor complexes at the cell membrane will tend to be conserved across different botanical families. The efficiency in *N. benthamiana* of laboratory techniques such as transient gene expression, VIGS and luminol-based ROS burst measurements, combined with the use of a novel method for quantification of the HR, facilitated the evaluation of various hypotheses generated from *Arabidopsis* data. Our analysis of microarray data from *Arabidopsis* revealed that

genes coding for known components of the SOBIR1 complex are co-expressed. These genes belong to a transcriptional cluster that is enriched in genes related to the plant immune responses. We propose the use of this cluster, or list of genes, as a tool to prioritize candidates obtained from wet-lab techniques, such as mass spectrometry-based methods using affinity purification or proximity-dependent labelling in Solanaceae. Besides this, our experiments in *N. benthamiana* provide insight into the processes regulating the ROS burst and the HR that is activated upon elicitor perception, and provide observations suggesting a guarding mechanism acting on the SOBIR1-complex (Figure 11).

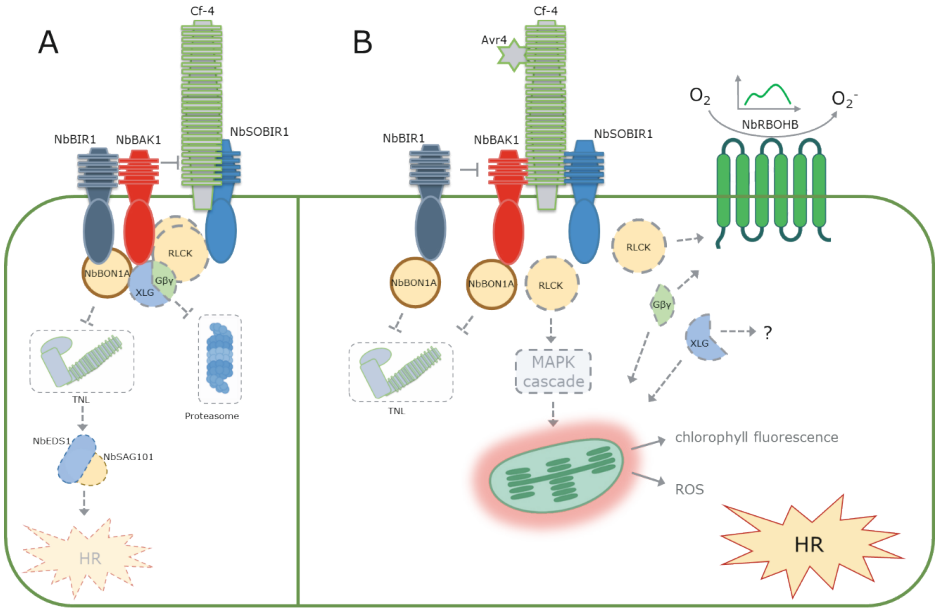

Figure 11. Model integrating the observations made in this study. (A) In the resting state, NbBIR1 interacts with NbBAK1, thereby preventing the activation of the SOBIR1 complex. G-proteins interact with components of the complex other than NbSOBIR1, and likely modulate its proteasomal degradation. NbBON1A interacts with NbBIR1 and NbBAK1 and negatively regulates a guarding mechanism acting on the SOBIR1 complex. (B) Perception of Avr4 triggers the recruitment of NbBAK1 to the Cf-4/SOBIR1 complex, resulting in the activation of NbRBOHB by phosphorylation through an activated RLCK and the dissociation of the G-protein complex. A parallel signalling pathway, in which a MAPK cascade is involved, causes the production of ROS from the chloroplasts, associated with an increase in chlorophyll fluorescence, which correlates with the intensity of the HR.

MATERIALS AND METHODS

Co-expression network analysis of *Arabidopsis* microarray data

The raw data of transcription profiling arrays by the GeneChip Arabidopsis ATH1 genome Array were downloaded from ArrayExpress (https://www.ebi.ac.uk/arrayexpress/). Specific treatments with *Arabidopsis* mutant lines were removed the dataset, and experiments with chemotherapeutics, UV radiation, and *Arabidopsis* mutant lines were not included.

The data were downloaded as CEL files and processed in R software using the Simpleaffy R package (version 2.48.0), from the BioConductor project (release 3.3) [302]. Array normalization was done using the Robust Multiarray Averaging (MRA) method and the pairwise comparisons between controls and treatments were computed using the default method, as follows:

log2FC= log2(mean (treatment replicates))-log2(mean (control replicates))

The log2FC for all the probes along all the treatments were compiled in one table, where each column represents a specific treatment and each row represents one of the 22,810 probes in the GeneChip Arabidopsis ATH1 Genome Array. From this table, the pair-wise Pearson Product Moment Correlations were calculated between all probes, and a correlation threshold was established to subset the data. Three known interactors, SOBIR1, BAK1 and BIR1, were used as guides to extract a subset of the network. The sub-network contains all the probes correlated to the guide genes, as well as all the correlations between all probes in the group.

The three groups (the SOBIR1, BAK1 and BIR1 groups) were uploaded to Cytoscape, version 3.9.1 [241] and merged to build one combined network. The network was analysed using NetworkAnalyzer [303], and the cut-off for correlation values was set as such that a scale-free network was formed in order to retrieve the network hubs using centrality measures; closeness centrality and betweenness centrality. Nodes that disconnect from the network while increasing the cut-off, where subsequently removed from the dataset.

The resulting list of nodes was annotated as follows: first, Affymetrix Arabidopsis ATH1 Genome Array annotation data [304] were used to map probe identifiers to TAIR

gene identifiers; second, the Cytoscape plug-in GeneMANIA [305] was used to retrieve the gene symbols and perform further functional annotation.

The Gene Ontology (GO) terms enrichment analysis was done using the Gene Ontology Consortium tool PANTHER [306]. Analysis type: PANTHER Overrepresentation Test (Released 20220202). Annotation Version and Release Date: PANTHER version 17.0 Released 2022-02-22. Reference List: *Arabidopsis thaliana* (all genes in database). Annotation data set: PANTHER GO-slim molecular function, PANTHER GO-slim biological process and PANTHER GO-slim cellular component.

In order to build a network representing the co-expression landscape of *Arabidopsis* after filtering out the proteins by their predicted localisation, all the pairs of probes whose Pearson Product Moment Correlation passed the selected threshold, were uploaded to Cytoscape, version 3.9.1 [241], and the nodes were filtered by predicted subcellular protein localisation according to annotation data from Arabidopsis.org (ftp://ftp.arabidopsis.org/home/tair/Proteins/Properties/, 2019). Nodes that disconnect from the network were removed from the dataset. The resulting network was visualized using the unweighted Prefuse Force-Directed Layout. The GO terms enrichment analysis of the resulting clusters was done as described previously but changing the Reference list to exclude the genes coding for proteins predicted to be located at the nucleus, chloroplast, mitochondria or Golgi bodies.

Phylogenetic analysis

Homologous protein sequences were retrieved by a BLAST search at The Sol Genomics Network (SGN) [307]. The alignments and phylogenies were done using the MAFFT web-server [308]. The protein sequences were aligned, selecting BLOSUM45 as a scoring matrix for amino acid sequences. The trees were built using the neighbour-joining method on the conserved sites with 100 bootstraps.

Plant material and growth conditions

N. benthamiana and transgenic *N. benthamiana* stably expressing Cf-4 (*N. bentamiana:Cf-4*) were grown in climate chambers under 16 hr of light, at 24°C and 8 hr of darkness, at 22 °C and at a RH of 75%.

Vectors for Agroinfiltration and virus-induced gene silencing

Tomato homologs of *Arabidopsis BON1, GPA2, XLG1, XLG2 and XLG4* were a amplified from tomato cDNA using Phusion Hot Start II High-Fidelity polymerase (Promega), and ligated to pENTR™/D-TOPO®. Then, the amplicons were transferred into the destination vectors using Gateway™ LR Clonase™ II Enzyme mix (Thermo Fisher Scientific). The primers used to clone the genes are listed in Table S6. The generated constructs are: pGWB20-35S::SlBON1A-10xMYC (SOL8614), pGWB20-35S::SlBON1B-10xMYC (SOL8615), pBin-GW-35S::SlBON1A-eGFP (SOL8619), pBinK-35S::SlBON1B-eGFP (SOL8620), pBIN-35S::SlXLG2-eGFP (SOL9312), pGWB20-35S::SlXLG2-10xMYC (SOL9313), pBIN-35S::SlGPA1-eGFP (SOL9314), pGWB20-35S::SlGPA1-10xmyc (SOL9315), pGWB6-35S::SlXLG1-sGFP (SOL9332), pGWB21-35S::SlXLG1-10xmyc (SOL9333), pGWB6-35S::SlXLG4-sGFP (SOL9318), pGWB21-35S::SlXLG4-10xmyc (SOL9319). The binary vectors pBIN-KS-35S::SlBIR1-eGFP (SOL 7105), pBIN-KS-35S::SlBIR2B-eGFP (SOL 7106), pBIN-KS-35S::SlSERK3a-eGFP (SOL2821), pBIN-KS-35S::GUS-eGFP (SOL5094), pBIN-KS-35S::SlSOBIR1–eGFP (Sol 2774), p2750-35S::GUS-10xMYC (SOL5822) have been described previously [66,102,309].

We used the SGN VIGS tool to generate the silencing constructs [307]. For the case of the silencing constructs pTRV2_NbBON1A (SOL8603), pTRV2_NbBON1B (SOL8604), pTRV2_NbBON1A/B (SOL8605), pTRV2_NbXLG1 (SOL9301), pTRV2_NbXLG2 (SOL7126), pTRV2_NbXLG3 (SOL7124), pTRV2_NbXLG4 (SOL9302), pTRV2_NbGPA1 (SOL9311), pTRV2_NbAGB1 (SOL7127), pTRV2_NbRBOHB (6975), and pTRV2_NbRBOHE (6976) we amplified fragments of ~200bp from *N. benthamiana* cDNA using Phusion Hot Start II High-Fidelity polymerase (Promega). The primers used to generate these constructs are listed in Table S6. The resulting fragments were ligated into the pCR™-Blunt II-TOPO® vector, and transferred into pTRV2 [310] by restriction digestion and ligation. For the case of the tandem silencing constructs pTRV2_NbXLG123, pTRV2_NbXLG1234, and pTRV2_NbXLG123GPA1, the fragments were fused by a PCR with overlapping primers, and ligated into pTRV2 [310]. The silencing construct TRV2_NbRBOHA is described in a published report [278]

Agrobacterium*-mediated transient transformation and virus-induced gene silencing (VIGS) in *N. benthamiana

For Co-immunoprecipitation and immunoblot assays, the agroinfiltrations were performed as previously described [206]. In brief, three to four weeks old *N. benthamiana*

were agroinfiltrated in the first fully expanded leave. The leaves were harvested for immunoprecipitation at 3 days after agroinfiltration.

VIGS using TRV-based vectors was performed in *N. benthamiana:Cf-4* as described previously [66,76]. In brief, 10 days old N. benthamiana were agroinfiltrated to express the designed TRV2 plasmid together with pTRV2-RNA1, each at an OD_{600} of 0.8. The plants were evaluated three weeks after agroinfiltration. The canopy area of the plants subjected to VIGS was estimated using ImageJ [311].

Bioassays for flg22- and Avr4-induced immunity

The intensity of the HR in the plant tissue was quantified by using the red-light imaging method using a Chemidoc XRS system (Bio-Rad). Pure Avr4 protein at 10 µM, diluted in MQ, was infiltrated into the leaves from the abaxial side. Two days after infiltration, the red light fluorescence emitted by the leaves was measured as described previously [235].

The apoplastic ROS burst was measured on 5mm leave discs taken from the first fully expanded leave of *N. benthamiana* plants. The leave discs were floated on 50 µL of Milli-Q water (MQ) in a 96-well plate and kept in the dark at room temperature overnight. The MQ was then removed using tissue paper, replaced by 50 µL of MQ, and kept in the dark for one hour. After this, a 50 µL solution containing 50 µM luminol L-012 (FUJIFILM), 10 µg horseradish peroxidase, and either 0.1 µM of Avr4 protein or 0.1 µM of the peptide flg22 (EZBiolab). The luminescence values were measured using a CLARIOstar plate reader (BMG LABTECH) for over five hours.

The DAB staining was performed on *N. benthamiana:Cf-4* leaves three hours after infiltration of 10 µM solutions of flg22 (EZBiolab) or Avr4 protein. The leaves were vacuum-infiltrated in DAB staining solution [312], incubated for 3 hours. Then, the leaves were destined by boiling for ten minutes in a 3:1:1 solution of ethanol, acetic acid and glycerol.

Co-immunoprecipitation assays

Co-immunoprecipitations (co-IPs) were performed as described previously [66]. The eGFP- or eYFP-tagged proteins were detected with αGFP-HRP (Miltenyi Biotec, 130-091-833). The Myc-tagged proteins were detected using αMyc (cMyc9E10, sc-40, Santa Cruz) and αMouse-HRP (GE healthcare) as a seconday antibody.

Production of Avr4 protein

The Avr4 protein was produced in *Pichia pastoris* [203]. The culture supernatant was concentrated using a VIVAFLOW 200 5000 MWCO (Sartorius) while kept at 4°C until reaching a final volume of ~100 mL/per liter of culture supernatant. The concentrated supernatant was dialyzed using Spectra/Por7 Dialysis Membrane pre-treated RC Tubing (Spectrum Labs; MWCO 3.5 kDa) and equilibration buffer (25 mM Tris, 25 mM NaCl, 10 mM Imidazole pH=7.5). The protein purification was performed using a Biologic LP Low pressure chromatography system (BIORAD) with 3 mL of His60 nickel resin beats Ni-NTA for His-tag purification (Takara Bio), and a 0 to 100% gradient withing 20 minutes of elution buffer (25 mM Tris, 25 mM NaCl, 200 mM Imidazole, pH=7.5). After this, the pure protein solution was dialyzed in MQ and store at -20°C. The resulting pure protein solution was quantified using Quick Start Bradford Protein Assay (BIORAD), and verified by immunoblotting using 6x-His Tag Monoclonal Antibody (Invitrogen, MA1-21315).

ACKNOWLEDGMENTS

Hirofumi Yoshioka provided the construct TRV2_NbRBOHA. Johannes Stuttmann provided *N. benthamiana* seeds of the Nbeds1, Nbpad4, and Nbbak1 mutants. Wen Huang provided seeds of *N. benthamiana sobir1 (-like)* and *N benthamiana:Cf-4 sobir1 (-like)*. We acknowledge Unifarm's personnel, especially Bert Essenstam, for the excellent plant care. S.L.V. is supported by the Peruvian Council for Science, Technology and Technological Innovation (CONCYTEC) and its executive unit FONDECYT.

SUPPLEMENTARY DATA

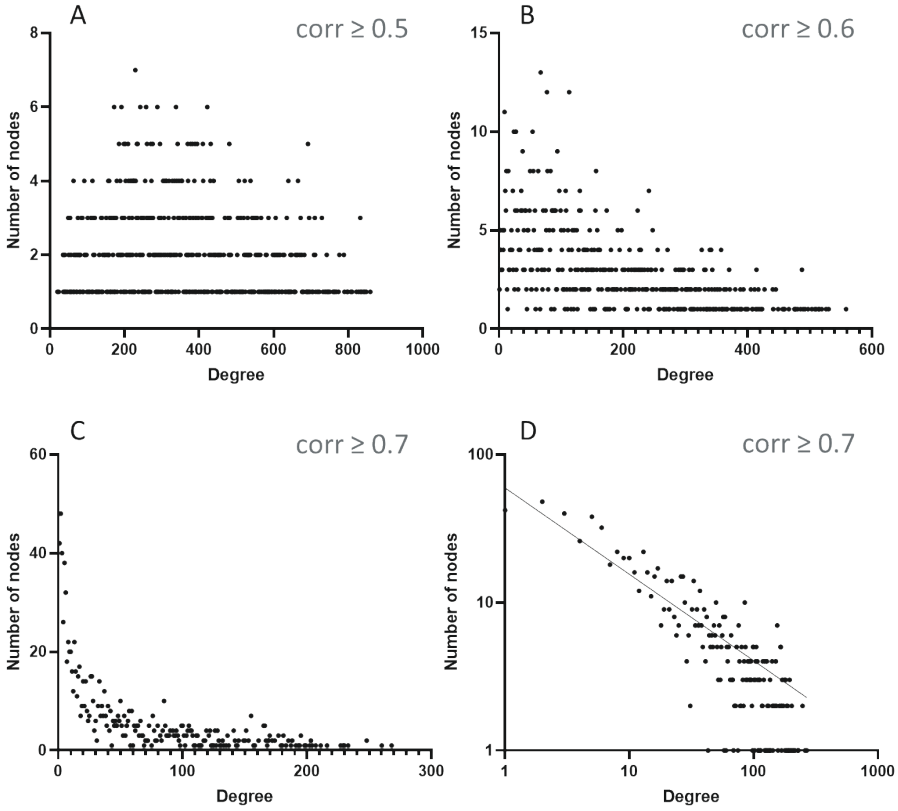

Figure S1. Node degree distribution with different correlation cut-offs. (A) Node degree distribution at correlation ≥ 0.5. (B) Node degree distribution at correlation ≥ 0.6. (C) Node degree distribution at correlation ≥ 0.7. (D) Degree distribution at correlation ≥ 0.7, with both axes in a logarithmic scale and a fitted line with the formula Y = 10^(a*log(X) + b), where a = -0.5835 and b = 1.775 (R-squared 0.8243).

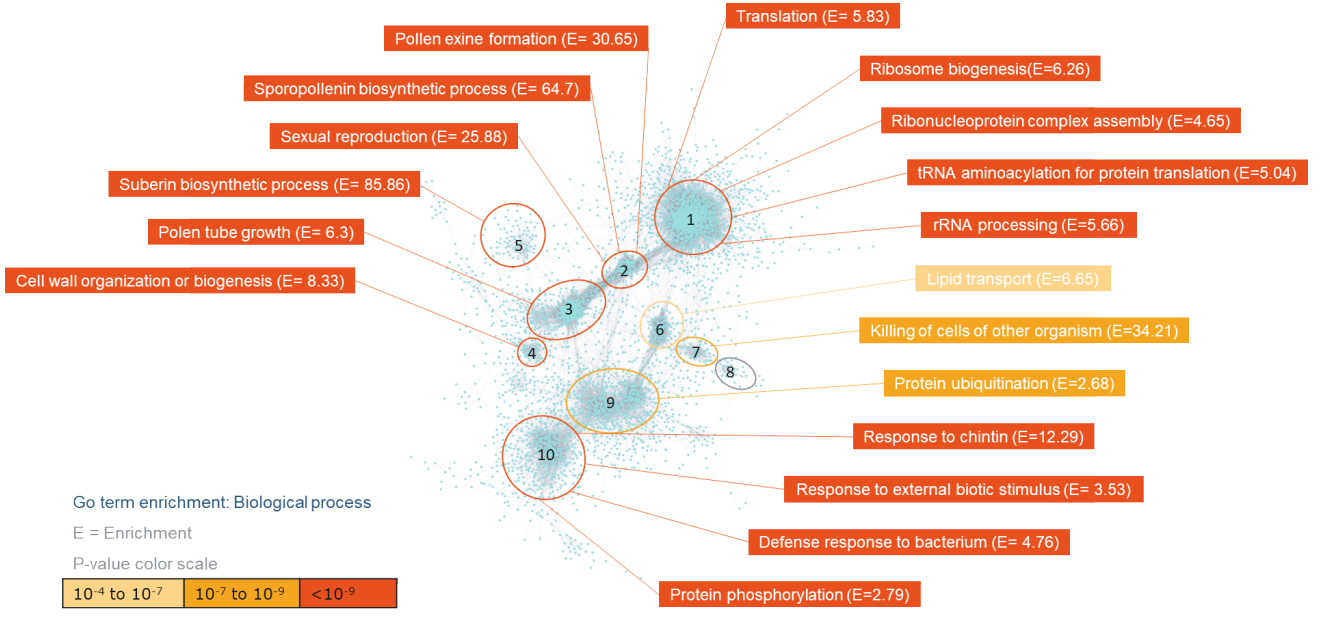

Figure S2. Gene ontology (GO) term enrichment analysis of the ten groups of highly interconnected nodes present in the co-expression landscape of *Arabidopsis*, after filtering out proteins predicted to localize at the nucleus, chloroplast, mitochondria and Golgi bodies. The graph only shows the most specific and most significantly enriched terms.

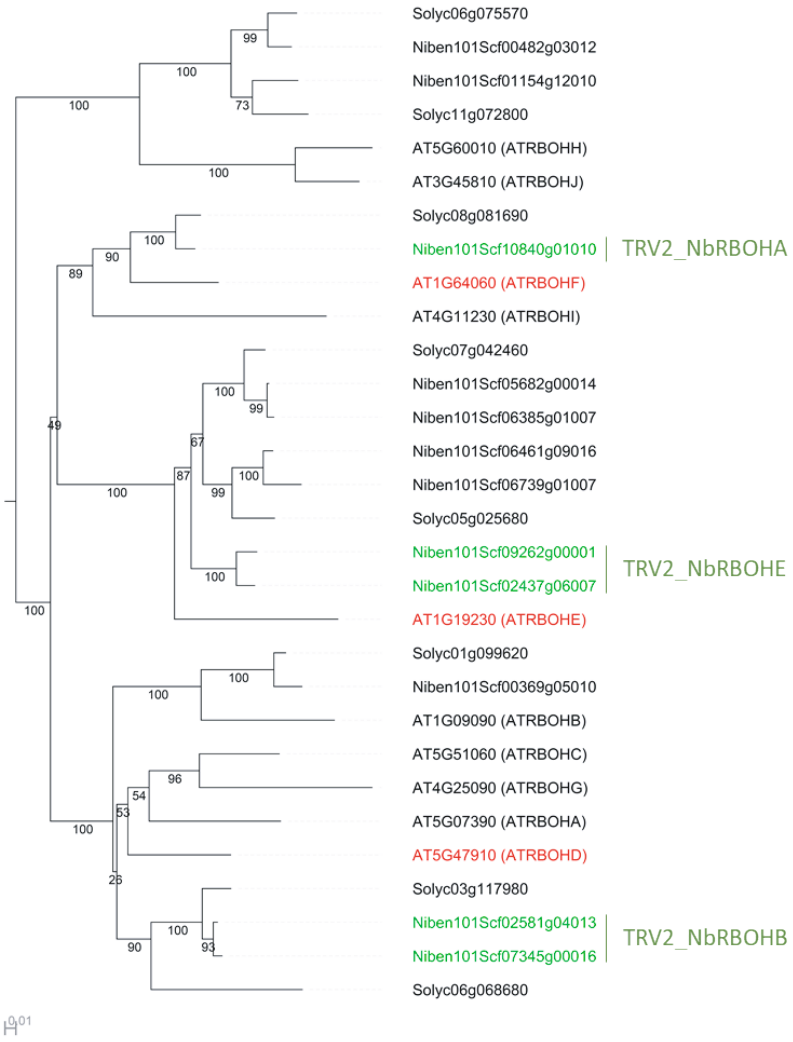

Figure S3. Phylogenetic tree of the respiratory burst oxidase homologue (RBOH) protein family of *Arabidopsis*, tomato and *N. benthamiana*. *Arabidopsis* proteins RBOHF, RBOHE and RBOHD are shown in red. *N. benthamiana* proteins selected for silencing of the encoding gene are shown in green. The branch length in the tree is proportional to the number of substitutions per site.

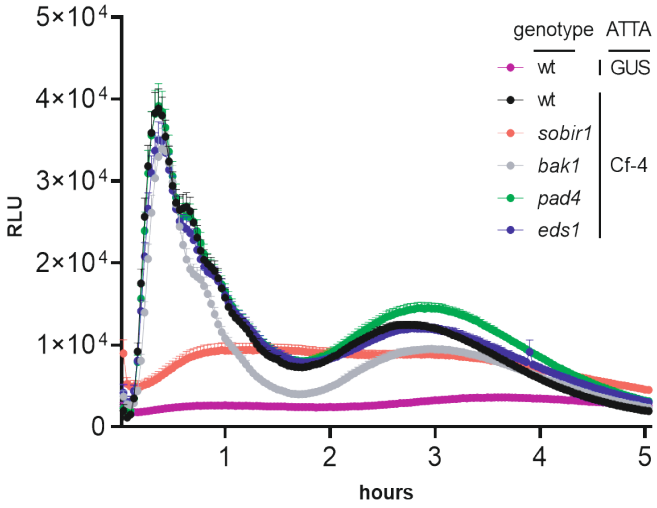

Figure S4. Luminol-based measurement of the Avr4-triggered ROS burst of different *N. benthamiana* knock-out lines, after transiently expressing GUS or Cf-4. Measurements were performed at three days after agroinfiltration at OD = 0.1. The error bars represent the SEM. The profiles are the result of a total of 48 measurements from four independent experiments. One leaf disc was considered as an outlier (as determined by the ROUT method) and was removed from the results of the *sobir1(-like)* genotype.

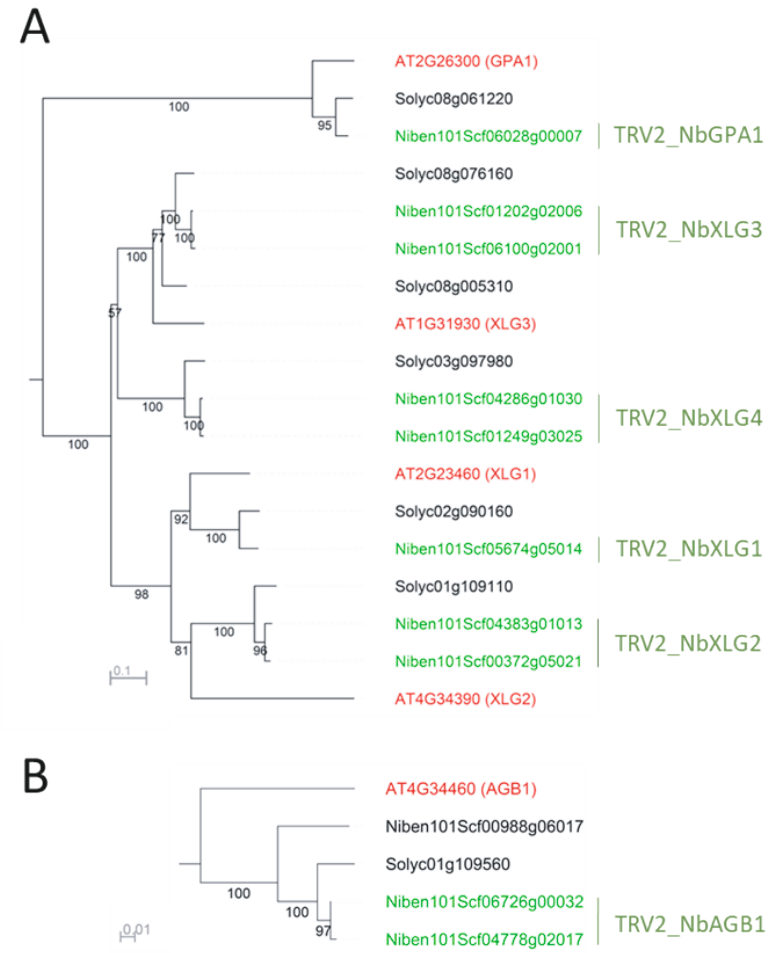

Figure S5. Phylogenetic tree with the homologs of the (A) Gα and (B) Gβ subunits of G-proteins present in *Arabidopsis*, tomato, and *N. benthamiana. Arabidopsis* proteins are shown in red. *N. benthamiana* proteins selected for silencing of the encoding gene are shown in green. The branch lengths in the trees are proportional to the number of substitutions per site.

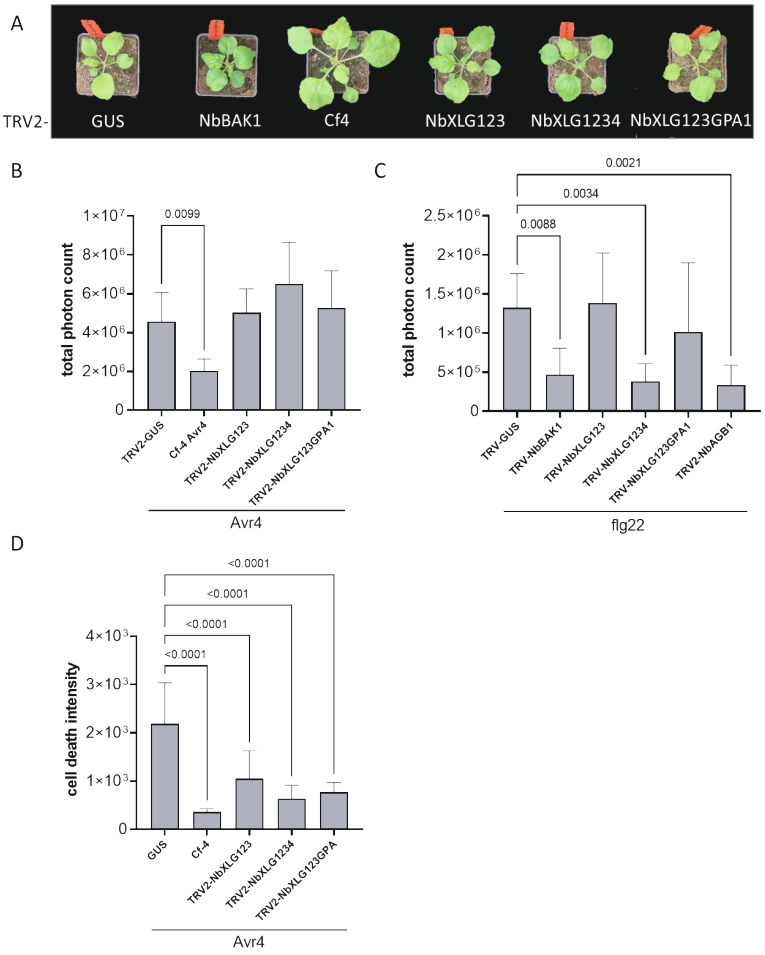

Figure S6. Extra-large G proteins redundantly regulate the flg22-triggered ROS burst in *N. benthamiana*. (A) Representative phenotypes of *N. benthamiana:Cf-4* plants agroinfiltrated with different TRV2 tandem constructs for VIGS. Pictures were taken three weeks after agroinfiltration. (B) Total amount of Avr4-triggered apoplastic ROS detected from leaf discs taken from *N. benthamiana:Cf-4* plants, subjected to VIGS. The leaf discs were exposed to 0.1 µM of Avr4 and ROS was measured over a period of 5 hours. N = 8, error bars show SD. P-values are indicated when ≤ 0.05 (ANOVA, Dunnett's test). (C) Total amount of flg22-triggered ROS detected from leaf discs taken from *N. benthamiana:Cf-4* plants, subjected to VIGS. The leaf discs were exposed to 0.1 µM of flg22 and ROS was measured over a period of 1 hour. N = 8, error bars show SD. P-values are indicated when ≤ 0.05 (ANOVA, Dunnett's test). (D) Quantification of the Avr4-triggered HR by means of red-light imaging in *N. benthamiana:Cf-4* plants, subjected to VIGS. Measurements were done at three days after infiltration of 10 µM of Avr4 protein in leaves of plants subjected to VIGS, using the indicated constructs. Error bars show the SD, n = 8. P-values are indicated when ≤ 0.05 (ANOVA, Dunnett's test).

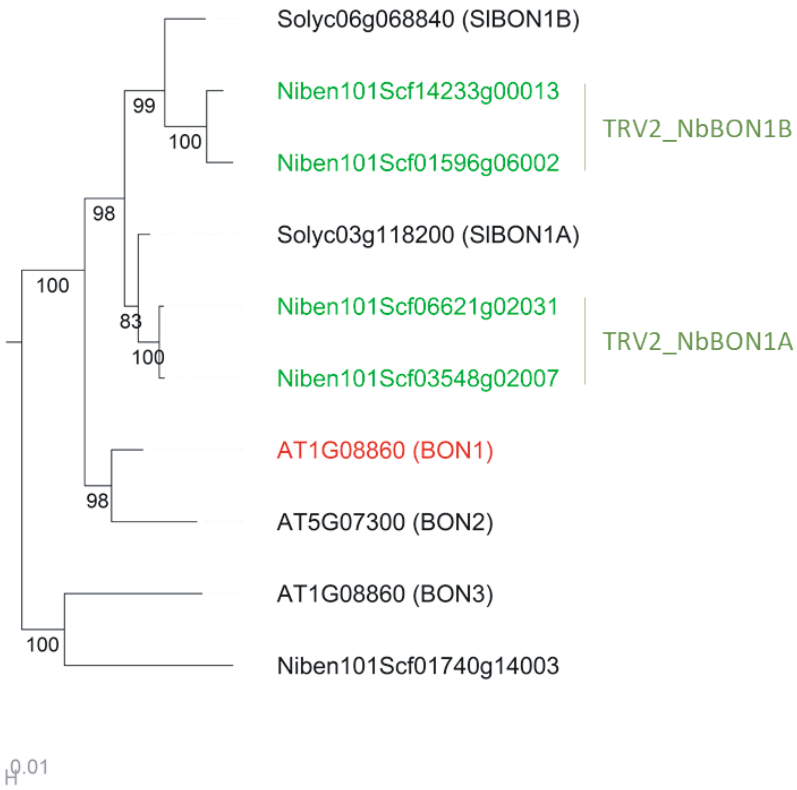

Figure S7. Part of the phylogenetic tree of the homologs of *Arabidopsis* BON1 found in tomato and *N. benthamiana*. The *Arabidopsis* BON1 protein is shown in red. *N. benthamiana* BON proteins selected for silencing of the corresponding gene are shown in green. The branch lengths in the tree are proportional to the number of substitutions per site.

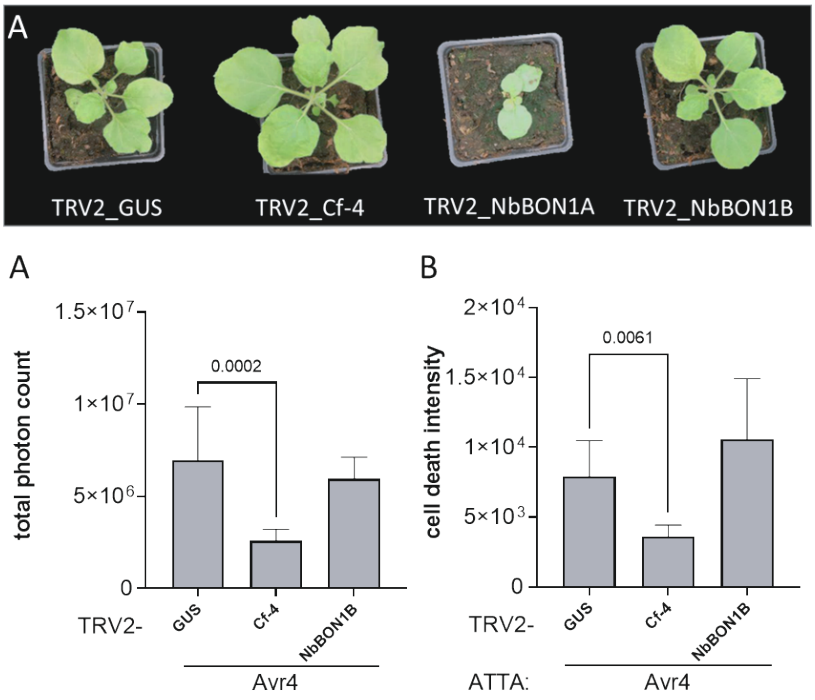

Figure S8. Immune responses upon Avr4 perception after silencing of *NbBON1B*. (A) Total amount of Avr4-triggered apoplastic ROS detected from leaf discs taken from *N. benthamiana:Cf-4* plants, subjected to VIGS. The leaf discs were exposed to 0.1 µM of Avr4 and ROS was measured over a period of 5 hours. N = 8, error bars show SD. P-values are indicated when ≤ 0.05 (ANOVA, Dunnett's test). (B) Quantification of the Avr4-triggered HR by means of red-light imaging in *N. benthamiana:Cf-4* plants. Measurements were done at three days after agroinfiltration for the expression of Avr4 (OD = 0.03) in leaves of plants subjected to VIGS. N = 8, error bars show SD. P-values are indicated when ≤ 0.05 (ANOVA, Dunnett's test).

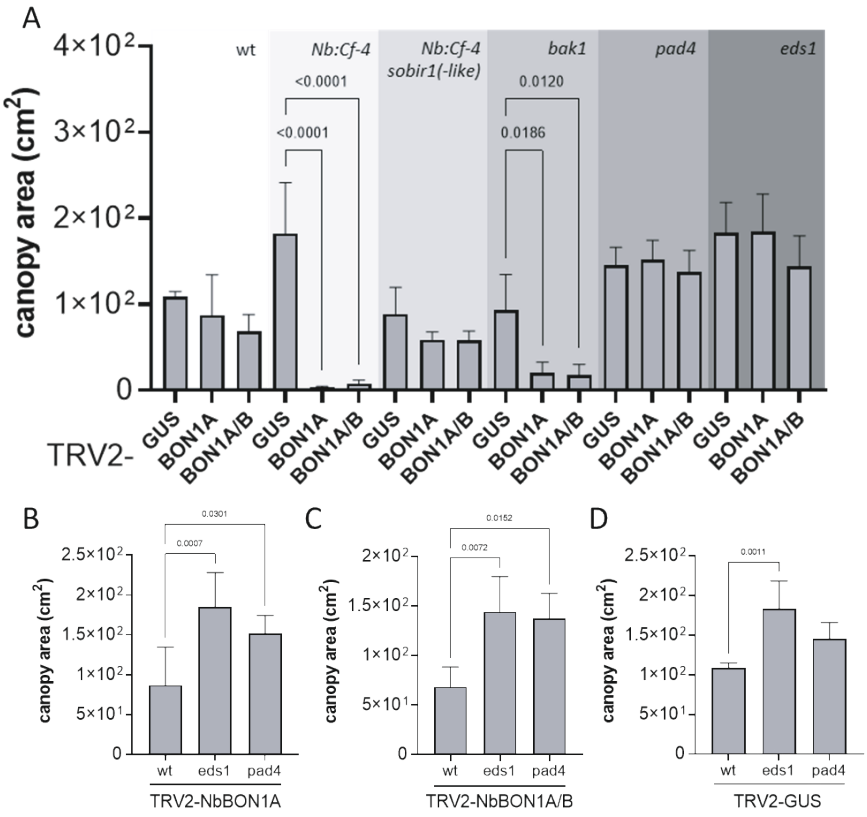

Figure S9. Quantification of the canopy area of the plants upon silencing of *BON1* homologs in different *N. benthamiana* genotypes. N = 5, error bars show SD. P-values are indicated when ≤ 0.05 (ANOVA, Dunnett's test). (A) Comparisons within each different genotype, and (B, C and D) comparison within each TRV2-VIGS construct.

Table S1. Accession number, title and number of treatments of the experiments of which the gene expression data were used for the analysis. Among the selected experiments, four include treatments of *Arabidopsis* mutant lines and these were excluded from the analysis (E-GEOD-39384, E-GEOD-5630, E-GEOD-5633 and E-GEOD-5632). In total, 19 treatments were removed, as these monitored gene expression in mutant plants.

Accession number	Title	included treatments	included measurements*
Treatment with pathogens and immunogenic patterns (IPs)			
E-GEOD-5615	Transcription profiling by array of *Arabidopsis* after treatment with LPS, HrpZ, flg-22 and NPP1	12	42
E-GEOD-5616	Transcription profiling by array of *Arabidopsis* after infection with *Phytophthora infestans*	3	18
E-GEOD-5684	Transcription profiling by array of *Arabidopsis* after infection with *Botrytis cinerea*	2	12
E-GEOD-5685	Transcription profiling by array of *Arabidopsis* after treatment with *Pseudomonas syringae*	15	32
E-GEOD-5686	Transcription profiling by array of *Arabidopsis* after inoculation with *Erysiphe orontii*	7	48
Treatment with hormones			
E-GEOD-5696	Transcription profiling by array of *Arabidopsis* after treatment with brassinosteroids	11	26
E-GEOD-5700	Transcription profiling by array of *Arabidopsis* after treatment with abscisic acid	3	8
E-GEOD-5701	Transcription profiling by array of *Arabidopsis* after treatment with gibberellin	3	13
E-GEOD-39384	The AtGenExpress: Basic hormone treatment of seedlings in *Arabidopsis*	21	48
E-GEOD-39385	The AtGenExpress: hormone inhibitor or other chemical treatment of seedlings in *Arabidopsis*	26	60
Different organs and developmental stages			
E-GEOD-5629	Transcription profiling by array of *Arabidopsis* at different developmental stages	2	24
E-GEOD-5620	Transcription profiling by array of *Arabidopsis* roots and shoots	14	36
E-GEOD-5632	Transcription profiling by array of *Arabidopsis* flowers and pollen at different developmental stages	14	45
E-GEOD-5633	Transcription profiling by array of *Arabidopsis* shoots and stems at different developmental stages	6	21
E-GEOD-5634	Transcription profiling by array of *Arabidopsis* seeds and siliques at different developmental stages	6	24
E-GEOD-5630	Transcription profiling by array of *Arabidopsis* leaves at different developmental stages grown in continuous light, short- or long-day conditions	16	57
E-GEOD-5631	Transcription profiling by array of *Arabidopsis* roots at different developmental stages after growth in continuous light or long-day conditions	4	21

Table S1. *(Continued)*

Accession number	Title	included treatments	included measurements*
Abiotic stress			
E-GEOD-5617	Transcription profiling by array of *Arabidopsis* after different light treatments	14	48
E-GEOD-5622	Transcription profiling by array of *Arabidopsis* after osmotic stress treatment	10	24
E-GEOD-5623	Transcription profiling by array of *Arabidopsis* after salt stress treatment	10	24
E-GEOD-5624	Transcription profiling by array of *Arabidopsis* after drought stress	10	28
E-GEOD-5628	Transcription profiling by array of *Arabidopsis* after exposure to heat stress	14	32
E-GEOD-5687	Transcription profiling by array of *Arabidopsis* seeds after incubation at different temperatures	1	4
E-GEOD-5688	Transcription profiling by array of *Arabidopsis* after growth in medium lacking sulphate	5	22
E-GEOD-33790	The response and recovery of *Arabidopsis* thaliana transcriptome to phosphate starvation	8	18
E-GEOD-5627	Transcription profiling by array of *Arabidopsis* after wounding	12	28
TOTAL		249	763

* The measurements include controls and treatments.

Table S2. Genes represented in the network that was built around known interactors of the SOBIR1-containing complex.

Probe ID	Identifier	Gene symbol	Description	BC	CC	Degree
251910_at	At3g53810	AT3G53810	L-type lectin-domain containing receptor kinase IV.2	0.019701014	0.5112219	268
253257_at	At4g34390	XLG2	XLG2 (extra-large GTP-binding protein 2)	0.019750539	0.5094433	260
252053_at	At3g52400	SYP122	SYP122 (SYNTAXIN OF PLANTS 122)	0.014725974	0.4978145	248
267028_at	At2g38470	WRKY33	WRKY33	0.010633755	0.4906654	248
250289_at	At5g13190	AT5G13190	GSH-induced LITAF domain protein	0.010170215	0.4844045	233
249264_s_at	At5g41740	AT5G41740 /// AT5G41750	TIR-NBS-LRR class disease resistance protein	0.005998108	0.4659091	230
258650_at	At3g09830	AT3G09830	protein kinase family protein	0.012312787	0.4927885	229
259312_at	At3g05200	ATL6	ATL6	0.034186771	0.504181	227
260477_at	At1g11050	AT1G11050	protein kinase superfamily protein	0.006076667	0.4763011	216
263379_at	At2g40140	CZF1	CZF1	0.004245946	0.4625451	211
256050_at	At1g07000	ATEXO70B2	ATEXO70B2 (exocyst subunit EXO70 family protein B2)	0.013992772	0.5017132	207
263182_at	At1g05575	AT1G05575	hypothetical protein	0.004009598	0.4531388	204
258787_at	At3g11840	PUB24	PUB24 (PLANT U-BOX 24)	0.016241173	0.5009775	203
264866_at	At1g24140	AT1G24140	putative metalloproteinase	0.006604435	0.4719153	203
259479_at	At1g19020	AT1G19020	hypothetical protein	0.008620855	0.4830349	202
265184_at	At1g23710	AT1G23710	hypothetical protein	0.003000382	0.4378471	199
258436_at	At3g16720	ATL2	ATL2	0.006542026	0.4633816	198
254432_at	At4g20830	AT4G20830	FAD-binding Berberine family protein	0.008414452	0.4867047	195
246777_at	At5g27420	CNI1	E3 ubiquitin-protein ligase ATL31	0.005419058	0.4816729	195
265375_at	At2g06530	VPS2.1	VPS2.1	0.013554027	0.4758589	195
246858_at	At5g25930	AT5G25930	protein kinase family protein with leucine-rich repeat domain	0.011002811	0.4904306	194
248327_at	At5g52750	AT5G52750	heavy metal transport/detoxification domain-containing protein	0.005548782	0.4734411	193
265725_at	At2g32030	AT2G32030	Acyl-CoA N-acyltransferases (NAT) superfamily protein	0.00404421	0.4592294	191

Table S2. *(Continued)*

Probe ID	Identifier	Gene symbol	Description	BC	CC	Degree
253414_at	At4g33050	EDA39	EDA39 (embryo sac development arrest 39)	0.012501975	0.4939759	188
246821_at	At5g26920	CBP60G	CBP60G (CAM-BINDING PROTEIN 60-LIKE.G)	0.006196576	0.4783014	188
252131_at	At3g50930	BCS1	BCS1 (CYTOCHROME BC1 SYNTHESIS)	0.004215485	0.4573851	187
266071_at	At2g18680	AT2G18670 /// AT2G18680	RING-H2 finger protein ATL56 hypothetical protein	0.014113458	0.4850923	185
254231_at	At4g23810	WRKY53	WRKY53	0.004103589	0.4635911	185
252278_at	At3g49530	anac062	anac062 (*Arabidopsis* NAC domain containing protein 62)	0.002427136	0.4339543	183
252470_at	At3g46930	AT3G46930	protein kinase family protein	0.010905656	0.4774103	181
262085_at	At1g56060	AT1G56060	hypothetical protein	0.007050236	0.4712644	181
261445_at	At1g28380	NSL1	NSL1 (necrotic spotted lesions 1)	0.005715843	0.462754	181
251636_at	At3g57530	CPK32	CPK32 (CALCIUM-DEPENDENT PROTEIN KINASE 32)	0.003026353	0.4270833	180
255599_at	At4g01010	ATCNGC13	ATCNGC13	0.012596435	0.4930255	179
251054_at	At5g01540	LECRKA4.1	LECRKA4.1 (LECTIN RECEPTOR KINASE A4.1)	0.010464488	0.4844045	177
258947_at	At3g01830	AT3G01830	putative calcium-binding protein CML40	0.003368404	0.4503515	177
250676_at	At5g06320	NHL3	NHL3	0.003345091	0.4371002	177
256756_at	At3g25610	AT3G25610	ATPase E1-E2 type family protein	0.009399947	0.4901961	174
248611_at	At5g49520	WRKY48	WRKY48	0.00402588	0.4511444	174
258606_at	At3g02840	AT3G02840	hypothetical protein	0.00230815	0.4346904	172
258792_at	At3g04640	AT3G04640	glycine-rich protein	0.001924738	0.4235537	172
251769_at	At3g55950	CCR3	CCR3 (*ARABIDOPSIS* THALIANA CRINKLY4 RELATED 3)	0.012274387	0.476966	170
249928_at	At5g22250	AT5G22250	CCR4-associated factor 1B	0.002426807	0.4454585	170
259792_at	At1g29690	CAD1	CAD1 (constitutively activated cell death 1)	0.005704019	0.4328547	170
266017_at	At2g18690	AT2G18690	hypothetical protein	0.020047885	0.4880952	169
261470_at	At1g28370	ERF11	ERF11 (ERF DOMAIN PROTEIN 11)	0.002188504	0.4292295	169

Table S2. *(Continued)*

Probe ID	Identifier	Gene symbol	Description	BC	CC	Degree
260399_at	At1g72520	AT1G72520	lipoxygenase 4	0.001930921	0.4233788	168
253284_at	At4g34150	AT4G34150	calcium-dependent lipid-binding domain-containing protein	0.001942514	0.4345061	167
261892_at	At1g80840	WRKY40	WRKY40	0.001265543	0.4247824	167
261526_at	At1g14370	APK2A	APK2A (PROTEIN KINASE 2A)	0.007289462	0.4894938	166
254241_at	At4g23190	CRK11	CRK11 (CYSTEINE-RICH RLK11)	0.0103851	0.4659091	166
262165_at	At1g75020	LPAT4	LPAT4 (LYSOPHOSPHATIDYL ACYLTRANSFERASE 4)	0.003143643	0.4418103	166
247137_at	At5g66210	CPK28	CPK28	0.004720937	0.4387842	166
251745_at	At3g55980	SZF1	SZF1 (SALT-INDUCIBLE ZINC FINGER 1)	0.001664783	0.4230293	166
246405_at	At1g57630	AT1G57630	Toll-Interleukin-Resistance domain-containing protein	0.015790615	0.4771881	165
246927_s_at	At5g25260	AT5G25250 /// AT5G25260	Flotillin-like protein 1 SPFH/Band 7	0.010483948	0.464221	165
247426_at	At5g62570	AT5G62570	calmodulin binding protein 60a	0.003931043	0.44604	165
261648_at	At1g27730	STZ	STZ (salt tolerance zinc finger)	0.001960388	0.4352442	165
245119_at	At2g41640	AT2G41640	Glycosyltransferase family 61 protein	0.001849623	0.4246065	165
267293_at	At2g23810	TET8	TET8 (TETRASPANIN8)	0.00287294	0.4399142	161
247708_at	At5g59550	AT5G59550	ABA- and drought-induced RING-DUF1117 protein	0.00133039	0.4202542	161
264008_at	At2g21120	AT2G21120	hypothetical protein	0.001741116	0.432307	158
247493_at	At5g61900	BON1	BON1 (BONZAI 1)	0.004468406	0.4648526	157
255967_at	At1g22280	PAPP2C	phytochrome-associated protein phosphatase type 2C	0.006698211	0.47942	155
250796_at	At5g05300	AT5G05300	hypothetical protein	0.006031171	0.4541427	155
262072_at	At1g59590	ZCF37	ZCF37	0.002500499	0.4527385	155
260401_at	At1g69840	AT1G69840	Hypersensitive-induced response protein 2	0.002290713	0.4523389	155
258682_at	At3g08720	S6K2	S6K2 (*ARABIDOPSIS* THALIANA SERINE/THREONINE PROTEIN KINASE 2)	0.00674546	0.451343	155
252592_at	At3g45640	ATMPK3	MITOGEN-ACTIVATED PROTEIN KINASE 3	0.001938492	0.4448785	155

Table S2. *(Continued)*

Probe ID	Identifier	Gene symbol	Description	BC	CC	Degree
253323_at	At4g33920	AT4G33920	putative protein phosphatase 2C 63	0.001723592	0.4299497	155
261718_at	At1g18390	AT1G18390	probable serine/threonine-protein kinase	0.012411191	0.4714811	153
260239_at	At1g74360	AT1G74360	putative LRR receptor-like serine/threonine-protein kinase	0.010871622	0.4659091	153
245051_at	At2g23320	WRKY15	WRKY15	0.00713064	0.4652746	151
259626_at	At1g42990	ATBZIP60	ATBZIP60 (BASIC REGION/LEUCINE ZIPPER MOTIF 60)	0.0058622	0.4600539	151
255844_at	At2g33580	AT2G33580	LysM-containing receptor-like kinase	0.006144419	0.4339543	151
256526_at	At1g66090	AT1G66090	TIR-NBS class of disease resistance protein	0.001058457	0.4328547	151
251507_at	At3g59080	AT3G59080	aspartyl protease family protein	0.003702258	0.4211175	150
247125_at	At5g66070	AT5G66070	RING/U-box superfamily protein	0.002000373	0.4190515	150
265723_at	At2g32140	AT2G32140	transmembrane receptor protein	0.003192011	0.4380342	149
267623_at	At2g39650	AT2G39650	hypothetical protein	0.000784	0.4086922	149
249987_at	At5g18490	AT5G18490	hypothetical protein	0.016485893	0.4850923	145
262901_at	At1g59910	AT1G59910	formin-like protein 7	0.001418968	0.4235537	145
263783_at	At2g46400	WRKY46	WRKY46	0.001820891	0.4279749	144
258786_at	At3g11820	SYP121	SYP121 (SYNTAXIN OF PLANTS 121)	0.005283914	0.4481854	143
245329_at	At4g14365	XBAT34	putative E3 ubiquitin-protein ligase XBAT34	0.005402842	0.4594352	142
247240_at	At5g64660	CMPG2	U-box domain-containing protein	0.001047596	0.4188803	142
257902_at	At3g28450	AT3G28450	leucine-rich repeat protein kinase-like protein	0.015984945	0.4883278	141
254592_at	At4g18880	HSF A4A	AT-HSFA4A	0.004574956	0.4693223	141
260804_at	At1g78410	AT1G78410	VQ motif-containing protein	0.006630088	0.4625451	141
255753_at	At1g18570	MYB51	MYB51 (MYB DOMAIN PROTEIN 51)	0.004275287	0.4615038	141
252679_at	At3g44260	AT3G44260	putative CCR4-associated factor 1	0.000657	0.3886993	137

Table S2. *(Continued)*

Probe ID	Identifier	Gene symbol	Description	BC	CC	Degree
263478_at	At2g31880	SOBIR1	leucine-rich repeat receptor-like serine/threonine/tyrosine-protein kinase SOBIR1	0.013735915	0.4631722	136
261719_at	At1g18380	AT1G18390	probable serine/threonine-protein kinase	0.009017687	0.4501537	136
249197_at	At5g42380	CML37	CML37 (CALMODULIN LIKE 37)	0.001346275	0.4131399	136
266658_at	At2g25735	AT2G25735	hypothetical protein	0.002704149	0.4235537	135
263800_at	At2g24600	AT2G24600	Ankyrin repeat family protein	0.00340704	0.4168361	133
258915_at	At3g10640	VPS60.1	VPS60.1	0.008581172	0.4730042	132
264107_s_at	At2g13790	SERK5	SERK5 (SOMATIC EMBRYOGENESIS RECEPTOR-LIKE KINASE 5)	0.007362967	0.4571811	132
256442_at	At3g10930	AT3G10930	hypothetical protein	0.000714	0.4033845	131
254926_at	At4g11280	ACS6	ACS6 (1-AMINOCYCLOPROPANE-1-CARBOXYLIC ACID (ACC) SYNTHASE 6)	0.000428	0.4057799	130
264660_at	At1g09940	HEMA2	HEMA2	0.003093096	0.4207718	129
253643_at	At4g29780	AT4G29780	hypothetical protein	0.000432	0.3889943	129
259550_at	At1g35230	AGP5	AGP5 (ARABINOGALACTAN-PROTEIN 5)	0.010730368	0.4596413	128
246943_at	At5g25440	AT5G25440	protein kinase family protein	0.004215814	0.4547471	128
245041_at	At2g26530	AR781	AR781	0.000585	0.4096723	128
252474_at	At3g46620	AT3G46620	E3 ligase RDUF1	0.000638	0.4048183	128
266800_at	At2g22880	AT2G22880	VQ motif-containing protein	0.001455738	0.432672	127
247571_at	At5g61210	SNAP33	SNAP33 (SOLUBLE N-ETHYLMALEIMIDE-SENSITIVE FACTOR ADAPTOR PROTEIN 33)	0.018027205	0.4723502	126
263565_at	At2g15390	FUT4	FUT4	0.007976778	0.466121	126
247655_at	At5g59820	RHL41	RHL41 (RESPONSIVE TO HIGH LIGHT 41)	0.000723	0.415316	126
245250_at	At4g17490	ATERF6	ATERF6 (ETHYLENE RESPONSIVE ELEMENT BINDING FACTOR 6)	0.00064	0.4073927	126
260296_at	At1g63750	AT1G63750	TIR-NBS-LRR class disease resistance protein	0.000808	0.4149798	125

Table S2. *(Continued)*

Probe ID	Identifier	Gene symbol	Description	BC	CC	Degree
251479_at	At3g59700	ATHLECRK	ATHLECRK (*ARABIDOPSIS* THALIANA LECTIN-RECEPTOR KINASE)	0.007247672	0.4397254	124
246988_at	At5g67340	AT5G67340	ARM repeat superfamily protein	0.008023532	0.4638009	123
254063_at	At4g25390	AT4G25390	receptor-like serine/threonine-protein kinase	0.009609456	0.4646419	122
254408_at	At4g21390	B120	B120	0.006996843	0.4485777	122
245247_at	At4g17230	SCL13	SCL13 (Scarecrow-like 13)	0.003756173	0.4233788	122
261650_at	At1g27770	ACA1	ACA1 (AUTO-INHIBITED CA2+-ATPASE 1)	0.002208023	0.4108216	122
261378_at	At1g18890	ATCDPK1	ATCDPK1 (CALCIUM-DEPENDENT PROTEIN KINASE 1)	0.009198004	0.4606742	121
246631_at	At1g50740	AT1G50740	transmembrane protein 14C	0.001209685	0.4294093	121
256755_at	At3g25600	AT3G25600	putative calcium-binding protein CML16	0.000527	0.4057799	121
246327_at	At1g16670	AT1G16670	putative serine/threonine kinase	0.00300615	0.464221	119
256633_at	At3g28340	GATL10	GATL10 (Galacturonosyltransferase-like 10)	0.000478	0.4019608	119
267069_at	At2g41010	ATCAMBP25	ATCAMBP25 (*ARABIDOPSIS* THALIANA CALMODULIN (CAM)-BINDING PROTEIN OF 25 KDA)	0.000303	0.3910721	119
254120_at	At4g24570	DIC2	mitochondrial substrate carrier family protein	0.000258	0.3807578	119
254869_at	At4g11890	AT4G11890	receptor-like cytosolic kinase ARCK1	0.00928234	0.4555556	118
265737_at	At2g01180	ATPAP1	ATPAP1 (PHOSPHATIDIC ACID PHOSPHATASE 1)	0.000634	0.4041798	118
264746_at	At1g62300	WRKY6	WRKY6	0.007940652	0.4594352	117
251884_at	At3g54150	AT3G54150	S-adenosyl-L-methionine-dependent methyltransferase-like protein	0.00286638	0.4472077	117
265841_at	At2g35710	AT2G35710	putative glucuronosyltransferase PGSIP8	0.000316	0.3870846	115
265670_s_at	At2g32210	AT2G32190 /// AT2G32210	hypothetical protein hypothetical protein	0.000961	0.440103	114
248981_at	At5g45110	NPR3	NPR3 (NPR1-LIKE PROTEIN 3)	0.000945	0.4151478	113
249237_at	At5g42050	AT5G42050	DCD (Development and Cell Death) domain protein	0.020477398	0.4640109	112
250829_at	At5g04720	ADR1-L2	ADR1-L2 (ADR1-like 2)	0.004747356	0.4468178	112

Table S2. *(Continued)*

Probe ID	Identifier	Gene symbol	Description	BC	CC	Degree
259826_at	At1g29340	PUB17	PUB17 (PLANT U-BOX 17)	0.001869815	0.4218107	112
258463_at	At3g17410	AT3G17410	putative serine/threonine protein kinase	0.012845879	0.4631722	111
259213_at	At3g09010	AT3G09010	protein kinase	0.007400201	0.4505495	111
252009_at	At3g52800	AT3G52800	zinc finger A20 and AN1 domain-containing stress-associated protein 6	0.002845924	0.4083665	111
261394_at	At1g79680	WAKL10	wall-associated receptor kinase-like 10	0.002891662	0.4372867	110
257022_at	At3g19580	AZF2	AZF2 (*ARABIDOPSIS* ZINC-FINGER PROTEIN 2)	0.003131699	0.4156529	109
246870_at	At5g26030	FC1	FC1 (ferrochelatase 1)	0.000722	0.4233788	108
261443_at	At1g28480	GRX480	GRX480	0.000846	0.4141414	108
251640_at	At3g57450	AT3G57450	hypothetical protein	0.00022	0.3769768	108
253273_at	At4g34180	AT4G34180	cyclase family protein	0.027358281	0.4533392	107
250335_at	At5g11650	AT5G11650	alpha/beta fold hydrolase family protein	0.000837	0.4267277	107
251336_at	At3g61190	BAP1	BAP1 (BON ASSOCIATION PROTEIN 1)	0.00021	0.3847598	107
254158_at	At4g24380	AT4G24380	hypothetical protein	0.000374	0.3836078	107
265597_at	At2g20145	AT2G20142	Toll-Interleukin-Resistance domain-containing protein	0.00230915	0.4399142	106
262228_at	At1g68690	AT1G68690	proline-rich receptor-like protein kinase PERK9	0.003260978	0.4391602	106
265674_at	At2g32190	AT2G32190	hypothetical protein	0.000861	0.432307	106
245840_at	At1g58420	AT1G58420	hypothetical protein	0.000705	0.4214638	106
256616_at	At3g22260	AT3G22260	OTU-like cysteine protease family protein	0.015333056	0.454949	105
247848_at	At5g58120	AT5G58120	TIR-NBS-LRR class disease resistance protein	0.003563422	0.4205991	105
245252_at	At4g17500	ATERF-1	ATERF-1 (ETHYLENE RESPONSIVE ELEMENT BINDING FACTOR 1)	0.000594	0.4141414	105
249903_at	At5g22690	AT5G22690	TIR-NBS-LRR class disease resistance protein	0.002687545	0.4113162	105
259979_at	At1g76600	AT1G76600	hypothetical protein	0.000321	0.3991433	105
251684_at	At3g56410	AT3G56410	hypothetical protein	0.001845843	0.4495614	104

Table S2. *(Continued)*

Probe ID	Identifier	Gene symbol	Description	BC	CC	Degree
246532_at	At5g15870	AT5G15870	glycosyl hydrolase family 81 protein	0.002625495	0.4431474	104
258282_at	At3g26910	AT3G26910	hydroxyproline-rich glycoprotein family protein	0.004948267	0.4399142	104
255095_at	At4g08500	MEKK1	MEKK1 (MAP KINASE KINASE KINASE 1)	0.005212503	0.4247824	104
263584_at	At2g17040	anac036	anac036 (*Arabidopsis* NAC domain containing protein 36)	0.003818668	0.4285117	103
266685_at	At2g19710	AT2G19710	Vps4 regulator of MVB pathway	0.001141715	0.420082	103
251259_at	At3g62260	AT3G62260	putative protein phosphatase 2C 49	0.001696869	0.4119775	103
250098_at	At5g17350	AT5G17350	hypothetical protein	0.000194	0.3789279	102
249417_at	At5g39670	AT5G39670	putative calcium-binding protein CML45	0.00327066	0.4391602	101
267357_at	At2g40000	HSPRO2	HSPRO2 (*ARABIDOPSIS* ORTHOLOG OF SUGAR BEET HS1 PRO-1 2)	0.003952731	0.3979037	101
253915_at	At4g27280	AT4G27280	EF-hand, calcium binding motif-containing protein	0.000267	0.3764231	101
252862_at	At4g39830	AT4G39830	putative L-ascorbate oxidase	0.00326292	0.4359847	100
254204_at	At4g24160	AT4G24160	lysophosphatidic acid acyltransferase	0.000451	0.4225062	100
252346_at	At3g48650	---	---	0.000877	0.4207718	100
261193_at	At1g32920	AT1G32920	hypothetical protein	0.00034	0.3882576	100
266316_at	At2g27080	AT2G27080	late embryogenesis abundant hydroxyproline-rich glycoprotein	0.000329	0.3715114	100
256793_at	At3g22160	AT3G22160	VQ motif-containing protein	0.001789285	0.4474029	99
251901_at	At3g54100	AT3G54100	O-fucosyltransferase family protein	0.002564696	0.4350594	99
265461_at	At2g46500	PI4K GAMMA 4	phosphoinositide 4-kinase gamma 4	0.002370354	0.4332206	99
255733_at	At1g25400	AT1G25400	hypothetical protein	0.002306775	0.3957529	99
248448_at	At5g51190	AT5G51190	ethylene-responsive transcription factor ERF105	0.000191	0.3768382	99
248164_at	At5g54490	PBP1	PBP1 (PINOID-BINDING PROTEIN 1)	0.000146	0.3934741	98
261973_at	At1g64610	AT1G64610	WD40 domain-containing protein	0.003394232	0.4397254	97
261005_at	At1g26420	AT1G26420	FAD-binding and BBE domain-containing protein	0.003971847	0.4306723	97

Table S2. *(Continued)*

Probe ID	Identifier	Gene symbol	Description	BC	CC	Degree
245755_at	At1g35210	AT1G35210	hypothetical protein	0.000974	0.4098361	96
256522_at	At1g66160	CMPG1	U-box domain-containing protein	0.000215	0.379911	96
257407_at	At1g27100	AT1G27100	Actin cross-linking protein	0.00036	0.375183	96
250990_at	At5g02290	NAK	NAK	0.002490944	0.4485777	95
261506_at	At1g71697	ATCK1	ATCK1 (CHOLINE KINASE 1)	0.00207934	0.4431474	95
255884_at	At1g20310	AT1G20310	hypothetical protein	0.000793	0.4008604	95
249339_at	At5g41100	AT5G41100	hypothetical protein	0.00213126	0.4007037	95
256922_at	At3g19010	AT3G19010	2-oxoglutarate (2OG) and Fe(II)-dependent oxygenase superfamily protein	0.0036588	0.4617117	94
250809_at	At5g05140	AT5G05140	transcription elongation factor (TFIIS) family protein	0.002616786	0.4274395	94
246270_at	At4g36500	AT4G36500	hypothetical protein	0.001781424	0.4207718	94
249485_at	At5g39020	AT5G39020	putative receptor-like protein kinase	0.001532248	0.4348748	93
249770_at	At5g24110	WRKY30	WRKY30	0.003225806	0.4178557	93
248799_at	At5g47230	ERF5	ERF5 (ETHYLENE RESPONSIVE ELEMENT BINDING FACTOR 5)	0.00024	0.3881106	93
259428_at	At1g01560	ATMPK11	ATMPK11	0.001724372	0.4376601	92
257751_at	At3g18690	MKS1	MKS1 (MAP kinase substrate 1)	0.001594498	0.4046585	92
264232_at	At1g67470	AT1G67470	inactive serine/threonine-protein kinase	0.000558	0.4033845	92
249746_at	At5g24590	TIP	TIP (TCV-INTERACTING PROTEIN)	0.000218	0.3753204	92
259410_at	At1g13340	AT1G13340	Regulator of Vps4 activity in the MVB pathway protein	0.004439283	0.4594352	90
267246_at	At2g30250	WRKY25	WRKY25	0.002309213	0.4511444	90
253147_at	At4g35600	CONNEXIN 32	CONNEXIN 32	0.002514066	0.4450716	90
245731_at	At1g73500	MKK9	MKK9 (MAP KINASE KINASE 9)	0.000705	0.4061014	90
249983_at	At5g18470	AT5G18470	curculin-like (mannose-binding) lectin family protein	0.005823325	0.4606742	89
261748_at	At1g76070	AT1G76070	hypothetical protein	0.003354069	0.4313973	89

Table S2. *(Continued)*

Probe ID	Identifier	Gene symbol	Description	BC	CC	Degree
254784_at	At4g12720	NUDT7	NUDT7	0.001382611	0.415316	89
260243_at	At1g63720	AT1G63720	hypothetical protein	0.003890357	0.4363559	88
254660_at	At4g18250	AT4G18250	putative receptor serine/threonine kinase	0.001863048	0.420082	88
264757_at	At1g61360	AT1G61360	G-type lectin S-receptor-like serine/threonine-protein kinase	0.001523622	0.4180261	88
267134_at	At2g23450	AT2G23450	wall-associated receptor kinase-like 14	0.012958596	0.4425734	87
262381_at	At1g72900	AT1G72900	Toll-Interleukin-Resistance domain-containing protein	0.00236257	0.4384089	87
250821_at	At5g05190	AT5G05190	hypothetical protein	0.001118861	0.4192229	87
248322_at	At5g52760	AT5G52760	copper transport family protein	0.001718686	0.4328547	86
260046_at	At1g73800	AT1G73805	protein SAR Deficient 1	0.003372193	0.4256645	86
248123_at	At5g54720	AT5G54720	ankyrin repeat-containing protein	0.000844	0.4131399	86
248487_at	At5g51070	ERD1	ERD1 (EARLY RESPONSIVE TO DEHYDRATION 1)	0.011468222	0.3946862	86
266834_s_at	At2g30020	AT2G30020 /// AT3G27140 /// AT4G08260	putative protein phosphatase 2C	0.000154	0.3793486	86
256735_at	At3g29400	ATEXO70E1	ATEXO70E1 (exocyst subunit EXO70 family protein E1)	0.002282011	0.4431474	85
252908_at	At4g39670	AT4G39670	glycolipid transfer protein	0.001898329	0.434322	85
254103_at	At4g25030	AT4G25030	hypothetical protein	0.00369076	0.4317607	85
261021_at	At1g26380	AT1G26380	FAD-binding and BBE domain-containing protein	0.001777721	0.4272614	85
254847_at	At4g11850	PLDGAMMA1	PLDGAMMA1	0.009218614	0.424255	85
259887_at	At1g76360	AT1G76360	putative protein kinase	0.00170539	0.4239041	85
257919_at	At3g23250	MYB15	MYB15 (MYB DOMAIN PROTEIN 15)	0.001230122	0.399922	85
264655_at	At1g09070	SRC2	SRC2 (SOYBEAN GENE REGULATED BY COLD-2)	0.000208	0.3846154	85
260656_at	At1g19380	AT1G19380	hypothetical protein	0.000417	0.3831776	85
262382_at	At1g72920	AT1G72920	Toll-Interleukin-Resistance domain-containing protein	0.000146	0.3778105	85

Table S2. *(Continued)*

Probe ID	Identifier	Gene symbol	Description	BC	CC	Degree
249550_at	At5g38210	AT5G38210	protein kinase family protein	0.001673559	0.4444926	84
252977_at	At4g38560	AT4G38560	phospholipase like protein (PEARLI 4)	0.00353528	0.4412398	84
263704_at	At1g31130	AT1G31130	hypothetical protein	0.000837	0.4310345	84
256763_at	At3g16860	COBL8	COBL8 (COBRA-LIKE PROTEIN 8 PRECURSOR)	0.000154	0.3816083	84
253485_at	At4g31800	WRKY18	WRKY18	0.000576	0.3979037	83
247543_at	At5g61600	ERF104	ethylene-responsive transcription factor ERF104	7.89E-05	0.3700361	83
258665_at	At3g08710	ATH9	ATH9 (thioredoxin H-type 9)	0.001415074	0.4335871	82
252483_at	At3g46600	AT3G46600	scarecrow-like protein 30	0.000348	0.3985226	82
253992_at	At4g26060	AT4G26060	ribosomal protein L18ae family protein	0.011241527	0.3962118	82
254694_at	At4g17900	AT4G17900	PLATZ transcription factor family protein	0.008647337	0.4328547	80
265853_at	At2g42360	AT2G42360	E3 ubiquitin-protein ligase ATL41	0.007957876	0.4267277	80
254605_at	At4g18950	AT4G18950	Integrin-linked protein kinase family protein	0.002067543	0.4176854	80
266452_at	At2g43320	AT2G43320	S-adenosyl-L-methionine-dependent methyltransferase-like protein	0.001901111	0.4148118	80
247811_at	At5g58430	ATEXO70B1	ATEXO70B1 (exocyst subunit EXO70 family protein B1)	0.000643	0.4025923	80
252906_at	At4g39640	GGT1	GGT1 (GAMMA-GLUTAMYL TRANSPEPTIDASE 1)	0.000328	0.4119775	79
247707_at	At5g59450	AT5G59450	GRAS family transcription factor	0.000282	0.4051383	79
257700_at	At3g12740	ALIS1	ALIS1 (ALA-INTERACTING SUBUNIT 1)	0.008739654	0.4435309	78
256958_at	At3g13430	AT3G13430	RING/U-box superfamily protein	0.005055103	0.4258413	78
257950_at	At3g21780	UGT71B6	UGT71B6 (UDP-glucosyl transferase 71B6)	0.003881525	0.4372867	77
265075_at	At1g55450	AT1G55450	S-adenosyl-L-methionine-dependent methyltransferases superfamily protein	0.004319436	0.4239041	77
256238_at	At3g12400	ELC	ELC	0.004245567	0.4161592	77
261143_at	At1g19770	ATPUP14	ATPUP14	0.000223	0.3876702	77

Table S2. *(Continued)*

Probe ID	Identifier	Gene symbol	Description	BC	CC	Degree
254255_at	At4g23220	CRK14	cysteine-rich receptor-like protein kinase 14	0.001649808	0.4385965	76
259211_at	At3g09020	AT3G09020	alpha 1,4-glycosyltransferase family protein	0.00100436	0.4371002	76
248821_at	At5g47070	AT5G47070	protein kinase family protein	0.000365	0.4193944	76
266835_at	At2g29990	NDA2	NDA2 (ALTERNATIVE NAD(P)H DEHYDROGENASE 2)	0.009950701	0.4104926	76
246368_at	At1g51890	AT1G51890	probable LRR receptor-like protein kinase	0.004993521	0.4082039	76
253124_at	At4g36030	ARO3	ARO3 (ARMADILLO REPEAT ONLY 3)	0.000118	0.3956002	76
245251_at	At4g17615	CBL1	CBL1 (CALCINEURIN B-LIKE PROTEIN 1)	0.000174	0.3921194	76
264951_at	At1g76970	AT1G76970	Target of Myb protein 1	0.005260941	0.4404813	75
253664_at	At4g30210	ATR2	ATR2 (*ARABIDOPSIS* P450 REDUCTASE 2)	0.000272	0.4297694	73
255116_at	At4g08850	AT4G08850	probable LRR receptor-like serine/threonine-protein kinase	0.007545829	0.4279749	73
246370_at	At1g51920	AT1G51920	hypothetical protein	0.001437729	0.4052985	73
266037_at	At2g05940	AT2G05940	RPM1-induced protein kinase	0.000256	0.3778105	73
259518_at	At1g20510	OPCL1	OPCL1 (OPC-8:0 COA LIGASE1)	0.000174	0.3689705	73
248934_at	At5g46080	AT5G46080	protein kinase family protein	0.004993628	0.4308533	72
267288_at	At2g23680	AT2G23680	Cold acclimation protein WCOR413 family	0.003891174	0.4272614	72
258207_at	At3g14050	RSH2	RSH2 (RELA-SPOT HOMOLOG 2)	0.008834195	0.4221582	71
265620_at	At2g27310	AT2G27310	F-box protein	0.001039575	0.4151478	71
257061_at	At3g18250	AT3G18250	putative membrane lipoprotein	0.001767973	0.4178557	70
262571_at	At1g15430	AT1G15430	hypothetical protein	0.000622	0.4061014	70
248775_at	At5g47850	CCR4	CCR4 (*ARABIDOPSIS* THALIANA CRINKLY4 RELATED 4)	0.003295975	0.4029088	69
260772_at	At1g49050	AT1G49050	aspartyl protease	0.003721076	0.4295893	68
260648_at	At1g08050	AT1G08050	C3HC4-type RING finger-containing protein	0.008512078	0.4292295	68
267436_at	At2g19190	FRK1	FRK1 (FLG22-INDUCED RECEPTOR-LIKE KINASE 1)	0.003182042	0.390923	68

Table S2. *(Continued)*

Probe ID	Identifier	Gene symbol	Description	BC	CC	Degree
252533_at	At3g46110	AT3G46110	hypothetical protein	0.00023	0.420082	67
254229_at	At4g23610	AT4G23610	late embryogenesis abundant hydroxyproline-rich glycoprotein	0.003154789	0.4185382	67
260068_at	At1g73805	AT1G73805	protein SAR Deficient 1	0.00202202	0.4085293	67
256046_at	At1g07135	AT1G07135	glycine-rich protein	0.00116979	0.4339543	66
256366_at	At1g66880	AT1G66880	serine/threonine protein kinase	0.001542083	0.4240794	66
263076_at	At2g17520	IRE1A	IRE1A	0.010446711	0.4124748	66
248964_at	At5g45340	CYP707A3	CYP707A3	6.81E-05	0.3560264	66
262481_at	At1g17080	AT1G17080	ribosomal protein L18ae family protein	0.004622032	0.3557792	66
261405_at	At1g18740	AT1G18740	hypothetical protein	7.94E-05	0.3517502	66
245197_at	At1g67800	AT1G67800	Copine (Calcium-dependent phospholipid-binding protein) family protein	0.001847873	0.4199099	65
258203_at	At3g13950	AT3G13950	hypothetical protein	0.004209127	0.406746	65
266010_at	At2g37430	AT2G37430	zinc finger protein ZAT11	0.001316082	0.3925699	65
246600_at	At5g14930	SAG101	SAG101 (SENESCENCE-ASSOCIATED GENE 101)	0.002644098	0.4258413	64
247740_at	At5g58940	CRCK1	CRCK1 (CALMODULIN-BINDING RECEPTOR-LIKE CYTOPLASMIC KINASE 1)	0.003200917	0.4204266	64
250858_at	At5g04760	AT5G04760	duplicated SANT DNA-binding domain-containing protein	0.001878064	0.407879	64
259879_at	At1g76650	CML38	calcium-binding EF hand family protein	6.64E-05	0.3566458	64
260227_at	At1g74450	AT1G74450	hypothetical protein	3.99E-05	0.3504274	64
259841_at	At1g52200	AT1G52200	PLAC8 family protein	0.00675651	0.4141414	63
252825_at	At4g39890	AtRABH1c	AtRABH1c (*Arabidopsis* Rab GTPase homolog H1c)	0.002108384	0.4114813	63
256017_at	At1g19180	JAZ1	JAZ1 (JASMONATE-ZIM-DOMAIN PROTEIN 1)	0.000216	0.3775322	63
264772_at	At1g22930	AT1G22930	T-complex protein 11	0.002864892	0.3734062	63
253628_at	At4g30280	XTH18	XTH18 (XYLOGLUCAN ENDOTRANSGLUCOSYLASE/HYDROLASE 18)	0.000116	0.3636041	63

Table S2. *(Continued)*

Probe ID	Identifier	Gene symbol	Description	BC	CC	Degree
253377_at	At4g33300	ADR1-L1	ADR1-L1 (ADR1-like 1)	0.004111113	0.423204	62
258855_at	At3g02070	AT3G02070	cysteine proteinase-like protein	0.000879	0.406746	62
263948_at	At2g35980	YLS9	YLS9 (YELLOW-LEAF-SPECIFIC GENE 9)	0.000983	0.4049783	62
245613_at	At4g14450	ATBET12	ATBET12	0.00141956	0.3940792	62
266101_at	At2g37940	AtIPCS2	inositol phosphorylceramide synthase 2	0.001233782	0.4308533	61
250818_at	At5g04930	ALA1	ALA1 (aminophospholipid ATPase1)	0.004084014	0.4230293	61
264867_at	At1g24150	FH4	FH4 (FORMIN HOMOLOGUE 4)	0.001758216	0.4219844	61
247145_at	At5g65600	AT5G65600	concanavalin A-like lectin kinase-like protein	0.001961967	0.3924196	61
260206_at	At1g70740	AT1G70740	protein kinase family protein	0.000164	0.3765614	61
264851_at	At2g17290	CPK6	CPK6 (CALCIUM-DEPENDENT PROTEIN KINASE 6)	0.007188774	0.4357993	60
247554_at	At5g61010	ATEXO70E2	ATEXO70E2 (EXOCYST SUBUNIT EXO70 FAMILY PROTEIN E2)	0.011577827	0.4303107	59
266231_at	At2g02220	PSKR1	PSKR1 (PHYTOSULFOKIN RECEPTOR 1)	0.008363992	0.4303107	59
245662_at	At1g28190	AT1G28190	hypothetical protein	0.000616	0.4141414	59
262772_at	At1g13210	ACA.I	ACA.I (autoinhibited Ca2+/ATPase II)	0.000295	0.4133065	59
251176_at	At3g63380	AT3G63380	putative calcium-transporting ATPase 12	0.000822	0.3980583	59
255340_at	At4g04490	CRK36	cysteine-rich receptor-like protein kinase 36	0.002292097	0.3962118	59
253632_at	At4g30430	TET9	TET9 (TETRASPANIN9)	0.000182	0.3667263	59
266181_at	At2g02390	ATGSTZ1	ATGSTZ1 (*ARABIDOPSIS* THALIANA GLUTATHIONE S-TRANSFERASE ZETA 1)	0.002119609	0.3582663	59
263804_at	At2g40270	AT2G40270	Protein kinase family protein	0.000581	0.3988327	58
264434_at	At1g10340	AT1G10340	ankyrin repeat-containing protein	0.000949	0.4123089	57
259272_at	At3g01290	AT3G01290	SPFH/Band 7/PHB domain-containing membrane-associated protein	0.005366535	0.4113162	57
267300_at	At2g30140	AT2G30140	UDP-glycosyltransferase 87A2	0.004005666	0.4025923	57

Table S2. *(Continued)*

Probe ID	Identifier	Gene symbol	Description	BC	CC	Degree
245711_at	At5g04340	ZAT6	ZAT6 (ZINC FINGER OF *ARABIDOPSIS* THALIANA 6)	0.000769	0.4010172	57
246453_at	At5g16830	SYP21	SYP21 (SYNTAXIN OF PLANTS 21)	0.000428	0.3957529	57
260411_at	At1g69890	AT1G69890	hypothetical protein	0.000511	0.3934741	57
256093_at	At1g20823	AT1G20823	RING-H2 finger protein ATL80	0.000324	0.3599017	57
245777_at	At1g73540	atnudt21	atnudt21 (*Arabidopsis* thaliana Nudix hydrolase homolog 21)	2.09E-05	0.3480475	57
253046_at	At4g37370	CYP81D8	CYP81D8	0.001863206	0.4170057	56
259876_at	At1g76700	AT1G76700	chaperone protein dnaJ 10	0.004488543	0.4156529	56
245599_at	At4g14220	RHF1A	RHF1A (RING-H2 GROUP F1A)	0.001075647	0.4040205	56
249918_at	At5g19240	AT5G19240	GPI-anchored glycoprotein membrane precursor	0.000154	0.3925699	56
246406_at	At1g57650	AT1G57650	ATP binding protein	0.000748	0.3894377	56
253735_at	At4g29160	SNF7.1	SNF7.1	0.002645256	0.3605346	56
263472_at	At2g31950	CNX2	CNX2 (COFACTOR OF NITRATE REDUCTASE AND XANTHINE DEHYDROGENASE 2)	0.004885409	0.4003906	55
257478_at	At1g16130	WAKL2	WAKL2 (wall associated kinase-like 2)	0.000204	0.3907739	55
260744_at	At1g15010	AT1G15010	hypothetical protein	4.47E-05	0.3588936	55
253832_at	At4g27654	AT4G27654	hypothetical protein	1.75E-05	0.3420087	55
254106_at	At4g24990	ATGP4	ATGP4	0.003226543	0.3360656	55
248698_at	At5g48380	BIR1	BAK1-interacting receptor-like kinase BIR1	0.003124116	0.4285117	54
248983_at	At5g45130	RHA1	RHA1 (RAB HOMOLOG 1)	0.004539302	0.3992988	54
248259_at	At5g53330	AT5G53330	ubiquitin-associated/translation elongation factor EF1B protein	0.001724482	0.3576413	54
264178_at	At1g02170	AMC1	AMC1 (METACASPASE 1)	0.001332711	0.4319427	53
253827_at	At4g28085	AT4G28085	hypothetical protein	0.000613	0.4185382	53
253324_at	At4g33940	AT4G33940	RING/U-box domain-containing protein	0.00322997	0.4075547	53

Table S2. *(Continued)*

Probe ID	Identifier	Gene symbol	Description	BC	CC	Degree
256583_at	At3g28850	AT3G28850	Glutaredoxin-like protein	0.001966274	0.4033845	53
252993_at	At4g38540	AT4G38540	FAD/NAD(P)-binding oxidoreductase family protein	0.003082688	0.4002343	53
254256_at	At4g23180	CRK10	CRK10 (CYSTEINE-RICH RLK10)	0.001075496	0.3948382	53
246108_at	At5g28630	AT5G28630	glycine-rich protein	4.09E-05	0.3639915	53
255502_at	At4g02410	AT4G02410	L-type lectin-domain containing receptor kinase IV.3	0.001016132	0.4218107	52
253796_at	At4g28460	AT4G28460	hypothetical protein	0.000948	0.3916699	52
267083_at	At2g41100	TCH3	TCH3 (TOUCH 3)	0.000975	0.3907739	52
262082_s_at	At1g56120	AT1G56120 /// AT1G56130 /// AT1G56140	Leucine-rich repeat transmembrane protein kinase putative LRR receptor-like serine	0.000463	0.4070691	51
246099_at	At5g20230	ATBCB	ATBCB (*ARABIDOPSIS* BLUE-COPPER-BINDING PROTEIN)	7.28E-05	0.4051383	51
247071_at	At5g66640	DAR3	DAR3 (DA1-RELATED PROTEIN 3)	0.000614	0.3931722	51
257644_at	At3g25780	AOC3	AOC3 (ALLENE OXIDE CYCLASE 3)	0.000122	0.3841829	51
256044_at	At1g07160	AT1G07160	putative protein phosphatase 2C 2	0.003531491	0.3761468	51
266615_s_at	At2g29720	CTF2A	CTF2A	0.000415	0.423204	50
252170_at	At3g50480	HR4	HR4 (HOMOLOG OF RPW8 4)	0.001508601	0.4164974	50
264223_s_at	At1g67520	CES101	CES101 (CALLUS EXPRESSION OF RBCS 101)	0.003269764	0.4144763	50
247819_at	At5g58350	WNK4	WNK4 (WITH NO K (=LYSINE) 4)	0.002841661	0.4073927	50
262930_at	At1g65690	AT1G65690	late embryogenesis abundant (LEA) hydroxyproline-rich glycoprotein	0.002146508	0.3996101	50
263222_at	At1g30640	AT1G30640	protein kinase family protein	0.003521653	0.3927203	50
264580_at	At1g05340	AT1G05340	hypothetical protein	0.00353019	0.3913708	50
246495_at	At5g16200	AT5G16200	50S ribosomal protein related protein	9.46E-05	0.3853383	50
261474_at	At1g14540	AT1G14540	peroxidase 4	0.00057	0.3782288	50
253830_at	At4g27652	AT4G27652	hypothetical protein	2.36E-05	0.3452341	50

Table S2. *(Continued)*

Probe ID	Identifier	Gene symbol	Description	BC	CC	Degree
250301_at	At5g11970	AT5G11970	hypothetical protein	0.004288812	0.4292295	49
265385_at	At2g20900	DGK5	diacylglycerol kinase 5	0.000583	0.4133065	49
252345_at	At3g48640	AT3G48640	hypothetical protein	0.002870189	0.4121431	49
264645_at	At1g08940	AT1G08940	phosphoglycerate mutase-like protein	0.002108771	0.4059406	49
259546_at	At1g35350	AT1G35350	phosphate transporter PHO1-8	0.006800476	0.4057799	49
248794_at	At5g47220	ERF2	ERF2 (ETHYLENE RESPONSIVE ELEMENT BINDING FACTOR 2)	5.57E-05	0.3901789	49
254707_at	At4g18010	AT5PTASE2	AT5PTASE2 (MYO-INOSITOL POLYPHOSPHATE 5-PHOSPHATASE 2)	0.000369	0.4123089	48
249835_s_at	At5g23510	AT5G23490 /// AT5G23510	hypothetical protein hypothetical protein	0.000577	0.406746	48
253747_at	At4g29050	AT4G29050	Concanavalin A-like lectin protein kinase family protein	0.000518	0.4037022	48
261155_at	At1g04960	AT1G04960	hypothetical protein	0.004186114	0.4011742	48
266247_at	At2g27660	AT2G27660	cysteine/histidine-rich C1 domain-containing protein	0.002919684	0.3939277	48
260798_at	At1g78280	AT1G78280	F-box protein	0.000165	0.3780893	48
251097_at	At5g01560	LECRKA4.3	LECRKA4.3 (LECTIN RECEPTOR KINASE A4.3)	0.001016594	0.3685725	48
249188_at	At5g42830	AT5G42830	HXXXD-type acyl-transferase-like protein	0.000637	0.4065847	47
260405_at	At1g69930	ATGSTU11	ATGSTU11 (GLUTATHIONE S-TRANSFERASE TAU 11)	0.000618	0.3913708	47
260310_at	At1g70590	AT1G70590	F-box protein	0.000812	0.3863551	47
252068_at	At3g51440	AT3G51440	strictosidine synthase family protein	0.002290605	0.361552	47
262384_at	At1g72950	AT1G72950	TIR-NBS class of disease resistance protein	0.000481	0.3578911	47
262832_s_at	At1g14870	PCR1 /// PCR2	cadmium resistance protein 1 cadmium resistance protein 2	0.00288478	0.4161592	46
252976_s_at	At4g38550	AT4G38550	phospholipase like protein (PEARLI 4) family	0.002727512	0.4133065	46
252060_at	At3g52430	PAD4	PAD4 (PHYTOALEXIN DEFICIENT 4)	0.001165338	0.4044988	46
254857_at	At4g12120	SEC1B	SEC1B	0.000648	0.3965184	46
252940_at	At4g39270	AT4G39270	leucine-rich repeat protein kinase-like protein	0.002174074	0.3894377	46

Table S2. *(Continued)*

Probe ID	Identifier	Gene symbol	Description	BC	CC	Degree
258201_at	At3g13910	AT3G13910	hypothetical protein	0.002720426	0.3696358	46
263457_at	At2g22300	SR1	SR1 (SIGNAL RESPONSIVE 1)	0.001932591	0.4064235	45
257623_at	At3g26210	CYP71B23	CYP71B23	0.002974943	0.3986776	45
256177_at	At1g51620	AT1G51620	protein kinase superfamily protein	0.00176364	0.3804751	45
245866_s_at	At1g57990	ATPUP18	ATPUP18	0.00014	0.3660714	45
254500_at	At4g20110	VSR7	vacuolar-sorting receptor 7	0.004039343	0.3645092	45
266993_at	At2g39210	AT2G39210	major facilitator protein	0.003251479	0.4214638	44
246529_at	At5g15730	AT5G15730	probable leucine-rich repeat receptor-like serine/threonine-protein kinase	0.007561376	0.3979037	44
266782_at	At2g29120	ATGLR2.7	ATGLR2.7	0.002511693	0.3966718	44
248904_at	At5g46295	AT5G46295	hypothetical protein	0.000513	0.3916699	44
260225_at	At1g74590	GSTU10	GSTU10 (GLUTATHIONE S-TRANSFERASE TAU 10)	0.001069014	0.3863551	44
257053_at	At3g15210	ERF4	ERF4 (ETHYLENE RESPONSIVE ELEMENT BINDING FACTOR 4)	3.04E-05	0.3481658	44
249050_at	At5g44290	AT5G44290	serine/threonine protein kinase	0.001896454	0.413807	43
265583_at	At2g20010	AT2G20010	hypothetical protein	0.002349113	0.3851935	42
248665_at	At5g48655	AT5G48655	RING/U-box domain-containing protein	0.000565	0.3850488	42
259033_at	At3g09410	AT3G09405	pectinacetylesterase family protein	0.001722347	0.3792083	42
253455_at	At4g32020	AT4G32020	hypothetical protein	6.16E-05	0.3746345	42
259230_at	At3g07780	OBE1	OBE1 (OBERON1)	0.006430628	0.3735423	42
265207_at	At2g36680	AT2G36680	vacuolar protein-sorting-associated protein 37-2	0.001378	0.3582663	42
253466_at	At4g32040	KNAT5	KNAT5 (KNOTTED1-LIKE HOMEOBOX GENE 5)	0.002217363	0.3481658	42
266096_at	At2g38020	VCL1	VCL1 (VACUOLELESS 1)	0.001472746	0.337393	42
265446_at	At2g37110	AT2G37110	PLAC8 domain-containing protein	0.000431	0.415316	41
258173_at	At3g21630	CERK1	CERK1 (CHITIN ELICITOR RECEPTOR KINASE 1)	0.002666391	0.4005471	41

Table S2. *(Continued)*

Probe ID	Identifier	Gene symbol	Description	BC	CC	Degree
247677_at	At5g59420	ORP3C	ORP3C (OSBP(OXYSTEROL BINDING PROTEIN)-RELATED PROTEIN 3C)	0.00327465	0.3900304	41
251790_at	At3g55470	AT3G55470	calcium-dependent lipid-binding domain-containing protein	0.001833375	0.3768382	41
257972_at	At3g27560	ATN1	ATN1	0.001666223	0.4106571	40
264351_at	At1g03370	AT1G03370	C2 calcium/lipid-binding and GRAM domain containing protein	0.001270309	0.4064235	40
258277_at	At3g26830	PAD3	PAD3 (PHYTOALEXIN DEFICIENT 3)	0.00053	0.3882576	40
254271_at	At4g23150	CRK7	cysteine-rich receptor-like protein kinase 7	0.002709695	0.378648	40
261063_at	At1g07520	AT1G07520	GRAS family transcription factor	0.00039	0.3776713	40
264000_at	At2g22500	UCP5	UCP5 (UNCOUPLING PROTEIN 5)	8.61E-05	0.3720508	40
264533_s_at	At1g55730	CAX5	ATCAX5	0.002266677	0.3709736	40
266901_at	At2g34600	JAZ7	JAZ7 (JASMONATE-ZIM-DOMAIN PROTEIN 7)	2.93E-05	0.34971	40
265732_at	At2g01300	AT2G01300	hypothetical protein	1.27E-05	0.3405316	40
254524_at	At4g20000	AT4G20000	VQ motif-containing protein	0.000352	0.3857734	39
252334_at	At3g48850	PHT3;2	phosphate transporter 3	0.000464	0.3824627	39
255605_at	At4g01090	AT4G01090	hypothetical protein	3.10E-05	0.3665951	39
267381_at	At2g26190	AT2G26190	calmodulin-binding protein	2.87E-05	0.3659407	39
246289_at	At3g56880	AT3G56880	VQ motif-containing protein	6.53E-05	0.3535702	39
256183_at	At1g51660	MKK4	ATMKK4 (*ARABIDOPSIS* THALIANA MITOGEN-ACTIVATED PROTEIN KINASE KINASE 4)	0.000792	0.3903275	38
259512_at	At1g12360	KEU	KEU (keule)	0.00497744	0.3886993	38
265648_at	At2g27500	AT2G27500	putative glucan endo-1,3-beta-glucosidase	0.002252304	0.3787879	38
255568_at	At4g01250	WRKY22	WRKY22	2.49E-05	0.3600281	38
261037_at	At1g17420	LOX3	LOX3	2.57E-05	0.3581412	38
245796_at	At1g32230	RCD1	RCD1 (RADICAL-INDUCED CELL DEATH1)	0.00083	0.3369494	38

Table S2. *(Continued)*

Probe ID	Identifier	Gene symbol	Description	BC	CC	Degree
247275_at	At5g64370	BETA-UP	BETA-UP (beta-ureidopropionase)	0.00155238	0.3187189	38
256013_at	At1g19270	DA1	DA1 (DA 1)	0.001509182	0.4101641	37
259440_at	At1g01550	BPS1	BPS1 (BYPASS 1)	0.005918891	0.3949904	37
250575_at	At5g08240	AT5G08240	hypothetical protein	0.000346	0.3943825	37
265221_s_at	At2g02010	GAD3	GAD3 (glutamate decarboxylase 3)	4.84E-05	0.3888467	37
266992_at	At2g39200	MLO12	MLO12 (MILDEW RESISTANCE LOCUS O 12)	0.001018557	0.386064	37
261763_at	At1g15520	PDR12	PDR12 (PLEIOTROPIC DRUG RESISTANCE 12)	0.000168	0.3853383	37
257363_at	At2g45760	BAP2	BAP2 (BON ASSOCIATION PROTEIN 2)	0.000438	0.3841829	37
263935_at	At2g35930	PUB23	PUB23 (PLANT U-BOX 23)	7.36E-05	0.3804751	37
247215_at	At5g64905	PROPEP3	PROPEP3 (Elicitor peptide 3 precursor)	0.000788	0.3787879	37
255923_at	At1g22180	AT1G22180	Sec14p-like phosphatidylinositol transfer family protein	0.002021379	0.3755955	37
267550_at	At2g32800	AP4.3A	AP4.3A	0.004116187	0.3719158	37
262607_at	At1g13990	AT1G13990	hypothetical protein	0.000714	0.338731	37
264936_at	At1g61140	EDA16	EDA16 (embryo sac development arrest 16)	0.000817	0.3972868	36
262408_at	At1g34750	AT1G34750	putative protein phosphatase 2C 10	0.001798649	0.3817505	36
260255_at	At1g74330	AT1G74330	putative serine/threonine kinase	9.70E-05	0.3775322	36
248124_at	At5g54730	ATG18F	AtATG18f	0.000571	0.3735423	36
261449_at	At1g21120	AT1G21120	O-methyltransferase family protein	0.000274	0.3731343	36
248132_at	At5g54840	SGP1	SGP1	0.001957543	0.3681753	36
259443_at	At1g02360	AT1G02360	putative chitinase	0.000514	0.3660714	36
252133_at	At3g50900	AT3G50900	hypothetical protein	0.002098963	0.4080414	35
267624_at	At2g39660	BIK1	BIK1 (BOTRYTIS-INDUCED KINASE1)	0.001579585	0.4054589	35

Table S2. *(Continued)*

Probe ID	Identifier	Gene symbol	Description	BC	CC	Degree
249252_at	At5g42010	AT5G42010 /// RBCS1A	WD40 domain-containing protein ribulose bisphosphate carboxylase small chain 1A	0.000301	0.3869385	35
264883_s_at	At1g61250	SC3	SC3 (SECRETORY CARRIER 3)	0.015420008	0.3782288	35
254265_s_at	At4g23140	CRK6	CRK6 (CYSTEINE-RICH RLK 6)	0.008855673	0.3715114	35
260915_at	At1g02660	AT1G02660	alpha/beta-Hydrolases superfamily protein	0.000151	0.3641208	35
266832_at	At2g30040	MAPKKK14	MAPKKK14	8.57E-06	0.354794	35
260988_at	At1g53570	MAP3KA	MAP3KA	0.000675	0.3362861	35
260690_at	At1g32340	NHL8	NHL8	0.000794	0.3283152	35
262540_at	At1g34260	FAB1D	putative 1-phosphatidylinositol-3-phosphate 5-kinase	0.000359	0.3881106	34
256169_at	At1g51800	AT1G51800	putative leucine-rich repeat protein kinase	0.001496245	0.3810409	34
261938_at	At1g22510	AT1G22510	C3HC4-type RING finger protein	0.000519	0.3676471	34
267546_at	At2g32680	AtRLP23	AtRLP23 (Receptor Like Protein 23)	0.003938561	0.3541811	34
261231_at	At1g20110	AT1G20110	RING/FYVE/PHD zinc finger-containing protein	0.001529175	0.3408713	34
254765_at	At4g13270	AT4G13270	late embryogenesis abundant hydroxyproline-rich glycoprotein	0.000361	0.322327	34
259610_at	At1g52320	AT1G52320	hypothetical protein	0.000739	0.3060615	34
254557_at	At4g19140	AT4G19140	hypothetical protein	0.000423	0.3924196	33
252329_at	At3g48760	AT3G48760	putative S-acyltransferase	0.001991011	0.3881106	33
257846_at	At3g12910	AT3G12910	no apical meristem domain-containing transcriptional regulator	0.000198	0.384039	33
251895_at	At3g54420	ATEP3	ATEP3	0.000246	0.3828913	33
253780_at	At4g28400	AT4G28400	putative protein phosphatase 2C 58	0.002406436	0.3818927	33
252331_s_at	At3g48790	SPT1	SPT1 (SERINE PALMITOYLTRANSFERASE 1)	0.000291	0.3794891	33
251300_at	At3g61980	AT3G61980	serine protease inhibitor, Kazal-type family protein	0.000163	0.3721859	33
251096_at	At5g01550	LECRKA4.2	LECRKA4.2 (LECTIN RECEPTOR KINASE A4.1)	0.000133	0.3717809	33

Table S2. *(Continued)*

Probe ID	Identifier	Gene symbol	Description	BC	CC	Degree
258577_at	At3g04220	AT3G04220	TIR-NBS-LRR class disease resistance protein	0.000303	0.3697691	33
257785_at	At3g26980	MUB4	MUB4 (MEMBRANE-ANCHORED UBIQUITIN-FOLD PROTEIN 4 PRECURSOR)	0.000199	0.3688377	33
253819_at	At4g28350	AT4G28350	concanavalin A-like lectin kinase-like protein	0.000202	0.3660714	33
255504_at	At4g02200	AT4G02200	protein dehydration-INDUCED 19-5	0.000339	0.3566458	33
254897_at	At4g11470	CRK31	putative cysteine-rich receptor-like protein kinase 31	0.000146	0.353083	33
254393_at	At4g21580	AT4G21580	oxidoreductase, zinc-binding dehydrogenase family protein	0.001656599	0.3264331	33
253702_at	At4g29900	ACA10	ACA10 (AUTOINHIBITED CA(2+)-ATPASE 10)	0.00075	0.4002343	32
264841_at	At1g03740	AT1G03740	protein kinase	0.000154	0.3897338	32
251475_at	At3g59660	AT3G59660	C2 domain and GRAM domain-containing protein	0.003303793	0.3775322	32
255319_at	At4g04220	AtRLP46	AtRLP46 (Receptor Like Protein 46)	0.004206703	0.3771155	32
250260_at	At5g13810	AT5G13810	Glutaredoxin family protein	0.001046057	0.3719158	32
248875_at	At5g46470	RPS6	protein RESISTANT TO P. SYRINGAE 6	2.36E-05	0.3696358	32
267393_at	At2g44500	AT2G44500	O-fucosyltransferase family protein	6.84E-05	0.3489956	32
247177_at	At5g65300	AT5G65300	hypothetical protein	5.35E-06	0.343729	32
259205_at	At3g09030	AT3G09030	BTB/POZ domain-containing protein	0.000825	0.3238547	32
249481_at	At5g38900	AT5G38900	Thioredoxin superfamily protein	0.000176	0.3620629	31
249001_at	At5g44990	AT5G44990	Glutathione S-transferase family protein	9.83E-05	0.3511477	31
262183_at	At1g77900	AT1G77890	DNA-directed RNA polymerase II protein	9.72E-05	0.3972868	30
249423_at	At5g39785	AT5G39785	hypothetical protein	2.22E-05	0.3846154	30
257784_at	At3g26970	MUB4	MUB4 (MEMBRANE-ANCHORED UBIQUITIN-FOLD PROTEIN 4 PRECURSOR)	4.76E-05	0.3588936	30
249974_at	At5g18780	AT5G18780	F-box domain-containing protein	0.001737908	0.3517502	30
248032_at	At5g55860	AT5G55860	hypothetical protein	0.000836	0.3307519	30

Table S2. *(Continued)*

Probe ID	Identifier	Gene symbol	Description	BC	CC	Degree
247545_at	At5g61530	AT5G61530	uncharacterized Rho GTPase-activating protein	0.00036	0.3303255	30
255740_at	At1g25390	AT1G25390	protein kinase superfamily protein	0.002387364	0.3898821	29
248868_at	At5g46780	AT5G46780	VQ motif-containing protein	8.74E-05	0.3776713	29
255926_at	At1g22190	AT1G22190	ethylene-responsive transcription factor RAP2.4	3.00E-05	0.3659407	29
252117_at	At3g51430	YLS2	YLS2	0.000997	0.3356254	29
259445_at	At1g02400	GA2OX6	GA2OX6 (GIBBERELLIN 2-OXIDASE 6)	0.000119	0.3934741	28
259019_at	At3g07370	CHIP	CHIP (CARBOXYL TERMINUS OF HSC70-INTERACTING PROTEIN)	0.000423	0.384039	28
261027_at	At1g01340	ATCNGC10	ATCNGC10 (CYCLIC NUCLEOTIDE GATED CHANNEL 10)	0.001105814	0.3806164	28
260568_at	At2g43570	CHI	putative chitinase	0.001106762	0.3747715	28
265008_at	At1g61560	MLO6	MLO6 (MILDEW RESISTANCE LOCUS O 6)	0.000122	0.3708394	28
252417_at	At3g47480	AT3G47480	putative calcium-binding protein CML47	0.001476972	0.3696358	28
254249_at	At4g23280	CRK20	putative cysteine-rich receptor-like protein kinase 20	0.000125	0.3623188	28
267384_at	At2g44370	AT2G44370	cysteine/histidine-rich C1 domain-containing protein	0.000467	0.3420087	28
259489_at	At1g15790	AT1G15790	hypothetical protein	0.003288906	0.3362861	28
266235_at	At2g02360	AtPP2-B10	AtPP2-B10 (Phloem protein 2-B10)	0.00057	0.3122144	28
253338_at	At4g33430	BAK1	BAK1 (BRI1-ASSOCIATED RECEPTOR KINASE)	6.47E-05	0.4003906	27
252310_at	At3g49350	AT3G49350	RabGAP/TBC domain-containing protein	0.000349	0.3959058	27
249346_at	At5g40780	LTH1	LHT1	0.000734	0.3957529	27
252602_at	At3g45040	AT3G45040	putative dolichol kinase	0.00126423	0.3915202	27
247394_at	At5g62860	AT5G62865	hypothetical protein	5.68E-05	0.3915202	27
257010_at	At3g14090	ATEXO70D3	ATEXO70D3 (exocyst subunit EXO70 family protein D3)	0.004009735	0.3900304	27
265276_at	At2g28400	AT2G28400	hypothetical protein	0.000182	0.3776713	27
251603_at	At3g57760	AT3G57760	protein kinase family protein	1.51E-05	0.3769768	27

Table S2. *(Continued)*

Probe ID	Identifier	Gene symbol	Description	BC	CC	Degree
254948_at	At4g11000	AT4G11000	ankyrin repeat-containing protein	0.000264	0.3740876	27
260754_at	At1g49000	AT1G49000	hypothetical protein	0.000226	0.3588936	27
263570_at	At2g27150	AAO3	AAO3 (Abscisic ALDEHYDE OXIDASE 3)	0.000275	0.3516295	27
264616_at	At2g17740	AT2G17740	cysteine/histidine-rich C1 domain-containing protein	0.000295	0.3447696	27
266447_at	At2g43290	MSS3	MSS3 (multicopy suppressors of snf4 deficiency in yeast 3)	3.66E-05	0.3337675	27
260943_at	At1g45145	ATTRX5	ATTRX5	0.000249	0.3264331	27
248615_at	At5g49570	AtPNG1	AtPNG1 (*Arabidopsis* thaliana peptide-N-glycanase 1)	0.002504108	0.3144172	27
247351_at	At5g63790	ANAC102	ANAC102 (*ARABIDOPSIS* NAC DOMAIN CONTAINING PROTEIN 102)	0.000304	0.3918196	26
256337_at	At1g72060	AT1G72060	serine-type endopeptidase inhibitor	0.00035	0.3876702	26
254861_at	At4g12040	AT4G12040	zinc finger A20 and AN1 domain-containing stress-associated protein 7	0.000199	0.3849042	26
258351_at	At3g17700	CNBT1	CNBT1 (CYCLIC NUCLEOTIDE-BINDING TRANSPORTER 1)	0.000887	0.3826055	26
255716_at	At4g00330	CRCK2	CRCK2	0.001751924	0.3821775	26
251624_at	At3g57280	AT3G57280	transmembrane protein 14C	0.001495061	0.3800519	26
261450_s_at	At1g21110	AT1G21110 /// AT1G21120	O-methyltransferase family protein O-methyltransferase family protein	4.28E-05	0.3747715	26
247044_at	At5g66850	MAPKKK5	MAPKKK5	0.000914	0.3725918	26
266792_at	At2g02860	SUT2	SUT2 (SUCROSE TRANSPORTER 2)	0.000188	0.3717809	26
263216_s_at	At1g30720	AT1G30720 /// AT1G30730	FAD-binding Berberine family protein FAD-binding and BBE domain-containing protein	0.001114383	0.3709736	26
248146_at	At5g54940	AT5G54940	translation initiation factor SUI1 family protein	0.001202361	0.3689705	26
249652_at	At5g37070	AT5G37070	hypothetical protein	0.002189634	0.351268	26
254741_s_at	At4g13900	AtRLP49	AtRLP49 (Receptor Like Protein 49)	0.001113167	0.3379492	26
266052_at	At2g40740	WRKY55	WRKY55	6.86E-05	0.3375041	26
249618_at	At5g37490	AT5G37490	U-box domain-containing protein 21	7.83E-05	0.3342028	26

Table S2. *(Continued)*

Probe ID	Identifier	Gene symbol	Description	BC	CC	Degree
254289_at	At4g22980	AT4G22980	hypothetical protein	0.001250809	0.3921194	25
259109_at	At3g05580	AT3G05580	serine/threonine-protein phosphatase PP1 isozyme 9	5.08E-05	0.3700361	25
246018_at	At5g10695	AT5G10695	hypothetical protein	9.79E-05	0.3575166	25
261242_at	At1g32960	SBT3.3	SBT3.3	3.90E-05	0.3570185	25
246653_at	At5g35200	AT5G35200	putative clathrin assembly protein	0.000913	0.3567699	25
251970_at	At3g53150	UGT73D1	UGT73D1 (UDP-glucosyl transferase 73D1)	0.000112	0.3539365	25
263378_at	At2g40180	ATHPP2C5	ATHPP2C5	0.000103	0.340758	25
261756_at	At1g08320	AT1G08315	armadillo/beta-catenin-like repeat-containing protein	0.000256	0.3913708	24
251400_at	At3g60420	AT3G60420	phosphoglycerate mutase family protein	0.004057366	0.3856283	24
247305_at	At5g63905	AT5G63905	hypothetical protein	0.000777	0.3773932	24
249418_at	At5g39780	AT5G39785	hypothetical protein	9.95E-05	0.3760088	24
263931_at	At2g36220	AT2G36220	hypothetical protein	1.07E-05	0.3749086	24
261339_at	At1g35710	AT1G35710	putative leucine-rich repeat receptor-like protein kinase	0.008400218	0.3523548	24
250279_at	At5g13200	AT5G13200	GRAM domain family protein	0.002194277	0.3824627	23
249719_at	At5g35735	AT5G35735	putative auxin-responsive protein	0.000597	0.3760088	23
252134_at	At3g50910	AT3G50910	hypothetical protein	0.000108	0.3743608	23
255406_at	At4g03450	AT4G03450	ankyrin repeat-containing protein	0.000236	0.3736785	23
247949_at	At5g57220	CYP81F2	CYP81F2	0.000407	0.3727273	23
256306_at	At1g30370	AT1G30370	DAD1-like acylhydrolase	9.16E-05	0.3456998	23
262932_at	At1g65820	AT1G65820	putative glutathione S-transferase	0.005426388	0.3337675	23
258954_at	At3g01400	AT3G01400	armadillo/beta-catenin-like repeat-containing protein	0.000508	0.308642	23
252214_at	At3g50260	CEJ1	CEJ1 (COOPERATIVELY REGULATED BY ETHYLENE AND JASMONATE 1)	6.39E-06	0.3946862	22
254759_at	At4g13180	AT4G13180	Rossmann-fold NAD(P)-binding domain-containing protein	0.000493	0.3873772	22

Table S2. *(Continued)*

Probe ID	Identifier	Gene symbol	Description	BC	CC	Degree
250493_at	At5g09800	AT5G09800	ARM repeat superfamily protein	9.21E-05	0.3783684	22
267490_at	At2g19130	AT2G19130	G-type lectin S-receptor-like serine/threonine-protein kinase	0.003654361	0.3764231	22
249078_at	At5g44070	CAD1	CAD1 (CADMIUM SENSITIVE 1)	0.001869822	0.3708394	22
253625_at	At4g30600	AT4G30600	signal recognition particle receptor subunit alpha	0.000433	0.3675152	22
257540_at	At3g21520	DMP1	DUF679 domain membrane protein 1	2.52E-05	0.3645092	22
266761_at	At2g47130	AT2G47130	short-chain dehydrogenase reductase 3	0.000129	0.3616796	22
252648_at	At3g44630	AT3G44630	TIR-NBS-LRR class disease resistance protein	3.23E-05	0.3593969	22
255564_s_at	At4g01750	RGXT2	RGXT2 (rhamnogalacturonan xylosyltransferase 2)	0.000395	0.3510274	22
250415_at	At5g11210	GLR2.5	ATGLR2.5	4.52E-05	0.3498294	22
251832_at	At3g55150	ATEXO70H1	ATEXO70H1 (exocyst subunit EXO70 family protein H1)	0.000115	0.3228346	22
249930_at	At5g22360	ATVAMP714	ATVAMP714 (VESICLE-ASSOCIATED MEMBRANE PROTEIN 714)	0.000701	0.3213166	22
262567_at	At1g34300	AT1G34300	G-type lectin S-receptor-like serine/threonine-protein kinase	0.001434277	0.3101362	22
264635_at	At1g65500	AT1G65500	hypothetical protein	0.00016	0.3837514	21
248134_at	At5g54860	AT5G54860	probable folate-biopterin transporter 4	4.53E-06	0.3836078	21
257038_at	At3g19260	LOH2	LOH2 (LAG ONE HOMOLOGUE 2)	0.000549	0.3778105	21
247940_at	At5g57190	PSD2	PSD2 (phosphatidylserine decarboxylase 2)	6.52E-05	0.3676471	21
253808_at	At4g28300	AT4G28300	hypothetical protein	0.000825	0.3591451	21
256969_at	At3g21080	AT3G21080	ABC transporter-like protein	0.000124	0.3486395	21
253113_at	At4g35985	AT4G35985	senescence/dehydration-associated protein	3.17E-06	0.3425802	21
257791_at	At3g27110	AT3G27110	peptidase family M48 family protein	0.000489	0.3311793	21
254060_at	At4g25350	SHB1	SHB1 (SHORT HYPOCOTYL UNDER BLUE1)	0.000332	0.3241619	21
266983_at	At2g39400	AT2G39400	alpha/beta-Hydrolases superfamily protein	9.86E-05	0.3879637	20
262803_at	At1g21000	AT1G21000	PLATZ transcription factor family protein	0.000567	0.3744976	20

Table S2. *(Continued)*

Probe ID	Identifier	Gene symbol	Description	BC	CC	Degree
257466_at	At1g62840	AT1G62840	hypothetical protein	0.000416	0.3715114	20
247864_s_at	At5g57890	ASB1	ASB1 (ANTHRANILATE SYNTHASE BETA SUBUNIT 1)	0.001046824	0.3704373	20
262896_at	At1g59820	ALA3	ALA3 (Aminophospholipid ATPase3)	5.26E-05	0.3683076	20
253647_at	At4g29950	AT4G29950	RabGAP/TBC domain-containing protein	0.000167	0.3672519	20
246607_at	At5g35370	AT5G35370	G-type lectin S-receptor-like serine/threonine-protein kinase	0.000435	0.3648985	20
245654_at	At1g56540	AT1G56540	TIR-NBS-LRR class disease resistance protein	1.44E-05	0.3533264	20
262360_at	At1g73080	PEPR1	PEPR1 (PEP1 receptor 1)	1.24E-05	0.3464008	20
247314_at	At5g64000	SAL2	SAL2	0.000386	0.3443063	20
248719_at	At5g47910	RBOHD	RBOHD (RESPIRATORY BURST OXIDASE HOMOLOGUE D)	1.13E-05	0.3439597	20
256170_at	At1g51790	AT1G51790	leucine-rich repeat protein kinase-like protein	0.000283	0.3406447	20
251342_at	At3g60690	AT3G60690	SAUR-like auxin-responsive protein	9.92E-05	0.3244698	20
245787_at	At1g32130	IWS1	IWS1-like protein	0.000237	0.3229364	20
263419_at	At2g17220	AT2G17220	putative serine/threonine-specific protein kinase kin3	3.65E-05	0.3846154	19
260878_at	At1g21450	SCL1	SCL1 (SCARECROW-LIKE 1)	0.000647	0.3692363	19
264619_at	At2g17760	AT2G17760	aspartyl protease family protein	0.001083602	0.3689705	19
259629_at	At1g56510	WRR4	WRR4 (WHITE RUST RESISTANCE 4)	0.001314436	0.353083	19
251145_at	At3g63500	AT3G63500	PHD-finger TITANIA 2	0.002075667	0.3404185	19
260015_at	At1g67980	CCOAMT	CCoAMT	9.35E-06	0.3363965	19
246384_at	At1g77370	AT1G77370	glutaredoxin-C3	0.000848	0.328105	19
246366_at	At1g51850	AT1G51850	Leucine-rich repeat protein kinase family protein	3.20E-05	0.3062444	19
253564_at	At4g31170	AT4G31170	protein kinase family protein	0.002322808	0.2928571	19
245038_at	At2g26560	PLA2A	PLA2A (PHOSPHOLIPASE A 2A)	2.22E-06	0.3668576	18
246305_at	At3g51890	AT3G51890	Clathrin light chain protein	0.000265	0.3593969	18

Table S2. *(Continued)*

Probe ID	Identifier	Gene symbol	Description	BC	CC	Degree
256185_at	At1g51700	ADOF1	ADOF1	2.28E-05	0.3503076	18
254652_at	At4g18170	WRKY28	WRKY28	3.64E-05	0.3493524	18
258982_at	At3g08870	AT3G08870	concanavalin A-like lectin protein kinase family protein	0.000929	0.3180267	18
261709_at	At1g32790	CID11	RNA-binding protein, putative	0.000656	0.3017368	18
252587_at	At3g45620	AT3G45620	DWD motif protein	0.000845	0.29962	18
248686_at	At5g48540	AT5G48540	receptor-like protein kinase-related family protein	5.58E-05	0.3776713	17
260635_at	At1g62420	AT1G62422	hypothetical protein	0.000604	0.3743608	17
266182_at	At2g02370	AT2G02370	SNARE associated Golgi protein	0.002477662	0.3689705	17
261413_at	At1g07630	PLL5	PLL5	0.000232	0.3665951	17
262229_at	At1g68620	AT1G68620	probable carboxylesterase 6	0.000466	0.3636041	17
253181_at	At4g35180	LHT7	LHT7 (Lys/His transporter 7)	7.45E-06	0.361935	17
248901_at	At5g46410	SSP4	SCP1-like small phosphatase 4	0.000315	0.3616796	17
261161_at	At1g34420	AT1G34420	leucine-rich repeat transmembrane protein kinase-like protein	0.001495077	0.3606615	17
262367_at	At1g73030	VPS46.2	VPS46.2	0.003909502	0.3575166	17
254014_at	At4g26120	AT4G26120	regulatory protein NPR2	4.69E-05	0.3571429	17
255301_at	At4g04800	ATMSRB3	methionine sulfoxide reductase domain-containing protein	0.000414	0.3489956	17
264592_at	At2g17720	AT2G17720	prolyl 4-hydroxylase 5	0.004423199	0.3487581	17
261458_at	At1g21080	AT1G21080	DNAJ heat shock N-terminal domain-containing protein	0.000241	0.3458165	17
250984_at	At5g02800	AT5G02800	protein CDG1-LIKE 1	0.00031	0.3417806	17
251877_at	At3g54300	ATVAMP727	ATVAMP727 (VESICLE-ASSOCIATED MEMBRANE PROTEIN 727)	0.00043	0.3050595	17
256431_s_at	At3g11010	AtRLP34	AtRLP34 (Receptor Like Protein 34)	0.000978	0.2995324	17
264172_at	At1g02120	VAD1	VAD1 (VASCULAR ASSOCIATED DEATH1)	0.000367	0.292106	17
258194_at	At3g29170	AT3G29170	hypothetical protein	2.82E-05	0.3804751	16

Table S2. *(Continued)*

Probe ID	Identifier	Gene symbol	Description	BC	CC	Degree
245566_at	At4g14610	---	---	0.002057647	0.3728629	16
257536_at	At3g02800	AT3G02800	atypical dual-specificity phosphatase	2.10E-05	0.3700361	16
262731_at	At1g16420	MC8	MC8 (METACASPASE 8)	1.24E-05	0.3668576	16
266292_at	At2g29350	SAG13	SAG13	0.000396	0.361552	16
250477_at	At5g10190	AT5G10190	major facilitator protein	0.00184106	0.3609155	16
245369_at	At4g15975	AT4G15975	RING-H2 finger protein ATL17	6.42E-05	0.3587679	16
263228_at	At1g30700	AT1G30700	FAD-binding Berberine family protein	3.75E-05	0.3471046	16
260350_at	At1g69410	ELF5A-3	ELF5A-3 (EUKARYOTIC ELONGATION FACTOR 5A-3)	0.00150772	0.3423514	16
248298_at	At5g53110	AT5G53110	Wall-associated receptor kinase and RING-finger domain-containing protein	8.67E-05	0.3404185	16
263541_at	At2g24860	AT2G24860	DnaJ/Hsp40 cysteine-rich domain-containing protein	0.000948	0.3320376	16
252511_at	At3g46280	AT3G46280	protein kinase-like protein	3.52E-05	0.3112663	16
249081_at	At5g44090	AT5G44090	serine/threonine protein phosphatase 2A regulatory subunit B''alpha	0.00067	0.3095741	16
263075_at	At2g17570	AT2G17570	cis-prenyltransferase 1	0.00012	0.3056052	16
252335_at	At3g48860	AT3G48860	hypothetical protein	0.000229	0.2927735	16
265772_at	At2g48010	RKF3	RKF3 (RECEPTOR-LIKE KINASE IN IN FLOWERS 3)	0.000408	0.3692363	15
252126_at	At3g50950	ZAR1	protein HOPZ-ACTIVATED RESISTANCE 1	0.004111852	0.3597754	15
255654_at	At4g00970	CRK41	cysteine-rich receptor-like protein kinase 41	1.13E-05	0.3551629	15
263799_at	At2g24550	AT2G24550	hypothetical protein	0.000185	0.3536922	15
251625_at	At3g57260	BGL2	BGL2 (BETA-1,3-GLUCANASE 2)	0.001638766	0.3369494	15
249032_at	At5g44910	AT5G44910	Toll-Interleukin-Resistance domain-containing protein	5.47E-05	0.3363965	15
247930_at	At5g57060	AT5G57060	hypothetical protein	7.63E-05	0.333225	15
256181_at	At1g51820	AT1G51820	putative LRR receptor-like serine/threonine protein kinase	7.37E-05	0.3322528	15

Table S2. *(Continued)*

Probe ID	Identifier	Gene symbol	Description	BC	CC	Degree
266749_at	At2g47060	AT2G47060	Pto-interacting 1-4	2.61E-05	0.3276854	15
251034_at	At5g02040	PRA1.A1	PRA1.A1 (PRENYLATED RAB ACCEPTOR 1.A1)	4.86E-05	0.3057876	15
261677_at	At1g18470	AT1G18470	transmembrane Fragile-X-F-associated protein	0.000143	0.3043349	15
262671_at	At1g76040	CPK29	CPK29	3.36E-05	0.3740876	14
254571_at	At4g19370	AT4G19370	hypothetical protein	1.37E-05	0.3719158	14
246993_at	At5g67450	AZF1	AZF1 (*ARABIDOPSIS* ZINC-FINGER PROTEIN 1)	0.000107	0.3709736	14
248726_at	At5g47960	ATRABA4C	ATRABA4C	2.93E-06	0.3650285	14
263274_at	At2g11520	CRCK3	CRCK3	3.82E-05	0.3641208	14
265132_at	At1g23830	AT1G23830	hypothetical protein	0.00195357	0.3616796	14
249221_at	At5g42440	AT5G42440	protein kinase family protein	7.19E-06	0.3605346	14
257206_at	At3g16530	AT3G16530	legume lectin-like protein	6.83E-05	0.3573919	14
257185_at	At3g13100	ATMRP7	ATMRP7	0.000132	0.3559028	14
266348_at	At2g01450	ATMPK17	ATMPK17	0.000302	0.3480475	14
257216_at	At3g14990	AT3G14990	protein DJ-1-like A	0.000556	0.3429241	14
253535_at	At4g31550	WRKY11	WRKY11	2.72E-05	0.3347485	14
259385_at	At1g13470	AT1G13470	hypothetical protein	0.000768	0.329582	14
257100_at	At3g25010	AtRLP41	AtRLP41 (Receptor Like Protein 41)	0.000227	0.3057876	14
248703_at	At5g48430	AT5G48430	aspartyl protease family protein	2.01E-05	0.3039739	14
247114_at	At5g65910	AT5G65910	BSD domain-containing protein	5.32E-05	0.2904506	14
245167_s_at	At2g33120	ATVAMP723	ATVAMP723 (VESICLE-ASSOCIATED MEMBRANE PROTEIN 723)	0.00013	0.3749086	13
266746_s_at	At2g02930	ATGSTF3	ATGSTF3 (GLUTATHIONE S-TRANSFERASE F3)	0.00016	0.3729985	13
252234_at	At3g49780	ATPSK4	ATPSK4 (PHYTOSULFOKINE 4 PRECURSOR)	5.90E-05	0.3667263	13
251848_at	At3g54620	BZIP25	BZIP25 (BASIC LEUCINE ZIPPER 25)	3.31E-05	0.3658101	13

Table S2. *(Continued)*

Probe ID	Identifier	Gene symbol	Description	BC	CC	Degree
250944_at	At5g03380	AT5G03380	heavy metal transport/detoxification domain-containing protein	0.001350637	0.3651585	13
260899_at	At1g21370	AT1G21370	hypothetical protein	0.002243175	0.3597754	13
249988_at	At5g18310	AT5G18310	hypothetical protein	0.000513	0.3587679	13
262845_at	At1g14740	AT1G14740	Protein OBERON 3	0.000179	0.3573919	13
246440_at	At5g17650	AT5G17650	glycine/proline-rich protein	0.003455762	0.3571429	13
250673_at	At5g07070	CIPK2	CIPK2 (CBL-INTERACTING PROTEIN KINASE 2)	2.69E-05	0.3560264	13
246448_at	At5g16800	AT5G16800	GCN5-related N-acetyltransferase (GNAT) family protein	0.00024	0.3533264	13
253779_at	At4g28490	HAE	HAE (HAESA)	0.000857	0.3410982	13
247618_at	At5g60280	AT5G60280	concanavalin A-like lectin kinase-like protein	6.57E-05	0.3406447	13
246744_at	At5g27760	AT5G27760	hypoxia-responsive family protein	0.000443	0.3403054	13
254673_at	At4g18430	AtRABA1e	AtRABA1e (*Arabidopsis* Rab GTPase homolog A1e)	5.99E-06	0.3383955	13
255243_at	At4g05590	AT4G05590	hypothetical protein	0.000208	0.3317152	13
255630_at	At4g00700	AT4G00700	C2 calcium/lipid-binding plant phosphoribosyltransferase family protein	0.000289	0.308178	13
261692_at	At1g08450	CRT3	CRT3 (CALRETICULIN 3)	0.003580672	0.2992701	13
248169_at	At5g54610	ANK	ANK (ankyrin)	0.000626	0.2977055	13
250423_s_at	At5g10610	CYP81K2	CYP81K2	1.90E-05	0.2974463	13
266520_at	At2g23980	ATCNGC6	ATCNGC6	6.34E-05	0.2968433	13
248221_at	At5g53530	VPS26A	VPS26A (VACUOLAR PROTEIN SORTING 26A)	2.52E-05	0.277027	13
259937_s_at	At1g71330	ATNAP5	ATNAP5	2.97E-05	0.3637331	12
263539_at	At2g24850	TAT3	TAT3 (TYROSINE AMINOTRANSFERASE 3)	8.40E-05	0.3620629	12
266396_at	At2g38790	AT2G38790	hypothetical protein	1.00E-04	0.3581412	12
247793_at	At5g58650	PSY1	PSY1 (plant peptide containing sulfated tyrosine 1)	0.000485	0.3519918	12

Table S2. *(Continued)*

Probe ID	Identifier	Gene symbol	Description	BC	CC	Degree
254318_at	At4g22530	AT4G22530	S-adenosyl-L-methionine-dependent methyltransferase domain-containing protein	6.12E-05	0.3475754	12
245986_at	At5g13160	PBS1	PBS1 (avrPphB susceptible 1)	0.000156	0.3471046	12
261711_at	At1g32700	AT1G32700	PLATZ transcription factor domain-containing protein	0.00039	0.3455833	12
256930_at	At3g22460	OASA2	OASA2 (O-ACETYLSERINE (THIOL) LYASE (OAS-TL) ISOFORM A1)	4.21E-05	0.3375041	12
249936_at	At5g22450	AT5G22450	hypothetical protein	0.000335	0.337282	12
266779_at	At2g29100	ATGLR2.9	ATGLR2.9	2.16E-05	0.3349673	12
262383_at	At1g72940	AT1G72940	Toll-Interleukin-Resistance domain-containing protein	2.74E-05	0.316945	12
266967_at	At2g39530	AT2G39530	hypothetical protein	3.90E-05	0.307623	12
256487_at	At1g31540	AT1G31540	TIR-NBS-LRR class disease resistance protein	4.34E-06	0.3656796	11
254447_at	At4g20860	AT4G20860	FAD-binding Berberine family protein	9.54E-06	0.3621908	11
250323_at	At5g12880	AT5G12880	proline-rich family protein	1.41E-05	0.3532047	11
254922_at	At4g11370	RHA1A	RHA1A	2.83E-05	0.3523548	11
254167_at	At4g24400	CIPK8	CIPK8 (CBL-INTERACTING PROTEIN KINASE 8)	0.001814876	0.3505472	11
254243_at	At4g23210	CRK13	protein kinase family protein	4.96E-05	0.3499488	11
255342_at	At4g04510	CRK38	cysteine-rich receptor-like protein kinase 38	4.76E-05	0.3494715	11
248162_at	At5g54500	FQR1	FQR1 (FLAVODOXIN-LIKE QUINONE REDUCTASE 1)	0.00027	0.3485209	11
259249_at	At3g07790	AT3G07790	DGCR14-like protein	3.42E-06	0.3433836	11
250655_at	At5g06960	OBF5	OBF5 (OCS-ELEMENT BINDING FACTOR 5)	9.06E-05	0.3365069	11
262177_at	At1g74710	EDS16	isochorismate synthase 1 (ICS1) / isochorismate mutase	2.55E-05	0.3363965	11
259850_at	At1g72240	AT1G72240	hypothetical protein	8.98E-07	0.3312864	11
259484_at	At1g12580	PEPKR1	PEPKR1 (Phosphoenolpyruvate carboxylase-related kinase 1)	1.17E-07	0.3287364	11
246987_at	At5g67300	MYBR1	MYBR1 (MYB DOMAIN PROTEIN R1)	3.26E-07	0.3242645	11

Table S2. *(Continued)*

Probe ID	Identifier	Gene symbol	Description	BC	CC	Degree
246302_at	At3g51860	CAX3	CAX3 (CATION EXCHANGER 3)	0.000174	0.3131683	11
247602_at	At5g60900	RLK1	RLK1 (RECEPTOR-LIKE PROTEIN KINASE 1)	0.001465918	0.286553	11
266476_at	At2g31090	AT2G31090	hypothetical protein	5.52E-05	0.3646389	10
259764_at	At1g64280	NPR1	NPR1 (NONEXPRESSER OF PR GENES 1)	2.64E-05	0.359523	10
248250_at	At5g53130	CNGC1	CNGC1 (CYCLIC NUCLEOTIDE GATED CHANNEL 1)	0.00016	0.3593969	10
266259_at	At2g27830	AT2G27830	hypothetical protein	4.11E-05	0.3505472	10
264717_at	At1g70140	ATFH8	ATFH8 (formin 8)	3.73E-05	0.3453504	10
265189_at	At1g23840	AT1G23840	hypothetical protein	4.68E-05	0.3445378	10
264663_at	At1g09970	LRR XI-23	LRR XI-23	3.89E-05	0.3428094	10
251633_at	At3g57460	AT3G57460	putative protein metalloendopeptidase NRD2 convertase	0.000214	0.3424658	10
245738_at	At1g44130	AT1G44130	aspartyl protease family protein	8.58E-05	0.3413253	10
250286_at	At5g13320	PBS3	PBS3 (AVRPPHB SUSCEPTIBLE 3)	1.70E-05	0.3358453	10
263854_at	At2g04430	atnudt5	atnudt5 (*Arabidopsis* thaliana Nudix hydrolase homolog 5)	2.16E-05	0.33453	10
249754_at	At5g24530	DMR6	DMR6 (DOWNY MILDEW RESISTANT 6)	0.000806	0.3293702	10
247327_at	At5g64120	AT5G64120	peroxidase 71	0.002022461	0.3276854	10
252422_at	At3g47550	AT3G47550	RING/FYVE/PHD zinc finger superfamily protein	0.000932	0.3135515	10
255595_at	At4g01700	AT4G01700	Chitinase family protein	0.000135	0.3135515	10
253503_at	At4g31950	CYP82C3	CYP82C3	1.76E-06	0.3047874	10
249486_at	At5g39030	AT5G39030	putative receptor-like protein kinase	9.46E-05	0.2981385	10
254975_at	At4g10500	AT4G10500	oxidoreductase, 2OG-Fe(II) oxygenase family protein	0.00048	0.2873563	10
265661_at	At2g24360	AT2G24360	putative serine/threonine/tyrosine kinase	0.001029868	0.2869541	10
257612_at	At3g26600	ARO4	ARO4 (ARMADILLO REPEAT ONLY 4)	0.000287	0.2676939	10
264774_at	At1g22890	AT1G22890	hypothetical protein	1.71E-06	0.3683076	9

Table S2. *(Continued)*

Probe ID	Identifier	Gene symbol	Description	BC	CC	Degree
255280_at	At4g04960	AT4G04960	concanavalin A-like lectin kinase-like protein	1.31E-05	0.367779	9
265450_at	At2g46620	AT2G46620	P-loop containing nucleoside triphosphate hydrolases superfamily protein	6.34E-05	0.3529614	9
260602_at	At1g55920	ATSERAT2;1	ATSERAT2	0.001636601	0.3513884	9
257264_at	At3g22060	AT3G22060	Receptor-like protein kinase-related family protein	5.01E-05	0.3500683	9
256933_at	At3g22600	AT3G22600	protease inhibitor/seed storage/lipid transfer protein (LTP) family protein	4.10E-05	0.3494715	9
252921_at	At4g39030	EDS5	EDS5 (ENHANCED DISEASE SUSCEPTIBILITY 5)	4.09E-05	0.3474576	9
264766_at	At1g61420	AT1G61420	G-type lectin S-receptor-like serine/threonine-protein kinase	2.97E-05	0.3418946	9
253292_at	At4g33985	AT4G33985	hypothetical protein	0.00139333	0.3416667	9
249896_at	At5g22530	AT5G22530	hypothetical protein	1.28E-05	0.3381722	9
261754_at	At1g76130	AMY2	AMY2 (ALPHA-AMYLASE-LIKE 2)	0.000103	0.337393	9
247065_s_at	At5g66900	NRG1	CC-NB-LRR class disease resistance protein	0.002042289	0.33453	9
260116_at	At1g33960	AIG1	AIG1 (AVRRPT2-INDUCED GENE 1)	7.78E-05	0.333985	9
251786_at	At3g55270	MKP1	MKP1 (MITOGEN-ACTIVATED PROTEIN KINASE PHOSPHATASE 1)	6.43E-05	0.3335503	9
251683_at	At3g57120	AT3G57120	protein kinase family protein	6.42E-06	0.3289474	9
248551_at	At5g50200	WR3	WR3 (WOUND-RESPONSIVE 3)	0.000109	0.3237524	9
245694_at	At5g04170	AT5G04170	putative calcium-binding protein CML50	0.000248	0.3100423	9
254262_at	At4g23480	AT4G23470	PLAC8 family protein	0.00122944	0.2971014	9
262220_at	At1g74740	CPK30	CPK30 (CALCIUM-DEPENDENT PROTEIN KINASE 30)	3.96E-05	0.2920228	9
265324_at	At2g18250	ATCOAD	ATCOAD (4-phosphopantetheine adenylyltransferase)	1.21E-05	0.2879213	9
252450_s_at	At3g47090	AT3G47090 /// AT3G47580	leucine-rich repeat protein kinase-like protein	2.10E-06	0.3474576	8
258941_at	At3g09940	MDHAR	MDHAR (MONODEHYDROASCORBATE REDUCTASE)	3.23E-05	0.3466351	8
256968_at	At3g21070	NADK1	NADK1 (NAD KINASE 1)	1.09E-05	0.3455833	8
247205_at	At5g64890	PROPEP2	PROPEP2 (Elicitor peptide 2 precursor)	3.30E-05	0.3423514	8

Table S2. *(Continued)*

Probe ID	Identifier	Gene symbol	Description	BC	CC	Degree
258683_at	At3g08760	ATSIK	ATSIK	0.000176	0.3415528	8
263797_at	At2g24570	WRKY17	WRKY17	7.36E-06	0.3400796	8
256981_at	At3g13380	BRL3	BRL3 (BRI1-LIKE 3)	1.25E-05	0.3382838	8
264648_at	At1g09080	BIP3	BIP3	1.27E-06	0.33453	8
253476_at	At4g32300	SD2-5	SD2-5 (S-DOMAIN-2 5)	3.99E-05	0.3326842	8
255880_at	At1g67060	AT1G67060	hypothetical protein	5.98E-05	0.3260178	8
257277_at	At3g14470	AT3G14470	NB-ARC domain-containing disease resistance protein	2.06E-05	0.3240594	8
254093_at	At4g25110	AtMC2	AtMC2 (metacaspase 2)	9.39E-06	0.3216191	8
258953_at	At3g01430	AT3G01430	hypothetical protein	6.83E-07	0.319713	8
256989_at	At3g28580	AT3G28580	AAA-type ATPase family protein	7.89E-06	0.3193146	8
250302_at	At5g11920	AtcwINV6	AtcwINV6 (6-&1-fructan exohydrolase)	1.25E-05	0.3186198	8
257088_at	At3g20510	AT3G20510	transmembrane protein 14C	6.20E-05	0.3154817	8
251930_at	At3g53780	ATRBL4	rhomboid family protein	0.00118941	0.293949	8
263776_s_at	At2g46440	ATCNGC3	ATCNGC3 (CYCLIC NUCLEOTIDE GATED CHANNEL 3)	0.000308	0.2884074	8
264219_at	At1g60420	AT1G60420	protein reduce transmission through pollen	1.66E-05	0.2850389	8
250445_at	At5g10760	AT5G10760	aspartyl protease family protein	0.000861	0.2808989	8
252486_at	At3g46510	PUB13	PUB13 (PLANT U-BOX 13)	0.002046243	0.2745046	8
255148_at	At4g08470	MAPKKK10	MAPKKK10	0.000256	0.2612796	8
265136_at	At1g51280	AT1G51270	vesicle-associated protein 1-4	9.50E-07	0.3614245	7
255479_at	At4g02380	SAG21	SAG21 (SENESCENCE-ASSOCIATED GENE 21)	1.01E-06	0.3597754	7
253637_at	At4g30390	AT4G30390	hypothetical protein	4.08E-05	0.3472222	7
263928_at	At2g36330	AT2G36330	hypothetical protein	1.66E-05	0.3421228	7
249140_at	At5g43190	AT5G43190	F-box/kelch-repeat protein	8.79E-06	0.3412117	7

Table S2. *(Continued)*

Probe ID	Identifier	Gene symbol	Description	BC	CC	Degree
251406_at	At3g60260	AT3G60260	ELMO/CED-12 domain-containing protein	1.46E-06	0.3395164	7
245200_at	At1g67850	AT1G67850	hypothetical protein	9.38E-06	0.3391794	7
265460_at	At2g46600	AT2G46600	Calcium-binding EF-hand family protein	2.94E-05	0.337282	7
267289_at	At2g23770	AT2G23770	lysin motif receptor-like kinase	1.78E-06	0.3337675	7
262660_at	At1g14000	VIK	VIK (VH1-INTERACTING KINASE)	8.66E-06	0.3309655	7
253401_at	At4g32870	AT4G32870	SRPBCC ligand-binding domain-containing protein	4.92E-06	0.3260178	7
253321_at	At4g33910	AT4G33910	oxidoreductase, 2OG-Fe(II) oxygenase family protein	0.000309	0.3250872	7
246955_at	At5g04870	CPK1	CPK1 (CALCIUM DEPENDENT PROTEIN KINASE 1)	1.43E-06	0.3226314	7
259076_at	At3g02140	TMAC2	TMAC2 (TWO OR MORE ABRES-CONTAINING GENE 2)	9.64E-07	0.3220232	7
262899_at	At1g59870	PEN3	PEN3 (PENETRATION 3)	0.001329431	0.3165534	7
256428_at	At3g11080	AtRLP35	AtRLP35 (Receptor Like Protein 35)	0.001567953	0.3162604	7
250983_at	At5g02780	GSTL1	glutathione transferase lambda 1	1.30E-05	0.31023	7
256121_at	At1g18160	AT1G18160	protein kinase family protein	0.001970804	0.2779284	7
260345_at	At1g69270	RPK1	RPK1 (RECEPTOR-LIKE PROTEIN KINASE 1)	3.52E-05	0.3627035	6
260880_at	At1g21380	AT1G21380	Target of Myb protein 1	4.65E-07	0.3572673	6
245457_s_at	At4g16960	AT4G16940 /// AT4G16960	TIR-NBS-LRR class disease resistance protein	0	0.3478113	6
264506_at	At1g09560	GLP5	GLP5 (GERMIN-LIKE PROTEIN 5)	2.38E-05	0.3465179	6
255344_s_at	At4g04540	CRK39 /// CRK40	putative cysteine-rich receptor-like protein kinase 39	0.000664	0.3440752	6
262119_s_at	At1g02930	ATGSTF6	ATGSTF6 (GLUTATHIONE S-TRANSFERASE)	9.58E-07	0.340758	6
247429_at	At5g62620	AT5G62620	putative beta-1,3-galactosyltransferase	0.000154	0.3398541	6
255543_at	At4g01870	AT4G01870	tolB-related protein	2.88E-06	0.337393	6
246916_at	At5g25910	AtRLP52	AtRLP52 (Receptor Like Protein 52)	9.75E-05	0.336728	6
254253_at	At4g23320	CRK24	cysteine-rich receptor-like protein kinase 24	2.25E-05	0.3360656	6

Table S2. *(Continued)*

Probe ID	Identifier	Gene symbol	Description	BC	CC	Degree
248932_at	At5g46050	PTR3	PTR3 (PEPTIDE TRANSPORTER 3)	1.45E-05	0.3344209	6
251248_at	At3g62150	PGP21	PGP21 (P-GLYCOPROTEIN 21)	9.54E-07	0.3336589	6
256425_at	At1g33560	ADR1	ADR1 (ACTIVATED DISEASE RESISTANCE 1)	5.96E-05	0.3335503	6
251121_at	At3g63420	AGG1	AGG1 (*Arabidopsis* Ggamma-subunit 1)	6.06E-05	0.3315006	6
248312_at	At5g52580	AT5G52580	RabGAP/TBC domain-containing protein	1.89E-05	0.3302191	6
250435_at	At5g10380	RING1	RING1	4.64E-06	0.329053	6
252373_at	At3g48090	EDS1	EDS1 (enhanced disease susceptibility 1)	5.35E-07	0.329053	6
252484_at	At3g46690	AT3G46690	UDP-glycosyltransferase 76E4	6.67E-06	0.3278951	6
266070_at	At2g18660	EXLB3	EXLB3 (EXPANSIN-LIKE B3 PRECURSOR)	0.000959	0.3275807	6
248971_at	At5g45000	AT5G45000	TIR-NBS-LRR class disease resistance protein	3.80E-06	0.3232419	6
265733_at	At2g01190	AT2G01190	Octicosapeptide/Phox/Bem1p family protein	2.54E-05	0.3219221	6
250267_at	At5g12930	AT5G12930	hypothetical protein	7.92E-05	0.3206131	6
247753_at	At5g59070	AT5G59070	glycosyl transferase family protein	4.98E-06	0.3160654	6
245334_at	At4g15800	RALFL33	RALFL33 (ralf-like 33)	6.79E-07	0.3121194	6
247835_at	At5g57910	AT5G57910	hypothetical protein	1.43E-06	0.3114555	6
261860_at	At1g50600	SCL5	SCL5	0.000304	0.3046062	6
257828_at	At3g26670	AT3G26670	hypothetical protein	0.000103	0.3037037	6
257535_at	At3g09490	AT3G09490	tetratricopeptide repeat domain-containing protein	0.00019	0.3008512	6
256233_at	At3g12360	ITN1	ITN1 (INCREASED TOLERANCE TO NACL)	0.000214	0.2921893	6
254425_at	At4g21450	AT4G21450	PapD-like superfamily protein	2.63E-05	0.2780792	6
257025_at	At3g19190	ATG2	unknown protein	4.08E-06	0.2701634	6
259561_at	At1g21250	WAK1	WAK1 (CELL WALL-ASSOCIATED KINASE)	2.05E-05	0.2677638	6
259495_at	At1g15890	AT1G15890	CC-NB-LRR class disease resistance protein	1.85E-06	0.3534483	5

Table S2. *(Continued)*

Probe ID	Identifier	Gene symbol	Description	BC	CC	Degree
266371_at	At2g41410	AT2G41410	putative calcium-binding protein CML35	1.61E-05	0.3532047	5
250670_at	At5g06860	PGIP1	PGIP1 (POLYGALACTURONASE INHIBITING PROTEIN 1)	9.33E-07	0.3506671	5
245765_at	At1g33600	AT1G33600	leucine-rich repeat-containing protein	0.000539	0.3484024	5
245209_at	At5g12340	AT5G12340	hypothetical protein	7.21E-06	0.3475754	5
245370_at	At4g16840	AT4G16840	hypothetical protein	6.24E-07	0.3474576	5
252421_at	At3g47540	AT3G47540	putative chitinase	5.30E-06	0.3466351	5
249777_at	At5g24210	AT5G24210	lipase class 3 family protein	1.02E-05	0.3413253	5
254924_at	At4g11330	ATMPK5	ATMPK5 (MAP KINASE 5)	5.66E-06	0.3413253	5
254385_s_at	At4g21830	ATMSRB7	methionine sulfoxide reductase domain-containing protein	2.97E-06	0.3410982	5
245543_at	At4g15260	AT4G15260	UDP-glycosyltransferase	2.41E-06	0.3404185	5
264780_at	At1g08720	EDR1	EDR1 (ENHANCED DISEASE RESISTANCE 1)	2.58E-05	0.338731	5
258617_at	At3g03000	AT3G03000	putative calcium-binding protein CML18	3.28E-06	0.3366174	5
253953_at	At4g26750	AT4G26750	LYST INTERACTING PROTEIN 5	2.66E-06	0.3363965	5
249730_at	At5g24430	AT5G24430	CDPK-related kinase 4 (AtCRK4)	4.17E-05	0.335296	5
249984_at	At5g18400	AT5G18400	anamorsin homolog	1.10E-06	0.333985	5
252681_at	At3g44350	anac061	anac061 (*Arabidopsis* NAC domain containing protein 61)	6.39E-06	0.3312864	5
247532_at	At5g61560	AT5G61560	U-box domain-containing protein 51	5.25E-06	0.3277902	5
252136_at	At3g50770	CML41	putative calcium-binding protein CML41	9.20E-05	0.327476	5
251528_at	At3g58600	AT3G58600	Adaptin ear-binding coat-associated protein 1 NECAP-1	0.000106	0.3273714	5
260327_at	At1g63840	AT1G63840	RING/U-box domain-containing protein	0.001959404	0.3266412	5
258275_at	At3g15760	AT3G15760	hypothetical protein	2.05E-06	0.3233438	5
262782_at	At1g13195	AT1G13195	RING/U-box domain-containing protein	4.00E-06	0.322733	5
259932_at	At1g34370	STOP1	STOP1 (sensitive to proton rhizotoxicity 1)	3.70E-05	0.3215182	5

Table S2. *(Continued)*

Probe ID	Identifier	Gene symbol	Description	BC	CC	Degree
245760_s_at	At1g66920	AT1G66910 /// AT1G66920	putative protein kinase putative serine/threonine protein kinase	9.56E-05	0.3185208	5
262919_at	At1g79380	AT1G79380	ubiquitin ligase	0.001244993	0.3172392	5
262126_at	At1g59620	CW9	CW9	0.000173	0.3133598	5
250644_at	At5g06750	AT5G06750	putative protein phosphatase 2C	0.001978619	0.3062444	5
255341_at	At4g04500	CRK37	cysteine-rich receptor-like protein kinase 37	2.62E-05	0.3019146	5
259426_at	At1g01470	LEA14	LEA14 (LATE EMBRYOGENESIS ABUNDANT 14)	0.001953339	0.2961572	5
247282_at	At5g64240	AtMC3	AtMC3 (metacaspase 3)	0.002033261	0.2936963	5
254858_at	At4g12070	AT4G12070	hypothetical protein	0.000848	0.2886511	5
256103_at	At1g13540	AT1G13540	hypothetical protein	7.24E-06	0.2819807	5
254521_at	At5g44810	AT5G44820	Nucleotide-diphospho-sugar transferase family protein	0.001966136	0.2819032	5
257989_at	At3g19770	VPS9A	VPS9A	5.42E-07	0.2783057	5
257754_at	At3g18820	ATRAB7B	ATRAB7B (*ARABIDOPSIS* RAB GTPASE HOMOLOG G3F)	3.31E-06	0.2634284	5
258000_at	At3g28940	AT3G28940	AIG2-like protein	0.002121972	0.262484	5
246029_at	At5g21090	AT5G21090	leucine-rich repeat-containing protein	0.00018	0.25	5
265728_at	At2g31990	AT2G31990	Exostosin family protein	4.62E-06	0.3454668	4
254242_at	At4g23200	CRK12	putative cysteine-rich receptor-like protein kinase 12	1.15E-07	0.3383955	4
246214_at	At4g36990	HSF4	HSF4 (HEAT SHOCK FACTOR 4)	2.14E-05	0.3378378	4
256799_at	At3g18560	AT3G18560	hypothetical protein	5.09E-06	0.3327922	4
247630_at	At5g60420	SIZ1	SIZ1	1.34E-05	0.3313935	4
246293_at	At3g56710	SIB1	SIB1 (SIGMA FACTOR BINDING PROTEIN 1)	0	0.329688	4
255627_at	At4g00955	AT4G00955	hypothetical protein	2.47E-07	0.3291586	4
263459_at	At2g31820	AT2G31820	ankyrin repeats-containing protein	3.73E-06	0.3243671	4
249940_at	At5g22380	anac090	anac090 (*Arabidopsis* NAC domain containing protein 90)	9.12E-07	0.323957	4

Table S2. *(Continued)*

Probe ID	Identifier	Gene symbol	Description	BC	CC	Degree
253140_at	At4g35480	RHA3B	RHA3B	1.59E-05	0.3192152	4
249393_at	At5g40170	AtRLP54	AtRLP54 (Receptor Like Protein 54)	0.000494	0.3148034	4
267375_at	At2g26300	GP ALPHA 1	GP ALPHA 1 (G PROTEIN ALPHA SUBUNIT 1)	5.82E-06	0.3128816	4
249459_at	At5g39580	AT5G39580	peroxidase 62	1.93E-05	0.3090142	4
252037_at	At3g51920	CAM9	CAM9 (CALMODULIN 9)	1.69E-05	0.308828	4
252684_at	At3g44400	AT3G44400	TIR-NBS-LRR class disease resistance protein	2.04E-06	0.3069781	4
267392_at	At2g44490	PEN2	PEN2 (PENETRATION 2)	1.12E-05	0.3062444	4
254331_s_at	At4g22710	CYP706A2	CYP706A2	2.11E-05	0.3054231	4
251773_at	At3g55960	AT3G55960	Haloacid dehalogenase-like hydrolase (HAD) superfamily protein	0.001958106	0.3052412	4
257621_at	At3g20410	CPK9	CPK9 (calmodulin-domain protein kinase 9)	6.33E-05	0.3038838	4
254248_at	At4g23270	CRK19	cysteine-rich receptor-like protein kinase 19	4.43E-05	0.302896	4
260852_at	At1g21900	AT1G21900	p24 subfamily delta 5	0.000951	0.3023599	4
259745_at	At1g71190	SAG18	SAG18 (SENESCENCE ASSOCIATED GENE 18)	5.27E-06	0.2920228	4
254266_at	At4g23130	CRK5	CRK5 (CYSTEINE-RICH RLK5)	7.30E-05	0.2802844	4
259925_at	At1g75040	PR5	PR5 (PATHOGENESIS-RELATED GENE 5)	0	0.27952	4
266911_at	At2g45910	AT2G45910	U-box domain-containing protein 33	1.27E-07	0.2618135	4
250298_at	At5g11860	SSP5	SCP1-like small phosphatase 5	2.40E-06	0.2596251	4
247448_at	At5g62770	AT5G62770	hypothetical protein	1.91E-06	0.3516295	3
259734_at	At1g77500	AT1G77500	hypothetical protein	1.75E-07	0.3452341	3
253173_at	At4g35110	AT4G35110	phospholipase-like (PEARLI 4) family protein	0	0.3430388	3
261110_at	At1g75440	UBC16	UBC16 (ubiquitin-conjugating enzyme 16)	2.71E-06	0.3403054	3
256231_at	At3g12630	AT3G12630	E3 ligase SAP5	4.96E-06	0.339404	3
264522_at	At1g10050	AT1G10050	putative glycosyl hydrolase	6.18E-06	0.338731	3

Table S2. *(Continued)*

Probe ID	Identifier	Gene symbol	Description	BC	CC	Degree
260829_s_at	At1g06870	AT1G06870 /// TPP	putative thylakoidal processing peptidase 2 thylakoid processing peptide	0	0.3311793	3
257690_at	At3g12830	AT3G12830	SAUR-like auxin-responsive protein	5.29E-07	0.3271625	3
246976_s_at	At5g24810	AT5G24810	ABC1 family protein	4.20E-07	0.3263292	3
258063_at	At3g14620	CYP72A8	CYP72A8	1.88E-05	0.3249841	3
251282_at	At3g61630	CRF6	CRF6 (CYTOKININ RESPONSE FACTOR 6)	9.73E-07	0.3219221	3
254559_at	At4g19200	AT4G19200	proline-rich family protein	1.41E-05	0.3199126	3
247104_at	At5g66620	DAR6	DAR6 (DA1-RELATED PROTEIN 6)	0	0.3178295	3
260005_at	At1g67920	AT1G67920	hypothetical protein	0	0.3175341	3
261899_at	At1g80820	CCR2	CCR2 (CINNAMOYL COA REDUCTASE)	0	0.3172392	3
265034_at	At1g61660	AT1G61660	transcription factor bHLH112	4.67E-06	0.316945	3
246831_at	At5g26340	MSS1	MSS1	0	0.3159679	3
260303_at	At1g70520	CRK2	cysteine-rich receptor-like protein kinase 2	5.68E-05	0.3151907	3
255511_at	At4g02075	PIT1	PIT1 (pitchoun 1)	0	0.3052412	3
249321_at	At5g40920	---	---	0.00195122	0.3046968	3
260362_at	At1g70530	CRK3	cysteine-rich receptor-like protein kinase 3	2.36E-05	0.3039739	3
258544_at	At3g07040	RPM1	RPM1 (RESISTANCE TO P. SYRINGAE PV MACULICOLA 1)	7.76E-07	0.3037037	3
253332_at	At4g33420	AT4G33420	probable peroxidase	2.26E-05	0.3017368	3
263806_at	At2g04305	AT2G04305	Magnesium transporter CorA-like family protein	2.95E-06	0.3017368	3
258049_at	At3g16220	AT3G16220	putative eukaryotic LigT protein	0.00202072	0.3015593	3
260651_at	At1g32460	AT1G32460	hypothetical protein	1.11E-05	0.3015593	3
251916_at	At3g53960	AT3G53960	probable peptide/nitrate transporter	3.32E-06	0.3014706	3
265040_at	At1g03970	GBF4	GBF4	5.28E-06	0.3007629	3
251621_at	At3g57700	AT3G57700	putative protein kinase	3.18E-06	0.2978785	3

Table S2. *(Continued)*

Probe ID	Identifier	Gene symbol	Description	BC	CC	Degree
248994_at	At5g45250	RPS4	RPS4 (RESISTANT TO P. SYRINGAE 4)	0	0.294964	3
255895_at	At1g17990	AT1G17990 /// AT1G18020	putative 12-oxophytodienoate reductase-like protein 2A	2.63E-06	0.2926899	3
248330_at	At5g52810	AT5G52810	NAD(P)-binding Rossmann-fold superfamily protein	0.000172	0.2852769	3
247604_at	At5g60950	COBL5	COBL5 (COBRA-LIKE PROTEIN 5 PRECURSOR)	1.49E-06	0.2850389	3
252462_at	At3g47250	AT3G47250	hypothetical protein	3.60E-05	0.2836978	3
263221_at	At1g30620	MUR4	MUR4 (MURUS 4)	7.47E-07	0.2801312	3
252915_at	At4g38810	AT4G38810	SnRK2-interacting calcium sensor SCS	0	0.2760571	3
250803_at	At5g04980	AT5G04980	DNAse I-like superfamily protein	4.21E-05	0.2743576	3
266737_at	At2g47140	AT2G47140	short-chain dehydrogenase reductase 5	0	0.2736252	3
259992_at	At1g67970	HSFA8	AT-HSFA8	3.27E-05	0.2686763	3
260671_at	At1g19310	AT1G19310	RING/U-box superfamily protein	2.00E-05	0.2654753	3
246009_at	At5g08335	ATSTE14B	ATSTE14B	0	0.328	2
266968_at	At2g39360	AT2G39360	putative receptor-like protein kinase	0	0.3202124	2
246796_at	At5g26770	AT5G26770	hypothetical protein	3.64E-05	0.3172392	2
260919_at	At1g21520	AT1G21520	hypothetical protein	0	0.3158706	2
257805_at	At3g18830	ATPLT5	ATPLT5 (POLYOL TRANSPORTER 5)	0	0.3155788	2
250999_at	At5g02630	AT5G02630	Lung seven transmembrane receptor family protein	0	0.308642	2
259071_at	At3g11650	NHL2	NHL2	0	0.3082707	2
246146_at	At5g20050	AT5G20050	putative receptor-like protein kinase	0	0.3055142	2
255596_at	At4g01720	WRKY47	WRKY47	0	0.3052412	2
258731_at	At3g11880	AT3G11880	hypothetical protein	1.06E-05	0.3037937	2
254247_at	At4g23260	CRK18	cysteine-rich receptor-like protein kinase 18	1.34E-05	0.3031647	2
258262_at	At3g15770	AT3G15770	hypothetical protein	0	0.3023599	2

Table S2. *(Continued)*

Probe ID	Identifier	Gene symbol	Description	BC	CC	Degree
260211_at	At1g74440	AT1G74440	hypothetical protein	3.43E-07	0.3021816	2
255039_at	At4g09570	CPK4	CPK4	1.81E-07	0.3007629	2
250692_at	At5g06560	AT5G06560	hypothetical protein	0	0.2997076	2
264685_at	At1g65610	KOR2	KOR2	0	0.29962	2
251879_at	At3g54200	AT3G54200	late embryogenesis abundant hydroxyproline-rich glycoprotein	0	0.2990954	2
263722_at	At2g13650	GONST1	GONST1 (Golgi Nucleotide Sugar Transporter 1)	0.003898628	0.298312	2
264624_at	At1g08930	ERD6	ERD6 (EARLY RESPONSE TO DEHYDRATION 6)	0	0.2981385	2
258100_at	At3g23550	AT3G23550	MATE efflux family protein LAL5	1.81E-06	0.2968433	2
252378_at	At3g47570	AT3G47570	putative LRR receptor-like serine/threonine-protein kinase	0	0.2944556	2
263582_at	At2g17120	LYM2	LYM2 (LYSM DOMAIN GPI-ANCHORED PROTEIN 2 PRECURSOR)	0	0.2943711	2
247389_at	At5g63490	AT5G63490	CBS / octicosapeptide/Phox/Bemp1 domain-containing protein	0	0.2922726	2
254244_at	At4g23230	CRK15	cysteine-rich receptor-like protein kinase 15	0	0.2884074	2
265479_at	At2g15760	AT2G15760	hypothetical protein	0	0.2851182	2
253204_at	At4g34460	AGB1	AGB1 (GTP BINDING PROTEIN BETA 1)	0	0.2848013	2
258084_at	At3g26020	AT3G26020	protein phosphatase 2A regulatory subunit B′ eta	0	0.2812843	2
253997_at	At4g26090	RPS2	RPS2 (RESISTANT TO P. SYRINGAE 2)	1.04E-05	0.2805913	2
257734_at	At3g18370	ATSYTF	ATSYTF	0	0.2777025	2
265433_at	At2g20950	AT2G20950	phospholipase-like protein (PEARLI 4) domain-containing protein	2.40E-06	0.2756117	2
245768_at	At1g33590	AT1G33590	leucine-rich repeat (LRR) family protein	2.10E-06	0.2754636	2
258537_at	At3g04210	AT3G04210	TIR-NBS class disease resistance protein	0	0.2682544	2
262076_at	At1g59580	ATMPK2	ATMPK2 (*ARABIDOPSIS* THALIANA MITOGEN-ACTIVATED PROTEIN KINASE HOMOLOG 2)	5.18E-06	0.2668576	2
262374_s_at	At1g72930	TIR	TIR (TOLL/INTERLEUKIN-1 RECEPTOR-LIKE)	0.00195122	0.2647895	2

Table S2. *(Continued)*

Probe ID	Identifier	Gene symbol	Description	BC	CC	Degree
261176_at	At1g04780	AT1G04780	ankyrin repeat-containing protein	7.03E-06	0.2643115	2
263631_at	At2g04900	AT2G04900	hypothetical protein	0	0.2636995	2
256058_at	At1g07240	UGT71C5	UGT71C5 (UDP-GLUCOSYL TRANSFERASE 71C5)	0.000103	0.2617467	2
263583_at	At2g17130	IDH2	IDH2 (ISOCITRATE DEHYDROGENASE SUBUNIT 2)	3.70E-05	0.2613463	2
260993_at	At1g12140	FMO GS-OX5	FMO GS-OX5 (FLAVIN-MONOOXYGENASE GLUCOSINOLATE S-OXYGENASE 5)	9.74E-07	0.2610135	2
252549_at	At3g45860	CRK4	cysteine-rich receptor-like protein kinase 4	0	0.2606816	2
265993_at	At2g24160	---	---	0	0.2606816	2
264999_at	At1g67310	AT1G67310	calmodulin-binding transcription activator 4	3.07E-06	0.2554199	2
266385_at	At2g14610	PR1	PR1 (PATHOGENESIS-RELATED GENE 1)	0	0.2552291	2
265659_at	At2g25440	AtRLP20	AtRLP20 (Receptor Like Protein 20)	2.97E-06	0.2449809	2
267165_at	At2g37710	RLK	RLK (receptor lectin kinase)	1.29E-05	0.2367206	2
253646_at	At4g29810	ATMKK2	ATMKK2 (*ARABIDOPSIS* THALIANA MAP KINASE KINASE 2)	0	0.2307519	2
248769_at	At5g47730	AT5G47730	Sec14p-like phosphatidylinositol transfer family protein	0.00195122	0.2299237	2
262926_s_at	At1g65790	ARK1	ARK1 (A. THALIANA RECEPTOR KINASE 1)	3.18E-07	0.2231657	2
247874_at	At5g57710	AT5G57710	protein SUPPRESSOR OF MAX2 1	0	0.335296	1
257766_at	At3g23030	IAA2	IAA2 (INDOLE-3-ACETIC ACID INDUCIBLE 2)	0	0.335296	1
251705_at	At3g56400	WRKY70	WRKY70	0	0.3166512	1
254291_at	At4g23010	UTR2	UDP-galactose transporter-related	0	0.3154817	1
264756_at	At1g61370	AT1G61370	S-locus lectin protein kinase family protein	0	0.3097613	1
258616_at	At3g02880	AT3G02880	leucine-rich repeat protein kinase family protein	0	0.3021816	1
261836_at	At1g16090	WAKL7	WAKL7 (wall associated kinase-like 7)	0	0.3012048	1
249029_at	At5g44870	AT5G44870	TIR-NBS-LRR class disease resistance protein LAZ5	0	0.2997953	1

Table S2. *(Continued)*

Probe ID	Identifier	Gene symbol	Description	BC	CC	Degree
258566_at	At3g04110	GLR1.1	GLR1.1 (GLUTAMATE RECEPTOR 1.1)	0	0.2994449	1
251643_at	At3g57550	AGK2	AGK2 (GUANYLATE KINASE)	0	0.2991827	1
248415_at	At5g51620	AT5G51620	hypothetical protein	0	0.2987467	1
252832_at	At4g39910	ATUBP3	ATUBP3 (*ARABIDOPSIS* THALIANA UBIQUITIN-SPECIFIC PROTEASE 3)	0	0.2987467	1
248851_s_at	At5g46490	AT5G46260 /// AT5G46490	TIR-NBS-LRR class disease resistance protein	0	0.2961572	1
267486_at	At2g02800	APK2B	APK2B (PROTEIN KINASE 2B)	0	0.2936963	1
256129_at	At1g18210	AT1G18210	putative calcium-binding protein CML27	0	0.2847222	1
260103_at	At1g35430	AT1G35430	hypothetical protein	0	0.2847222	1
255742_at	At1g25560	TEM1	TEM1 (TEMPRANILLO 1)	0	0.2836193	1
265810_at	At2g18090	AT2G18090	PHD finger, SWIB/MDM2 and GYF domain-containing protein	0	0.2832274	1
263145_at	At1g54090	ATEXO70D2	ATEXO70D2 (exocyst subunit EXO70 family protein D2)	0	0.2806681	1
261402_at	At1g79670	RFO1	RFO1 (RESISTANCE TO FUSARIUM OXYSPORUM 1)	0	0.2805913	1
267104_at	At2g41430	ERD15	ERD15 (EARLY RESPONSIVE TO DEHYDRATION 15)	0	0.2764293	1
256891_at	At3g19030	AT3G19030	hypothetical protein	0	0.2747989	1
257545_at	At3g23200	AT3G23200	hypothetical protein	0	0.2656817	1
245740_at	At1g44100	AAP5	AAP5	0	0.2632255	1
245266_at	At4g17070	AT4G17070	peptidyl-prolyl cis-trans isomerase	0	0.2586424	1
248521_s_at	At5g50630	AT5G50520 /// AT5G50630	major facilitator protein major facilitator protein	0	0.2507339	1
249581_at	At5g37600	GSR 1	ATGSR1	0	0.2503053	1
250090_at	At5g17330	GAD	GAD	0	0.246869	1
264005_at	At2g22470	AGP2	AGP2 (ARABINOGALACTAN PROTEIN 2)	0	0.2462758	1
249806_at	At5g23850	AT5G23850	hypothetical protein	0	0.2345001	1

Table S2. *(Continued)*

Probe ID	Identifier	Gene symbol	Description	BC	CC	Degree
248195_at	At5g54110	ATMAMI	ATMAMI (*ARABIDOPSIS* THALIANA MEMBRANE-ASSOCIATED MANNITOL-INDUCED)	0	0.2339115	1
249320_at	At5g40910	AT5G40910	TIR-NBS-LRR class disease resistance protein	0	0.2335916	1
259752_at	At1g71040	LPR2	LPR2 (Low Phosphate Root2)	0	0.2317432	1
264787_at	At2g17840	ERD7	ERD7 (EARLY-RESPONSIVE TO DEHYDRATION 7)	0	0.2285396	1
266265_at	At2g29340	AT2G29340	tropinone reductase-like protein	0	0.2270713	1
258401_at	At3g15430	AT3G15430	regulator of chromosome condensation 1	0	0.2265694	1
249021_at	At5g44820	AT5G44820	Nucleotide-diphospho-sugar transferase family protein	0	0.2199571	1
247419_at	At5g63080	AT5G63080	HR demethylase JMJ20	0	0.2175297	1
258614_at	At3g02770	AT3G02770	ribonuclease E inhibitor RraA/Dimethylmenaquinone methyltransferase	0	0.2154267	1
249480_s_at	At5g38990	AT5G38990 /// AT5G39000	putative receptor-like protein kinase putative receptor-like protein kinase	0	0.2093973	1
250339_at	At5g11670	ATNADP-ME2	ATNADP-ME2 (NADP-malic enzyme 2)	0	0.2079529	1
252652_at	At3g44720	ADT4	ADT4 (arogenate dehydratase 4)	0	0.1869756	1

Genes ordered according to their number of connections (degrees). BC: betweenness centrality, CC: closeness centrality.

Table S3. Go-slim analysis of the network, by cellular component.

	Arabidopsis (reference)		In the network			
PANTHER GO-Slim Cellular Component	#	#	expected	Fold enrichment	p-value	FDR
extrinsic component of cytoplasmic side of plasma membrane (GO:0031234)	5	3	0.18	16.44	2.13E-03	2.65E-02
extrinsic component of plasma membrane (GO:0019897)	5	3	0.18	16.44	2.13E-03	2.57E-02
cytoplasmic side of plasma membrane (GO:0009898)	9	4	0.33	12.18	8.47E-04	1.29E-02
ESCRT I complex (GO:0000813)	9	4	0.33	12.18	8.47E-04	1.24E-02
cytoplasmic side of membrane (GO:0098562)	15	4	0.55	7.31	3.88E-03	3.67E-02
side of membrane (GO:0098552)	15	4	0.55	7.31	3.88E-03	3.58E-02
leaflet of membrane bilayer (GO:0097478)	15	4	0.55	7.31	3.88E-03	3.50E-02
exocyst (GO:0000145)	36	7	1.31	5.33	6.99E-04	1.16E-02
endosome membrane (GO:0010008)	47	9	1.72	5.25	1.37E-04	3.89E-03
late endosome (GO:0005770)	36	6	1.31	4.57	3.33E-03	3.39E-02
vesicle tethering complex (GO:0099023)	67	8	2.45	3.27	4.82E-03	4.26E-02
cytoplasmic vesicle membrane (GO:0030659)	104	11	3.8	2.9	2.48E-03	2.74E-02
vesicle membrane (GO:0012506)	104	11	3.8	2.9	2.48E-03	2.66E-02
endosome (GO:0005768)	158	16	5.77	2.77	4.56E-04	9.05E-03
intracellular vesicle (GO:0097708)	278	23	10.15	2.27	6.94E-04	1.25E-02
cytoplasmic vesicle (GO:0031410)	278	23	10.15	2.27	6.94E-04	1.20E-02
cell periphery (GO:0071944)	2092	141	76.34	1.85	8.51E-12	1.13E-09
plasma membrane (GO:0005886)	1918	129	69.99	1.84	9.15E-11	9.08E-09

Table S4. Go-slim analysis of the network, by biological process.

	Arabidopsis thaliana (REF)		In the network			
PANTHER GO-Slim Biological Process	#	#	expected	Fold enrichment	p-value	FDR
phospholipid translocation (GO:0045332)	13	4	0.47	8.43	2.52E-03	4.59E-02
multivesicular body sorting pathway (GO:0071985)	27	7	0.99	7.1	1.54E-04	5.22E-03
protein autophosphorylation (GO:0046777)	65	14	2.37	5.9	6.07E-07	6.48E-05
vesicle fusion to plasma membrane (GO:0099500)	55	11	2.01	5.48	1.78E-05	1.06E-03
exocytic process (GO:0140029)	55	11	2.01	5.48	1.78E-05	1.02E-03
exocytosis (GO:0006887)	55	11	2.01	5.48	1.78E-05	9.86E-04
response to external biotic stimulus (GO:0043207)	68	13	2.48	5.24	4.83E-06	4.51E-04
response to other organism (GO:0051707)	68	13	2.48	5.24	4.83E-06	4.25E-04
response to biotic stimulus (GO:0009607)	68	13	2.48	5.24	4.83E-06	4.01E-04
defense response to other organism (GO:0098542)	68	13	2.48	5.24	4.83E-06	3.80E-04
cell surface receptor signaling pathway (GO:0007166)	37	7	1.35	5.18	8.06E-04	2.01E-02
biological process involved in interspecies interaction between organisms (GO:0044419)	72	13	2.63	4.95	8.35E-06	5.94E-04
secretion by cell (GO:0032940)	61	11	2.23	4.94	4.13E-05	2.13E-03
export from cell (GO:0140352)	61	11	2.23	4.94	4.13E-05	2.06E-03
secretion (GO:0046903)	61	11	2.23	4.94	4.13E-05	1.99E-03
defense response (GO:0006952)	102	16	3.72	4.3	3.99E-06	3.98E-04
response to external stimulus (GO:0009605)	113	16	4.12	3.88	1.27E-05	7.93E-04
endosomal transport (GO:0016197)	59	8	2.15	3.72	2.38E-03	4.40E-02
organelle fusion (GO:0048284)	98	13	3.58	3.64	1.46E-04	5.09E-03
peptidyl-serine phosphorylation (GO:0018105)	93	12	3.39	3.54	3.28E-04	1.00E-02
peptidyl-serine modification (GO:0018209)	93	12	3.39	3.54	3.28E-04	9.80E-03
vesicle fusion (GO:0006906)	94	12	3.43	3.5	3.58E-04	1.05E-02

Table S4. *(Continued)*

	Arabidopsis thaliana (REF)			In the network		
organelle membrane fusion (GO:0090174)	97	12	3.54	3.39	4.63E-04	1.28E-02
membrane fusion (GO:0061025)	101	12	3.69	3.26	6.43E-04	1.66E-02
signal transduction (GO:0007165)	442	46	16.13	2.85	1.71E-09	3.65E-07
signaling (GO:0023052)	447	46	16.31	2.82	2.36E-09	4.41E-07
intracellular signal transduction (GO:0035556)	206	21	7.52	2.79	5.84E-05	2.64E-03
cell communication (GO:0007154)	472	48	17.22	2.79	1.51E-09	3.76E-07
protein phosphorylation (GO:0006468)	344	32	12.55	2.55	5.83E-06	4.36E-04
vesicle organization (GO:0016050)	197	17	7.19	2.36	2.04E-03	3.97E-02
phosphorylation (GO:0016310)	406	35	14.82	2.36	9.87E-06	6.71E-04
membrane organization (GO:0061024)	303	25	11.06	2.26	3.71E-04	1.07E-02
vesicle-mediated transport (GO:0016192)	390	28	14.23	1.97	1.17E-03	2.78E-02
cellular response to stimulus (GO:0051716)	796	56	29.05	1.93	1.08E-05	7.04E-04
response to stimulus (GO:0050896)	1098	76	40.07	1.9	3.85E-07	4.42E-05
phosphate-containing compound metabolic process (GO:0006796)	811	53	29.6	1.79	1.04E-04	3.88E-03
phosphorus metabolic process (GO:0006793)	826	53	30.14	1.76	1.73E-04	5.76E-03
cellular protein modification process (GO:0006464)	1062	65	38.76	1.68	9.74E-05	4.05E-03
protein modification process (GO:0036211)	1062	65	38.76	1.68	9.74E-05	3.94E-03

Table S5. Go-slim analysis of the network, by molecular function.

	Arabidopsis thaliana (REF)	In the network				
PANTHER GO-Slim Molecular Function	#	#	expected	Fold enrichment	p-value	FDR
calmodulin binding (GO:0005516)	48	13	1.75	7.42	1.62E-07	8.90E-06
calcium ion binding (GO:0005509)	69	11	2.52	4.37	1.11E-04	3.76E-03
protein kinase activity (GO:0004672)	431	43	15.73	2.73	1.79E-08	3.94E-06
protein serine/threonine kinase activity (GO:0004674)	323	32	11.79	2.71	1.35E-06	6.58E-05
kinase activity (GO:0016301)	571	51	20.84	2.45	2.86E-08	4.19E-06
phosphotransferase activity, alcohol group as acceptor (GO:0016773)	534	47	19.49	2.41	1.46E-07	9.20E-06
transferase activity, transferring phosphorus-containing groups (GO:0016772)	697	52	25.44	2.04	4.29E-06	1.89E-04
catalytic activity, acting on a protein (GO:0140096)	1305	80	47.62	1.68	1.76E-05	7.02E-04

Table S6. Primers used.

name	SOL-number	gene ID	sequence
SlBON1A_Fw	SO33	Solyc03g118200	caccATGGGAAATTGCTGCTCTG
SlBON1A_Rv	SO34		CAAAGTTGGCTGTATCTTTCTGGA
SlBON1B_Fw	SO31	Solyc06g068840	caccATGGGAAATTGCTGCTCC
SlBON1B_Rv	SO32		AGTTGGCTGGATCCTTTTGAG
SlXLG1_FW	SO53	Solyc02g090160	caccATGTCGCCGGAACTGG
SlXLG1_RV	SO54		AGGTGAGAAGGAACTTGCATC
SlXLG2_FW	SO9	Solyc01g109110	caccATGGCTGCAATCTTGAAAAGTCTTTTCCC
SlXLG2_RV	SO10		TGTAGTTGTGCTAGCCTCCAGTGTTG
SlXLG3_FW	SO11	Solyc08g076160	caccATGGAGAAAAAAGATGGAGAGCATTGGAAG
SlXLG3_RV	SO12		CTCCTGTCGGAAGAAAGGAGACGAG

Table S6. *(Continued)*

name	SOL-number	gene ID	sequence
SlXLG4_FW	MO1	Solyc03g097980	caccATGACTGAGCCATACGC
SlXLG4_RV	MO2		ATCGTTAAAAGAAATGCTATACTCC
SlGPA1_Fw	MO3	Solyc08g061220	caccATGCTGTCGGTGGTTTTC
SlGPA1_Rv	MO4		TAATAAACCTGCTTCGAAGAGA
vigs_NbBON1A	SO35	Niben101Scf06621g02031 Niben101Scf03548g02007	CTTATCtctagaTGGCCCAGTTTCTCATTGC
vigs_NbBON1A	SO36		CTTATCggtaccactagtCGAAATACTTCCGCTCACTG
vigs_NbBON1B	SO37	Niben101Scf01596g06002 Niben101Scf14233g00013	CTTATCtctagaAGGCCAAATGCTTATCAGAAAG
vigs_NbBON1B	SO38		CTTATCggtaccactagtAAATGAAACATTAAAAAGGGCACTC
vigs_NbXLG1_Fw	MO5	Niben101Scf05674g05014	actgatctagaCAGGTCTATATAAATGGCCGTG
vigs_NbXLG1_Rv	MO6		atcagctcgaggctagcACTGGAAGAGAGAGTACGG
vigs_NbXLG1_Fw	MO43		CAGGTCTATATAAATGGCCGTGAG
vigs_NbXLG1_Rv	Mo44		ACTGGAAGAGAGAGTACGGCACA
vigs_NbXLG2a_Fw	SO21	Niben101Scf04383g01013	tctagaCCCGACTGCCTCAGTTGTTGC
vigs_NbXLG2a_Rv	SO22		ccatgggctagcAGGTACCAGAACTTTCAATTCCATCTGATACTC
vigs_NbXLG2b_Fw	SO23	Niben101Scf00372g05021	tctagaCGGGAAATTACACAAGTAGAGCTGTTGATG
vigs_NbXLG2b_Rv	SO24		ccatgggctagcCACTGCACGAGTCACCTACATCC
vigs_NbXLG2ab_Fw	MO36	Niben101Scf04383g01013 Niben101Scf00372g05021	TCTAGACCCGACTGCCTCA
vigs_NbXLG2ab_Rv	MO37		CGGGAAATTACACAAGTAGAGC
vigs_NbXLG3_Fw	SO25	Niben101Scf01202g02006 Niben101Scf06100g02001	tctagaGAATTTCTCAGATTGGCTACTGGATATTATAGCAACCG
vigs_NbXLG3_Rv	SO26		ccatgggctagcCCTTGGGTAACTCCTTCTGCATACAAAATGTC
vigs_NbXLG4_FW	MO7	Niben101Scf04286g01030 Niben101Scf01249g03025	actgatctagaCCTGATACTGCTAAATATTTCCTG
vigs_NbXLG4_Rv	MO8		atcagctcgaggctagcCTTGGTCCAAGGAGGTTC
vigs_NbXLG4_RV	MO9		CTTGGTCCAAGGAGGTTCG

Table S6. *(Continued)*

name	SOL-number	gene ID	sequence
vigs_NbGPA1_FW	MO31	Niben101Scf06028g00007 niben101scf01380g03018	GGATGAAAGAAAGAACCGAATG
vigs_NbGPA1_RV	MO32		CAATCTCTTGTTTTCCTGTTGAAA
vigs_NbAGB1_Fw	SO27	Niben101Scf04778g02017 Niben101Scf06726g00032	tctagaGCCTTCTCTCCTAGTGGGCAGTC
vigs_NbAGB1_Rv	SO28		ccatgggctagcAGTTATATCCCAAAGAACACATGTTTGATCACCAGAAC
vigs_NbXLG3_overhangXLG2_Fw	MO38		TCTACTTGTGTAATTTCCCGGAATTTCTCAGATTGGCTACTG
vigs_NbXLG3_overhangXLG1_Fw	MO39		GCCGTACTCTCTCTTCCAGTGAATTTCTCAGATTGGCTACTG
vigs_NbXLG2_overhangXLG1_Fw	MO40		GCCGTACTCTCTCTTCCAGTCCCGACTGCCTCAGTT
vigs_NbGPA1_overhangXLG3_Fw	MO41		GCAGAAGGAGTTACCCAAGGGGATGAAAGAAAGAACCGAATG
vigs_NbXLG4_overhangXLG3_Fw	MO42		GCAGAAGGAGTTACCCAAGGCCTGATACTGCTAAATATTTCCTG
vigs_NbRBOHB_Fw	SO55	Niben101Scf02581g04013 Niben101Scf07345g00016	CTTATCtctagaAGTCTAAGGAATTTGCTGTAGAGCTATATGATGCG
vigs_NbRBOHB_Rv	SO56		CTTATCggtaccactagtGGTTGTTAGGATCCAACTCTTC
vigs_NbRBOHE_Fw	SO181	Niben101Scf09262g00001 Niben101Scf02437g06007	CGACGACGTCAAACTCTCG
vigs_NbRBOHE_Rv	SO182		AAACGTGATCATCATCCACGTC

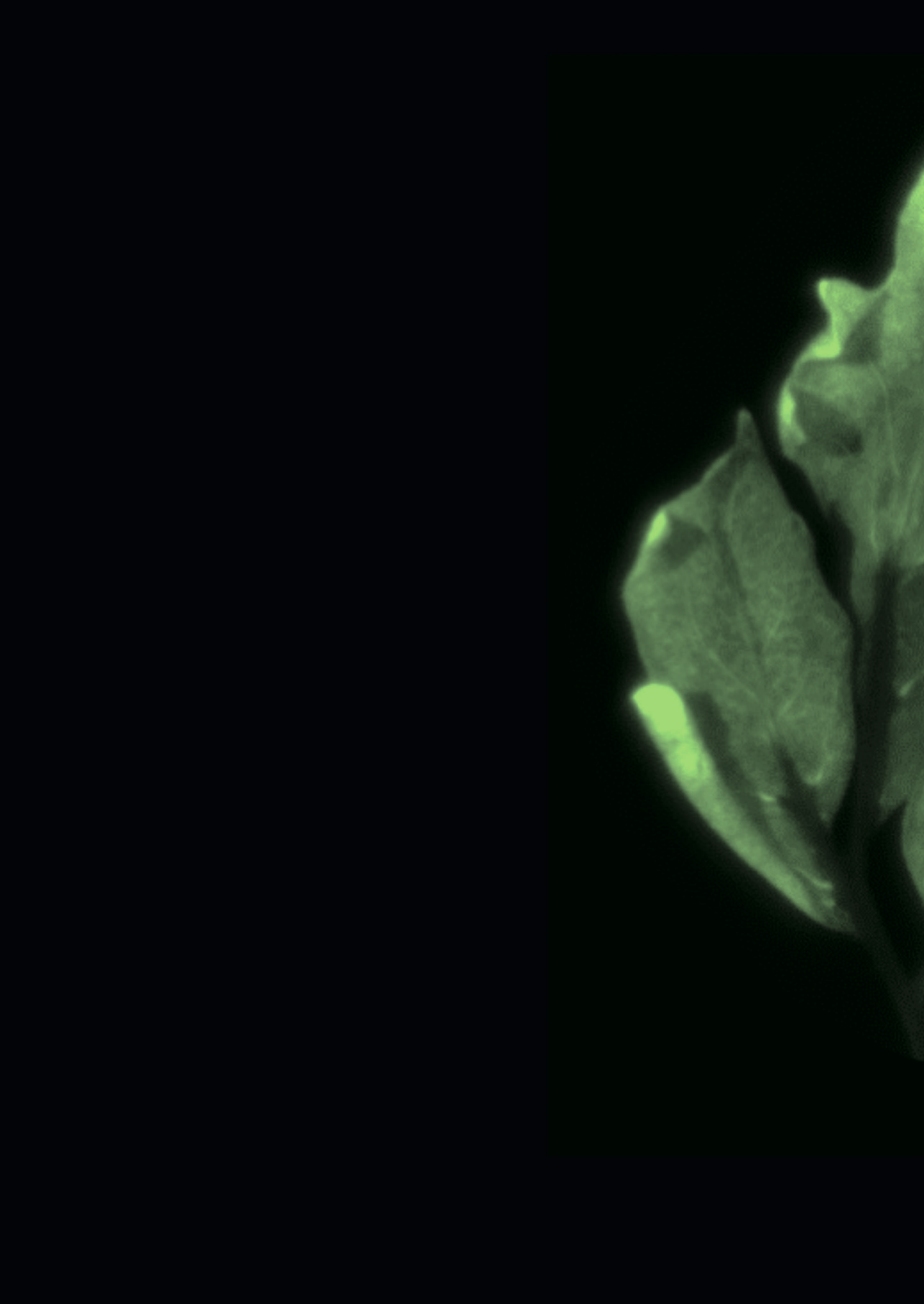

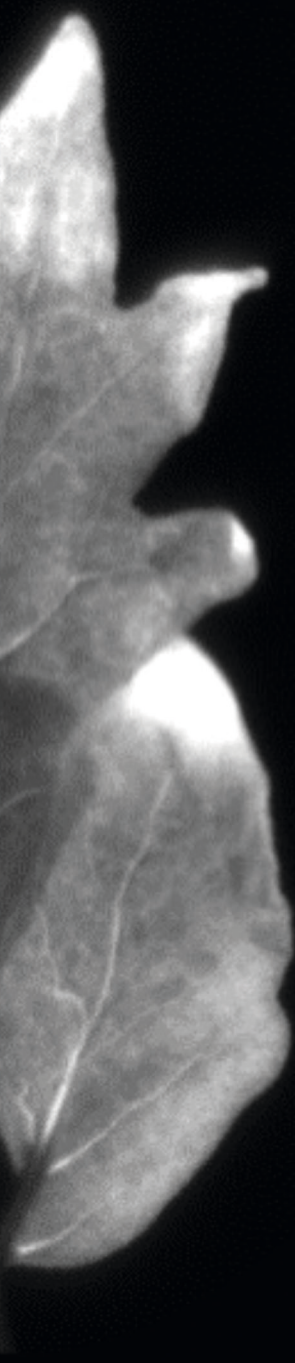

CHAPTER 4

Implementation of TurboID-based proximity-dependent labelling of cell-surface receptor complexes in *Nicotiana benthamiana*

Sergio Landeo Villanueva[a], José Juan Piña[a], Christiaan Schol[a], Esranur Budak[a], Casper ter Waarbeek[a], Matthieu H.A.J. Joosten[a]

[a] Laboratory of Phytopathology, Wageningen University & Research, Droevendaalsesteeg 1, 6708 PB Wageningen, The Netherlands

ABSTRACT

Studies on the molecular mechanisms mediating the perception of pathogens by cell-surface receptors, and the composition of the downstream signalling cascade that is subsequently activated, often requires the detection of weak and transient protein interactions with membrane-bound proteins. Frequently used methods for unbiased detection of protein-protein interactions, such as yeast-based screenings and affinity purification followed by mass spectrometry, have limitations that affect their applicability for the study of the interactions of cytoplasmic signalling partners with cell-surface receptors in plants. Recently, proximity-dependent biotinylation has emerged as an alternative technique to identify interactors based on their physical proximity to a protein of interest. In this study, we implemented the use of the biotin ligase TurboID (TbID) for the dissection of the Cf-4/SOBIR1 cell-surface receptor complex in *Nicotiana benthamiana*. We generated a series of constructs encoding signalling-competent TbID-tagged fusion proteins, adapted a protocol for proximity-dependent biotinylation *in planta,* and showed that TbID-tagged fusion proteins can specifically biotinylate cell-surface receptor on the cytoplasmic or the apoplastic side of the plasma membrane. These results show that proximity-dependent labelling not only can be used for the dissection of receptor complexes by mass spectrometry, but it could also allow for the identification of an unknown cell-surface receptor of a particular effector in resistant plants.

INTRODUCTION

As introduced in Chapter 1, defence against pathogens is based on the perception of danger signals and the subsequent activation of immune responses [170]. In plants, the first layer of the immune system comprises a plethora of cell-surface receptors at the plasma membrane (PM) [20]. These immune receptors perform their biological function through the swift recruitment of additional signalling partners upon signal perception, which are either cell-surface co-receptors or components that form part of the downstream signalling cascade [25]. Hence, the elucidation of what kind of protein-protein interactions occur upon pathogen perception and subsequent initiation of downstream signalling, represents a key aspect of the studies on deciphering the molecular mechanisms that form the basis of the first line of the plant immune response.

Frequently used methods for unbiased detection of interacting proteins in plants include yeast two-hybrid (Y2H) and split-ubiquitin screens, as well as affinity purification of the protein of interest, followed by mass spectrometry (AP-MS) [313,314]. These techniques all face significant drawbacks that limit their applicability. The Y2H method is, for example, based on the ability of hybrid transcription factor domains to associate with, and activate the expression of, reporter genes in the nucleus of yeast cells. Hence, this technique requires the interaction partners to localize in the nucleus, which is a very different environment from that of immune receptor complexes that are localised at the PM of plants. The split-ubiquitin yeast system represents an alternative method that is more suitable for the identification of proteins interacting with membrane-associated proteins [315,316]. This system is based on the co-expression of two split fragments of ubiquitin, which is a highly conserved eukaryotic protein involved in protein degradation [317]. Once reconstituted, ubiquitin-specific proteases cleave the ubiquitin from the reconstituted complex, allowing the release of a reporter transcription factor. This approach has been successfully implemented to identify interactions with membrane-associated proteins involved in plant immune responses [244,318–321]. However, as is for the case of Y2H, the split-ubiquitin system involves the screening of a cDNA library in yeast cells, making these methods prone to generate spurious interactions and false positives [314,322]. With the AP-MS method, tagged-proteins of interest are expressed as baits. The tag is then used to isolate the bait protein from the plant tissue by affinity purification, thereby recovering also co-purifying, interacting proteins that can be identified by MS. This approach allows

for the screening of protein-protein interactions in their native context inside the cell. However, this method requires the interacting partners to remain bound to each other during all steps of protein extraction, precipitation, washing and subsequent isolation [313,323]. This is not always the case for membrane-associated proteins and furthermore, their isolation requires the use of detergents to solubilize them, and this can affect their folding and disrupt protein-protein interactions, causing the loss of signalling partners [324–326]. Recent progress in chemical crosslinking, combined with mass spectrometry, offers alternatives to preserve and detect weak or only transient protein-protein interactions, providing additional information about the sites of physical interaction. However, this strategy generally results in low levels of detection, mainly because of the low efficiency of the crosslinking reagents [327,328].

Recently, enzyme-catalysed proximity-dependent labelling (PL) has emerged as an alternative tool to study the composition of protein complexes. PL techniques involve the conversion of an inert substrate, most often biotin, into a short-lived reactive species that is covalently bound to proteins that are in the vicinity of the bait protein, which in the case of the use of biotin, is fused to a biotin-ligase that performs the labelling. This method allows to perform labelling in living cells and bypasses the necessity to maintain the integrity of the interactions during the processing of the sample [329]. The strength of the biotin-streptavidin interaction allows for the purification of the biotinylated proteins using streptavidin-coated beads. The coupling of this method with an MS analysis of the isolated proteins (PL-MS), is emerging as a very appropriate technique for identifying *in vivo* protein-protein interactions and determining the composition of large protein complexes [329–331]. There are two major classes of enzymes that have been adapted for PL-MS: peroxidases and biotin ligases [269]. The peroxidases require activation with H_2O_2 to oxidize phenol derivatives, such as biotin-phenol, to phenoxyl radicals. These reactive radicals can then covalently react with electron-rich amino acids, like tyrosine, resulting in proximity-dependent labelling of the proteins that surround the bait protein to which the peroxidase is fused. However, the cellular toxicity of H_2O_2 and the poor membrane permeability of the biotin-phenol derivative, prevents its application in plant tissues. In contrast, the biotin ligases adapted for PL only require the addition of biotin, which is an endogenous compound that is membrane-permeable and non-toxic [329]. The best characterized biotin ligase, and also the origin of several novel enzymes adapted for PL, is the BIFUNCTIONAL LIGASE/REPRESSOR A (BirA) enzyme. This 35 KDa DNA-binding biotin ligase from the bacterium *Escherichia coli* catalyses the transfer of biotin to

a specific acceptor peptide sequence of acetyl-CoA carboxylase and also functions as a repressor of the biotin biosynthetic operon [332]. The biotin ligation reaction that is catalysed by BirA is a two-step process. First, biotin is fused to ATP, resulting in a reactive biotinyl-5'-AMP (bioAMP) molecule. Then, this bioAMP is bound within the BirA active site and transferred to a specific lysine residue in the biotin acceptor domain of acetyl-CoA carboxylase [332]. The characterization of mutants, like BirA R118G (called BirA*), that prematurely releases the reactive bioAMP and is defective in DNA binding [333,334], opened the door for the application of BirA* as a tool for PL-MS [335,336]. In the presence of biotin and ATP, the expression of BirA* fused to a protein of interest results in the generation of a cloud of reactive and labile bioAMP molecules around the enzyme. Within this cloud, which is estimated to have a radius of 10nm [337], the bioAMP reacts with lysine residues in proximal proteins, resulting in their covalent biotinylation. The search for even better promiscuous biotin ligases led to the development of several alternatives to BirA* [329]. Among these alternatives, one of the most promising enzymes, TurboID (TbID), was engineered from BirA*, using yeast display-based directed evolution [338]. The TbID enzyme produces, in animal cells, as much biotinylated product within 10 min as BirA* gives in 18 hours of treatment with biotin, thereby generating a biotinylation cloud with an estimated radius of at least 35nm [339]. Since its development in 2018, TbID has been successfully used for PL-MS in various systems, including animals and plants [331,338,340–342]. PL techniques cannot discriminate between whether there is actually a physical, and thereby probably a functional, interaction between the bait and prey proteins, or whether they are just in close proximity. Instead, PL provides a qualitative metric of the proximity between them. Beside this limitation, PL is a very useful approach for studying low-affinity and transient protein-protein interactions, as well as for the identification of the composition of protein complexes present at the PM [269,329,330].

As mentioned in Chapter 1, plant cell-surface receptors mediating immune responses upon pathogen detection can be categorised as receptor-like kinases (RLKs) and receptor-like proteins (RLPs). RLKs are single-pass transmembrane proteins with an extracellular domain for danger perception and a cytoplasmic kinase domain for the initiation of downstream signalling. RLPs mediating immune responses lack any intracellular signalling domain and form bi-molecular receptor-like kinases by their constitutive interaction with the adaptor regulatory RLK SUPPRESSOR OF BIR1-1 (SOBIR1) [18,61]. The tomato Cf-4 protein is an example of such an RLP mediating immune responses. This RLP mediates resistance against strains of the leaf

mould fungus *Cladosporium fulvum* that secrete the effector protein Avr4, which is a chitin-binding lectin that protects fungal cell walls against hydrolysis by plant chitinases [40,70,343]. The assumed direct interaction of Avr4 with the extracellular leucine-rich repeat (LRR) domain of Cf-4 triggers the recruitment of the RLK BRI1-ASSOCIATED KINASE 1 (BAK1) [76], after which a subsequent series of transphosphorylation events between the cytoplasmic kinase domains of SOBIR1 and BAK1 initiates an immune signalling cascade [77]. There is evidence suggesting that BAK1 recruitment is negatively regulated by its interaction with the RLK BAK1-INTERACTING RECEPTOR KINASE 1 (BIR1) [93,100]. However, not much more is known regarding the interaction partners of RLP/SOBIR1 receptor complexes mediating immune responses in solanaceous plants. It is also still unclear whether the Avr4 protein binds directly to the extracellular LRRs of Cf-4 or whether Avr4 recognition by Cf-4 requires additional interaction partners. Furthermore, no immediate downstream signalling components have been found to interact with the cytoplasmic kinase domain of SOBIR1 in solanaceous plants. In this study, we have generated constructs encoding multiple bait-TbID fusion proteins and have adapted a protocol to explore the cytoplasmic interactors of RLP/SOBIR1 receptor complexes by proximity-dependent labelling. We have generated TbID-tagged fusion proteins based on known components of the complex, such as the RLP Cf-4 and the RLK SOBIR1, and a putative additional component, which is the copine protein BONSAI 1 (BON1) [238]. We have also generated fusion proteins to be used as negative controls, including the TbID-tagged β-glucuronidase (GUS) protein and the small trans-membrane protein LOW TEMPERATURE-INDUCED PROTEIN 6B (LTI6b) [344]. We have subsequently evaluated the capacity of these bait-TbID fusion proteins to biotinylate their known interactors, aiming at paving the way for the identification of potential novel interactors by PL-MS.

RESULTS

The various bait -YFP-TbID fusion proteins accumulate upon their transient expression in *Nicotiana benthamiana*

To evaluate the use of TbID-based proximity-dependent labelling on dissecting the composition of RLP/SOBIR1-containing complexes in *N. benthamiana*, with the overall aim to identify novel interactors present in such complexes, we inserted a series of open reading frames (ORFs) into the gateway-compatible 35S-YFP-TbID vector

[341]. These ORFs encode known, as well as putative components of the Cf-4/SOBIR1 complex, in addition to proteins to be used as negative controls.

We first set out to assess the accumulation of the various bait proteins fused to YFP-TbID and their association with known interactors. For this purpose, C-terminally GFP- and YFP-TbID-tagged NbSOBIR1 or -GUS were transiently co-expressed in *N. benthamiana* with C-terminally Myc-tagged Cf-4 or -GUS. Two days after agroinfiltration, we extracted and immunoprecipitated the proteins using GFP-trap agarose beads. The isolated proteins were then subjected to immunoblotting with either anti-GFP or anti-Myc antibodies. The anti-GFP blot showed that the fusion proteins NbSOBIR1-YFP-TbID and GUS-YFP-TbID properly accumulate *in planta*, both represented by bands corresponding to ~140KDa (red arrows, Figure 1A, upper panel). When compared with their GFP-tagged versions, the absence of the TbID enzyme of approximately ~37KDa in molecular weight was reflected by the faster migration of the corresponding bands (blue arrows, Figure 1A, upper panel). Immunoblotting of the isolated proteins with anti-Myc antibodies evidenced that the NbSOBIR1-YFP-TbID fusion protein, like its GFP-tagged version, constitutively interacts with the Cf-4-Myc fusion protein (black arrows, Figure 1A, second panel from above). However, the anti-Myc antibodies also revealed strong signals from the GUS-Myc negative control co-purifying with NbSOBIR1-GFP and NbSOBIR1-YFP-TbID (orange arrows, Figure 1A, second panel from above), and from Cf-4-Myc co-purifying with GUS-GFP and GUS-YFP-TbID (green arrows, Figure 1A, second panel from above). This shows the need for further optimisation of the protocol, as GFP- and Myc-tagged GUS accumulate at high levels in the total protein extract (grey arrows, Figure 1A, third and fourth panel from above). The intense band representing Cf-4-Myc co-purifying with GUS-YFP-TbID, suggests a limitation for the use of this TbID-tagged fusion protein as a negative control for further PL experiments.

We then evaluated the behaviour of SlBON1-YFP-TbID, which is a tagged version of a putative component of RLP/SOBIR1 receptor complexes (Chapter 3), and YFP-YFP-TbID, which is a fusion protein that we aimed to use as an alternative negative control. For this purpose, C-terminally GFP- and YFP-TbID-tagged SlBON1 or -GUS, as well as YFP-YFP-TbID, were transiently co-expressed in *N. benthamiana* with C-terminally Myc-tagged SlBAK1 or -GUS. Again, two days after agroinfiltration, total protein extracts from the agroinfiltrated leaves were subjected to immunoprecipitation using GFP-trap agarose beads, and immunoblotting with anti-GFP antibodies

revealed the accumulation of SlBON1-YFP-TbID and SlBON1-GFP as bands corresponding to ~140KDa and ~100KDa, respectively (red and blue arrows, respectively, Figure 1B, upper panel). The YFP-YFP-TbID fusion protein accumulated a high level and was visible as a band at ~95KDa after the pull-down with GFP beads and in the input (black arrows, Figure 1B, upper and third panel from above, respectively). However, after the pull-down, the main band was accompanied by a high number of additional bands, suggesting aggregation and degradation of the YFP-YFP-TbID fusion protein. Immunoblotting with anti-Myc antibodies failed to reveal proper evidence for an interaction between SlBON1-GFP, or SlBON1-YFP-TbID, and SlBAK1-Myc. This was likely because of the high accumulation level of GUS-Myc, as evidenced by the strong bands at 110Kda in the immunoprecipitated samples and in the total protein extract (input) (grey arrows, Figure 1B, second and fourth panel from above). Bands at ~110KDa indicating SlBAK1-Myc co-purifying with SlBON1-GFP and with SlBON1-YFP-TbID, were only very faint in comparison with the bands corresponding to the negative control, GUS-Myc. Therefore, to visualise the band corresponding to SlBAK1-Myc, co-purifying with SlBON1-YFP-TbID, it was even necessary to expose the blot for a longer time (orange arrows, Figure 1B, second panel from above).

Overall, these results show that the different bait-YFP-TbID fusion protein do successfully accumulate upon their transient expression in *N. benthamiana*. However, the high level of the background signals from the negative controls, suggesting that the protein-protein interactions that we observe are not specific, prevents us from coming to conclusions about a possible interference of the TbID enzyme with the protein-protein interactions in which the bait proteins are anticipated to be involved.

The TbID element present in the various fusion proteins is enzymatically active in *N. benthamiana*.

To evaluate whether the YFP-TbID-tagged bait proteins can be used as a tool to identify interacting candidates of the Cf-4/SOBIR1 receptor complex, it will be necessary to first test whether the TbID element is capable to biotinylate known interactors of the complex. The TbID enzyme produces a biotinylation cloud with a radius of at least ~35nm [339]. Hence, besides the ability to self-biotinylate, the bait-YFP-TbID fusion proteins are expected to biotinylate proteins that are present in their vicinity. We first tested the biotinylation of Myc-tagged SlBAK1 by the NbSOBIR1-YFP-TbID fusion protein. Although BAK1 is specifically recruited to the Cf-4/SlSOBIR1 complex upon Avr4 perception [76,102], BAK1 is expected to be in the proximity of our bait protein,

SOBIR1, also in the pre-activation state. We anticipate this, as when transiently expressed in *N. benthamiana*, SlSOBIR1 co-purifies with SlBAK1, independently of the presence of Avr4 [76]. Therefore, we performed the biotinylation assays in a *N. benthamiana* line stably expressing the *Cf-4* transgene (*N. benthamiana:Cf-4*), either in the presence or absence of Avr4. For this, YFP-YFP-TbID, GUS-YFP-TbID, NbSOBIR1-GFP, and NbSOBIR1-YFGP-TbID were all transiently expressed in *N. benthamiana*, together with SlBAK1-Myc. Two days after agroinfiltration, the leaves were infiltrated with a biotin solution at a concentration of 200µM. Three hours after the infiltration of biotin, the leaves were infiltrated again with either a solution containing Avr4 or MilliQ water (MQ) and harvested one hour later. Total protein extracts from the harvested leaves were desalted to remove the free biotin, after which the extracts were incubated with streptavidin-coated magnetic beads to capture the biotinylated proteins, followed by immunoblotting of the captured proteins. When developing the blot with anti-GFP antibodies, the YFP-YFP-TbID and GFP-YFP-TbID fusion proteins were visible as bands at ~95KDa and 140KDa, respectively (indicated by the blue and red arrows, respectively, in Figure 2A, upper panel). NbSOBIR1-YFP-TbID was visible as a faint band that needed a longer exposure time to become clearly visible (see the red and green rectangles in Figure 2A, upper panel). Together with the absence of NbSOBIR1-GFP on the blot, this result shows that the different YFP-TbID-tagged bait proteins do self-biotinylate when expressed in *N. benthamiana*. When developing the blot with anti-Myc antibodies, bands at ~110KDa, corresponding with SlBAK1-Myc, revealed that all the YFP-TbID-tagged fusion proteins biotinylated SlBAK1-Myc (indicated by an orange arrow, Figure 2A, second panel from above). We detected biotinylation of SlBAK1-Myc by NbSOBIR1-YFP-TbID independently of the presence of Avr4. However, the procedure was found to be not specific enough, as SlBAK1-Myc was also biotinylated by the fusion proteins YFP-YFP-TbID and GUS-YFP-TbID, which were included as negative controls.

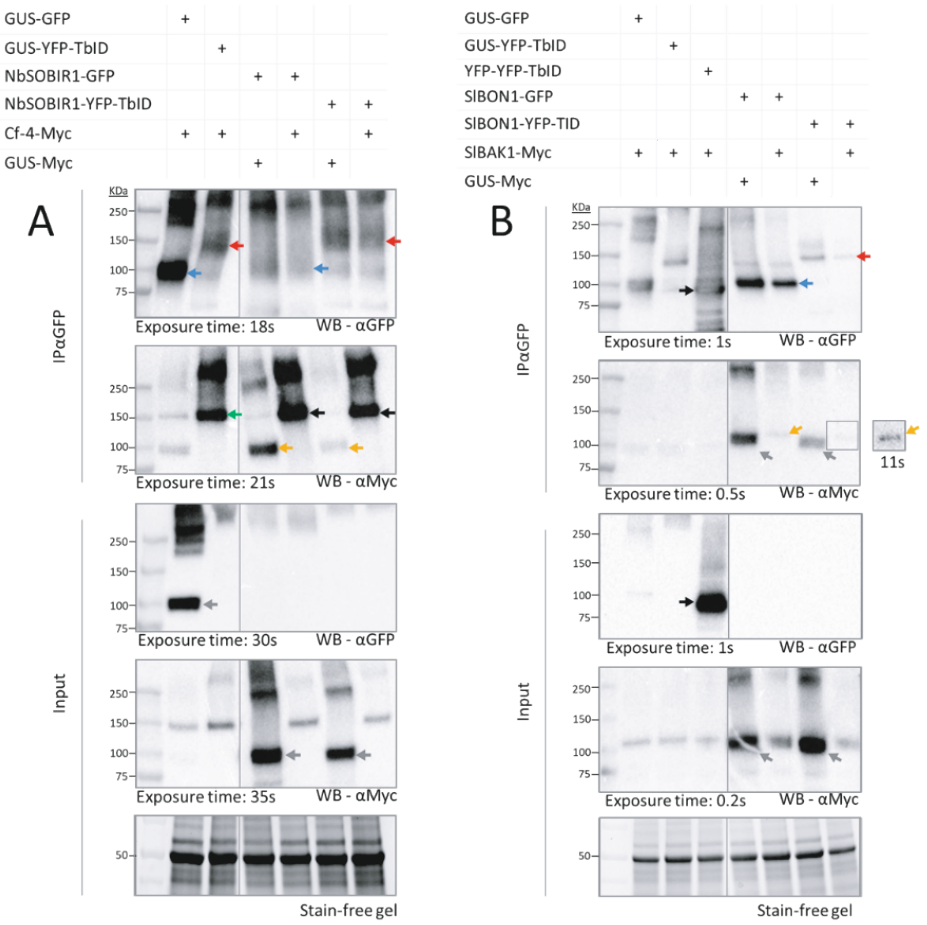

Figure 1. The various bait-YFP-TbID fusion proteins successfully accumulate *in planta*. The various bait-YFP-TbID proteins were agroinfiltrated together with Cf-4-Myc, GUS-Myc or BAK1-Myc in leaves of *N. benthamiana*, with an OD_{600}=0.5 per construct. Two days after agroinfiltration, leaves were harvested and subjected to a total protein extraction. The protein extracts were incubated with GFP-trap beads and the immuno- precipitate was analysed by immunoblotting. The intensity of the Rubisco band in the different input samples (Stain-free gel) shows equal loading. (A) Proper accumulation of YFP-TbID-tagged NbSOBIR1 and GUS takes place. The red arrows in the upper panel indicate the GUS-YFP-TbID and NbSOBIR1-YFP-TbID bands, whereas the blue arrows point to the GFP-tagged versions of the bait proteins. The slower migration of the bands that are observed upon loading of the corresponding YFP-TbID-tagged bait proteins indicates that these actually represent the YFP-TbID-tagged versions. The black and green arrows in the second panel from above point to Cf-4-Myc, whereas the orange arrows indicate GUS-Myc in the immunoprecipitated samples. The detection of Cf-4-Myc co-purifying with GUS-YFP-TbID, and GUS-Myc co-purifying with NbSOBIR1-GFP and with NbSOBIR1-YFP-TbID prevent us from drawing conclusions about the specificity of the various interactions that we observe. In the third and fourth panel from above,

the grey arrows indicate GFP- and Myc-tagged GUS, as present in the total protein extract (input), respectively. (B) Proper accumulation of YFP-TbID-tagged SlBON1 and YFP-YFP-TbID. The red and blue arrows in the upper panel indicate SlBON1-YFP-TbID and SlBON1-GFP, respectively, and the presence of these bands evidences the stability of the YFP-TbID-tagged fusion proteins. The black arrow in this panel and in the third panel from above indicates YFP-YFP-TbID, whereas the grey arrows in the second and fourth panel from above point to GUS-Myc. The orange arrows in the second panel from above indicate SlBAK1-Myc co-purifying with GFP- and YFP-TbID-tagged versions of SlBON1. The detection of GUS-Myc co-purifying with GPF- and YFP-TbID-tagged versions of SlBON1 also here prevents us from assessing the specificity of the various interactions that we observe.

The TbID element present in the various fusion proteins is enzymatically active in *N. benthamiana*.

To evaluate whether the YFP-TbID-tagged bait proteins can be used as a tool to identify interacting candidates of the Cf-4/SOBIR1 receptor complex, it will be necessary to first test whether the TbID element is capable to biotinylate known interactors of the complex. The TbID enzyme produces a biotinylation cloud with a radius of at least ~35nm [339]. Hence, besides the ability to self-biotinylate, the bait-YFP-TbID fusion proteins are expected to biotinylate proteins that are present in their vicinity. We first tested the biotinylation of Myc-tagged SlBAK1 by the NbSOBIR1-YFP-TbID fusion protein. Although BAK1 is specifically recruited to the Cf-4/SlSOBIR1 complex upon Avr4 perception [76,102], BAK1 is expected to be in the proximity of our bait protein, SOBIR1, also in the pre-activation state. We anticipate this, as when transiently expressed in *N. benthamiana*, SlSOBIR1 co-purifies with SlBAK1, independently of the presence of Avr4 [76]. Therefore, we performed the biotinylation assays in a *N. benthamiana* line stably expressing the *Cf-4* transgene (*N. benthamiana:Cf-4*), either in the presence or absence of Avr4. For this, YFP-YFP-TbID, GUS-YFP-TbID, NbSOBIR1-GFP, and NbSOBIR1-YFGP-TbID were all transiently expressed in *N. benthamiana*, together with SlBAK1-Myc. Two days after agroinfiltration, the leaves were infiltrated with a biotin solution at a concentration of 200µM. Three hours after the infiltration of biotin, the leaves were infiltrated again with either a solution containing Avr4 or MilliQ water (MQ) and harvested one hour later. Total protein extracts from the harvested leaves were desalted to remove the free biotin, after which the extracts were incubated with streptavidin-coated magnetic beads to capture the biotinylated proteins, followed by immunoblotting of the captured proteins. When developing the blot with anti-GFP antibodies, the YFP-YFP-TbID and GFP-YFP-TbID fusion proteins were visible as bands at ~95KDa and 140KDa, respectively (indicated by the blue

and red arrows, respectively, in Figure 2A, upper panel). NbSOBIR1-YFP-TbID was visible as a faint band that needed a longer exposure time to become clearly visible (see the red and green rectangles in Figure 2A, upper panel). Together with the absence of NbSOBIR1-GFP on the blot, this result shows that the different YFP-TbID-tagged bait proteins do self-biotinylate when expressed in *N. benthamiana*. When developing the blot with anti-Myc antibodies, bands at ~110KDa, corresponding with SlBAK1-Myc, revealed that all the YFP-TbID-tagged fusion proteins biotinylated SlBAK1-Myc (indicated by an orange arrow, Figure 2A, second panel from above). We detected biotinylation of SlBAK1-Myc by NbSOBIR1-YFP-TbID independently of the presence of Avr4. However, the procedure was found to be not specific enough, as SlBAK1-Myc was also biotinylated by the fusion proteins YFP-YFP-TbID and GUS-YFP-TbID, which were included as negative controls.

In a second assay, we reduced the time between the infiltration of biotin and the harvesting of the leaves from four hours to one hour and included tests in which we did not infiltrate any biotin. This was all done to render the biotinylation process more specific. We also decided not to infiltrate the Avr4 protein, and to reduce the amount of the suspension of streptavidin-coated beads that we use to recover the biotinylated proteins from the total protein extract by half (from 100µL to 50µL of suspension per sample). Furthermore, we now also again included the tomato BON1 protein. Two days after agroinfiltration for transient expression of YFP-YFP-TbID, GUS-YFP-TbID, NbSOBIR1-GFP, NbSOBIR1-YFP-TbID, SlBON1-GFP and SlBON1-YFP-TbID, together with SlBAK1-Myc in *N. benthamiana*, we infiltrated a biotin solution at 200µM and harvested the leaves after one hour. In addition, two samples include agroinfiltration of GUS and NbSOBIR1, both tagged with YFP-TbID and co-expressed with SlBAK1-Myc, but not treated afterwards with the biotin solution. Upon total protein extraction plus removal of free biotin, again a streptavidin pull-down and immunoblotting were performed. Developing of the blot with anti-GFP initially only detected the bands corresponding to YFP-YFP-TbID and GUS-YFP-TbID (indicated by blue and red arrows, respectively, Figure 2B, upper panel).

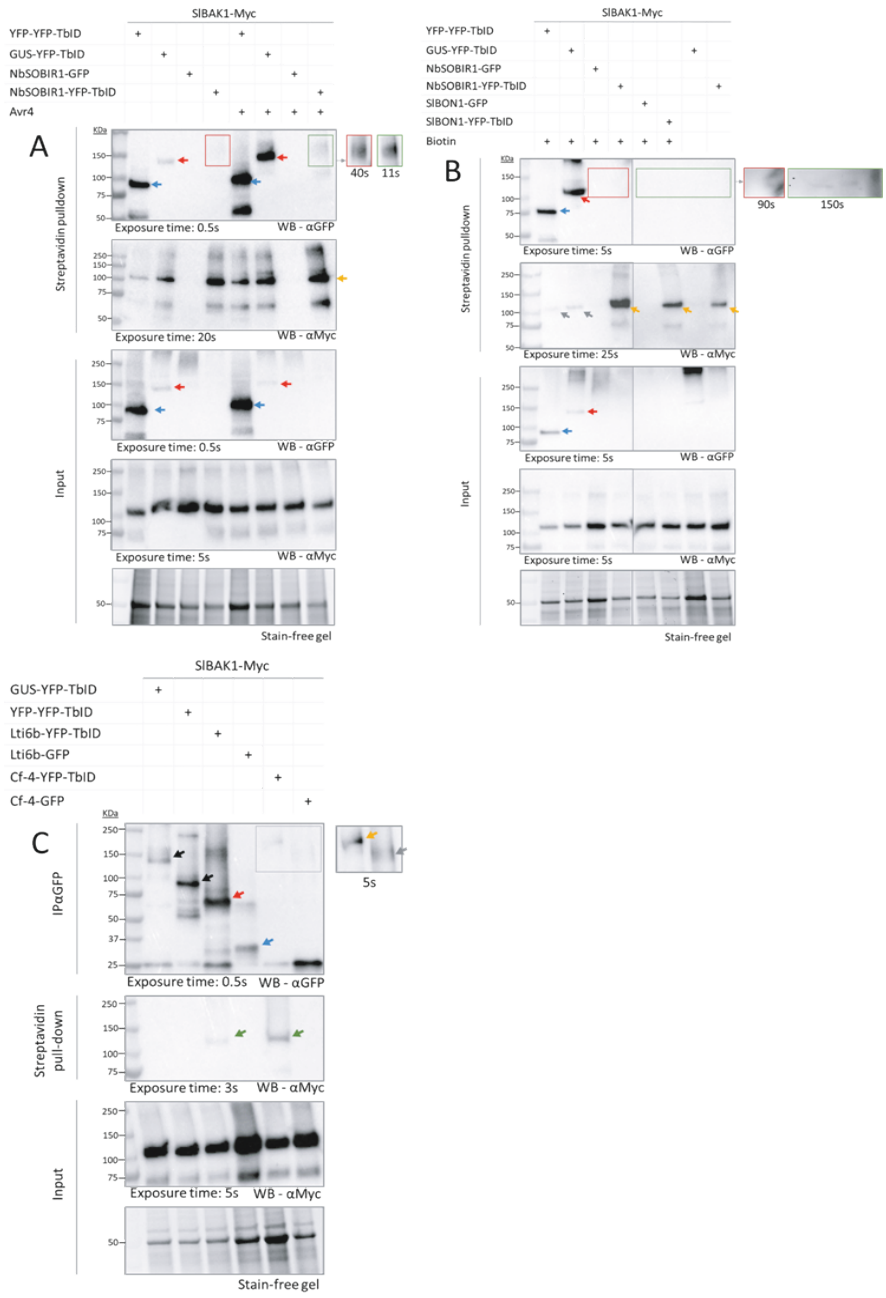

Figure 2. Proximity-dependent labelling (PL) employing various YFP-TbID-tagged bait proteins in *N. benthamiana*. A series of YFP-TbID- and GFP-tagged fusion proteins were transiently expressed in leaves of *N. benthamiana*, together with SlBAK1-Myc. Agroinfiltrations were performed at an OD_{600} of 0.5 per fusion protein. (A) Evaluation of PL, including four hours of biotin treatment

and infiltration with Avr4 protein where indicated. Two days after agroinfiltration, leaves were infiltrated with a solution containing biotin at 200μM (pH=8, 10 mM MES). Three hours later, the leaves were infiltrated with either a solution containing Avr4 (26 μM) or MQ, and harvested after one hour. Total protein extracts from the agroinfiltrated leaves were desalted to remove the free biotin, incubated with streptavidin-coated beads and analysed by immunoblotting. In the upper panel, as well as in the third panel from above that represents the input, the blue and red arrows indicate YFP-YFP-TbID and GUS-YFP-TbID, respectively, whereas the red and green rectangles indicate the bands evidencing self-biotinylation of NbSOBIR1-YFP-TbID. In the second panel from above, the orange arrow indicates the position of SlBAK1-Myc, which has been biotinylated by the YFP-TbID-tagged fusion proteins, as it has been captured by the streptavidin-coated beads. (B) Evaluation of PL, with and without one hour of biotin treatment. Two days after agroinfiltration, leaves transiently expressing the various fusion proteins were infiltrated with a solution of biotin at 200μM where indicated (pH=8, 10 mM MES), and the leaves were harvested one hour later, after which protein accumulation and PL were analysed by immunoblotting. In the upper panel, as well as in the third panel from above that represents the input, the blue and red arrows indicate YFP-YFP-TbID and GUS-YFP-TbID, respectively, whereas the red and green rectangles indicate the presence of faint bands that suggest self-biotinylation of NbSOBIR1-YFP-TbID, SlBON1-YFP-TbID and GUS-YFP-TbID. The orange arrows in the second panel from above indicate the position of Sl-BAK1-Myc, which appears to have been biotinylated by the YFP-TbID-tagged versions of its known interactors, NbSOBIR1 and SlBON1. The grey arrows in this panel indicate SlBAK1-Myc which has been biotinylated by the negative control fusion proteins YFP-YFP-TbID and GUS-YFP-TbID. (C) Evaluation of PL using YFP-TbID-tagged versions of the negative control membrane protein LTI6b, and Cf-4. Two days after agroinfiltration, the leaves were infiltrated with a solution of biotin at 200μM (pH=8, 10 mM MES), and harvested after one hour. Desalted total protein extracts of the agroinfiltrated leaves were either incubated with GFP-trap beads or with streptavidin-coated beads and analysed by immunoblotting. In the upper panel, the black arrows indicate the position of GUS-YFP-TbID and YFP-YFP-TbID, whereas the red and the blue arrows indicate LTI6b-YFP-TbID and LTI6b-GFP, respectively. The orange and grey arrows point to Cf-4-YFP-TbID and Cf-4-GFP, respectively. The green arrows in the second panel from above evidence biotinylation of SlBAK1-Myc, as in these treatments the protein is captured by a streptavidin pull-down.

Again, self-biotinylation of NbSOBIR1-YFP-TBID and SlBON1-YFP-TbID was detected as faint bands after a longer exposure time (see the red and green rectangles, Figure 2B, upper panel), suggesting low levels of self-biotinylation. Developing of the blot with anti-Myc antibodies revealed that SlBAK1-Myc was biotinylated by NbSOBIR1-YFP-TbID and by SlBON1-YFP-TbID (indicated with an orange arrow, Figure 2B, second panel from above). The reduction of the time in between the infiltration of the biotin solution and the harvest of the plant material for total protein extraction, has successfully improved the specificity of the procedure, as among the treatments in which biotin was infiltrated prior to harvesting the plant material, co-expression

of SlBAK1-Myc with YFP-YFP-TbID or GUS-YFP-TbID only resulted in faint bands (indicated by the grey arrows, Figure 2B, second panel from above). These bands were very faint when compared with the bands resulting from the co-expression of SlBAK1-Myc with NbSOBIR1-YFP-TbID or with SlBON1-YFP-TbID, indicating that only in the latter case substantial biotinylation took place. Analysis of the samples that originated from leaf material that was not supplemented with biotin revealed that the different YFP-TbID-tagged bait proteins can sufficiently biotinylate proximal proteins by using only the endogenous biotin that is present in the leaves of *N. benthamiana*. Not infiltrating any additional biotin resulted in a more specific biotinylation process, as there was no band visible indicating biotinylation of SlBAK1-Myc by GUS-YFP-TbID (Figure 2B, second panel from above).

We next tested our protocol with two additional YFP-TbID-tagged bait proteins. One of the baits is based on LOW TEMPERATURE-INDUCED PROTEIN 6B (LTI6b), which is a small transmembrane protein that is commonly used as a PM-localised negative control [331,344–347], and another one is based on the tomato RLP Cf-4 [40,70,343]. After generating the expression constructs, we agroinfiltrated the constructs GUS-YFP-TbID, YFP-YFP-TbID, LTI6b-YFP-TbID, LTi6b-GFP, Cf-4-YFP-TbID and Cf-4-GFP, all in combination with SlBAK1-Myc, in *N. benthamiana*. Two days after agroinfiltration, the leaves were infiltrated with a biotin solution at 200µM and harvested after one hour. Total protein extracts from the infiltrated leaves were first desalted to remove the free biotin, and then separated into two halves, of which one half was incubated with GFP-trap beads (for a GFP pull-down) and the other half was incubated with streptavidin-coated beads (for a streptavidin pull-down of the biotinylated proteins). Immunoblotting with anti-GFP antibodies of the GFP pull-downs evidenced the expression of the GUS-YFP-TbID and YFP-YFP-TbID bait proteins (indicated by black arrows, Figure 2C, upper panel), whereas the LTI6b-YFP-TbID fusion protein was visible as a band corresponding to ~74Kda (indicated by a red arrow, Figure 2C, upper panel), and LTI6b-GFP was visible as a lower band corresponding to ~34KDa (see the blue arrow, Figure 2C, upper panel). The YFP-TbID- and GFP-tagged versions of Cf-4 needed a longer exposure time to become visible and appeared as bands corresponding to 190Kda (indicated by the orange arrow, Figure 2C, upper panel) and to ~150KDa (indicated by the grey arrow, Figure 2C, upper panel), respectively. These results show that also YFP-TbID-tagged LTI6b and the Cf-4 fusion proteins properly accumulate in leaves of *N. benthamiana* upon their transient expression. In order to reveal a possible interaction of the various transiently expressed proteins with

SlBAK1-Myc and its resulting biotinylation, the fractions of the total protein extracts that were subjected to a streptavidin pull-down were analysed by immunoblotting using anti-Myc antibodies. The result revealed that SlBAK1-Myc was biotinylated by Cf-4-YFP-TbID, and also by the negative control LTI6b-YFP-TbID, albeit to a much lower level (indicated by the green arrows in Figure 2C, second panel from above). In this experiment, we did not detect biotinylation of SlBAK1-Myc by the negative controls GUS-YFP-TbID and YFP-YFP-TbID. These results show that the YFP-TbID-tagged bait proteins properly accumulate in *N. benthamiana* and in the case of Cf-4 specifically biotinylates proteins in its vicinity. The result also suggests that, even in the absence of Avr4 perception by Cf-4, SlBAK1-Myc localises in the proximity of Cf-4-YFP-TbID when transiently co-expressed in *N. benthamiana*.

All together, these results indicate that the various YFP-TbID-tagged fusion proteins that we have generated can covalently attach biotin to other proteins that are present in their vicinity. Also, the results confirm previous reports indicating that a long labelling time after the infiltration of the biotin solution affects the specificity of the biotinylation process [330,341].

NbSOBIR1-YFP-TbID and Cf-4-YFP-TBID fusion proteins retain their biological function, as they mediate the Avr4-triggered hypersensitive response (HR) and reactive oxygen species (ROS) burst.

We then set out to investigate whether the NbSOBIR1-YFP-TbID and Cf-4-YFP-TbID fusion proteins are still immune signalling-competent. We first evaluated the capacity of NbSOBIR1-YFP-TbID to complement *N. benthamiana:Cf-4 sobir1(-like)* knock-out plants. This is a *N. benthamiana* line that stably expresses the *Cf-4* transgene, and in which *SOBIR1* and its close paralog *SOBIR1-like* were knocked out by CRISPR/Cas technology [253]. We transiently expressed NbSOBIR1-YFP-TbID and NbSOBIR1-GFP by agroinfiltration, together with either Avr4 or Avr9, after which the leaf tissue was visualised by red light imaging [235] at six days after agroinfiltration. Clear evidence of a hypersensitive response (HR) was observed upon co-expression of each of the fusion proteins together with Avr4, but not with Avr9 or upon the expression of Avr4 alone (Figure 3A). We also evaluated the capacity of these fusion proteins to restore the Avr4-triggered production of reactive oxygen species (ROS) in the apoplast. This ROS burst is an early downstream response upon immune activation that is not strictly coupled with the development of an HR (Chapter 3).

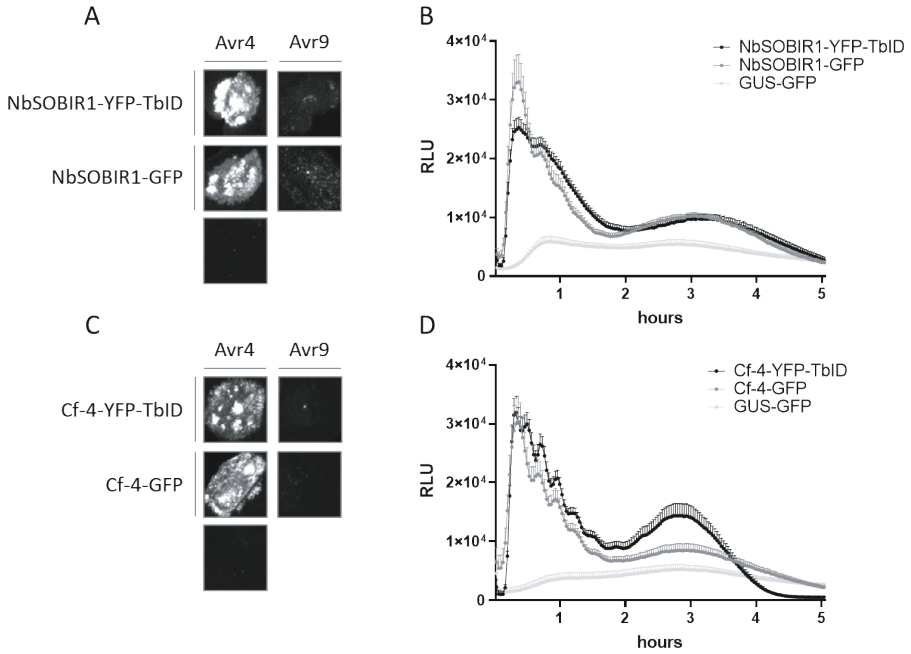

Figure 3. YFP-TbID-tagged versions of NbSOBIR1 and Cf-4 are signalling competent. (A) NbSOBIR1-YFP-TbID and NbSOBIR1-GFP, together with Avr4 and Avr9, were transiently expressed by agroinfiltration in ***N. benthamiana:Cf-4 sobir1(-like)*** plants. The occurrence of an HR was evaluated at six days after agroinfiltration by red light imaging [235]. An OD_{600} of 0.5 was employed for the expression of both fusion proteins, and an OD_{600} of 0.1 was used for both Avr4 and Avr9. (B) NbSOBIR1-YFP-TbID, NbSOBIR1-GFP and the negative control GUS-GFP were expressed by agroinfiltration in ***N. benthamiana:Cf-4 sobir1(-like)*** plants, after which the Avr4-triggered ROS was monitored two days later, by using a luminol-based assay in which Avr4 protein was added at a concentration of 0.1μM (N=12). Error bars show the standard error. (C) Cf-4-YFP-TbID and Cf-4-GFP, together with Avr4 and Avr9, were transiently expressed by agroinfiltration in ***N. benthamiana*** wild-type (WT) plants. The occurrence of an HR was monitored by red light imaging [235] at six days after agroinfiltration. OD_{600}=0.5 for GFP- and YFP-TbID-tagged Cf-4, and OD_{600}=0.1 for Avr4 and Avr9. (D) Cf-4-YFP-TbID, Cf-4-GFP and the negative control GUS-GFP were expressed by agroinfiltration in ***N. benthamiana*** WT at an OD_{600} of 0.1. The Avr4-triggered ROS burst was monitored two days later, by using a luminol-based assay in which Avr4 protein was added at a concentration of 0.1μM (N=12). Error bars show the standard error.

For this purpose, we transiently expressed NbSOBIR1-YFP-TbID, NbSOBIR1-GFP and the GUS-GFP negative control in *N. benthamiana:Cf-4 sobir1(-like)* knock-out plants and monitored the Avr4-triggered ROS burst two days after agroinfiltration, using a luminol-based assay. While the expression of both NbSOBIR1 fusion proteins restored the typical biphasic Avr4-triggered ROS burst, expression of GUS-GFP only caused a basal generation of ROS, likely because of priming of the tissue due to perception of the infiltrated Agrobacterium (Figure 3B).

We then evaluated the capacity of the Cf-4-YFP-TbID fusion protein to activate immune responses upon recognition of Avr4. For this, we transiently expressed Cf-4-GFP and Cf-4-YFP-TbID, together with either Avr4 or Avr9, in leaves of *N. benthamiana* wild-type (WT) plants. We visualised the tissue by red light imaging [235] at six days after agroinfiltration, and observed a clear HR when Cf-4-GFP and Cf-4-YFP-TbID were expressed together with Avr4, but not when expressed with Avr9, or when Avr4 was expressed alone (Figure 3C). As for NbSOBIR1, we also monitored the capacity of the Cf-4 fusion proteins to trigger a ROS burst upon perception of Avr4. For this, we transiently expressed Cf-4-GFP, Cf-4-YFP-TbID and the negative control GUS-GFP in *N. benthamiana* WT plants and monitored the capacity of the leaves to generate an Avr4-triggered ROS burst at two days after agroinfiltration. Expression of both Cf-4-GFP and Cf-4-YFP-TbID, resulted in the production of the typical biphasic Avr4-triggered ROS burst, while the expression of GUS-GFP again resulted in a basal production of ROS, probably because of the perception of Agrobacterium (Figure 3D).

Altogether, these results show that the NbSOBIR1-YFP-TBID and Cf-4-YFP-TbID fusion proteins are signalling-competent, in addition to being able to biotinylate their signalling partners when transiently expressed in *N. benthamiana*.

Transient expression of secreted Avr4-YFP-TbID results in biotinylation of Cf-4-Myc in *N. benthamiana*.

We then evaluated whether proximity-dependent labelling can also be applied in the apoplast of the leaves of *N. benthamiana*. For this purpose, we generated a YFP-TbID-bait fusion protein containing the primary translation product of the *Avr4* gene of 135 amino acids. The resulting fusion protein contains the original fungal Avr4 signal peptide for extracellular targeting [40]. To evaluate whether proper expression and secretion of the Avr4 fusion protein in the apoplast of *N. benthamiana* leaves

takes place, we isolated apoplastic fluid (AF) of the leaves at three days after agroinfiltration of the Avr4-YFP-TbID construct. SDS-PAGE, followed by immunoblotting of the proteins present in the AF with anti-TbID antibodies confirmed proper secretion of the intact fusion protein into the apoplast, as a band at ~80KDa was present, indicating the accumulation of Avr4-YFP-TbID (see red arrow, Figure 4A). The presence of several bands representing faster migrating proteins that were also detected with the anti-TbID antibodies, suggested that there is degradation of the fusion protein taking place in the apoplast. These bands included one at ~70KDa, corresponding with the mass of the -YFP-TbID fragment (indicated with a blue arrow, Figure 4A), and another band at ~36KDa that corresponds with the predicted mass of the -TbID element itself (see orange arrow, Figure 4A).

We also infiltrated this AF into *N. benthamiana:Cf-4* and *N. benthamiana* wild-type plants. Two days after infiltration, the *N. benthamiana:Cf-4* plants showed symptoms of chlorosis in the infiltrated areas, while the wild-type plants showed no response to the AF (upper panel, Figure 4B). Red light imaging of the infiltrated leaves evidenced that the AF indeed triggers a cell death response in *N. benthamiana:Cf-4*, but not in *N. benthamiana* wild-type plants (lower panel, Figure 4B). We then tested whether biotinylation of Cf-4-Myc takes place by the Avr4-YFP-TbID fusion protein, which would suggest that Cf-4 and Avr4 interact, either directly or indirectly. For this purpose, we transiently expressed Avr4-YFP-TbID together with either Cf-4-Myc or FLS2-Cf-9-Myc. FLS2-Cf-9-Myc is a chimeric protein resulting from fusing the extracellular LRR domain of FLS2 to the transmembrane and cytoplasmic portion of the RLP Cf-9. FLS2-Cf-9-Myc was used as a negative control for the specificity of the biotinylation process, as this protein also accumulates in the PM and interacts constitutively with SOBIR1 in *N. benthamiana*, but is not expected to interact with Avr4-YFP-TbID [348]. Two days after agroinfiltration, the leaves were infiltrated with a solution containing 200µM of biotin and they were harvested one hour later. Total protein extracts were desalted to remove the free biotin from the samples, subsequently incubated with streptavidin-coated beads, after which the precipitate was analysed by immunoblotting. Development of the blot with anti-GFP antibodies showed a band at ~80KDa, corresponding to the Avr4-YFP-TbID fusion protein which was self-biotinylated. Development of blot with anti-Myc antibodies revealed that Cf-4-Myc was biotinylated by Avr4-YFP-TbID as it had been captured by the streptavidin-coated beads, whereas FLS2-Cf-9-Myc was not biotinylated by Avr4-YFP-TbID as a band representing the FLS2-Cf-9-Myc fusion protein was not visible (Figure 4C).

All together, these results suggest that Avr4 appears to have either direct or indirect affinity for Cf-4, and not for FLS2, and that it is possible to specifically biotinylate plant cell-surface receptors in the apoplast using TbID-tagged versions of the matching secreted effector proteins.

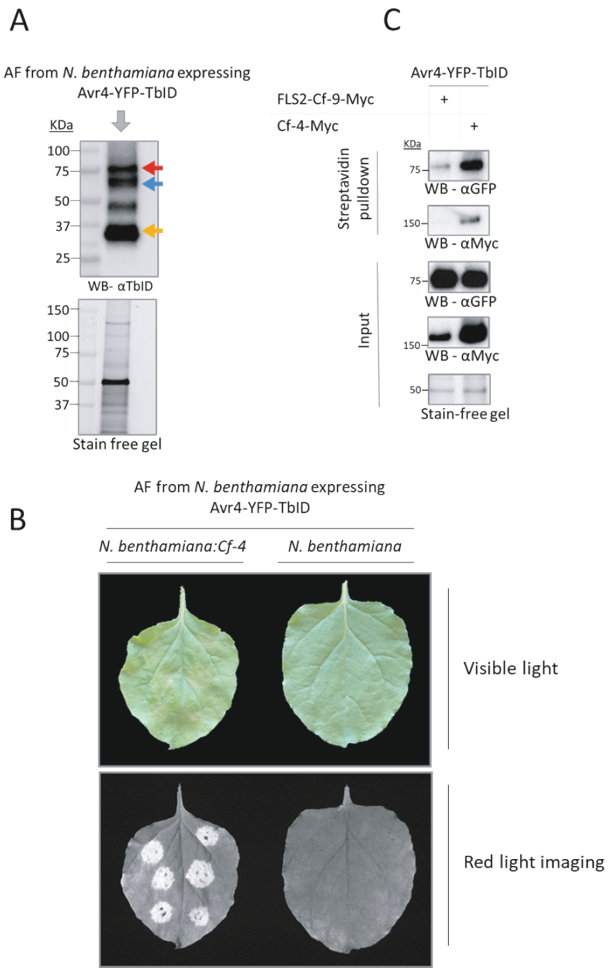

Figure 4. Proximity-dependent labelling (PL) of the cell-surface receptor Cf-4 by a YFP-TbID-tagged version of its matching secreted effector protein, Avr4. (A) Immunoblot of apoplastic fluid (AF) containing the Avr4-YFP-TbID fusion protein. Avr4-YFP-TbID was expressed by agroinfiltration in ***N. benthamiana***, at an OD_{600} of 2. Three days later, AF was isolated from the leaves, and the proteins present in the AF were analysed by immunoblotting. The red arrow indicates the band that corresponds to the full-length fusion protein Avr4-YFP-TbID. The blue and the orange arrows indicate bands that correspond to the predicted migration of the -YFP-TbID and -TbID elements,

respectively. The possible identity of the 45KDa band is not clear. (B) Elicitor activity of the AF containing Avr4-YFP-TbID. The AF analysed in (A) was also infiltrated in ***N. benthamiana:Cf-4*** and in ***N. benthamiana*** wild-type plants, at six sites per leaf, after which the occurrence of an HR was assessed at two days after infiltration. (C) PL of Cf-4-Myc by Avr4-YFP-TbID. Avr4-YFP-TbID was transiently expressed together with either Cf-4-Myc or FLS2-Cf-4-Myc, in ***N. benthamiana***, as indicated. For Avr4-YFP-TbID, the OD_{600} was 0.03, whereas for the other constructs an OD_{600} of 0.5 was used. At two days after agroinfiltration, the leaves were infiltrated with a solution containing biotin at 200µM (pH=8, 10 mM MES), and they were harvested after one hour. Total protein extracts were desalted, subsequently incubated with streptavidin-coated beads and the precipitate was analysed by immunoblotting.

DISCUSSION

Proximity-dependent labelling techniques have emerged as powerful tools to study protein-protein interactions. For our studies, these novel techniques overcome the classical limitations of affinity purifications, facilitating the study of weak or transient interactions of PM-associated proteins [269,329,330]. In this study, we have generated several YFP-TbID-tagged fusion proteins and evaluated their potential application in determining the overall composition of SOBIR1-containing cell-surface receptor complexes. The different fusion proteins were capable of biotinylating their known interactors at either the cytoplasmic side or the apoplastic side of the PM. On the cytoplasmic side of the PM, co-expression of YFP-TbID-tagged versions of NbSOBIR1, Cf-4 and SlBON1 resulted in biotinylation of SlBAK1-Myc (Figures 2A-C). On the apoplastic side of the PM, the co-expression of Avr4-YFP-TbID resulted in biotinylation of its receptor Cf-4-Myc (Figures 4C). The detection of both the YFP-TbID- and the GFP-tagged versions of the various bait proteins upon GFP pull-down, at similar levels, suggests that fusion to the biotin ligase TurboID does not significantly affect the accumulation of the bait proteins. For example, the accumulation levels of the YFP-TbID-tagged versions of NbSOBIR1, Cf-4 and LTI6b were not lower than the accumulation levels of their GFP-tagged versions (Figures 1A and 2C). We observed a lower accumulation level of GUS-YFP-TbID when compared to GUS-GFP, and an even more pronounced reduction of the accumulation of SlBON1-YFP-TbID, when compared to SlBON1-GFP. However, this lower accumulation level does not affect the potential application of these fusion proteins for PL, as we were able to show that SlBON1-YFP-TbID biotinylates one of its interacting proteins, which is the RLK SlBAK1 (Figure 2). Previous reports on mammalian model systems described significant levels of cellular toxicity when using the TurboID enzyme [338,339].

This toxicity does not seem to be an issue for plant systems, as the various reports on TurboID-based PL in plants do not mention a toxic effect [331,341,342]. In our experiments in *N. benthamiana*, we observed no evidence for possible cell death caused by the expression of the various fusion proteins containing the promiscuous biotin ligase TurboID.

The results from the streptavidin pull-down assays showed that the protocol that we have developed based on the method published by Kim and co-workers [341], is suitable for PL in *N. benthamiana* (Figures 2 and 4). The reduction of the labelling time upon biotin supplementation from four hours to only one hour, diminished the non-specific biotinylation of SlBAK1 by the YFP-TbID-tagged negative controls GUS and YFP. We also detected biotinylation of BAK1-Myc by NbSOBIR1-YFP-TbID, even without biotin supplementation (Figure 2B), evidencing that the endogenous levels of free biotin in *N. benthamiana* are already sufficient to support PL. Considering the balance between the strong specific biotinylation signals of our target proteins and the relatively low levels of background signals from the negative controls, we retained the supplementation with 200µM of biotin, in combination with allowing the labelling reaction to proceed over a period of one hour, as part of the protocol.

Immunoblot analysis with anti-GFP antibodies of the streptavidin pull-downs suggested the occurrence of low levels of self-biotinylation of the GUS-YFP-TbID, NbSOBIR1-YFP-TbID and SlBON1-YFP-TbID fusion proteins (Figures 2A and B). However, follow-up experiments resulted in inconsistent detection of the biotinylated YFP-TbID-tagged proteins with anti-GFP antibodies. This prevented us from drawing a conclusion about the apparent limited self-biotinylation that was observed. For instance, immunoblotting with anti-GFP antibodies failed to detect the accumulation of Avr4-YFP-TbID in the AF obtained from agroinfiltrated leaves of *N. benthamiana* plants (data not shown). Still, developing of the same blot using anti-TbID antibodies revealed bands corresponding to the Avr4-YFP-TbID fusion protein, as well as to the -YFP-TbID and -TbID fragments derived from this fusion protein (Figure 4A). However, unlike what is the case for classical co-immunoprecipitations, our experiments suggest that a low level of expression of the TbID-tagged baits is already sufficient for detectable biotinylation levels of the interacting target proteins. This was for example observed for the Cf-4-YFP-TbID fusion protein. SOBIR1 is required for the accumulation of Cf-4 [66] and therefore agroinfiltration for expression of the fusion proteins Cf-4-YFP-TbID and Cf-4-GFP, without co-expressing also SOBIR1, yielded

only limited amounts of recombinant Cf-4 protein accumulation, as observed upon GFP pull-down (Figure 2C). However, this low accumulation did not prevent the Cf-4-YFP-TbID fusion protein from catalysing the biotinylation of detectable levels of BAK1-Myc (Figure 4C). This result also shows that, when both fusion proteins are over-expressed in *N. benthamiana*, SlBAK1 and Cf-4 localize in close-proximity to each other, even in the absence of the Avr4 effector that is recognised by Cf-4 and triggers specific recruitment of BAK1 to the Cf-4/SOBIR1 complex [76].

The addition of epitope tags can affect the biological function of RLKs. For instance, C-terminally tagged versions of BAK1 are impaired in their capacity to mediate immune responses [349,350]. This observation can limit the application of TbID-tagged bait proteins for PL-MS. Fortunately, GFP-tagged versions of SOBIR1 are able to complement the Avr4-triggered HR and ROS burst in *SOBIR1(-like)* knock-out lines of *N. benthamiana:Cf-4* [253]. Furthermore, GFP-tagged Cf-4 induces the development of an HR [66] and the production of ROS upon Avr4 perception, when transiently expressed in *N. benthamiana* (this thesis, Chapter 3). When evaluating the functionality of the YFP-TbID-tagged versions of NbSOBIR1 and Cf-4, we observed that both fusion proteins do mediate the development of an HR upon perception of Avr4 (Figure 3), evidencing the signalling competence of these fusion proteins.

The promising results observed when performing PL of trans-membrane proteins having TbID fused to their C-terminus, present at the inner, cytoplasmic, side of the PM, prompted us to evaluate the use of TbID at the apoplastic side of the PM. This would allow to study which proteins are actually involved in the recognition of effectors in the apoplast, such as the protein Avr4. In addition to the identification of possible host virulence targets of the apoplastic effectors of *C. fulvum*, this approach might also facilitate the identification of unknown cell-surface receptors of particular TbID-tagged effectors present in plants resistant to the pathogen of interest. We tested this option by focusing on the recognition of Avr4 by the LRR-RLP Cf-4. The *Avr4* gene of *C. fulvum* codes for a pre-pro-protein of 135 amino acids, including an N-terminal signal peptide for extracellular targeting [40]. Once secreted, the Avr4 pro-protein, comprising 117 amino acids, is processed at its N- and C-termini by apoplastic proteases into the mature and stable Avr4 elicitor of 86 amino acids [351]. This N- and C-terminal processing implies that the expression of a full-length version of Avr4, fused to a C-terminal YFP-TbID tag, might result in the accumulation of an untagged Avr4 elicitor because of proteolytic processing. Indeed, immunoblot

analysis of AF isolated from *N. benthamiana* transiently expressing a C-terminally YFP-TbID-tagged fusion protein containing the primary 135 amino acid expression product of the *Avr4* gene revealed high levels of degradation of the fusion protein (Figure 4A). However, besides an intense band at ~37KDa, corresponding to the TbID element itself, the presence of additional higher bands on the immunoblot suggests that there is still a small pool of YFP-TbID tagged Avr4 protein present. Indeed, the band at ~80KDa (indicated by the red arrow in Figure 4A) corresponds to the predicted mass of Avr4-YFP-TbID. This observation points to the accumulation of at least some residual amount of the complete Avr4-YFP-TbID fusion protein in the apoplast of *N. benthamiana*. Infiltration of this AF in leaves of *N. benthamiana:Cf-4* induced an HR (Figure 4B). However, we cannot exclude that the observed HR originates from the untagged and mature form of the Avr4 protein that will accumulate due to proteolytic degradation of the fusion protein, in addition to the induction of an HR by the Avr4-YFP-TbID fusion protein. The observation that co-expression of Avr4-YFP-TbID and Cf-4-Myc results in a specific biotinylation of the Cf-4 receptor, suggests that either an (indirect) interaction between the receptor and the full-length Avr4 fusion protein takes place (Figure 4C), or that the Cf-4 protein and Avr4 are at least in close vicinity. The possible recognition of Avr4, present as a fusion protein, by the LRRs of Cf-4 might be responsible for keeping the TbID enzyme in the proximity of the receptor.

A versatile method for the identification of an unknown host cell-surface receptor of a particular secreted effector protein of a pathogen by PL-MS should work without knowledge on possible apoplastic processing of the effector and, ideally, with no need for expression of the TbID-fused effector protein from the host tissue itself. Our results suggest that, at least when properly secreted by the host cells, even unstable TbID-tagged effector pro-proteins can biotinylate the corresponding receptor possibly already before being processed, and degraded, by proteases. This process may be facilitated by the short delivery route of the fusion protein, as effector proteins secreted by the host itself do not have to pass the cell wall to come into contact with their matching cell-surface receptors, thereby reducing the possibility of degradation of the fusion protein in the apoplast before biotinylation of the receptor can occur. This option was for example proposed to explain why unstable isoforms of the Avr4 effector from strains of *C. fulvum* that are virulent on Cf-4-containing tomato, still elicit immune responses when expressed by Cf-4-tomato itself, but not when expressed by *C. fulvum* during colonisation of the leaf apoplast of Cf-4-tomato [351]. The

need for the expression of the TbID-tagged fusion protein from the host tissue itself might be bypassed by the infiltration of AF taken from leaves of *N. benthamiana* expressing the fused, secreted, effector protein. The accumulation of TbID-tagged effector proteins in the AF of *N. benthamiana* could possibly be enhanced by the infiltration of protease inhibitors such as phenylmethylsulfonyl fluoride (PMSF), or by the transient co-expression of protease inhibitors, such as Extracellular protease inhibitor 1 (Epi1) from *Phytophthora infestans* [352]. It has yet to be tested whether it will be possible to obtain detectable levels of biotinylation of the Cf-4 receptor after infiltration of AF isolated from *N. benthamiana* expressing secreted Avr4-YFP-TbID. If successful, this would be a more convenient approach than for example the heterologous production of the fusion protein in the bacterium *Escherichia coli* or the yeast *Pichia pastoris*. Still, the major barriers for the binding of an unstable TbID-tagged fusion protein by a cell-surface receptor, followed by its biotinylation, are the proteases that are present in the apoplast [351,353,354]. Another option to try to identify matching cell-surface receptors of certain effectors by PL-MS in plant species that are recalcitrant to transient expression by agroinfiltration, could be to perform the PL in transfected protoplasts.

In this study, we implemented the use of the promiscuous biotin ligase TurboID for the determination of the overall composition of Cf-4/SOBIR1-containing immune receptor complexes. The adapted protocol proved to be useful to selectively biotinylate known components of the complex either at the cytoplasmic side or the apoplastic side of the PM. We have now generated a validated series of TbID-fused bait proteins that can be used to identify novel components of the Cf-4/SOBIR1 complex by PL-MS. Additionally, we present data suggesting that it is possible to use PL-MS to identify an unknown cell-surface receptor of a particular secreted effector of a pathogen, in plants resistant to that particular pathogen. This could potentially speed up the process of the identification of economically relevant cell-surface receptors acting as resistance proteins in plants, and thereby revolutionize resistance breeding.

METHODS

Plant material and growth conditions

N. benthamiana and transgenic *N. benthamiana* stably expressing Cf-4 (*N. bentamiana:Cf-4*) were grown in climate chambers under 16 hr of light, at 24˚C and 8 hr of darkness, at 22 ˚C and at an RH of 75%.

Vectors for Agroinfiltrations

The different bait-TbID fusion proteins were generated using a gateway-compatible 35S-YFP-TbID expression vector based on pEarleyGate101 (pEG101) [341]. To generate C-terminally fused Avr4-YFP-TbID, the sequence encoding the primary translation product of the *Avr4* gene of 135 amino acids was amplified from the pMOG800-Avr4 (SOL6783) plasmid and inserted into the destination vector using the ClonExpress MultiS One Step Cloning Kit. For constructing LTI6b-YFP-TbID (SOL9208), the sequence encoding LTI6b was amplified from pBIB-35S-LTI6b-eGFP [344], cloned into pENTR/D-Topo, and transferred into the destination vector using the Gateway® LR Clonase® II enzyme mix. The vectors GUS-YFP-TbID (SOL9203), NbSOBIR1-YFP-TbID (SOL9201), SlBON1-YFP-TbID (SOL9205), and Cf4-YFP-TBID were generated by LR reactions from the gateway entry vectors SOL2685, SOL4064, SOL8609, and SOL2520, respectively. The primers that were used are listed in Table S1.

Agrobacterium-mediated transient transformation

Agrobacterium-mediated transient transformations (agroinfiltrations) were performed as previously described [206]. For protein expression, we infiltrated the first fully expanded leaf of three to four weeks old *N. benthamiana* plants at the indicated OD_{600}. For co-immunoprecipitation and streptavidin-pull downs, the leaves were harvested at two days after agroinfiltration.

Bioassays for determining the Avr4-triggered HR and ROS burst

The intensity of the HR in the leaf tissue of *N. benthamiana* was quantified by red-light imaging using a Chemidoc XRS system (Bio-Rad). We observed that the fluorescence produced by the -eYFP tag that is present in the various fusion proteins that we generated interferes with visualisation of the HR when using the protocol as described in Chapter 2. To prevent this, visualisation of the strong necrotic responses shown in Figures 3A and 3C was performed at six days after agroinfiltration, once the signal from the -eYFP tag had faded away because of the transient nature

of the accumulation of the various recombinant, transiently expressed proteins. In the case of the weak HR observed upon infiltration of AF containing Avr4-YFP-TbID in *N. benthamiana:Cf-4*, the images shown in Figure 4B were acquired upon excitation by a light source in the red visible spectrum (Red LED Module kit no. 1708283), and using the emission filter 695/55, thereby avoiding the fluorescence emitted by the -eYFP tag.

Co-immunoprecipitation assays and immunoblots

Co-immunoprecipitations (co-IPs) were performed as described previously [66]. The eGFP- or eYFP-tagged proteins were detected with αGFP-HRP antibodies (Miltenyi Biotec, 130-091-833), whereas Myc-tagged proteins were detected using αMyc antibodies (cMyc9E10, sc-40, Santa Cruz), with αMouse-HRP (GE healthcare) as a secondary antibody. Presence of the TurboID element was detected by using αBirA antibodies (Agrisera, AS20 4440-ALP).

Proximity-dependent labelling (PL)

An adjusted protocol for the PL was used for the experiments of which the results are shown in Figures 2C and 4C. For these assays, two days after agroinfiltration, the leaves were infiltrated with a biotin solution (200µM, pH=8, 10 mM MES), harvested after one hour and kept in liquid nitrogen or at -80°C, after which the samples were ground in liquid nitrogen using a mortar and pestle. The pulverized samples were then transferred to pre-cooled 50mL V-shape tubes, weighed, and resuspended in 2mL/gram of extraction buffer (EB; pH=8.0, 150 mM NaCl, 1.0% [v/v] IGEPAL®CA-630 (NP-40), 50 mM Tris (Sigma) and 1 tablet of protease inhibitor cocktail (manufacturer) per 50 mL). The samples were subsequently centrifuged at 13,000 rpm for 30 minutes at 4°C in a Sigma 4-16K Centrifuge. To prevent saturation of the streptavidin beads with the free biotin remaining in the samples, the centrifuged protein extracts were desalted at 4°C using MiniTrap PD-10 desalting columns (GE Healthcare), following the manufacturer's gravity protocol for removing salt. An aliquot of 45µL of each desalted extract was collected as an input sample, mixed with 15µL of 4 x Laemmli loading buffer (4xLB; 200 mM Tris-HCl pH=6.8, 8% SDS, 40% glycerol, 400 mM DTT and 0.2% of Bromophenol blue), incubated at 95°C for 5 minutes and kept at -20°C until further processing for western blotting. For each sample, 2mL of desalted extracts were incubated for 1 hour at 4°C (at 10 rpm in an SB3 tube rotator, STUART) with 100µL of Dynabeads™ MyOne™ Streptavidin C1 (previously washed according to the manufacturers' protocol). After incubation, the beads were transferred into

new 2mL Eppendorf tubes using a magnetic separation rack, washed three times with 1mL of EB, and eventually resuspended in 30 µL of EB. To each sample 10µL of 4xLB was added, after which they were incubated at 95˚C for 5 minutes and subsequently kept at -20˚C until further processing for western blotting as described previously [66].

For the PL assay of which the result is shown in Figure 2A, we applied a longer biotin treatment. Here, at two days after agroinfiltration, the leaves were infiltrated with the biotin solution and after three hours, the leaves were infiltrated with either MQ or a solution containing pure Avr4 protein (26µM) and harvested after one hour.

Isolation of apoplastic fluid from agroinfiltrated *N. benthamiana* leaves

The isolation of apoplastic fluid was performed as described previously [355]. The samples were kept at -20˚C.

ACKNOWLEDGMENTS

Octavina Sukarta and Paul Alexander Niederau from the Laboratory of Nematology at WUR provided the construct to express the control YFP-YFP-TbID recombinant protein. We acknowledge the personnel of UNIFARM, especially Bert Essenstam, for excellent plant care. S.L.V. is supported by the Peruvian Council for Science, Technology and Technological Innovation (CONCYTEC) and its executive unit FONDECYT.

SUPPLEMENTARY DATA

Table S1. Nucleotide sequences of the primers that were used.

name	SOL-number	sequence
LTI6b-Fw	JO20	caccATGAGTACAGCCACTTTCG
LTI6b-Rv	JO21	CTTGGTGATGATATAAAGAGCG
Avr4-Fw	SO195	gagaggacacgctcgagatcATGCACTACACAACCCTC
Avr4-Rv	SO196	cccttgctcaccctaggcacATAGCCAGGATGTCCAAC
pEG101-Fw	JO28	GTGCCTAGGGTGAGCAAGGG
pEG101-Rv	JO29	GATCTCGAGCGTGTCCTCTCC
NbSOBIR1-Fw	JO4	TTCTTGAAGGTCATGTGCC
YFP-Rv	JO6	CTCAGGTAGTGGTTGTCGG
TurboID-Rv	JO8	GCAGATACAGGTCATTGGG
GUS-Fw	JO9	GGTTATCTCTATGAACTGTGCG
SlBON1-Fw	JO11	CTGAAAGTGGAATTGTCGTTCC

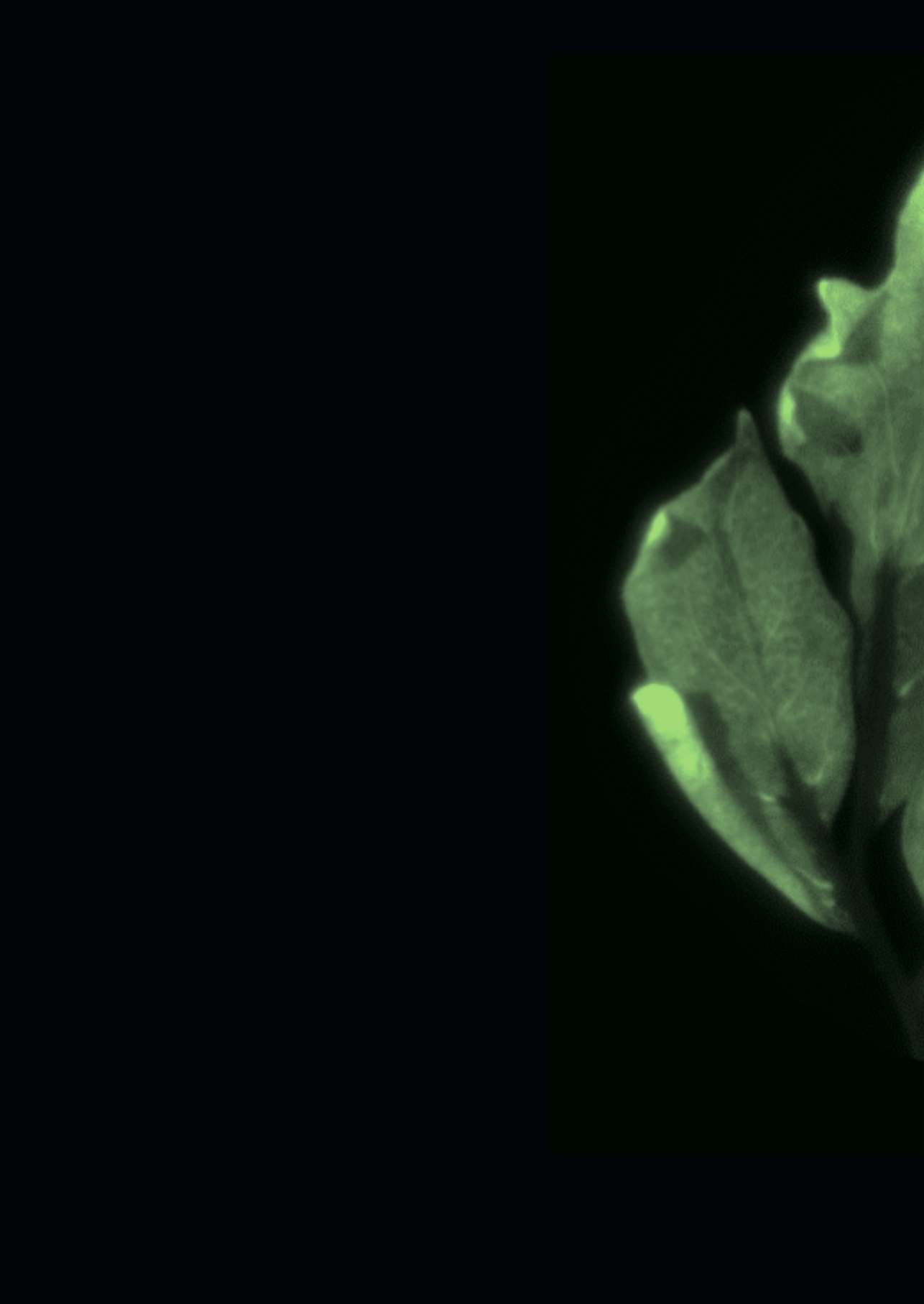

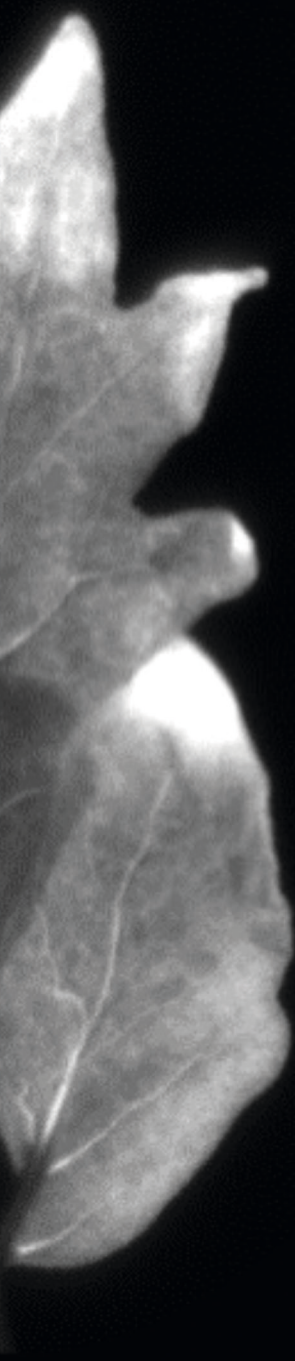

CHAPTER 5

Proximity-dependent labelling, followed by mass spectrometry analysis, of the Cf-4/SOBIR1-containing immune complex in *Nicotiana benthamiana* reveals that the co-receptor SOBIR1 functionally connects the Cf-4 receptor with the cytoplasmic immune signalling machinery

Sergio Landeo Villanueva[a], José Juan Piña[a], Sjef Boeren[b], Matthieu H.A.J. Joosten[a]

[a] Laboratory of Phytopathology, Wageningen University & Research, Droevendaalsesteeg 1, 6708 PB Wageningen, The Netherlands

[b] Laboratory of Biochemistry, Wageningen University, Stippeneng 4, 6708 PB Wageningen, The Netherlands

ABSTRACT

The first layer of the plant immune system consists of a set of cell-surface receptors that perceive immunogenic patterns (IPs) and subsequently trigger appropriate immune responses against invading pathogens. These cell-surface receptors are either receptor-like kinases (RLKs), comprising an extracellular domain for IP recognition and a cytoplasmic kinase domain for the initiation of downstream signalling by phosphorylation of signalling partners, or receptor-like proteins (RLPs) that lack such a cytoplasmic signalling domain. RLPs constitutively interact with the RLK SUPPRESSOR OF BIR1-1 (SOBIR1), thereby forming a bimolecular RLK that is capable of initiating downstream signalling through the kinase domain of SOBIR1. Upon IP perception, the RLP/SOBIR1 complex recruits the RLK BRI1-ASSOCIATED KINASE 1 (BAK1), thereby triggering a signalling cascade that activates plant immune responses. The weak and transient nature of the interactions of these receptor complexes that are located at the plasma membrane (PM) with their downstream cytoplasmic signalling partners, complicate the identification of such partners, and hamper dissection of the receptor complex. Proximity-dependent labelling by biotinylation, followed by identification of the biotinylated proteins by mass spectrometry analysis, is currently emerging as a very important tool for the dissection of the composition of receptor complexes. In this study, we deploy the promiscuous biotin ligase TurboID to identify the proximal proteome of an RLP/SOBIR1 receptor complex in the model plant *Nicotiana benthamiana* (*Nb*). TurboID-tagged versions of the tomato RLP Cf-4, providing resistance against strains of the extracellular pathogenic fungus *Cladosporium fulvum* secreting the IP Avr4, and the Cf-4-interacting RLK NbSOBIR1, were used as baits to identify a set of proteins that are members of the receptor complex. The identified proximal proteome of the Cf-4/NbSOBIR1 complex revealed proteins that possibly play a role in the functioning of the complex itself, such as a phosphatase 2C, as well as downstream signalling partners that are potentially activated by the complex upon IP recognition, including receptor-like cytoplasmic kinases (RLCKs) and mitogen-activated protein kinases (MAP3Ks). Furthermore, the proximal proteome that we identified suggests that Cf-4/SOBIR1 receptor complexes reside at the PM in nanodomains, as we also detected hypersensitive induced response proteins (HIRs) and remorins, and provides a snapshot of the molecular components of such nanodomains.

INTRODUCTION

Plants are constantly threatened by a wide range of pathogenic micro-organisms. Unlike vertebrates, plants lack mobile immune cells mediating adaptive immunity and instead they fully rely on their innate immune system to perceive, and subsequently eliminate, microbial pathogens. The innate immune system of plants is broadly organised into two interconnected tiers, one at the level of the plasma membrane (PM) and one at the level of the cytoplasm [6,7]. At the level of the PM, cell-surface receptors have the function to perceive extracellular immunogenic patterns (ExIPs), either directly or indirectly derived from pathogens, and these receptors represent the first layer of the plant innate immune system [356]. The perceived ExIPs can be structural components of the microbial pathogen, like so-called microbe-associated molecular patterns (MAMPs), and can also be modified components of the host, like host-derived damage-associated molecular patterns (DAMPs). In addition, secreted virulence factors of the pathogen, referred to as effectors, which are generally produced to suppress the initial immune response of the plant, can also act as ExIPs. At the level of the cytoplasm, nucleotide-binding leucine-rich repeat-containing immune receptors (NB-LRRs or NLRs) perceive effector proteins that are transferred to the cytoplasm of the host cells, either directly or by sensing the perturbation of host target proteins with the aim to suppress host immune responses. Perception of pathogen effectors, either by cell-surface receptors or by NLRs, triggers an immune response that is often associated with the hypersensitive response (HR), which is a form of programmed cell death (PCD) [7,18,20].

Cell-surface receptors are single pass transmembrane proteins that possess an extracellular domain, in most cases consisting of leucine-rich repeats (LRRs), which mediates recognition of proteinaceous ExIPs. These immune receptors can be categorised into receptor-like kinases (RLKs) and receptor-like proteins (RLPs), according to the presence or absence of an intracellular C-terminal kinase domain, respectively. As RLPs lack an intracellular domain for the initiation of downstream signal transduction, these cell-surface receptors constitutively associate with an adaptor RLK to mediate downstream signalling. Indeed, the RLK SUPPRESSOR OF BIR1-1 (SOBIR1) was found to be a common adaptor for LRR-RLPs mediating immune responses [61,66]. An example of such an RLP is the tomato Cf-4 protein, which is a cell-surface receptor conferring resistance to races of the tomato pathogen *Cladosporium fulvum* secreting the matching fungal effector Avr4. Upon Avr4 perception,

the Cf-4/SOBIR1 receptor complex recruits the RLK BRI1-ASSOCIATED KINASE 1 (BAK1), leading to a series of phosphorylation events between the cytoplasmic kinase domains of SOBIR1 and BAK1 that have come in close proximity, eventually activating a downstream immune signalling cascade [76]. This process triggers an immune response that includes a fast production of reactive oxygen species (ROS) in the apoplast by respiratory burst oxidase homologs (RBOHs) and eventually an HR is activated (Chapter 3). In the resting state, the Cf-4/SOBIR1 receptor complex is negatively regulated by the interaction of BAK1 with the RLK BAK1-INTERACTING RECEPTOR-LIKE KINASE 1 (BIR1) [100]. Knocking out *BIR1* in *Arabidopsis thaliana* (*Arabidopsis*) or silencing of its homologs in *N. benthamiana*, results in a constitutive activation of immune responses that depends on the RLKs SOBIR1 and BAK1 [93,100]. Currently, very little is known regarding the immediate downstream signalling components of RLP/SOBIR1-containing complexes mediating immune responses in solanaceous plants. For instance, receptor-like cytoplasmic kinases (RLCKs) are common signalling components interacting with RLKs, such as FLAGELLIN-SENSITIVE 2 (FLS2) from *Arabidopsis*. This is particularly the case for the RLCKs belonging to the group VII (RCLK-VII) [25,154]. Interestingly, the tomato RLCK-VII AVR9/CF-9-INDUCED KINASE 1 (ACIK1), has been found to be required for the immune responses triggered by Cf proteins, including Cf-4 [164]. However, its exact position in the immune signalling cascade is still unknown. In *Arabidopsis*, which is a member of the *Brassicaceae* family, only higher order knock-out mutant plants in subgroups of RLCK-VII are compromised in ROS production upon activation of several RLKs [113]. This indicates that there is functional redundancy among the various RLCK VII members, which renders their individual evaluation by virus-induced gene silencing (VIGS) in *Nicotiana benthamiana* difficult.

The identification of interaction partners is a critical step in deciphering the various components of the signalling cascade that is activated by cell-surface receptors. Commonly used approaches to identify protein-protein interactions that are based on affinity purification, followed by mass spectrometry to identify co-purifying signalling partners, requires the interacting partners to remain bound to each other during the process of protein isolation and purification [313,323]. This requirement limits the application of regular affinity purification approaches for the study of membrane-associated proteins engaging in weak or transient protein-protein interactions. Recently, proximity-dependent labelling through biotinylation, coupled with mass spectrometry (PL-MS), has been emerging as an alternative approach

to identify proteins that only weakly or transiently interact with the target protein [329,330]. The fusion of a promiscuous biotin ligase to a protein of interest results in the biotinylation of endogenous proteins that interact with this protein in a proximity-dependent manner. The biotinylated proteins can subsequently be captured by streptavidin-based affinity purification and identified by mass spectrometry analysis. Several modified enzymes have been developed for PL, with TurboID (TbID) being one of the most promising ones [342]. This enzyme was developed based on the *Escherichia coli* biotin ligase BirA, using yeast display-based directed evolution [338], and it possesses fast labelling kinetics and requires biotin, which is a non-toxic, membrane-permeable substrate that is already naturally present in plant tissues. Of note, PL-MS cannot discriminate whether two proteins are actually physically interacting with each other or whether they are just in close vicinity. Instead, the method provides an indication of the physical proximity between the promiscuous biotin ligase that is fused to the bait protein and the proteins that are biotinylated by the ligase. In animal cells, the TbID enzyme will biotinylate proteins within a radius of at least 35nm over a period of 10 minutes after biotin supplementation [339]. However, this distance depends on the specific experimental conditions [330,341] and cannot be directly extrapolated to plant systems. In plants there is less control over the biotinylation process, as plants synthesise biotin endogenously, allowing the biotinylation of proximal proteins to take place even in the absence of biotin supplementation (see Chapter 4).

In this study, we have performed TbID-based PL-MS with the aim to identify downstream signalling components of the Cf-4/SOBIR1-containing receptor complex in *N. benthamiana*. We employed the previously validated NbSOBIR1 and Cf-4 TbID-tagged fusion proteins as baits (Chapter 4) and have identified a large set of proteins that are predicted to be located in close-proximity to the cytoplasmic kinase domain of NbSOBIR1, and which are promising candidates for further validation. When using NbSOBIR1-TbID as a bait, the identified candidates include proteins that are anticipated to be functionally related to the Cf-4/SOBIR1 complex, like RLCKs belonging to group VII, mitogen-activated protein kinases (MAP3Ks) and the RBOH enzyme that is responsible for the swift production of apoplastic ROS upon perception of Avr4. Interestingly, such signalling partners were not identified when Cf-4-TbID was used as a bait. Our results are consistent with a role of SOBIR1 as an integral part of the signalling cascade, acting as a bridge between the Cf-4 receptor and the cytoplasmic immune signalling machinery.

RESULTS

Proximity-dependent biotinylation from *Nb*SOBIR1 in *N. benthamiana*.

To identify proteins that are present in close-proximity of the co-receptor SOBIR1, when transiently expressed in a Cf-4 background, we performed a series of TbID-based PL-MS experiments in which we expressed previously validated bait-TbID fusion proteins in *N. benthamiana* stably expressing Cf-4 (Chapter 4). For the first set of samples to be generated, we transiently expressed the fusion proteins *Nb*SOBIR1-YFP-TbID and the control GUS-YFP-TbID in *N. benthamiana:Cf-4 sobir1(-like)* knock-out plants (Table S1). This transgenic *N. benthamiana* line stably expresses the RLP Cf-4 and is a CRISPR/Cas-mediated knock-out mutant of *SOBIR1* and its close paralog *SOBIR1-like* [253]. The samples were prepared in triplicate, expressing each TbID-tagged bait protein in 15 *N. benthamiana:Cf-4 sobir1(-like)* plants (one leaf per plant), and combining the agroinfiltrated leaves of five plants to generate each individual sample. Two days after agroinfiltration for driving the expression of the TbID-tagged fusion proteins, the leaves were infiltrated with a biotin solution at 200µM and harvested after one hour. Total protein extracts from the harvested leaves were desalted to remove the free biotin, and the desalted protein extracts were subsequently incubated with streptavidin-coated beads for one hour to capture the biotinylated proteins. After this incubation, the streptavidin-coated beads were collected and washed three times with a detergent-free version of the buffer used for protein extraction. The disulphide bonds in the captured proteins were then reduced using DTT, and the sulfhydryl groups were alkylated with acrylamide. Peptides from the captured proteins were released from the beads by tryptic digestion and subsequently analysed by nano-LC-MS/MS, using label-free relative quantitation. Although the data could still be used, because of the presence of residual detergent in the first set of samples, the second and the third set of samples for PL-MS received three additional washing steps with ammonium bicarbonate buffer after incubation with the streptavidin-coated beads. Besides this modification, we included LOW TEMPERATURE-INDUCED PROTEIN 6B (Lti6b)-YFP-TbID as an additional control. Lti6b is a small transmembrane protein that is commonly used as a PM marker in plant cell biology (Figure 1A) [331,344–347]. We used MaxQuant to identify the peptides and to quantify the relative amount of each biotinylated protein [357]. To determine the relative enrichment level, we used Perseus [358] to calculate two-sample t-tests, comparing the samples for which our TbID-tagged baits and control proteins were expressed.

The peptides that were significantly enriched in the samples expressing NbSOBIR1-YFP-TbID from the first, second, and third PL-MS experiment, when compared to the control, mapped to 209, 572 and 577 proteins, respectively. From those proteins, 81 were significantly enriched in all three independent PL-MS experiments in which NbSOBIR1-YFP-TbID was used as a bait protein (Figure 1B and 1C). Gene ontology (GO) terms enrichment analysis of this group of overlapping proteins revealed enrichment within two categories: "molecular function" (MF) and "biological process" (BP), with the most highly enriched term for each category being "protein serine/threonine kinase activity" (GO:0004674) and "protein phosphorylation" (GO:0006468), respectively (Figure 1D). Of these 81 reproducibly enriched proteins (Figure 1B and 1C, and Table 1), 22 are classified as protein kinases [359], including seven RLKs, five RLCKs, five MAP3Ks, a calcium-dependent protein kinase (CDPK), two homologs of the *Arabidopsis* blue light receptor PHOTOTROPIN 2 (PHOT2) [360], and a homolog of the *Arabidopsis* NON-RACE-SPECIFIC DISEASE RESISTANCE 1 (NDR1) protein [361]. Among the non-kinases included in this list, we find the RLP Cf-4, a phosphatase 2C, the RESPIRATORY BURST OXIDASE HOMOLOG B (RBOHB), three binding proteins (BiPs) involved in endoplasmic reticulum quality control (ER-QC) [207,362], five remorins, six homologs of the *Arabidopsis* immune repressor RPM1-INTERACTING PROTEIN 4 (RIN4) [363], four hypersensitive-induced reaction (HIR) proteins, nine proteins involved in chloroplast relocation [364], and several proteins involved in endocytosis and vesicular trafficking. No RLP other than Cf-4 was detected in any of the three sets of samples. Furthermore, we did find peptides matching with GUS, but we found no peptides mapping to the control Lti6b (Figure 1C), likely because of the protein being very small and relatively hydrophobic (Figure 1A). In relation to this observation, we also found no peptides mapping to the transmembrane domain of the identified RLKs and additional membrane-associated proteins that were significantly enriched in all three independent PL-MS experiments (Figure S1). Furthermore, we detected a significant enrichment of peptides originating from both homeologs of SOBIR1, Niben101Scf03816g01001 (NbSOBIR1a) and Niben101Scf04099g05004 (NbSOBIR1b) (Figure 1C and S2). However, the NbSOBIR1-YFP-TbID fusion protein that we generated is based on NbSOBIR1a, and label-free quantitation (LFQ) of the peptides that mapped uniquely to NbSOBIR1b did not result in any peptides. Therefore, the detection of NbSOBIR1b is probably an artifact of the mapping of the detected peptides, as due to their high homology, peptides matching NbSOBIR1a also in some cases match NbSOBIR1b.

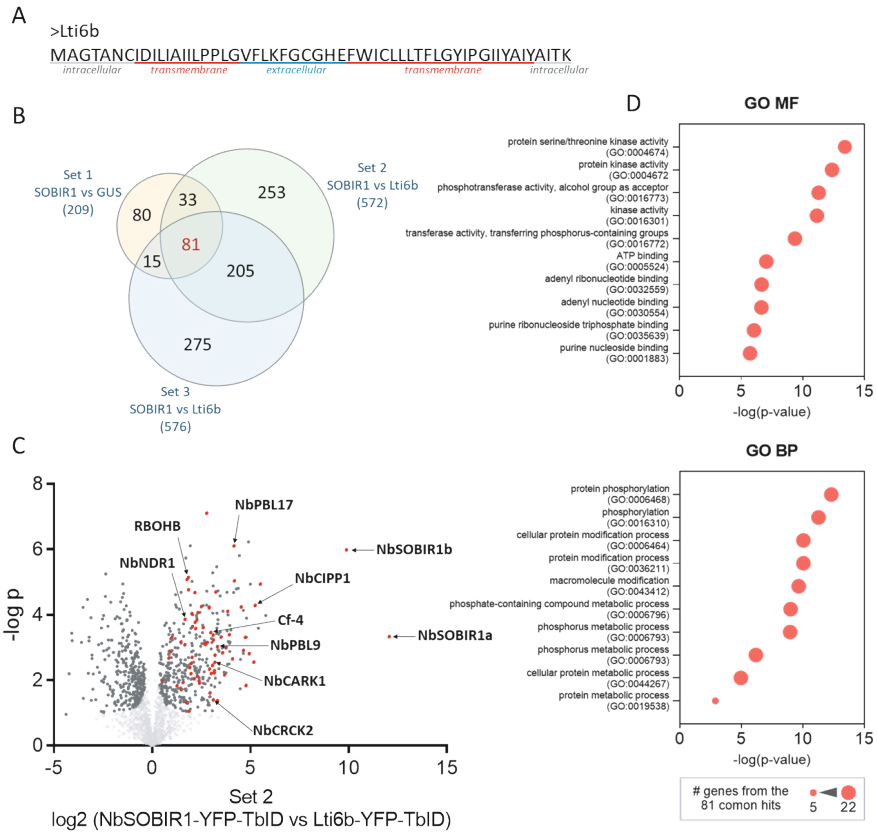

Figure 1. TbID-based PL-MS from NbSOBIR1 in *N. benthamiana*. TbID-tagged NbSOBIR1 and the GUS and Lti6b control proteins were transiently expressed by agroinfiltration in leaves of *N. benthamiana:Cf-4 sobir1(-like)*. Two days after agroinfiltration, the treated leaves were infiltrated with a solution containing 200µM of biotin and they were harvested after one hour. After total protein extraction, the extract was desalted to remove the free biotin and the biotinylated proteins were isolated using streptavidin-coated beads, subsequently on-bead digested with trypsin, and then analysed by nano-LC-MS/MS using label-free quantification (LFQ). In each PL-MS experiment, three replicates were included. The enrichment of the detected peptides was calculated by a two-sample t-test based on the LFQ intensities, with a false discovery rate (FDR) set to 0.05 and an S0 set to 0.1. (A) Amino acid sequence of the control Lti6b protein with the predicted transmembrane topology indicated [365]. (B) Venn diagram showing the number of significantly enriched proteins detected in the three independent PL-MS experiments, using NbSOBIR1-YFP-TbID as a transiently expressed bait protein in *N. benthamiana:Cf-4 sobir1(-like)*. Set 1 of three replicates used GUS-YFP-TbID as a control, whereas Set 2 and Set 3 of three replicates each, included Lti6b-YFP-TbID as a control. The areas in the Venn diagram are proportional to the number of proteins in each group [366]. (C) Representative volcano plot showing the proteins identified in the PL-MS analysis. Proteins enriched in the samples expressing NbSOBIR1-YFP-TbID are shown on the right,

and proteins enriched in the samples expressing the control Lti6b-YFP-TbID are shown on the left. Proteins crossing the threshold of significance are shown as dark grey dots, and the proteins that are not significantly enriched are shown as light grey crosses. Proteins belonging to the group of 81 that are significantly enriched in all three PL-MS experiments are shown in red. (D) GO-terms enrichment analysis of the group of 81 proteins significantly enriched in all three independent PL-MS experiments, using NbSOBIR1-YFP-TbID as a bait. The top 10 of the most highly enriched terms is shown for the categories "molecular function" (MF) and "biological process" (BP). No enrichment was found in the category of "cellular component".

Table 1. The 81 proteins reproducibly found to be biotinylated in all three independent PL-MS experiments, transiently expressing NbSOBIR1-YFP-TbID in *N. benthamiana:Cf-4 sobir1(-like)*. The proteins are grouped according to their functional annotation and are shown next to their *Arabidopsis* best blast hit (The *Arabidopsis* Information Resource, TAIR). The *N. benthamiana* identifiers that are depicted in bold indicate the proteins that were also significantly enriched in at least one PL-MS experiment using Cf-4-YFP-TbID as a bait. Asterisks next to the name of the corresponding *Arabidopsis* homologs indicate that the encoding gene is co-expressed with *AtSOBIR1* according to the data described in Chapter 3. The complete list of proteins detected in one, two and three PL-MS experiments is shown in Table S2.

Kinases		
group	Bentha ID	*Arabidopsis* best blast hit
RLKs	**Niben101Scf07619g00006**	AT3G51550 / FERONIA
	Niben101Scf02854g02005	AT1G48480 / RKL1
	Niben101Scf11524g00007	
	Niben101Scf03816g01001	AT2G31880 /SOBIR1 *
	Niben101Scf04099g05004	
	Niben101Scf08151g00006	AT3G24550 / PERK1
	Niben101Scf10330g02004	AT5G02070
RLCKs	Niben101Scf05118g10007	AT4G00330 / CRCK2 *
	Niben101Scf03216g00001	
	Niben101Scf00012g00012	AT1G07570 / PBL9
	Niben101Scf10157g01009	AT2G07180 / PBL17
	Niben101Scf01671g04002	AT3G17410 / CARK1 *
MAP3K	Niben101Scf02437g02021	AT2G24360 / STYK *
	Niben101Scf02836g02006	AT4G31170 / RAF28 *
	Niben101Scf07584g02008	AT5G50000 / CBC2
	Niben101Scf02237g07012	
	Niben101Scf03469g03002	AT3G22750

Table 1. *(Continued)*

Kinases		
other kinases	Niben101Scf03438g06004	AT3G57530 / CPK32 *
	Niben101Scf13290g00001	AT4G14350 / NDR1
	Niben101Scf11383g03008	AT5G58140 / PHOT2
	Niben101Scf02804g00010	
	Niben101Scf04396g02009	AT1G54610
Non-kinases		
RLP Cf-4	_	_
phosphatase 2C	Niben101Scf02133g02001	AT1G34750 / CIPP1 *
RBOHB	Niben101Scf02581g04013	AT5G47910 / RBOHD *
ER-quality control	**Niben101Scf02972g05008**	AT5G28540 / BIP1
	Niben101Scf15536g02038	
	Niben101Scf08590g00005	AT5G42020 / BIP2
remorins	Niben101Scf08587g00002	AT5G23750 / REM1.4
	Niben101Scf17127g00017	
	Niben101Scf04804g01002	
	Niben101Scf02910g01040	
guarded by NLRs	Niben101Scf08799g00001	AT3G25070 / RIN4
	Niben101Scf03479g05049	
	Niben101Scf08899g00008	
	Niben101Scf03488g06005	
	Niben101Scf07498g02020	
	Niben101Scf13593g00007	
hypersensitive-induced reaction proteins	Niben101Scf00593g03012	AT5G62740 / HIR4
	Niben101Scf04407g02005	
	Niben101Scf00593g03002	
	Niben101Scf00488g00003	
	Niben101Scf05166g07012	
chloroplast relocation	Niben101Scf00132g01003	AT1G64500 / THRUMIN1
	Niben101Scf03491g01021	AT1G42550 / PMI1
	Niben101Scf03738g00006	
	Niben101Scf06394g04009	AT1G66840 / PMI2
	Niben101Scf09172g01012	AT1G75100 / JAC1 *
	Niben101Scf18348g00015	
	Niben101Scf01085g02012	AT2G30520 / RPT2
	Niben101Scf03549g00004	AT5G67385 / NCH1
	Niben101Scf00709g04010	

Table 1. *(Continued)*

Kinases		
endocytosis and vesicle organisation	Niben101Scf01063g04003	AT5G16880 / TOL1
	Niben101Scf05049g00003	AT1G06210 / TOL2
	Niben101Scf05049g00008	
	Niben101Scf02637g00012	AT1G21380 / TOL3
	Niben101Scf00712g10025	AT1G20760 / ATEH1
	Niben101Scf02569g03013	AT1G12360 / KEU *
	Niben101Scf07294g00014	AT3G09740 / SYP71
	Niben101Scf01236g01010	AT3G17440 / NPSN13
	Niben101Scf18014g00014	
	Niben101Scf00199g03003	AT3G63460 / SEC31B
	Niben101Scf00257g00006	AT2G25430 / ATECA4
	Niben101Scf01489g00009	AT2G35190 / NSPN11
others	Niben101Scf03930g04011	AT1G15400 / MASS2
	Niben101Scf03979g02010	AT2G18960 / HA1
	Niben101Scf00593g01002	AT5G62670 / HA11
	Niben101Scf01812g05008	AT1G08680 / AGD14
	Niben101Scf00416g06002	AT1G16860 / SHOU4L
	Niben101Scf00898g02014	AT1G27100 *
	Niben101Scf06218g01003	AT1G30755 / PSI2
	Niben101Scf06172g01003	AT1G74690 / IQ31
	Niben101Scf08390g06006	AT2G01650 / PUX2
	Niben101Scf07305g00002	AT2G12462
	Niben101Scf12211g02007	
	Niben101Scf02280g04002	AT2G40070 / BPP1
	Niben101Scf12852g03012	AT3G05900
	Niben101Scf15536g02006	AT4G10840 / KLCR1
	Niben101Scf00700g05004	AT4G20260 / PCAP1
	Niben101Scf06815g01013	AT4G24630
	Niben101Scf02525g03002	AT5G43310

These results show that TbID-based PL-MS allows to detect proteins that are located in the vicinity of NbSOBIR1 in *N. benthamiana*, as suggested by the detection of Cf-4 and RLCKs belonging to group VII. In our search for functional components of SOBIR1-containing cell-surface receptor complexes, this approach resulted in the identification of a large set of proteins that merit further experimental validation (Table 1 and Table S2).

Proximity-dependent biotinylation from Cf-4 in *N. benthamiana*.

SOBIR1 and Cf-4 interact constitutively, thereby forming a bimolecular RLK [66]. Hence, we anticipated that performing PL-MS from both components of the complex would improve the identification of proteins that are in close-proximity to the Cf-4/SOBIR1 receptor complex and that possibly play a role in its functioning. Following this reasoning, three sets of samples for PL-MS analysis also included samples in which we transiently expressed the fusion protein Cf-4-YFP-TbID (Chapter 4) in leaves of *N. benthamiana* (Table S1).

The peptides that were significantly enriched in the samples obtained upon expressing Cf-4-YFP-TbID from the first, second, and third PL-MS experiment mapped to 307, 577, and 327 proteins, respectively (Figure 2A). From those proteins, 59 were enriched in all three independent PL-MS experiments in which Cf-4-YFP-TbID was used as a bait protein (Figure 2B, Table 2). This group of 59 proteins was subsequently characterised by a GO terms enrichment analysis (Figure 2C), and in the category of cellular components we found enrichment of GO terms related to components of the nucleus, with the highest enrichment corresponding to the "nucleosome" (GO:0000786). In the category of molecular function, we found enrichment for the GO terms: "protein heterodimerization activity" (GO:0046982), "protein dimerization activity" (GO:00046983), "unfolded protein binding" (GO:0051082), "DNA binding" (GO:0003677), "protein binding" (GO:0003677), and "nucleic acid binding" (GO:0003676). For the category of biological process, we found enrichment of GO terms related to the organisation of the DNA in the nucleus, with the highest enrichment corresponding to "nucleosome organisation" (GO:0.0034728). Overall, this GO terms enrichment analysis described a set of proteins very different from the one detected after performing PL-MS experiments with NbSOBIR1-YFP-TbID. This analysis suggests that the fusion protein Cf-4-YFP-TbID is locating at the membrane of the nucleus, besides its expected location at the PM [76]. From the 59 proteins that were significantly enriched in all three independent PL-MS experiments when using Cf-4-YFP-TbID as a bait, 18 are histones (Table 2).

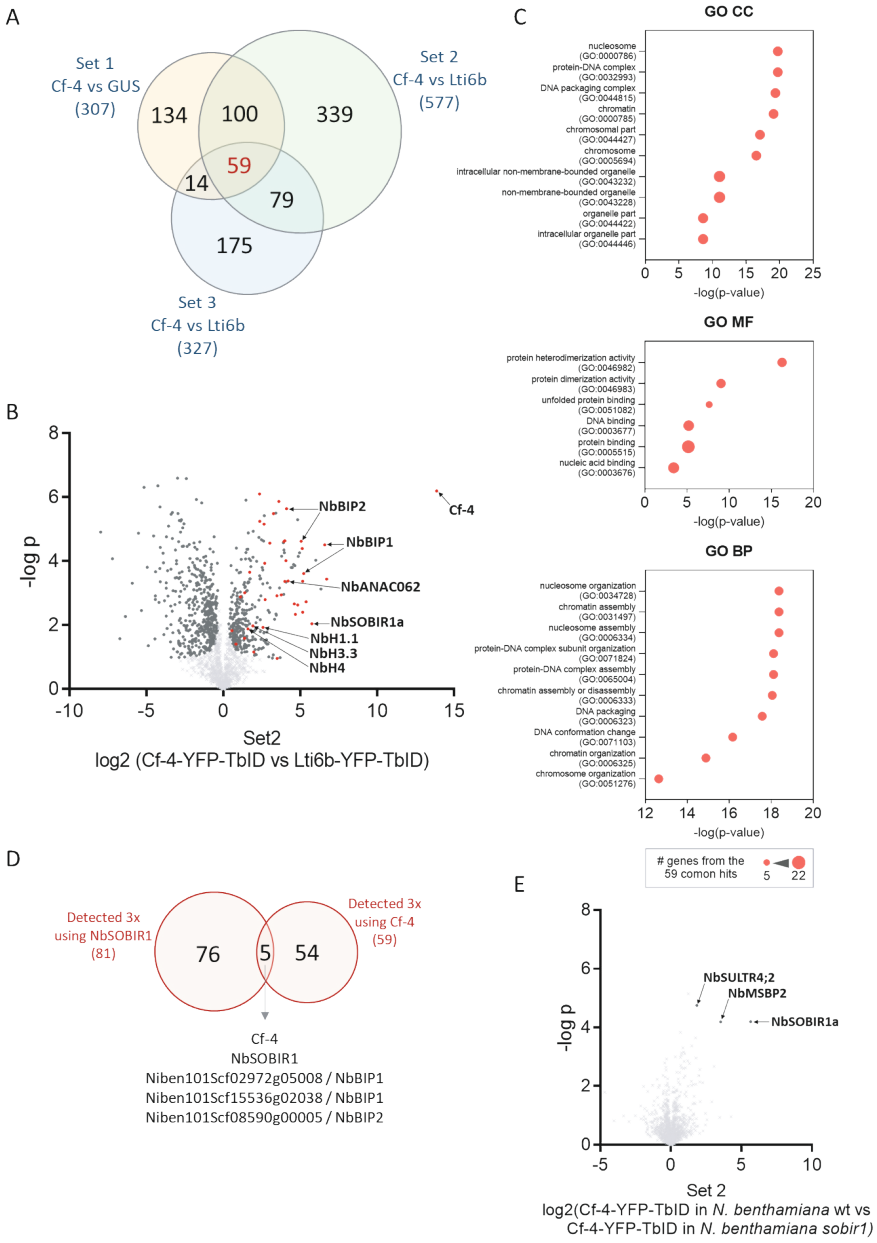

Figure 2. TbID-based PL-MS from Cf-4 in *N. benthamiana*. The TbID-tagged Cf-4 fusion protein was transiently expressed both in *N. benthamiana* wild-type (WT) and in *N. benthamiana:Cf-4 sobir1(-like)*, whereas the controls GUS- and Lti6b-YFP-TbID were expressed in *N. benthamiana:Cf-4 sobir1(-like).* Two days after agroinfiltration, the leaves were infiltrated with a biotin solution at 200µM and were harvested after one hour. After total protein extraction, the extract was desalted

to remove the free biotin and the biotinylated proteins were isolated using streptavidin-coated beads. The captured proteins were on-bead digested with trypsin, and the released peptides were subsequently analysed by nano-LC-MS/MS using LFQ. In each PL-MS experiment three replicates were included. The relative protein quantification of the sample compared to the to control was performed by applying a two-sample t-test on the LFQ intensities, with an FDR=0.05 and an S0=0.1. (A) Venn diagram showing the number of proteins significantly enriched in the three independent PL-MS experiments, using Cf-4-YFP-TbID as a bait protein. Set 1 used GUS-YFP-TbID as a control, whereas Set 2 and Set 3 used Lti6b-YFP-TbID as a control. The areas in the Venn diagram are proportional to the number of proteins in each group [366]. (B) Representative volcano plot showing the proteins identified in the PL-MS analysis using TbID-tagged Cf-4. Proteins enriched in the samples expressing Cf-4-YFP-TbID are shown on the right, and the proteins enriched in the samples expressing the control Lti6b-YFP-TbiD are shown on the left. Proteins passing the threshold for significance are shown as dark grey dots, and the proteins that are not significantly enriched are shown as light grey crosses. Proteins belonging to the group of 59 that were significantly enriched in three PL-MS experiments using Cf-4-YFP-TbID are shown in red. (C) GO-term enrichment analysis of the group of 59 proteins found to be enriched in three independent PL-MS experiments, using Cf-4-YFP-TbID as a bait. The top 10 of the most highly enriched terms is shown. (D) Venn diagram showing the overlap between the proteins that were significantly enriched in all three independent PL-MS experiments using NbSOBIR1-YFP-TbID and using Cf-4-YFP-TbID as a bait. The areas are proportional to the numbers in each group [366]. (E) Volcano plot showing the result of performing PL-MS upon transiently expressing Cf-4-YFP-TbID in *N. benthamiana*, in either the presence or absence of SOBIR1 homologs. Proteins enriched in samples expressing TbID-tagged Cf-4 in *N. benthamiana sobir1(-like)* are shown on the left, and proteins enriched in samples expressing TbID-tagged Cf-4 in WT *N. benthamiana* are shown on the right. Significantly enriched proteins are shown as dark grey dots, and the proteins that did not pass the threshold for significance are shown as light grey crosses. The arrows point at Niben101Scf01035g05012 (NbMSBP2), Niben101Scf30418g00019 (SULTR4;2), and Niben101Scf03816g01001 (NbSOBR1a).

However, from this group, 13 are H4 histones that are detected as a single protein group because of their small size and sequence similarity. Among the detected proteins we also found four proteins involved in vesicle-mediated protein transport, and several chaperones involved in the endoplasmic reticulum (ER) quality-control pathway, including binding proteins (BiPs), and homologs of the *Arabidopsis* transcription factor ANAC062, which is a PM-tethered transcription factor that is involved in the unfolded protein response [207,367]. No protein kinase, other than NbSOBIR1 itself, is part of the list of proteins that are significantly enriched in the three independent PL-MS experiments using Cf-4-YFP-TbID as a bait. From the 81 proteins found to be enriched in all three PL-MS experiments using NbSOBIR1-YFP-TbID as a bait, 17 were also enriched at least in one of the PL-MS experiments in which Cf-4-YFP-TbID was used as a bait (Table S2). Only five proteins were found to be enriched in all three

independent experiments when using both baits, these are Cf-4 and NbSOBIR1 themselves, and three BiP proteins (Figure 2D).

Table 2. The 59 proteins detected in three independent PL-MS experiments expressing Cf-4-YFP-TbID in *N. benthamiana*. The proteins are grouped according to their functional annotations and are shown next to their *Arabidopsis* best blast hit (TAIR). *N. benthamiana* identifiers depicted in bold refer to the proteins that are significantly enriched in at least one PL-MS experiment using NbSOBIR1-YFP-TbID as a bait. Asterisks next to the name of the *Arabidopsis* homologs indicate that the protein is co-expressed with SOBIR1 according to the data described in Chapter 3. The complete list of proteins detected in one, two and three PL-MS experiments is shown in Table S2.

Group	bentha ID	*Arabidopsis* best blast hit
RLP Cf-4	**Cf-4**	
RLK	**Niben101Scf03816g01001**	SOBIR1 *
ER-quality control / protein folding	**Niben101Scf01596g11007**	AT5G61790 / CNX1
	Niben101Scf03777g00018	
	Niben101Scf03349g00008	AT3G62600 / ATERDJ3B
	Niben101Scf03390g09001	
	Niben101Scf04331g09018	AT4G24190 / HSP90
	Niben101Scf27914g00006	
	Niben101Scf06091g00010	AT2G25110 / SDF2
	Niben101Scf02972g05008	AT5G28540 / BIP1
	Niben101Scf13703g01006	
	Niben101Scf02030g04003	
	Niben101Scf15536g02038	
	Niben101Scf00369g07016	AT5G42020 / BIP2
	Niben101Scf08590g00005	
	Niben101Scf00308g01003	AT3G49530 / ANAC062 *
	Niben101Scf02983g01003	
	Niben101Scf04779g01020	AT4G12400 / HOP3
	Niben101Scf09387g03018	
vesicle-mediated transport	**Niben101Scf01773g07014**	AT4G01810 / SEC23A
	Niben101Scf01750g14033	AT5G22360 / VAMP714 *
	Niben101Scf00173g04010	AT2G36300
	Niben101Scf03413g00005	
translational machinery	**Niben101Scf06761g01029**	AT5G23740 / RPS11-BETA
	Niben101Scf14636g02013	AT1G61580 / ARP2
	Niben101Scf01968g00002	AT3G53740
	Niben101Scf24868g00002	
	Niben101Scf00863g02001	AT1G76810

Table 2. *(Continued)*

Group	bentha ID	*Arabidopsis* best blast hit
histones	Niben101Scf04361g01001	AT1G06760 / H1.1
	Niben101Scf06590g03003	
	Niben101Scf07945g01002	AT5G10980 / H3.3
	Niben101Scf02537g02033	
	Niben101Ctg14707g00002	AT5G59970 / H4
	Niben101Scf00482g03005	
	Niben101Scf01154g17005	
	Niben101Scf01579g00002	
	Niben101Scf02441g01009	
	Niben101Scf03088g01003	
	Niben101Scf05373g02004	
	Niben101Scf05579g00001	
	Niben101Scf06238g01004	
	Niben101Scf07275g00004	
	Niben101Scf07650g02006	
	Niben101Scf10015g01010	
	Niben101Scf16416g02012	
	Niben101Scf23814g00038	
others	**Niben101Scf02829g06001**	AT1G03090 / MCCA
	Niben101Scf07382g01007	AT1G52670 / BADC2
	Niben101Scf12266g02002	
	Niben101Scf10152g03006	AT3G56130 / BADC1
	Niben101Scf07459g00017	AT2G45790 / PMM
	Niben101Scf00704g04019	AT4G31080 / LNP2.2
	Niben101Scf00972g01011	
	Niben101Scf01727g03003	AT1G14340 / BPL3
	Niben101Scf00634g04004	AT1G20330 / SMT2
	Niben101Scf00355g01008	AT3G17000 / UBC32
	Niben101Scf04325g01023	AT5G59210
	Niben101Scf01623g14008	AT3G62580
	Niben101Scf10338g00011	

The RLK SOBIR1 and the RLP Cf-4 constitutively interact and SOBIR1 is required for proper accumulation and functionality of Cf-4 [66,253]. To evaluate the effect of the absence of SOBIR1 on the detection of proteins that are in the proximity of Cf-4, we included samples in which we expressed Cf-4-YFP-TbID in *N. benthamiana sobir1(-like)* knock-out mutant lines [253] in our PL-MS experiments, and compared the detected peptides with the ones detected in the samples in which we expressed the same bait in *N. benthamiana* wild-type (WT) plants. We observed a significant enrichment of peptides mapping to three particular proteins in the samples originating from *N. benthamiana* WT plants (Figure 2E). Besides NbSOBIR1 itself, the other two detected proteins are homologs of *Arabidopsis* MEMBRANE STEROID BINDING PROTEIN 2 (MSBP2) and SULFATE TRANSPORTER 4;2 (SULTR4;2). From these three proteins, only NbSOBIR1 belongs to the group of proteins detected in the three independent PL-MS experiments in which Cf-4-YFP-TbID was used as bait.

Overall, these results suggest that Cf-4 itself is not in close-proximity to the expected signalling components that play a role downstream of the Cf-4/NbSOBIR1 receptor complex, like RLCKs and MAP3Ks. It appears that NbSOBIR1 is an integral part of the signalling pathway, connecting the cell-surface receptor Cf-4 with its downstream signalling partners.

Comparing GUS and Lti6b as controls for PL-MS using SOBIR1 and Cf-4

To compare the implications of using TbID-tagged GUS or Lti6b as controls for our PL-MS experiments, the third set of samples included both controls (Table S1). For the case of NbSOBIR1-YFP-TbID, the use of GUS-YFP-TbID as a control produced a list of significantly enriched peptides that mapped to 1091 proteins being biotinylated by GUS-YFP-TbID, which is a much larger set than the one generated when using Lti6b-YFP-TbID as a control (Figure 3A). From the set of 81 candidate proteins detected in the three PL-MS experiments using NbSOBIR1-YFP-TbID as a bait (Figure 1 and Table 1), only two were missed when using GUS-YFP-TbID as a control in the third set of samples, these are Niben101Scf00898g02014 and Niben101Scf12852g03012, which are two proteins of unknown function (Figure 3A, Table 1). For the case of Cf-4-YFP-TbID, the use of GUS-YFP-TbID as a control produced a list of significantly enriched peptides that mapped to 753 proteins (Figure 3B), which is also a larger set that the one generated when using Lti6b-YFP-TbID as a control.

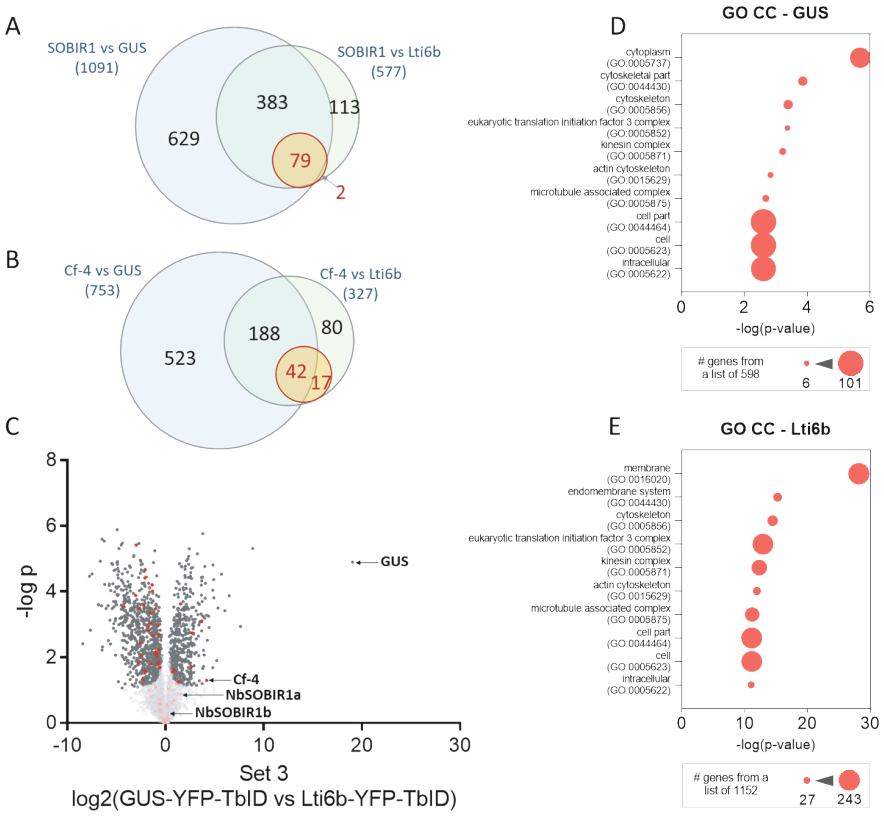

Figure 3. Comparison of GUS and Lti6b as controls for TbID-based PL-MS on the cell-surface receptors SOBIR1 and Cf-4. TbID-tagged GUS, Lti6b, and NbSOBIR1, were transiently expressed in *N. benthamiana:Cf-4 sobir1(-like).* TbID-tagged Cf-4 was expressed in *N. benthamiana* WT. Two days after agroinfiltration, the leaves were infiltrated with a solution containing 200µM of biotin and were harvested after one hour. Total protein extracts from the treated leaves were desalted, and the biotinylated proteins were isolated using streptavidin-coated beads. Peptides from the captured proteins were released from the beads by tryptic digestion and they were analysed by nano-LC-MS/MS, using label free quantification (LFQ). Three replicates were included. The enrichment of the detected proteins was calculated by a two-sample t-test based on the LFQ intensities, with a FDR set to 0.05 and S0 set to 0.1. (A) Area-proportional Venn diagram [366] showing the number of significantly enriched proteins detected when using NbSOBIR1-YFP-TbID as a bait, and either GUS-YFP-TbID or Lti6b-YFP-TbID as a control. The red circle indicates the 81 proteins found to be significantly enriched in three independent PL-MS experiments, using NbSOBIR1-YFP-TbID as a bait (Figure 1). (B) Area-proportional Venn diagram [366] showing the number of proteins corresponding to the significantly enriched peptides when using Cf-4-YFP-TbID as a bait, and either GUS-YFP-TbID or Lti6b-FYP-TbID as a control. The red circle indicates the 59 proteins found to be significantly enriched in the three independent PL-MS experiments, using Cf-4-YFP-TbID as a bait (Figure 2).

(C) Volcano-plot showing the proteins identified by PL-MS when comparing the samples obtained upon expression of GUS-YFP-TbID with the samples that were obtained upon expression of Lti6b-YFP-TbID. The change in colour, from light grey to dark grey, indicates the threshold for statistical significance. The proteins that were significantly enriched in three independent experiments in which NbSOBIR1-YFP-TbID was used as a bait (indicated with the red dots in Figure 1C) are shown in red; as red dots if they pass the threshold for statistical significance and as light red crosses if they were not significantly enriched in neither GUS-YFP-TbID nor Lti6b-YFP-TbID. (D-E) GO-term enrichment analysis of the cellular component's category, showing the top 10 of most enriched terms in samples obtained upon expression of (D) GUS-YFP-TbID or (E) Lti6b-YFP-TbID.

From the 59 proteins detected to be significantly enriched in the three PL-MS experiments using Cf-4-YFP-TbID as a bait, 17 were missed when using GUS-YFP-TbID as a control in the third set of samples. These are the ribosomal proteins Niben101Scf06761g01029 and Niben101Scf14636g02013, and a set of histone proteins including Niben101Scf06590g03003, Niben101Scf07945g01002, Niben101Scf02537g02033, and 12 histones H4 that were detected as a single protein group because of their small size and sequence similarity. The shorter list of significantly enriched proteins that was detected when using Lti6b instead of GUS as a control for NbSOBIR1 and Cf-4 is consistent with Lti6b being a membrane-bound protein. When using TbID-tagged GUS and Lti6b as a control for each other (Figure 3C), the GO term enrichment analysis in the category of cellular components clearly reflects the cytoplasmic location of GUS (Figure 3D), and the membrane-bound nature of Lti6b (Figure 3E). These results suggest that the smaller set of candidates obtained from the first set of samples (Figure 1A) is not a consequence of having used GUS as a control, instead of Lti6b. However, it is likely a consequence of the lower quality of the samples, as indicated by the quality control of the LC-MS dataset (data not shown).

Proximity-dependent biotinylation from the Cf-4/NbSOBIR1 receptor complex does not detect significant alterations among the labelled components upon perception of Avr4.

Activation of cell-surface receptor complexes involves changes in protein-protein interactions, followed by phosphorylation events. For instance, perception of Avr4 by Cf-4 triggers the recruitment of the RLK BAK1 to the Cf-4/SOBIR1 receptor complex [76]. This process brings the cytoplasmic kinase domains of BAK1 and SOBIR1 in close-proximity, and initiates a series of phosphorylation events between both kinase domains that are essential for the activation of the downstream signalling

cascade, eventually leading to the HR [77]. RLKs generally interact with downstream cytoplasmic RLCKs that dissociate from the receptor complex upon their activation by phosphorylation, and which act as executors of downstream signalling events [25,154]. To evaluate whether the PL-MS approach can provide the resolution required to detect the specific recruitment or dissociation of immune signalling components, we prepared samples for which we transiently expressed either NbSOBIR1-YFP-TbID in *N. benthamiana:Cf-4 sobir1(-like)* or Cf-4-YFP-TbID in WT *N. benthamiana* and supplemented the biotin solution with either 10μM of pure Avr4 protein, or not (Table S1). In this way, we were able to compare the sets of significantly enriched peptides from samples treated with, and without Avr4. The results of the PL-MS using TbID-tagged NbSOBIR1 and Cf-4 as baits showed no relevant differences between the sets of detected proteins when comparing the samples including Avr4, or not (Figure 4A and 4B). For the samples for which NbSOBIR1-YFP-TbID was a used as bait protein, the only significantly enriched peptides upon treatment with Avr4 mapped to the Avr4 protein itself (Figure 4A). Besides this, another set of peptides mapping to a hydroxyproline-rich glycoprotein of unknown function (Niben101Scf00109g02013) was significantly enriched in the samples that were not treated with Avr4 protein. Similar results were obtained with the samples in which Cf-4-YFP-TbID was used as a bait (Figure 4B). For these samples, the infiltration of Avr4 protein before harvesting the plant material resulted in an enrichment of a set of peptides mapping to Avr4 and Niben101Scf13971g00002, which is a homolog of the *Arabidopsis* CTC-INTERACTING DOMAIN 7 (CID7) protein, which is associated with the modulation of RNA metabolism [368]. The samples that were not treated with Avr4 were significantly enriched in peptides mapping to two uncharacterised proteins with 95% of sequence similarity (Niben101Scf08157g02042 and Niben101Scf02778g04003). Our PL-MS experiments revealed no significant impact of the perception of Avr4 on the composition of the set of proteins found to be in the vicinity of the Cf-4/NbSOBIR1 receptor complex. We did not detect the recruitment of BAK1, or its close paralogs, to the receptor complex upon the addition of the Avr4 protein. Intriguingly, we also did not detect any peptides mapping to the different BAK1 homologs in any of our PL-MS experiments when using TbID-tagged NbSOBIR1 or Cf-4 as a bait.

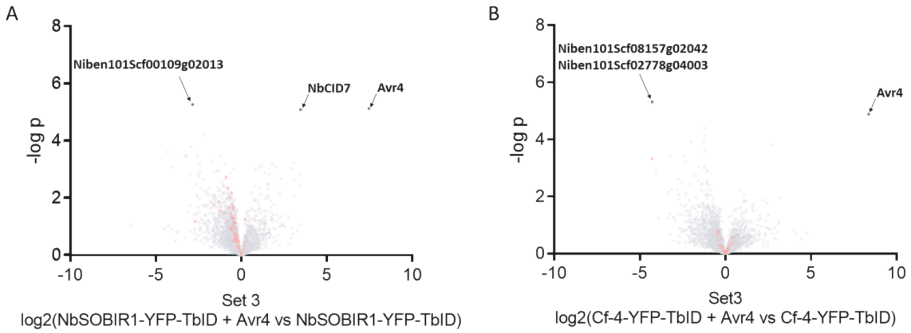

Figure 4. The impact of Avr4 perception on the composition of the set of proteins detected by PL-MS, using TbID-tagged NbSOBIR1 and Cf-4 as a bait in *N. benthamiana*. NbSOBIR1-YFP-TbID was expressed in *N. benthamiana:Cf-4 sobir1(-like)*, whereas Cf-4-YFP-TbID was expressed in *N. benthamiana* WT. Two days after agroinfiltration, the leaves were infiltrated with either a solution containing 200µM of biotin complemented with 10µM of Avr4, or with a solution only containing 200µM of biotin, after which the leaves were harvested after one hour. Total proteins were extracted, after which the biotinylated proteins were isolated from the desalted total protein extracts using streptavidin-coated beads. Peptides were released from the captured proteins by on-bead tryptic digestion, and they were analysed by nano-LC-MS/MS using label free quantification. (A-B) Volcano plots depicting the enrichment of the proteins when using (A) NbSOBIR1-YFP-TbID and (B) Cf-4-YFP-TbID, in the presence or in the absence of Avr4. Proteins enriched in the samples treated with Avr4 are shown on the right, whereas proteins enriched in the samples without Avr4 treatment are shown on the left. Proteins passing the threshold of significance are indicated with arrows. The proteins that were significantly enriched in three independent PL-MS experiments, using (A) NbSOBIR1-YFP-TbID (shown as red dots in Figure 1C) and (B) Cf-4-YFP-TbID (shown as red dots in Figure 2B), as baits are shown as light red crosses.

DISCUSSION

TurboID-based PL-MS generates noisy datasets in *N. benthamiana*.

Proximity-dependent labelling followed by mass spectrometry (PL-MS) is emerging as an attractive alternative to yeast-based screenings and classical affinity purifications for the study of weak or transient protein-protein interactions involving membrane-bound proteins, with the aim to dissect the composition of receptor complexes localised at the cell surface [369]. However, PL-MS does not provide conclusive evidence of a direct physical and functional interaction between the bait protein and the identified biotinylated proteins, as it merely gives an indication of the physical proximity between two proteins. Furthermore, this technique reveals the proximity

relationships that are present during the entire life-cycle of a bait protein, from its synthesis until its degradation [269,330]. Therefore, the generated datasets are inherently noisy with regard to the search for specific functional protein-protein interactions. In this study, we performed a series of PL-MS experiments in *N. benthamiana* using two key components of an RLP/SOBIR1 receptor complex; the RLK NbSOBIR1 and the RLP Cf-4 themselves, as a bait. We identified a set of proteins that was consistently found to be in the proximity of our TbID-tagged bait proteins in three independent PL-MS experiments. From the total amount of proteins that was observed to be significantly enriched in at least one out of three PL-MS experiments, only 8.6% and 6.5% were consistently enriched in all three independent experiments that were performed using TbID-tagged versions of NbSOBIR1 and Cf-4, respectively. Our results suggest the need for a cautious interpretation of PL-MS datasets, especially when obtained through PL-MS experiments performed only one time. An example of such a dataset that was generated deploying the TbID biotinylating enzyme in *N. benthamiana*, is the published proteome that is proximal to the cytoplasmic immune receptor N [342], which is an NLR that confers resistance to Tobacco mosaic virus (TMV) [370]. In this study, a PL-MS experiment using a TbID-tagged version of N resulted in the identification of a set of 374 proteins that were significantly enriched in the samples expressing the bait protein. Experimental evaluation of 10 of these proteins resulted in the identification of a putative E3 ubiquitin ligase that interacts with and regulates the stability of N. Besides being an example of a successful application of PL-MS in *N. benthamiana*, the numbers in this report evidence the limitation of PL-MS for the unbiased discovery of functionally relevant interacting proteins. Our results suggest that multiple independent PL-MS experiments are necessary to define a reproducible set of proteins that locates in the vicinity of a TbID-tagged bait protein. Yet, the need for replicate PL-MS experiments to reduce the large number of false positives, imposes a significant impact on the required budget. Further optimisation of our protocol for PL-MS in *N. benthamiana* should evaluate the possibilities for a reduction of the time between the infiltration of biotin and harvesting of the leaf samples, as well as a reduction in the concentration of biotin supplemented to the leaf tissue. Our previous results showed that the endogenous levels of biotin in *N. benthamiana* are already sufficient for the application of TbID-based PL (Chapter 4). Besides this, the bimolecular nature of RLP/SOBIR1 receptor complexes might allow the use of split versions of promiscuous biotin ligases, such as split-TurboID [371]. Instead of using a full-length enzyme, this method is based on the use of two inactive fragments of the biotin ligase, which are brought

together and subsequently result in an active enzyme as a result of protein-protein interaction. This could lead to a more focused view of the proximal interactomes of different RLP/SOBIR1 receptor complexes, as biotinylation of proximal proteins will only take place when a functional, signalling-competent, RLP/SOBIR1 receptor complex is present, and thereby reducing the number of false positives.

TbID-based PL-MS consistently identifies proteins that are functionally involved in RLP/SOBIR1-containing receptor complexes.

Besides the indicated noisiness of the obtained datasets of our PL-MS experiments in *N. benthamiana*, our approach resulted in a set of proteins that was consistently detected to be in close-proximity to our TbID-tagged bait proteins. In the case of NbSOBIR1, this group comprised a set of 81 proteins, including proteins that are known to be functionally involved in RLP/SOBIR1-containing complexes (Tables 1 and S2). In the case of Cf-4, we identified a set of 59 proteins, which did not include proteins that could be related to the signal transduction cascade that is expected to be activated downstream of RLP/SOBIR1-containing immune complexes upon ligand perception. Besides NbSOBIR1 and Cf-4 themselves, the only proteins that were consistently detected to be in close-proximity of both TbID-tagged bait proteins were endoplasmic reticulum (ER)-resident chaperones HSP70-related binding proteins (BiPs), which interact with transmembrane (co-)receptors and are required for their proper folding [207,372,373]. The signalling components present in the detected proximal proteome of NbSOBIR1 are anticipated not to be specific for the Cf-4/NbSOBIR1 receptor complex. NbSOBIR1 will interact with additional RLPs in *N. benthamiana*, and the signalling mechanism downstream of different RLP/SOBIR1 complexes may differ, as not all of them trigger an HR [18]. We expressed our TbID-tagged NbSOBIR1 fusion protein in a *N. benthamiana* line that expresses the transgene *Cf-4* and is a knock-out mutant of *SOBIR1* [253]. The observation that Cf-4 was the only RLP detected to be in close-proximity of NbSOBIR1, suggests that Cf-4 accumulates at relatively high levels when compared with the endogenous RLPs. Because of this reason, it is possible that a potentially specific Cf-4/NbSOBIR1 proximal proteome is enriched in the set of proteins that was found to be in close-proximity of the TbID-tagged NbSOBIR1 bait.

The set of proteins detected to be in close proximity to NbSOBIR1 includes functionally related proteins, such as RBOHB (Chapter 3). This enzyme is responsible for the extracellular ROS burst that takes place upon perception of apoplastic im-

munogenic patterns, such as the fungal effector Avr4 by Cf-4 (Chapter 3) and the flagellin-derived peptide flg22 [280]. The flg22 peptide is perceived by the RLK FLS2 [36], which also recruits the RLK BAK1 to activate immune responses [51]. The proximal proteome of NbSOBIR1 contains also five RLCKs, which were detected in all three independent replicate experiments using NbSOBIR1-YFP-TbID as a bait. The RLCKs form a large family of protein kinases that are divided into 17 groups [374]. These proteins act either as downstream signalling partners of cell-surface receptors, or as intracellular sensors of the effectors of pathogens [112]. One of these consistently detected RLCKs, Niben101Scf01671g04002, is a homolog of the tomato RLCK-VIII PTO-INTERACTING 1 (PTI1), which is required for the flg22-induced ROS burst [375]. Another two of the consistently detected RLCKs, Niben101Scf00012g00012 and Niben101Scf10157g01009, belong to subgroups 8 and 6 of RLCK group VII, respectively. Interestingly, there is ample evidence describing that the RLCK-VII group members acts downstream of cell-surface receptors [112]. In *Arabidopsis*, two close paralogs belonging to the RLCK-VII-8 subgroup, BOTRYTIS-INDUCED KINASE 1 (BIK1) and PBS1-LIKE 1 (PBL1), have been shown to interact with the RLK FLS2 and are indeed required for various FLS2-mediated immune responses [115,376]. Upon flg22 perception and BAK1 recruitment to the FLS2-BIK1 (or FLS2-PBL1) complex, these RLCKs activate the *Arabidopsis* homolog of *N. benthamiana* RBOHB by phosphorylation [210]. Additionally, higher order knock-out mutants of the RLCK-VII-8 subgroup showed a compromised ROS burst upon perception of different apoplastic immunogenic patterns in *Arabidopsis*, evidencing functional redundancy [113]. In the solanaceous plants tomato and *N. benthamiana*, the RLCK-VII-6 AVR9/CF-9 INDUCED KINASE 1 (ACIK1) is required for the immune responses triggered by Cf-4, and also by the RLP Cf-9, the latter which recognises the *C. fulvum* effector Avr9 [164,212]. Although we base the description of the obtained dataset as shown in Table S2 on the proteins that were consistently found to be significantly enriched in all three PL-MS experiments using TbID-tagged NbSOBIR1 (Table 1), it is also possible of having identified functionally relevant proteins among those proteins that were detected with less consistency. Of the 253 proteins that were significantly enriched in only two out of three of our PL-MS experiments using TbID-tagged NbSOBIR1, 20 are RLCKs, of which eight are RLCK-VII members (Figure 1B and Table S3). These RLCK-VII members are: four close paralogs that are members of the RLCK-VII-8 subgroup; two homeologs that are members of RLCK-VII-6; one RLCK-VII-4 member that is a homolog of *Arabidopsis* PCRK1, which functions downstream of the RLK FLS2 [377,378]; and one member of the RLCK-VII-1 subgroup, which is a homolog of *Arabidopsis* AVRPPHB-SUSCEPTIBLE 1

(PBS1) that acts as a sensor for the bacterial effector AvrPphB and activates immunity through its interaction with the NLR protein RESISTANCE TO PSEUDOMONAS SYRINGAE 5 (RPS5) [379,380].

TbID-based PL-MS has generated a set of novel candidates for signalling components of RLP/SOBIR1-containing receptor complexes.

Protein proximity represents weak evidence of a functional relationship. However, the presence of proteins that are known to be required for the functioning of RLP/SOBIR1-containing complexes, among those proteins that were consistently detected by PL-MS using TbID-tagged NbSOBIR1, invites to speculate about the potential roles of the other detected proteins in RLP/SOBIR1-mediated immune signalling (Tables 1 and S2). This is especially relevant when considering the different molecular processes that are expected to take place downstream of RLP/SOBIR1-containing complexes triggering immune responses. For instance, MAP kinase cascades represent key signalling modules that are activated by RLCKs downstream of cell-surface receptors [160,381]. These signal amplification cascades comprise three levels of protein phosphorylation: upstream MAPK kinase kinases (MAP3Ks), middle MAPK kinases (MAP2Ks), and bottom tier MAP kinases (MAPKs) [382]. Recognition of Avr4 by the Cf-4/SOBIR1 receptor complex indeed requires activation of a MAPK cascade for proper induction of defence responses, as silencing of the genes encoding the tomato MAPKs LeMPK1, LeMPK2, and LeMPK3 compromises the Cf-4-induced resistance to *C. fulvum* [205]. Interestingly, the set of proteins consistently detected to be in close proximity to NbSOBIR1 also includes five MAP3Ks. Two of these belong to the clade C6 of the MAP3Ks (Niben101Scf02437g02021 and Niben101Scf02836g02006) and the other three belong the clade C7 (Niben101Scf03469g03002, and the two homeologs Niben101Scf07584g02008 and Niben101Scf02237g07012) [382]. MAP3Ks are classified into two groups, MEKKs and RAF-like, and the consistently detected proteins all belong to the RAF-like group of MAP3Ks [382]. So far, unlike what has been shown for the MEKKs, there is no biochemical evidence showing that RAF-like MAP3Ks can activate downstream MAP2Ks-MAPKs cascades [160]. When looking at the proteins that were significantly enriched in two out of three PL-MS experiments using TbID-tagged NbSOBIR1, we find 12 MAP3K, of which four are indeed MEKKs (Figure 2A, Table S4). These are the two homeologs of *Arabidopsis* MAPKKK3 (Niben101Scf09063g00003 and Niben101Scf01795g10003), and the two homeologs of *Arabidopsis* MAPKKK7 (Niben101Scf03861g02013 and Niben101Scf01587g02009. MAPKKK3 forms part of the module MAPKKK3/MAPKKK5-MKK4/MKK5-MPK3/

MPK6, which is required for immune responses triggered by apoplastic immunogenic patterns [383,384]. In *N. benthamiana*, VIGS of these *MAPKKK3* homologs results in a reduction of the HR that is triggered upon co-expression of Cf-9 with Avr9 [385]. Likewise, VIGS of the detected homologs of *MAPKKK7* results in a reduction of the HR that is activated upon co-expression of Cf-4 with Avr4, and of Cf-9 with Avr9 [386].

The signalling mechanism of immune receptors needs to be regulated tightly because of the occurrence of growth-defence trade-offs [219]. Therefore, another molecular mechanism that is expected to be represented in the proximal proteome of SOBIR1 is the regulation of the phosphorylation status of its kinase domain by protein phosphatases of the type 2C (PP2C) [154,387]. Such a process was proposed to explain why the overexpression of *Arabidopsis* SOBIR1 triggers MAPK activation and an HR in *N. tabacum* and in *N. benthamiana*, whereas overexpression of the tomato and *N. benthamiana* homologs of SOBIR1 does not trigger such responses in these plants [388]. It was hypothesised that endogenous phosphatases of *N. tabacum* and *N. benthamiana* are able to properly regulate solanaceous SOBIR1 immune signalling by dephosphorylation, while having a lower affinity for more distantly related *Arabidopsis* SOBIR1 [388]. The list of proteins that are consistently detected to be in close-proximity of the kinase domain of NbSOBIR1 includes one PP2C-type protein phosphatase that is a homolog of the *Arabidopsis* CERK1-INTERACTING PROTEIN PHOSPHATASE 1 (CIPP1) (Table 1). *Arabidopsis* CIPP1 negatively regulates signalling by CHITIN ELICITOR RECEPTOR KINASE 1 (CERK1), which is an RLK that perceives chitin, a component of oomycete and fungal cell walls [389,390]. It has not yet been established whether CIPP1 is a specific negative regulator of CERK1-mediated immunity, or whether this particular phosphatase is a promiscuous enzyme involved in negatively regulating various RLKs. Possibly, the PP2C-type protein phosphatase that we identified is indeed a negative regulator of RLP/SOBIR1 complexes.

Some signalling components and interacting proteins anticipated to be identified, are missing from the detected proximal proteome of the Cf-4/SOBIR1 receptor complex.

Experimental evidence indicates a role of cytoplasmic NLR immune receptors downstream of SOBIR1-containing immune complexes. For example, in *Arabidopsis*, the constitutive activation of immune responses that causes cell death in knock-out mutants of BIR1, which is a negative regulator of RLP/SOBIR1/BAK1 complex formation, partially depends on PHYTOALEXIN DEFICIENT 4 (PAD4), ENHANCED DIS-

EASE SUSCEPTIBILITY 1 (EDS1), and NON RACE-SPECIFIC DISEASE RESISTANCE 1 (NDR1) [93,100]. PAD4 and EDS1 are part of a signalling module that is required for NLRs containing an N-terminal Toll-interleukin-1 (TIR) domain (TIR-NLRs or TNLs), while NDR1 is required for NLRs having an N-terminal coiled-coil (CC) domain (CC-NLRs or CNLs) [391]. In *Arabidopsis*, EDS1 and PAD4 have been shown to associate with SOBIR1 and to mediate immune responses triggered by RLPs and RLKs [162,163]. However, in *N. benthamiana*, where PAD4 seems to be dispensable for TNL immune signalling [301], neither EDS1 nor PAD4 are required for the HR and ROS burst triggered by the RLP Cf-4 [392], and knock-out mutants of *EDS1* or *PAD4* cannot rescue the lethal phenotype produced when silencing the homologs of *BIR1* in *N. benthamiana* (Chapter 3). Consistent with these observations, our PL-MS experiments in *N. benthamiana* did not detect a proximity of NbSOBIR1 with the homologs of EDS1 or PAD4. It was recently found that NB-LRR PROTEIN REQUIRED FOR HR-ASSOCIATED CELL DEATH 3 (NRC3), which is a helper CNL required for the activity of sensor CNLs, is required for the HR triggered by the RLP Cf-4 [165]. However, the processes connecting RLP/SOBIR1/BAK1 complex formation and signalling with the activation of downstream NRC3-dependent processes, likely through an uncharacterised sensor CNL, remain obscure. Our TbID-based PL-MS experiments with NbSOBIR1 did not detect any NLR in any of the three experiments that were performed (Table S2). The only potential links with the activity of CNLs downstream of the Cf-4/SOBIR1 complex are represented by proteins that are guarded by these immune receptors. The detected proximal proteome of the kinase domain of NbSOBIR1 includes six homologs of *Arabidopsis* RIN4, as well as homologs of the RIN4-associated proteins NDR1 [393] and a H^+-ATPASE 1 (HA1) [394] (Table 1). RIN4 is a negative regulator of defence responses that is targeted by several pathogen effectors in order to perturb plant immune signalling [363]. This protein is guarded by the CNLs RESISTANCE TO *P. SYRINGAE PV MACULICOLA* 1 (RPM1) and RESISTANT TO *P. SYRINGAE* 2 (RPS2), which monitor its phosphorylation status and its integrity, respectively [395,396]. Other members of the detected proximal proteome of NbSOBIR1 that could be guarded by CNLs are Niben101Scf05118g10007 and Niben101Scf03216g00001, which are the two homeologs of the *Arabidopsis* RLCK-IV CALMODULIN-BINDING RECEPTOR-LIKE CYTOPLASMIC KINASE 2 (CRCK2). In *Arabidopsis* a close paralog of CRCK2, CRCK3, is guarded by the CNL SUPPRESSOR OF MKK1 MKK2 2 (SUMM2), which monitors the phosphorylation status of CRCK3 [397].

The absence of known interactors in PL-MS datasets has been described in previous reports. The first application of PL-MS deployed a mutant version (R118G) of the biotin ligase BirA in mammalian cells and failed to detect one of the known interactors of the fusion protein that was used as bait [336]. More recently, the application of PL-MS in *N. benthamiana* using a TbID-tagged version of the TNL N failed to detect N RECEPTOR-INTERACTING PROTEIN 1 (NRIP1) and SQUAMOSA PROMOTER BINDING PROTEIN-LIKE 6 (SPL6) [342]. These two proteins are known to associate with N upon the activation of the immune response [398,399]. Our application of PL-MS in *N. benthamiana* using TbID-tagged NbSOBIR1 and Cf-4 for example failed to detect the recruitment of BAK1 homologs to the Cf-4/SOBIR1 complex upon treatment with Avr4. This was an unexpected result, considering that upon co-expression by agroinfiltration in *N. benthamiana*, TbID-tagged NbSOBIR1 and Cf-4 do biotinylate the tomato homolog of BAK1 in the absence of Avr4 (Chapter 4). In our experiments, treatment with Avr4 did not result in a relevant change in the proximal proteome of our TbID-tagged bait proteins (Figures 4A and 4B). This was expected in the case of proteins that dissociate from the receptor complex, as the endogenous level of biotin in *N. benthamiana* allows for biotinylation to take place before the infiltration of the solution containing both biotin and Avr4 (Chapter 4). Therefore, any dissociating protein would likely already be biotinylated and purified anyway by the pull-down with the streptavidin-coated beads and identified by the mass spectrometry analysis. However, it should be possible to detect the specific recruitment of proteins to the Cf-4/SOBIR1-containing receptor complex. The plant material was harvested one hour after the infiltration of a solution containing biotin and Avr4, and the recruitment of BAK1 is expected to happen within one minute after elicitation with Avr4 [76]. Possibly, the relatively high levels of protein accumulation achieved in *N. benthamiana* upon transient expression of the TbID-fused versions of SOBIR1 and Cf-4, employing the constitutive 35S promoter, causes aberrant localisation of the bait proteins, increasing the level of non-relevant background proteins and reducing the sensitivity of this PL method for endogenous interacting proteins that are only expressed at low levels. This could explain why our TbID-tagged Cf-4 protein seems to also locate at the nuclear membrane, besides its known localisation at the cell surface [76], as suggested by the biotinylation of histone proteins (Table 2). Also, this would explain why the absence of NbSOBIR1 has no effect on the detected proximal proteome of Cf-4 (Figure 2E), as only a fraction of the ectopically expressed Cf-4 protein would form a complex with the endogenous NbSOBIR1. Lastly, this could also explain why only Cf-4, as expressed by the *Cf-4* transgene in *N. benthamiana:Cf-4*

sobir1(-like), was found to interact with NbSOBIR1 and not any additional endogenous RLP. Further PL-MS experiments in *N. benthamiana* should consider the use of endogenous, or at least weaker, promoters for transient expression of the TbID-tagged baits. For the application of PL-MS in solanaceous crops such as tomato and potato, our results suggest that the relatively low levels of protein accumulation that are usually achieved by agroinfiltration in the leaves of these plants may be favourable for the biotinylation and subsequent detection of functionally relevant endogenous proteins.

The TbID-based PL-MS approach provides information about the molecular environment of RLP/SOBIR1-containing receptor complexes.

Besides the identification of candidate proteins that represent downstream signalling partners of RLP/SOBIR1-containing complexes, the application of PL-MS also provides information about the molecular environment in which these complexes are organized at the PM. The PM is a heterogenous organelle that can be subdivided into lateral compartments, with compositions and biological functions distinct from the surrounding membrane [400]. One of these levels of organization, referred to as nanodomains, consists of submicron assemblies of protein complexes and lipids that are visual as punctuate structures at the cell surface upon applying fluorescent microscopy techniques [401,402]. These nanodomains are hypothesized to act as platforms involved in the maintenance of signalling specificity of the different receptor complexes that share the same signalling components [403]. For instance, the RLK BRASSINOSTEROID INSENSITIVE 1 (BRI1) regulates developmental processes by perceiving brassinosteroid hormones [404], and shares signalling components with the RLK FLS2, including their co-receptor BAK1 and the RLCK BIK1 [405–407]. The spatial separation of FLS2 and BRI1 over different nanodomains is proposed to be a means to generate and preserve the signalling specificities of receptor complexes regulating growth and immune responses [403]. The detected TbID-based proximal proteome of NbSOBIR1 suggests that RLP/SOBIR1-containing receptor complexes also localize in nanodomains, as the proximal proteome of NbSOBIR1 includes several proteins known to be associated with these structures, like RBOHB [408,409], and also proteins that are considered to be markers for nanodomains, such as five hypersensitive-induced response proteins (HIRs) and four remorins (Table 1) [402,403,410–412].

HIRs are plant-specific members of a large family of stomatin/prohibitin/flotillin/HflK/C (SPFH) domain-containing proteins [410]. SPFH domain-containing proteins

are widespread, from prokaryotes to eukaryotes, and they are associated with nanodomains located at the PM and in various intracellular compartments [413]. HIRs associate with the inner side of the PM, likely through myristoylation and/or palmitoylation at their N-termini. These proteins are positive regulators of plant immune responses and their overexpression promotes the HR [410,414–416]. *Arabidopsis* possesses four HIRs and at least two of these, HIR1 and HIR2, form complexes with the CNL RPS2 [415]. Thirteen HIRs have been described in *N. benthamiana* [416], and the five HIRs that were found to be in close-proximity to NbSOBIR1 share strong similarity with HIR4 from *Arabidopsis* (Table 1).

Remorins were initially described in potato and tomato as pp34, being small 34KDa proteins associated with the PM that are phosphorylated upon perception of oligogalacturonides [417–419]. These proteins were later renamed as remorins due to their hydrophobicity and their ability to attach to the PM [420]. Remorins form a family of plant-specific membrane-associated proteins that are classified into six groups [421]. The five remorins that were found to be in close proximity to NbSOBIR1 belong to group 1, which is the group of the canonical remorins. These proteins are characterised by the presence of the domains Remorin_N and Remorin_C, and they associate with the PM as a result of palmitoylation of their C-terminal hydrophobic core [422,423]. These remorins are associated with the initiation of plant defence responses [423–427], and the overexpression of multiple canonical remorins from tomato induces cell death in *N. benthamiana* leaves [427]. In *Arabidopsis*, REM1.2, a canonical remorin, co-purifies with RPS2 upon affinity purification of RIN4 [394]. *Arabidopsis* possesses four canonical remorins [421], whereas *N. benthamiana* has at least eight of these proteins [421,423]. The remorins that were found to be in close proximity to NbSOBIR1 share more similarity with REM1.4 than with the other remorins of *Arabidopsis* (Table 1).

The proximal proteome of NbSOBIR1 also includes the two *N. benthamiana* homeologs of *Arabidopsis* PHOTOTROPIN 2 (PHOT2). Phototropins are blue-light receptors comprising an N-terminal photosensory region containing two Light, Oxygen or Voltage (LOV) domains and a C-terminal Ser/Thr kinase domain [360]. Sensing of blue light induces autophosphorylation of phototropins and subsequent phosphorylation of their substrate proteins [428]. Phototropins regulate multiple processes related to the perception of light, such as chloroplast relocation [364], stomatal opening [429] and phototropism [430,431]. *Arabidopsis* possesses two phototropins, PHOT1 and PHOT2, and both co-purify with the CNL RPS2 [432,433]. Interestingly, recent evidence points to a role

of phototropins in the modulation of plant defence responses. In *N. benthamiana*, overexpression of the potato homologs of PHOT1 and PHOT2 promotes infection by *Phytophthora infestans*. Inversely, silencing of the *N. benthamiana* homologs of *PHOT1* and *PHOT2* reduces colonisation of the leaves by this oomycete [434]. In addition, a recent study on the model bryophyte *Marchantia polymorpha* found that the phototropin MpPHOT is phosphorylated upon perception of chitin, and is involved in negative feedback regulation of defence-related gene expression [435].

Although the physical proximity of two proteins does not necessarily imply a functional relation, it still calls to our attention that, besides phototropins, several components involved in phototropin-mediated chloroplast movement are part of the proximal proteome of NbSOBIR1 (Table 1). Among the proteins consistently detected to be in close-proximity to NbSOBIR1, we for example also found ROOT PHOTOTROPISM 2 (RPT2), PLASTID MOVEMENT IMPAIRED 1 (PMI1), PMI2, J-DOMAIN PROTEIN REQUIRED FOR CHLOROPLAST ACCUMULATION RESPONSE 1 (JAC1) and THRUMIN1. All these proteins are molecular components regulating light-induced chloroplast movements [364]. Considering that the movement of the chloroplasts towards the nucleus of the cell, referred to as chloroplast perinuclear clustering, is a general response upon immune activation [436], the physical proximity of the different molecular components involved in these two cellular processes suggests that there is a crosstalk between light perception through phototropins and the immune responses triggered by RLP/SOBIR1-containing receptor complexes.

CONCLUSIONS

In this study, we performed a series of PL-MS experiments in *N. benthamiana* with the aim of identifying candidate proteins representing downstream signalling components of an RLP/SOBIR1-containing receptor complex. By using previously validated TbID-tagged fusion proteins (as described in Chapter 4), we identified the proximal proteomes of the RLP Cf-4 and the RLK NbSOBIR1, which constitutively interact. Our PL-MS experiments identified several proteins that were already known to be functionally related to RLP/SOBIR1-containing receptor complexes, as well as multiple novel candidates for downstream signalling components (Figure 5). Our results also suggest that PL-MS using cell-surface receptors as baits can be used as a tool to characterise the nanodomains in which different receptor complexes localise.

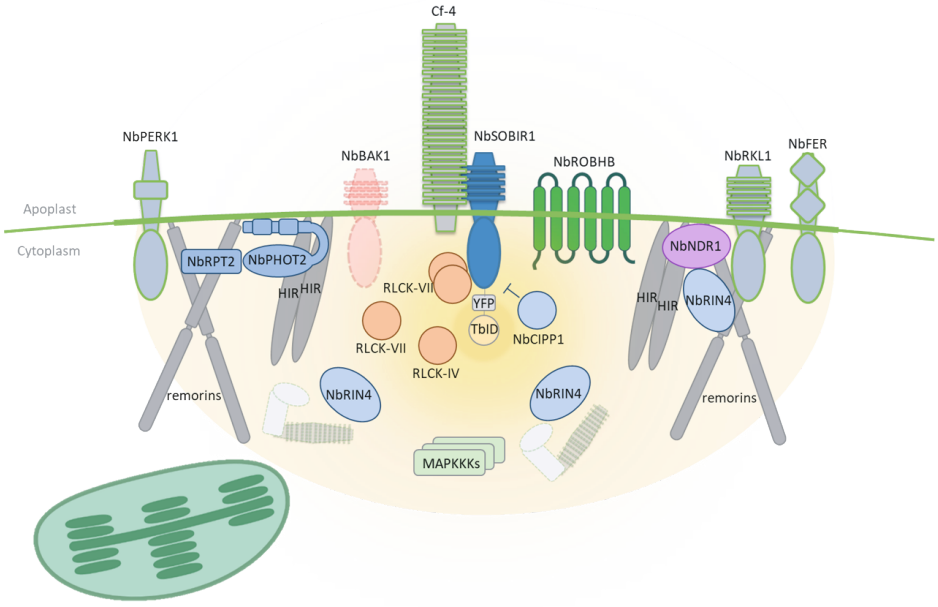

Figure 5. Diagram showing a selection of the proteins found to be in close-proximity to the Cf-4/NbSOBIR1 complex by TbID-based proximity labelling. In the presence of ATP and biotin, the promiscuous biotin ligase, TbID, produces a "cloud" of reactive and labile biotinyl-5'-AMP (bioAMP), shown as a yellow background. These bioAMP molecules react with primary amines, such as the lysines that are present in proteins, resulting in the covalent attachment of biotin to the proteins that are present within the biotinylation cloud. Subsequent extraction of the total proteins, followed by purification of the biotinylated proteins with streptavidin-coated beads and subsequent mass spectrometry analysis, allows to identify the proteins that reside in the vicinity of the TbID-tagged bait protein, which in this figure is NbSOBIR1. The identifiers of the proteins shown in the diagram are listed in Table 1. Proteins like NbBAK1 that are depicted with dotted lines are expected to be present but were not detected by PL-MS.

MATERIALS AND METHODS

Plant material and growth conditions

N. benthamiana, *N. benthamiana sobir1(-like), and N. benthamiana:Cf-4* were grown in climate chambers under 16 hr of light at 24°C, and 8 hr of darkness at 22 °C, and at an RH of 75%.

Phylogenetic analysis of the RLK-Pelle_LRR-XI group

The phylogenetic tree of the members of the group RLK-Pelle_LRR-XI in *Arabidopsis*, tomato and *N. benthamiana* was built after retrieving the protein sequences already classified at iTAK - Plant Transcription factor & Protein Kinase Identifier and Classifier [359]. The protein sequences were then aligned using the MAFFT web-server using the default settings [308], and the phylogenetic tree was built using the neighbour-joining method on the conserved sites with 100 bootstraps.

Agrobacterium-mediated transient transformation

Agrobacterium-mediated transient transformations (agroinfiltrations) were performed as previously described [206]. The constructs used for the PL-MS experiments were Lti6b-YFP-TbID (SOL9208), GUS-YFP-TbID (SOL9203), NbSOBIR1-YFP-TbID (SOL9201), and Cf4-YFP-TBID (SOL9210). We performed the agroinfiltrations in the first fully expanded leaf of three to four weeks old *N. benthamiana* plants of the indicated genotypes, at an OD_{600}=0.5. Each sample expressing one of the TbID-tagged fusion proteins was prepared in triplicate. For each replicate, we infiltrated one leaf per plant, in a total of five plants.

Streptavidin-pull down for mass spectrometry analysis

Two days after agroinfiltration, the leaves were infiltrated with a solution containing biotin (200 µM, pH=8, 10 mM MES) and harvested after one hour. For the treatments using Avr4, this protein was included in the biotin solution at a concentration of 10 µM. For each replicate, the five treated leaves were harvested, combined, wrapped in aluminium foil, and kept in liquid nitrogen or at -80˚C until further use.

The frozen samples were ground to a fine powder in liquid nitrogen using a mortar and pestle. Then, the pulverized samples were transferred to pre-cooled 50mL V-shape tubes, weighed, and resuspended in 2mL/g of extraction buffer (EB; pH=8.0, 150 mM NaCl, 1.0% [v/v] IGEPAL®CA-630 (=NP-40), 50 mM Tris, Sigma protease inhibitor cocktail = 1 tablet per 50 mL). For this resuspension, the frozen samples with the EB were vortexed at room temperature and kept on ice once melted. Then, the samples were centrifuged at 13,000rpm for 30 minutes at 4˚C in a Sigma 4-16K centrifuge .

To prevent saturation of the streptavidin beads with the free biotin remaining in the samples, 10mL of the centrifuged protein extracts were desalted using PD MiniTrap

PD-10 desalting columns (GE Healthcare). This process was done at 4°C, following the manufacturer's gravity protocol for removing salt.

The desalted protein extracts were transferred into pre-cooled 15mL tubes, and incubated for one hour at 4°C (10 rpm in an SB3 tube rotator, STUART), with 200µL of Dynabeads™ MyOne™ Streptavidin C1 (washed before use according to the manufacturer's protocol). After incubation, the beads were washed three times with 1mL of EB, without NP-40, and were resuspended in 45uL of EB buffer. Because of the presence of residual detergent in the first set of samples, the second and third set of samples were subjected to three additional washing steps with 1ml of ABC buffer (ammonium bicarbonate, 50 mM, pH=8), and were eventually resuspended in 45uL of ABC buffer.

Sample preparation for proteomics by mass spectrometry

While still on the beads, the disulphide bonds in the captured proteins were reduced by adding 5µL of DTT (150 mM) and incubating the samples at 45°C for 30 minutes. The sulfhydryl groups were subsequently alkylated by adding 6µL of acrylamide (200 mM) and incubating the samples for 10 minutes at room temperature.

The peptides to be measured by mass spectrometry were subsequently released from the streptavidin-coated beads by tryptic digestion. For this, a stock solution of trypsin (0.5 µg/µL of trypsin in 1 mM HCl, pH 3) was diluted 100 times in ABC buffer (ammonium bicarbonate, 50 mM, pH=8) and 100µL of the diluted trypsin solution was added to each sample. The samples were then incubated overnight at room temperature, with mild agitation, after which they were acidified to pH=3 using trifluoroacetic acid, and cleaned-up using µColumns according to the method published by Wendrich and co-workers [437].

LC-MS/MS Analysis

For the LC-MS/MS analysis, the peptides were separated by reverse-phase nano liquid chromatography using a Thermo nLC1000 column and they were measured using an Orbitrap Exploris 480 mass spectrometer. The peptide spectra were searched in Maxquant (version 2.0.3.0) [438], using the Andromeda search engine [439] with label-free quantification (LFQ), against the version Niben1.0.1 of the *N. benthamiana* proteome dataset, including the protein sequence of Cf-4 (O50025), Avr4

(Q00363), LTI6b (AT3G05890), GUS (P05804) and frequently occurring contaminants.

The identified protein groups were then analysed using Perseus (version 1.6.2.3) [358]. Reverse and contaminant proteins, and those only identified by matching, were filtered out. Then, protein groups identified in less than three replicate samples were also filtered out. The LFQ values were log2 transformed, and the missing values were assigned assuming a normal distribution. The relative protein quantitation of the samples relative to the controls were calculated applying both-sided Student's t tests, using a permutation-based adjustment (FDR=0.05, 250 randomizations, and S0 set to 0.1).

ACKNOWLEDGMENTS

We acknowledge the personnel of UNIFARM, especially Bert Essenstam, for excellent plant care. S.L.V. is supported by the Peruvian Council for Science, Technology and Technological Innovation (CONCYTEC) and its executive unit FONDECYT.

SUPPLEMENTARY DATA

Figure S1. Mapping of the peptides corresponding to transmembrane proteins that were detected by PL-MS using TbID-tagged NbSOBIR1. Legend: signal peptide, underlined in orange; extracellular domain, underlined in blue; transmembrane, underlined in red; intracellular, underlined in grey; peptides detected by mass spectrometry are highlighted in yellow.

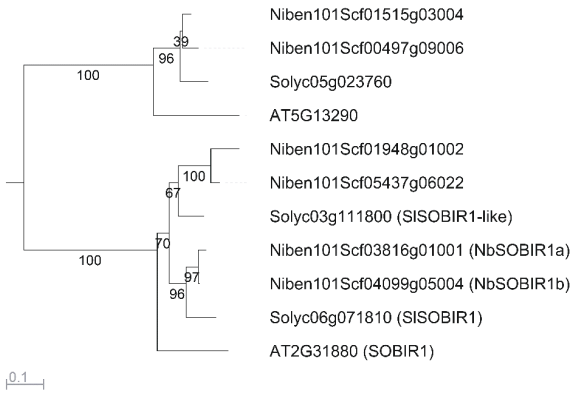

Figure S2. Phylogenetic tree depicting the members of the family of kinases belonging to RLK-Pelle_LRR-XI in *Arabidopsis*, tomato, and *N. benthamiana*. The branch lengths in the tree are proportional to the number of substitutions per site.

Table S1. Sets of samples prepared for PL-MS and analysed in this study. The first column refer to the TbID-tagged fusion proteins that were expressed by agroinfiltration. It also indicates for which samples the biotin solutions were supplemented with 10 µM of Avr4 protein. The second column indicates the genotypes of *N. benthamiana* that were used. The third and fourth columns indicate the amount of plants that were used and the amount of samples that were prepared, respectively.

First set of samples			
Bait	Genotype	# of plants	# of samples
*Nb*SOBIR1a-YFP-TbID	*N. benthamiana:Cf-4 sobir1(/sobir1-like)*	15	3
Cf-4-YFP-TbID	*N. benthamiana* WT	15	3
GUS-YFP-TbID	*N. benthamiana:Cf-4 sobir1(/sobir1-like)*	15	3
Second set of samples			
Bait	Genotype	#plants	# of samples
*Nb*SOBIR1a-YFP-TbID	*N. benthamiana:Cf-4 sobir1(/sobir1-like)*	15	3
Cf-4-YFP-TbID	*N. benthamiana* WT	15	3
Cf-4-YFP-TbID	*N. benthamiana sobir1(/sobir1-like)*	15	3
Lti6b-TbID	*N. benthamiana:Cf-4 sobir1(/sobir1-like)*	15	3
Third set of samples			
Bait	Genotype	#plants	# of samples
*Nb*SOBIR1a-YFP-TbID	*N. benthamiana:Cf-4 sobir1(/sobir1-like)*	15	3
*Nb*SOBIR1a-YFP-TbID + Avr4	*N. benthamiana:Cf-4 sobir1(/sobir1-like)*	15	3
Cf-4-YFP-TbID	*N. benthamiana* WT	15	3
Cf-4-YFP-TbID + Avr4	*N. benthamiana* WT	15	3
Lti6b-TbID	*N. benthamiana:Cf-4 sobir1(/sobir1-like)*	15	3
GUS-YFP-TbID	*N. benthamiana:Cf-4 sobir1(/sobir1-like)*	15	3

Table S2. Proteins detected by PL-MS, upon transient expression of TbID-tagged versions of NbSOBRI1 and tomato Cf-4 in *N. benthamiana*. The first column, # Cf-4-TbID, refers to the number of the PL-MS experiment using TbID-tagged Cf-4, in which the protein was also detected. The second column, *N. benthamiana ID*, refers to the protein identifier according to the Niben1.0.1 version of the proteome of *N. benthamiana*. The third column, Avr4 vs GUS 16h, refers to unpublished expression data obtained by RNA-seq of *N. benthamiana:Cf-4* at sixteen hours after agroinfiltration of Avr4, when compared with agroinfiltration of GUS. The fourth and the fifth column contain the annotation of the *N. benthamiana* proteins according to the SOL genomics website [307], that were significantly enriched in the different PL-MS experiments when using NbSOBIR1-YFP-TbID as a bait.

Significantly enriched in three independent PL-MS experiments when using NbSOBIR1-YFP-TbID as a bait				
# Cf-4-TbID	*N. benthamiana* ID	Avr4 vs GUS 16h	Blast Hit Accession	Description
0	Niben101Scf08799g00001	4.503148356	gb|ACZ64224.1|	RPM1 interacting protein 4 transcript 2 [*Lactuca saligna*]
0	Niben101Scf10330g02004	4.425524979	sp|Q9LIG2|RLK6_ARATH	Receptor-like protein kinase
0	Niben101Scf02581g04013	4.29148232	sp|Q2HXL0|RBOHC_SOLTU	Respiratory burst oxidase homolog protein C
0	Niben101Scf03479g05049	4.176715872	gb|ACZ64221.1|	RPM1 interacting protein 4 transcript 2 [*Lactuca saligna*]
0	Niben101Scf08151g00006	3.915118238	sp|Q9FN94|RLK7_ARATH	Receptor-like protein kinase
0	Niben101Scf03438g06004	3.524214348	AT3G57530.1	calcium-dependent protein kinase 32 LENGTH=538
0	Niben101Scf02637g00012	3.378542076	sp|Q0U4Z8|VPS27_PHANO	Vacuolar protein sorting-associated protein 27
1	Niben101Scf00257g00006	3.315891346	sp|O55012|PICAL_RAT	Phosphatidylinositol-binding clathrin assembly protein
0	Niben101Scf05118g10007	3.263679282	AT4G00330	Receptor-like protein kinase
0	Niben101Scf08899g00008	2.850576141	gb|ACZ64221.1|	RPM1 interacting protein 4 transcript 2 [*Lactuca saligna*]
0	Niben101Scf00012g00012	2.758018695	AT1G07570	Receptor-like protein kinase
0	Niben101Scf01063g04003	2.57529432	sp|P0CR79|HSE1_CRYNB	Class E vacuolar protein-sorting machinery protein HSE1
0	Niben101Scf08390g06006	1.927247658	sp|Q9BZV1|UBXN6_HUMAN	UBX domain-containing protein 6
0	Niben101Scf00593g03012	1.788673298	sp|Q9FM19|HIR1_ARATH	Hypersensitive-induced response protein 1
0	Niben101Scf01671g04002	1.581673496	AT3G17410	Receptor-like protein kinase
0	Niben101Scf02133g02001	1.522880001	AT1G34750.1	Protein phosphatase 2C family protein LENGTH=282
3	Niben101Scf08590g00005	1.455863099	sp|P54652|HSP72_HUMAN	Heat shock-related 70 kDa protein 2
3	Niben101Scf03816g01001	1.440506333	sp|P47735|RLK5_ARATH	Receptor-like protein kinase 5

Table S2. *(Continued)*

0	Niben101Scf06815g01013	1.280655523	ref|XP_002869709.1|	zinc ion binding protein [*Arabidopsis lyrata* subsp. *lyrata*]
0	Niben101Scf03930g04011	1.144909708	AT5G20100.1	unknown protein
0	Niben101Scf04407g02005	1.074322926	sp|Q9FM19|HIR1_ARATH	Hypersensitive-induced response protein 1
0	Niben101Scf00898g02014	0.894195994	emb|CDY14706.1|	BnaC05g19630D [*Brassica napus*]
0	Niben101Scf00712g10025	0.835845637	AT1G20760.1	Calcium-binding EF hand family protein LENGTH=1019
0	Niben101Scf00700g05004	0.826567991	sp|Q96262|PCAP1_ARATH	Plasma membrane-associated cation-binding protein 1
0	Niben101Scf01236g01010	0.82104059	sp|Q9LRP1|NPS13_ARATH	Novel plant SNARE 13
2	Niben101Scf00199g03003	0.710729275	ref|XP_002527953.1|	nucleotide binding protein, putative [*Ricinus communis*]
1	Niben101Scf07619g00006	0.390166263	sp|Q9LIG2|RLK6_ARATH	AT3G51550
0	Niben101Scf01489g00009	0.386995879	sp|Q944A9|NPS11_ARATH	Novel plant SNARE 11
3	Niben101Scf02972g05008	0.384302531	sp|P27541|HSP70_BRUMA	Heat shock 70 kDa protein
0	Niben101Scf00593g03002	0.346627311	sp|Q9FM19|HIR1_ARATH	Hypersensitive-induced response protein 1
0	Niben101Scf15536g02006	0.201630716	sp|Q5R581|KLC1_PONAB	Kinesin light chain 1
0	Niben101Scf02437g02021	0.097528705	AT2G24360	Protein kinase superfamily protein LENGTH=411
0	Niben101Scf07294g00014	-0.032021271	sp|Q9SF29|SYP71_ARATH	Syntaxin-71
0	Niben101Scf10157g01009	-0.449835485	AT2G07180	Receptor-like protein kinase
0	Niben101Scf01812g05008	-0.592568602	sp|Q8VHH5|AGAP3_MOUSE	Arf-GAP with GTPase, ANK repeat and PH domain-containing protein 3
0	Niben101Scf02280g04002	-0.918125063	emb|CDY07628.1|	BnaA03g18830D [*Brassica napus*]
0	Niben101Scf03488g06005	-0.935135013	gb|ACZ64220.1|	RPM1 interacting protein 4 transcript 2 [*Lactuca saligna*]
0	Niben101Scf07584g02008	-1.064767103	AT5G50000	Protein kinase superfamily protein LENGTH=385
1	Niben101Scf00593g01002	-1.153354929	sp|P20431|PMA3_ARATH	ATPase 3, plasma membrane-type
0	Niben101Scf07498g02020	-1.190490624	gb|ACZ64225.1|	RPM1 interacting protein 4 transcript 2 [*Lactuca saligna*]
0	Niben101Scf08587g00002	-1.26112475	sp|P93788|REMO_SOLTU	Remorin
0	Niben101Scf02237g07012	-1.30573091	AT5G50000	Protein kinase superfamily protein LENGTH=385
0	Niben101Scf00132g01003	-1.989890164	AT1G64500.1	Glutaredoxin family protein LENGTH=368

Table S2. *(Continued)*

1	Niben101Scf06394g04009	-2.014048757	sp|Q9C9N6|PMI2_ARATH	Protein PLASTID MOVEMENT IMPAIRED 2
0	Niben101Scf06172g01003	-2.057048782	sp|Q8L4D8|IQD31_ARATH	Protein IQ-DOMAIN 31
0	Niben101Scf02854g02005	-2.14412876	AT1G48480.1	receptor-like kinase 1 LENGTH=655
0	Niben101Scf02525g03002	-2.144146005	AT5G43310.1	COP1-interacting protein-related LENGTH=1237
0	Niben101Scf07305g00002	-2.425876955	AT1G15760.1	Sterile alpha motif (SAM) domain-containing protein LENGTH=202
0	Niben101Scf04804g01002	-2.476938867	sp|P93788|REMO_SOLTU	Remorin
0	Niben101Scf17127g00017	-2.718599983	sp|P93788|REMO_SOLTU	Remorin
0	Niben101Scf12852g03012	-3.041569238	ref|XP_002512588.1|	GRIP and coiled-coil domain-containing protein, putative [*Ricinus communis*]
0	Niben101Scf12211g02007	-3.197148851	AT1G80520.1	Sterile alpha motif (SAM) domain-containing protein LENGTH=192
0	Niben101Scf03491g01021	-3.315151488	AT1G42550.1	plastid movement impaired1 LENGTH=843
0	Niben101Scf02910g01040	-3.376178888	sp|P93788|REMO_SOLTU	Remorin
2	Niben101Scf11383g03008	-3.597715912	AT5G40030.1	Protein kinase superfamily protein LENGTH=499
0	Niben101Scf03549g00004	-3.779225653	AT5G67385.1	Phototropic-responsive NPH3 family protein LENGTH=604
0	Niben101Scf09172g01012	-3.879558958	sp|Q9C9Q4|JAC1_ARATH	J domain-containing protein required for chloroplast accumulation response 1
0	Niben101Scf18348g00015	-4.001539193	sp|Q9C9Q4|JAC1_ARATH	J domain-containing protein required for chloroplast accumulation response 1
3	Cf-4	_	NA	NA
1	Niben101Scf13290g00001	_	AT1G03920.1	Protein kinase family protein LENGTH=569
1	Niben101Scf02804g00010	_	AT5G40030.1	Protein kinase superfamily protein LENGTH=499
0	Niben101Scf04396g02009	_	AT5G10270.1	cyclin-dependent kinase C;1 LENGTH=505
0	Niben101Scf11524g00007	_	AT1G48480.1	receptor-like kinase 1 LENGTH=655
0	Niben101Scf04099g05004	_	sp|P93194|RPK1_IPONI	Receptor-like protein kinase
0	Niben101Scf03216g00001	_	AT4G00330	Receptor-like protein kinase
0	Niben101Scf02836g02006	_	AT4G31170	Protein kinase superfamily protein LENGTH=412

Table S2. *(Continued)*

0	Niben101Scf03469g03002	_	AT3G22750	Protein kinase superfamily protein LENGTH=378
3	Niben101Scf15536g02038	_	sp|Q9TUG3|HSP72_CAPHI	Heat shock-related 70 kDa protein 2
1	Niben101Scf00416g06002	_	AT1G16860.1	Ubiquitin-specific protease family C19-related protein LENGTH=474
1	Niben101Scf03979g02010	_	sp|P22180|PMA1_SOLLC	Plasma membrane ATPase 1
1	Niben101Scf05049g00003	_	sp|P0CR79|HSE1_CRYNB	Class E vacuolar protein-sorting machinery protein HSE1
1	Niben101Scf05049g00008	_	AT1G06210.1	ENTH/VHS/GAT family protein LENGTH=383
0	Niben101Scf00488g00003	_	sp|Q9FM19|HIR1_ARATH	Hypersensitive-induced response protein 1
0	Niben101Scf00709g04010	_	AT5G67385.1	Phototropic-responsive NPH3 family protein LENGTH=604
0	Niben101Scf01085g02012	_	AT2G30520.1	Phototropic-responsive NPH3 family protein LENGTH=593
0	Niben101Scf02569g03013	_	sp|Q54QC8|SEC1_DICDI	Protein transport protein sec1
0	Niben101Scf03738g00006	_	AT1G42550.1	plastid movement impaired1 LENGTH=843
0	Niben101Scf05166g07012	_	sp|Q9FM19|HIR1_ARATH	Hypersensitive-induced response protein 1
0	Niben101Scf06218g01003	_	AT1G30755.1	Protein of unknown function (DUF668) LENGTH=615
0	Niben101Scf13593g00007	_	gb|ACZ64221.1|	RPM1 interacting protein 4 transcript 2 [*Lactuca saligna*]
0	Niben101Scf18014g00014	_	sp|Q9LRP1|NPS13_ARATH	Novel plant SNARE 13

Significantly enriched in two independent PL-MS experiments when using NbSOBIR1-YFP-TbID as a bait				
# Cf-4-TbID	*N. benthamiana* ID	Avr4 vs GUS 16h	Blast Hit Accession	Description
0	Niben101Scf01376g04031	6.828213225	sp|Q9SEE4|PIRL_SOLLC	Pirin-like protein
0	Niben101Scf10524g04001	5.413906661	sp|O23429|VA724_ARATH	Vesicle-associated membrane protein 724
0	Niben101Scf07345g00016	5.201647061	sp|Q2HXL0|RBOHC_SOLTU	Respiratory burst oxidase homolog protein C
0	Niben101Scf00595g08043	4.899087992	sp|P39062|ACSA_BACSU	Acetyl-coenzyme A synthetase
0	Niben101Scf05149g00006	4.469226693	AT3G16510.1	Calcium-dependent lipid-binding (CaLB domain) family protein LENGTH=360
0	Niben101Scf01534g02014	4.27316194	AT5G28680.1	Unknown protein

Table S2. *(Continued)*

0	Niben101Scf15752g00002	4.017033845	AT3G57530.1	calcium-dependent protein kinase 32 LENGTH=538
0	Niben101Scf06394g08019	3.965433421	AT1G66880	Receptor-like protein kinase
0	Niben101Scf04146g01012	3.756280705	AT5G10270.1	cyclin-dependent kinase C;1 LENGTH=505
0	Niben101Scf01691g01017	3.679139801	AT1G29690.1	MAC/Perforin domain-containing protein LENGTH=561
0	Niben101Scf17164g00028	3.549914401	AT5G40380	Receptor-like protein kinase
0	Niben101Scf00109g02013	3.505511802	AT2G33490.1	hydroxyproline-rich glycoprotein family protein LENGTH=623
0	Niben101Scf05901g01008	3.443659844	AT4G15755.1	Calcium-dependent lipid-binding (CaLB domain) family protein LENGTH=289
0	Niben101Scf00404g01014	3.375133751	sp|Q7F613|SCAM2_ORYSJ	Secretory carrier-associated membrane protein 2
0	Niben101Scf00369g02005	3.315032793	AT4G15755.1	Calcium-dependent lipid-binding (CaLB domain) family protein LENGTH=289
0	Niben101Scf00381g03001	3.239297135	sp|P70587|LRRC7_RAT	Leucine-rich repeat-containing protein 7
0	Niben101Scf09248g01010	2.993330917	AT2G38410.1	ENTH/VHS/GAT family protein LENGTH=671
0	Niben101Scf03362g05002	2.88692082	AT1G70530	Receptor-like protein kinase 2
0	Niben101Scf09203g00003	2.860045111	AT3G22750	Protein kinase superfamily protein LENGTH=378
0	Niben101Scf01586g01011	2.82607506	sp|Q3UHD9|AGAP2_MOUSE	Arf-GAP with GTPase, ANK repeat and PH domain-containing protein 2
0	Niben101Scf07729g03014	2.677500261	sp|Q8LPL6|AP2A1_ARATH	AP-2 complex subunit alpha-1
0	Niben101Scf00024g04005	2.613972021	AT1G74740.1	calcium-dependent protein kinase 30 LENGTH=541
0	Niben101Scf01529g01009	2.55730122	sp|Q9P0L0|VAPA_HUMAN	Vesicle-associated membrane protein-associated protein A
0	Niben101Scf03202g12016	2.48429138	AT5G01550.1	lectin receptor kinase a4.1 LENGTH=688
0	Niben101Scf01984g00024	2.481604959	AT1G70520	Receptor-like protein kinase
0	Niben101Scf01378g00004	2.460732939	AT1G07570	Receptor like protein kinase S.2
3	Niben101Scf00173g04010	2.357777152	AT2G36300.1	Integral membrane Yip1 family protein LENGTH=255
0	Niben101Scf01735g02019	2.317408903	AT4G00340.1	receptor-like protein kinase 4 LENGTH=818
0	Niben101Scf07829g02001	2.265400424	AT5G20100.1	unknown protein

Table S2. *(Continued)*

0	Niben101Scf00149g10020	2.253841606	AT1G21270.1	wall-associated kinase 2 LENGTH=732
1	Niben101Scf05912g02005	2.215901235	AT5G23700.1	unknown protein
0	Niben101Scf01413g05008	2.153898638	sp|Q7F613|SCAM2_ORYSJ	Secretory carrier-associated membrane protein 2
0	Niben101Scf00149g10001	2.093319248	AT1G21210	Wall-associated receptor kinase 4
0	Niben101Scf01557g00014	2.090005964	sp|Q8LPL6|AP2A1_ARATH	AP-2 complex subunit alpha-1
0	Niben101Scf01519g01007	2.082479449	AT1G53430	Receptor-like protein kinase 5
0	Niben101Scf05081g01018	2.037292758	AT3G09830	Receptor-like protein kinase
0	Niben101Scf09119g01011	2.021882332	sp|Q9S9T7|VP282_ARATH	Vacuolar protein sorting-associated protein 28 homolog 2
0	Niben101Scf08176g00005	1.878552252	AT2G24360	Protein kinase superfamily protein LENGTH=411
0	Niben101Scf06200g02013	1.823344561	AT1G28380.1	MAC/Perforin domain-containing protein LENGTH=612
1	Niben101Scf08804g00003	1.815570227	AT5G23700.1	unknown protein
0	Niben101Scf01897g08006	1.81133873	AT3G08890.1	Protein of unknown function, DUF538 LENGTH=170
0	Niben101Scf04664g02002	1.77718372	AT4G34660.1	SH3 domain-containing protein LENGTH=368
0	Niben101Scf12754g00010	1.68226288	AT2G11520	Receptor-like protein kinase
0	Niben101Scf04007g07024	1.616523341	sp|O48724|WEB1_ARATH	Protein WEAK CHLOROPLAST MOVEMENT UNDER BLUE LIGHT 1
0	Niben101Scf00279g06016	1.585850345	AT3G08890.1	Protein of unknown function, DUF538 LENGTH=170
0	Niben101Scf01370g03003	1.562418482	AT1G34750.1	Protein phosphatase 2C family protein LENGTH=282
0	Niben101Scf26330g00002	1.5238062	sp|Q9LIG2|RLK6_ARATH	Receptor-like protein kinase
1	Niben101Scf16015g04006	1.523096264	gb|AER52053.1|	vWA domain containing protein [Oryza sativa Japonica Group]
1	Niben101Scf00168g06003	1.511639129	sp|Q503V0|CHMP6_DANRE	Charged multivesicular body protein 6
0	Niben101Scf00279g09002	1.469225785	sp|Q5R977|F126B_PONAB	Protein FAM126B
0	Niben101Scf02335g03002	1.454968145	sp|Q8C729|F126B_MOUSE	Protein FAM126B
0	Niben101Scf00180g10016	1.402114131	gb|KEH43480.1|	microtubule organization protein [*Medicago truncatula*]
0	Niben101Scf03855g05006	1.365292296	AT5G10270.1	cyclin-dependent kinase C;1 LENGTH=505
0	Niben101Scf11886g02001	1.332711626	sp|Q96262|PCAP1_ARATH	Plasma membrane-associated cation-binding protein 1

Table S2. *(Continued)*

0	Niben101Scf01066g03011	1.295174844	AT3G59350	Protein kinase superfamily protein LENGTH=408
2	Niben101Scf03777g00002	1.288184182	sp|Q39817|CALX_SOYBN	Calnexin homolog
1	Niben101Scf00149g00008	1.233194755	AT5G01460.1	LMBR1-like membrane protein LENGTH=509
0	Niben101Scf02996g03008	1.169470182	AT5G13160	Receptor-like protein kinase
0	Niben101Scf18955g00001	1.140559915	sp|Q6IRE4|TS101_RAT	Tumor susceptibility gene 101 protein
1	Niben101Scf11631g00005	1.097049949	sp|Q5ZJL8|ABHDD_CHICK	Alpha/beta hydrolase domain-containing protein 13
0	Niben101Scf02098g02033	1.092483362	AT4G12770.1	Chaperone DnaJ-domain superfamily protein LENGTH=891
0	Niben101Scf08609g00018	1.08296797	ref|XP_007014605.1|	Transducin/WD40 repeat-like superfamily protein isoform 1
0	Niben101Scf00229g07003	1.064106625	AT5G02290	Receptor-like protein kinase 2
0	Niben101Scf01791g01001	1.06041143	gb|ABF98470.1|	expressed protein [Oryza sativa Japonica Group]
3	Niben101Scf02983g01003	1.011602029	sp|Q9FFI5|NAC86_ARATH	NAC domain-containing protein 86
0	Niben101Scf27671g00007	0.977481779	AT2G40980.1	Protein kinase superfamily protein LENGTH=617
1	Niben101Scf04722g04012	0.970998825	AT5G01460.1	LMBR1-like membrane protein LENGTH=509
0	Niben101Scf04864g03005	0.917772535	AT3G56760.1	Protein kinase superfamily protein LENGTH=577
0	Niben101Scf06424g02029	0.895483281	AT1G73390.1	Endosomal targeting BRO1-like domain-containing protein
0	Niben101Scf16132g00002	0.894952071	AT1G08720	Protein kinase superfamily protein LENGTH=933
0	Niben101Scf00083g02012	0.856297406	sp|Q9S9T7|VP282_ARATH	Vacuolar protein sorting-associated protein 28 homolog 2
0	Niben101Scf06516g04018	0.768440835	sp|Q6ZKC0|14333_ORYSJ	14-3-3-like protein GF14-C
0	Niben101Scf00713g04002	0.713544834	sp|Q62848|ARFG1_RAT	ADP-ribosylation factor GTPase-activating protein 1
0	Niben101Scf03861g02013	0.694172258	AT3G13530	mitogen-activated protein kinase kinase kinase 7 LENGTH=1368
0	Niben101Scf00058g00001	0.673652071	gb|AGZ88227.1|	cytokinesis protein, partial [Polypodium glycyrrhiza]
0	Niben101Scf00294g01016	0.664943031	sp|O93277|WDR1_CHICK	WD repeat-containing protein 1
0	Niben101Scf07937g02011	0.629337555	sp|Q8BGK5|S35F1_MOUSE	Solute carrier family 35 member F1
0	Niben101Scf03045g11001	0.584585067	AT3G26600.1	armadillo repeat only 4 LENGTH=615
0	Niben101Scf04396g04016	0.531421426	AT1G08720	Protein kinase superfamily protein LENGTH=933

Table S2. *(Continued)*

3	Niben101Scf01773g07014	0.494584041	sp|A5DA00|SEC23_PICGU	Protein transport protein SEC23
1	Niben101Scf11383g00020	0.469743251	sp|P21335|TADA_BACSU	tRNA-specific adenosine deaminase
0	Niben101Scf06933g02001	0.46206826	AT2G24360	Protein kinase superfamily protein LENGTH=411
0	Niben101Scf14915g00001	0.436817182	AT3G15220	Serine/threonine-protein kinase 4 homolog B
2	Niben101Scf06461g06012	0.420369089	AT2G07360.2	SH3 domain-containing protein LENGTH=1198
2	Niben101Scf11646g03017	0.403735988	gb|AAO72706.1|	heavy meromyosin-like protein [Oryza sativa Japonica Group]
0	Niben101Scf05955g00002	0.361032039	sp|Q9SFX2|PUB43_ARATH	U-box domain-containing protein 43
0	Niben101Scf02605g01003	0.360294863	sp|Q9P0L0|VAPA_HUMAN	Vesicle-associated membrane protein-associated protein A
0	Niben101Scf12653g00011	0.302076395	AT3G26600.1	armadillo repeat only 4 LENGTH=615
2	Niben101Scf16376g00001	0.301305864	AT5G32440.3	Ubiquitin system component Cue protein LENGTH=265
0	Niben101Scf01334g04008	0.290511947	AT3G62220	Receptor-like protein kinase
0	Niben101Scf09063g00003	0.276347972	AT1G53570	mitogen-activated protein kinase kinase kinase 3 LENGTH=609
0	Niben101Scf09234g02008	0.25020328	sp|Q86TI4|WDR86_HUMAN	WD repeat-containing protein 86
0	Niben101Scf01849g03013	0.22442359	AT2G04410.1	RPM1-interacting protein 4 (RIN4) family protein LENGTH=73
2	Niben101Scf00616g00002	0.222430715	sp|Q9Z1Z0|USO1_MOUSE	General vesicular transport factor p115
2	Niben101Scf01922g08010	0.136082941	gb|AAO72706.1|	heavy meromyosin-like protein [Oryza sativa Japonica Group]
0	Niben101Scf03444g03015	0.11685559	ref|XP_003601496.1|	Membrane protein, putative [*Medicago truncatula*]
1	Niben101Scf16244g01002	0.111558173	AT5G06970.1	Protein of unknown function (DUF810) LENGTH=1101
0	Niben101Scf02133g10015	0.108260143	sp|Q9LVQ4|Y5586_ARATH	WEB family protein
0	Niben101Scf00155g03002	0.093759427	sp|Q9SF29|SYP71_ARATH	Syntaxin-71
0	Niben101Scf02367g04001	0.089965696	sp|Q6ZKC0|14333_ORYSJ	14-3-3-like protein GF14-C
1	Niben101Scf02525g02005	0.074215168	AT1G03920.1	Protein kinase family protein LENGTH=569
0	Niben101Scf04953g06007	0.052868573	sp|Q9SF29|SYP71_ARATH	Syntaxin-71
0	Niben101Scf05434g03014	-9.59E-05	AT1G70940.1	Auxin efflux carrier family protein LENGTH=640
0	Niben101Scf08203g00021	-0.058788382	sp|Q6NRL1|AGAP1_XENLA	Arf-GAP with GTPase, ANK repeat and PH domain-containing protein 1

Table S2. *(Continued)*

0	Niben101Scf03202g04017	-0.064283713	AT1G21270	Wall-associated receptor kinase 2
0	Niben101Scf01032g02002	-0.073102668	sp|O48724|WEB1_ARATH	Protein WEAK CHLOROPLAST MOVEMENT UNDER BLUE LIGHT 1
0	Niben101Scf02133g07001	-0.101374236	AT5G47750.1	D6 protein kinase like 2 LENGTH=586
0	Niben101Scf09234g03023	-0.106534368	AT5G10270.1	cyclin-dependent kinase C;1 LENGTH=505
1	Niben101Scf25768g00010	-0.113443399	sp|Q9LIG2|RLK6_ARATH	AT3G51550
2	Niben101Scf07278g00012	-0.114063119	AT4G34030.1	3-methylcrotonyl-CoA carboxylase LENGTH=587
2	Niben101Scf01814g05011	-0.125001891	AT3G50590.1	Transducin/WD40 repeat-like superfamily protein LENGTH=1614
0	Niben101Scf02441g04008	-0.126185258	AT3G46290	Receptor-like protein kinase
0	Niben101Scf14771g00001	-0.194464252	AT1G16860.1	Ubiquitin-specific protease family C19-related protein LENGTH=474
0	Niben101Scf03888g01021	-0.207304806	AT1G66150	Receptor-like protein kinase
3	Niben101Scf01750g14033	-0.223416157	sp|Q9FMR5|VA714_ARATH	Vesicle-associated membrane protein 714
3	Niben101Scf07459g00017	-0.23188408	sp|Q1W375|PMM_TOBAC	Phosphomannomutase
2	Niben101Scf09812g01018	-0.262708468	sp|Q05B78|ZFY21_BOVIN	Zinc finger FYVE domain-containing protein 21
2	Niben101Scf12084g01001	-0.324836934	sp|P35283|RAB12_MOUSE	Ras-related protein Rab-12
0	Niben101Scf07008g00030	-0.329112931	AT3G16060.1	ATP binding microtubule motor family protein LENGTH=684
0	Niben101Scf00837g00016	-0.351885651	AT4G35230	Receptor like protein kinase S.3
1	Niben101Scf06876g01037	-0.392655686	AT5G28050.2	Cytidine/deoxycytidylate deaminase family protein LENGTH=204
0	Niben101Scf05368g03010	-0.424907827	AT3G08890.1	Protein of unknown function, DUF538 LENGTH=170
2	Niben101Scf02631g01015	-0.481290633	ref|WP_027830635.1|	methylcrotonoyl-CoA carboxylase [Marinobacter sp. HL-58]
3	Niben101Scf02829g06001	-0.498948172	sp|P11029|ACAC_CHICK	Acetyl-CoA carboxylase
1	Niben101Scf00488g02003	-0.56169466	sp|P54211|PMA1_DUNBI	Plasma membrane ATPase
0	Niben101Scf02030g00023	-0.624024522	AT5G25590.1	Protein of unknown function (DUF630 and DUF632) LENGTH=775
0	Niben101Scf02085g20005	-0.628164996	AT5G37070.1	Protein of unknown function, DUF538 LENGTH=170
0	Niben101Scf04099g05003	-0.633041778	sp|D7MMW4|CSPLJ_ARALL	CASP-like protein 4A2
0	Niben101Scf05369g00007	-0.652950179	AT1G14390	Receptor-like protein kinase

Table S2. *(Continued)*

3	Niben101Scf00369g07016	-0.662405398	sp|P0CB32|HS71L_BOVIN	Heat shock 70 kDa protein 1-like
0	Niben101Scf04627g03001	-0.714906859	sp|Q9FJX6|FH6_ARATH	Formin-like protein 6
0	Niben101Scf03184g01010	-0.739039536	AT1G16860.1	Ubiquitin-specific protease family C19-related protein LENGTH=474
0	Niben101Scf04233g01015	-0.77328231	sp|Q96B97|SH3K1_HUMAN	SH3 domain-containing kinase-binding protein 1
1	Niben101Scf07352g00001	-0.842278045	AT3G14940.1	phosphoenolpyruvate carboxylase 3 LENGTH=968
2	Niben101Scf06256g01001	-0.92707682	sp|O04153|CALR3_ARATH	Calreticulin-3
0	Niben101Scf07590g02006	-0.984939389	AT2G44870.1	unknown protein
0	Niben101Scf00355g04013	-1.004745689	AT3G23750	Receptor-like protein kinase
0	Niben101Scf12582g01003	-1.023614895	AT3G08890.1	Protein of unknown function, DUF538 LENGTH=170
0	Niben101Scf00152g19010	-1.029973001	sp|Q9FXI5|IQD32_ARATH	Protein IQ-DOMAIN 32
0	Niben101Scf05476g01001	-1.042127729	AT2G28930	Receptor-like protein kinase
0	Niben101Scf21817g00005	-1.051723098	sp|Q9SF32|IQD1_ARATH	Protein IQ-DOMAIN 1
0	Niben101Scf08552g00011	-1.056693484	AT5G19473.1	RPM1-interacting protein 4 (RIN4) family protein LENGTH=99
0	Niben101Scf02712g00006	-1.076142853	sp|Q9LIG2|RLK6_ARATH	Receptor-like protein kinase
0	Niben101Scf00046g07018	-1.088442656	ref|XP_003601496.1|	Membrane protein, putative [*Medicago truncatula*]
1	Niben101Scf01485g00002	-1.098083166	sp|Q503V9|ENDUB_DANRE	Poly(U)-specific endoribonuclease-B
0	Niben101Scf02427g03008	-1.127109567	AT3G19540.1	Protein of unknown function (DUF620) LENGTH=485
0	Niben101Scf11899g00015	-1.134440498	sp|P92934|AAP6_ARATH	Amino acid permease 6
1	Niben101Scf00170g05014	-1.138905471	sp|Q9LVG9|Y5600_ARATH	BTB/POZ domain-containing protein
0	Niben101Scf01283g01015	-1.154448902	sp|P47735|RLK5_ARATH	Receptor-like protein kinase 5
0	Niben101Scf01507g01017	-1.168157995	AT2G42960	Receptor-like protein kinase
0	Niben101Scf04801g01026	-1.172853785	AT5G50000	Protein kinase superfamily protein LENGTH=385
0	Niben101Scf13404g00002	-1.191658501	sp|Q9LHP4|RCH2_ARATH	Receptor-like protein kinase 2
0	Niben101Scf04216g03017	-1.233167127	AT1G34320.1	Protein of unknown function (DUF668) LENGTH=657
0	Niben101Scf03407g02009	-1.427560316	AT5G54380	Receptor-like protein kinase

Table S2. *(Continued)*

0	Niben101Scf01976g00011	-1.436281156	AT5G54380	Receptor-like protein kinase
0	Niben101Scf00435g02010	-1.477649817	AT1G50700.1	calcium-dependent protein kinase 33 LENGTH=521
0	Niben101Scf04995g15004	-1.486155907	AT3G19540.1	Protein of unknown function (DUF620) LENGTH=485
1	Niben101Scf07183g00018	-1.489311089	AT4G32410.1	cellulose synthase 1 LENGTH=1081
0	Niben101Scf12708g02026	-1.522306952	AT2G31820.1	Ankyrin repeat family protein LENGTH=662
0	Niben101Scf10650g01009	-1.582597987	AT1G51940	Receptor-like protein kinase
1	Niben101Scf00170g05007	-1.594770758	AT2G44830.1	Protein kinase superfamily protein LENGTH=765
0	Niben101Scf08898g00003	-1.713959488	AT5G56460	Receptor-like protein kinase
0	Niben101Scf06507g00014	-1.847504495	sp|Q66GP0|Y5738_ARATH	BTB/POZ domain-containing protein
0	Niben101Scf11142g00012	-1.852037739	AT1G18160	Protein kinase superfamily protein LENGTH=992
1	Niben101Scf08089g00005	-1.90327402	AT5G13260.1	unknown protein
0	Niben101Scf04995g00014	-1.934960371	AT4G02630	Receptor-like protein kinase
0	Niben101Scf07741g05001	-1.94185248	AT1G16860.1	Ubiquitin-specific protease family C19-related protein LENGTH=474
1	Niben101Scf09570g00018	-2.084076442	sp|Q9SF32|IQD1_ARATH	Protein IQ-DOMAIN 1
0	Niben101Scf00129g01001	-2.087015561	AT4G02630	Receptor-like protein kinase
0	Niben101Scf01063g01004	-2.233016336	emb|CDY16984.1|	BnaC09g41110D [*Brassica napus*]
0	Niben101Scf00024g04006	-2.296064971	sp|P83970|PMA1_WHEAT	Plasma membrane ATPase
0	Niben101Scf01326g08021	-2.567882677	sp|Q8L4D8|IQD31_ARATH	Protein IQ-DOMAIN 31
0	Niben101Scf08078g00005	-2.584653255	sp|Q0WSY2|FPP4_ARATH	Filament-like plant protein 4
0	Niben101Scf03371g01037	-2.736885832	AT3G26700	Receptor-like protein kinase
0	Niben101Scf09552g01001	-2.922149478	sp|B4S6P7|DNAK_PROA2	Chaperone protein DnaK
0	Niben101Scf02992g03010	-3.111376481	sp|F4JGP4|ATK5_ARATH	Kinesin-5
0	Niben101Scf06504g01026	-3.302540887	AT1G64500.1	Glutaredoxin family protein LENGTH=368
1	Niben101Scf01284g02011	-3.319917206	sp|Q11180|WHT1_CAEEL	ABC transporter ATP-binding protein/permease wht-1
0	Niben101Scf06528g03001	-3.378583293	AT4G31820.1	Phototropic-responsive NPH3 family protein LENGTH=571

Table S2. *(Continued)*

0	Niben101Scf02581g05010	-3.471594042	sp|Q3J5H6|GLND_RHOS4	Bifunctional uridylyltransferase/uridylyl-removing enzyme
0	Niben101Scf04706g01026	-3.517860175	sp|Q9US60|KLP3_SCHPO	Kinesin-like protein 3
0	Niben101Scf00167g03014	-3.597181592	ref|NP_001067921.1|	product [Oryza sativa Japonica Group]
0	Niben101Scf00988g00002	-3.657370256	AT2G37180.1	Aquaporin-like superfamily protein LENGTH=285
0	Niben101Scf01338g03019	-3.856861845	AT3G25690.1	Hydroxyproline-rich glycoprotein family protein LENGTH=1004
0	Niben101Scf09296g01009	_	AT5G19450.1	calcium-dependent protein kinase 19 LENGTH=533
0	Niben101Scf01992g01013	_	AT5G54380	Receptor-like protein kinase
0	Niben101Scf02449g02004	_	AT3G46290	Receptor-like protein kinase
0	Niben101Scf21897g00005	_	AT5G01550.1	lectin receptor kinase a4.1 LENGTH=688
0	Niben101Scf10608g00008	_	AT1G66150	Receptor-like protein kinase
0	Niben101Scf16185g00007	_	sp|P93194|RPK1_IPONI	Receptor-like protein kinase
0	Niben101Scf08874g01003	_	AT1G14390	Receptor-like protein kinase
0	Niben101Scf03021g01006	_	sp|Q9LIG2|RLK6_ARATH	Receptor-like protein kinase
0	Niben101Scf01683g11003	_	AT4G39400	Receptor-like protein kinase 2
0	Niben101Scf01374g13005	_	AT1G51940	Receptor-like protein kinase
0	Niben101Scf05035g01015	_	AT3G24550	Receptor-like protein kinase
0	Niben101Scf06678g03002	_	AT2G11520	Receptor-like protein kinase
0	Niben101Scf04617g00001	_	AT3G26700	Receptor-like protein kinase
0	Niben101Scf00402g02004	_	AT1G56720	Receptor-like protein kinase
0	Niben101Scf00635g04002	_	AT5G02290	Receptor-like protein kinase
0	Niben101Scf03396g00005	_	AT5G56460	Receptor-like protein kinase
0	Niben101Scf02175g03013	_	AT4G35230	Receptor like protein kinase S.3
0	Niben101Scf03340g05001	_	AT4G00340.1	receptor-like protein kinase 4 LENGTH=818
0	Niben101Scf13018g00012	_	sp|Q9LIG2|RLK6_ARATH	Receptor-like protein kinase
0	Niben101Scf01795g10003	_	AT1G53570	mitogen-activated protein kinase kinase kinase 3 LENGTH=609

Table S2. *(Continued)*

0	Niben101Scf02526g02006	_	AT4G10730	Serine/threonine-protein kinase 4 homolog B
0	Niben101Scf08652g01010	_	AT4G10730	Serine/threonine-protein kinase 4
0	Niben101Scf01587g02009	_	AT3G13530	Serine/threonine-protein kinase 3
0	Niben101Scf06164g00002	_	AT5G50000	Protein kinase superfamily protein LENGTH=385
3	Niben101Scf03413g00005	_	AT2G36300.1	Integral membrane Yip1 family protein LENGTH=255
3	Niben101Scf04325g01023	_	gb|AAO72598.1|	myosin-like protein [Oryza sativa Japonica Group]
3	Niben101Scf13703g01006	_	sp|P17066|HSP76_HUMAN	Heat shock 70 kDa protein 6
2	Niben101Scf00110g05007	_	sp|A5DA00|SEC23_PICGU	Protein transport protein SEC23
2	Niben101Scf00265g01015	_	AT3G50590.1	Transducin/WD40 repeat-like superfamily protein LENGTH=1614
2	Niben101Scf01434g03006	_	sp|Q41238|LOX16_SOLTU	Linoleate 9S-lipoxygenase 6
2	Niben101Scf02755g06016	_	sp|P54652|HSP72_HUMAN	Heat shock-related 70 kDa protein 2
2	Niben101Scf10834g03005	_	sp|O04153|CALR3_ARATH	Calreticulin-3
1	Niben101Scf00491g04001	_	AT1G49040.1	stomatal cytokinesis defective / SCD1 protein (SCD1) LENGTH=1187
1	Niben101Scf00508g06005	_	sp|Q0WSY2|FPP4_ARATH	Filament-like plant protein 4
1	Niben101Scf03351g04001	_	sp|Q503V0|CHMP6_DANRE	Charged multivesicular body protein 6
1	Niben101Scf07824g00009	_	AT4G32410.1	cellulose synthase 1 LENGTH=1081
0	Niben101Ctg15555g00001	_	sp|Q13492|PICAL_HUMAN	Phosphatidylinositol-binding clathrin assembly protein
0	Niben101Scf00381g09020	_	AT1G21630.2	Calcium-binding EF hand family protein LENGTH=1247
0	Niben101Scf01190g04005	_	AT4G34660.1	SH3 domain-containing protein LENGTH=368
0	Niben101Scf01232g05005	_	gb|ABF98470.1|	expressed protein [Oryza sativa Japonica Group]
0	Niben101Scf01374g04004	_	AT3G16060.1	ATP binding microtubule motor family protein LENGTH=684
0	Niben101Scf01448g02005	_	gb|KEH17617.1|	structural constituent of cell wall protein, putative
0	Niben101Scf01826g01004	_	AT5G50380.1	exocyst subunit exo70 family protein F1 LENGTH=683
0	Niben101Scf02190g04003	_	AT2G31820.1	Ankyrin repeat family protein LENGTH=662
0	Niben101Scf02354g13005	_	AT4G32760.2	ENTH/VHS/GAT family protein LENGTH=676

Table S2. *(Continued)*

0	Niben101Scf02537g00004	_	sp|Q6ZKC0|14333_ORYSJ	14-3-3-like protein GF14-C
0	Niben101Scf02752g02003	_	sp|Q9MA55|ACBP4_ARATH	Acyl-CoA-binding domain-containing protein 4
0	Niben101Scf03015g03010	_	sp|Q6ZKC0|14333_ORYSJ	14-3-3-like protein GF14-C
0	Niben101Scf03152g00012	_	ref|XP_007014605.1|	Transducin/WD40 repeat-like superfamily protein isoform 1
0	Niben101Scf03546g01013	_	sp|Q6NKW9|E138_ARATH	Glucan endo-1,3-beta-glucosidase 8
0	Niben101Scf04098g00012	_	AT5G06970.1	Protein of unknown function (DUF810) LENGTH=1101
0	Niben101Scf04384g04005	_	sp|Q5N749|MOR1_ORYSJ	Protein MOR1
0	Niben101Scf04608g05035	_	AT5G03540.3	exocyst subunit exo70 family protein A1 LENGTH=664
0	Niben101Scf04714g03015	_	sp|O22151|GOS12_ARATH	Golgi SNAP receptor complex member 1-2
0	Niben101Scf05044g04023	_	AT5G25590.1	Protein of unknown function (DUF630 and DUF632) LENGTH=775
0	Niben101Scf05051g02002	_	AT2G37180.1	Aquaporin-like superfamily protein LENGTH=285
0	Niben101Scf05061g02010	_	sp|Q9M5P2|SCAM3_ARATH	Secretory carrier-associated membrane protein 3
0	Niben101Scf05149g00005	_	AT3G16510.1	Calcium-dependent lipid-binding (CaLB domain) family protein
0	Niben101Scf05301g00016	_	AT1G03445.1	Serine/threonine protein phosphatase family protein LENGTH=793
0	Niben101Scf07510g00018	_	sp|Q9P0L0|VAPA_HUMAN	Vesicle-associated membrane protein-associated protein A
0	Niben101Scf07515g03006	_	sp|O55012|PICAL_RAT	Phosphatidylinositol-binding clathrin assembly protein
0	Niben101Scf08415g00010	_	sp|P39062|ACSA_BACSU	Acetyl-coenzyme A synthetase
0	Niben101Scf08482g00017	_	AT2G44870.1	unknown protein
0	Niben101Scf09467g02010	_	AT4G32760.2	ENTH/VHS/GAT family protein LENGTH=676
0	Niben101Scf10224g01005	_	sp|Q8LPL6|AP2A1_ARATH	AP-2 complex subunit alpha-1
0	Niben101Scf10277g01006	_	sp|Q9LRP1|NPS13_ARATH	Novel plant SNARE 13
0	Niben101Scf12202g00012	_	sp|A2QW93|HSE1_ASPNC	Class E vacuolar protein-sorting machinery protein hse1

Table S2. *(Continued)*

Significantly enriched in one of the PL-MS experiments when using NbSOBIR1-YFP-TbID as a bait				
# Cf-4-TbID	*N. benthamiana* ID	Avr4 vs GUS 16h	Blast Hit Accession	Description
0	Niben101Scf11175g00005	6.646103187	emb|CDY22603.1|	BnaC08g42370D [*Brassica napus*]
0	Niben101Scf06245g01017	6.11155454	sp|B9SBU9|TPS5_RICCO	Terpene synthase 5
0	Niben101Scf02093g00004	5.507988751	sp|Q9ZSD4|SY121_ARATH	Syntaxin-121
1	Niben101Scf16022g04010	5.16267327	sp|Q54UK0|PLDA_DICDI	Phospholipase D A
0	Niben101Scf11684g00005	4.981623794	AT2G02800	Receptor-like protein kinase
0	Niben101Scf01887g02002	4.805550935	ref|XP_003589248.1|	Pheromone receptor-like protein [*Medicago truncatula*]
0	Niben101Scf19766g00001	4.718514165	emb|CDY14706.1|	BnaC05g19630D [*Brassica napus*]
0	Niben101Scf02222g00005	4.698351178	AT1G65690.1	Late embryogenesis abundant (LEA) hydroxyproline-rich glycoprotein
0	Niben101Scf08111g02011	4.548985714	sp|Q9LQU4|PCR2_ARATH	Protein PLANT CADMIUM RESISTANCE 2
1	Niben101Scf00332g06012	4.46630641	sp|P21616|AVP_VIGRR	Pyrophosphate-energized vacuolar membrane proton pump
0	Niben101Scf07792g02034	4.343291387	sp|Q94KB7|MLO6_ARATH	MLO-like protein 6
0	Niben101Scf02918g00003	4.294429554	sp|Q43792|ACCO_TOBAC	1-aminocyclopropane-1-carboxylate oxidase
0	Niben101Scf01521g08013	4.227851553	emb|CDY45142.1|	BnaA09g14500D [*Brassica napus*]
0	Niben101Scf02262g01020	4.130072478	sp|Q94B77|FH5_ARATH	Formin-like protein 5
0	Niben101Scf08057g00006	4.06392295	sp|Q9LQU4|PCR2_ARATH	Protein PLANT CADMIUM RESISTANCE 2
0	Niben101Scf02278g01011	3.858983513	sp|Q9FN94|RLK7_ARATH	Receptor-like protein kinase
0	Niben101Scf08376g00012	3.834546763	AT1G75170.1	Sec14p-like phosphatidylinositol transfer family protein LENGTH=296
0	Niben101Scf00873g02006	3.811906672	sp|Q6K5F8|CDKG1_ORYSJ	Cyclin-dependent kinase G-1
0	Niben101Scf21770g00007	3.761878592	AT1G03445.1	Serine/threonine protein phosphatase family protein LENGTH=793
0	Niben101Scf01319g04019	3.652623468	AT1G30755.1	Protein of unknown function (DUF668) LENGTH=615
0	Niben101Scf00560g10001	3.63336663	sp|B9M4V3|NQOR_GEODF	NAD(P)H dehydrogenase (quinone)
0	Niben101Scf02816g01009	3.602629489	AT2G19710.1	Regulator of Vps4 activity in the MVB pathway protein LENGTH=937
0	Niben101Scf01239g02002	3.597675313	AT5G54160.1	O-methyltransferase 1 LENGTH=363

Table S2. *(Continued)*

0	Niben101Scf07442g00008	3.561185445	sp|Q7NZU6|MSBA_CHRVO	Lipid A export ATP-binding/permease protein MsbA
0	Niben101Scf02812g00002	3.553586217	sp|Q80TE7|LRRC7_MOUSE	Leucine-rich repeat-containing protein 7
1	Niben101Scf01719g08001	3.513917274	sp|Q7PC83|AB41G_ARATH	ABC transporter G family member 41
0	Niben101Scf16150g00002	3.450956497	sp|Q9FN94|RLK7_ARATH	Receptor-like protein kinase
2	Niben101Scf04099g08003	3.405152038	sp|Q9FFI5|NAC86_ARATH	NAC domain-containing protein 86
0	Niben101Scf04231g02014	3.39897532	ref|NP_001149203.1|	seed specific protein Bn15D1B [Zea mays]
1	Niben101Scf15391g01009	3.312910879	emb|CDX96276.1|	BnaA07g28870D [*Brassica napus*]
0	Niben101Scf01322g04020	3.21471847	AT2G25800.1	Protein of unknown function (DUF810) LENGTH=987
1	Niben101Scf07261g01014	3.197696589	AT1G60140.1	trehalose phosphate synthase LENGTH=861
0	Niben101Scf04406g08002	3.196124573	AT2G33490.1	hydroxyproline-rich glycoprotein family protein LENGTH=623
0	Niben101Scf12205g00010	3.165998081	AT1G18160	Protein kinase superfamily protein LENGTH=992
0	Niben101Scf00047g03013	2.97447449	AT1G14780.1	MAC/Perforin domain-containing protein LENGTH=627
0	Niben101Scf08341g06012	2.968212366	sp|Q3UHD9|AGAP2_MOUSE	Arf-GAP with GTPase, ANK repeat and PH domain-containing protein 2
0	Niben101Scf01453g06010	2.924079053	sp|Q96520|PER12_ARATH	Peroxidase 12
0	Niben101Scf00369g08005	2.915226628	sp|P15252|REF_HEVBR	Rubber elongation factor protein
0	Niben101Scf01429g01016	2.911532556	sp|Q9ZSD4|SY121_ARATH	Syntaxin-121
0	Niben101Scf02907g06031	2.876169375	sp|P42327|ADH2_GEOSE	Alcohol dehydrogenase
0	Niben101Scf00176g07004	2.851644493	sp|Q9M0X5|CRK25_ARATH	Cysteine-rich receptor-like protein kinase 25
0	Niben101Scf03751g01004	2.844554968	AT5G42830.1	HXXXD-type acyl-transferase family protein LENGTH=450
0	Niben101Scf05262g00022	2.811014249	sp|E9Q634|MYO1E_MOUSE	Unconventional myosin-Ie
0	Niben101Scf04991g00004	2.684135452	sp|C4XGC2|NQOR_DESMR	NAD(P)H dehydrogenase (quinone)
0	Niben101Scf03376g05017	2.670608572	sp|A0L4Z2|DNAK_MAGSM	Chaperone protein DnaK
0	Niben101Scf02790g05007	2.638773416	sp|Q54DB1|CM2A2_DICDI	Charged multivesicular body protein 2a homolog 2
0	Niben101Scf00449g03001	2.619402469	sp|Q2LVL0|MSBA_SYNAS	Lipid A export ATP-binding/permease protein MsbA
0	Niben101Scf00821g16005	2.598338618	AT2G33490.1	hydroxyproline-rich glycoprotein family protein LENGTH=623

Table S2. *(Continued)*

1	Niben101Scf36191g00003	2.537187709	AT3G45640	mitogen-activated protein kinase 3 LENGTH=370
0	Niben101Scf09527g01016	2.532536397	sp|Q54DB1|CM2A2_DICDI	Charged multivesicular body protein 2a homolog 2
0	Niben101Scf08566g02005	2.459237654	AT1G34750.1	Protein phosphatase 2C family protein LENGTH=282
0	Niben101Scf32086g00002	2.401481898	AT1G34750.1	Protein phosphatase 2C family protein LENGTH=282
0	Niben101Scf21242g00003	2.367459104	sp|Q94KB7|MLO6_ARATH	MLO-like protein 6
2	Niben101Scf04285g03020	2.365249326	AT2G02860.1	sucrose transporter 2 LENGTH=594
0	Niben101Scf02440g00006	2.31032419	sp|C4XGC2|NQOR_DESMR	NAD(P)H dehydrogenase (quinone)
0	Niben101Scf35444g00004	2.274848367	sp|Q9SR36|GSTU8_ARATH	Glutathione S-transferase U8
0	Niben101Scf06569g01020	2.244718783	sp|Q99614|TTC1_HUMAN	Tetratricopeptide repeat protein 1
0	Niben101Scf06822g01006	2.181656903	sp|O23140|AP2M_ARATH	AP-2 complex subunit mu
0	Niben101Scf10757g00001	2.165089415	sp|Q6ZKC0|14333_ORYSJ	14-3-3-like protein GF14-C
0	Niben101Scf10332g02006	2.112508673	AT1G18160	Protein kinase superfamily protein LENGTH=992
1	Niben101Scf05705g00009	2.049194582	AT4G26060.1	Ribosomal protein L18ae family LENGTH=133
0	Niben101Scf01745g04011	2.047282605	AT5G47070	Receptor-like protein kinase
0	Niben101Scf02467g01048	2.034457191	AT5G35200.1	ENTH/ANTH/VHS superfamily protein LENGTH=544
0	Niben101Scf05804g01017	2.003574022	AT5G35200.1	ENTH/ANTH/VHS superfamily protein LENGTH=544
0	Niben101Scf05301g04003	1.974132494	sp|Q9FN94|RLK7_ARATH	Receptor-like protein kinase
0	Niben101Scf04504g01003	1.94745972	sp|Q6NRL1|AGAP1_XENLA	Arf-GAP with GTPase, ANK repeat and PH domain-containing protein 1
0	Niben101Scf00987g00004	1.927189236	AT4G14340.1	casein kinase I LENGTH=457
0	Niben101Scf12653g00012	1.903307134	sp|Q8SWN8|ACT_ENCCU	Actin
0	Niben101Scf01326g11012	1.872796734	sp|P47735|RLK5_ARATH	Receptor-like protein kinase 5
0	Niben101Scf09025g01006	1.869373674	AT5G50380.1	exocyst subunit exo70 family protein F1 LENGTH=683
0	Niben101Scf08723g01003	1.851527771	AT5G66200.1	armadillo repeat only 2 LENGTH=651
0	Niben101Scf07953g02010	1.84614553	sp|Q6K5F8|CDKG1_ORYSJ	Cyclin-dependent kinase G-1
1	Niben101Scf07247g04003	1.808772276	sp|O23144|PPI1_ARATH	Proton pump-interactor 1

Table S2. *(Continued)*

0	Niben101Scf08230g00016	1.790770846	AT5G03540.3	exocyst subunit exo70 family protein A1 LENGTH=664
0	Niben101Scf02913g00012	1.760742917	AT5G08570.1	Pyruvate kinase family protein LENGTH=510
0	Niben101Scf06461g04011	1.730839159	AT4G31170	Protein kinase superfamily protein LENGTH=412
0	Niben101Scf01999g06011	1.721579438	sp|Q0BW82|DNAK_GRABC	Chaperone protein DnaK
2	Niben101Scf04639g03005	1.702927543	sp|B4U7U4|FTSH_HYDS0	ATP-dependent zinc metalloprotease FtsH
1	Niben101Scf13098g00013	1.687880041	sp|A2XUW1|CDKG2_ORYSI	Cyclin-dependent kinase G-2
0	Niben101Scf03069g01001	1.679670475	AT1G12310.1	Calcium-binding EF-hand family protein LENGTH=148
0	Niben101Scf03731g02014	1.6762952	sp|Q6NRL1|AGAP1_XENLA	Arf-GAP with GTPase, ANK repeat and PH domain-containing protein 1
0	Niben101Scf04955g07012	1.662274974	sp|Q9M9F9|ICR4_ARATH	Interactor of constitutive active ROPs 4
0	Niben101Scf07027g06012	1.659718009	AT1G21630.2	Calcium-binding EF hand family protein LENGTH=1247
2	Niben101Scf07423g05003	1.658115892	sp|P54775|PRS6B_MOUSE	26S protease regulatory subunit 6B
0	Niben101Scf08721g01033	1.641363062	AT4G02860.1	Phenazine biosynthesis PhzC/PhzF protein LENGTH=313
1	Niben101Scf05080g01012	1.641337932	sp|Q55B11|VTA1_DICDI	Vacuolar protein sorting-associated protein VTA1 homolog
0	Niben101Scf06688g01008	1.622966514	sp|Q9SF32|IQD1_ARATH	Protein IQ-DOMAIN 1
3	Niben101Scf01727g03003	1.611225177	sp|Q9DF42|RB8AA_XENLA	RNA-binding protein 8A-A
1	Niben101Scf06128g00010	1.610541882	sp|Q9SA23|SYP51_ARATH	Syntaxin-51
0	Niben101Scf01163g04023	1.573871513	gb|ABF98470.1|	expressed protein [Oryza sativa Japonica Group]
3	Niben101Scf01968g00002	1.569413283	sp|Q9M352|RL362_ARATH	60S ribosomal protein L36-2
0	Niben101Scf04608g05036	1.557492245	AT5G03540.3	exocyst subunit exo70 family protein A1 LENGTH=664
0	Niben101Scf01481g00009	1.548810556	sp|Q9Y169|EXT2_DROME	Exostosin-2
0	Niben101Scf01066g01009	1.523438938	sp|O95208|EPN2_HUMAN	Epsin-2
0	Niben101Scf01664g03005	1.503037459	sp|Q949R4|DIOXL_ARATH	Extradiol ring-cleavage dioxygenase
0	Niben101Scf05720g06006	1.496428043	AT4G32285.1	ENTH/ANTH/VHS superfamily protein LENGTH=635
0	Niben101Scf10254g01002	1.483223143	sp|Q9FUT0|GSTU9_ARATH	Glutathione S-transferase U9
0	Niben101Scf04973g02006	1.476700556	sp|C8V212|BRO1_EMENI	Vacuolar protein-sorting protein bro1

Table S2. *(Continued)*

0	Niben101Scf07939g00002	1.438382869	AT4G31170	Protein kinase superfamily protein LENGTH=412
0	Niben101Scf00337g01007	1.403966161	AT1G69030.1	BSD domain-containing protein LENGTH=317
1	Niben101Scf03592g02001	1.39542407	emb|CDY14195.1|	BnaA08g13260D [*Brassica napus*]
0	Niben101Scf09908g00005	1.389189918	AT2G17890.1	calcium-dependent protein kinase 16 LENGTH=571
0	Niben101Scf01375g09028	1.374828524	ref|NP_568790.1|	ubiquitin-associated/translation elongation factor EF1B protein
3	Niben101Scf01596g11007	1.372361321	sp|Q39817|CALX_SOYBN	Calnexin homolog
0	Niben101Scf05805g02006	1.358769754	AT2G17890.1	calcium-dependent protein kinase 16 LENGTH=571
0	Niben101Scf00744g02013	1.317396564	AT5G65520.1	Tetratricopeptide repeat (TPR)-like superfamily protein LENGTH=206
0	Niben101Scf01441g02001	1.301530213	sp|Q8TAG9|EXOC6_HUMAN	Exocyst complex component 6
0	Niben101Scf01489g00004	1.297409292	AT5G47070	Receptor-like protein kinase
0	Niben101Scf11491g02021	1.291258243	AT1G48790.1	associated molecule with the SH3 domain of STAM 1 LENGTH=507
0	Niben101Scf02039g04010	1.287220564	sp|Q9SF32|IQD1_ARATH	Protein IQ-DOMAIN 1
3	Niben101Scf00355g01008	1.237719385	AT3G17000.1	ubiquitin-conjugating enzyme 32 LENGTH=309
0	Niben101Scf09089g01025	1.208635951	sp|Q9FG38|SNX1_ARATH	Sorting nexin 1
0	Niben101Scf07381g02007	1.19264038	sp|Q06967|14336_ORYSJ	14-3-3-like protein GF14-F
0	Niben101Scf08130g00016	1.159194435	sp|Q9SR36|GSTU8_ARATH	Glutathione S-transferase U8
0	Niben101Scf10749g02005	1.15884548	AT1G50700.1	calcium-dependent protein kinase 33 LENGTH=521
1	Niben101Scf00916g01007	1.132922102	sp|Q9SIQ9|VA712_ARATH	Vesicle-associated membrane protein 712
1	Niben101Scf03100g01016	1.130048776	AT5G32440.3	Ubiquitin system component Cue protein LENGTH=265
0	Niben101Scf02583g06016	1.12255515	AT5G66200.1	armadillo repeat only 2 LENGTH=651
0	Niben101Scf02622g09004	1.109015029	AT5G04520.1	Protein of unknown function DUF455 LENGTH=291
0	Niben101Scf00128g02010	1.030930565	sp|Q9LHP4|RCH2_ARATH	Receptor-like protein kinase 2
1	Niben101Scf00905g12005	1.025863093	gb|KEH17617.1|	structural constituent of cell wall protein, putative [*Medicago truncatula*]
1	Niben101Scf02585g00029	1.008973902	gb|KEH17617.1|	structural constituent of cell wall protein, putative [*Medicago truncatula*]
1	Niben101Scf00777g06012	1.004868831	sp|Q9LK09|SYP32_ARATH	Syntaxin-32

Table S2. *(Continued)*

0	Niben101Scf01267g11013	0.976126686	gb|AFW56318.1|	ABA-responsive protein [Zea mays]
1	Niben101Scf02508g03006	0.96242023	gb|AAO72706.1|	heavy meromyosin-like protein [Oryza sativa Japonica Group]
0	Niben101Scf01010g00009	0.958142314	AT5G19760.1	Mitochondrial substrate carrier family protein LENGTH=298
1	Niben101Scf03341g02011	0.94396846	sp|Q9LN71|RING1_ARATH	E3 ubiquitin-protein ligase
1	Niben101Scf14394g01020	0.942508299	sp|P27541|HSP70_BRUMA	Heat shock 70 kDa protein
1	Niben101Scf01276g02007	0.938406084	sp|O82703|VATG2_TOBAC	V-type proton ATPase subunit G 2
1	Niben101Scf02111g11001	0.911694091	AT3G17000.1	ubiquitin-conjugating enzyme 32 LENGTH=309
0	Niben101Scf04699g00014	0.903059367	AT1G03445.1	Serine/threonine protein phosphatase family protein LENGTH=793
0	Niben101Scf10152g04002	0.898656183	sp|B9DFS6|SNX2B_ARATH	Sorting nexin 2B
0	Niben101Scf02502g12001	0.876818707	sp|Q3EBL9|VP372_ARATH	Vacuolar protein-sorting-associated protein 37 homolog 2
1	Niben101Scf03580g01006	0.876081073	sp|Q86A67|ALF_DICDI	Fructose-bisphosphate aldolase
0	Niben101Scf01222g01011	0.869252518	AT1G70940.1	Auxin efflux carrier family protein LENGTH=640
0	Niben101Scf09876g00009	0.842811807	sp|Q68F45|WIPI3_XENLA	WD repeat domain phosphoinositide-interacting protein 3
0	Niben101Scf10015g10014	0.834024589	AT3G12360.1	Ankyrin repeat family protein LENGTH=590
0	Niben101Scf01980g12010	0.819169864	sp|Q6ZKC0|14333_ORYSJ	14-3-3-like protein GF14-C
0	Niben101Scf05901g03008	0.807312905	sp|Q9MA55|ACBP4_ARATH	Acyl-CoA-binding domain-containing protein 4
1	Niben101Scf07187g01003	0.798031265	sp|Q94KK7|SYP52_ARATH	Syntaxin-52
0	Niben101Scf15532g01008	0.795281635	ref|XP_002885363.1|	calcium-binding EF hand family protein
0	Niben101Scf04703g00002	0.793946638	sp|O22151|GOS12_ARATH	Golgi SNAP receptor complex member 1-2
0	Niben101Scf16132g00001	0.784800416	AT1G08720.1	Protein kinase superfamily protein LENGTH=933
0	Niben101Scf07438g04016	0.783920861	sp|Q9LHA4|VA0D2_ARATH	V-type proton ATPase subunit d2
0	Niben101Scf10366g00012	0.743627113	sp|P46824|KLC_DROME	Kinesin light chain
0	Niben101Scf03202g13014	0.725478991	ref|NP_001059890.1|	OsJ_24600 [Oryza sativa Japonica Group]
0	Niben101Scf02972g07003	0.696357318	AT4G10730	Serine/threonine-protein kinase 4
0	Niben101Scf04122g05011	0.696063289	sp|Q9P0L0|VAPA_HUMAN	Vesicle-associated membrane protein-associated protein A

Table S2. *(Continued)*

0	Niben101Scf03011g01012	0.678103413	sp|Q9LIG2|RLK6_ARATH	Receptor-like protein kinase
0	Niben101Scf01701g07009	0.676808892	AT1G19730.1	Thioredoxin superfamily protein LENGTH=119
1	Niben101Scf00302g01002	0.670913073	sp|Q86A67|ALF_DICDI	Fructose-bisphosphate aldolase
1	Niben101Scf02401g02014	0.66518067	AT5G19010	mitogen-activated protein kinase 16 LENGTH=567
0	Niben101Scf25021g01021	0.657956031	sp|O48724|WEB1_ARATH	Protein WEAK CHLOROPLAST MOVEMENT UNDER BLUE LIGHT 1
0	Niben101Scf01240g04010	0.654369785	sp|Q9SH88|RRS1_ARATH	Ribosome biogenesis regulatory protein homolog
1	Niben101Scf11161g00006	0.653525343	sp|Q66I12|CCD47_DANRE	Coiled-coil domain-containing protein 47
0	Niben101Scf06093g00001	0.649627893	AT5G19450.1	calcium-dependent protein kinase 19 LENGTH=533
0	Niben101Scf04968g00011	0.64681321	tpg|DAA39002.1|	TPA: hypothetical protein ZEAMMB73_375277 [Zea mays]
0	Niben101Scf02849g07001	0.641310676	sp|Q11SV1|GPMA_CYTH3	2,3-bisphosphoglycerate-dependent phosphoglycerate mutase
0	Niben101Scf02468g02007	0.637978997	AT3G05420.2	acyl-CoA binding protein 4 LENGTH=669
0	Niben101Scf02646g02009	0.634616594	sp|F1MCA7|LRRC7_BOVIN	Leucine-rich repeat-containing protein 7
3	Niben101Scf00634g04004	0.619021089	AT1G20330.1	sterol methyltransferase 2 LENGTH=361
1	Niben101Scf05982g01005	0.596833745	sp|Q4V8C4|WDR5B_RAT	WD repeat-containing protein 5B
0	Niben101Scf04078g02006	0.596072105	AT1G69960.1	serine/threonine protein phosphatase 2A LENGTH=307
0	Niben101Scf03129g03013	0.594742714	AT3G16060.1	ATP binding microtubule motor family protein LENGTH=684
0	Niben101Scf04103g07019	0.582945529	sp|P62191|PRS4_HUMAN	26S protease regulatory subunit 4
0	Niben101Scf00428g16011	0.571145999	sp|Q9LJI5|VA0D1_ARATH	V-type proton ATPase subunit d1
0	Niben101Scf01784g05010	0.5702173	sp|O48724|WEB1_ARATH	Protein WEAK CHLOROPLAST MOVEMENT UNDER BLUE LIGHT 1
0	Niben101Scf19779g00007	0.541582413	AT4G32760.2	ENTH/VHS/GAT family protein LENGTH=676
0	Niben101Scf04671g06008	0.534915776	AT1G03445.1	Serine/threonine protein phosphatase family protein LENGTH=793
0	Niben101Scf06825g00010	0.526242541	AT1G73390.1	Endosomal targeting BRO1-like domain-containing protein LENGTH=419
0	Niben101Scf01849g05008	0.519428132	sp|Q9LVQ4|Y5586_ARATH	WEB family protein
0	Niben101Scf13289g00009	0.518217476	sp|Q9NGQ2|KIF1_DICDI	Kinesin-related protein 1
0	Niben101Scf07395g00029	0.505402279	sp|Q9LV10|PTR53_ARATH	Protein NRT1/ PTR FAMILY 2.11

Table S2. *(Continued)*

0	Niben101Scf01150g05006	0.485654114	AT1G76850.1	exocyst complex component sec5 LENGTH=1090
0	Niben101Scf02979g03004	0.481411916	sp|B0UTU8|SYN_HISS2	Asparagine--tRNA ligase
0	Niben101Scf03894g01016	0.462424664	AT4G10730	Serine/threonine-protein kinase 4
1	Niben101Scf01090g05008	0.461858475	sp|P0CR79|HSE1_CRYNB	Class E vacuolar protein-sorting machinery protein HSE1
1	Niben101Scf03486g02009	0.444532377	sp|Q12788|TBL3_HUMAN	Transducin beta-like protein 3
0	Niben101Scf00466g04036	0.435043923	sp|Q40401|CALR_NICPL	Calreticulin
0	Niben101Scf04145g00026	0.427789428	sp|Q9FGY4|FB341_ARATH	F-box protein
0	Niben101Scf05468g10026	0.381908286	AT3G59770.3	sacI domain-containing protein / WW domain-containing protein
1	Niben101Scf02108g02018	0.367584441	AT1G73460.1	Protein kinase superfamily protein LENGTH=1169
0	Niben101Scf02044g02006	0.3634823	gb|ACG40676.1|	p8MTCP1 [Zea mays]
2	Niben101Scf00204g00004	0.354627722	sp|Q876F5|SC242_SACU7	Protein transport protein SEC24-2
0	Niben101Scf00606g00010	0.353358206	AT1G19730.1	Thioredoxin superfamily protein LENGTH=119
3	Niben101Scf02030g04003	0.350971223	sp|P17156|HSP72_MOUSE	Heat shock-related 70 kDa protein 2
0	Niben101Scf10176g01002	0.326854052	sp|Q64VI7|DNAJ_BACFR	Chaperone protein DnaJ
1	Niben101Scf05904g00005	0.322434566	sp|P93654|SYP22_ARATH	Syntaxin-22
0	Niben101Scf02919g00020	0.321899554	AT3G17850.1	Protein kinase superfamily protein LENGTH=1296
2	Niben101Scf09977g00011	0.318445567	gb|AIU51078.1|	AT4G29520-like protein, partial [Solanum tuberosum]
0	Niben101Scf09014g01003	0.31746576	sp|Q86A67|ALF_DICDI	Fructose-bisphosphate aldolase
0	Niben101Scf00961g03002	0.289135668	AT4G32760.2	ENTH/VHS/GAT family protein LENGTH=676
0	Niben101Scf02639g03014	0.286363232	AT3G12360.1	Ankyrin repeat family protein LENGTH=590
2	Niben101Scf05154g01024	0.283683767	sp|Q9M376|VA727_ARATH	Vesicle-associated membrane protein 727
0	Niben101Scf02733g00018	0.279802271	sp|Q9FN94|RLK7_ARATH	Receptor-like protein kinase
0	Niben101Scf01243g01007	0.265460869	sp|O80856|ARC1A_ARATH	Actin-related protein 2/3 complex subunit 1A
0	Niben101Scf02902g03008	0.254667224	AT1G76850.1	exocyst complex component sec5 LENGTH=1090
0	Niben101Scf01745g04006	0.239734669	sp|Q944A9|NPS11_ARATH	Novel plant SNARE 11

Table S2. *(Continued)*

0	Niben101Scf08001g01004	0.207150083	sp|Q9N4Y9|ZFPL1_CAEEL	Zinc finger protein-like 1 homolog
0	Niben101Scf02318g00005	0.203623015	AT3G15220	Serine/threonine-protein kinase 4 homolog B
0	Niben101Scf04403g03001	0.198998639	AT1G69220	Serine/threonine-protein kinase 10
0	Niben101Scf10278g01002	0.184348133	sp|Q6ZKC0|14333_ORYSJ	14-3-3-like protein GF14-C
0	Niben101Scf06080g04001	0.174061208	sp|C1DFM2|DNAJ_AZOVD	Chaperone protein DnaJ
1	Niben101Scf01305g02004	0.153594537	sp|P93654|SYP22_ARATH	Syntaxin-22
0	Niben101Scf11895g03027	0.150698359	sp|Q5E9R3|EHD1_BOVIN	EH domain-containing protein 1
1	Niben101Scf00747g01011	0.144933084	sp|Q9LTR9|NMT1_ARATH	Glycylpeptide N-tetradecanoyltransferase 1
0	Niben101Scf03734g00001	0.142777499	sp|Q9SCP9|VP371_ARATH	Vacuolar protein-sorting-associated protein 37 homolog 1
1	Niben101Scf16457g00008	0.138218968	sp|Q9N0E7|MOCOS_BOVIN	Molybdenum cofactor sulfurase
1	Niben101Scf06187g01021	0.136850714	emb|CDY15385.1|	BnaC04g42380D [*Brassica napus*]
0	Niben101Scf14996g00009	0.134942197	sp|Q9M5L6|CATA_CAPAN	Catalase
0	Niben101Scf09781g00016	0.113000638	sp|Q9SMX9|SPL1_ARATH	Squamosa promoter-binding-like protein 1
0	Niben101Ctg15209g00004	0.11077857	sp|O95208|EPN2_HUMAN	Epsin-2
0	Niben101Scf00103g00019	0.079399245	AT1G29690.1	MAC/Perforin domain-containing protein LENGTH=561
0	Niben101Scf04018g13004	0.063971947	sp|Q556Y4|KC1_DICDI	Casein kinase I
0	Niben101Scf00611g11028	0.055317989	sp|Q556Y4|KC1_DICDI	Casein kinase I
2	Niben101Scf04444g01004	0.050015225	sp|Q08069|RS8_MAIZE	40S ribosomal protein S8
0	Niben101Scf11960g01001	0.041169371	sp|Q8L7A9|AP4E_ARATH	AP-4 complex subunit epsilon
0	Niben101Scf03628g08003	0.026985778	sp|Q9CR95|NECP1_MOUSE	Adaptin ear-binding coat-associated protein 1
0	Niben101Scf06653g01003	0.020171266	sp|O80856|ARC1A_ARATH	Actin-related protein 2/3 complex subunit 1A
1	Niben101Scf07182g04010	0.017328662	sp|Q6ABS5|FTHS_PROAC	Formate--tetrahydrofolate ligase
0	Niben101Scf05415g01002	0	AT2G41970	Receptor-like protein kinase 5
1	Niben101Scf04083g01008	-0.001591427	sp|Q9M376|VA727_ARATH	Vesicle-associated membrane protein 727
0	Niben101Scf07790g01023	-0.01180246	sp|Q9S9T7|VP282_ARATH	Vacuolar protein sorting-associated protein 28 homolog 2

Table S2. *(Continued)*

0	Niben101Scf04039g00004	-0.025986883	sp|O95684|FR1OP_HUMAN	FGFR1 oncogene partner
2	Niben101Scf04301g01001	-0.026239465	gb|AAO72598.1|	myosin-like protein
0	Niben101Scf05959g01005	-0.045094679	sp|Q96300|14337_ARATH	14-3-3-like protein GF14 nu
0	Niben101Scf01515g07011	-0.060730577	sp|P62191|PRS4_HUMAN	26S protease regulatory subunit 4
2	Niben101Scf01752g10011	-0.062718009	sp|Q08069|RS8_MAIZE	40S ribosomal protein S8
0	Niben101Scf00927g02017	-0.063716679	sp|Q55512|DHAS_SYNY3	Aspartate-semialdehyde dehydrogenase
1	Niben101Scf10200g00007	-0.071693459	AT5G19010	mitogen-activated protein kinase 16 LENGTH=567
0	Niben101Scf01478g08020	-0.076859065	AT5G08580.1	Calcium-binding EF hand family protein LENGTH=391
0	Niben101Scf06211g01011	-0.100058827	sp|A4QK54|RK14_ARAHI	50S ribosomal protein L14, chloroplastic
1	Niben101Scf02470g00003	-0.102481627	sp|Q4QQS1|T184A_RAT	Transmembrane protein 184A
0	Niben101Scf02752g05009	-0.105054014	AT5G18610	Receptor-like protein kinase
0	Niben101Scf07533g01002	-0.111910614	sp|Q91790|DUS1A_XENLA	Dual specificity protein phosphatase 1-A
0	Niben101Scf04899g05008	-0.132219867	AT5G58950	Protein kinase superfamily protein LENGTH=525
0	Niben101Scf10490g00011	-0.145899882	AT1G19730.1	Thioredoxin superfamily protein LENGTH=119
0	Niben101Scf07672g00018	-0.162851089	sp|P56252|ENO_HOMGA	Enolase
0	Niben101Scf04475g00005	-0.167563801	sp|Q6ZKC0|14333_ORYSJ	14-3-3-like protein GF14-C
0	Niben101Scf03036g04004	-0.171420484	AT3G59350	Receptor-like protein kinase
0	Niben101Scf05588g03007	-0.18198742	emb|CDX93559.1|	BnaA06g04890D [*Brassica napus*]
0	Niben101Scf10384g02005	-0.189716303	sp|Q9BPL7|ENO2_TOXGO	Enolase 2
0	Niben101Scf01478g08021	-0.196195014	AT3G19960.2	myosin 1 LENGTH=1176
1	Niben101Scf16022g04001	-0.197157188	sp|Q5BJQ2|FA63A_RAT	Protein FAM63A
1	Niben101Scf05827g00005	-0.20544108	sp|P62427|RL7A_NANEQ	50S ribosomal protein L7Ae
0	Niben101Scf01721g02001	-0.212662376	sp|Q54KZ4|CHMP6_DICDI	Charged multivesicular body protein 6
1	Niben101Scf08523g00013	-0.225387727	AT3G27190.1	uridine kinase-like 2 LENGTH=483
0	Niben101Scf00747g01016	-0.225953611	sp|Q556Y4|KC1_DICDI	Casein kinase I

Table S2. *(Continued)*

0	Niben101Scf06912g01020	-0.234379673	sp|Q6BK66|CCS1_DEBHA	Superoxide dismutase 1 copper chaperone
0	Niben101Scf09792g02018	-0.235178761	sp|Q6NVL7|CHM2B_XENTR	Charged multivesicular body protein 2b
0	Niben101Scf00270g03014	-0.250481656	AT3G59350	Receptor-like protein kinase
0	Niben101Scf13002g03023	-0.256558492	AT2G41970	Protein kinase superfamily protein LENGTH=365
0	Niben101Scf01975g03009	-0.263590006	sp|Q9LIG2|RLK6_ARATH	Receptor-like protein kinase
0	Niben101Scf03377g05003	-0.297539373	AT5G03540.3	exocyst subunit exo70 family protein A1 LENGTH=664
0	Niben101Scf07488g00024	-0.298911991	sp|P47735|RLK5_ARATH	Receptor-like protein kinase 5
0	Niben101Scf03634g06015	-0.326788863	sp|Q9LHA4|VA0D2_ARATH	V-type proton ATPase subunit d2
0	Niben101Scf11497g02007	-0.336557534	sp|Q5JIR1|VATD_THEKO	V-type ATP synthase subunit D
3	Niben101Scf04331g09018	-0.343102256	AT4G24190.1	Chaperone protein htpG family protein LENGTH=823
0	Niben101Scf00730g01013	-0.344062522	sp|Q9SF32|IQD1_ARATH	Protein IQ-DOMAIN 1
0	Niben101Scf17538g00008	-0.356458104	sp|Q0WUQ1|BAG1_ARATH	BAG family molecular chaperone regulator 1
0	Niben101Scf24322g00012	-0.371267237	emb|CDY07628.1|	BnaA03g18830D [*Brassica napus*]
0	Niben101Scf01157g01014	-0.383769475	AT4G35230	Receptor like protein kinase S.3
0	Niben101Scf01859g07007	-0.395225636	sp|A1JPA1|MDTK_YERE8	Multidrug resistance protein MdtK
0	Niben101Scf13221g00005	-0.410113868	gb|AER52053.1|	vWA domain containing protein [Oryza sativa Japonica Group]
0	Niben101Scf00528g00013	-0.420034982	sp|Q8K9Y9|DNAJ_BUCAP	Chaperone protein DnaJ
0	Niben101Scf10980g00002	-0.421134064	AT5G63640.1	ENTH/VHS/GAT family protein LENGTH=447
0	Niben101Scf00674g00009	-0.429117859	AT5G66200.1	armadillo repeat only 2 LENGTH=651
0	Niben101Scf02911g06011	-0.438467203	sp|Q9H9S4|CB39L_HUMAN	Calcium-binding protein 39-like
1	Niben101Scf02395g02002	-0.444991333	sp|A5D2S3|TRUB_PELTS	tRNA pseudouridine synthase B
0	Niben101Scf04216g07018	-0.453536781	AT1G66220.1	Subtilase family protein LENGTH=753
1	Niben101Scf04995g18023	-0.471835359	sp|Q9STX1|ACBP3_ARATH	Acyl-CoA-binding domain-containing protein 3
1	Niben101Scf16332g01002	-0.493813204	sp|Q20365|RAB33_CAEEL	Ras-related protein Rab-33
2	Niben101Scf00752g03013	-0.5021311	sp|Q9HBF4|ZFYV1_HUMAN	Zinc finger FYVE domain-containing protein 1

Table S2. *(Continued)*

0	Niben101Scf04122g05014	-0.507798108	AT1G11260.1	sugar transporter 1 LENGTH=522
0	Niben101Scf07035g02001	-0.512485319	emb|CDX93559.1|	BnaA06g04890D [*Brassica napus*]
0	Niben101Scf10557g01002	-0.531279198	AT3G56240.1	copper chaperone LENGTH=121
0	Niben101Scf24238g00004	-0.544995175	sp|Q9SE94|MTHR1_MAIZE	Methylenetetrahydrofolate reductase 1
0	Niben101Scf00745g02009	-0.545932411	sp|P97377|CDK2_MOUSE	Cyclin-dependent kinase 2
0	Niben101Scf03877g00007	-0.549722508	sp|Q42029|PSBP1_ARATH	Oxygen-evolving enhancer protein 2-1, chloroplastic
1	Niben101Scf08293g02002	-0.55768247	sp|B6I2D2|MSRA_ECOSE	Peptide methionine sulfoxide reductase MsrA
0	Niben101Scf00578g05006	-0.560644106	sp|A8GCS6|NQOR_SERP5	NAD(P)H dehydrogenase (quinone)
1	Niben101Scf04555g02006	-0.570226846	AT4G21380.1	receptor kinase 3 LENGTH=850
1	Niben101Scf08522g02011	-0.594020021	AT4G16340.1	guanyl-nucleotide exchange factors
0	Niben101Scf05271g00004	-0.595633576	ref|XP_010092339.1|	Protein kinase G11A [Morus notabilis]
1	Niben101Scf05552g08006	-0.651293962	sp|Q8LGM7|MOCOS_SOLLC	Molybdenum cofactor sulfurase
1	Niben101Scf01888g01004	-0.667137647	AT1G72420.1	NADH:ubiquinone oxidoreductase intermediate-associated protein 30
0	Niben101Scf01668g00002	-0.692952754	emb|CDY58982.1|	BnaA04g28680D [*Brassica napus*]
3	Niben101Scf06761g01029	-0.69452999	sp|Q089P5|RS17_SHEFN	30S ribosomal protein S17
0	Niben101Scf06349g02002	-0.694923517	AT5G14720	Serine/threonine-protein kinase 3
0	Niben101Scf20077g00018	-0.69580819	sp|O43001|SYJ1_SCHPO	Inositol-1,4,5-trisphosphate 5-phosphatase 1
1	Niben101Scf06509g05011	-0.702364127	sp|Q93ZY3|STT3A_ARATH	Dolichyl-diphosphooligosaccharide-protein glycosyltransferase subunit STT3A
0	Niben101Scf09808g01002	-0.704903697	sp|Q1LUM3|ENDUC_DANRE	Poly(U)-specific endoribonuclease-C
0	Niben101Scf06423g03030	-0.710851815	AT5G47750.1	D6 protein kinase like 2 LENGTH=586
0	Niben101Scf07437g04001	-0.713669056	AT1G70950.1	TPX2 (targeting protein for Xklp2) protein family LENGTH=478
0	Niben101Scf03711g01021	-0.722231766	sp|Q9XEX2|PRX2B_ARATH	Peroxiredoxin-2B
1	Niben101Scf04528g11001	-0.748026758	sp|A2BMB2|RL2_HYPBU	50S ribosomal protein L2
1	Niben101Scf13874g01006	-0.750815304	AT5G13710.1	sterol methyltransferase 1 LENGTH=336

Table S2. *(Continued)*

1	Niben101Scf01395g00005	-0.777356333	sp|Q8L7G3|CRK7_ARATH	Cysteine-rich receptor-like protein kinase 7
1	Niben101Scf03949g06008	-0.778155523	gb|ACG38839.1|	snRK1-interacting protein 1 [Zea mays]
2	Niben101Scf00126g06014	-0.782605619	sp|F4I4W2|HCS2_ARATH	Biotin--protein ligase 2
1	Niben101Scf12266g02003	-0.785143567	sp|B5X8M4|BRCC3_SALSA	Lys-63-specific deubiquitinase BRCC36
0	Niben101Scf04669g02010	-0.825987473	sp|Q9CR95|NECP1_MOUSE	Adaptin ear-binding coat-associated protein 1
0	Niben101Scf03687g01001	-0.844609909	sp|P30819|NADC_PSEAE	Nicotinate-nucleotide pyrophosphorylase [carboxylating]
0	Niben101Scf01218g01007	-0.85336103	sp|O55012|PICAL_RAT	Phosphatidylinositol-binding clathrin assembly protein
0	Niben101Scf01958g02008	-0.856680308	sp|Q9H9S4|CB39L_HUMAN	Calcium-binding protein 39-like
1	Niben101Scf07304g07011	-0.860812642	sp|Q08436|PMA3_NICPL	Plasma membrane ATPase 3
0	Niben101Scf05440g00014	-0.864187083	sp|Q9FN94|RLK7_ARATH	Receptor-like protein kinase
0	Niben101Scf03157g00006	-0.879027967	emb|CDY70616.1|	BnaA03g54770D [*Brassica napus*]
0	Niben101Scf02188g02028	-0.879953983	AT3G27000.1	actin related protein 2 LENGTH=389
2	Niben101Scf03880g00003	-0.884624395	sp|Q55EI6|ATX10_DICDI	Ataxin-10 homolog
0	Niben101Scf03208g01009	-0.902965044	sp|Q69ZF3|GBA2_MOUSE	Non-lysosomal glucosylceramidase
0	Niben101Scf01580g02004	-0.919567646	sp|F4IME2|MSL8_ARATH	Mechanosensitive ion channel protein 8
0	Niben101Scf01556g04009	-0.938826194	AT4G22290.1	Ubiquitin-specific protease family C19-related protein LENGTH=445
0	Niben101Scf05989g01008	-0.941612888	sp|Q33DL3|CFI_TOBAC	Chalcone--flavonone isomerase
2	Niben101Scf32851g00036	-0.945033953	sp|P46300|RS4_SOLTU	40S ribosomal protein S4
1	Niben101Scf01375g07001	-0.946559069	sp|P23935|NDUA5_BOVIN	NADH dehydrogenase [ubiquinone] 1 alpha subcomplex subunit 5
0	Niben101Scf00090g01010	-0.94727607	sp|Q9C9X3|ANXD5_ARATH	Annexin D5
1	Niben101Scf00860g03019	-0.950332176	sp|Q57GH3|MSRA_SALCH	Peptide methionine sulfoxide reductase MsrA
1	Niben101Scf05399g03003	-0.953060759	AT5G13110.1	glucose-6-phosphate dehydrogenase 2 LENGTH=596
2	Niben101Scf12165g00003	-0.962527797	sp|Q06881|BCCP_NOSS1	Biotin carboxyl carrier protein of acetyl-CoA carboxylase
0	Niben101Scf06290g03007	-0.973038673	sp|P97377|CDK2_MOUSE	Cyclin-dependent kinase 2

Table S2. *(Continued)*

0	Niben101Scf08522g02016	-0.979497604	AT4G16340.1	guanyl-nucleotide exchange factors;GTPase binding;GTP binding LENGTH=1830
0	Niben101Scf01529g02004	-0.98327445	AT1G11260.1	sugar transporter 1 LENGTH=522
0	Niben101Scf03070g08001	-0.993232072	sp|Q9SEE5|GALK1_ARATH	Galactokinase
0	Niben101Scf06183g03009	-0.995045868	AT2G42590.3	general regulatory factor 9 LENGTH=276
0	Niben101Scf09703g00001	-1.004827002	sp|Q9SEE5|GALK1_ARATH	Galactokinase
0	Niben101Scf05692g07002	-1.014698077	ref|XP_002885363.1|	calcium-binding EF hand family protein
0	Niben101Scf01940g00012	-1.055030153	AT3G17850.1	Protein kinase superfamily protein LENGTH=1296
0	Niben101Scf18000g00028	-1.082584234	AT1G72410.2	COP1-interacting protein-related LENGTH=1270
1	Niben101Scf09792g03014	-1.099458149	sp|Q93XX8|NOP10_ARATH	H/ACA ribonucleoprotein complex subunit 3-like protein
0	Niben101Scf01236g02003	-1.104725156	AT3G17410	Receptor-like protein kinase
0	Niben101Scf07008g01017	-1.105046193	sp|Q9LIG2|RLK6_ARATH	Receptor-like protein kinase
0	Niben101Scf02622g07005	-1.10826962	sp|P34885|KPC1B_CAEEL	Protein kinase C-like 1B
2	Niben101Scf04292g01004	-1.11770678	sp|Q06881|BCCP_NOSS1	Biotin carboxyl carrier protein of acetyl-CoA carboxylase
0	Niben101Scf07498g02003	-1.134142841	sp|F4JUL9|ARPC4_ARATH	Actin-related protein 2/3 complex subunit 4
1	Niben101Scf03936g01006	-1.146250829	sp|Q93ZY3|STT3A_ARATH	Dolichyl-diphosphooligosaccharide--protein glycosyltransferase subunit STT3A
0	Niben101Scf01559g03017	-1.170492408	ref|NP_001148046.1|	LOC100281655 [Zea mays] gb|ACG29576.1| metal ion binding protein [Zea mays]
0	Niben101Scf04216g02006	-1.183179361	ref|WP_002796693.1|	Phot [Microcystis aeruginosa PCC 9809]
0	Niben101Scf00595g02001	-1.205503403	AT1G63700	Protein kinase superfamily protein LENGTH=883
0	Niben101Scf02357g08010	-1.209431516	sp|Q9FN94|RLK7_ARATH	Receptor-like protein kinase
2	Niben101Scf06956g00014	-1.21094284	ref|XP_007049662.1|	P-loop containing nucle , putative [Theobroma cacao]
0	Niben101Scf00294g02004	-1.218138744	sp|Q9SF32|IQD1_ARATH	Protein IQ-DOMAIN 1
1	Niben101Scf30418g00019	-1.219540979	AT5G13550.1	sulfate transporter 4.1 LENGTH=685
1	Niben101Scf00031g00003	-1.234769769	AT3G14940.1	phosphoenolpyruvate carboxylase 3 LENGTH=968

Table S2. *(Continued)*

0	Niben101Scf03222g01012	-1.241441926	AT4G32410.1	cellulose synthase 1 LENGTH=1081
0	Niben101Scf06186g06008	-1.249332406	AT1G63700	Serine/threonine-protein kinase 24
1	Niben101Scf03257g02001	-1.249906161	gb|ACG38839.1|	snRK1-interacting protein 1 [Zea mays]
1	Niben101Scf03576g00007	-1.255127559	AT1G42960.1	expressed protein localized to the inner membrane of the chloroplast
1	Niben101Scf05183g01003	-1.256074845	sp|A6TB06|RSMF_KLEP7	Ribosomal RNA small subunit methyltransferase F
0	Niben101Scf07109g01003	-1.256451238	AT2G20990.3	synaptotagmin A LENGTH=579
0	Niben101Scf09725g00020	-1.279283757	ref|XP_007030054.1|	Nucleic acid binding protein, putative isoform 2
0	Niben101Scf03687g01012	-1.309875021	sp|P30819|NADC_PSEAE	Nicotinate-nucleotide pyrophosphorylase [carboxylating]
0	Niben101Scf04788g00023	-1.321441424	sp|P30819|NADC_PSEAE	Nicotinate-nucleotide pyrophosphorylase [carboxylating]
0	Niben101Scf08621g04007	-1.352464671	AT5G16620.1	hydroxyproline-rich glycoprotein family protein LENGTH=447
0	Niben101Scf06678g02006	-1.362859335	sp|Q94BT0|SPSA1_ARATH	Sucrose-phosphate synthase 1
0	Niben101Scf01388g01020	-1.398761015	sp|Q8R550|SH3K1_MOUSE	SH3 domain-containing kinase-binding protein 1
0	Niben101Scf06525g01002	-1.433563785	sp|P46629|RAB25_RABIT	Ras-related protein Rab-25
1	Niben101Scf02976g00007	-1.435057994	sp|P43510|CPR6_CAEEL	Cathepsin B-like cysteine proteinase 6
0	Niben101Scf00090g08013	-1.435283221	sp|O48724|WEB1_ARATH	Protein WEAK CHLOROPLAST MOVEMENT UNDER BLUE LIGHT 1
1	Niben101Scf04420g02003	-1.440717764	sp|Q0S0L7|KGUA_RHOJR	Guanylate kinase
0	Niben101Scf16022g04004	-1.448739334	AT1G63000.1	nucleotide-rhamnose synthase/epimerase-reductase LENGTH=301
0	Niben101Scf00991g08004	-1.455992796	sp|Q9FJX6|FH6_ARATH	Formin-like protein 6
1	Niben101Scf03326g05014	-1.461664741	AT3G02900.1	unknown protein
1	Niben101Scf00712g09038	-1.522963773	AT1G42960.1	expressed protein localized to the inner membrane of the chloroplast
0	Niben101Scf08804g03006	-1.542366821	AT3G17850.1	Protein kinase superfamily protein LENGTH=1296
0	Niben101Scf08566g01006	-1.615816962	sp|Q9KWS6|DNAJ_GEOTM	Chaperone protein DnaJ
0	Niben101Scf07465g01016	-1.622436649	sp|Q9FXI5|IQD32_ARATH	Protein IQ-DOMAIN 32
0	Niben101Scf08322g00001	-1.622497467	sp|Q9C6X2|SCAM4_ARATH	Secretory carrier-associated membrane protein 4
0	Niben101Scf03076g01026	-1.628028829	sp|Q869Q3|NAPA_DICDI	Nck-associated protein 1 homolog

Table S2. *(Continued)*

0	Niben101Scf01763g00004	-1.634339831	AT1G56720	Receptor-like protein kinase
1	Niben101Scf10259g00009	-1.682398461	AT3G61050.1	Calcium-dependent lipid-binding (CaLB domain) family protein LENGTH=510
0	Niben101Scf03264g01004	-1.729109369	sp|P80680|FTRV_MAIZE	Ferredoxin-thioredoxin reductase, variable chain
0	Niben101Scf07113g00007	-1.737135246	gb|AFV66582.1|	LSG [Saccharum hybrid cultivar]
0	Niben101Scf05929g02003	-1.737141217	sp|Q75AA5|NTF2_ASHGO	Nuclear transport factor 2
2	Niben101Scf02003g01001	-1.764997385	sp|Q6ZPJ0|TEX2_MOUSE	Testis-expressed sequence 2 protein
0	Niben101Scf03817g15014	-1.779600885	AT3G22190.1	IQ-domain 5 LENGTH=422
2	Niben101Scf10532g00001	-1.801725575	sp|Q1XDK5|BCCP_PYRYE	Biotin carboxyl carrier protein of acetyl-CoA carboxylase
0	Niben101Scf04007g01012	-1.811429683	sp|P25792|CYSP_SCHMA	Cathepsin B-like cysteine proteinase
0	Niben101Scf10595g00008	-1.819988903	AT1G63000.1	nucleotide-rhamnose synthase/epimerase-reductase LENGTH=301
0	Niben101Scf04585g00006	-1.830124657	sp|Q9P4D1|ACT_PICPG	Actin
1	Niben101Scf06671g03027	-1.831688971	sp|P23935|NDUA5_BOVIN	NADH dehydrogenase [ubiquinone] 1 alpha subcomplex subunit 5
0	Niben101Scf00055g04003	-1.84812975	sp|Q9LIG2|RLK6_ARATH	Receptor-like protein kinase
0	Niben101Scf08580g00015	-1.849915971	sp|Q9SF32|IQD1_ARATH	Protein IQ-DOMAIN 1
1	Niben101Scf02474g01021	-1.8575464	sp|P31414|AVP1_ARATH	Pyrophosphate-energized vacuolar membrane proton pump 1
0	Niben101Scf05191g00013	-1.868464014	AT4G15080.1	DHHC-type zinc finger family protein LENGTH=718
1	Niben101Scf01369g05022	-1.87369071	AT1G42960.1	expressed protein localized to the inner membrane of the chloroplast
0	Niben101Scf07402g00012	-1.909026651	AT4G22290.1	Ubiquitin-specific protease family C19-related protein LENGTH=445
0	Niben101Scf05102g02013	-1.936618855	AT5G16620.1	hydroxyproline-rich glycoprotein family protein LENGTH=447
0	Niben101Scf04316g05002	-1.948315139	sp|Q9M9F9|ICR4_ARATH	Interactor of constitutive active ROPs 4
0	Niben101Scf01989g00011	-2.018414985	emb|CDY70616.1|	BnaA03g54770D [*Brassica napus*]
0	Niben101Scf03714g00006	-2.046259605	sp|Q3E7D0|NAT12_ARATH	Nucleobase-ascorbate transporter 12
0	Niben101Scf00869g06027	-2.066479488	sp|P80680|FTRV_MAIZE	Ferredoxin-thioredoxin reductase, variable chain
0	Niben101Scf00606g02018	-2.10017644	sp|Q72MG4|IPYR_LEPIC	Inorganic pyrophosphatase

Table S2. *(Continued)*

1	Niben101Scf00140g00002	-2.106136131	emb|CDY63903.1|	BnaA01g34680D [*Brassica napus*]
0	Niben101Scf03503g00003	-2.108244422	AT1G76040.2	calcium-dependent protein kinase 29 LENGTH=561
0	Niben101Scf01175g06002	-2.157862138	AT5G10270.1	cyclin-dependent kinase C;1 LENGTH=505
1	Niben101Scf04943g00013	-2.168393463	sp|Q9LIG2|RLK6_ARATH	Receptor-like protein kinase
0	Niben101Scf05047g03010	-2.175067197	AT5G52430.1	hydroxyproline-rich glycoprotein family protein LENGTH=438
0	Niben101Scf01819g02019	-2.180371589	AT2G02170.1	Remorin family protein LENGTH=486
1	Niben101Scf02562g04001	-2.192944091	sp|P21616|AVP_VIGRR	Pyrophosphate-energized vacuolar membrane proton pump
0	Niben101Scf07247g01002	-2.217302183	AT5G10270.1	cyclin-dependent kinase C;1 LENGTH=505
2	Niben101Scf05269g04001	-2.219039862	AT1G36160.1	acetyl-CoA carboxylase 1 LENGTH=2254
1	Niben101Scf01048g00008	-2.276134106	AT4G37900.1	Protein of unknown function (duplicated DUF1399) LENGTH=787
1	Niben101Scf05080g01011	-2.282435245	sp|Q9FLP0|MA651_ARATH	65-kDa microtubule-associated protein 1
0	Niben101Scf06715g02001	-2.285737012	sp|Q9C6X2|SCAM4_ARATH	Secretory carrier-associated membrane protein 4
0	Niben101Scf03875g00008	-2.287737703	AT2G03350.1	Protein of unknown function, DUF538 LENGTH=179
0	Niben101Scf02908g01016	-2.308941055	ref|WP_026735795.1|	molecular chaperone DnaJ [Fischerella sp. PCC 9605]
0	Niben101Scf00089g02001	-2.358872336	ref|XP_007022165.1|	Interactor of constitutive active rops 1 isoform 2 [Theobroma cacao]
0	Niben101Scf07162g04010	-2.362733579	AT2G39770.1	Glucose-1-phosphate adenylyltransferase family protein LENGTH=361
0	Niben101Scf04206g01012	-2.417282966	tpg|DAA62158.1|	TPA: hypothetical protein ZEAMMB73_942245 [Zea mays]
0	Niben101Scf04007g04002	-2.430094733	AT4G02630	Receptor-like protein kinase
0	Niben101Scf02660g04001	-2.437779975	AT4G14740.1	Plant protein of unknown function (DUF828)
0	Niben101Scf16278g00004	-2.462174335	sp|Q7JZB4|GMPPB_DROME	Mannose-1-phosphate guanyltransferase beta
0	Niben101Scf11756g03011	-2.483702172	ref|XP_007022164.1|	Interactor of constitutive active rops 1 isoform 1 [Theobroma cacao]
1	Niben101Scf05385g04007	-2.539296972	gb|ADQ73987.1|	dehydrin [Solanum peruvianum]
0	Niben101Scf31796g00003	-2.602642775	tpg|DAA62158.1|	TPA: hypothetical protein ZEAMMB73_942245 [Zea mays]
1	Niben101Scf03224g07001	-2.631841975	sp|P21616|AVP_VIGRR	Pyrophosphate-energized vacuolar membrane proton pump
1	Niben101Scf01154g02003	-2.658002726	AT2G44830.1	Protein kinase superfamily protein LENGTH=765

Table S2. *(Continued)*

0	Niben101Scf01497g04006	-2.670386009	AT4G35730.1	Regulator of Vps4 activity in the MVB pathway protein LENGTH=466
0	Niben101Scf14009g02003	-2.736352476	ref|XP_002521463.1|	Microtubule-associated protein futsch, putative [*Ricinus communis*]
0	Niben101Scf00490g01036	-2.755138769	AT4G22890.1	PGR5-LIKE A LENGTH=324
1	Niben101Scf04708g00011	-2.840403479	AT5G64740.1	cellulose synthase 6 LENGTH=1084
0	Niben101Scf00309g00001	-2.860243937	gb|KEH41061.1|	auxin canalization protein [*Medicago truncatula*]
1	Niben101Scf03840g02006	-2.878999404	sp|O84100|RS1_CHLTR	30S ribosomal protein S1
1	Niben101Scf01369g05023	-2.954661824	sp|P94915|G3P_MYCAV	Glyceraldehyde-3-phosphate dehydrogenase
0	Niben101Scf01656g00015	-2.959988647	AT3G59700.1	lectin-receptor kinase LENGTH=661
0	Niben101Scf01273g00002	-2.979997569	AT5G08570.1	Pyruvate kinase family protein LENGTH=510
1	Niben101Scf25430g00015	-2.989392488	AT1G53310.1	phosphoenolpyruvate carboxylase 1 LENGTH=967
0	Niben101Scf02440g01037	-3.010267395	AT4G21380.1	receptor kinase 3 LENGTH=850
0	Niben101Scf03768g03025	-3.029155725	AT5G01560.1	lectin receptor kinase a4.3 LENGTH=691
0	Niben101Scf01036g03007	-3.108520233	AT4G03520.1	Thioredoxin superfamily protein LENGTH=186
0	Niben101Scf05824g12003	-3.122118658	AT4G31820.1	Phototropic-responsive NPH3 family protein LENGTH=571
0	Niben101Scf00571g10002	-3.23628927	AT5G19760.1	Mitochondrial substrate carrier family protein LENGTH=298
0	Niben101Scf11689g02005	-3.302609648	AT2G37180.1	Aquaporin-like superfamily protein LENGTH=285
0	Niben101Scf01735g00005	-3.325278471	AT1G37130.1	nitrate reductase 2 LENGTH=917
0	Niben101Scf25768g00021	-3.442794908	gb|AAT74390.1|	rapid alkalinization factor 5 [*Solanum chacoense*]
0	Niben101Scf03816g02010	-3.520539764	sp|P74227|EFTU_SYNY3	Elongation factor Tu
0	Niben101Scf02602g00001	-3.530141485	AT4G03520.1	Thioredoxin superfamily protein LENGTH=186
0	Niben101Scf02576g00011	-3.546317372	AT2G37180.1	Aquaporin-like superfamily protein LENGTH=285
0	Niben101Scf02004g00032	-4.089992356	sp|Q9KUT3|MDH_VIBCH	Malate dehydrogenase
1	Niben101Scf01025g01013	-4.843286635	AT4G38970.1	fructose-bisphosphate aldolase 2 LENGTH=398
0	Niben101Scf01596g01023	_	AT3G17850.1	Protein kinase superfamily protein LENGTH=1296
0	Niben101Scf05697g00006	_	sp|P34885|KPC1B_CAEEL	Protein kinase C-like 1B

Table S2. *(Continued)*

0	Niben101Scf00539g05012	_	AT1G76040.2	calcium-dependent protein kinase 29 LENGTH=561
0	Niben101Scf01269g08008	_	AT1G50700.1	calcium-dependent protein kinase 33 LENGTH=521
0	Niben101Scf14322g00008	_	AT3G56760.1	Protein kinase superfamily protein LENGTH=577
0	Niben101Scf02031g00029	_	AT1G72710.1	casein kinase 1-like protein 2 LENGTH=465
0	Niben101Scf16152g00007	_	sp|Q556Y4|KC1_DICDI	Casein kinase I
0	Niben101Scf02217g05009	_	sp|P97377|CDK2_MOUSE	Cyclin-dependent kinase 2
0	Niben101Scf06698g01004	_	sp|P97377|CDK2_MOUSE	Cyclin-dependent kinase 2
1	Niben101Scf04123g01031	_	sp|Q9LIG2|RLK6_ARATH	Receptor-like protein kinase
0	Niben101Scf01025g10006	_	sp|Q9FN94|RLK7_ARATH	Receptor-like protein kinase
0	Niben101Scf01192g05016	_	sp|Q9FN94|RLK7_ARATH	Receptor-like protein kinase
0	Niben101Scf01374g03007	_	sp|Q9LIG2|RLK6_ARATH	Receptor-like protein kinase
0	Niben101Scf01415g01005	_	sp|Q9LIG2|RLK6_ARATH	Receptor-like protein kinase
0	Niben101Scf02015g01014	_	AT4G00330	Receptor-like protein kinase
0	Niben101Scf04144g00001	_	AT3G59110	Receptor-like protein kinase
0	Niben101Scf04343g00001	_	AT5G13160	Receptor-like protein kinase
0	Niben101Scf05202g00005	_	AT5G18610	Receptor-like protein kinase
0	Niben101Scf05916g00004	_	AT2G02800	Receptor-like protein kinase
0	Niben101Scf10970g00025	_	AT5G47070	Receptor-like protein kinase
0	Niben101Scf05713g04009	_	AT5G58950	Protein kinase superfamily protein LENGTH=525
3	Niben101Scf03777g00018	_	sp|Q39817|CALX_SOYBN	Calnexin homolog
3	Niben101Scf24868g00002	_	sp|Q9M352|RL362_ARATH	60S ribosomal protein L36-2
3	Niben101Scf27914g00006	_	AT4G24190.1	Chaperone protein htpG family protein LENGTH=823
2	Niben101Scf00837g11004	_	AT4G24190.1	Chaperone protein htpG family protein LENGTH=823
2	Niben101Scf01596g12004	_	sp|Q39817|CALX_SOYBN	Calnexin homolog
2	Niben101Scf04083g04040	_	sp|P27541|HSP70_BRUMA	Heat shock 70 kDa protein

Table S2. *(Continued)*

2	Niben101Scf06976g03021	_	sp|Q93ZE8|SDF2_ARATH	Stromal cell-derived factor 2-like protein
2	Niben101Scf13802g03003	_	sp|Q6FWD3|SC242_CANGA	Protein transport protein SEC24-2
2	Niben101Scf14717g00010	_	sp|P46300|RS4_SOLTU	40S ribosomal protein S4
1	Niben101Scf00254g05005	_	sp|Q9Z1Z0|USO1_MOUSE	General vesicular transport factor p115
1	Niben101Scf00430g01027	_	AT1G17350.2	NADH:ubiquinone oxidoreductase intermediate-associated protein 30
1	Niben101Scf00472g07004	_	sp|Q66I12|CCD47_DANRE	Coiled-coil domain-containing protein 47
1	Niben101Scf00507g00008	_	sp|Q5ZJL8|ABHDD_CHICK	Alpha/beta hydrolase domain-containing protein 13
1	Niben101Scf00544g00003	_	sp|Q2JUX7|RS12_SYNJA	30S ribosomal protein S12
1	Niben101Scf00747g01026	_	sp|Q9LTR9|NMT1_ARATH	Glycylpeptide N-tetradecanoyltransferase 1
1	Niben101Scf00870g15011	_	sp|Q9LTR9|NMT1_ARATH	Glycylpeptide N-tetradecanoyltransferase 1
1	Niben101Scf01175g03010	_	sp|O23144|PPI1_ARATH	Proton pump-interactor 1
1	Niben101Scf01795g20002	_	sp|Q3SRZ7|KGUA_NITWN	Guanylate kinase
1	Niben101Scf02007g06001	_	AT5G13110.1	glucose-6-phosphate dehydrogenase 2 LENGTH=596
1	Niben101Scf02192g01015	_	sp|Q9LK09|SYP32_ARATH	Syntaxin-32
1	Niben101Scf02243g01029	_	sp|Q93XX8|NOP10_ARATH	H/ACA ribonucleoprotein complex subunit 3-like protein
1	Niben101Scf02306g02017	_	sp|A6TB06|RSMF_KLEP7	Ribosomal RNA small subunit methyltransferase F
1	Niben101Scf02353g01008	_	AT1G17820.1	Putative integral membrane protein conserved region (DUF2404)
1	Niben101Scf02455g01011	_	sp|P31414|AVP1_ARATH	Pyrophosphate-energized vacuolar membrane proton pump 1
1	Niben101Scf02613g02021	_	AT3G27190.1	uridine kinase-like 2 LENGTH=483
1	Niben101Scf03107g00001	_	sp|Q9SA23|SYP51_ARATH	Syntaxin-51
1	Niben101Scf03115g02008	_	sp|P40918|HSP70_DAVTA	Heat shock 70 kDa protein
1	Niben101Scf03392g10005	_	AT3G59770.3	sacI homology domain-containing protein / WW domain-containing protein
1	Niben101Scf03867g02046	_	sp|Q5R6D1|CATB_PONAB	Cathepsin B
1	Niben101Scf04549g09017	_	sp|Q96SK2|TM209_HUMAN	Transmembrane protein 209

Table S2. *(Continued)*

1	Niben101Scf04562g03001	_	sp|P21616|AVP_VIGRR	Pyrophosphate-energized vacuolar membrane proton pump
1	Niben101Scf05364g00007	_	sp|O82703|VATG2_TOBAC	V-type proton ATPase subunit G 2
1	Niben101Scf06583g03009	_	sp|Q7PC88|AB31G_ARATH	ABC transporter G family member 31
1	Niben101Scf06814g01018	_	sp|P93654|SYP22_ARATH	Syntaxin-22
1	Niben101Scf07103g01009	_	sp|Q8DLG8|ATPB_THEEB	ATP synthase subunit beta
1	Niben101Scf11895g01001	_	sp|Q9FLP0|MA651_ARATH	65-kDa microtubule-associated protein 1
1	Niben101Scf13643g01008	_	gb|KEH17617.1|	structural constituent of cell wall protein, putative [*Medicago truncatula*]
1	Niben101Scf13764g00003	_	emb|CDY03722.1|	BnaA02g15150D [*Brassica napus*]
0	Niben101Ctg12940g00001	_	sp|Q6QNM1|KC1_TOXGO	Casein kinase I
0	Niben101Ctg14382g00002	_	sp|Q96299|14339_ARATH	14-3-3-like protein GF14 mu
0	Niben101Ctg14629g00001	_	sp|Q9XEX2|PRX2B_ARATH	Peroxiredoxin-2B
0	Niben101Ctg14686g00002	_	emb|CDY37195.1|	BnaC02g35030D [*Brassica napus*]
0	Niben101Ctg16374g00004	_	sp|Q94B77|FH5_ARATH	Formin-like protein 5
0	Niben101Scf00028g03009	_	sp|Q110B7|RL14_TRIEI	50S ribosomal protein L14
0	Niben101Scf00117g02019	_	sp|B2S0M0|DNAK_BORHD	Chaperone protein DnaK
0	Niben101Scf00270g15010	_	AT1G14780.1	MAC/Perforin domain-containing protein LENGTH=627
0	Niben101Scf00305g05031	_	sp|Q72MG4|IPYR_LEPIC	Inorganic pyrophosphatase
0	Niben101Scf00332g06011	_	sp|Q40401|CALR_NICPL	Calreticulin
0	Niben101Scf00570g03008	_	ref|XP_003589006.1|	Chloroplast unusual p [*Medicago truncatula*]
0	Niben101Scf00668g02007	_	sp|P0CR79|HSE1_CRYNB	Class E vacuolar protein-sorting machinery protein HSE1
0	Niben101Scf00683g02004	_	AT5G55530.1	Calcium-dependent lipid-binding (CaLB domain) family protein LENGTH=405
0	Niben101Scf00786g00015	_	AT3G27000.1	actin related protein 2 LENGTH=389
0	Niben101Scf00851g03005	_	AT1G03445.1	Serine/threonine protein phosphatase family protein LENGTH=793
0	Niben101Scf00861g02013	_	sp|Q11180|WHT1_CAEEL	ABC transporter ATP-binding protein/permease wht-1

Table S2. *(Continued)*

0	Niben101Scf00917g03010	_	gb|ACG26510.1|	FIP1 [Zea mays]
0	Niben101Scf00941g00013	_	sp|Q94AI6|SEC6_ARATH	Exocyst complex component SEC6
0	Niben101Scf01005g02012	_	AT5G64330.1	Phototropic-responsive NPH3 family protein LENGTH=746
0	Niben101Scf01078g00006	_	AT3G48200.1	unknown protein
0	Niben101Scf01346g01021	_	sp|Q96NW7|LRRC7_HUMAN	Leucine-rich repeat-containing protein 7
0	Niben101Scf01376g04032	_	sp|Q9SEE4|PIRL_SOLLC	Pirin-like protein
0	Niben101Scf01453g06003	_	sp|Q96520|PER12_ARATH	Peroxidase 12
0	Niben101Scf01453g09001	_	ref|XP_002869709.1|	zinc ion binding protein [*Arabidopsis* lyrata subsp. lyrata]
0	Niben101Scf01695g03013	_	AT3G16060.1	ATP binding microtubule motor family protein LENGTH=684
0	Niben101Scf01750g06009	_	AT1G03445.1	Serine/threonine protein phosphatase family protein LENGTH=793
0	Niben101Scf01764g03017	_	sp|P46824|KLC_DROME	Kinesin light chain
0	Niben101Scf01937g02005	_	sp|Q8YWD8|MSRA2_NOSS1	Peptide methionine sulfoxide reductase MsrA 2
0	Niben101Scf02042g00014	_	sp|O95208|EPN2_HUMAN	Epsin-2
0	Niben101Scf02114g00010	_	sp|P49420|DHAS_PROMA	Aspartate-semialdehyde dehydrogenase
0	Niben101Scf02168g04008	_	AT5G19760.1	Mitochondrial substrate carrier family protein LENGTH=298
0	Niben101Scf02307g02016	_	AT1G20760.1	Calcium-binding EF hand family protein LENGTH=1019
0	Niben101Scf02353g05007	_	sp|Q9XTT8|PP4C2_CAEEL	Serine/threonine-protein phosphatase 4 catalytic subunit 2
0	Niben101Scf02420g08013	_	sp|Q6L545|GID1_ORYSJ	Gibberellin receptor GID1
0	Niben101Scf02538g03016	_	sp|Q9C9N6|PMI2_ARATH	Protein PLASTID MOVEMENT IMPAIRED 2
0	Niben101Scf02680g01006	_	sp|Q94KB7|MLO6_ARATH	MLO-like protein 6
0	Niben101Scf02896g00004	_	sp|Q2LVL0|MSBA_SYNAS	Lipid A export ATP-binding/permease protein MsbA
0	Niben101Scf02913g00013	_	AT5G08570.1	Pyruvate kinase family protein LENGTH=510
0	Niben101Scf03069g01002	_	AT1G12310.1	Calcium-binding EF-hand family protein LENGTH=148
0	Niben101Scf03103g00015	_	AT5G19760.1	Mitochondrial substrate carrier family protein LENGTH=298
0	Niben101Scf03326g01016	_	sp|Q0U4Z8|VPS27_PHANO	Vacuolar protein sorting-associated protein 27

Table S2. *(Continued)*

0	Niben101Scf03326g04013	_	emb|CDY16984.1|	BnaC09g41110D [*Brassica napus*]
0	Niben101Scf03377g05004	_	sp|O35250|EXOC7_MOUSE	Exocyst complex component 7
0	Niben101Scf03396g07029	_	AT5G19760.1	Mitochondrial substrate carrier family protein LENGTH=298
0	Niben101Scf03488g06006	_	sp|F4JUL9|ARPC4_ARATH	Actin-related protein 2/3 complex subunit 4
0	Niben101Scf03526g01002	_	sp|Q8NJ52|NTF2_DAVTA	Nuclear transport factor 2
0	Niben101Scf03577g00001	_	sp|P46629|RAB25_RABIT	Ras-related protein Rab-25
0	Niben101Scf03600g04008	_	AT5G40760.1	glucose-6-phosphate dehydrogenase 6 LENGTH=515
0	Niben101Scf03865g05006	_	sp|F4IME2|MSL8_ARATH	Mechanosensitive ion channel protein 8
0	Niben101Scf04099g03003	_	sp|P74227|EFTU_SYNY3	Elongation factor Tu
0	Niben101Scf04109g03009	_	sp|C8V212|BRO1_EMENI	Vacuolar protein-sorting protein bro1
0	Niben101Scf04284g00021	_	AT1G16860.1	Ubiquitin-specific protease family C19-related protein LENGTH=474
0	Niben101Scf04400g01006	_	ref|XP_007045932.1|	Nodulin-related protein 1, putative [Theobroma cacao]
0	Niben101Scf04431g01010	_	AT3G22190.1	IQ-domain 5 LENGTH=422
0	Niben101Scf04556g02009	_	sp|Q8TUS9|VATD_METKA	V-type ATP synthase subunit D
0	Niben101Scf04639g06007	_	sp|Q01520|EF1A_PODAS	Elongation factor 1-alpha
0	Niben101Scf04779g01029	_	AT4G12520.1	Bifunctional inhibitor/lipid-transfer protein/seed storage 2S albumin superfamily protein
0	Niben101Scf04782g01001	_	sp|O22193|PUB4_ARATH	U-box domain-containing protein 4
0	Niben101Scf05077g00012	_	sp|Q54UC9|KIF3_DICDI	Kinesin-related protein 3
0	Niben101Scf05226g08017	_	AT5G52430.1	hydroxyproline-rich glycoprotein family protein LENGTH=438
0	Niben101Scf05241g02004	_	AT1G16220.1	Protein phosphatase 2C family protein LENGTH=491
0	Niben101Scf05247g01011	_	sp|O95208|EPN2_HUMAN	Epsin-2
0	Niben101Scf05409g00003	_	sp|Q6Z844|COPZ2_ORYSJ	Coatomer subunit zeta-2
0	Niben101Scf05694g00009	_	sp|Q9ZSD4|SY121_ARATH	Syntaxin-121
0	Niben101Scf05711g04009	_	sp|Q8T135|KIF5_DICDI	Kinesin-related protein 5

Table S2. *(Continued)*

0	Niben101Scf05731g00008	_	sp|P0CW07|DNAJ_METMA	Chaperone protein DnaJ
0	Niben101Scf05764g05016	_	AT1G19730.1	Thioredoxin superfamily protein LENGTH=119
0	Niben101Scf05813g08004	_	sp|Q11SV1|GPMA_CYTH3	2,3-bisphosphoglycerate-dependent phosphoglycerate mutase
0	Niben101Scf05961g03007	_	sp|Q9SU08|AUXI1_ARATH	Auxilin-related protein 1
0	Niben101Scf06125g01005	_	sp|Q9Y169|EXT2_DROME	Exostosin-2
0	Niben101Scf07288g08019	_	sp|Q8L7A9|AP4E_ARATH	AP-4 complex subunit epsilon
0	Niben101Scf07493g04001	_	AT5G42830.1	HXXXD-type acyl-transferase family protein LENGTH=450
0	Niben101Scf07532g02009	_	AT1G12310.1	Calcium-binding EF-hand family protein LENGTH=148
0	Niben101Scf07532g02010	_	AT1G12310.1	Calcium-binding EF-hand family protein LENGTH=148
0	Niben101Scf07549g02022	_	sp|Q9C9X3|ANXD5_ARATH	Annexin D5
0	Niben101Scf07585g00047	_	sp|Q5XAD7|DNAJ_STRP6	Chaperone protein DnaJ
0	Niben101Scf07591g00002	_	AT1G48790.1	associated molecule with the SH3 domain of STAM 1 LENGTH=507
0	Niben101Scf07623g01035	_	sp|Q3J5H6|GLND_RHOS4	Bifunctional uridylyltransferase/uridylyl-removing enzyme
0	Niben101Scf07798g02004	_	AT1G72410.2	COP1-interacting protein-related LENGTH=1270
0	Niben101Scf08026g02006	_	sp|O23140|AP2M_ARATH	AP-2 complex subunit mu
0	Niben101Scf08160g02006	_	AT1G75170.1	Sec14p-like phosphatidylinositol transfer family protein LENGTH=296
0	Niben101Scf08263g01014	_	AT1G03445.1	Serine/threonine protein phosphatase family protein LENGTH=793
0	Niben101Scf08527g01006	_	sp|Q6ZKC0|14333_ORYSJ	14-3-3-like protein GF14-C
0	Niben101Scf09238g02007	_	sp|Q9BZV1|UBXN6_HUMAN	UBX domain-containing protein 6
0	Niben101Scf09392g00008	_	sp|Q62848|ARFG1_RAT	ADP-ribosylation factor GTPase-activating protein 1
0	Niben101Scf09725g00022	_	sp|Q3SNK1|METE_NITWN	5-methyltetrahydropteroyltriglutamate–homocysteine methyltransferase
0	Niben101Scf10007g00001	_	AT5G19473.1	RPM1-interacting protein 4 (RIN4) family protein LENGTH=99
0	Niben101Scf10205g00006	_	sp|Q9ZW24|GSTU7_ARATH	Glutathione S-transferase U7

Table S2. *(Continued)*

0	Niben101Scf10314g04006	_	sp|Q5E9G1|P2R3C_BOVIN	Serine/threonine-protein phosphatase 2A regulatory subunit B" subunit gamma
0	Niben101Scf10329g03026	_	AT5G08580.1	Calcium-binding EF hand family protein LENGTH=391
0	Niben101Scf10412g01012	_	sp|Q9NV70|EXOC1_HUMAN	Exocyst complex component 1
0	Niben101Scf10737g01013	_	sp|Q54B27|EXOC6_DICDI	Exocyst complex component 6
0	Niben101Scf11253g00004	_	sp|Q63347|PRS7_RAT	26S protease regulatory subunit 7
0	Niben101Scf11383g00021	_	sp|Q99W51|TADA_STAAM	tRNA-specific adenosine deaminase
0	Niben101Scf11496g01003	_	sp|A8X2R2|ZFPL1_CAEBR	Zinc finger protein-like 1 homolog
0	Niben101Scf12017g05002	_	AT4G16340.1	guanyl-nucleotide exchange factors;GTPase binding;GTP binding LENGTH=1830
0	Niben101Scf12653g01003	_	AT5G08570.1	Pyruvate kinase family protein LENGTH=510
0	Niben101Scf12754g00011	_	sp|Q94BT0|SPSA1_ARATH	Sucrose-phosphate synthase 1
0	Niben101Scf13150g04023	_	AT1G34760.1	general regulatory factor 11 LENGTH=255
0	Niben101Scf13203g01005	_	AT1G29690.1	MAC/Perforin domain-containing protein LENGTH=561
0	Niben101Scf13741g04011	_	gb|ACG40676.1|	p8MTCP1 [Zea mays]
0	Niben101Scf14269g00008	_	AT4G12770.1	Chaperone DnaJ-domain superfamily protein LENGTH=891
0	Niben101Scf14394g01038	_	sp|Q07866|KLC1_HUMAN	Kinesin light chain 1
0	Niben101Scf15541g00007	_	sp|O48724|WEB1_ARATH	Protein WEAK CHLOROPLAST MOVEMENT UNDER BLUE LIGHT 1
0	Niben101Scf15568g00037	_	sp|P93788|REMO_SOLTU	Remorin
0	Niben101Scf18589g00012	_	sp|Q9H9S4|CB39L_HUMAN	Calcium-binding protein 39-like
0	Niben101Scf18725g00006	_	sp|Q9S9T7|VP282_ARATH	Vacuolar protein sorting-associated protein 28 homolog 2
0	Niben101Scf19779g00010	_	AT4G32760.2	ENTH/VHS/GAT family protein LENGTH=676
0	Niben101Scf21125g00005	_	sp|Q54GX7|ACT10_DICDI	Actin-10
1	Niben101Scf06332g03011	_	sp|A2BMB2|RL2_HYPBU	50S ribosomal protein L2

Table S2. *(Continued)*

Significantly enriched in PL-MS experiments when using Cf-4-TbID as a bait				
# Cf-4-TbID	*N. benthamiana* ID	Avr4 vs GUS 16h	Blast Hit	Description
3	Niben101Scf04361g01001	1.732326676	sp|P37218|H1_SOLLC	Histone H1
3	Niben101Scf06590g03003	1.708541749	sp|Q71V09|H4_CAPAN	Histone H4
3	Niben101Scf01623g14008	1.526913273	sp|Q6GPW4|TM205_XENLA	Transmembrane protein 205
3	Niben101Scf06091g00010	1.525304647	AT2G25110.1	stromal cell-derived factor 2-like protein precursor
3	Niben101Scf00972g01011	1.42556233	sp|Q5R891|LNP_PONAB	Protein lunapark
3	Niben101Scf00704g04019	1.271974668	sp|Q5R891|LNP_PONAB	Protein lunapark
3	Niben101Scf03390g09001	1.177333871	sp|Q5HNW7|DNAJ_STAEQ	Chaperone protein DnaJ
3	Niben101Scf03349g00008	0.880999067	sp|Q6G1F8|DNAJ_BARQU	Chaperone protein DnaJ
3	Niben101Scf02537g02033	0.797503331	sp|P59169|H33_ARATH	Histone H3.3
3	Niben101Scf00308g01003	0.733707351	sp|Q9FFI5|NAC86_ARATH	NAC domain-containing protein 86
3	Niben101Scf00482g03005	0.689077351	sp|Q71V09|H4_CAPAN	Histone H4
3	Niben101Scf05579g00001	0.545220753	sp|Q71V09|H4_CAPAN	Histone H4
3	Niben101Scf00863g02001	0.242547774	sp|B0RDY9|IF2_CLAMS	Translation initiation factor IF-2
3	Niben101Scf16416g02012	0.212287501	sp|Q9U7D0|H4_MASBA	Histone H4
3	Niben101Scf07275g00004	0.009119348	sp|Q71V09|H4_CAPAN	Histone H4
3	Niben101Scf07945g01002	-0.361676294	sp|P84227|H32_BOVIN	Histone H3.2
3	Niben101Scf02441g01009	-0.491232028	sp|Q71V09|H4_CAPAN	Histone H4
3	Niben101Scf14636g02013	-0.603898142	sp|Q8ZW52|RL3_PYRAE	50S ribosomal protein L3
3	Niben101Scf01579g00002	-0.911096181	sp|Q71V09|H4_CAPAN	Histone H4
3	Niben101Scf06238g01004	-0.948841141	sp|Q71V09|H4_CAPAN	Histone H4
3	Niben101Scf07382g01007	-1.001008011	sp|Q06881|BCCP_NOSS1	Biotin carboxyl carrier protein of acetyl-CoA carboxylase
3	Niben101Scf23814g00038	-1.14172635	sp|P59259|H4_ARATH	Histone H4
3	Niben101Scf03088g01003	-1.290532379	sp|Q71V09|H4_CAPAN	Histone H4

Table S2. *(Continued)*

3	Niben101Scf10152g03006	-1.48166826	sp|Q06881|BCCP_NOSS1	Biotin carboxyl carrier protein of acetyl-CoA carboxylase
3	Niben101Scf07650g02006	-1.647169961	sp|Q71V09|H4_CAPAN	Histone H4
3	Niben101Scf10015g01010	-1.829614842	sp|P59259|H4_ARATH	Histone H4
3	Niben101Scf05373g02004	-1.982261343	sp|Q9U7D0|H4_MASBA	Histone H4
3	Niben101Ctg14707g00002	_	sp|P59259|H4_ARATH	Histone H4
3	Niben101Scf01154g17005	_	sp|Q71V09|H4_CAPAN	Histone H4
3	Niben101Scf04779g01020	_	sp|Q95LY5|TTC12_MACFA	Tetratricopeptide repeat protein 12
3	Niben101Scf09387g03018	_	sp|Q95LY5|TTC12_MACFA	Tetratricopeptide repeat protein 12
3	Niben101Scf10338g00011	_	sp|Q6GPW4|TM205_XENLA	Transmembrane protein 205
3	Niben101Scf12266g02002	_	sp|Q06881|BCCP_NOSS1	Biotin carboxyl carrier protein of acetyl-CoA carboxylase
2	Niben101Scf01704g00002	2.982205382	sp|Q73IV4|DNAJ_WOLPM	Chaperone protein DnaJ
2	Niben101Scf05506g02016	2.841893372	sp|P82888|H4_OLILU	Histone H4
2	Niben101Scf07035g07011	2.320838529	sp|Q08752|PPID_HUMAN	Peptidyl-prolyl cis-trans isomerase D
2	Niben101Scf01150g02009	2.231581053	sp|P84227|H32_BOVIN	Histone H3.2
2	Niben101Scf02315g01009	1.96929109	sp|P62191|PRS4_HUMAN	26S protease regulatory subunit 4
2	Niben101Scf07748g01001	1.926793251	sp|P37218|H1_SOLLC	Histone H1
2	Niben101Scf08515g00019	1.5207125	sp|Q9FMR5|VA714_ARATH	Vesicle-associated membrane protein 714
2	Niben101Scf07827g00014	1.235415762	emb|CDY14195.1|	BnaA08g13260D [*Brassica napus*]
2	Niben101Scf01687g01001	1.166689501	sp|Q7ZX41|GNL3_XENLA	Guanine nucleotide-binding protein-like 3
2	Niben101Scf02819g05019	1.151451464	sp|P49972|SR542_SOLLC	Signal recognition particle 54 kDa protein 2
2	Niben101Scf07152g04015	0.878572733	sp|Q9LQQ4|H2B1_ARATH	Histone H2B.1
2	Niben101Scf01035g05012	0.703391337	sp|Q9M2Z4|MSBP2_ARATH	Membrane steroid-binding protein 2
2	Niben101Scf05487g01009	0.601901552	sp|P37218|H1_SOLLC	Histone H1
2	Niben101Scf02909g02010	0.348610575	AT1G50920.1	Nucleolar GTP-binding protein LENGTH=671
2	Niben101Scf00270g05019	0.21235553	sp|Q54GN8|NSA2_DICDI	Ribosome biogenesis protein NSA2 homolog

Table S2. *(Continued)*

2	Niben101Scf03488g06007	0.13950263	sp|Q8VDI7|UBAC1_MOUSE	Ubiquitin-associated domain-containing protein 1
2	Niben101Scf01956g01003	0.137503424	sp|P62980|RS27A_SOLLC	Ubiquitin-40S ribosomal protein S27a
2	Niben101Scf01927g09005	0.099948928	sp|P49689|RS30_ARATH	40S ribosomal protein S30
2	Niben101Scf02699g01012	0.092318514	AT1G03350.1	BSD domain-containing protein LENGTH=470
2	Niben101Scf05845g03012	0.058519189	sp|P49689|RS30_ARATH	40S ribosomal protein S30
2	Niben101Scf20596g00004	0.002291755	sp|Q86YN1|DOPP1_HUMAN	Dolichyldiphosphatase 1
2	Niben101Scf00558g00006	0	sp|A4QJT5|RR4_OLIPU	30S ribosomal protein S4, chloroplastic
2	Niben101Scf11178g01003	0	sp|P31562|ACCD_CUSRE	Acetyl-coenzyme A carboxylase carboxyl transferase subunit beta
2	Niben101Scf00181g00004	-0.017953591	sp|B0RDY9|IF2_CLAMS	Translation initiation factor IF-2
2	Niben101Scf06819g02006	-0.044545114	sp|Q8LC83|RS242_ARATH	40S ribosomal protein S24-2
2	Niben101Scf03488g09019	-0.121559556	sp|Q8TT43|RL13_METAC	50S ribosomal protein L13
2	Niben101Scf00078g02001	-0.145135369	sp|P49210|RL9_ORYSJ	60S ribosomal protein L9
2	Niben101Scf01374g03036	-0.162534149	sp|Q8LEM8|RL373_ARATH	60S ribosomal protein L37-3
2	Niben101Scf07393g00003	-0.217248036	sp|O65743|RL24_CICAR	60S ribosomal protein L24
2	Niben101Scf08633g01003	-0.229904522	sp|O59299|RS9_PYRHO	30S ribosomal protein S9
2	Niben101Scf03202g13010	-0.238682909	sp|P93028|UBE11_ARATH	Ubiquitin-activating enzyme E1 1
2	Niben101Scf12159g00012	-0.262947051	sp|Q8LC83|RS242_ARATH	40S ribosomal protein S24-2
2	Niben101Scf08774g00012	-0.263635263	sp|Q7U4J2|RL29_SYNPX	50S ribosomal protein L29
2	Niben101Scf02756g00005	-0.27401353	sp|Q08069|RS8_MAIZE	40S ribosomal protein S8
2	Niben101Scf11325g00032	-0.274679128	sp|P51414|RL261_ARATH	60S ribosomal protein L26-1
2	Niben101Scf02227g00003	-0.277845656	sp|Q9SF40|RL4A_ARATH	60S ribosomal protein L4-1
2	Niben101Scf00496g01001	-0.309497833	sp|Q9XF97|RL4_PRUAR	60S ribosomal protein L4
2	Niben101Scf00409g00002	-0.327158398	sp|Q72W01|AROC_LEPIC	Chorismate synthase
2	Niben101Scf00130g01022	-0.368681581	sp|Q5U241|PD5BB_XENLA	Sister chromatid cohesion protein PDS5 homolog B-B
2	Niben101Scf03534g01011	-0.370744004	sp|O59299|RS9_PYRHO	30S ribosomal protein S9

Table S2. *(Continued)*

2	Niben101Scf00961g02009	-0.393116132	sp|P52478|UBC1_CAEEL	Ubiquitin-conjugating enzyme E2 1
2	Niben101Scf02752g07003	-0.412187498	sp|O65743|RL24_CICAR	60S ribosomal protein L24
2	Niben101Scf05018g00001	-0.4718516	sp|P41129|RL132_BRANA	60S ribosomal protein L13-2
2	Niben101Scf00408g09007	-0.475566776	sp|P49692|RL7A1_ARATH	60S ribosomal protein L7a-1
2	Niben101Scf07323g02009	-0.503961872	sp|Q54GN8|NSA2_DICDI	Ribosome biogenesis protein NSA2 homolog
2	Niben101Scf05997g00002	-0.529202093	sp|Q9SIM4|RL141_ARATH	60S ribosomal protein L14-1
2	Niben101Scf00864g00004	-0.539127567	sp|Q22053|FBRL_CAEEL	rRNA 2′-O-methyltransferase fibrillarin
2	Niben101Scf02852g00013	-0.544294778	AT2G04030.1	Chaperone protein htpG family protein LENGTH=780
2	Niben101Scf02639g03012	-0.552819222	sp|Q97EI6|RL29_CLOAB	50S ribosomal protein L29
2	Niben101Scf00542g07012	-0.558039056	sp|O42993|FKBP_SCHPO	Peptidyl-prolyl cis-trans isomerase
2	Niben101Scf01689g06005	-0.571975573	sp|P49689|RS30_ARATH	40S ribosomal protein S30
2	Niben101Scf04727g04007	-0.581172091	sp|B7ZAQ6|GPHRA_HUMAN	Golgi pH regulator A
2	Niben101Scf03779g07007	-0.590295821	sp|Q9C912|R35A3_ARATH	60S ribosomal protein L35a-3
2	Niben101Scf08833g01006	-0.592120838	sp|P84227|H32_BOVIN	Histone H3.2
2	Niben101Scf03273g02008	-0.598645025	sp|P49692|RL7A1_ARATH	60S ribosomal protein L7a-1
2	Niben101Scf00168g08008	-0.620832071	sp|P14030|RL6_METVA	50S ribosomal protein L6
2	Niben101Scf05017g04011	-0.63841943	sp|Q9C912|R35A3_ARATH	60S ribosomal protein L35a-3
2	Niben101Scf02912g00004	-0.640093581	sp|Q08069|RS8_MAIZE	40S ribosomal protein S8
2	Niben101Scf06447g00005	-0.643022502	sp|Q8LC83|RS242_ARATH	40S ribosomal protein S24-2
2	Niben101Scf07320g00021	-0.644436565	sp|Q9C912|R35A3_ARATH	60S ribosomal protein L35a-3
2	Niben101Scf00343g05008	-0.674981226	AT1G22610.1	C2 calcium/lipid-binding plant phosphoribosyltransferase
2	Niben101Scf03412g05009	-0.680847403	sp|P81898|PNAA_PRUDU	Peptide-N4-(N-acetyl-beta-glucosaminyl)asparagine amidase A
2	Niben101Scf03734g04015	-0.733341669	sp|O65743|RL24_CICAR	60S ribosomal protein L24
2	Niben101Scf09564g00010	-0.736666553	sp|O65743|RL24_CICAR	60S ribosomal protein L24
2	Niben101Scf06954g03017	-0.753075375	sp|A1RSE1|RL13_PYRIL	50S ribosomal protein L13

Table S2. *(Continued)*

2	Niben101Scf06876g01025	-0.757231322	sp|Q8LC83|RS242_ARATH	40S ribosomal protein S24-2
2	Niben101Scf00853g07006	-0.791913989	sp|Q30Z53|RL24_DESAG	50S ribosomal protein L24
2	Niben101Scf00527g05007	-0.799021385	sp|Q9P0L0|VAPA_HUMAN	Vesicle-associated membrane protein-associated protein A
2	Niben101Scf02502g15014	-0.838535634	sp|O65743|RL24_CICAR	60S ribosomal protein L24
2	Niben101Scf03321g04018	-0.86150037	sp|Q2NFX3|RL6_METST	50S ribosomal protein L6
2	Niben101Scf05588g05006	-0.864143346	sp|Q089P5|RS17_SHEFN	30S ribosomal protein S17
2	Niben101Scf03156g00009	-0.87936854	sp|P46300|RS4_SOLTU	40S ribosomal protein S4
2	Niben101Scf11802g02006	-0.882756345	sp|Q089P5|RS17_SHEFN	30S ribosomal protein S17
2	Niben101Scf07311g01004	-0.890847869	sp|Q9C912|R35A3_ARATH	60S ribosomal protein L35a-3
2	Niben101Scf09116g03007	-0.901203765	sp|Q9SIM4|RL141_ARATH	60S ribosomal protein L14-1
2	Niben101Scf02280g01015	-0.902413973	sp|Q9C912|R35A3_ARATH	60S ribosomal protein L35a-3
2	Niben101Scf02249g02011	-0.90753366	sp|P41127|RL131_ARATH	60S ribosomal protein L13-1
2	Niben101Scf02073g00008	-0.91681659	sp|Q9LZH9|RL7A2_ARATH	60S ribosomal protein L7a-2
2	Niben101Scf20261g00003	-0.938329547	sp|P49692|RL7A1_ARATH	60S ribosomal protein L7a-1
2	Niben101Scf08447g02008	-0.957705394	sp|Q08069|RS8_MAIZE	40S ribosomal protein S8
2	Niben101Scf02216g02012	-0.959335521	sp|P84227|H32_BOVIN	Histone H3.2
2	Niben101Scf09432g00008	-0.973214343	sp|Q9C912|R35A3_ARATH	60S ribosomal protein L35a-3
2	Niben101Scf03468g03025	-0.974900081	sp|Q0WL80|UGGG_ARATH	UDP-glucose:glycoprotein glucosyltransferase
2	Niben101Scf02240g02009	-0.975608876	sp|P41129|RL132_BRANA	60S ribosomal protein L13-2
2	Niben101Scf01148g02008	-0.976768297	sp|Q6UNT2|RL5_CUCSA	60S ribosomal protein L5
2	Niben101Scf00646g04009	-1.006472364	sp|O59418|RL3_PYRHO	50S ribosomal protein L3
2	Niben101Scf07428g01005	-1.062930603	sp|P49199|RS8_ORYSJ	40S ribosomal protein S8
2	Niben101Scf09242g00008	-1.12423077	sp|P41127|RL131_ARATH	60S ribosomal protein L13-1
2	Niben101Scf03000g01002	-1.147121555	AT2G04030.1	Chaperone protein htpG family protein LENGTH=780
2	Niben101Scf05391g02005	-1.166390437	sp|P68429|H32_MEDSA	Histone H3.2

Table S2. *(Continued)*

2	Niben101Scf08523g00026	-1.237692377	sp|Q9ATF5|RL18A_CASSA	60S ribosomal protein L18a
2	Niben101Scf02459g03003	-1.336283465	sp|Q9LZH9|RL7A2_ARATH	60S ribosomal protein L7a-2
2	Niben101Scf05665g00012	-1.385955953	AT3G10560.1	Cytochrome P450 superfamily protein LENGTH=514
2	Niben101Scf05892g00006	-1.406115022	sp|P84227|H32_BOVIN	Histone H3.2
2	Niben101Scf05676g06017	-1.431565998	sp|Q97EI6|RL29_CLOAB	50S ribosomal protein L29
2	Niben101Scf04436g03001	-1.478564453	sp|P49199|RS8_ORYSJ	40S ribosomal protein S8
2	Niben101Scf04665g02018	-1.490119054	AT3G57880.1	CaLB domain plant phosphoribosyltransferase family protein
2	Niben101Scf01718g07005	-1.526705848	AT1G20330.1	sterol methyltransferase 2 LENGTH=361
2	Niben101Scf02902g00007	-1.564950775	sp|P84227|H32_BOVIN	Histone H3.2
2	Niben101Scf06869g02006	-1.603219418	sp|P68432|H31_BOVIN	Histone H3.1
2	Niben101Scf00960g15006	-1.621263699	AT1G36160.1	acetyl-CoA carboxylase 1 LENGTH=2254
2	Niben101Scf00653g01010	-1.783736593	sp|Q06881|BCCP_NOSS1	Biotin carboxyl carrier protein of acetyl-CoA carboxylase
2	Niben101Scf02318g02002	-1.796897369	sp|B7JWV1|RS20_CYAP8	30S ribosomal protein S20
2	Niben101Scf09742g00031	-1.899298192	sp|B1XIR0|RL35_SYNP2	50S ribosomal protein L35
2	Niben101Scf17973g00015	-2.029211503	sp|Q8DJN4|RS20_THEEB	30S ribosomal protein S20
2	Niben101Scf01994g02012	-2.056103554	sp|Q9XF97|RL4_PRUAR	60S ribosomal protein L4
2	Niben101Scf06128g00002	-2.070376248	sp|P11891|PSRP5_PEA	50S ribosomal protein 5, chloroplastic
2	Niben101Scf03154g03001	-2.144195213	sp|B1L938|RL1_THESQ	50S ribosomal protein L1
2	Niben101Scf03736g00002	-2.289977438	sp|Q2LR20|RL35_SYNAS	50S ribosomal protein L35
2	Niben101Scf03253g02006	-2.365169194	sp|B1L938|RL1_THESQ	50S ribosomal protein L1
2	Niben101Scf12789g00006	-2.386745736	sp|Q9LV60|CRR55_ARATH	Cysteine-rich repeat secretory protein 55
2	Niben101Scf01436g03010	-2.447373129	sp|Q5Z1Q5|RS5_NOCFA	30S ribosomal protein S5
2	Niben101Scf01440g02013	-2.680186302	sp|Q9X248|FABG_THEMA	3-oxoacyl-[acyl-carrier-protein] reductase FabG
2	Niben101Scf15760g00012	-2.945144413	sp|Q9SCU0|SDR2A_ARATH	Short-chain dehydrogenase reductase 2a
2	Niben101Scf02982g03003	-3.011424021	AT4G13840.1	HXXXD-type acyl-transferase family protein LENGTH=428

Table S2. *(Continued)*

2	Niben101Scf17834g00014	-3.591686729	sp|A0PMB8|RL17_MYCUA	50S ribosomal protein L17
2	Niben101Scf10780g00002	-3.88728238	sp|Q9XF43|KCS6_ARATH	3-ketoacyl-CoA synthase 6
2	Niben101Scf00111g01016	_	sp|O65743|RL24_CICAR	60S ribosomal protein L24
2	Niben101Scf00294g03034	_	sp|Q9XF97|RL4_PRUAR	60S ribosomal protein L4
2	Niben101Scf00528g01012	_	sp|P59226|H32_ARATH	Histone H3.2
2	Niben101Scf00679g02011	_	ref|NP_001054228.1|	product [Oryza sativa Japonica Group]
2	Niben101Scf00687g03008	_	sp|P62980|RS27A_SOLLC	Ubiquitin-40S ribosomal protein S27a
2	Niben101Scf01094g01011	_	sp|P08903|H32_ENCAL	Histone H3.2
2	Niben101Scf01150g02010	_	sp|P84227|H32_BOVIN	Histone H3.2
2	Niben101Scf01502g00018	_	AT1G50920.1	Nucleolar GTP-binding protein LENGTH=671
2	Niben101Scf01773g03023	_	sp|P62980|RS27A_SOLLC	Ubiquitin-40S ribosomal protein S27a
2	Niben101Scf01851g03014	_	sp|O65743|RL24_CICAR	60S ribosomal protein L24
2	Niben101Scf02122g02021	_	sp|Q0WL80|UGGG_ARATH	UDP-glucose:glycoprotein glucosyltransferase
2	Niben101Scf02282g00001	_	sp|P51414|RL261_ARATH	60S ribosomal protein L26-1
2	Niben101Scf02296g00019	_	sp|Q54GN8|NSA2_DICDI	Ribosome biogenesis protein NSA2 homolog
2	Niben101Scf02802g00009	_	sp|A3DNA4|RL3_STAMF	50S ribosomal protein L3
2	Niben101Scf02915g08013	_	sp|P59277|SYP81_ARATH	Syntaxin-81
2	Niben101Scf03113g02002	_	sp|Q9HPB8|RL6_HALSA	50S ribosomal protein L6
2	Niben101Scf03114g09011	_	sp|Q80WS3|FBLL1_MOUSE	rRNA/tRNA 2'-O-methyltransferase fibrillarin-like protein 1
2	Niben101Scf03350g06021	_	AT1G22610.1	C2 calcium/lipid-binding plant phosphoribosyltransferase protein
2	Niben101Scf04395g00022	_	sp|P84227|H32_BOVIN	Histone H3.2
2	Niben101Scf04664g03006	_	sp|P17093|RS11_SOYBN	40S ribosomal protein S11
2	Niben101Scf05767g04004	_	sp|Q9FKC0|R13A4_ARATH	60S ribosomal protein L13a-4
2	Niben101Scf05800g02020	_	sp|Q5U241|PD5BB_XENLA	Sister chromatid cohesion protein PDS5 homolog B-B
2	Niben101Scf06094g07001	_	ref|NP_001054228.1|	product [Oryza sativa Japonica Group]

Table S2. *(Continued)*

2	Niben101Scf07498g02004	_	sp|Q5ZJI9|UBAC1_CHICK	Ubiquitin-associated domain-containing protein 1
2	Niben101Scf09523g01007	_	sp|P84227|H32_BOVIN	Histone H3.2
2	Niben101Scf10676g01010	_	sp|Q08069|RS8_MAIZE	40S ribosomal protein S8
2	Niben101Scf11306g00009	_	sp|P93028|UBE11_ARATH	Ubiquitin-activating enzyme E1 1
2	Niben101Scf11383g00015	_	sp|Q8LC83|RS242_ARATH	40S ribosomal protein S24-2
2	Niben101Scf22792g00002	_	sp|Q8DMM5|RL16_THEEB	50S ribosomal protein L16
2	Niben101Scf23355g00004	_	sp|Q8XSF6|MNTH_RALSO	Divalent metal cation transporter MntH
2	Niben101Scf32453g00001	_	sp|P41129|RL132_BRANA	60S ribosomal protein L13-2
1	Niben101Scf07586g00004	4.352465503	sp|Q9M7R0|ALL8_OLEEU	Calcium-binding allergen Ole e 8
1	Niben101Scf08926g01025	3.627203496	sp|Q9FIH9|CML37_ARATH	Calcium-binding protein CML37
1	Niben101Scf02296g00016	3.26952452	AT5G40760.1	glucose-6-phosphate dehydrogenase 6 LENGTH=515
1	Niben101Scf00213g01002	2.970796608	AT5G60900.1	receptor-like protein kinase 1 LENGTH=748
1	Niben101Scf15153g02001	2.695333599	sp|A4YL90|PCKA_BRASO	Phosphoenolpyruvate carboxykinase [ATP]
1	Niben101Scf03953g01007	2.635918748	sp|P84976|GRP2_POPEU	Glycine-rich RNA-binding protein 2 (Fragments)
1	Niben101Scf03374g05008	2.517250833	sp|Q54Y27|FKBP6_DICDI	FK506-binding protein 6
1	Niben101Scf02063g05005	2.295331696	AT5G43400.1	Uncharacterised conserved protein UCP015417, vWA LENGTH=655
1	Niben101Scf04377g01001	2.266680054	sp|Q9C7S7|ERO1_ARATH	Endoplasmic reticulum oxidoreductin-1
1	Niben101Scf02581g03002	2.188811896	sp|Q9BXT4|TDRD1_HUMAN	Tudor domain-containing protein 1
1	Niben101Scf00370g04028	2.029924721	AT5G27490.1	Integral membrane Yip1 family protein LENGTH=282
1	Niben101Scf07402g00014	2.029429832	sp|Q9BTZ2|DHRS4_HUMAN	Dehydrogenase/reductase SDR family member 4
1	Niben101Scf05588g04010	1.98389353	sp|P0C1I1|PPID_RHIO9	Peptidyl-prolyl cis-trans isomerase D
1	Niben101Scf02807g11016	1.902690974	emb|CDY48281.1|	BnaA05g10730D [*Brassica napus*]
1	Niben101Scf04225g02006	1.833237324	sp|Q9C7S7|ERO1_ARATH	Endoplasmic reticulum oxidoreductin-1
1	Niben101Scf01402g02022	1.789567519	sp|O64740|SC13B_ARATH	Protein transport protein SEC13 homolog B
1	Niben101Scf06397g00015	1.692239293	sp|Q86YN1|DOPP1_HUMAN	Dolichyldiphosphatase 1

Table S2. *(Continued)*

1	Niben101Scf03341g01002	1.69104054	emb|CDX93551.1|	BnaA06g04970D [*Brassica napus*]
1	Niben101Scf23954g00005	1.61343676	AT3G53710.1	ARF-GAP domain 6 LENGTH=459
1	Niben101Scf22781g00001	1.586285655	AT1G13220.2	nuclear matrix constituent protein-related LENGTH=1128
1	Niben101Scf02164g05014	1.554988042	sp|Q9SIM4|RL141_ARATH	60S ribosomal protein L14-1
1	Niben101Scf03099g01010	1.431151286	sp|A0PZN1|SYT_CLONN	Threonine--tRNA ligase
1	Niben101Scf00332g04004	1.369844067	sp|P21195|PDIA1_RABIT	Protein disulfide-isomerase
1	Niben101Scf02816g07016	1.362673124	gb|AIU51078.1|	AT4G29520-like protein, partial [Solanum tuberosum]
1	Niben101Scf03202g05005	1.356459464	sp|P0CW07|DNAJ_METMA	Chaperone protein DnaJ
1	Niben101Scf02290g07003	1.34972548	sp|O35685|NUDC_MOUSE	Nuclear migration protein nudC
1	Niben101Scf06280g02016	1.345509769	sp|O64740|SC13B_ARATH	Protein transport protein SEC13 homolog B
1	Niben101Scf03337g03016	1.287310913	sp|A2VDZ9|VAPB_BOVIN	Vesicle-associated membrane protein-associated protein B
1	Niben101Scf01933g07001	1.271983289	AT5G65910.1	BSD domain-containing protein LENGTH=432
1	Niben101Scf00262g03003	1.262965574	sp|P93847|RL10_SOLME	60S ribosomal protein L10
1	Niben101Scf05279g01002	1.231899402	sp|P84977|GRP3_POPEU	Glycine-rich RNA-binding protein 3 (Fragments)
1	Niben101Scf02658g01005	1.209906001	sp|Q41188|CSP2_ARATH	Cold shock protein 2
1	Niben101Scf09156g00023	1.204500218	sp|Q9Y259|CHKB_HUMAN	Choline/ethanolamine kinase
1	Niben101Scf02062g03003	1.183102209	sp|O76094|SRP72_HUMAN	Signal recognition particle subunit SRP72
1	Niben101Scf04871g23001	1.159485805	sp|Q93VI3|RL171_ARATH	60S ribosomal protein L17-1
1	Niben101Scf00536g01002	1.142714442	sp|A5UL75|RL5_METS3	50S ribosomal protein L5
1	Niben101Scf20077g00030	1.092753961	sp|Q9Y259|CHKB_HUMAN	Choline/ethanolamine kinase
1	Niben101Scf12711g01009	1.090645414	sp|O81644|VILI2_ARATH	Villin-2
1	Niben101Scf00369g18020	1.044026291	sp|Q9H6B9|EPHX3_HUMAN	Epoxide hydrolase 3
1	Niben101Scf07763g01012	0.985972611	sp|Q94AU2|SEC22_ARATH	25.3 kDa vesicle transport protein
1	Niben101Scf00149g12016	0.967061803	sp|Q2YT48|DNAJ_STAAB	Chaperone protein DnaJ
1	Niben101Scf04847g03018	0.96653482	sp|Q1CZI7|HTPG_MYXXD	Chaperone protein HtpG

Table S2. *(Continued)*

1	Niben101Scf05929g06002	0.965548707	AT3G24315.1	Sec20 family protein LENGTH=293
1	Niben101Scf08566g07003	0.949222189	sp|Q803I2|ERGI3_DANRE	Endoplasmic reticulum-Golgi intermediate compartment protein 3
1	Niben101Scf00612g02001	0.943697845	gb|AAO72706.1|	heavy meromyosin-like protein [Oryza sativa Japonica Group]
1	Niben101Scf14022g00011	0.938798667	AT2G26710.1	Cytochrome P450 superfamily protein LENGTH=520
1	Niben101Scf08334g03001	0.87163899	sp|Q93Y22|COPD_ARATH	Coatomer subunit delta
1	Niben101Scf00486g03003	0.834227335	sp|Q4PE39|SEC23_USTMA	Protein transport protein SEC23
1	Niben101Scf05804g04012	0.800019735	sp|Q5XIA4|CNO10_RAT	CCR4-NOT transcription complex subunit 10
1	Niben101Scf11291g00012	0.781588942	sp|Q00004|SRP68_CANFA	Signal recognition particle subunit SRP68
1	Niben101Scf04436g06002	0.736043183	sp|P93847|RL10_SOLME	60S ribosomal protein L10
1	Niben101Scf03015g06008	0.724339946	sp|Q05462|RL27_PEA	60S ribosomal protein L27
1	Niben101Scf16178g00008	0.67753872	sp|A6ZXP4|SUB2_YEAS7	ATP-dependent RNA helicase SUB2
1	Niben101Scf20652g01025	0.620372285	AT1G62020.1	Coatomer, alpha subunit LENGTH=1216
1	Niben101Scf00127g01005	0.612484854	AT1G52360.2	Coatomer, beta' subunit LENGTH=970
1	Niben101Scf06734g02019	0.608191921	sp|A7FY87|SYT_CLOB1	Threonine--tRNA ligase
1	Niben101Scf04490g00001	0.584850922	sp|P34931|HS71L_HUMAN	Heat shock 70 kDa protein 1-like
1	Niben101Scf03036g05003	0.584408837	sp|Q92575|UBXN4_HUMAN	UBX domain-containing protein 4
1	Niben101Scf09363g00016	0.580665679	sp|O64740|SC13B_ARATH	Protein transport protein SEC13 homolog B
1	Niben101Scf01221g05018	0.577711089	AT3G24315.1	Sec20 family protein LENGTH=293
1	Niben101Scf06825g04006	0.57601055	sp|Q5SMI4|RL393_ORYSJ	60S ribosomal protein L39-3
1	Niben101Scf03572g04014	0.574443101	ref|XP_002527953.1|	nucleotide binding protein, putative [*Ricinus communis*]
1	Niben101Scf01233g00001	0.556625042	sp|Q2JL77|RL36_SYNJB	50S ribosomal protein L36
1	Niben101Scf03964g04005	0.554051967	sp|Q91Z38|TTC1_MOUSE	Tetratricopeptide repeat protein 1
1	Niben101Scf03456g00002	0.552684831	sp|P42696|RBM34_HUMAN	RNA-binding protein 34
1	Niben101Scf01523g00023	0.538405841	sp|Q6GQ69|FAF2B_XENLA	FAS-associated factor 2-B
1	Niben101Scf01911g15015	0.509810116	sp|P48601|PRS4_DROME	26S protease regulatory subunit 4

Table S2. *(Continued)*

1	Niben101Scf07183g00016	0.466567255	sp|A6R603|SUB2_AJECN	ATP-dependent RNA helicase SUB2
1	Niben101Scf03197g06003	0.462045456	sp|P35469|CH601_RHIME	60 kDa chaperonin 1
1	Niben101Scf00197g02006	0.444322537	AT1G62020.1	Coatomer, alpha subunit LENGTH=1216
1	Niben101Scf06091g06020	0.403293899	sp|P49972|SR542_SOLLC	Signal recognition particle 54 kDa protein 2
1	Niben101Scf06228g00010	0.391939249	AT1G62020.1	Coatomer, alpha subunit LENGTH=1216
1	Niben101Scf04175g00017	0.389977021	sp|Q54YW1|ELMOA_DICDI	ELMO domain-containing protein A
1	Niben101Scf01214g02004	0.341745197	sp|Q6GQ69|FAF2B_XENLA	FAS-associated factor 2-B
1	Niben101Scf02690g01006	0.340085043	sp|O81644|VILI2_ARATH	Villin-2
1	Niben101Scf06856g00007	0.330128134	sp|P55034|PSMD4_ARATH	26S proteasome non-ATPase regulatory subunit 4 homolog
1	Niben101Scf00388g08017	0.325919057	AT1G13220.2	nuclear matrix constituent protein-related LENGTH=1128
1	Niben101Scf00603g08024	0.319716475	sp|P62302|RS13_SOYBN	40S ribosomal protein S13
1	Niben101Scf00920g01006	0.317346506	sp|Q8CI11|GNL3_MOUSE	Guanine nucleotide-binding protein-like 3
1	Niben101Scf10747g00012	0.305219038	sp|Q7U4J2|RL29_SYNPX	50S ribosomal protein L29
1	Niben101Scf13231g02006	0.30253198	sp|A5UL75|RL5_METS3	50S ribosomal protein L5
1	Niben101Scf05298g06002	0.298703755	sp|P42791|RL182_ARATH	60S ribosomal protein L18-2
1	Niben101Scf10388g00004	0.295162951	sp|Q7X923|SPT16_ORYSJ	FACT complex subunit SPT16
1	Niben101Scf08892g00008	0.293262063	AT1G74040.1	2-isopropylmalate synthase 1 LENGTH=631
1	Niben101Scf07695g00001	0.2869543	sp|Q54M20|TTC4_DICDI	Tetratricopeptide repeat protein 4 homolog
1	Niben101Scf00318g11015	0.27461094	ref|XP_007026671.1|	Transducin family protein / WD-40 repeat family protein
1	Niben101Scf07201g01007	0.273094378	AT5G63310.1	nucleoside diphosphate kinase 2 LENGTH=231
1	Niben101Scf04659g00004	0.269461067	sp|P84977|GRP3_POPEU	Glycine-rich RNA-binding protein 3 (Fragments)
1	Niben101Scf04907g01014	0.257141229	sp|Q04W40|AROC_LEPBJ	Chorismate synthase
1	Niben101Scf02381g08015	0.245499457	sp|A4FWA8|RL5_METM5	50S ribosomal protein L5
1	Niben101Scf05233g00010	0.220223151	AT2G32910.1	DCD (Development and Cell Death) domain protein LENGTH=691
1	Niben101Scf05378g01017	0.193851856	sp|O82491|SPT16_ARATH	FACT complex subunit SPT16

Table S2. *(Continued)*

1	Niben101Scf04327g02018	0.193664618	sp|Q41188|CSP2_ARATH	Cold shock protein 2
1	Niben101Scf09153g05036	0.163879501	sp|Q9LN01|PPR21_ARATH	Pentatricopeptide repeat-containing protein
1	Niben101Scf02949g03001	0.149490095	sp|Q5R5C8|TCPH_PONAB	T-complex protein 1 subunit eta
1	Niben101Scf00626g01002	0.138192586	sp|Q9M352|RL362_ARATH	60S ribosomal protein L36-2
1	Niben101Scf00078g02005	0.126790107	sp|P41101|RL27_SOLTU	60S ribosomal protein L27
1	Niben101Scf04732g01002	0.122480993	sp|Q9SMU7|SRP09_ARATH	Signal recognition particle 9 kDa protein
1	Niben101Scf02614g00010	0.109296764	sp|P93847|RL10_SOLME	60S ribosomal protein L10
1	Niben101Scf02098g02013	0.102580906	sp|Q6UNT2|RL5_CUCSA	60S ribosomal protein L5
1	Niben101Scf02902g01014	0.067643073	sp|A0AUR5|F188A_DANRE	Protein FAM188A
1	Niben101Scf06677g01002	0.05550016	sp|P41127|RL131_ARATH	60S ribosomal protein L13-1
1	Niben101Scf00412g01010	0.052846426	sp|Q6P011|EMC4_DANRE	ER membrane protein complex subunit 4
1	Niben101Scf19230g01011	0.016061541	sp|Q8PV45|RL22_METMA	50S ribosomal protein L22
1	Niben101Scf08470g00002	0.009865913	AT1G04220.1	3-ketoacyl-CoA synthase 2 LENGTH=528
1	Niben101Scf03209g00029	0.00322283	sp|P34091|RL6_MESCR	60S ribosomal protein L6
1	Niben101Scf00929g00007	0	AT4G13850.1	glycine-rich RNA-binding protein 2 LENGTH=158
1	Niben101Scf02606g00007	0	sp|Q54XP6|IF2P_DICDI	Eukaryotic translation initiation factor 5B
1	Niben101Scf03076g00018	0	sp|P46301|RS25_SOLLC	40S ribosomal protein S25
1	Niben101Scf09577g00007	0	sp|Q3ZCC9|SEC13_BOVIN	Protein SEC13 homolog
1	Niben101Scf00414g06008	-0.00167568	sp|Q1CZI7|HTPG_MYXXD	Chaperone protein HtpG
1	Niben101Scf04895g00007	-0.003342439	sp|Q1W375|PMM_TOBAC	Phosphomannomutase
1	Niben101Scf06332g00010	-0.005498432	sp|Q8X132|H2A_NEUCR	Histone H2A
1	Niben101Scf02972g07001	-0.007408962	sp|Q6GQ69|FAF2B_XENLA	FAS-associated factor 2-B
1	Niben101Scf08724g04008	-0.008594718	sp|P41098|RL34_TOBAC	60S ribosomal protein L34
1	Niben101Scf03541g00012	-0.018082373	sp|A8A8W3|RS4_IGNH4	30S ribosomal protein S4
1	Niben101Scf03264g03001	-0.033038926	sp|Q08752|PPID_HUMAN	Peptidyl-prolyl cis-trans isomerase D

Table S2. *(Continued)*

1	Niben101Scf01281g10027	-0.046005087	sp|P49211|RL321_ARATH	60S ribosomal protein L32-1
1	Niben101Scf04032g00002	-0.055829606	gb|AAO72598.1|	myosin-like protein [Oryza sativa Japonica Group]
1	Niben101Scf01051g09003	-0.056612341	sp|Q99L47|F10A1_MOUSE	Hsc70-interacting protein
1	Niben101Scf17221g00007	-0.061803529	sp|P59277|SYP81_ARATH	Syntaxin-81
1	Niben101Scf11936g01021	-0.067983438	sp|Q5SMI4|RL393_ORYSJ	60S ribosomal protein L39-3
1	Niben101Scf03374g06003	-0.069663825	sp|Q96AY4|TTC28_HUMAN	Tetratricopeptide repeat protein 28
1	Niben101Scf05845g03009	-0.078112711	sp|Q9V195|RS9_PYRAB	30S ribosomal protein S9
1	Niben101Scf02316g03040	-0.089506285	sp|P93847|RL10_SOLME	60S ribosomal protein L10
1	Niben101Scf02459g09004	-0.096045585	sp|O82528|RL15_PETHY	60S ribosomal protein L15
1	Niben101Scf04528g13017	-0.119364387	sp|Q4HTT1|H2A_GIBZE	Histone H2A
1	Niben101Scf08843g01010	-0.143528418	sp|Q9STX1|ACBP3_ARATH	Acyl-CoA-binding domain-containing protein 3
1	Niben101Scf03977g01005	-0.158404551	sp|P34091|RL6_MESCR	60S ribosomal protein L6
1	Niben101Scf09169g01002	-0.164605392	sp|Q2FT38|RL5_METHJ	50S ribosomal protein L5
1	Niben101Scf03277g02012	-0.165046747	sp|P35065|H2A1_TETTS	Histone H2A.1
1	Niben101Scf07638g04005	-0.165323712	sp|A7EIX7|SUB2_SCLS1	ATP-dependent RNA helicase sub2
1	Niben101Scf09268g00007	-0.166847333	sp|P84977|GRP3_POPEU	Glycine-rich RNA-binding protein 3 (Fragments)
1	Niben101Scf04993g01010	-0.167258016	sp|A8A8W3|RS4_IGNH4	30S ribosomal protein S4
1	Niben101Scf02830g02032	-0.168864026	sp|B0R660|RS19_HALS3	30S ribosomal protein S19
1	Niben101Scf00730g00026	-0.173338285	sp|A2BN38|RS12_HYPBU	30S ribosomal protein S12
1	Niben101Scf02897g01002	-0.173481919	sp|Q8EUM4|DNAJ_MYCPE	Chaperone protein DnaJ
1	Niben101Scf05824g13011	-0.187653985	sp|P49211|RL321_ARATH	60S ribosomal protein L32-1
1	Niben101Scf02401g01001	-0.195424199	sp|Q61011|GBB3_MOUSE	Guanine nucleotide-binding protein G(I)/G(S)/G(T) subunit beta-3
1	Niben101Scf02764g05010	-0.198027712	ref|XP_007008941.1|	Transducin family protein / WD-40 repeat family protein
1	Niben101Scf07031g00004	-0.199210165	sp|Q971C9|RL7A_SULTO	50S ribosomal protein L7Ae
1	Niben101Scf02836g00008	-0.213272757	sp|Q76FK4|NOL8_HUMAN	Nucleolar protein 8

Table S2. *(Continued)*

1	Niben101Scf02232g00014	-0.217556035	sp|Q8TRR0|RS11_METAC	30S ribosomal protein S11
1	Niben101Scf00858g00009	-0.24476763	sp|P40282|H2A_PLAFA	Histone H2A
1	Niben101Scf07728g00002	-0.253028143	sp|Q9ATF5|RL18A_CASSA	60S ribosomal protein L18a
1	Niben101Scf00271g02002	-0.259663216	AT3G55600.1	Membrane fusion protein Use1 LENGTH=240
1	Niben101Scf11009g00008	-0.284226904	sp|A2BN38|RS12_HYPBU	30S ribosomal protein S12
1	Niben101Scf13776g01016	-0.284556687	ref|WP_029317398.1|	copper oxidase [Bacillus subtilis]
1	Niben101Scf00117g02009	-0.286688995	sp|Q93Y22|COPD_ARATH	Coatomer subunit delta
1	Niben101Scf03214g01013	-0.289633988	sp|P46301|RS25_SOLLC	40S ribosomal protein S25
1	Niben101Scf03532g00003	-0.298279764	sp|Q7U4J2|RL29_SYNPX	50S ribosomal protein L29
1	Niben101Scf04436g13024	-0.313635174	sp|Q6UNT2|RL5_CUCSA	60S ribosomal protein L5
1	Niben101Scf02354g02009	-0.314562542	sp|Q8LFH7|RL371_ARATH	60S ribosomal protein L37-1
1	Niben101Scf09590g03007	-0.316607736	sp|Q08507|ACCO3_PETHY	1-aminocyclopropane-1-carboxylate oxidase 3
1	Niben101Scf00494g04009	-0.321282262	gb|ELR52794.1|	Retrograde Golgi transport protein RGP1-like protein
1	Niben101Scf00735g06004	-0.325149605	sp|P25087|ERG6_YEAST	Sterol 24-C-methyltransferase
1	Niben101Scf05892g00003	-0.327202951	sp|A2SPL5|RL5_METLZ	50S ribosomal protein L5
1	Niben101Scf16244g02036	-0.335133489	sp|A6VGV7|RS10_METM7	30S ribosomal protein S10
1	Niben101Scf01061g00001	-0.349018876	sp|P49211|RL321_ARATH	60S ribosomal protein L32-1
1	Niben101Scf04448g02007	-0.370694146	sp|A0RY01|RS13_CENSY	30S ribosomal protein S13
1	Niben101Scf06382g02016	-0.37295082	sp|Q96499|RL44_GOSHI	60S ribosomal protein L44
1	Niben101Scf04081g02005	-0.374189726	sp|A7I5P3|RS19_METB6	30S ribosomal protein S19
1	Niben101Scf03147g07006	-0.380565771	sp|Q971C9|RL7A_SULTO	50S ribosomal protein L7Ae
1	Niben101Scf01764g00009	-0.381710605	sp|O82204|RL281_ARATH	60S ribosomal protein L28-1
1	Niben101Scf04290g04018	-0.386629668	sp|P41098|RL34_TOBAC	60S ribosomal protein L34
1	Niben101Scf00568g04011	-0.387890851	sp|B2LMI9|PSBC_GUIAB	Photosystem II CP43 reaction center protein
1	Niben101Scf03037g00008	-0.391000392	sp|Q2JL77|RL36_SYNJB	50S ribosomal protein L36

Table S2. *(Continued)*

1	Niben101Scf04614g08001	-0.392853083	sp|O26125|RS14Z_METTH	30S ribosomal protein S14 type Z
1	Niben101Scf00288g16005	-0.398566359	sp|P46300|RS4_SOLTU	40S ribosomal protein S4
1	Niben101Scf08143g00006	-0.399258647	sp|Q8TRR0|RS11_METAC	30S ribosomal protein S11
1	Niben101Scf01628g04009	-0.408972042	sp|P42791|RL182_ARATH	60S ribosomal protein L18-2
1	Niben101Scf00428g05013	-0.415085413	sp|Q96499|RL44_GOSHI	60S ribosomal protein L44
1	Niben101Scf00360g01005	-0.420530702	sp|Q9M3V8|RS6_ASPOF	40S ribosomal protein S6
1	Niben101Scf15166g03015	-0.422686896	sp|Q1CZI7|HTPG_MYXXD	Chaperone protein HtpG
1	Niben101Scf10431g00005	-0.425551934	sp|A6VGV7|RS10_METM7	30S ribosomal protein S10
1	Niben101Scf02457g01001	-0.442872107	AT2G32910.1	DCD (Development and Cell Death) domain protein
1	Niben101Scf09552g01014	-0.447422695	sp|Q93Y22|COPD_ARATH	Coatomer subunit delta
1	Niben101Scf00736g00015	-0.464382275	sp|Q32LS6|ABHDD_DANRE	Alpha/beta hydrolase domain-containing protein 13
1	Niben101Scf10737g00008	-0.468640355	sp|P42791|RL182_ARATH	60S ribosomal protein L18-2
1	Niben101Scf17473g00009	-0.490008284	sp|P46300|RS4_SOLTU	40S ribosomal protein S4
1	Niben101Scf23111g00011	-0.498108207	sp|Q8LFH7|RL371_ARATH	60S ribosomal protein L37-1
1	Niben101Scf02182g18008	-0.528042835	sp|O82528|RL15_PETHY	60S ribosomal protein L15
1	Niben101Scf03738g03024	-0.548377928	sp|Q971C9|RL7A_SULTO	50S ribosomal protein L7Ae
1	Niben101Scf13167g00007	-0.551373809	sp|A5D2S3|TRUB_PELTS	tRNA pseudouridine synthase B
1	Niben101Scf09082g00015	-0.55321971	sp|P14029|RL5_METVA	50S ribosomal protein L5
1	Niben101Scf09592g00006	-0.563237864	sp|Q96499|RL44_GOSHI	60S ribosomal protein L44
1	Niben101Scf06105g01001	-0.570004304	sp|P35685|RL7A_ORYSJ	60S ribosomal protein L7a
1	Niben101Scf00736g04011	-0.57661754	sp|Q6LXE7|RS3_METMP	30S ribosomal protein S3
1	Niben101Scf10798g00006	-0.588400031	sp|Q9LHP1|RL74_ARATH	60S ribosomal protein L7-4
1	Niben101Scf05582g03004	-0.594637679	sp|P49098|CYB5_TOBAC	Cytochrome b5
1	Niben101Scf01150g03006	-0.603443293	sp|A0AUR5|F188A_DANRE	Protein FAM188A
1	Niben101Scf00478g06002	-0.603675384	sp|Q9M3V8|RS6_ASPOF	40S ribosomal protein S6

Table S2. *(Continued)*

1	Niben101Scf03471g01013	-0.608985326	sp|P40282|H2A_PLAFA	Histone H2A
1	Niben101Scf04195g01006	-0.610363058	sp|Q1JDX0|VATA_STRPB	V-type ATP synthase alpha chain
1	Niben101Scf03565g00006	-0.61926887	sp|Q9M352|RL362_ARATH	60S ribosomal protein L36-2
1	Niben101Scf22195g00025	-0.624478518	sp|Q8LC83|RS242_ARATH	40S ribosomal protein S24-2
1	Niben101Scf01764g02003	-0.640074479	sp|Q09903|DRS1_SCHPO	ATP-dependent RNA helicase drs1
1	Niben101Scf04608g01007	-0.642570525	sp|P49215|RS17_SOLLC	40S ribosomal protein S17
1	Niben101Scf05551g00009	-0.644984726	sp|Q96499|RL44_GOSHI	60S ribosomal protein L44
1	Niben101Scf05002g03030	-0.648547627	sp|Q6LXE7|RS3_METMP	30S ribosomal protein S3
1	Niben101Scf23557g00012	-0.649900079	emb|CDX73753.1|	BnaC08g22500D [*Brassica napus*]
1	Niben101Scf00912g04004	-0.65832907	sp|P49215|RS17_SOLLC	40S ribosomal protein S17
1	Niben101Scf00015g01003	-0.662021564	sp|Q9FDZ9|RL212_ARATH	60S ribosomal protein L21-2
1	Niben101Scf01568g01024	-0.665845279	sp|Q089P5|RS17_SHEFN	30S ribosomal protein S17
1	Niben101Scf02637g02013	-0.669957565	sp|A6UWV8|RS5_META3	30S ribosomal protein S5
1	Niben101Scf00206g00033	-0.691400405	sp|O82204|RL281_ARATH	60S ribosomal protein L28-1
1	Niben101Scf01579g01046	-0.691712687	sp|Q9LQQ4|H2B1_ARATH	Histone H2B.1
1	Niben101Scf01658g02008	-0.694284273	sp|Q8LFH7|RL371_ARATH	60S ribosomal protein L37-1
1	Niben101Scf03824g02001	-0.705508708	sp|P08283|H1_PEA	Histone H1
1	Niben101Scf12270g02001	-0.711748397	sp|Q2NFZ5|RS11_METST	30S ribosomal protein S11
1	Niben101Scf00825g03003	-0.71317701	sp|P49211|RL321_ARATH	60S ribosomal protein L32-1
1	Niben101Scf01958g03003	-0.71459918	sp|P34091|RL6_MESCR	60S ribosomal protein L6
1	Niben101Scf01945g01012	-0.72613625	sp|P95987|RS4_SULSO	30S ribosomal protein S4
1	Niben101Scf00088g01010	-0.728483633	sp|P46301|RS25_SOLLC	40S ribosomal protein S25
1	Niben101Scf01905g01002	-0.729861003	sp|Q5SMI4|RL393_ORYSJ	60S ribosomal protein L39-3
1	Niben101Scf05529g00001	-0.732041196	sp|Q8NBP0|TTC13_HUMAN	Tetratricopeptide repeat protein 13
1	Niben101Scf01440g02010	-0.735277328	sp|P49215|RS17_SOLLC	40S ribosomal protein S17

Table S2. *(Continued)*

1	Niben101Ctg14963g00002	-0.743003821	sp|P41101|RL27_SOLTU	60S ribosomal protein L27
1	Niben101Scf12414g01019	-0.743231871	sp|P62302|RS13_SOYBN	40S ribosomal protein S13
1	Niben101Scf04233g00002	-0.743396544	sp|P49211|RL321_ARATH	60S ribosomal protein L32-1
1	Niben101Scf01779g05002	-0.761639492	sp|Q9M3V8|RS6_ASPOF	40S ribosomal protein S6
1	Niben101Scf09089g01036	-0.764438348	sp|B6YSQ2|RS11_THEON	30S ribosomal protein S11
1	Niben101Scf12585g00006	-0.773709229	AT1G68100.1	ZIP metal ion transporter family LENGTH=469
1	Niben101Scf07165g01002	-0.774696052	sp|Q9XEG7|RS3A_TORRU	40S ribosomal protein S3a
1	Niben101Scf01585g01017	-0.779222604	sp|Q9LHP1|RL74_ARATH	60S ribosomal protein L7-4
1	Niben101Scf00527g01005	-0.780127338	sp|P62302|RS13_SOYBN	40S ribosomal protein S13
1	Niben101Scf13099g00013	-0.78203273	sp|B1YC32|RL13_PYRNV	50S ribosomal protein L13
1	Niben101Scf02494g08002	-0.789470242	sp|P62302|RS13_SOYBN	40S ribosomal protein S13
1	Niben101Scf02637g01005	-0.790314135	sp|A6UWV8|RS5_META3	30S ribosomal protein S5
1	Niben101Scf11361g00001	-0.807904923	sp|P62302|RS13_SOYBN	40S ribosomal protein S13
1	Niben101Scf04181g00034	-0.822614388	emb|CDX73753.1|	BnaC08g22500D [*Brassica napus*]
1	Niben101Scf25768g00009	-0.823631046	sp|Q5SMI4|RL393_ORYSJ	60S ribosomal protein L39-3
1	Niben101Scf11491g02007	-0.824074173	sp|Q9ZNS1|RS7_AVIMR	40S ribosomal protein S7
1	Niben101Scf04740g00005	-0.837388782	AT5G06850.1	C2 calcium/lipid-binding plant phosphoribosyltransferase
1	Niben101Scf02562g00024	-0.857547757	ref|WP_025880009.1|	MULTISPECIES: hypothetical protein [Prochlorococcus]
1	Niben101Scf02821g04003	-0.862374422	sp|Q609G2|UBIG_METCA	Ubiquinone biosynthesis O-methyltransferase
1	Niben101Scf04926g06003	-0.869757105	sp|B4EAW5|DER_BURCJ	GTPase Der
1	Niben101Scf07532g02017	-0.877843589	sp|P62302|RS13_SOYBN	40S ribosomal protein S13
1	Niben101Scf32526g00010	-0.908970088	AT5G23390.1	Plant protein of unknown function (DUF639) LENGTH=730
1	Niben101Scf36191g00005	-0.910614647	sp|A2BN38|RS12_HYPBU	30S ribosomal protein S12
1	Niben101Scf02927g09007	-0.911030352	sp|Q9FDZ9|RL212_ARATH	60S ribosomal protein L21-2
1	Niben101Scf01797g01008	-0.915289579	sp|P49211|RL321_ARATH	60S ribosomal protein L32-1

Table S2. *(Continued)*

1	Niben101Scf02477g00012	-0.917367756	sp|Q9M0E2|RL282_ARATH	60S ribosomal protein L28-2
1	Niben101Scf00117g00006	-0.939361859	sp|Q975I1|RL3_SULTO	50S ribosomal protein L3
1	Niben101Scf04784g03005	-0.940905445	sp|P46301|RS25_SOLLC	40S ribosomal protein S25
1	Niben101Scf03284g06010	-0.942184083	sp|Q93Z16|RPN2_ARATH	Dolichyl-diphosphooligosaccharide-protein glycosyltransferase
1	Niben101Scf12318g00006	-0.943254004	sp|Q9FK53|NLAL2_ARATH	H/ACA ribonucleoprotein complex subunit 1-like protein 2
1	Niben101Scf10228g00002	-0.954333321	sp|Q9SF40|RL4A_ARATH	60S ribosomal protein L4-1
1	Niben101Scf38997g00004	-0.962198533	sp|Q9M9W1|RL222_ARATH	60S ribosomal protein L22-2
1	Niben101Scf05955g00013	-0.966560543	sp|O29136|RS9_ARCFU	30S ribosomal protein S9
1	Niben101Scf03138g01041	-0.977973711	sp|P49215|RS17_SOLLC	40S ribosomal protein S17
1	Niben101Scf03747g04010	-0.979621195	sp|A1SNK7|RL24_NOCSJ	50S ribosomal protein L24
1	Niben101Scf06183g07014	-0.983871769	sp|Q46GA8|RL5_METBF	50S ribosomal protein L5
1	Niben101Scf03790g00014	-0.984185295	ref|WP_025880009.1|	MULTISPECIES: hypothetical protein [Prochlorococcus]
1	Niben101Scf00858g05001	-0.99826063	sp|Q3IMY5|RL2_NATPD	50S ribosomal protein L2
1	Niben101Scf00301g00001	-1.024455164	AT3G57880.1	CaLB domain plant phosphoribosyltransferase protein
1	Niben101Scf07449g00006	-1.032010394	sp|Q8SRB0|GBLP_ENCCU	Guanine nucleotide-binding protein subunit beta-like protein
1	Niben101Scf04627g02010	-1.035890698	sp|A1SNK7|RL24_NOCSJ	50S ribosomal protein L24
1	Niben101Scf10055g10004	-1.086017891	sp|Q9LHP1|RL74_ARATH	60S ribosomal protein L7-4
1	Niben101Scf05634g00003	-1.0889067	sp|A3PA97|NDK_PROM0	Nucleoside diphosphate kinase
1	Niben101Scf04632g03007	-1.0949056	sp|Q8TRR0|RS11_METAC	30S ribosomal protein S11
1	Niben101Scf01834g04007	-1.097402518	sp|P49215|RS17_SOLLC	40S ribosomal protein S17
1	Niben101Scf02319g06012	-1.100080004	sp|Q8LFH7|RL371_ARATH	60S ribosomal protein L37-1
1	Niben101Scf01945g01009	-1.111665816	sp|P61992|RS4_PYRAB	30S ribosomal protein S4
1	Niben101Scf04323g04023	-1.113595884	sp|P46301|RS25_SOLLC	40S ribosomal protein S25
1	Niben101Scf00991g05009	-1.113848419	sp|P51414|RL261_ARATH	60S ribosomal protein L26-1
1	Niben101Scf01049g02006	-1.122254403	sp|Q6ZLK0|OST48_ORYSJ	Dolichyl-diphosphooligosaccharide-protein glycosyltransferase

Table S2. *(Continued)*

1	Niben101Scf04044g01026	-1.153276149	AT2G38140.1	plastid-specific ribosomal protein 4 LENGTH=118
1	Niben101Scf14144g00024	-1.161790766	sp|Q5SMI4|RL393_ORYSJ	60S ribosomal protein L39-3
1	Niben101Scf00110g01011	-1.162565937	sp|Q9V195|RS9_PYRAB	30S ribosomal protein S9
1	Niben101Scf09801g01006	-1.168171307	sp|P41098|RL34_TOBAC	60S ribosomal protein L34
1	Niben101Scf12063g00001	-1.168224136	sp|P59259|H4_ARATH	Histone H4
1	Niben101Scf11491g00006	-1.170256879	AT1G48840.1	Plant protein of unknown function (DUF639) LENGTH=691
1	Niben101Scf01018g01010	-1.180667502	sp|P49098|CYB5_TOBAC	Cytochrome b5
1	Niben101Scf06078g02032	-1.223914775	gb|AAF14244.1|AF110228_1	nuclear RNA binding protein A [Spinacia oleracea]
1	Niben101Scf00057g00033	-1.225723926	sp|Q9LH74|MSL5_ARATH	Mechanosensitive ion channel protein 5
1	Niben101Scf00121g00019	-1.229474664	sp|Q8SRB0|GBLP_ENCCU	Guanine nucleotide-binding protein subunit beta-like protein
1	Niben101Scf04077g03006	-1.246310038	sp|E9Q4Z2|ACACB_MOUSE	Acetyl-CoA carboxylase 2
1	Niben101Scf04375g08024	-1.257699787	sp|Q42533|BCCP1_ARATH	Biotin carboxyl carrier protein of acetyl-CoA carboxylase 1
1	Niben101Ctg16374g00011	-1.266735251	sp|Q4R3X5|H2AJ_MACFA	Histone H2A.J
1	Niben101Scf03214g00006	-1.271307922	AT4G13850.1	glycine-rich RNA-binding protein 2 LENGTH=158
1	Niben101Scf05413g01015	-1.287240651	sp|A2BMB2|RL2_HYPBU	50S ribosomal protein L2
1	Niben101Scf13622g00001	-1.29641379	sp|Q0KL01|UBX2B_MOUSE	UBX domain-containing protein 2B
1	Niben101Scf09123g00004	-1.308649011	sp|B0TI32|ACCA_HELMI	Acetyl-coenzyme A carboxylase carboxyl transferase subunit alpha
1	Niben101Scf00428g12016	-1.313002486	gb|AAF14244.1|AF110228_1	nuclear RNA binding protein A [Spinacia oleracea]
1	Niben101Scf09100g03002	-1.3245104	AT5G35790.1	glucose-6-phosphate dehydrogenase 1 LENGTH=576
1	Niben101Scf04082g00008	-1.325172552	AT1G04220.1	3-ketoacyl-CoA synthase 2 LENGTH=528
1	Niben101Scf09467g02007	-1.347583673	sp|A6UWV8|RS5_META3	30S ribosomal protein S5
1	Niben101Scf03939g06022	-1.369299116	sp|Q96499|RL44_GOSHI	60S ribosomal protein L44
1	Niben101Scf00944g06005	-1.385618829	sp|Q9T043|RL142_ARATH	60S ribosomal protein L14-2
1	Niben101Scf10440g01002	-1.396726403	sp|P62980|RS27A_SOLLC	Ubiquitin-40S ribosomal protein S27a
1	Niben101Scf10986g00001	-1.45642598	sp|Q9LV60|CRR55_ARATH	Cysteine-rich repeat secretory protein 55

Table S2. *(Continued)*

1	Niben101Scf06888g02020	-1.462248836	sp|O81154|CYSK_SOLTU	Cysteine synthase
1	Niben101Scf04294g01001	-1.471637255	AT5G60620.1	glycerol-3-phosphate acyltransferase 9 LENGTH=376
1	Niben101Scf02262g01009	-1.487841426	sp|Q3IMY5|RL2_NATPD	50S ribosomal protein L2
1	Niben101Scf14210g00010	-1.505232196	sp|Q5HQ75|ODPB_STAEQ	Pyruvate dehydrogenase E1 component subunit beta
1	Niben101Scf00578g00010	-1.529782961	sp|Q3IMY5|RL2_NATPD	50S ribosomal protein L2
1	Niben101Scf05060g01010	-1.614050193	sp|P41098|RL34_TOBAC	60S ribosomal protein L34
1	Niben101Scf11724g04003	-1.659351179	ref|NP_175508.2|	cell redox home [*Arabidopsis thaliana*]
1	Niben101Scf04558g02002	-1.692466942	AT5G20990.1	molybdopterin biosynthesis CNX1 protein
1	Niben101Scf13823g02004	-1.693929116	AT5G63140.1	purple acid phosphatase 29 LENGTH=389
1	Niben101Scf10885g00015	-1.697414724	sp|Q8PV45|RL22_METMA	50S ribosomal protein L22
1	Niben101Scf01339g06010	-1.733179278	sp|Q97BW2|RS14Z_THEVO	30S ribosomal protein S14 type Z
1	Niben101Scf01994g02009	-1.739955918	sp|A7I4X6|RS12_METB6	30S ribosomal protein S12
1	Niben101Scf15437g02016	-1.742770033	sp|Q0TMQ7|RL24_CLOP1	50S ribosomal protein L24
1	Niben101Scf01326g04004	-1.797819041	sp|P41098|RL34_TOBAC	60S ribosomal protein L34
1	Niben101Scf06910g05004	-1.828855058	sp|Q31KX4|PROA_SYNE7	Gamma-glutamyl phosphate reductase
1	Niben101Scf06734g00014	-1.841908248	AT1G70280.2	NHL domain-containing protein LENGTH=509
1	Niben101Scf03082g01001	-1.850008532	sp|Q3V096|ANR42_MOUSE	Ankyrin repeat domain-containing protein 42
1	Niben101Scf02207g05005	-1.854184949	sp|Q96499|RL44_GOSHI	60S ribosomal protein L44
1	Niben101Scf02016g00005	-1.869470896	sp|Q8N9V6|ANR53_HUMAN	Ankyrin repeat domain-containing protein 53
1	Niben101Scf06171g00001	-1.942164238	sp|Q1J0V5|RL31_DEIGD	50S ribosomal protein L31
1	Niben101Scf00582g01035	-1.961907162	sp|P16866|H2A4_VOLCA	Histone H2A-IV
1	Niben101Scf10328g00024	-2.037458938	sp|Q7VQV0|RL34_BLOFL	50S ribosomal protein L34
1	Niben101Scf01971g01006	-2.106092843	gb|AIT42208.1|	Kunitz-type inhibitor C [Solanum tuberosum]
1	Niben101Scf01318g00005	-2.151602132	sp|O80439|RR31_ARATH	30S ribosomal protein S31, chloroplastic
1	Niben101Scf06131g00004	-2.151676436	sp|P93847|RL10_SOLME	60S ribosomal protein L10

Table S2. *(Continued)*

1	Niben101Scf00133g04024	-2.176138852	sp|P81898|PNAA_PRUDU	Peptide-N4-(N-acetyl-beta-glucosaminyl)asparagine amidase A
1	Niben101Scf01448g02025	-2.229122256	sp|A8F997|RL5_BACP2	50S ribosomal protein L5
1	Niben101Scf02994g03003	-2.232349261	ref|WP_024571788.1|	copper oxidase [Bacillus subtilis]
1	Niben101Scf00151g07009	-2.238028455	ref|XP_002523935.1|	hydrolase, hydrolyzing O-glycosyl compounds
1	Niben101Scf00207g05027	-2.268813907	sp|Q3SER0|RL34_THIDA	50S ribosomal protein L34
1	Niben101Scf01681g02007	-2.32994377	AT1G74040.1	2-isopropylmalate synthase 1 LENGTH=631
1	Niben101Scf04113g01012	-2.354851056	sp|A0Q316|RL31_CLONN	50S ribosomal protein L31
1	Niben101Scf05712g03021	-2.355375185	AT1G04220.1	3-ketoacyl-CoA synthase 2 LENGTH=528
1	Niben101Scf06078g00003	-2.363634862	sp|A5G0G7|RL19_ACICJ	50S ribosomal protein L19
1	Niben101Scf11689g01017	-2.37790825	sp|A2C0L8|MURE_PROM1	UDP-N-acetylmuramoyl-L-alanyl-D-glutamate--2,6-diaminopimelate ligase
1	Niben101Scf03056g02008	-2.438482755	sp|Q3A9T5|RL15_CARHZ	50S ribosomal protein L15
1	Niben101Scf03628g14021	-2.461416923	AT1G53310.1	phosphoenolpyruvate carboxylase 1 LENGTH=967
1	Niben101Scf04289g01011	-2.530439461	AT1G70280.2	NHL domain-containing protein LENGTH=509
1	Niben101Scf00428g15006	-2.5424288	sp|Q1GPJ8|RL19_SPHAL	50S ribosomal protein L19
1	Niben101Scf08724g02009	-2.548210797	sp|Q9MB58|F26_ARATH	6-phosphofructo-2-kinase/fructose-2,6-bisphosphatase
1	Niben101Scf03801g00003	-2.70133326	sp|Q31KX4|PROA_SYNE7	Gamma-glutamyl phosphate reductase
1	Niben101Scf02320g00019	-2.711507551	sp|A1SNI7|RL17_NOCSJ	50S ribosomal protein L17
1	Niben101Scf05697g02007	-2.783874288	AT3G52990.1	Pyruvate kinase family protein LENGTH=527
1	Niben101Scf19612g01003	-2.896458538	AT5G35790.1	glucose-6-phosphate dehydrogenase 1 LENGTH=576
1	Niben101Scf04198g01002	-2.977381057	sp|P55038|GLTS_SYNY3	Ferredoxin-dependent glutamate synthase 2
1	Niben101Scf23355g00024	-3.061722285	sp|Q9NW13|RBM28_HUMAN	RNA-binding protein 28
1	Niben101Scf01291g04005	-3.107475911	sp|B2HCX5|RL17_MYCMM	50S ribosomal protein L17
1	Niben101Scf21202g00009	-3.229693034	sp|B9K895|RS17_THENN	30S ribosomal protein S17
1	Niben101Scf03396g03006	-3.278013707	AT2G42850.1	cytochrome P450, family 718 LENGTH=485

Table S2. *(Continued)*

1	Niben101Scf01249g03027	-3.378402448	sp|B0KCK8|RL29_THEP3	50S ribosomal protein L29
1	Niben101Scf15752g00007	-3.402302018	AT4G02930.1	GTP binding Elongation factor Tu family protein LENGTH=454
1	Niben101Scf06349g02015	-3.470106912	sp|Q8KG16|RL7_CHLTE	50S ribosomal protein L7/L12
1	Niben101Scf01912g01003	-3.65092917	sp|Q1MPU3|RL7_LAWIP	50S ribosomal protein L7/L12
1	Niben101Scf02156g00008	-3.70224962	sp|Q9FSB8|CHS2_RUTGR	Chalcone synthase 2
1	Niben101Scf05220g00005	-3.741604425	sp|P21616|AVP_VIGRR	Pyrophosphate-energized vacuolar membrane proton pump
1	Niben101Scf02757g01001	-4.022509265	AT4G29060.1	elongation factor Ts family protein LENGTH=953
1	Niben101Scf05737g00003	-4.089984482	sp|O78502|PSAD_GUITH	Photosystem I reaction center subunit II
1	Niben101Scf00493g00020	-4.128093575	sp|P94040|GL31_ARATH	Germin-like protein subfamily 3 member 1
1	Niben101Scf00797g18009	-4.357466164	sp|Q56YA5|SGAT_ARATH	Serine--glyoxylate aminotransferase
1	Niben101Scf02749g04008	-4.535332496	sp|P94072|GL33_ARATH	Germin-like protein subfamily 3 member 3
1	Niben101Ctg11493g00003	_	sp|Q9CQE7|ERGI3_MOUSE	Endoplasmic reticulum-Golgi intermediate compartment protein 3
1	Niben101Ctg12179g00003	_	sp|Q9M3V8|RS6_ASPOF	40S ribosomal protein S6
1	Niben101Ctg14099g00002	_	sp|Q2TA14|PCP_BOVIN	Lysosomal Pro-X carboxypeptidase
1	Niben101Ctg15214g00001	_	AT1G20330.1	sterol methyltransferase 2 LENGTH=361
1	Niben101Scf00163g07005	_	sp|B2JIU7|DER_BURP8	GTPase Der
1	Niben101Scf00262g02011	_	sp|C0Q9U6|RL17_DESAH	50S ribosomal protein L17
1	Niben101Scf00307g01038	_	sp|Q9LIG2|RLK6_ARATH	Receptor-like protein kinase
1	Niben101Scf00311g00001	_	sp|O82528|RL15_PETHY	60S ribosomal protein L15
1	Niben101Scf00332g11005	_	sp|Q9M352|RL362_ARATH	60S ribosomal protein L36-2
1	Niben101Scf00343g05011	_	sp|Q65JE5|MIAB_BACLD	tRNA-2-methylthio-N(6)-dimethylallyladenosine synthase
1	Niben101Scf00438g02016	_	sp|A5V3X3|ATPA_SPHWW	ATP synthase subunit alpha
1	Niben101Scf00466g04033	_	sp|Q5R5B6|PDIA1_PONAB	Protein disulfide-isomerase
1	Niben101Scf00508g01009	_	sp|Q9LH74|MSL5_ARATH	Mechanosensitive ion channel protein 5
1	Niben101Scf00519g00014	_	sp|Q8DMM5|RL16_THEEB	50S ribosomal protein L16

Table S2. *(Continued)*

1	Niben101Scf00545g00013	_	sp|P33731|SRP72_CANFA	Signal recognition particle subunit SRP72
1	Niben101Scf00558g00004	_	emb|CED79771.1|	acetyl-CoA carboxylase beta subunit (chloroplast)
1	Niben101Scf00597g08029	_	ref|XP_007050168.1|	Nuclear transport factor 2 family protein with RNA binding domain
1	Niben101Scf00631g01020	_	sp|A2BN38|RS12_HYPBU	30S ribosomal protein S12
1	Niben101Scf00693g02022	_	sp|Q1CZI7|HTPG_MYXXD	Chaperone protein HtpG
1	Niben101Scf00713g02004	_	sp|P73314|RS3_SYNY3	30S ribosomal protein S3
1	Niben101Scf00800g04004	_	AT4G02930.1	GTP binding Elongation factor Tu family protein LENGTH=454
1	Niben101Scf00858g01009	_	sp|Q0TMQ7|RL24_CLOP1	50S ribosomal protein L24
1	Niben101Scf00904g01001	_	sp|Q5SMI4|RL393_ORYSJ	60S ribosomal protein L39-3
1	Niben101Scf00966g01002	_	sp|P41098|RL34_TOBAC	60S ribosomal protein L34
1	Niben101Scf01100g01004	_	sp|Q6DDW6|GPHR_XENLA	Golgi pH regulator
1	Niben101Scf01181g00019	_	sp|Q8SRB0|GBLP_ENCCU	Guanine nucleotide-binding protein subunit beta-like protein
1	Niben101Scf01250g01002	_	sp|Q74N79|RL5_NANEQ	50S ribosomal protein L5
1	Niben101Scf01285g04011	_	sp|P41098|RL34_TOBAC	60S ribosomal protein L34
1	Niben101Scf01304g13012	_	sp|Q9M0E2|RL282_ARATH	60S ribosomal protein L28-2
1	Niben101Scf01374g00008	_	sp|B9K895|RS17_THENN	30S ribosomal protein S17
1	Niben101Scf01391g04001	_	AT4G13110.1	BSD domain-containing protein LENGTH=316
1	Niben101Scf01418g03019	_	sp|Q2H4D0|SUB2_CHAGB	ATP-dependent RNA helicase SUB2
1	Niben101Scf01628g02006	_	sp|Q9H6B9|EPHX3_HUMAN	Epoxide hydrolase 3
1	Niben101Scf01689g06004	_	sp|Q9YB48|RS9_AERPE	30S ribosomal protein S9
1	Niben101Scf01734g01048	_	sp|A7M907|ACCD_CUSGR	Acetyl-coenzyme A carboxylase carboxyl transferase subunit beta
1	Niben101Scf01816g00009	_	sp|B1LVH1|ATPA_METRJ	ATP synthase subunit alpha
1	Niben101Scf01922g05005	_	sp|A8LJP9|CH60_DINSH	60 kDa chaperonin
1	Niben101Scf01980g02001	_	AT1G36160.1	acetyl-CoA carboxylase 1 LENGTH=2254
1	Niben101Scf02027g01022	_	sp|Q9BXT4|TDRD1_HUMAN	Tudor domain-containing protein 1

Table S2. *(Continued)*

1	Niben101Scf02073g04012	_	sp|O82528|RL15_PETHY	60S ribosomal protein L15
1	Niben101Scf02077g10001	_	sp|Q96499|RL44_GOSHI	60S ribosomal protein L44
1	Niben101Scf02145g01003	_	sp|Q0KL01|UBX2B_MOUSE	UBX domain-containing protein 2B
1	Niben101Scf02171g00001	_	sp|A2BN38|RS12_HYPBU	30S ribosomal protein S12
1	Niben101Scf02182g18003	_	sp|O82528|RL15_PETHY	60S ribosomal protein L15
1	Niben101Scf02354g02008	_	sp|Q8LEM8|RL373_ARATH	60S ribosomal protein L37-3
1	Niben101Scf02425g00020	_	sp|Q32LS6|ABHDD_DANRE	Alpha/beta hydrolase domain-containing protein 13
1	Niben101Scf02426g02028	_	sp|Q8CH18|CCAR1_MOUSE	Cell division cycle and apoptosis regulator protein 1
1	Niben101Scf02467g01008	_	sp|Q5XIA4|CNO10_RAT	CCR4-NOT transcription complex subunit 10
1	Niben101Scf02585g00014	_	sp|Q5WLQ0|RL5_BACSK	50S ribosomal protein L5
1	Niben101Scf02706g04005	_	sp|Q00004|SRP68_CANFA	Signal recognition particle subunit SRP68
1	Niben101Scf02734g01027	_	ref|NP_004308.2|	ATPase ASNA1 [Homo sapiens] ref|NP_001092334.1|
1	Niben101Scf02747g00011	_	sp|Q94AU2|SEC22_ARATH	25.3 kDa vesicle transport protein
1	Niben101Scf02790g05015	_	sp|Q9FJA6|RS33_ARATH	40S ribosomal protein S3-3
1	Niben101Scf02837g07011	_	sp|Q5HQ75|ODPB_STAEQ	Pyruvate dehydrogenase E1 component subunit beta
1	Niben101Scf02949g14009	_	sp|P42791|RL182_ARATH	60S ribosomal protein L18-2
1	Niben101Scf03044g00006	_	ref|NP_175508.2|	cell redox home [*Arabidopsis thaliana*]
1	Niben101Scf03080g04029	_	emb|CDY02278.1|	BnaA03g38890D [*Brassica napus*]
1	Niben101Scf03113g02012	_	sp|P41101|RL27_SOLTU	60S ribosomal protein L27
1	Niben101Scf03138g01017	_	sp|P49215|RS17_SOLLC	40S ribosomal protein S17
1	Niben101Scf03142g02005	_	AT4G29060.1	elongation factor Ts family protein LENGTH=953
1	Niben101Scf03203g07006	_	sp|A0RY01|RS13_CENSY	30S ribosomal protein S13
1	Niben101Scf03371g01018	_	emb|CDY15385.1|	BnaC04g42380D [*Brassica napus*]
1	Niben101Scf03432g00012	_	sp|Q9FKC0|R13A4_ARATH	60S ribosomal protein L13a-4
1	Niben101Scf03599g01016	_	sp|Q9P0L0|VAPA_HUMAN	Vesicle-associated membrane protein-associated protein A

Table S2. *(Continued)*

1	Niben101Scf03706g02013	_	sp|Q9LUQ6|RL192_ARATH	60S ribosomal protein L19-2
1	Niben101Scf04286g01033	_	sp|B0KCK8|RL29_THEP3	50S ribosomal protein L29
1	Niben101Scf04294g03011	_	gb|AAD40381.1|	vesicle transport-related protein [Homo sapiens]
1	Niben101Scf04328g00019	_	AT5G63310.1	nucleoside diphosphate kinase 2 LENGTH=231
1	Niben101Scf04377g02011	_	sp|Q96499|RL44_GOSHI	60S ribosomal protein L44
1	Niben101Scf04418g12003	_	sp|Q6UNT2|RL5_CUCSA	60S ribosomal protein L5
1	Niben101Scf04489g00008	_	AT1G15440.1	periodic tryptophan protein 2 LENGTH=900
1	Niben101Scf04528g13006	_	sp|Q4HTT1|H2A_GIBZE	Histone H2A
1	Niben101Scf04592g00016	_	sp|A2BN38|RS12_HYPBU	30S ribosomal protein S12
1	Niben101Scf04633g02005	_	sp|B4U736|RL7_HYDS0	50S ribosomal protein L7/L12
1	Niben101Scf04665g02021	_	AT5G06850.1	C2 calcium/lipid-binding plant phosphoribosyltransferase protein
1	Niben101Scf04703g11023	_	sp|P62302|RS13_SOYBN	40S ribosomal protein S13
1	Niben101Scf04714g01004	_	sp|A5GFS8|VAPB_PIG	Vesicle-associated membrane protein-associated protein B
1	Niben101Scf04739g02010	_	sp|Q1CZI7|HTPG_MYXXD	Chaperone protein HtpG
1	Niben101Scf04787g02004	_	sp|P49211|RL321_ARATH	60S ribosomal protein L32-1
1	Niben101Scf04879g06001	_	AT1G74040.1	2-isopropylmalate synthase 1 LENGTH=631
1	Niben101Scf04918g05001	_	sp|P21616|AVP_VIGRR	Pyrophosphate-energized vacuolar membrane proton pump
1	Niben101Scf05222g05008	_	sp|Q8XIT1|DNAJ_CLOPE	Chaperone protein DnaJ
1	Niben101Scf05229g04013	_	sp|Q9FLF0|RS92_ARATH	40S ribosomal protein S9-2
1	Niben101Scf05317g00004	_	sp|P62302|RS13_SOYBN	40S ribosomal protein S13
1	Niben101Scf05379g00001	_	AT4G13850.1	glycine-rich RNA-binding protein 2 LENGTH=158
1	Niben101Scf05440g06004	_	ref|NP_001054228.1|	product [Oryza sativa Japonica Group]
1	Niben101Scf05545g00003	_	sp|Q9ZNS1|RS7_AVIMR	40S ribosomal protein S7
1	Niben101Scf05750g04010	_	sp|Q8PV45|RL22_METMA	50S ribosomal protein L22
1	Niben101Scf06078g02031	_	gb|AAF14244.1|AF110228_1	nuclear RNA binding protein A [Spinacia oleracea]

Table S2. *(Continued)*

1	Niben101Scf06080g04011	_	sp|Q9FKQ3|H3L5_ARATH	Histone H3-like 5
1	Niben101Scf06221g03002	_	sp|A5VSE3|ATPA_BRUO2	ATP synthase subunit alpha
1	Niben101Scf06236g01011	_	sp|P62302|RS13_SOYBN	40S ribosomal protein S13
1	Niben101Scf06365g00001	_	sp|Q9LHP1|RL74_ARATH	60S ribosomal protein L7-4
1	Niben101Scf06375g05001	_	AT1G36160.1	acetyl-CoA carboxylase 1 LENGTH=2254
1	Niben101Scf06759g00005	_	sp|Q3IMY5|RL2_NATPD	50S ribosomal protein L2
1	Niben101Scf06829g02007	_	sp|Q28559|ACACA_SHEEP	Acetyl-CoA carboxylase 1
1	Niben101Scf06840g00012	_	sp|Q8DMM5|RL16_THEEB	50S ribosomal protein L16
1	Niben101Scf06849g00011	_	sp|A4YKD8|ATPA_BRASO	ATP synthase subunit alpha
1	Niben101Scf06986g02010	_	sp|Q3C1P7|RR15_NICSY	30S ribosomal protein S15, chloroplastic
1	Niben101Scf07008g00005	_	sp|Q8LEM8|RL373_ARATH	60S ribosomal protein L37-3
1	Niben101Scf07123g00001	_	sp|Q56YA5|SGAT_ARATH	Serine--glyoxylate aminotransferase
1	Niben101Scf07183g00017	_	sp|P0CQ97|SUB2_CRYNB	ATP-dependent RNA helicase SUB2
1	Niben101Scf07221g00001	_	sp|A9LYE2|RK2_ACOAM	50S ribosomal protein L2, chloroplastic
1	Niben101Scf07223g01007	_	sp|Q9SF40|RL4A_ARATH	60S ribosomal protein L4-1
1	Niben101Scf07250g03025	_	sp|P55034|PSMD4_ARATH	26S proteasome non-ATPase regulatory subunit 4 homolog
1	Niben101Scf07288g01005	_	sp|Q609G2|UBIG_METCA	Ubiquinone biosynthesis O-methyltransferase
1	Niben101Scf07724g00005	_	sp|Q9C6I8|NOG1_ARATH	Nucleolar GTP-binding protein 1
1	Niben101Scf07741g03005	_	sp|A2BN38|RS12_HYPBU	30S ribosomal protein S12
1	Niben101Scf08523g00022	_	AT2G26640.1	3-ketoacyl-CoA synthase 11 LENGTH=509
1	Niben101Scf08776g02028	_	sp|Q9P6I1|UBC16_SCHPO	Ubiquitin-conjugating enzyme E2 16
1	Niben101Scf08792g00007	_	sp|Q9ATF5|RL18A_CASSA	60S ribosomal protein L18a
1	Niben101Scf09304g00002	_	sp|B0C431|RS11_ACAM1	30S ribosomal protein S11
1	Niben101Scf09816g00003	_	sp|P0CQ97|SUB2_CRYNB	ATP-dependent RNA helicase SUB2
1	Niben101Scf10200g01004	_	sp|Q5SMI4|RL393_ORYSJ	60S ribosomal protein L39-3
1	Niben101Scf10277g00009	_	sp|P48601|PRS4_DROME	26S protease regulatory subunit 4

Table S2. *(Continued)*

1	Niben101Scf10314g01001	_	sp|Q18CG9|RL29_PEPD6	50S ribosomal protein L29
1	Niben101Scf10390g00003	_	sp|P21874|ODPB_GEOSE	Pyruvate dehydrogenase E1 component subunit beta
1	Niben101Scf10796g00009	_	sp|Q1CZI7|HTPG_MYXXD	Chaperone protein HtpG
1	Niben101Scf11368g00015	_	gb|KFP22985.1|	Retrograde Golgi transport protein RGP1, partial [Egretta garzetta]
1	Niben101Scf11416g00016	_	sp|P42794|RL112_ARATH	60S ribosomal protein L11-2
1	Niben101Scf12017g05016	_	AT4G16340.1	guanyl-nucleotide exchange factors
1	Niben101Scf12258g01006	_	AT4G28080.1	Tetratricopeptide repeat (TPR)-like superfamily protein
1	Niben101Scf12695g00005	_	ref|XP_003074807.1|	Hsp27-ERE-TATA-binding protein/Scaffold attachment factor (SAF-B) (ISS)
1	Niben101Scf12966g00005	_	sp|P55038|GLTS_SYNY3	Ferredoxin-dependent glutamate synthase 2
1	Niben101Scf14268g00001	_	sp|A7TEF4|FAL1_VANPO	ATP-dependent RNA helicase FAL1
1	Niben101Scf14294g01005	_	sp|A2BYS9|RL16_PROM5	50S ribosomal protein L16
1	Niben101Scf14325g00009	_	sp|Q6P011|EMC4_DANRE	ER membrane protein complex subunit 4
1	Niben101Scf15106g00004	_	sp|P49211|RL321_ARATH	60S ribosomal protein L32-1
1	Niben101Scf15836g01009	_	ref|XP_007015446.1|	N-terminal isoform 1 [Theobroma cacao] gb|EOY33065.1|
1	Niben101Scf16178g00002	_	sp|P0CQ97|SUB2_CRYNB	ATP-dependent RNA helicase SUB2
1	Niben101Scf16292g00002	_	sp|Q11A13|RS15_TRIEI	30S ribosomal protein S15
1	Niben101Scf19719g00009	_	sp|B6YSQ2|RS11_THEON	30S ribosomal protein S11
1	Niben101Scf19975g01003	_	sp|Q6KAJ8|RL391_ORYSJ	60S ribosomal protein L39-1
1	Niben101Scf20576g01002	_	sp|Q110B5|RL29_TRIEI	50S ribosomal protein L29
1	Niben101Scf21026g00011	_	emb|CDY48281.1|	BnaA05g10730D [*Brassica napus*]
1	Niben101Scf21171g00004	_	sp|O82528|RL15_PETHY	60S ribosomal protein L15
1	Niben101Scf29115g00001	_	sp|Q06H01|PSBC_DRIGR	Photosystem II CP43 reaction center protein
1	Niben101Scf31501g00001	_	sp|Q0VS07|MURE_ALCBS	UDP-N-acetylmuramoyl-L-alanyl-D-glutamate--2,6-diaminopimelate ligase
1	Niben101Scf32851g00006	_	sp|P49211|RL321_ARATH	60S ribosomal protein L32-1

Table S3. RLCKs detected in two out of three PL-MS experiments for which the NbSOBIR1-YFP-TbID fusion protein was transiently expressed as a bait in *N. benthamiana*. The *N. benthamiana* IDs refer to the protein identifiers according to the Niben1.0.1 version of the proteome of *N. benthamiana*. Asterisks next to the name of the *Arabidopsis* homologs in the second column indicate that the protein is co-expressed with SOBIR1 according to the data described in Chapter 3. The third column indicates the classification as protein kinases according to Zheng, ***et. al.*** [359].

RLCKs significantly enriched in two independent PL-MS experiments when using NbSOBIR1-YFP-TbID as a bait		
N. benthamiana ID	*Arabidopsis* best blast hit	Classification as a kinase [359]
Niben101Scf12754g00010	AT2G11520 / CRCK3 *	RLK-Pelle_RLCK-IV
Niben101Scf06678g03002		
Niben101Scf01507g01017	AT2G42960	RLK-Pelle_RLCK-V
Niben101Scf04995g00014	AT4G02630	RLK-Pelle_RLCK-V
Niben101Scf00129g01001		
Niben101Scf00402g02004	AT1G56720	RLK-Pelle_RLCK-V
Niben101Scf02996g03008	AT5G13160 / PBS1 *	RLK-Pelle_RLCK-VII-1
Niben101Scf05081g01018	AT3G09830 / PCRK1 *	RLK-Pelle_RLCK-VII-4
Niben101Scf08898g00003	AT5G56460 / PBL16	RLK-Pelle_RLCK-VII-6
Niben101Scf03396g00005		
Niben101Scf01378g00004	AT1G07570 / PBL17	RLK-Pelle_RLCK-VII-8
Niben101Scf00229g07003	AT5G02290 / NAK *	RLK-Pelle_RLCK-VII-8
Niben101Scf05476g01001	AT2G28930 / PK1B	RLK-Pelle_RLCK-VII-8
Niben101Scf00635g04002	AT5G02290 / NAK *	RLK-Pelle_RLCK-VII-8
Niben101Scf01066g03011	AT3G59350 / MAZ	RLK-Pelle_RLCK-VIII
Niben101Scf01334g04008	AT3G62220 / CARK2	RLK-Pelle_RLCK-VIII
Niben101Scf03371g01037	AT3G26700	RLK-Pelle_RLCK-IX
Niben101Scf04617g00001		
Niben101Scf00837g00016	AT4G35230 / BSK1	RLK-Pelle_RLCK-XII
Niben101Scf02175g03013		

Table S4. List of mitogen-activated protein kinases detected in two out of three PL-MS experiments for which the NbSOBIR1-YFP-TbID fusion protein was transiently expressed as a bait in *N. benthamiana*. The first column refers to the protein identifiers according to the Niben1.0.1 version of the proteome of *N. benthamiana*. Asterisks next to the name of the *Arabidopsis* homologs in the second column indicate that the protein is co-expressed with SOBIR1 according to the data described in Chapter 3. The third column indicates the classification as protein kinases according to Zheng, ***et. al.*** [359]. The fourth column indicates the classification as mitogen-activated protein kinase according to Ichimura, ***et. al.*** [382].

Mitogen-activated protein kinases significantly enriched in two independent PL-MS experiment using NbSOBIR1-YFP-TbID			
N. benthamiana ID	*Arabidopsis* best blast hit	Classification as kinase [359]	Classification as MAPKKK [382]
Niben101Scf09063g00003	AT1G53570 / MAPKKK3 *	STE_STE11	clade A2 (RAF-like)
Niben101Scf01795g10003			
Niben101Scf03861g02013	AT3G13530 / MAPKKK7	STE_STE-PI	clade A4 (RAF-like)
Niben101Scf01587g02009			
Niben101Scf11142g00012	AT1G18160 /M3KDELTA7 *	TKL_CTR1-DRK-2	clade B3 (MEKK-like)
Niben101Scf16132g00002	AT1G08720 / EDR1 *	TKL_CTR1-DRK-2	clade B3 (MEKK-like)
Niben101Scf04396g04016			
Niben101Scf08176g00005	AT2G24360 / RAF22 *	TKL-PI-4	clade C6 (MEKK-like)
Niben101Scf06933g02001			
Niben101Scf09203g00003	AT3G22750	TKL-PI-4	clade C7 (MEKK-like)
Niben101Scf06164g00002	AT5G50000 / CBC2	TKL-PI-4	clade C7 (MEKK-like)
Niben101Scf04801g01026			
Niben101Scf14915g00001	AT3G15220	STE_STE20-YSK (MAPKKKK)	-
Niben101Scf02526g02006	AT4G10730	STE_STE20-Fray (MAPKKKK)	-
Niben101Scf08652g01010			

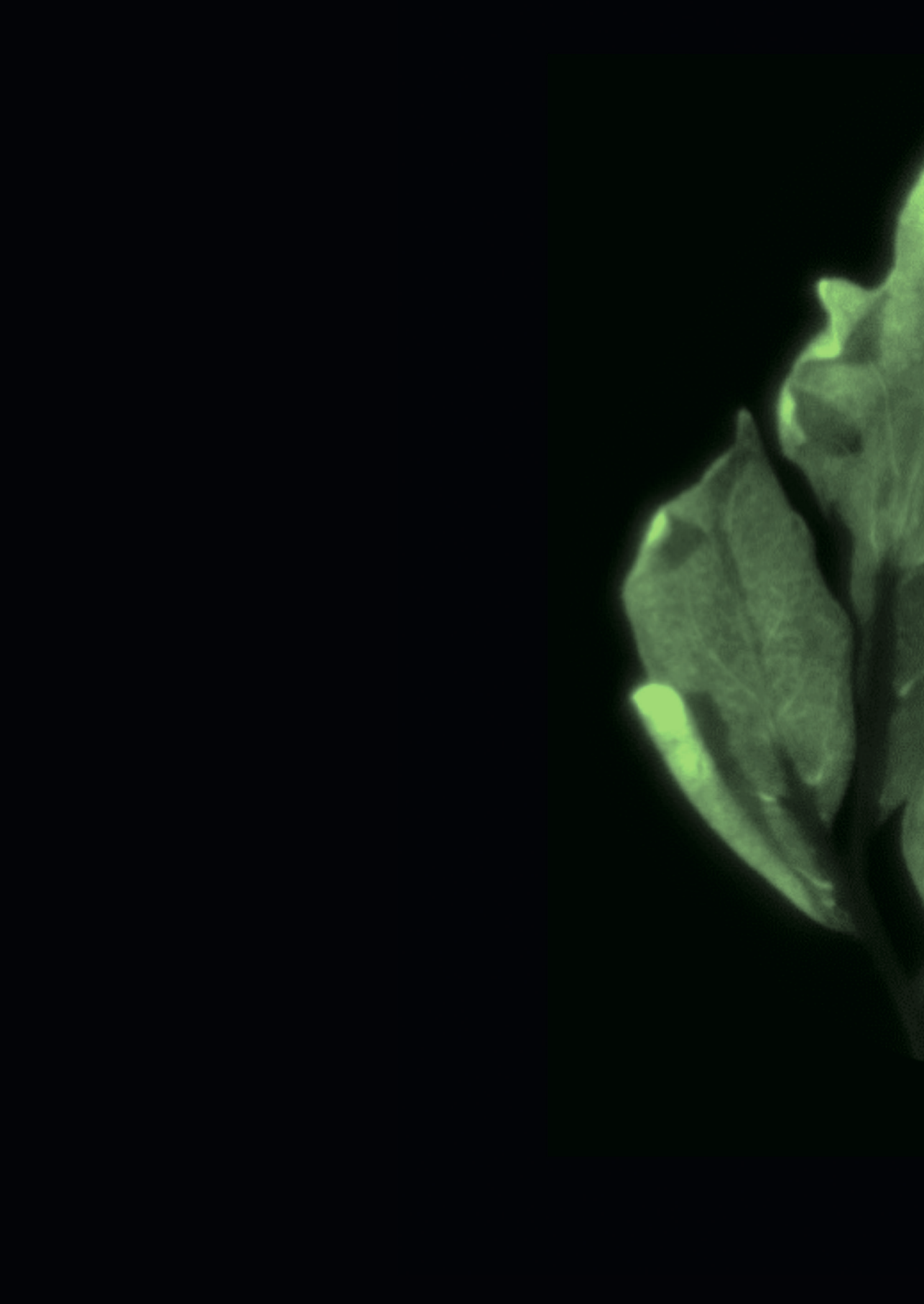

CHAPTER 6

General discussion

Cells are the functional unit of life. There are very many cells in multicellular organisms, such as in plants. Multicellularity evolved, so that cells can cooperate to achieve more than they would be able to achieve individually. The benefits associated with multicellularity include: size-related advantages, functional specialisation, and metabolic cooperation [440]. Cell death is a vital process for multicellular organisms, and plants use a series of regulatory pathways to program the end of a cell's life. Programmed cell death (PCD) is a highly regulated process that directs a cell to eliminate itself, for the overall benefit of the organism. In plants, PCD has been reported to play a role in developmental processes such as xylem formation, gametophyte maturation, degeneration of embryo suspensor cells, root development, and senescence [441]. Furthermore, PCD processes have important roles in mediating plant responses to abiotic stress and invading pathogens [183,442–447].

This General Discussion provides an overview of the major PCD pathways that have recently been described in eukaryotes and highlights the roles of these pathways in the interactions of plants with their microbial pathogens. The aim of this chapter is to place the findings described in this thesis, regarding the Cf-4/Avr4-triggered immune responses, within the broader context of the research into the molecular mechanisms of PCD in plants.

Programmed cell death as a survival mechanism

There are different ways by which a cell can commit suicide. Studies on the regulatory processes mediating PCD are dominated by the research on mammalian systems, in which several cell death programs have been described, including apoptosis, pyroptosis, necroptosis and autophagy [448–451.]

Apoptosis is a highly regulated process, because it directs the demise of the cell, while preventing the leakage of intracellular material. In mammals, at the end of this process, the cells are broken down into membrane-enclosed vesicles called "apoptotic bodies", which are rapidly phagocytosed by macrophages [452]. The degree

by which the process of apoptosis is conserved in plants when compared to mammals, is subject to a debate in the literature, and the term apoptotic-like cell death is often used [181,185,453–456]. Apoptosis is largely mediated by the activity of a class of cysteine aspartate-specific proteases, known as caspases [457,458]. Caspases are not conserved in plants, and this, together with the absence of circulating phagocytic cells, is presented as arguments against the use of the term apoptosis regarding PCD in plants. Nevertheless, caspase-like activity has been observed during plant PCD [459,460], and the genome of plants codes for caspase-like proteases, including vacuolar processing enzymes (VPEs) [461], serine-dependent subtilisin-like proteases (saspases) [462], and metacaspases which are plant proteases that are most similar to caspases [463–466]. Moreover, many of the hallmark features of apoptotic cell death are conserved in plants, including plasma membrane (PM) blebbing, cytoplasmic and nuclear shrinkage, chromatin condensation and fragmentation, and cytochrome c release [467].

Unlike what is the case for apoptosis, during which the integrity of the PM is maintained until late stages of the process, pyroptosis and necroptosis involve the release of lytic content to the extracellular space and rupture of the PM, prior to cellular demise. Pyroptosis in mammals is typically initiated upon perception of pathogens by their innate immune system. This process is mediated by a subset of caspases that cleave gasdermin family members (GSDM), of which gasdermin D (GSDMD) is one of the most extensively studied [468–470]. GSDMs typically consist of two domains, an N-terminal pore-forming domain and a C-terminal repressor domain. Upon cleavage of these proteins by caspases, the N-terminal domain oligomerizes and forms pores in the PM. As a consequence, the water entering through the pores causes cell swelling and osmotic lysis [471,472]. Pore-forming GSDMs are widespread across the tree of life [470]. Even in prokaryotes, GSDMs are processed by bacterial caspase-like proteases that remove their C-terminal inhibitory peptide and thereby activate them to oligomerize and form pores in the PM [473]. However, notably, GSMDs are absent in plants. So, pyroptosis, when defined as GSDM-mediated cell death [474], is not a process that is conserved in plants. In contrast to apoptosis and pyroptosis, necroptosis does not require caspase activity [451,475]. Necroptosis is also activated upon pathogen perception by the innate immune system of mammalian cells. However, this program requires the inhibition of apoptosis and caspase activity. As a consequence, necroptosis is generally regarded as a backup mechanism of apoptosis [476]. The key step committing a cell to undergo necroptosis is the oligomerization of the protein

kinase RECEPTOR-INTERACTING SERINE/THREONINE-PROTEIN KINASE 3 (RIPK3) and the recruitment of the related protein kinase RIPK1. The activated complex then recruits, and phosphorylates, the pseudokinase MIXED LINEAGE KINASE-LIKE (MLKL). Once activated, MLKL oligomerizes and associates with the PM causing its permeabilisation, likely through PM pore formation [475–477]. Although pyroptosis and necroptosis represent pathways mediating PCD in mammalian cells, recent discoveries on the mechanisms mediating PCD upon pathogen perception in plants (see Chapter one) shows that alteration of the integrity of the PM by pore-forming proteins is a common mechanism to trigger PCD, used by both mammalian and plant cells [127,128,478].

In addition to the classical pathways described to eventually trigger PCD in mammalian cells, autophagy, which is a conserved process in eukaryotes, also plays an important role in modulating PCD. Autophagy refers to a range of cellular processes involving the degradation and recycling of cytoplasmic material, through their delivery to the lysosome in animal cells, or to the vacuole in yeast and plant cells [448,479]. These are, in general, survival processes. However, under certain circumstances, autophagic processes can either modulate or lead to PCD [480,481]. There are three major types of autophagy: chaperone-mediated autophagy, micro-autophagy, and macro-autophagy. Chaperone-mediated autophagy involves the direct transport of cytoplasmic proteins across the lysosomal membrane and has only been documented in animal cells [482,483]. In micro-autophagy, the lysosome, or the vacuole itself, engulfs a portion of cytoplasm, either by invagination or protrusion of their membranes to surround the cytosol or organelles [484]. In plants, micro-autophagy for example mediates the degradation of anthocyanin aggregates [485], the elimination of photo-damaged chloroplasts [486,487], and is induced in root cells as a mechanism to recycle cellular components in response to starvation [488]. Macro-autophagy is the most extensively studied type of autophagy, and is usually referred to simply as autophagy [182,448,489–491]. This process is mediated by the formation of double-membraned vesicles, known as autophagosomes, that engulf cytosolic cargo and deliver it to a lytic organelle. The development of autophagosomes requires the concerted activity of different autophagy-related (ATG) proteins, many of which are also required for micro-autophagy [448,492]. In plants, the contribution of autophagy to the maintenance of cellular homeostasis becomes evident when growing autophagy-defective plants (atg mutants) under nutrient-deficient conditions. The resulting phenotypes are slow growth, enhanced senescence, lower fecundity, and reduced survival [492]. The

cellular machinery for macro-autophagy is also involved in the regulation of plant PCD, and autophagy-dependent cell death has been defined as a form of PCD that can be retarded by pharmacological or genetic inhibition of macro-autophagy [448].

The demise of plant cells is often accompanied by autolysis. This process involves the permeabilisation and rupture of the vacuolar membrane, thereby releasing hydrolases directly into the cytoplasm, causing the degradation of cytoplasmic material. As there is no phagocytosis in plants, autolysis often represents the final stages of developmental PCD [493,494], and it has also been observed as part of the immune response triggered in *Nicotiana benthamiana* against tobacco mosaic virus (TMV) [444]. This process has been proposed as a fourth type of autophagy in plant cells, termed mega-autophagy [492,495]. However, mega-autophagy does not involve the delivery of cytoplasmic material to the vacuole. Hence, this process should not be considered as a type of autophagy, and the processes involving the rupture of the vacuole and the release of its lytic content, should be described as different forms of autolysis.

PCD in plant-microbe interactions

The battle between plants and their challenging microbial pathogens is largely dictated by the interaction of the pathogens with the innate immune system of the plant. The plant immune system is governed by the ability to perceive immunogenic patterns (IPs) originating from the microbial pathogen by a series of immune receptors either present at the PM or in the cytoplasm (for an overview, see Chapter 1). These IPs can be of a different nature. They can be microbe-associated molecular patterns (MAMPs), which are conserved structural components of all microbes, including microbial pathogens. IPs can also be damage-associated molecular patterns (DAMPs), which are host-derived danger signals released in response to pathogen invasion. Furthermore, proteins released by the pathogen to enhance virulence, referred to as effectors, also represent IPs when perceived by host immune receptors. In plants, MAMPs and DAMPs are perceived by cell-surface receptors and elicit largely overlapping downstream immune responses [14]. Activation of these cell-surface receptors triggers a series of physiological responses that include the closure of the stomata, the liberation of reactive oxygen species (ROS) into the apoplast, the deposition of callose in the cell walls, and a transcriptional reprogramming favouring the activation of defence responses [25]. Effector proteins are recognised by immune receptors that are either located on the cell surface or present in the cytoplasm. Their perception is generally associated with more pronounced and sustained

immune responses. Recognition of effectors by plant immune receptors usually leads to a hypersensitive response (HR), which represents a rapid localized PCD that occurs at the point of pathogen ingress and is associated with disease resistance [44]. Together, these cell-surface and cytoplasmic immune receptors enable plants to mount a swift and effective immune response against most plant pathogens [6,18,20]. In order to colonize the host tissue, adapted pathogens deploy a series of strategies attempting to evade their detection, to suppress plant defence responses, or to manipulate the plant physiology to facilitate the infection process [15,186,496,497].

Cell death processes play a critical role in the outcome of the interaction between plants and microbial pathogens. Depending on the pathogen's lifestyle and how the PCD is carried out, the cell death can be beneficial or detrimental to the plant [181,498]. Archetypical examples of cell death processes in plant-microbe interactions include the cell death induced by necrotrophic pathogens and the HR that is triggered as a defence mechanism against biotrophic and hemibiotrophic pathogens. Compelling evidence for the relevance of apoptotic, or apoptotic-like, PCD in plants in relation to their interaction with microbial pathogens, and its interplay with autophagic PCD, comes from the interaction between necrotrophic pathogens and their hosts. For instance, *Sclerotinia sclerotiorum*, which is a necrotrophic ascomycete with a broad host range, secretes the non-selective phytotoxin oxalic-acid (OA) as an effector to promote its virulence [499]. Infection of *Arabidopsis* by *S. sclerotiorum* results in a spreading of the cell death and an infection displaying apoptotic features in the host cells, such as DNA laddering and chromatin condensation [443,500]. However, inoculation of an OA-deficient mutant onto *Arabidopsis* results in localized cell death and restriction of the mycelial growth, which is a situation reminiscent of the HR observed in incompatible interactions of plants with biotrophic pathogens [442]. This incompatible interaction between *Arabidopsis* and an OA-deficient mutant of *S. sclerotiorum* displays autophagic features in the host cells, including the production of autophagosomes [501]. Additionally, the expression of the antiapoptotic *CELL DEATH ABNORMALITY-9* (*CED-9*) gene from *C. elegans* in *Arabidopsis* results in host resistance and a suppression of the spreading necrosis after inoculation with *S. sclerotiorum* [445], without affecting the localized cell death that is triggered upon inoculation with an OA-deficient mutant [501]. Conversely, the use of *Arabidopsis* autophagy-defective mutants, or tomato leaves that were pre-treated with chemical inhibitors of autophagy, restored the pathogenicity of the OA-deficient mutant and had no effect on wild type *S. sclerotiorum* infection [501]. In general, the expression

of anti-apoptotic genes in plants tends to confer resistance to infection by necrotrophic fungi [445,502,503], while autophagy-defective plants show spreading necrotic lesions and enhanced susceptibility upon their inoculation with necrotrophic fungi [504–506]. Other necrotrophic fungal pathogens deploy host-specific toxins to hijack host defence mechanisms, for example activating host immune receptors to promote their virulence [507]. The fungal pathogen *Cochliobolus victoriae*, causal agent of Victoria blight on oat (*Avena sativa*), produces the host-specific toxin victorin to induce a type of PCD that exhibits several apoptotic hallmarks [183,508–511]. Susceptibility to Victoria blight disease is conferred by the dominant *VICTORIA BLIGHT* (*Vb*) gene. Interestingly, the *Vb* gene is proposed to be the same as the *PUCCINIA CORONATE-2* (*Pc2*) gene, that confers resistance to the biotrophic fungal pathogen *Puccinia coronate* [512–514]. This is further supported by research on *Arabidopsis* and bean (*Phaseolus vulgaris*) that identified the cytoplasmic immune receptor LOCUS ORCHESTRATING VICTORIN EFFECTS-1 (LOV1) as the determinant of the sensitivity to victorin [446,515–517]. These observations exemplify that a strict control of cell death is crucial, with PCD having different outcomes depending on which organism, either the host or the invading pathogen, is dictating the process.

Unlike the clear trends observed in the interaction between plants and necrotrophic pathogens, autophagy plays both a positive and a negative role in modulating the PCD occurring upon infection of plants by biotrophic and hemibiotrophic pathogens. Autophagy is for example required to restrict the cell death to the infection sites in plants mounting an HR in response to infection by the pathogenic bacterium *Pseudomonas syringae* pv. *tomato* DC3000 and TMV [518–520]. Conversely, leaves of *Arabidopsis* and *N. benthamiana* silenced or knocked-out in *ATG* genes display spreading necrosis upon activation of several immune receptors perceiving effector proteins at the PM or in the cytoplasm [518]. Furthermore, autophagy negatively regulates *Arabidopsis* cell death and suppresses resistance to infection by the obligate biotrophic powdery mildew pathogens *Golovinomyces cichoracearum* and *Erysiphe cruciferarum* [505,521]. In contrast, *Arabidopsis* mutants deficient in autophagy show a reduced HR upon recognition of the effector protein Avr4RPS4 produced by *P. syringae* [522]. This effector is recognised by the pair of cytoplasmic immune receptors RESISTANCE TO RALSTONIA SOLANACEARUM 1 (RRS1) and RESISTANCE TO PSEUDOMONAS SYRINGAE 4 (RPS4), which cooperate by forming a receptor complex [121]. The contribution of autophagy to the HR seems to depend on the type of immune receptor that is activated. Cytoplasmic immune receptors are nucleotide-binding

domain and leucine-rich repeat-containing proteins (NLRs). NLRs perceiving pathogen effectors can be broadly classified according to their N-terminal domains into TOLL/INTERLEUKIN-1 (IL1) receptor-like (TIR)-type NLRs (TNLs) and coiled-coil (CC)-type NLRs (CNLs) [523]. In Arabidopsis, the HR triggered upon activation of the TNLs RPS4 and RECOGNITION OF PERONOSPORA PARASITICA 1 (RPP1) requires the activity of *ATG* genes, while these are dispensable for the HR triggered by the CNLs RESISTANCE TO P. SYRINGAE PV MACULICOLA 1 (RPM1) and RESISTANT TO P. SYRINGAE 2 (RPS2) [522]. In *N. benthamiana*, the HR and resistance against TMV mediated by the TNL resistance protein N are enhanced as a result of the constitutive activation of autophagy, whereas the disruption of autophagy results in more TMV accumulation [518,524].

Autophagy refers to more than the non-selective bulk recycling of cytoplasmic components. Autophagy can operate in a very specific manner, through mechanisms involving the recognition of autophagy substrates by dedicated receptors that drive the selective engagement of the autophagy machinery [525]. Selective autophagy in plants allows for the removal of specific proteins, protein aggregates, organelles, and viruses [448,492]. Some pathogens have evolved mechanisms to modulate these autophagic processes for their own benefit. For instance, the bacterial pathogen *Ralstonia solanacearum* secretes the effector AWR5, named like this after a conserved alanine-tryptophan-arginine triad, to activate autophagy with the likely aim to contribute to pathogenicity by promoting nutrient availability during the necrotrophic phase of the bacterial infection [526]. Also, the oomycete pathogen *Phytophthora infestans* secretes the effector protein PexRD54, referring to *P. infestans* extracellular (Pex) proteins containing an RXLR-DEER motif (PexRD), to interfere with the host's autophagy, thereby stimulating the formation of autophagosomes [527,528]. This process is proposed to outcompete selective autophagy pathways that would otherwise contribute to the plant's defence responses, or to activate selective autophagy to eliminate defence-related compounds. In addition, the pathogen could also benefit from the redistribution of nutrients that are released when the cellular material is broken down via autophagy [527,528].

Recent breakthrough studies have shown that the activation of plant NLRs leads to the formation of large wheel-like structures, referred to as resistosomes [104,105,109,127]. This name highlights their structural similarities to mammalian apoptosomes and inflammasomes, which are macromolecular complexes that play central roles in

apoptosis and pyroptosis, respectively [478]. The activation of these resistosomes results in the formation of pores in the PM, resembling the mechanisms by which pyroptosis and necroptosis cause the death of animal cells [127,128,153,529]. The first resistosome described in plants corresponds to the activated form of the *Arabidopsis* CNL HOPZ-ACTIVATED RESISTANCE 1 (ZAR1) [127]. ZAR1 is part of a pentameric resistosome that is formed upon perception of the effector protein AvrAC, produced by the plant-pathogenic bacterium *Xanthomonas campestris* pv. *campestris* [118]. In the ZAR1 resistosome, the N-terminal helices of the five protomers form a funnel-shaped structure to create a pore in the PM, which is crucial to induce HR and bacterial resistance [127,128]. Unlike CNLs, the activation of TNLs results in the formation of tetrameric resistosomes that display multiple enzymatic activities and produce signalling molecules. For instance, in *Arabidopsis*, perception of the effector protein *ARABIDOPSIS THALIANA* RECOGNISED 1 (ATR1), produced by the oomycete *Hyaloperonospora arabidopsidis*, triggers the oligomerization of RPP1 into an active TNL resistosome [106,107,132,133]. Active TNLs produce signalling molecules, resulting in the activation of a small set of helper NLRs that are characterized by having a CC domain similar to the resistance protein RESISTANCE TO POWDERY MILDEW 8 (RPW8), and that are referred to as RNLs (or CC_R-type NLR) [42,530]. In *Arabidopsis* the N REQUIREMENT GENE 1 (NRG1) and ACTIVATED DISEASE RESISTANCE 1 (ADR1) subfamilies of RNLs are required as helper NLRs for TNL-mediated immunity, while in *N. benthamiana* TNLs signal primarily through NRG1 [142,145–147]. The transduction of the signals from TNLs to RNLs is mediated by a small family of lipase-like proteins comprising ENHANCED DISEASE SUSCEPTIBILITY 1 (EDS1), SENESCENCE-ASSOCIATED GENE 101 (SAG101), and PHYTOALEXIN-DEFICIENT 4 (PAD4) [148]. EDS1 forms mutually exclusive heterodimers with SAG101 or PAD4, which are required for the activation of NRG1s and ADR1s, respectively [148–150]. Similar to CNLs, the activation of RNLs results in their oligomerization into pentameric resistosomes and the formation of Ca^{2+}-permeable channels to induce an HR [153,391]. It is not yet known which mechanism mediates plant cell death after the induction of the Ca^{2+} influx into the cytoplasm. Resistance and HR upon activation of NLRs can be uncoupled, suggesting the existence of additional signalling requirements beyond the formation of pores in the PM and an increase in the cytoplasmic Ca^{2+} concentration [531–534]. Evidence suggests a role of the vacuole in regulating NLR-mediated cell death. For instance, autophagic components are necessary for the cell death mediated by the TNLs RRS1/RPS4 and RPP1 [522], and activation of the TNL N is followed by the disruption of the vacuole in a process that depends on the vacuolar protease VACUOLAR

PROCESSING ENZYME 1 (VPE1) [444]. Additionally, the activation of the CNLs RPM1 and RPS2 induces the fusion of the central vacuole with the PM, resulting in the discharge of vacuolar proteins with antibacterial and cell death induction activity into the apoplast [460].

Dissection of the cell-surface receptor complex triggering PCD

The activation of plant cell-surface receptors mediating immune responses is typically associated with the perception of MAMPs and DAMPs, and the resulting activation of defence responses, without triggering an HR [19,535]. However, a subset of cell-surface receptors triggers an HR upon perception of their corresponding IPs [18]. The tomato resistance protein Cf-4 is a representative of this group. The work described in this thesis focuses on the study of the early signalling mechanisms underlying the Cf-4-triggered immune responses leading to resistance. Cf-4 is a cell-surface receptor that confers resistance to strains of the hemibiotrophic fungal pathogen *Cladosporium fulvum* (Syn. *Fulvia fulva*), expressing the effector protein Avr4 [40,67,68]. This effector binds to chitin, and is secreted by the pathogen to contribute to virulence by protecting the fungal hyphae against degradation by host chitinases that are released into the tomato apoplast during infection [70,71,536].

Red light imaging as a proxy for monitoring cell death in green plant tissue

Most of the previous research on the signalling mechanisms downstream of Cf-4 was performed by evaluating the intensity of the HR by a visual assessment of the necrotic lesions that are formed on the leaves after Cf-4 activation [40,66,68,76,77,102,165,201,253,537]. This approach hinders the evaluation of the contribution of regulatory components that modulate the intensity of the HR. For this reason, in Chapter 2, we propose a new method for visualisation and quantification of the intensity of cell death in green plant tissues [235].

The actual moment when cells die is difficult to define. Cells undergoing PCD are engaged in a process that is reversible until the first irreversible point-of-no-return is crossed. The complete loss of PM integrity is a generally accepted operational definition of cell death in plant biology [467,538]. This is a point-of-no-return, as cells cannot maintain homeostasis in a space that is not physically defined. Vitality dyes, such as fluorescein diacetate (FDA) and propidium iodide (PI), are often used in combination with fluorescence microscopy to distinguish between live and dead cells and to quantify their relative proportions [128,539,540]. In viable cells with an active

metabolism, intracellular esterases hydrolyse FDA producing the green fluorescent compound fluorescein. In dead cells with a permeabilised PM, PI can enter the cell and binds to the DNA present in the nucleus, resulting in red fluorescence. The most widely used method to visualise cell death in plant tissues is staining using trypan blue (TB) [541,542]. TB selectively stains cells that have a PM with a compromised integrity, resulting in a blue colouration. However, this method requires the use of harmful chemicals, such as phenol, and provides a qualitative rather than a quantitative assessment of cell death. A quantitative alternative for assessing the cell death intensity in plant tissue is the measurement of ion leakage [543]. When a cell loses the integrity of the PM, electrolytes leak out of the cell and this process can be monitored by measuring the electrolytic conductivity of the water in which leaf discs are incubated. Although it is a versatile method, it is labour-intensive and the destructive nature limits its applicability.

The newly proposed method (Chapter 2) is not based on assessing the integrity of the PM but exploits the increase in red light fluorescence of plant tissue undergoing cell death. We propose that the increased fluorescence is caused by the disassembly of the thylakoid membranes in the chloroplast and the resulting halt of the electron flow, causing the release of the excitation energy as fluorescence. The intensity of the red light signal shows a dose-dependent response upon infiltration of different cell death-inducing agents and correlates with the severity of the visual signs of cell death, such as the collapse of leaf tissue. Moreover, this non-destructive approach allows for monitoring the development of necrotic lesions over time in inoculation assays. However, the presented validation of the method does not further explore whether the emission of red light fluorescence occurs before or after the disruption of the PM, which is the generally accepted moment of plant cell death. The moment when red light fluorescence starts to be emitted could depend on the particular trigger of cell death. The increased emission of red light fluorescence is likely a post-mortem process in the case of cell death induced by NECROSIS- AND ETHYLENE-INDUCING PROTEIN 1 (NEP1)-like proteins (NLPs) that are produced by several bacterial, fungal and oomycete plant pathogens [544]. NLPs target the outer leaflet of the PM and exert their cytolytic activity by eventually disrupting the integrity of the PM [545,546]. In contrast, the increased emission of red light fluorescence may be a pre-mortem process in the case of cell death triggered by the activation of NLRs. The activation of the CNL ZAR1 results in damage to the chloroplasts prior to the rupture of the cell [128], and the activation of the TNL RPS4 induces chloroplast

degradation via autophagy [547]. Further research is needed to assess whether the detected increase in red light fluorescence represents a point-of-no-return in the chain of events leading to cell death, or whether there are physiologically relevant processes in which this could be a reversible process. Despite this uncertainty, since its publication as a method [235], red light imaging has been used by various research groups to visualise and quantify the intensity of the cell death triggered by cell death-inducing proteins from necrotrophic pathogens [546,548], activated cell-surface receptors [549–551] and activated NLRs [392,552], and in inoculation assays with fungal [553,554] and oomycete pathogens [555].

Main aspects of the immune signalling cascade downstream of Cf-4 in *N. benthamiana*

Cell-surface receptors can be classified into receptor-like kinases (RLKs) and receptor-like proteins (RLPs). RLKs are single-pass transmembrane proteins with an extracellular domain for recognising apoplastic IPs and a cytoplasmic kinase domain for the initiation of downstream signalling. RLPs lack such a cytoplasmic signalling domain and form bi-molecular receptor complexes with adaptor kinases to activate cytoplasmic signalling cascades [61]. Different extracellular domains can recognise different types of IPs. Most RLKs and RLPs with leucine-rich repeats (LRRs) in their extracellular domains recognise proteinaceous IPs. LRR-RLKs and LRR-RLPs make up the largest groups of cell-surface receptors and will be further referred to simply as RLKs and RLPs, respectively [34,35]. One of the best characterised RLKs mediating plant immune responses is FLAGELLIN SENSING 2 (FLS2), which has been extensively studied, particularly in *Arabidopsis*. FLS2 recognises the flagellin epitope flg22, which is a MAMP derived from the bacterial flagellum [36,50]. The tomato immune receptor Cf-4, instead, is an RLP. Cf-4 constitutively interacts with the RLK SUPPRESSOR OF BIR1-1 (SOBIR1), thereby forming a bi-molecular receptor that, unlike FLS2, triggers an HR upon its activation [66]. This constitutive interaction with SOBIR1 appears to be a general feature of all RLPs mediating immune responses and these RLPs are thereby expected to activate similar downstream immune signalling events [18,20,61].

A common step upon recognition of IPs by both RLKs and constitutive RLP/SOBIR1 receptor complexes is the recruitment of the RLK BRASSINOSTEROID-INSENSITIVE 1 (BRI1)-ASSOCIATED KINASE (BAK1) and its closely related paralogs [58,209] (Figure 1). Indeed, both FLS2 and Cf-4/SOBIR1 recruit these regulatory RLKs, starting a series

of phosphorylation events that eventually result in the activation of the receptor complexes [51,52,54,57,76]. Subsequent cytoplasmic signalling downstream of all cell-surface receptor complexes that have been characterised up till now is mediated by receptor-like cytoplasmic kinases (RLCKs) [25,112,154]. RLCKs form a large family of protein kinases, which are classified into 17 different groups [374]. RLCKs belonging to group VII (RLCK-VII) have prominent roles downstream of cell-surface receptors [113,549,556]. The RLCK-VII members are further classified into nine subgroups, exhibiting a significant functional redundancy downstream of different RLKs [113,549,556]. One well-studied representative of the RLCK-VII group is BOTRYTIS-INDUCED KINASE 1 (BIK1), which constitutively interacts with FLS2 and BAK1. Upon perception of flg22, BIK1 undergoes a rapid phosphorylation and subsequent dissociation from the receptor complex [115,157]. Activated BIK1 then phosphorylates the PM-associated RESPIRATORY BURST OXIDASE HOMOLOG D (RBOHD) and CYCLIC NUCLEOTIDE-GATED CHANNEL 4 (CNGC4) proteins, resulting in a swift production of ROS in the apoplast and an increase in the concentration of cytosolic Ca^{2+}, respectively [159,557]. Next, mitogen-activated protein kinases (MAPKs) and calcium-dependent protein kinases (CDPKs) act as signal transducers, resulting in a massive transcriptional reprogramming to activate further downstream defence responses [25,160,161].

Similar to FLS2, the activation of Cf-4/SOBIR1 in *N. benthamiana* plants also induces the production of apoplastic ROS through the activation of RBOHB, which is the *N. benthamiana* ortholog of *Arabidopsis* RBOHD [278] (Figure 1). However, it has been observed that recognition of flg22 and Avr4 elicits clearly distinguishable ROS burst profiles (Chapter 3). While the perception of flg22 by FLS2 triggers a monophasic burst of ROS, the perception of Avr4 by the Cf-4/SOBIR1 complex produces a more prolonged and biphasic profile of the ROS burst. A similar ROS burst profile has been described for *Cf-9*-transgenic tobacco (*Nicotiana tabacum*) plants that were challenged with the Avr9 effector [274]. Cf-9 is a tomato RLP that has a very similar overall structure as Cf-4 and triggers an HR upon recognition of the secreted effector Avr9 from *C. fulvum* [212]. Similar to what has been reported for Cf-9, virus-induced gene silencing (VIGS) experiments in *N. benthamiana* plants revealed that the activity of RBOHB is not only dispensable for the onset of the Cf-4-triggered HR, but even has a negative regulatory effect, as the intensity of the HR increases upon silencing of *RBOHB* (Chapter 3) [558].

The development of an HR is also associated with the generation of ROS from the chloroplasts [251,559] (Figure 1). The staining of leaves with 3,3′-Diaminobenzidine (DAB), which allows for intracellular ROS detection [247,282], revealed that the perception of Avr4, rather than flg22, triggers a ROS production that is independent of the apoplastic ROS burst generated by RBOHB (Chapter 3). These findings align with previous observations in tobacco, showing that the activation of MAPK signalling triggers a light-dependent burst of ROS from the chloroplasts and a subsequent HR-like cell death [247,560]. Our results indicate that the ROS burst generated by RBOHB, and the HR represent different branches of the immune signalling cascade that is activated downstream of the Cf-4/SOBIR1 complex.

The identification of downstream signalling components associated with RLP/SOBIR1 complexes has proven to be difficult because of technical limitations associated with detecting weak and transient protein-protein interactions with membrane-bound proteins. Previous attempts using affinity purification, followed by mass spectrometry did not significantly detect any RLCK interacting with the kinase domain of SOBIR1 in *N. benthamiana* [102]. To overcome these limitations, we implemented the use of TurboID-based proximity-dependent labelling (PL) for the dissection of the Cf-4/SOBIR1 receptor complex in *N. benthamiana* (Chapter 4). This approach involves fusing the PM-associated proteins of interest to TurboID, which is a promiscuous biotin ligase, enabling the biotinylation of endogenous proteins that are in close-proximity to the TurboID-tagged bait protein. The biotinylated proteins are then purified using streptavidin-coated beads [338,341]. The application of PL, using a TurboID-tagged version of SOBIR1, followed by the identification of the biotinylated proteins by mass spectrometry analysis (PL-MS), revealed a set of 81 proteins that was consistently detected to be in close-proximity to the TurboID-tagged SOBIR1 fusion protein, across multiple experiments (Chapter 5). This proximal proteome of SOBIR1 in *Cf-4*-transgenic *N. benthamiana* plants includes proteins that are functionally related to the Cf-4/SOBIR1 complex, such as RBOHB and Cf-4 itself. Moreover, it includes five RLCKs, with two of them belonging to the RLCK-IV group, two belonging to the RLCK-VII group, and one belonging to the RLCK-VIII group. The detected RLCK-VIIs belong to the subgroups -6 and -8. Interestingly, it has been found that higher-order mutants of the RLCKs belonging to these subgroups in *Cf-4*-transgenic *N. benthamiana* plants display an impaired ROS burst production upon recognition of flg22 and Avr4 [549]. While *rlck-VII-8* knock-out lines show a reduction of the overall biphasic profile of the Avr4-triggered ROS burst,

rlck-VII-6 knock-out lines seem to be particularly compromised in the ROS burst belonging to the second phase that is produced by RBOHB upon perception of Avr4. Among the other detected RLCKs, the one belonging to RLCK-VIII is a homolog of the tomato RLCK PTO-INTERACTING 1 (PTI1), which is required for the flg22-induced ROS burst [375].

The immune responses elicited by cell-surface receptors and NLRs have long been considered to be separate pathways [6,19]. Recently, emerging evidence shows that immune signalling by cell-surface receptors and NLRs are interconnected [9,10,162,163]. For example, the activation of cell-surface receptors is required for the HR triggered by multiple NLRs. In addition, EDS1 complexes and their associated RNLs are required for many immune responses mediated by RLKs and RLPs in *Arabidopsis* [162,163]. The emerging model is that immune signalling by cell-surface receptors and NLRs mutually potentiate each other by enhancing transcription of their core components. Consistent with these observations, our gene co-expression network analysis of publicly available *Arabidopsis* microarray data revealed that genes encoding downstream signalling components of cell-surface receptors and NLRs are part of the same transcriptional cluster in the context of the *Arabidopsis* co-expression landscape (Chapter 3). In *N. benthamiana*, EDS1-containing complexes are neither required for the Avr4- or flg22-triggered apoplastic ROS burst, nor for the Avr4-triggered HR (Chapter 3). Recently, the Cf-4-triggered HR was shown to be largely mediated by the CNL NB-LRR REQUIRED FOR HR-ASSOCIATED CELL DEATH-3 (NRC3) [165,201] (Figure 1). NRCs form a clade of helper NLRs that are required for many sensor CNLs in solanaceous plants [43]. It is not yet known how the signal originating from sensor CNLs is transduced to helper NRCs. An activation-and-release working model has been proposed, in which the IP-triggered activation of a sensor CNL leads to conformational changes that allow them to signal to NRCs, possibly via transient interactions [151,152]. The activated NRCs then oligomerise into pore-forming resistosomes, triggering cell death.

Our PL-MS experiments in *N. benthamiana* revealed a proximal proteome of SOBIR1 that also includes a set of novel candidates for signalling components downstream of RLP/SOBIR1-containing receptor complexes. Interestingly, the products of genes that we identified as being co-expressed with *SOBIR1* in our expression analysis of the *Arabidopsis* microarray data (Chapter 3), are overrepresented in the detected proximal proteome of SOBIR1 in *N. benthamiana* (Chapter 5). From the 57 *Arabi-*

dopsis homologs of the proteins detected to be in close-proximity to SOBIR1 in *N. benthamiana*, the genes encoding 11 of them are also co-expressed with *SOBIR1* in our gene co-expression network analysis of the *Arabidopsis* microarray data (hypergeometric p-value = 4e-05). These proteins include RLCKs, MAP3Ks, a phosphatase, a CDPK, and RBOHB. However, some expected signalling components and interacting proteins are missing from the detected proximal proteome of the Cf-4/SOBIR1 receptor complex. Our application of PL-MS in *N. benthamiana* using TurboID-tagged versions of SOBIR1 and Cf-4 for example failed to detect the recruitment of BAK1 homologs to the Cf-4/SOBIR1 complex upon treatment with Avr4. Furthermore, the detected proximal proteome of SOBIR1 did not include an endogenous RLP other than Cf-4, as being expressed by the *Cf-4*-transgene in *N. benthamiana:Cf-4 sobir1(-like)*. Consequently, we were unable to draw conclusions regarding the absence of any sensor CNL in the proximal proteome of SOBIR1 that could connect Cf-4/SOBIR1/BAK1 complex formation and signalling with the activation of downstream NRC3-dependent cell death. It is likely that this lack of resolution is a consequence of the relatively high levels of protein accumulation achieved in *N. benthamiana* upon transient expression of the TurboID-tagged fusion proteins employing the constitutive 35S promoter. To enhance the resolution, future PL-MS experiments should either use the endogenous promoters of the genes encoding the bait proteins or should express the TurboID-tagged bait proteins in alternative solanaceous plants, such as tomato and potato (*Solanum tuberosum*), which show lower levels of protein accumulation upon their agroinfiltration.

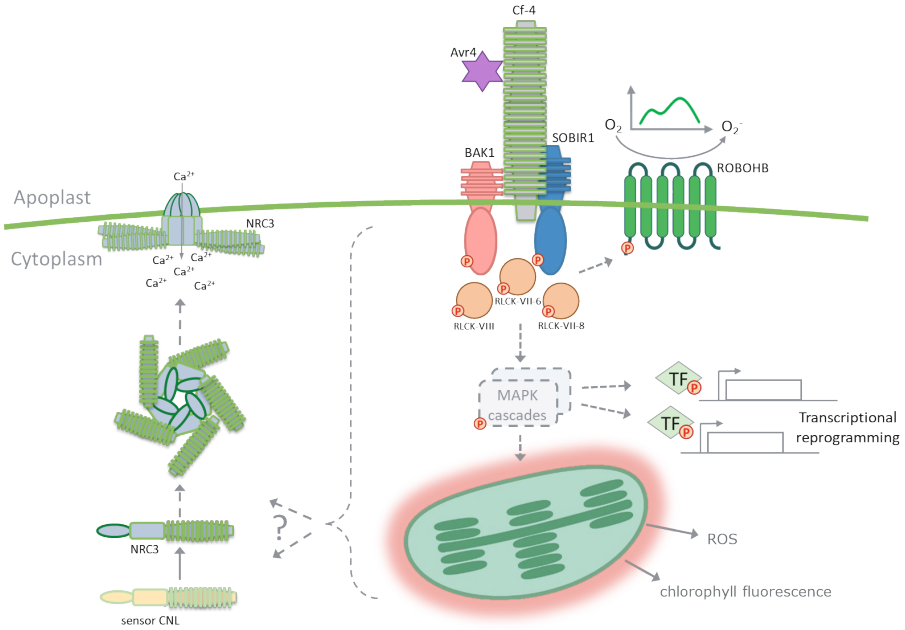

Figure 1. Main signalling events downstream of the Cf-4/SOBIR1 receptor complex in *N. benthamiana*. Perception of the *C. fulvum* effector Avr4 by the Cf-4/SOBIR1 receptor complex triggers the recruitment of BAK1. RLCKs serve as signal transducers for cell-surface receptors, and evidence suggests that members of the RLCK-VIII, RLCK-VII-6, and RLCK-VII-8 groups are required for the Avr4-triggered apoplastic ROS burst. Perception of Avr4 also triggers the activation of MAPK cascades, acting as downstream signal transducers, resulting in transcriptional reprogramming of the cell and the release of ROS from the chloroplast, with an associated HR. The Avr4-triggered HR has recently been found to be NRC3-dependent, possibly through the formation of an NRC3 resistosome, involving yet uncharacterised sensor-CNLs. TF, transcription factor; P in circle, phosphorylation.

Final remarks

PCD is a complex process with multiple dimensions. In the context of the interactions of plants with microbial pathogens, the morphological characteristics of the necrotic lesions, the underlying biochemical mechanisms triggering the process, and the ultimate outcome of the interaction, can vary in different manners depending on the context. The consequences of PCD activation, whether it leads to resistance or susceptibility allowing disease development, are intricately tied to the lifestyle of the pathogen involved. Moreover, unlike what is the case of the clear and defined molecular interactions we use to study the processes related to

PCD, the interactions actually taking place in nature involve a cross-talk between pathways that are activated by different IPs, originating from different microbial pathogens, and are also influenced by different abiotic stress conditions. Despite these complexities, plant immune receptors play significant roles in shaping the outcomes of these interactions.

Current scientific and technological limitations hinder the rational design of immune receptors to recognise specific IPs. As a result, we rely on exploring the existing natural biodiversity to identify immune receptors that can be deployed for crop protection. A profound understanding of the molecular mechanisms regulating plant immune receptors and the diverse physiological processes that they activate is crucial for their successful transfer and effective implementation in crop protection strategies. The work described in this thesis is the result from curiosity driven research into the early signalling mechanisms of the cell-surface receptor Cf-4 in the model solanaceous plant *N. benthamiana*. The work has resulted into a novel method for the assessment and quantification of cell death in green plant tissues, novel insights into the downstream immune signalling cascade that is activated, and a list of candidate proteins playing various roles in the functioning of the Cf-4/SOBIR1 receptor complex.

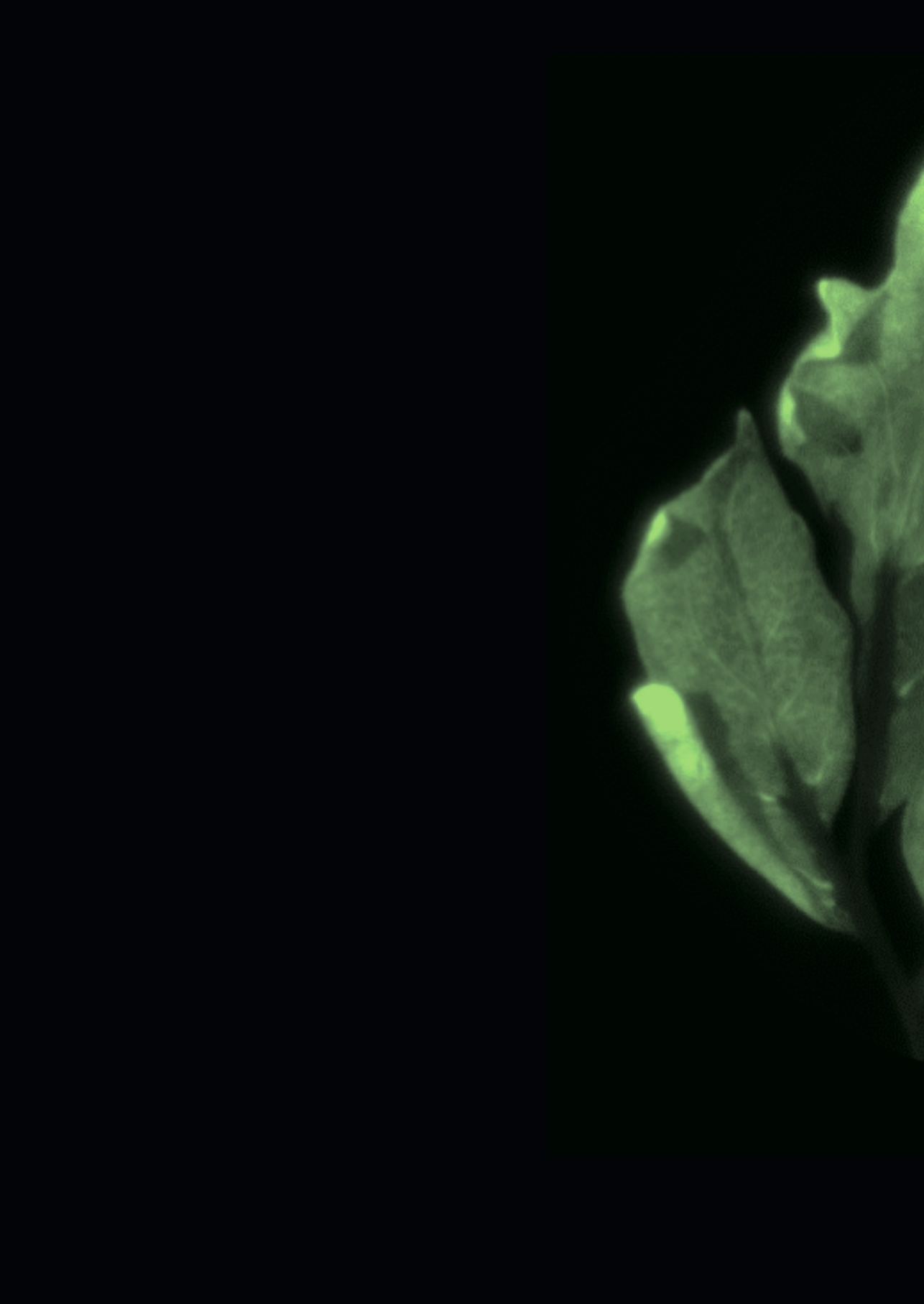

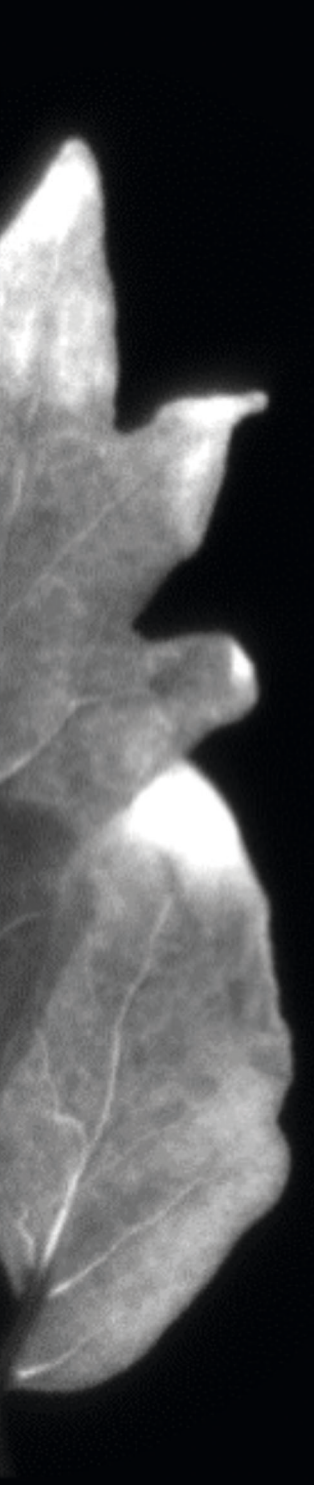

REFERENCES VOL

1. Savary, S. *et al.* The global burden of pathogens and pests on major food crops. *Nat. Ecol. Evol.* **3**, 430–439 (2019).
2. Lamichhane, J. R., Dachbrodt-Saaydeh, S., Kudsk, P. & Messéan, A. Conventional pesticides in agriculture: benefits versus risks. *Plant Dis.* **100**, 10–24 (2016).
3. Berger, S., El Chazli, Y., Babu, A. F. & Coste, A. T. Azole resistance in *Aspergillus fumigatus*: a consequence of antifungal use in agriculture? *Front. Microbiol.* **8**, 1–6 (2017).
4. Arya, G. C., Sarkar, S., Manasherova, E., Aharoni, A. & Cohen, H. The Plant Cuticle: an ancient guardian barrier set against long-standing rivals. *Front. Plant Sci.* **12**, (2021).
5. You, Y. & Kan, J. A. L. Bitter and sweet make tomato hard to (b)eat. *New Phytol.* **230**, 90–100 (2021).
6. Dodds, P. N. & Rathjen, J. P. Plant immunity: towards an integrated view of plant–pathogen interactions. *Nat. Rev. Genet.* **11**, 539–548 (2010).
7. Han, G. Origin and evolution of the plant immune system. *New Phytol.* **222**, 70–83 (2019).
8. Bernoux, M., Zetzsche, H. & Stuttmann, J. Connecting the dots between cell surface- and intracellular-triggered immune pathways in plants. *Curr. Opin. Plant Biol.* **69**, 102276 (2022).
9. Ngou, B. P. M., Ahn, H. K., Ding, P. & Jones, J. D. G. Mutual potentiation of plant immunity by cell-surface and intracellular receptors. *Nature* **592**, 110–115 (2021).
10. Yuan, M. *et al.* Pattern-recognition receptors are required for NLR-mediated plant immunity. *Nature* **592**, 105–109 (2021).
11. Felix, G., Duran, J. D., Volko, S. & Boller, T. Plants have a sensitive perception system for the most conserved domain of bacterial flagellin. *Plant J.* **18**, 265–276 (1999).
12. Felix, G., Regenass, M. & Boller, T. Specific perception of subnanomolar concentrations of chitin fragments by tomato cells: induction of extracellular alkalinization, changes in protein phosphorylation, and establishment of a refractory state. *Plant J.* **4**, 307–316 (1993).
13. Shibuya, N., Kaku, H., Kuchitsu, K. & Maliarik, M. J. Identification of a novel high-affinity binding site for N -acetylchitooligosaccharide elicitor in the membrane fraction from suspension-cultured rice cells. *FEBS Lett.* **329**, 75–78 (1993).
14. De Lorenzo, G. & Cervone, F. Plant immunity by damage-associated molecular patterns (DAMPs). *Essays Biochem.* **66**, 459–469 (2022).
15. Uhse, S. & Djamei, A. Effectors of plant-colonizing fungi and beyond. *PLOS Pathog.* **14**, e1006992 (2018).
16. Win, J. *et al.* Effector biology of plant-associated organisms: concepts and perspectives. *Cold Spring Harb. Symp. Quant. Biol.* **77**, 235–247 (2012).
17. Snelders, N. C. *et al.* Microbiome manipulation by a soil-borne fungal plant pathogen using effector proteins. *Nat. Plants* **6**, (2020).
18. van der Burgh, A. M. & Joosten, M. H. A. J. Plant Immunity: thinking outside and inside the box. *Trends Plant Sci.* **24**, 587–601 (2019).
19. Jones, J. D. G. & Dangl, J. L. The plant immune system. *Nature* **444**, 323–329 (2006).

20. Ngou, B. P. M., Ding, P. & Jones, J. D. G. Thirty years of resistance: zig-zag through the plant immune system. *Plant Cell* **34**, 1447–1478 (2022).

21. Dangl, J. L. & Jones, J. D. G. Plant pathogens and integrated defence responses to infection. *Nature* **411**, 826–833 (2001).

22. Kourelis, J. & Van Der Hoorn, R. A. L. Defended to the nines: 25 years of resistance gene cloning identifies nine mechanisms for R protein function. *Plant Cell* **30**, 285–299 (2018).

23. Van Der Hoorn, R. A. L., De Wit, P. J. G. M. & Joosten, M. H. A. J. Balancing selection favors guarding resistance proteins. *Trends Plant Sci.* **7**, 67–71 (2002).

24. Thomma, B. P. H. J., Nürnberger, T. & Joosten, M. H. A. J. Of PAMPs and effectors: The blurred PTI-ETI dichotomy. *Plant Cell* **23**, 4–15 (2011).

25. DeFalco, T. A. & Zipfel, C. Molecular mechanisms of early plant pattern-triggered immune signaling. *Mol. Cell* **81**, 3449–3467 (2021).

26. Gust, A. A., Willmann, R., Desaki, Y., Grabherr, H. M. & Nürnberger, T. Plant LysM proteins: modules mediating symbiosis and immunity. *Trends Plant Sci.* **17**, 495–502 (2012).

27. Zipfel, C. & Oldroyd, G. E. D. Plant signalling in symbiosis and immunity. *Nature* **543**, 328–336 (2017).

28. Choi, J. *et al.* Identification of a plant receptor for extracellular ATP. *Science.* **343**, 290–294 (2014).

29. Ranf, S. *et al.* A lectin S-domain receptor kinase mediates lipopolysaccharide sensing in *Arabidopsis thaliana*. *Nat. Immunol.* **16**, 426–433 (2015).

30. Catanzariti, A., Lim, G. T. T. & Jones, D. A. The tomato I-3 gene: a novel gene for resistance to *Fusarium* wilt disease. *New Phytol.* **207**, 106–118 (2015).

31. Kato, H. *et al.* Recognition of pathogen-derived sphingolipids in *Arabidopsis*. *Science.* **376**, 857–860 (2022).

32. Brutus, A., Sicilia, F., Macone, A., Cervone, F. & De Lorenzo, G. A domain swap approach reveals a role of the plant wall-associated kinase 1 (WAK1) as a receptor of oligogalacturonides. *Proc. Natl. Acad. Sci. U. S. A.* **107**, 9452–9457 (2010).

33. Kohorn, B. D. Cell wall-associated kinases and pectin perception. *J. Exp. Bot.* **67**, 489–494 (2016).

34. Li, L., Yu, Y., Zhou, Z. & Zhou, J. M. Plant pattern-recognition receptors controlling innate immunity. *Sci. China Life Sci.* **59**, 878–888 (2016).

35. Dievart, A., Gottin, C., Périn, C., Ranwez, V. & Chantret, N. Origin and diversity of plant receptor-like kinases. *Annu. Rev. Plant Biol.* **71**, 131–156 (2020).

36. Gómez-Gómez, L. & Boller, T. FLS2: An LRR Receptor–like kinase involved in the perception of the bacterial elicitor flagellin in *Arabidopsis*. *Mol. Cell* **5**, 1003–1011 (2000).

37. Zipfel, C. *et al.* Perception of the bacterial PAMP EF-Tu by the receptor EFR restricts *Agrobacterium*-mediated transformation. *Cell* **125**, 749–760 (2006).

38. Yamaguchi, Y., Huffaker, A., Bryan, A. C., Tax, F. E. & Ryan, C. A. PEPR2 is a second receptor for the Pep1 and Pep2 peptides and contributes to defense responses in *Arabidopsis*. *Plant Cell* **22**, 508–522 (2010).

39. Yamaguchi, Y., Pearce, G. & Ryan, C. A. The cell surface leucine-rich repeat receptor for AtPep1, an endogenous peptide elicitor in *Arabidopsis*, is functional in transgenic tobacco cells. *Proc. Natl. Acad. Sci. U. S. A.* **103**, 10104–10109 (2006).

40. Joosten, M. H. A. J. A. J., Cozijnsen, T. J. & De Wit, P. J. G. M. G. M. Host resistance to a fungal tomato pathogen lost by a single base-pair change in an avirulence gene. *Nature* **367**, 384–386 (1994).

41. Larkan, N. J. *et al.* The *Brassica napus* blackleg resistance gene LepR3 encodes a receptor-like protein triggered by the *Leptosphaeria maculans* effector AVRLM1. *New Phytol.* **197**, 595–605 (2013).

42. Collier, S. M., Hamel, L.-P. & Moffett, P. Cell death mediated by the N-terminal domains of a unique and highly conserved class of NB-LRR Protein. *Mol. Plant-Microbe Interact.* **24**, 918–931 (2011).

43. Wu, C. H. *et al.* NLR network mediates immunity to diverse plant pathogens. *Proc. Natl. Acad. Sci. U. S. A.* **114**, 8113–8118 (2017).

44. Balint-Kurti, P. The plant hypersensitive response: concepts, control and consequences. *Mol. Plant Pathol.* **20**, mpp.12821 (2019).

45. Hann, D. R. & Rathjen, J. P. Early events in the pathogenicity of Pseudomonas syringae on *Nicotiana benthamiana*. *Plant J.* **49**, 607–618 (2007).

46. Robatzek, S. *et al.* Molecular identification and characterization of the tomato flagellin receptor LeFLS2, an orthologue of *Arabidopsis* FLS2 exhibiting characteristically different perception specificities. *Plant Mol. Biol.* **64**, 539–547 (2007).

47. Takai, R., Isogai, A., Takayama, S. & Che, F.-S. Analysis of flagellin perception mediated by flg22 receptor OsFLS2 in rice. *Mol. Plant-Microbe Interact.* **21**, 1635–1642 (2008).

48. Boller, T. & Felix, G. A Renaissance of elicitors: perception of microbe-associated molecular patterns and danger signals by pattern-recognition receptors. *Annu. Rev. Plant Biol.* **60**, 379–406 (2009).

49. Shi, Q., Febres, V. J., Jones, J. B. & Moore, G. A. A survey of FLS2 genes from multiple citrus species identifies candidates for enhancing disease resistance to *Xanthomonas citri* ssp. citri. *Hortic. Res.* **3**, 16022 (2016).

50. Zipfel, C. *et al.* Bacterial disease resistance in *Arabidopsis* through flagellin perception. *Nature* **428**, 764–767 (2004).

51. Chinchilla, D. *et al.* A flagellin-induced complex of the receptor FLS2 and BAK1 initiates plant defence. *Nature* **448**, 497–500 (2007).

52. Heese, A. *et al.* The receptor-like kinase SERK3/BAK1 is a central regulator of innate immunity in plants. *Proc. Natl. Acad. Sci. U. S. A.* **104**, 12217–12222 (2007).

53. Sun, Y. *et al.* Structural basis for flg22-induced activation of the *Arabidopsis* FLS2-BAK1 immune complex. *Science.* **342**, 624–628 (2013).

54. Schulze, B. *et al.* Rapid heteromerization and phosphorylation of ligand-activated plant transmembrane receptors and their associated kinase BAK1. *J. Biol. Chem.* **285**, 9444–9451 (2010).

55. Huffaker, A. & Ryan, C. A. Endogenous peptide defense signals in *Arabidopsis* differentially amplify signaling for the innate immune response. *Proc. Natl. Acad. Sci. U. S. A.* **104**, 10732–10736 (2007).

56. Krol, E. *et al.* Perception of the *Arabidopsis* danger signal peptide 1 involves the pattern recognition receptor AtPEPR1 and its close homologue AtPEPR2. *J. Biol. Chem.* **285**, 13471–13479 (2010).

57. Roux, M. *et al.* The Arabidopsis leucine-rich repeat receptor-like kinases BAK1/SERK3 and BKK1/SERK4 are required for innate immunity to hemibiotrophic and biotrophic pathogens. *Plant Cell* **23**, 2440–2455 (2011).

58. Ma, X., Xu, G., He, P. & Shan, L. SERKing coreceptors for receptors. *Trends Plant Sci.* **21**, 1017–1033 (2016).

59. Santiago, J., Henzler, C. & Hothorn, M. Molecular mechanism for plant steroid receptor activation by somatic embryogenesis co-receptor kinases. *Science.* **341**, 889–892 (2013).

60. Sun, Y. *et al.* Structure reveals that BAK1 as a co-receptor recognizes the BRI1-bound brassinolide. *Cell Res.* **23**, 1326–1329 (2013).

61. Gust, A. A. & Felix, G. Receptor like proteins associate with SOBIR1-type of adaptors to form bimolecular receptor kinases. *Curr. Opin. Plant Biol.* **21**, 104–111 (2014).

62. Müller, R., Bleckmann, A. & Simon, R. The receptor kinase CORYNE of *Arabidopsis* transmits the stem cell-limiting signal CLAVATA3 independently of CLAVATA1. *Plant Cell* **20**, 934–946 (2008).

63. Bleckmann, A., Weidtkamp-Peters, S., Seidel, C. A. M. & Simon, R. Stem cell signaling in *Arabidopsis* requires CRN to localize CLV2 to the plasma membrane. *Plant Physiol.* **152**, 166–176 (2010).

64. Kaku, H. *et al.* Plant cells recognize chitin fragments for defense signaling through a plasma membrane receptor. *Proc. Natl. Acad. Sci. U. S. A.* **103**, 11086–11091 (2006).

65. Shimizu, T. *et al.* Two LysM receptor molecules, CEBiP and OsCERK1, cooperatively regulate chitin elicitor signaling in rice. *Plant J.* **64**, 204–214 (2010).

66. Liebrand, T. W. H. *et al.* Receptor-like kinase SOBIR1/EVR interacts with receptor-like proteins in plant immunity against fungal infection. *Proc. Natl. Acad. Sci. U. S. A.* **110**, 10010–10015 (2013).

67. Mesarich, C. H. *et al.* Beyond the genomes of Fulvia fulva (syn . Cladosporium fulvum) and *Dothistroma septosporum* : New insights into how these fungal pathogens interact with their host plants. 1–21 (2023) doi:https://doi.org/10.1111/mpp.13309.

68. Thomas, C. C. M. C. C. M. *et al.* Characterization of the tomato Cf-4 gene for resistance to *Cladosporium fulvum* identifies sequences that determine recognitional specificity in Cf-4 and Cf-9. *Plant Cell* **9**, 2209–2224 (1997).

69. Thomma, B. P. H. J., Van Esse, H. P., Crous, P. W. & De Wit, P. J. G. M. *Cladosporium fulvum* (syn. *Passalora fulva*), a highly specialized plant pathogen as a model for functional studies on plant pathogenic Mycosphaerellaceae. *Mol. Plant Pathol.* **6**, 379–393 (2005).

70. van den Burg, H. A., Harrison, S. J., Joosten, M. H. A. J., Vervoort, J. & de Wit, P. J. G. M. *Cladosporium fulvum* Avr4 protects fungal cell walls against hydrolysis by plant chitinases accumulating during infection. *Mol. Plant-Microbe Interact.* **19**, 1420–1430 (2006).

71. Esse, H. P. Van, Bolton, M. D., Stergiopoulos, I., Wit, P. J. G. M. De & Thomma, B. P. H. J. The chitin-binding *Cladosporium fulvum* effector protein Avr4 is a virulence factor. *Mol. Plant-Microbe Interact.* **20**, 1092–1101 (2007).

72. van den Burg, H. A. *et al.* Natural disulfide bond-disrupted mutants of AVR4 of the tomato pathogen *Cladosporium fulvum* are sensitive to proteolysis, circumvent Cf-4-mediated resistance, but retain their chitin binding ability. *J. Biol. Chem.* **278**, 27340–27346 (2003).

73. Van Den Burg, H. A. *et al.* Binding of the AVR4 elicitor of *Cladosporium fulvum* to chitotriose units is facilitated by positive allosteric protein-protein interactions: the chitin-binding site of AVR4 represents a novel binding site on the folding scaffold shared between the inverte. *J. Biol. Chem.* **279**, 16786–16796 (2004).

74. De Jonge, R. *et al.* Tomato immune receptor Ve1 recognizes effector of multiple fungal pathogens uncovered by genome and RNA sequencing. *Proc. Natl. Acad. Sci. U. S. A.* **109**, 5110–5115 (2012).

75. Kawchuk, L. M. *et al.* Tomato Ve disease resistance genes encode cell surface-like receptors. *Proc. Natl. Acad. Sci. U. S. A.* **98**, 6511–6515 (2001).

76. Postma, J. *et al.* Avr4 promotes Cf-4 receptor-like protein association with the BAK1/SERK3 receptor-like kinase to initiate receptor endocytosis and plant immunity. *New Phytol.* **210**, 627–642 (2016).

77. van der Burgh, A. M., Postma, J., Robatzek, S. & Joosten, M. H. A. J. Kinase activity of SOBIR1 and BAK1 is required for immune signalling. *Mol. Plant Pathol.* **20**, 410–422 (2019).

78. Fradin, E. F. *et al.* Genetic dissection of verticillium wilt resistance mediated by tomato ve1. *Plant Physiol.* **150**, 320–332 (2009).

79. Fradin, E. F. *et al.* Interfamily transfer of tomato ve1 mediates *Verticillium* resistance in *Arabidopsis*. *Plant Physiol.* **156**, 2255–2265 (2011).

80. Du, J. *et al.* Elicitin recognition confers enhanced resistance to *Phytophthora infestans* in potato. *Nat. Plants* **1**, 15034 (2015).

81. Chaparro-Garcia, A. *et al.* The receptor-like kinase SERK3/BAK1 is required for basal resistance against the late blight pathogen *Phytophthora infestans* in *Nicotiana benthamiana*. *PLoS One* **6**, (2011).

82. Domazakis, E. *et al.* The ELR-SOBIR1 complex functions as a two-component receptor-like Kinase to mount defense against *Phytophthora infestans*. *Mol. Plant-Microbe Interact.* **31**, 795–802 (2018).

83. Chen, Z. *et al.* Convergent evolution of immune receptors underpins distinct elicitin recognition in closely related Solanaceous plants. *Plant Cell* 1–16 (2023) doi:10.1093/plcell/koad002.

84. Ma, Z. *et al.* A *Phytophthora sojae* glycoside hydrolase 12 protein is a major virulence factor during soybean infection and is recognized as a PAMP. *Plant Cell* **27**, 2057–2072 (2015).

85. Wang, Y. Y. *et al.* Leucine-rich repeat receptor-like gene screen reveals that *Nicotiana* RXEG1 regulates glycoside hydrolase 12 MAMP detection. *Nat. Commun.* **9**, 594 (2018).

86. Oome, S. *et al.* Nep1-like proteins from three kingdoms of life act as a microbe-associated molecular pattern in *Arabidopsis*. *Proc. Natl. Acad. Sci. U. S. A.* **111**, 16955–16960 (2014).

87. Böhm, H. *et al.* A conserved peptide pattern from a widespread microbial virulence factor triggers pattern-induced immunity in *Arabidopsis*. *PLoS Pathog.* **10**, e1004491 (2014).

88. Bi, G. *et al. Arabidopsis thaliana* receptor-like protein AtRLP23 associates with the receptor-like kinase AtSOBIR1. *Plant Signal. Behav.* **9**, 1–5 (2014).

89. Albert, I. *et al.* An RLP23–SOBIR1–BAK1 complex mediates NLP-triggered immunity. *Nat. Plants* **1**, 15140 (2015).

90. Zhang, W. *et al.* Arabidopsis RECEPTOR-LIKE PROTEIN30 and receptor-like kinase SUPPRESSOR OF BIR1-1/EVERSHED mediate innate immunity to necrotrophic fungi. *Plant Cell* **25**, 4227–4241 (2013).

91. Zhang, L. *et al.* Fungal endopolygalacturonases are recognized as microbe-associated molecular patterns by the *Arabidopsis* receptor-like protein RESPONSIVENESS TO BOTRYTIS POLYGALACTURONASES1. *Plant Physiol.* **164**, 352–364 (2014).

92. Zhang, L. *et al.* Distinct immune sensor systems for fungal endopolygalacturonases in closely related Brassicaceae. *Nat. Plants* **7**, 1254–1263 (2021).

93. Gao, M. *et al.* Regulation of cell death and innate immunity by two receptor-like kinases in *Arabidopsis*. *Cell Host Microbe* **6**, 34–44 (2009).

94. Halter, T. *et al.* The leucine-rich repeat receptor kinase BIR2 is a negative regulator of BAK1 in plant immunity. *Curr. Biol.* **24**, 134–143 (2014).

95. Ma, C. *et al.* Structural basis for BIR1-mediated negative regulation of plant immunity. *Cell Res.* **27**, 1521–1524 (2017).

96. Imkampe, J. *et al.* The *Arabidopsis* leucine-rich repeat receptor kinase BIR3 negatively regulates BAK1 receptor complex formation and stabilizes BAK1. *Plant Cell* **29**, 2285–2303 (2017).

97. Hohmann, U., Nicolet, J., Moretti, A., Hothorn, L. A. & Hothorn, M. The SERK3 elongated allele defines a role for BIR ectodomains in brassinosteroid signalling. *Nat. Plants* **4**, 345–351 (2018).

98. Clouse, S. D., Langford, M. & McMorris, T. C. A brassinosteroid-insensitive mutant in *Arabidopsis thaliana* exhibits multiple defects in growth and development. *Plant Physiol.* **111**, 671–678 (1996).

99. Li, J. & Chory, J. A putative leucine-rich repeat receptor kinase involved in brassinosteroid signal transduction. *Cell* **90**, 929–938 (1997).

100. Liu, Y., Huang, X., Li, M., He, P. & Zhang, Y. Loss-of-function of *Arabidopsis* receptor-like kinase BIR1 activates cell death and defense responses mediated by BAK1 and SOBIR1. *New Phytol.* **212**, 637–645 (2016).

101. Huang, S. *et al.* SlBIR3 negatively regulates PAMP responses and cell death in tomato. *Int. J. Mol. Sci.* **18**, 1966 (2017).

102. van der Burgh, A. M. SOBIR1-containing immune complexes at the plant cell surface: partners and signalling. (Wageningen University, 2018). doi:10.18174/454717.

103. Jones, J. D. G., Vance, R. E. & Dangl, J. L. Intracellular innate immune surveillance devices in plants and animals. *Science.* **354**, (2016).

104. Martin, R. *et al.* Structure of the activated ROQ1 resistosome directly recognizing the pathogen effector XopQ. *Science.* **370**, (2020).

105. Ma, S. *et al.* Direct pathogen-induced assembly of an NLR immune receptor complex to form a holoenzyme. *Science.* **370**, (2020).

106. Botella, M. A. *et al.* Three genes of the *Arabidopsis* RPP1 complex resistance locus recognize distinct *Peronospora parasitica* avirulence determinants. *Plant Cell* **10**, 1847–1860 (1998).

107. Steinbrenner, A. D., Goritschnig, S. & Staskawicz, B. J. Recognition and Activation domains contribute to allele-specific responses of an *Arabidopsis* NLR receptor to an oomycete effector protein. *PLOS Pathog.* **11**, e1004665 (2015).

108. Schultink, A., Qi, T., Lee, A., Steinbrenner, A. D. & Staskawicz, B. Roq1 mediates recognition of the *Xanthomonas* and *Pseudomonas* effector proteins XopQ and HopQ1. *Plant J.* **92**, 787–795 (2017).

109. Förderer, A. *et al.* A wheat resistosome defines common principles of immune receptor channels. *Nature* **610**, 532–539 (2022).

110. Saintenac, C. *et al.* Identification of wheat gene Sr35 that confers resistance to Ug99 stem rust race group. *Science.* **341**, 783–786 (2013).

111. Salcedo, A. *et al.* Variation in the AvrSr35 gene determines Sr35 resistance against wheat stem rust race Ug99. *Science.* **358**, 1604–1606 (2017).

112. Liang, X. & Zhou, J.-M. Receptor-like cytoplasmic kinases: central players in plant receptor kinase–mediated signaling. *Annu. Rev. Plant Biol.* **69**, 267–299 (2018).

113. Rao, S. *et al.* Roles of receptor-like cytoplasmic kinase VII members in pattern-triggered immune signaling. *Plant Physiol.* **177**, pp.00486.2018 (2018).

114. Yamaguchi, K. *et al.* A receptor-like cytoplasmic kinase targeted by a plant pathogen effector is directly phosphorylated by the chitin receptor and mediates rice immunity. *Cell Host Microbe* **13**, 347–357 (2013).

115. Zhang, J. *et al.* Receptor-like cytoplasmic kinases integrate signaling from multiple plant immune receptors and are targeted by a *Pseudomonas syringae* effector. *Cell Host Microbe* **7**, 290–301 (2010).

116. Feng, F. *et al.* A *Xanthomonas* uridine 5′-monophosphate transferase inhibits plant immune kinases. *Nature* **485**, 114–118 (2012).

117. Irieda, H. *et al.* Conserved fungal effector suppresses PAMP-triggered immunity by targeting plant immune kinases. *Proc. Natl. Acad. Sci. U. S. A.* **116**, 496–505 (2019).

118. Wang, G. *et al.* The decoy substrate of a pathogen effector and a pseudokinase specify pathogen-induced modified-self recognition and immunity in plants. *Cell Host Microbe* **18**, 285–295 (2015).

119. Cesari, S., Bernoux, M., Moncuquet, P., Kroj, T. & Dodds, P. N. A novel conserved mechanism for plant NLR protein pairs: the "integrated decoy" hypothesis. *Front. Plant Sci.* **5**, 1–10 (2014).

120. Wu, C.-H., Krasileva, K. V., Banfield, M. J., Terauchi, R. & Kamoun, S. The "sensor domains" of plant NLR proteins: more than decoys? *Front. Plant Sci.* **6**, 5–7 (2015).

121. Sarris, P. F. *et al.* A plant immune receptor detects pathogen effectors that target WRKY transcription factors. *Cell* **161**, 1089–1100 (2015).

122. Le Roux, C. *et al.* A receptor pair with an integrated decoy converts pathogen disabling of transcription factors to immunity. *Cell* **161**, 1074–1088 (2015).

123. Deslandes, L. *et al.* Resistance to *Ralstonia solanacearum* in *Arabidopsis thaliana* is conferred by the recessive RRS1-R gene, a member of a novel family of resistance genes. *Proc. Natl. Acad. Sci. U. S. A.* **99**, 2404–2409 (2002).

124. Wani, S. H., Anand, S., Singh, B., Bohra, A. & Joshi, R. WRKY transcription factors and plant defense responses: latest discoveries and future prospects. *Plant Cell Rep.* **40**, 1071–1085 (2021).

125. Ma, Y. *et al.* Distinct modes of derepression of an *Arabidopsis* immune receptor complex by two different bacterial effectors. *Proc. Natl. Acad. Sci. U. S. A.* **115**, 10218–10227 (2018).

126. Förderer, A., Yu, D., Li, E. & Chai, J. Resistosomes at the interface of pathogens and plants. *Curr. Opin. Plant Biol.* **67**, (2022).

127. Wang, J. *et al.* Reconstitution and structure of a plant NLR resistosome conferring immunity. *Science.* **364**, (2019).

128. Bi, G. *et al.* The ZAR1 resistosome is a calcium-permeable channel triggering plant immune signaling. *Cell* **184**, 3528-3541.e12 (2021).

129. Zhao, Y. B. *et al.* Pathogen effector AvrSr35 triggers Sr35 resistosome assembly via a direct recognition mechanism. *Sci. Adv.* **8**, 1–12 (2022).

130. Wan, L. *et al.* TIR domains of plant immune receptors are NAD + -cleaving enzymes that promote cell death. *Science.* **365**, 799–803 (2019).

131. Horsefield, S. *et al.* NAD+ cleavage activity by animal and plant TIR domains in cell death pathways. *Science.* **365**, 793–799 (2019).

132. Jia, A. *et al.* TIR-catalyzed ADP-ribosylation reactions produce signaling molecules for plant immunity. *Science.* **377**, (2022).

133. Huang, S. *et al.* Identification and receptor mechanism of TIR-catalyzed small molecules in plant immunity. *Science.* **377**, (2022).

134. Adachi, H., Derevnina, L. & Kamoun, S. NLR singletons, pairs, and networks: evolution, assembly, and regulation of the intracellular immunoreceptor circuitry of plants. *Curr. Opin. Plant Biol.* **50**, 121–131 (2019).

135. Ashikawa, I. *et al.* Two adjacent nucleotide-binding site–leucine-rich repeat class genes are required to confer Pikm-specific rice blast resistance. *Genetics* **180**, 2267–2276 (2008).

136. Maqbool, A. *et al.* Structural basis of pathogen recognition by an integrated HMA domain in a plant NLR immune receptor. *Elife* **4**, 1–24 (2015).

137. Zdrzałek, R., Kamoun, S., Terauchi, R., Saitoh, H. & Banfield, M. J. The rice NLR pair Pikp-1/Pikp-2 initiates cell death through receptor cooperation rather than negative regulation. *PLoS One* **15**, e0238616 (2020).

138. Adachi, H. & Kamoun, S. NLR receptor networks in plants. *Essays Biochem.* **66**, 541–549 (2022).

139. Bendahmane, A., Kanyuka, K. & Baulcombe, D. C. The Rx gene from potato controls separate virus resistance and cell death responses. *Plant Cell* **11**, 781–791 (1999).

140. Vossen, E. A. G. *et al.* The Rpi-blb2 gene from *Solanum bulbocastanum* is an Mi-1 gene homolog conferring broad-spectrum late blight resistance in potato. *Plant J.* **44**, 208–222 (2005).

141. Shao, Z.-Q. *et al.* Large-Scale analyses of angiosperm nucleotide-binding site-leucine-rich repeat genes reveal three anciently diverged classes with distinct evolutionary patterns. *Plant Physiol.* **170**, 2095–2109 (2016).

142. Castel, B. *et al.* Diverse NLR immune receptors activate defence via the RPW8-NLR NRG1. *New Phytol.* **222**, 966–980 (2019).

143. Wu, Z. *et al.* Differential regulation of TNL-mediated immune signaling by redundant helper CNLs. *New Phytol.* **222**, 938–953 (2019).

144. Saile, S. C. *et al.* Two unequally redundant 'helper' immune receptor families mediate *Arabidopsis thaliana* intracellular 'sensor' immune receptor functions. *PLOS Biol.* **18**, e3000783 (2020).

145. Lapin, D. *et al.* A coevolved EDS1-SAG101-NRG1 module mediates cell death signaling by TIR-domain immune receptors. *Plant Cell* **31**, 2430–2455 (2019).

146. Peart, J. R., Mestre, P., Lu, R., Malcuit, I. & Baulcombe, D. C. NRG1, a CC-NB-LRR Protein, together with N, a TIR-NB-LRR Protein, mediates resistance against tobacco mosaic virus. *Curr. Biol.* **15**, 968–973 (2005).

147. Qi, T. *et al.* NRG1 functions downstream of EDS1 to regulate TIR-NLR-mediated plant immunity in *Nicotiana benthamiana*. *Proc. Natl. Acad. Sci. U. S. A.* **115**, E10979–E10987 (2018).

148. Lapin, D., Bhandari, D. D. & Parker, J. E. Origins and immunity networking functions of EDS1 family proteins. *Annu. Rev. Phytopathol.* **58**, 253–276 (2020).

149. Wagner, S. *et al.* Structural basis for signaling by exclusive EDS1 heteromeric complexes with SAG101 or PAD4 in plant innate immunity. *Cell Host Microbe* **14**, 619–630 (2013).

150. Sun, X. *et al.* Pathogen effector recognition-dependent association of NRG1 with EDS1 and SAG101 in TNL receptor immunity. *Nat. Commun.* **12**, 1–15 (2021).

151. Contreras, M. P. *et al.* Sensor NLR immune proteins activate oligomerization of their NRC helpers in response to plant pathogens. *EMBO J.* **42**, (2023).

152. Ahn, H. *et al.* Effector-dependent activation and oligomerization of plant NRC class helper NLRs by sensor NLR immune receptors Rpi-amr3 and Rpi-amr1. *EMBO J.* **42**, 1–15 (2023).

153. Jacob, P. *et al.* Plant "helper" immune receptors are Ca2+-permeable nonselective cation channels. *Science.* **373**, 420–425 (2021).

154. Couto, D. & Zipfel, C. Regulation of pattern recognition receptor signalling in plants. *Nat. Rev. Immunol.* **16**, 537–552 (2016).

155. Lin, W., Ma, X., Shan, L. & He, P. Big roles of small kinases: the complex functions of receptor-like cytoplasmic kinases in plant immunity and development. *J. Integr. Plant Biol.* **55**, 1188–1197 (2013).

156. Lehti-Shiu, M. D., Zou, C., Hanada, K. & Shiu, S. H. Evolutionary history and stress regulation of plant receptor-like kinase/pelle genes. *Plant Physiol.* **150**, 12–26 (2009).

157. Lu, D. *et al.* A receptor-like cytoplasmic kinase, BIK1, associates with a flagellin receptor complex to initiate plant innate immunity. *Proc. Natl. Acad. Sci. U. S. A.* **107**, 496–501 (2010).

158. Liu, Z. *et al.* BIK1 interacts with PEPRs to mediate ethylene-induced immunity. *Proc. Natl. Acad. Sci. U. S. A.* **110**, 6205–6210 (2013).

159. Kadota, Y., Shirasu, K. & Zipfel, C. Regulation of the NADPH oxidase RBOHD during plant immunity. *Plant Cell Physiol.* **56**, 1472–1480 (2015).

160. Zhang, M. & Zhang, S. Mitogen-activated protein kinase cascades in plant signaling. *J. Integr. Plant Biol.* **64**, 301–341 (2022).

161. Jiang, Y. & Ding, P. Calcium signaling in plant immunity: a spatiotemporally controlled symphony. *Trends Plant Sci.* **2**, 1–16 (2022).

162. Pruitt, R. N. *et al.* The EDS1–PAD4–ADR1 node mediates *Arabidopsis* pattern-triggered immunity. *Nature* **598**, 495–499 (2021).

163. Tian, H. *et al.* Activation of TIR signalling boosts pattern-triggered immunity. *Nature* **598**, 500–503 (2021).

164. Rowland, O. *et al.* Functional analysis of Avr9/Cf-9 rapidly elicited genes identifies a protein kinase, ACIK1, that is essential for full Cf-9-dependent disease resistance in tomato. *Plant Cell* **17**, 295–310 (2005).

165. Kourelis, J. *et al.* The helper NLR immune protein NRC3 mediates the hypersensitive cell death caused by the cell-surface receptor Cf-4. *PLOS Genet.* **18**, e1010414 (2021).

166. Cai, X., Takken, F. L. W., Joosten, M. H. A. J. & De Wit, P. J. G. M. Specific recognition of AVR4 and AVR9 results in distinct patterns of hypersensitive cell death in tomato, but similar patterns of defence-related gene expression. *Mol. Plant Pathol.* **2**, 77–86 (2001).

167. Yuan, M., Cai, B. & Xin, X.-F. Plant immune receptor pathways as a united front against pathogens. *PLOS Pathog.* **19**, e1011106 (2023).

168. Bjornson, M. & Zipfel, C. Plant immunity: crosstalk between plant immune receptors. *Curr. Biol.* **31**, R796–R798 (2021).

169. Kourelis, J. & Adachi, H. Activation and regulation of NLR immune receptor networks. *Plant Cell Physiol.* **63**, 1366–1377 (2022).

170. Gust, A. A., Pruitt, R. & Nürnberger, T. Sensing danger: key to activating plant immunity. *Trends Plant Sci.* **22**, 779–791 (2017).

171. Kanyuka, K. & Rudd, J. J. Cell surface immune receptors: the guardians of the plant's extracellular spaces. *Curr. Opin. Plant Biol.* **50**, 1–8 (2019).

172. Granado, J., Felix, G. & Boller, T. Perception of fungal sterols in plants (subnanomolar concentrations of ergosterol elicit extracellular alkalinization in tomato cells). *Plant Physiol.* **107**, 485–490 (1995).

173. Jourdan, E. *et al.* Insights into the defense-related events occurring in plant cells following perception of surfactin-type lipopeptide from *Bacillus subtilis*. *Mol. Plant-Microbe Interact.* **22**, 456–468 (2009).

174. Luna, E. *et al.* Callose deposition: a multifaceted plant defense response. *Mol. Plant-Microbe Interact.* **24**, 183–193 (2011).

175. Voigt, C. A. Callose-mediated resistance to pathogenic intruders in plant defense-related papillae. *Front. Plant Sci.* **5**, 1–6 (2014).

176. Turkan, I. ROS and RNS: key signalling molecules in plants. *J. Exp. Bot.* **69**, 3313–3315 (2018).

177. Grant, M. *et al.* The RPM1 plant disease resistance gene facilitates a rapid and sustained increase in cytosolic calcium that is necessary for the oxidative burst and hypersensitive cell death. *Plant J.* **23**, 441–450 (2000).

178. Jain, D. & Khurana, J. P. Role of pathogenesis-related (PR) proteins in plant defense mechanism. in *Molecular Aspects of Plant-Pathogen Interaction* (eds. Singh, A. & Singh, I. K.) 265–281 (Springer Singapore, 2018). doi:10.1007/978-981-10-7371-7_12.

179. Jeandet, P. Phytoalexins: current progress and future prospects. *Molecules* **20**, 2770–2774 (2015).

180. Cai, Q. *et al.* Plants send small RNAs in extracellular vesicles to fungal pathogen to silence virulence genes. *Science.* **360**, 1126–1129 (2018).

181. Kabbage, M., Kessens, R., Bartholomay, L. C. & Williams, B. The life and death of a plant cell. *Annu. Rev. Plant Biol.* **68**, 375–404 (2017).

182. Michaeli, S., Galili, G., Genschik, P., Fernie, A. R. & Avin-Wittenberg, T. Autophagy in plants – what's new on the menu? *Trends Plant Sci.* **21**, 134–144 (2016).

183. Curtis, M. J. & Wolpert, T. J. The victorin-induced mitochondrial permeability transition precedes cell shrinkage and biochemical markers of cell death, and shrinkage occurs without loss of membrane integrity. *Plant J.* **38**, 244–259 (2004).

184. VAN BAARLEN, P., STAATS, M. & VAN KAN, J. A. L. Induction of programmed cell death in lily by the fungal pathogen *Botrytis elliptica*. *Mol. Plant Pathol.* **5**, 559–574 (2004).

185. Dickman, M., Williams, B., Li, Y., de Figueiredo, P. & Wolpert, T. Reassessing apoptosis in plants. *Nat. Plants* **3**, 773–779 (2017).

186. Veloso, J. & van Kan, J. A. L. Many shades of grey in botrytis–host plant interactions. *Trends Plant Sci.* **23**, 613–622 (2018).

187. Ehrlich, P. Das Sauerstoff-Bedürfnis des Organismus. Eine farbenanalytische Studie. (1885).

188. Mott, F. W. The late professor Edwin Goldmann's investigations on the central nervous system by vital staining. *BMJ* **2**, 871–873 (1913).

189. Escamez, S., Bollhöner, B. & Tuominen, H. Quick histochemical staining methods to detect cell death in xylem elements of plant tissues. in *Methods in Molecular Biology* vol. 1544 27–36 (2017).

190. Johansson, O. N. *et al.* A quick and robust method for quantification of the hypersensitive response in plants. *PeerJ* **3**, e1469 (2015).

191. Takemoto, D., Hardham, A. R. & Jones, D. A. Differences in cell death induction by Phytophthora elicitins are determined by signal components downstream of MAP kinase kinase in different species of *Nicotiana* and cultivars of *Brassica rapa* and *Raphanus sativus*. *Plant Physiol.* **138**, 1491–1504 (2005).

192. Vogel, J. P., Raab, T. K., Somerville, C. R. & Somerville, S. C. Mutations in PMR5 result in powdery mildew resistance and altered cell wall composition. *Plant J.* **40**, 968–978 (2004).

193. Guo, Y. *et al.* Functional analysis of RXLR effectors from the New Zealand kauri dieback pathogen *Phytophthora agathidicida*. *Mol. Plant Pathol.* **21**, 1131–1148 (2020).

194. Schornack, S. *et al.* The tomato resistance protein Bs4 is a predicted non-nuclear TIR-NB-LRR protein that mediates defense responses to severely truncated derivatives of AvrBs4 and overexpressed AvrBs3. *Plant J.* **37**, 46–60 (2004).

195. Gabriëls, S. H. E. J. *et al.* An NB-LRR protein required for HR signalling mediated by both extra- and intracellular resistance proteins. *Plant J.* **50**, 14–28 (2007).

196. Jambunathan, N. Determination and detection of reactive oxygen species (ROS), lipid peroxidation, and electrolyte leakage in plants. in *Plant Stress Tolerance. Methods in Molecular Biology* 291–297 (Humana Press, 2010). doi:10.1007/978-1-60761-702-0_18.

197. Vishwakarma, A. *et al.* Current approaches to measure nitric oxide in plants. *J. Exp. Bot.* **70**, 4333–4343 (2019).

198. Bennett, M., Mehta, M. & Grant, M. Biophoton imaging: a nondestructive method for assaying r gene responses. *Mol. Plant-Microbe Interact.* **18**, 95–102 (2005).

199. Gómez-Gómez, L., Felix, G. & Boller, T. A single locus determines sensitivity to bacterial flagellin in *Arabidopsis thaliana*. *Plant J.* **18**, 277–284 (1999).

200. Baker, N. R. Chlorophyll fluorescence: a probe of photosynthesis in vivo. *Annu. Rev. Plant Biol.* **59**, 89–113 (2008).

201. Gabriëls, S. H. E. J. *et al.* cDNA-AFLP combined with functional analysis reveals novel genes involved in the hypersensitive response. *Mol. Plant-Microbe Interact.* **19**, 567–576 (2006).

202. Schouten, A., Van Baarlen, P. & Van Kan, J. A. L. Phytotoxic Nep1-like proteins from the necrotrophic fungus *Botrytis cinerea* associate with membranes and the nucleus of plant cells. *New Phytol.* **177**, 493–505 (2008).

203. van den Burg, H. A., de Wit, P. J. G. M. & Vervoort, J. Efficient 13C/15N double labeling of the avirulence protein AVR4 in a methanol-utilizing strain (Mut+) of *Pichia pastoris*. *J. Biomol. NMR* **20**, 251–261 (2001).

204. Etalo, D. W. *et al.* System-wide hypersensitive response-associated transcriptome and metabolome reprogramming in tomato. *Plant Physiol.* **162**, 1599–1617 (2013).

205. Stulemeijer, I. J. E., Stratmann, J. W. & Joosten, M. H. A. J. Tomato mitogen-activated protein kinases LeMPK1, LeMPK2, and LeMPK3 are activated during the Cf-4/Avr4-induced hypersensitive response and have distinct phosphorylation specificities. *Plant Physiol.* **144**, 1481–1494 (2007).

206. Van der Hoorn, R. A. L., Laurent, F., Roth, R. & De Wit, P. J. G. M. Agroinfiltration is a versatile tool that facilitates comparative analyses of Avr 9/ Cf-9 -induced and Avr 4/ Cf-4 -induced necrosis. *Mol. Plant-Microbe Interact*. **13**, 439–446 (2000).

207. Liebrand, T. W. H. *et al.* Endoplasmic reticulum-quality control chaperones facilitate the biogenesis of Cf receptor-like proteins involved in pathogen resistance of tomato. *Plant Physiol.* **159**, 1819–1833 (2012).

208. Ho, J. & Theg, S. M. The formation of stromules in vitro from chloroplasts isolated from *Nicotiana benthamiana*. *PLoS One* **11**, e0146489 (2016).

209. Chinchilla, D., Shan, L., He, P., de Vries, S. & Kemmerling, B. One for all: the receptor-associated kinase BAK1. *Trends Plant Sci.* **14**, 535–541 (2009).

210. Kadota, Y. *et al.* Direct regulation of the NADPH oxidase RBOHD by the PRR-associated kinase BIK1 during plant immunity. *Mol. Cell* **54**, 43–55 (2014).

211. Li, L. *et al.* The FLS2-associated kinase BIK1 directly phosphorylates the NADPH oxidase RbohD to control plant immunity. *Cell Host Microbe* **15**, 329–338 (2014).

212. Jones, D. A., Thomas, C. M., Hammond-Kosack, K. E., Balint-Kurti, P. J. & Jones, J. D. G. Isolation of the tomato Cf-9 gene for resistance to *Cladosporium fulvum* by Transposon tagging. *Science.* **266**, 789–793 (1994).

213. Hammond-Kosack, K. E., Tang, S., Harrison, K. & Jones, J. D. G. The tomato Cf-9 disease resistance gene functions in tobacco and potato to confer responsiveness to the fungal avirulence gene product Avr9. *Plant Cell* **10**, 1251–1266 (1998).

214. Jehle, A. K., Fürst, U., Lipschis, M., Albert, M. & Felix, G. Perception of the novel MAMP eMax from different *Xanthomonas* species requires the *Arabidopsis* receptor-like protein remax and the receptor kinase SOBIR1. *Plant Signal. Behav.* **8**, 11–13 (2013).

215. Ma, L. & Borhan, M. H. The receptor-like kinase SOBIR1 interacts with *Brassica napus* LepR3 and is required for *Leptosphaeria maculans* AvrLm1-triggered immunity. *Front. Plant Sci.* **6**, 1–10 (2015).

216. Hegenauer, V., Fürst, U., Kaiser, B., Smoker, M. & Zipfel, C. Detection of the plant parasite *Cuscuta reflexa* by a tomato cell surface receptor. *Science*. **353**, 478-481 (2016)

217. Catanzariti, A. M. *et al.* The tomato I gene for Fusarium wilt resistance encodes an atypical leucine-rich repeat receptor-like protein whose function is nevertheless dependent on SOBIR1 and SERK3/BAK1. *Plant J.* **89**, 1195–1209 (2017).

218. Wan, W. *et al.* Comparing *Arabidopsis* receptor kinase and receptor protein-mediated immune signaling reveals BIK1-dependent differences. *New Phytol.* **221**, 2080–2095 (2019).

219. Huot, B., Yao, J., Montgomery, B. L. & He, S. Y. Growth–defense tradeoffs in plants: a balancing act to optimize fitness. *Mol. Plant* **7**, 1267–1287 (2014).

220. Grigoriev, A. A relationship between gene expression and protein interactions on the proteome scale: analysis of the bacteriophage T7 and the yeast *Saccharomyces cerevisiae*. *Nucleic Acids Res.* **29**, 3513–3519 (2001).

221. Barabási, A. L. & Oltvai, Z. N. Network biology: understanding the cell's functional organization. *Nat. Rev. Genet.* **5**, 101–113 (2004).

222. Freeman, T. C. *et al.* Construction, visualisation, and clustering of transcription networks from microarray expression data. *PLoS Comput. Biol.* **3**, 2032–2042 (2007).

223. Albert, R. Scale-free networks in cell biology. *J. Cell Sci.* **118**, 4947–4957 (2005).

224. Erdös, P. & Rényi, A. On the evolution of random graphs. in *The Structure and Dynamics of Networks* vol. 9781400841 38–82 (Princeton University Press, 2011).

225. Barabási, A.-L. & Albert, R. Emergence of scaling in random networks. *Science.* **286**, 509–512 (1999).

226. Ebel, H., Mielsch, L.-I. & Bornholdt, S. Scale-free topology of e-mail networks. *Phys. Rev. E* **66**, 035103 (2002).

227. Kumar, R., Novak, J. & Tomkins, A. Structure and evolution of online social networks. in *Proceedings of the 12th ACM SIGKDD international conference on Knowledge discovery and data mining - KDD '06* 611 (ACM Press, 2006). doi:10.1145/1150402.1150476.

228. Mislove, A., Marcon, M., Gummadi, K. P., Druschel, P. & Bhattacharjee, B. Measurement and analysis of online social networks. in *Proceedings of the 7th ACM SIGCOMM conference on Internet measurement - IMC '07* 29 (ACM Press, 2007). doi:10.1145/1298306.1298311.

229. Albert, R., Jeong, H. & Barabási, A.-L. Diameter of the World-Wide Web. *Nature* **401**, 130–131 (1999).

230. Pastor-Satorras, R., Vázquez, A. & Vespignani, A. Dynamical and correlation properties of the internet. *Phys. Rev. Lett.* **87**, 258701 (2001).

231. Jeong, H., Tombor, B., Albert, R., Oltvai, Z. N. & Barabási, A.-L. The large-scale organization of metabolic networks. *Nature* **407**, 651–654 (2000).

232. Carter, S. L., Brechbuhler, C. M., Griffin, M. & Bond, A. T. Gene co-expression network topology provides a framework for molecular characterization of cellular state. *Bioinformatics* **20**, 2242–2250 (2004).

233. Zaidi, F. S., Fatima, U., Usmani, B. A. & Jafri, A. R. Comprehending nodes essentiality through centrality measures in biological networks. **19**, 65–75 (2019).

234. Jeong, H., Mason, S. P., Barabási, A. L. & Oltvai, Z. N. Lethality and centrality in protein networks. *Nature* **411**, 41–42 (2001).

235. Landeo Villanueva, S., Malvestiti, M. C., van Ieperen, W., Joosten, M. H. A. J. & van Kan, J. A. L. Red light imaging for programmed cell death visualization and quantification in plant–pathogen interactions. *Mol. Plant Pathol.* **22**, 361–372 (2021).

236. Rhee, S. Y. & Mutwil, M. Towards revealing the functions of all genes in plants. *Trends Plant Sci.* **19**, 212–221 (2014).

237. Torres, M. A., Dangl, J. L. & Jones, J. D. G. *Arabidopsis* gp91phox homologues Atrbohd and Atrbohf are required for accumulation of reactive oxygen intermediates in the plant defense response. *Proc. Natl. Acad. Sci. U. S. A.* **99**, 517–522 (2002).

238. Wang, Z., Meng, P., Zhang, X., Ren, D. & Yang, S. BON1 interacts with the protein kinases BIR1 and BAK1 in modulation of temperature-dependent plant growth and cell death in *Arabidopsis*. *Plant J.* **67**, 1081–1093 (2011).

239. Maruta, N., Trusov, Y., Brenya, E., Parekh, U. & Botella, J. R. Membrane-localized extra-large G proteins and Gβγ of the heterotrimeric G proteins form functional complexes engaged in plant immunity in *Arabidopsis*. *Plant Physiol.* **167**, 1004–1016 (2015).

240. Liu, J. *et al.* Heterotrimeric G proteins serve as a converging point in plant defense signaling activated by multiple receptor-like kinases. *Plant Physiol.* **161**, 2146–2158 (2013).

241. Shannon, P. *et al.* Cytoscape: A software environment for integrated models of biomolecular interaction networks. *Genome Res.* **13**, 2498–2504 (2003).

242. Koschützki, D. & Schreiber, F. Centrality analysis methods for biological networks and their application to gene regulatory networks. *Gene Regul. Syst. Bio.* **2**, GRSB.S702 (2008).

243. Berardini, T. Z. *et al.* The arabidopsis information resource: making and mining the 'gold standard' annotated reference plant genome. *Genesis* **53**, 474–485 (2015).

244. Aranda-Sicilia, M. N. *et al.* Heterotrimeric G proteins interact with defense-related receptor-like kinases in Arabidopsis. *J. Plant Physiol.* **188**, 44–48 (2015).

245. Liang, X. *et al.* Arabidopsis heterotrimeric G proteins regulate immunity by directly coupling to the FLS2 receptor. *Elife* **5**, 1–18 (2016).

246. Xie, H. T., Wan, Z. Y., Li, S. & Zhang, Y. Spatiotemporal production of reactive oxygen species by nadph oxidase is critical for tapetal programmed cell death and pollen development in Arabidopsis. *Plant Cell* **26**, 2007–2023 (2014).

247. Liu, Y. *et al.* Chloroplast-generated reactive oxygen species are involved in hypersensitive response-like cell death mediated by a mitogen-activated protein kinase cascade. *Plant J.* **51**, 941–954 (2007).

248. Zurbriggen, M. D. *et al.* Chloroplast-generated reactive oxygen species play a major role in localized cell death during the non-host interaction between tobacco and *Xanthomonas campestris* pv. *vesicatoria*. *Plant J.* **60**, 962–973 (2009).

249. Nanda, A. K., Andrio, E., Marino, D., Pauly, N. & Dunand, C. Reactive oxygen species during plant-microorganism early interactions. *J. Integr. Plant Biol.* **52**, 195–204 (2010).

250. Zurbriggen, M. D., Carrillo, N. & Hajirezaei, M. R. ROS signaling in the hypersensitive response: when, where and what for? *Plant Signal. Behav.* **5**, 393–396 (2010).

251. Shapiguzov, A., Vainonen, J. P., Wrzaczek, M. & Kangasjärvi, J. ROS-talk - how the apoplast, the chloroplast, and the nucleus get the message through. *Front. Plant Sci.* **3**, 1–9 (2012).

252. Li, M. & Kim, C. Chloroplast ROS and stress signaling. *Plant Commun.* **3**, 100264 (2022).

253. Huang, W. R. H., Schol, C., Villanueva, S. L., Heidstra, R. & Joosten, M. H. A. J. Knocking out SOBIR1 in *Nicotiana benthamiana* abolishes functionality of transgenic receptor-like protein Cf-4. *Plant Physiol.* **185**, 290–294 (2021).

254. Zönnchen, J. *et al.* Differential requirement for the EDS1 catalytic triad in *A. thaliana* and *N. benthamiana*. *bioRxiv* 2021.12.15.472806 (2021) doi:https://doi.org/10.1101/2021.12.15.472806.

255. Ordon, J. *et al.* Generation of chromosomal deletions in dicotyledonous plants employing a user-friendly genome editing toolkit. *Plant J.* **89**, 155–168 (2017).

256. Pandey, S. Heterotrimeric G-Protein signaling in plants: conserved and novel mechanisms. *Annu. Rev. Plant Biol.* **70**, 213–238 (2019).

257. Petutschnig, E. *et al.* EXTRA LARGE G-PROTEIN 2 (XLG2) mediates cell death and hyperimmunity via a novel, apoplastic ROS-independent pathway in *Arabidopsis thaliana*. *bioRxiv* **2**, 2021.10.08.463358 (2021).

258. Li, Y., Pennington, B. O. & Hua, J. Multiple R-like genes are negatively regulated by BON1 and BON3 in *Arabidopsis*. *Mol. Plant-Microbe Interact.* **22**, 840–848 (2009).

259. Hua, J., Grisafi, P., Cheng, S.-H. H. & Fink, G. R. Plant growth homeostasis is controlled by the *Arabidopsis* BON1 and BAP1 genes. *Genes Dev.* **15**, 2263–2272 (2001).

260. Yang, S. & Hua, J. A haplotype-specific Resistance gene regulated by BONZAI1 mediates temperature-dependent growth control in *Arabidopsis*. *Plant Cell* **16**, 1060–1071 (2004).

261. Yang, S. *et al.* The BON/CPN gene family represses cell death and promotes cell growth in *Arabidopsis*. *Plant J.* **45**, 166–179 (2006).

262. Zhang, B. & Horvath, S. A general framework for weighted gene co-expression network analysis. *Stat. Appl. Genet. Mol. Biol.* **4**, (2005).

263. Giorgi, F. M., Del Fabbro, C. & Licausi, F. Comparative study of RNA-seq- and Microarray-derived coexpression networks in *Arabidopsis thaliana*. *Bioinformatics* **29**, 717–724 (2013).

264. Azuaje, F. J. Selecting biologically informative genes in co-expression networks with a centrality score. *Biol. Direct* **9**, 1–23 (2014).

265. ZHU, J., LI, C. & JI, W. Identification of genes in ulcerative colitis associated colorectal cancer based on centrality analysis of co-expression network. *Neoplasma* **62**, 756–764 (2015).

266. van Noort, V., Snel, B. & Huynen, M. A. Predicting gene function by conserved co-expression. *Trends Genet.* **19**, 238–242 (2003).

267. Brückner, A., Polge, C., Lentze, N., Auerbach, D. & Schlattner, U. Yeast two-hybrid, a powerful tool for systems biology. *Int. J. Mol. Sci.* **10**, 2763–2788 (2009).

268. Morris, J. H. *et al.* Affinity purification-mass spectrometry and network analysis to understand protein-protein interactions. *Nat. Protoc.* **9**, 2539–2554 (2014).

269. Samavarchi-Tehrani, P., Samson, R. & Gingras, A. C. Proximity dependent biotinylation: key enzymes and adaptation to proteomics approaches. *Mol. Cell. Proteomics* **19**, 757–773 (2020).

270. Woodward, A. W. & Bartel, B. Biology in Bloom: A primer on the *Arabidopsis thaliana* model system. *Genetics* **208**, 1337–1349 (2018).

271. Liebrand, T. W. H., van den Burg, H. A. & Joosten, M. H. A. J. Two for all: receptor-associated kinases SOBIR1 and BAK1. *Trends Plant Sci.* **19**, 123–132 (2014).

272. Goodin, M. M., Zaitlin, D., Naidu, R. A. & Lommel, S. A. *Nicotiana benthamiana*: its history and future as a model for plant-pathogen interactions. *Mol. Plant-Microbe Interact.* **21**, 1015–1026 (2008).

273. Bally, J. *et al.* The rise and rise of *Nicotiana benthamiana*: a plant for all reasons. *Annu. Rev. Phytopathol.* **56**, 405–426 (2018).

274. Piedras, P., Hammond-Kosack, K. E., Harrison, K. & Jones, J. D. G. Rapid, Cf-9 - and Avr9-dependent production of active oxygen species in tobacco suspension cultures. *Mol. Plant-Microbe Interact.* **11**, 1155–1166 (1998).

275. Levine, A., Tenhaken, R., Dixon, R. & Lamb, C. H_2O_2 from the oxidative burst orchestrates the plant hypersensitive disease resistance response. *Cell* **79**, 583–593 (1994).

276. Baker, C. J. & Orlandi, E. W. Active oxygen in plant pathogenesis. *Annu. Rev. Phytopathol.* **33**, 299–321 (1995).

277. Chai, H. B. & Doke, N. Activation of the potential of potato leaf tissue to react hypersensitively to *Phytophthora infestans* by cytospore germination fluid and the enhancement of this potential by calcium ions. *Physiol. Mol. Plant Pathol.* **30**, 27–37 (1987).

278. Yoshioka, H. *et al. Nicotiana benthamiana* gp91phox homologs Nbrboha and Nbrbohb participate in H_2O_2 accumulation and resistance to *Phytophthora infestans*. *Plant Cell* **15**, 706–718 (2003).

279. Adachi, H. *et al.* WRKY transcription factors phosphorylated by MAPK regulate a plant immune NADPH oxidase in *Nicotiana benthamiana*. *Plant Cell* **27**, 2645–2663 (2015).

280. Segonzac, C. *et al.* Hierarchy and roles of pathogen-associated molecular pattern-induced responses in *Nicotiana benthamiana*. *Plant Physiol.* **156**, 687–699 (2011).

281. Almagro, L. *et al.* Class III peroxidases in plant defence reactions. *J. Exp. Bot.* **60**, 377–390 (2009).

282. Thordal-Christensen, H., Zhang, Z., Wei, Y. & Collinge, D. B. Subcellular localization of H_2O_2 in plants. H_2O_2 accumulation in papillae and hypersensitive response during the barley-powdery mildew interaction. *Plant J.* **11**, 1187–1194 (1997).

283. Song, W., Forderer, A., Yu, D. & Chai, J. Structural biology of plant defence. *New Phytol.* **229**, 692–711 (2021).

284. Llorente, F., Alonso-Blanco, C., Sánchez-Rodriguez, C., Jorda, L. & Molina, A. ERECTA receptor-like kinase and heterotrimeric G protein from *Arabidopsis* are required for resistance to the necrotrophic fungus *Plectosphaerella cucumerina*. *Plant J.* **43**, 165–180 (2005).

285. Tunc-Ozdemir, M. & Jones, A. M. Ligand-induced dynamics of heterotrimeric G protein-coupled receptor-like kinase complexes. *PLoS One* **12**, 1–16 (2017).

286. Zhong, C. L., Zhang, C. & Liu, J. Z. Heterotrimeric G protein signaling in plant immunity. *J. Exp. Bot.* **70**, 1109–1118 (2019).

287. Pandey, S. Plant receptor-like kinase signaling through heterotrimeric G-proteins. *J. Exp. Bot.* **71**, 1742–1751 (2020).

288. Ding, L., Pandey, S. & Assmann, S. M. *Arabidopsis* extra-large G proteins (XLGs) regulate root morphogenesis. *Plant J.* **53**, 248–263 (2008).

289. Urano, D. *et al.* Saltational evolution of the heterotrimeric G protein signaling mechanisms in the plant kingdom. *Sci. Signal.* **9**, 1–10 (2016).

290. Torres, M. A., Morales, J., Sánchez-Rodríguez, C., Molina, A. & Dangl, J. L. Functional interplay between arabidopsis NADPH oxidases and heterotrimeric G protein. *Mol. Plant-Microbe Interact.* **26**, 686–694 (2013).

291. Wang, J. *et al.* A regulatory module controlling homeostasis of a plant immune kinase. *Mol. Cell* **69**, 493-504.e6 (2018).

292. Zhang, W., He, S. Y. & Assmann, S. M. The plant innate immunity response in stomatal guard cells invokes G-protein-dependent ion channel regulation. *Plant J.* **56**, 984–996 (2008).

293. Zeng, W. & He, S. Y. A prominent role of the flagellin receptor FLAGELLIN-SENSING2 in mediating stomatal response to *Pseudomonas syringae* pv tomato DC3000 in *Arabidopsis*. *Plant Physiol.* **153**, 1188–1198 (2010).

294. Lee, S., Rojas, C. M., Ishiga, Y., Pandey, S. & Mysore, K. S. *Arabidopsis* heterotrimeric G-proteins play a critical role in host and nonhost resistance against *Pseudomonas syringae* pathogens. *PLoS One* **8**, e82445 (2013).

295. Creutz, C. E. *et al.* The copines, a novel class of c2 domain-containing, calcium-dependent, phospholipid-binding proteins conserved from *Paramecium* to Humans. *J. Biol. Chem.* **273**, 1393–1402 (1998).

296. Rizo, J. & Südhof, T. C. C2-domains, structure and function of a universal Ca^{2+}-binding domain. *J. Biol. Chem.* **273**, 15879–15882 (1998).

297. Whittaker, C. A. & Hynes, R. O. Distribution and evolution of von Willebrand/Integrin A domains: widely dispersed domains with roles in cell adhesion and elsewhere. *Mol. Biol. Cell* **13**, 3369–3387 (2002).

298. Jambunathan, N. A humidity-sensitive *Arabidopsis* copine mutant exhibits precocious cell death and increased disease resistance. *PLANT CELL ONLINE* **13**, 2225–2240 (2001).

299. Kemmerling, B. *et al.* The BRI1-ASSOCIATED KINASE 1, BAK1, has a brassinolide-independent role in plant cell-death control. *Curr. Biol.* **17**, 1116–1122 (2007).

300. He, K. *et al.* BAK1 and BKK1 regulate brassinosteroid-dependent growth and brassinosteroid-independent cell-death pathways. *Curr. Biol.* **17**, 1109–1115 (2007).

301. Gantner, J., Ordon, J., Kretschmer, C., Guerois, R. & Stuttmann, J. An EDS1-SAG101 complex is essential for TNL-mediated immunity in *Nicotiana benthamiana*. *Plant Cell* **31**, 2456–2474 (2019).

302. Wilson, C. L. & Miller, C. J. Simpleaffy: a bioconductor package for affymetrix quality control and data analysis. *Bioinformatics* **21**, 3683–3685 (2005).

303. Assenov, Y., Ramírez, F., Schelhorn, S. E. S. E., Lengauer, T. & Albrecht, M. Computing topological parameters of biological networks. *Bioinformatics* **24**, 282–284 (2008).

304. Carlson, M. ath1121501.db: Affymetrix *Arabidopsis* ATH1 genome array annotation data (chip ath1121501). (2014) doi:10.18129/B9.bioc.ath1121501.db.

305. Warde-Farley, D. *et al.* The GeneMANIA prediction server: biological network integration for gene prioritization and predicting gene function. *Nucleic Acids Res.* **38**, 214–220 (2010).

306. Thomas, P. D. *et al.* PANTHER: A library of protein families and subfamilies indexed by function. *Genome Res.* **13**, 2129–2141 (2003).

307. Fernandez-Pozo, N. *et al.* The Sol Genomics Network (SGN)—from genotype to phenotype to breeding. *Nucleic Acids Res.* **43**, D1036–D1041 (2015).

308. Katoh, K., Rozewicki, J. & Yamada, K. D. MAFFT online service: multiple sequence alignment, interactive sequence choice and visualization. *Brief. Bioinform.* **20**, 1160–1166 (2018).

309. Wu, J. Regulation and activation of SOBIR1-containing receptor complexes involved in plant immune signalling. (Wageningen University, 2020). doi:10.18174/504639.

310. Liu, Y., Schiff, M., Marathe, R. & Dinesh-Kumar, S. P. Tobacco Rar1, EDS1 and NPR1/NIM1 like genes are required for N-mediated resistance to tobacco mosaic virus. *Plant J.* **30**, 415–429 (2002).

311. Schneider, C. A., Rasband, W. S. & Eliceiri, K. W. NIH Image to ImageJ: 25 years of image analysis. *Nat. Methods* **9**, 671–675 (2012).

312. Daudi, A., O'Brien, J. A. & O'Brien, J. Detection of hydrogen peroxide by dab staining in *Arabidopsis* leaves. *BIO-PROTOCOL* **2**, 4–7 (2012).

313. Meyer, K. & Selbach, M. Quantitative affinity purification mass spectrometry: a versatile technology to study protein–protein interactions. *Front. Genet.* **6**, 1–7 (2015).

314. Xing, S., Wallmeroth, N., Berendzen, K. W. & Grefen, C. Techniques for the analysis of protein-protein interactions in vivo. *Plant Physiol.* **171**, 727–758 (2016).

315. Johnsson, N. & Varshavsky, A. Split ubiquitin as a sensor of protein interactions in vivo. *Proc. Natl. Acad. Sci. U. S. A.* **91**, 10340–10344 (1994).

316. Raquet, X., Eckert, J. H., Müller, S. & Johnsson, N. Detection of altered protein conformations in living cells. *J. Mol. Biol.* **305**, 927–938 (2001).

317. Glickman, M. H. & Ciechanover, A. The ubiquitin-proteasome proteolytic pathway: destruction for the sake of construction. *Physiol. Rev.* **82**, 373–428 (2002).

318. Grefen, C. *et al.* A vesicle-trafficking protein commandeers Kv channel voltage sensors for voltage-dependent secretion. *Nat. Plants* **1**, 15108 (2015).

319. Zhang, B. *et al.* The *Arabidopsis* R-SNARE VAMP721 Interacts with KAT1 and KC1 K^+ channels to moderate K^+ current at the plasma membrane. *Plant Cell* **27**, 1697–1717 (2015).

320. Wang, W. *et al.* Functional characterization of calcium-dependent protein kinase (CPK) 2 gene from oilseed rape (*Brassica napus* L.) in regulating reactive oxygen species signaling and cell death control. *Gene* **651**, 49–56 (2018).

321. Pan, G. *et al.* Rapeseed calcium-dependent protein kinase CPK6L modulates reactive oxygen species and cell death through interacting and phosphorylating RBOHD. *Biochem. Biophys. Res. Commun.* **518**, 719–725 (2019).

322. Fields, S. & Song, O. A novel genetic system to detect protein–protein interactions. *Nature* **340**, 245–246 (1989).

323. Dedecker, M., Van Leene, J. & De Jaeger, G. Unravelling plant molecular machineries through affinity purification coupled to mass spectrometry. *Curr. Opin. Plant Biol.* **24**, 1–9 (2015).

324. Privé, G. G. Detergents for the stabilization and crystallization of membrane proteins. *Methods* **41**, 388–397 (2007).

325. Babu, M. *et al.* Interaction landscape of membrane-protein complexes in *Saccharomyces cerevisiae*. *Nature* **489**, 585–589 (2012).

326. Lee, Y.-C. *et al.* Impact of detergents on membrane protein complex isolation. *J. Proteome Res.* **17**, 348–358 (2018).

327. Iacobucci, C., Götze, M. & Sinz, A. Cross-linking/mass spectrometry to get a closer view on protein interaction networks. *Curr. Opin. Biotechnol.* **63**, 48–53 (2020).

328. Low, T. Y. *et al.* Recent progress in mass spectrometry-based strategies for elucidating protein–protein interactions. *Cell. Mol. Life Sci.* **78**, 5325–5339 (2021).

329. Mair, A. & Bergmann, D. C. Advances in enzyme-mediated proximity labeling and its potential for plant research. *Plant Physiol.* **188**, 756–768 (2022).

330. Gingras, A. C., Abe, K. T. & Raught, B. Getting to know the neighborhood: using proximity-dependent biotinylation to characterize protein complexes and map organelles. *Curr. Opin. Chem. Biol.* **48**, 44–54 (2019).

331. Arora, D. *et al.* Establishment of proximity-dependent biotinylation approaches in different plant model systems. *Plant Cell* **32**, 3388–3407 (2020).

332. Chapman-Smith, A. & Cronan Jr, J. E. Molecular biology of biotin attachment to proteins. *J. Nutr.* **129**, 477S-484S (1999).

333. Kwon, K. & Beckett, D. Function of a conserved sequence motif in biotin holoenzyme synthetases. *Protein Sci.* **9**, 1530–1539 (2000).

334. Kwon, K., Streaker, E. D., Ruparelia, S. & Beckett, D. Multiple disordered loops function in corepressor-induced dimerization of the biotin repressor. *J. Mol. Biol.* **304**, 821–833 (2000).

335. Cronan, J. E. Targeted and proximity-dependent promiscuous protein biotinylation by a mutant *Escherichia coli* biotin protein ligase. *J. Nutr. Biochem.* **16**, 416–418 (2005).

336. Roux, K. J., Kim, D. I., Raida, M. & Burke, B. A promiscuous biotin ligase fusion protein identifies proximal and interacting proteins in mammalian cells. *J. Cell Biol.* **196**, 801–810 (2012).

337. Kim, D. I. *et al.* Probing nuclear pore complex architecture with proximity-dependent biotinylation. *Proc. Natl. Acad. Sci. U. S. A.* **111**, 2453–2461 (2014).

338. Branon, T. C. *et al.* Efficient proximity labeling in living cells and organisms with TurboID. *Nat. Biotechnol.* **36**, 880–898 (2018).

339. May, D. G., Scott, K. L., Campos, A. R. & Roux, K. J. Comparative application of BioID and TurboID for protein-proximity biotinylation. *Cells* **9**, 1070 (2020).

340. Larochelle, M., Bergeron, D., Arcand, B. & Bachand, F. Proximity-dependent biotinylation by TurboID to identify protein-protein interaction networks in yeast. *J. Cell Sci.* **132**, (2019).

341. Kim, T.-W. *et al.* Application of TurboID-mediated proximity labeling for mapping a GSK3 kinase signaling network in Arabidopsis. *bioRxiv* 636324 (2019) doi:10.1101/636324.

342. Zhang, Y. *et al.* TurboID-based proximity labeling reveals that UBR7 is a regulator of N NLR immune receptor-mediated immunity. *Nat. Commun.* **10**, 3252 (2019).

343. de Wit, P. J. G. M. *Cladosporium fulvum* effectors: weapons in the arms race with tomato. *Annu. Rev. Phytopathol.* **54**, 1–23 (2016).

344. Kurup, S. *et al.* Marking cell lineages in living tissues. *Plant J.* **42**, 444–453 (2005).

345. Cutler, S. R., Ehrhardt, D. W., Griffitts, J. S. & Somerville, C. R. Random GFP-cDNA fusions enable visualization of subcellular structures in cells of *Arabidopsis* at a high frequency. *Proc. Natl. Acad. Sci. U. S. A.* **97**, 3718–3723 (2000).

346. Ghareeb, H., Laukamm, S. & Lipka, V. COLORFUL-circuit: a platform for rapid multigene assembly, delivery, and expression in plants. *Front. Plant Sci.* **7**, 1–15 (2016).

347. Lee, D. H. *et al.* Regulation of reactive oxygen species during plant immunity through phosphorylation and ubiquitination of RBOHD. *Nat. Commun.* **11**, (2020).

348. Wu, J. *et al.* An EFR-Cf-9 chimera confers enhanced resistance to bacterial pathogens by SOBIR1- and BAK1-dependent recognition of elf18. *Mol. Plant Pathol.* **20**, 751–764 (2019).

349. Ntoukakis, V., Schwessinger, B., Segonzac, C. & Zipfel, C. Cautionary notes on the use of C-Terminal BAK1 fusion proteins for functional studies. *Plant Cell* **23**, 3871–3878 (2011).

350. Hurst, C. H. *et al.* Variable Effects of C-Terminal Fusions on FLS2 function: not all epitope tags are created equal. *Plant Physiol.* **177**, 522–531 (2018).

351. Joosten, M. H. A. J., Vogelsang, R., Cozijnsen, T. J., Verberne, M. C. & De Wit, P. J. G. M. The biotrophic fungus *Cladosporium fulvum* circumvents Cf-4-mediated resistance by producing unstable AVR4 elicitors. *Plant Cell* **9**, 367–379 (1997).

352. Tian, M., Huitema, E., da Cunha, L., Torto-Alalibo, T. & Kamoun, S. A Kazal-like extracellular serine protease inhibitor from *Phytophthora infestans* targets the tomato pathogenesis-related protease P69B. *J. Biol. Chem.* **279**, 26370–26377 (2004).

353. Misas-Villamil, J. C., Hoorn, R. A. L. & Doehlemann, G. Papain-like cysteine proteases as hubs in plant immunity. *New Phytol.* **212**, 902–907 (2016).

354. Schaller, A. *et al.* From structure to function - a family portrait of plant subtilases. *New Phytol.* **218**, 901–915 (2018).

355. Joosten, M. H. A. J. Isolation of apoplastic fluid from leaf tissue by the vacuum infiltration-centrifugation technique. in *Methods in Molecular Biology* vol. 835 603–610 (2012).

356. Schellenberger, R. *et al.* Apoplastic invasion patterns triggering plant immunity: plasma membrane sensing at the frontline. *Mol. Plant Pathol.* **20**, 1602–1616 (2019).

357. Tyanova, S., Temu, T. & Cox, J. The MaxQuant computational platform for mass spectrometry-based shotgun proteomics. *Nat. Protoc.* **11**, 2301–2319 (2016).

358. Tyanova, S. *et al.* The Perseus computational platform for comprehensive analysis of (prote) omics data. *Nat. Methods* **13**, 731–740 (2016).

359. Zheng, Y. *et al.* iTAK: A program for genome-wide prediction and classification of plant transcription factors, transcriptional regulators, and protein kinases. *Mol. Plant* **9**, 1667–1670 (2016).

360. Christie, J. M. Phototropin blue-light receptors. *Annu. Rev. Plant Biol.* **58**, 21–45 (2007).

361. Knepper, C., Savory, E. A. & Day, B. *Arabidopsis* NDR1 is an integrin-like protein with a role in fluid loss and plasma membrane-cell wall adhesion. *Plant Physiol.* **156**, 286–300 (2011).

362. Berka, M., Kopecká, R., Berková, V., Brzobohatý, B. & Černý, M. Regulation of heat shock proteins 70 and their role in plant immunity. *J. Exp. Bot.* **73**, 1894–1909 (2022).

363. Ray, S. K., Macoy, D. M., Kim, W. Y., Lee, S. Y. & Kim, M. G. Role of RIN4 in regulating pamp-triggered immunity and effector-triggered immunity: current status and future perspectives. *Mol. Cells* **42**, 503–511 (2019).

364. Suetsugu, N. & Wada, M. Signalling mechanism of phototropin-mediated chloroplast movement in *Arabidopsis*. *J. Plant Biochem. Biotechnol.* **29**, 580–589 (2020).

365. Hallgren, J. *et al.* DeepTMHMM predicts alpha and beta transmembrane proteins using deep neural networks. *bioRxiv* 2022.04.08.487609 (2022) doi:10.1101/2022.04.08.487609.

366. Hulsen, T. DeepVenn -- a web application for the creation of area-proportional Venn diagrams using the deep learning framework Tensorflow.js. *arXiv* (2022).

367. Sun, J.-L., Li, J.-Y., Wang, M.-J., Song, Z.-T. & Liu, J.-X. Protein quality control in plant organelles: current progress and future perspectives. *Mol. Plant* **14**, 95–114 (2021).

368. Bravo, J., Aguilar-Henonin, L., Olmedo, G. & Guzmán, P. Four distinct classes of proteins as interaction partners of the PABC domain of *Arabidopsis thaliana* Poly(A)-binding proteins. *Mol. Genet. Genomics* **272**, 651–665 (2005).

369. Zafra, F. & Piniella, D. Proximity labeling methods for proteomic analysis of membrane proteins. *J. Proteomics* **264**, 104620 (2022).

370. Whitham, S. *et al.* The product of the tobacco mosaic virus resistance gene n: similarity to toll and the interleukin-1 receptor. *Cell* **78**, 1101–1115 (1994).

371. Cho, K. F. *et al.* Split-TurboID enables contact-dependent proximity labeling in cells. *Proc. Natl. Acad. Sci. U. S. A.* **117**, 12143–12154 (2020).

372. Anelli, T. & Sitia, R. Protein quality control in the early secretory pathway. *EMBO J.* **27**, 315–327 (2008).

373. Liebrand, T. W. H. *et al.* Chaperones of the endoplasmic reticulum are required for Ve1-mediated resistance to *Verticillium*. *Mol. Plant Pathol.* **15**, 109–17 (2014).

374. Shiu, S.-H. *et al.* Comparative analysis of the receptor-like kinase family in *Arabidopsis* and rice. *Plant Cell* **16**, 1220–1234 (2004).

375. Schwizer, S. *et al.* The tomato kinase Pti1 contributes to production of reactive oxygen species in response to two flagellin-derived peptides and promotes resistance to *Pseudomonas syringae* infection. *Mol. Plant-Microbe Interact.* **30**, 725–738 (2017).

376. Lu, D. *et al.* A receptor-like cytoplasmic kinase, BIK1, associates with a flagellin receptor complex to initiate plant innate immunity. *Proc. Natl. Acad. Sci. U. S. A.* **107**, 496–501 (2010).

377. Sreekanta, S. *et al.* The receptor-like cytoplasmic kinase PCRK1 contributes to pattern-triggered immunity against *Pseudomonas syringae* in *Arabidopsis thaliana*. *New Phytol.* **207**, 78–90 (2015).

378. Kong, Q. *et al.* Two redundant receptor-like cytoplasmic kinases function downstream of pattern recognition receptors to regulate activation of SA biosynthesis in *Arabidopsis*. *Plant Physiol.* **171**, pp.01954.2015 (2016).

379. Swiderski, M. R. & Innes, R. W. The *Arabidopsis* PBS1 resistance gene encodes a member of a novel protein kinase subfamily. *Plant J.* **26**, 101–112 (2001).

380. Shao, F. *et al.* Cleavage of *Arabidopsis* PBS1 by a bacterial type iii effector. *Science.* **301**, 1230–1233 (2003).

381. Cui, F., Sun, W. & Kong, X. RLCKs bridge plant immune receptors and MAPK cascades. *Trends Plant Sci.* **23**, 1039–1041 (2018).

382. Ichimura, K. *et al.* Mitogen-activated protein kinase cascades in plants: a new nomenclature. *Trends Plant Sci.* **7**, 301–308 (2002).

383. Sun, T. *et al.* Antagonistic interactions between two MAP kinase cascades in plant development and immune signaling . *EMBO Rep.* **19**, 1–12 (2018).

384. Bi, G. *et al.* Receptor-like cytoplasmic kinases directly link diverse pattern recognition receptors to the activation of mitogen-activated protein kinase cascades in *Arabidopsis*. *Plant Cell* **30**, 1543–1561 (2018).

385. Pozo, O. del, Pedley, K. F. & Martin, G. B. MAPKKKα is a positive regulator of cell death associated with both plant immunity and disease. *EMBO J.* **23**, 3072–3082 (2004).

386. Melech-Bonfil, S. & Sessa, G. Tomato MAPKKKε is a positive regulator of cell-death signaling networks associated with plant immunity. *Plant J.* **64**, 379–391 (2010).

387. Schweighofer, A., Hirt, H. & Meskiene, I. Plant PP2C phosphatases: emerging functions in stress signaling. *Trends Plant Sci.* **9**, 236–243 (2004).

388. Wu, J. *et al.* The bacterial effector AvrPto targets the regulatory coreceptor SOBIR1 and suppresses defense signaling mediated by the receptor-like protein Cf-4. *Mol. Plant-Microbe Interact.* **31**, 75–85 (2018).

389. Liu, J. *et al.* A Tyrosine phosphorylation cycle regulates fungal activation of a plant receptor Ser/Thr kinase. *Cell Host Microbe* **23**, 241-253.e6 (2018).

390. Miya, A. *et al.* CERK1, a LysM receptor kinase, is essential for chitin elicitor signaling in *Arabidopsis*. *Proc. Natl. Acad. Sci. U. S. A.* **104**, 19613–19618 (2007).

391. Wang, J., Song, W. & Chai, J. Structure, biochemical function, and signaling mechanism of plant NLRs. *Mol. Plant* 1–21 (2022) doi:10.1016/j.molp.2022.11.011.

392. Zönnchen, J. *et al.* EDS1 complexes are not required for PRR responses and execute TNL-ETI from the nucleus in Nicotiana benthamiana. *New Phytol.* **236**, 2249–2264 (2022).

393. Day, B., Dahlbeck, D. & Staskawicz, B. J. NDR1 interaction with RIN4 mediates the differential activation of multiple disease resistance pathways in *Arabidopsis*. *Plant Cell* **18**, 2782–2791 (2006).

394. Liu, J. *et al.* RIN4 Functions with Plasma Membrane H^+-ATPases to regulate stomatal apertures during pathogen attack. *PLoS Biol.* **7**, e1000139 (2009).

395. Axtell, M. J., Chisholm, S. T., Dahlbeck, D. & Staskawicz, B. J. Genetic and molecular evidence that the *Pseudomonas syringae* type III effector protein AvrRpt2 is a cysteine protease. *Mol. Microbiol.* **49**, 1537–1546 (2003).

396. Mackey, D., Holt, B. F., Wiig, A. & Dangl, J. L. RIN4 interacts with *Pseudomonas syringae* type iii effector molecules and is required for RPM1-mediated resistance in *Arabidopsis*. *Cell* **108**, 743–754 (2002).

397. Zhang, Z. *et al.* The NLR protein SUMM2 senses the disruption of an immune signaling MAP kinase cascade via CRCK3. *EMBO Rep.* **18**, 292–302 (2017).

398. Caplan, J. L., Mamillapalli, P., Burch-Smith, T. M., Czymmek, K. & Dinesh-Kumar, S. P. Chloroplastic protein NRIP1 mediates innate immune receptor recognition of a viral effector. *Cell* **132**, 449–462 (2008).

399. Padmanabhan, M. S. *et al.* Novel positive regulatory role for the SPL6 transcription factor in the N TIR-NB-LRR receptor-mediated plant innate immunity. *PLoS Pathog.* **9**, e1003235 (2013).

400. Malinsky, J., Opekarová, M., Grossmann, G. & Tanner, W. Membrane microdomains, rafts, and detergent-resistant membranes in plants and fungi. *Annu. Rev. Plant Biol.* **64**, 501–529 (2013).

401. Ott, T. Membrane nanodomains and microdomains in plant–microbe interactions. *Curr. Opin. Plant Biol.* **40**, 82–88 (2017).

402. Jarsch, I. K. *et al.* Plasma membranes are subcompartmentalized into a plethora of coexisting and diverse microdomains in *Arabidopsis* and *Nicotiana benthamiana*. *Plant Cell* **26**, 1698–1711 (2014).

403. Bücherl, C. A. *et al.* Plant immune and growth receptors share common signalling components but localise to distinct plasma membrane nanodomains. *Elife* **6**, 1–28 (2017).

404. Wang, Z.-Y., Seto, H., Fujioka, S., Yoshida, S. & Chory, J. BRI1 is a critical component of a plasma-membrane receptor for plant steroids. *Nature* **410**, 380–383 (2001).

405. Li, J. *et al.* BAK1, an *Arabidopsis* LRR receptor-like protein kinase, interacts with BRI1 and modulates brassinosteroid signaling. *Cell* **110**, 213–222 (2002).

406. Nam, K. H. & Li, J. BRI1/BAK1, a receptor kinase pair mediating brassinosteroid signaling. *Cell* **110**, 203–212 (2002).

407. Lin, W. *et al.* Inverse modulation of plant immune and brassinosteroid signaling pathways by the receptor-like cytoplasmic kinase BIK1. *Proc. Natl. Acad. Sci. U. S. A.* **110**, 12114–12119 (2013).

408. Lherminier, J. *et al.* NADPH oxidase-mediated reactive oxygen species production: subcellular localization and reassessment of its role in plant defense. *Mol. Plant-Microbe Interact.* **22**, 868–881 (2009).

409. Hao, H. *et al.* Clathrin and membrane microdomains cooperatively regulate RbohD dynamics and activity in *Arabidopsis*. *Plant Cell* **26**, 1729–1745 (2014).

410. Daněk, M., Valentová, O. & Martinec, J. Flotillins, Erlins, and HIRs: from animal base camp to plant new horizons. *CRC. Crit. Rev. Plant Sci.* **35**, 191–214 (2016).

411. Xu, C. *et al.* Environmental cues contribute to dynamic plasma membrane organization of nanodomains containing Flotillin-1 and Hypersensitive Induced Reaction-1 proteins in *Arabidopsis thaliana*. *Front. Plant Sci.* **13**, 1–14 (2022).

412. Daněk, M. *et al.* Cell wall contributes to the stability of plasma membrane nanodomain organization of *Arabidopsis thaliana* FLOTILLIN2 and HYPERSENSITIVE INDUCED REACTION1 proteins. *Plant J.* **101**, 619–636 (2020).

413. Browman, D. T., Hoegg, M. B. & Robbins, S. M. The SPFH domain-containing proteins: more than lipid raft markers. *Trends Cell Biol.* **17**, 394–402 (2007).

414. Zhou, L. *et al.* Rice Hypersensitive Induced Reaction Protein 1 (OsHIR1) associates with plasma membrane and triggers hypersensitive cell death. *BMC Plant Biol.* **10**, 290 (2010).

415. Qi, Y. *et al.* Physical association of *Arabidopsis* Hypersensitive Induced Reaction Proteins (HIRs) with the immune receptor RPS2. *J. Biol. Chem.* **286**, 31297–31307 (2011).

416. Li, S. *et al.* The hypersensitive induced reaction 3 (HIR3) gene contributes to plant basal resistance via an EDS1 and salicylic acid-dependent pathway. *Plant J.* **98**, 783–797 (2019).

417. Jacinto, T., Farmer, E. E. & Ryan, C. A. Purification of potato leaf plasma membrane protein pp34, a protein phosphorylated in response to oligogalacturonide signals for defense and development. *Plant Physiol.* **103**, 1393–1397 (1993).

418. Farmer, E. E., Moloshok, T. D., Saxton, M. J. & Ryan, C. A. Oligosaccharide signaling in plants. Specificity of oligouronide-enhanced plasma membrane protein phosphorylation. *J. Biol. Chem.* **266**, 3140–3145 (1991).

419. Farmer, E. E., Pearce, G. & Ryan, C. A. In vitro phosphorylation of plant plasma membrane proteins in response to the proteinase inhibitor inducing factor. *Proc. Natl. Acad. Sci. U. S. A.* **86**, 1539–1542 (1989).

420. Reymond, P. *et al.* Cloning of a cDNA encoding a plasma membrane-associated, uronide binding phosphoprotein with physical properties similar to viral movement proteins. *Plant Cell* **8**, 2265–2276 (1996).

421. Raffaele, S., Mongrand, S., Gamas, P., Niebel, A. & Ott, T. Genome-wide annotation of remorins, a plant-specific protein family: evolutionary and functional perspectives. *Plant Physiol.* **145**, 593–600 (2007).

422. Konrad, S. S. A. *et al.* S-acylation anchors remorin proteins to the plasma membrane but does not primarily determine their localization in membrane microdomains. *New Phytol.* **203**, 758–769 (2014).

423. Fu, S. *et al.* Rice stripe virus interferes with s-acylation of remorin and induces its autophagic degradation to facilitate virus infection. *Mol. Plant* **11**, 269–287 (2018).

424. Raffaele, S. *et al.* Remorin, a solanaceae protein resident in membrane rafts and plasmodesmata, impairs potato virus X movement. *Plant Cell* **21**, 1541–1555 (2009).

425. Perraki, A. *et al.* Plasma membrane localization of *Solanum tuberosum* remorin from group 1, homolog 3 is mediated by conformational changes in a novel c-terminal anchor and required for the restriction of potato virus x movement. *Plant Physiol.* **160**, 624–637 (2012).

426. Bozkurt, T. O. *et al.* The plant membrane-associated REMORIN1.3 accumulates in discrete perihaustorial domains and enhances susceptibility to *Phytophthora infestans*. *Plant Physiol.* **165**, 1005–1018 (2014).

427. Cai, J., Chen, T., Wang, Y., Qin, G. & Tian, S. SIREM1 triggers cell death by activating an oxidative burst and other regulators. *Plant Physiol.* **183**, 717–732 (2020).

428. Łabuz, J., Sztatelman, O. & Hermanowicz, P. Molecular insights into the phototropin control of chloroplast movements. *J. Exp. Bot.* **73**, 6034–6051 (2022).

429. Inoue, S. & Kinoshita, T. Blue light regulation of stomatal opening and the plasma membrane H^+-ATPase. *Plant Physiol.* **174**, 531–538 (2017).

430. Briggs, W. R. Phototropism: Some history, some puzzles, and a look ahead. *Plant Physiol.* **164**, 13–23 (2014).

431. Christie, J. M. & Murphy, A. S. Shoot phototropism in higher plants: new light through old concepts. *Am. J. Bot.* **100**, 35–46 (2013).

432. Qi, Y. & Katagiri, F. Purification of low-abundance *Arabidopsis* plasma-membrane protein complexes and identification of candidate components. *Plant J.* **57**, 932–944 (2009).

433. Sakai, T. *et al.* Arabidopsis nph1 and npl1: Blue light receptors that mediate both phototropism and chloroplast relocation. *Proc. Natl. Acad. Sci. U. S. A.* **98**, 6969–6974 (2001).

434. Naqvi, S. *et al.* Blue-light receptor PHOTOTROPIN 1 suppresses immunity to promote *Phytophthora infestans* infection. *New Phytol.* **233**, 2282–2293 (2022).

435. Yotsui, I. *et al.* Genetic and phosphoproteomic basis of LysM-mediated immune signaling in *Marchantia polymorpha* highlights conserved elements and new aspect of pattern-triggered immunity in land plants. *bioRxiv* (2022) doi:10.1101/2022.12.28.521631.

436. Ding, X., Jimenez-Gongora, T., Krenz, B. & Lozano-Duran, R. Chloroplast clustering around the nucleus is a general response to pathogen perception in *Nicotiana benthamiana*. *Mol. Plant Pathol.* **20**, 1298–1306 (2019).

437. Wendrich, J. R., Boeren, S., Möller, B. K., Weijers, D. & De Rybel, B. In vivo identification of plant protein complexes using IP-MS/MS. *Plant Hormones. Methods in Molecular Biology* 147–158 (2017).

438. Cox, J. & Mann, M. MaxQuant enables high peptide identification rates, individualized p.p.b.-range mass accuracies and proteome-wide protein quantification. *Nat. Biotechnol.* **26**, 1367–1372 (2008).

439. Cox, J. *et al.* Andromeda: A peptide search engine integrated into the MaxQuant environment. *J. Proteome Res.* **10**, 1794–1805 (2011).

440. Grosberg, R. K. & Strathmann, R. R. The evolution of multicellularity: a minor major transition? *Annu. Rev. Ecol. Evol. Syst.* **38**, 621–654 (2007).

441. Van Hautegem, T., Waters, A. J., Goodrich, J. & Nowack, M. K. Only in dying, life: programmed cell death during plant development. *Trends Plant Sci.* **20**, 102–113 (2015).

442. Williams, B., Kabbage, M., Kim, H. J., Britt, R. & Dickman, M. B. Tipping the balance: *Sclerotinia sclerotiorum* secreted oxalic acid suppresses host defenses by manipulating the host redox environment. *PLoS Pathog.* **7**, (2011).

443. Kim, K. S., Min, J.-Y. & Dickman, M. B. Oxalic acid is an elicitor of plant programmed cell death during *Sclerotinia sclerotiorum* disease development. *Mol. Plant-Microbe Interact.* **21**, 605–612 (2008).

444. Hatsugai, N. *et al.* A plant vacuolar protease, VPE, mediates, virus-induced hypersensitive cell death. *Science.* **305**, 855–858 (2004).

445. Dickman, M. B. *et al.* Abrogation of disease development in plants expressing animal antiapoptotic genes. *Proc. Natl. Acad. Sci. U. S. A.* **98**, 6957–6962 (2001).

446. Lorang, J. *et al.* Tricking the guard: exploiting plant defense for disease susceptibility. *Science.* **338**, 659–662 (2012).

447. Doukhanina, E. V *et al.* Identification and functional characterization of the BAG protein family in *Arabidopsis thaliana*. *J. Biol. Chem.* **281**, 18793–18801 (2006).

448. Galluzzi, L. *et al.* Molecular definitions of autophagy and related processes. *EMBO J.* **36**, 1811–1836 (2017).

449. Galluzzi, L. *et al.* Molecular mechanisms of cell death: recommendations of the nomenclature committee on cell death 2018. *Cell Death Differ.* **25**, 486–541 (2018).

450. Tang, D., Kang, R., Berghe, T. Vanden, Vandenabeele, P. & Kroemer, G. The molecular machinery of regulated cell death. *Cell Res.* **29**, 347–364 (2019).

451. Hofmann, K. The evolutionary origins of programmed cell death signaling. *Cold Spring Harb. Perspect. Biol.* **12**, 1–16 (2020).

452. Nagata, S. Apoptosis and clearance of apoptotic cells. *Annu. Rev. Immunol.* **36**, 489–517 (2018).

453. Mukhtar, M. S., McCormack, M. E., Argueso, C. T. & Pajerowska-Mukhtar, K. M. Pathogen tactics to manipulate plant cell death. *Curr. Biol.* **26**, R608–R619 (2016).

454. Van Doorn, W. G. *et al.* Morphological classification of plant cell deaths. *Cell Death and Differentiation* vol. 18 1241–1246 (2011).

455. Reape, T. J. & McCabe, P. F. Apoptotic-like regulation of programmed cell death in plants. *Apoptosis* **15**, 249–56 (2010).

456. van Doorn, W. G. & Woltering, E. J. Many ways to exit? Cell death categories in plants. *Trends Plant Sci.* **10**, 117–122 (2005).

457. Kumar, S. Caspase function in programmed cell death. *Cell Death and Differentiation* vol. 14 32–43 (2007).

458. Shalini, S., Dorstyn, L., Dawar, S. & Kumar, S. Old, new and emerging functions of caspases. *Cell Death and Differentiation* vol. 22 526–539 (2015).

459. Tran, V., Weier, D., Radchuk, R., Thiel, J. & Radchuk, V. Caspase-like activities accompany programmed cell death events in developing barley grains. *PLoS One* **9**, (2014).

460. Hatsugai, N. *et al.* A novel membrane fusion-mediated plant immunity against bacterial pathogens. *Genes Dev.* **23**, 2496–2506 (2009).

461. Rojo, E. *et al.* VPEγ exhibits a caspase-like activity that contributes to defense against pathogens. *Curr. Biol.* **14**, 1897–1906 (2004).

462. Coffeen, W. C. & Wolpert, T. J. Purification and characterization of serine proteases that exhibit caspase-like activity and are associated with programmed cell death in *Avena sativa*. *Plant Cell* **16**, 857–873 (2004).

463. Uren, A. G. *et al.* Identification of paracaspases and metacaspases: Two ancient families of caspase-like proteins, one of which plays a key role in MALT lymphoma. *Mol. Cell* **6**, 961–967 (2000).

464. Carmona-Gutierrez, D., Fröhlich, K. U., Kroemer, G. & Madeo, F. Editorial: Metacaspases are caspases. Doubt no more. *Cell Death and Differentiation* vol. 17 377–378 (2010).

465. Enoksson, M. & Salvesen, G. S. Metacaspases are not caspases - Always doubt. *Cell Death and Differentiation* vol. 17 1221 (2010).

466. Minina, E. A., Coll, N. S., Tuominen, H. & Bozhkov, P. V. Metacaspases versus caspases in development and cell fate regulation. *Cell Death and Differentiation* vol. 24 1314–1325 (2017).

467. Dickman, M. B. & Fluhr, R. Centrality of host cell death in plant-microbe interactions. *Annu. Rev. Phytopathol.* **51**, 543–570 (2013).

468. Feng, S., Fox, D. & Man, S. M. Mechanisms of gasdermin family members in inflammasome signaling and cell death. *J. Mol. Biol.* **430**, 3068–3080 (2018).

469. Yu, P. *et al.* Pyroptosis: mechanisms and diseases. *Signal Transduct. Target. Ther.* **6**, (2021).

470. Devant, P. & Kagan, J. C. Molecular mechanisms of gasdermin D pore-forming activity. *Nat. Immunol.* (2023) doi:10.1038/s41590-023-01526-w.

471. Fink, S. L. & Cookson, B. T. Caspase-1-dependent pore formation during pyroptosis leads to osmotic lysis of infected host macrophages. *Cell. Microbiol.* **8**, 1812–1825 (2006).

472. Sun, G. W., Lu, J., Pervaiz, S., Cao, W. P. & Gan, Y.-H. Caspase-1 dependent macrophage death induced by *Burkholderia pseudomallei*. *Cell. Microbiol.* **7**, 1447–1458 (2005).

473. Johnson, A. G. *et al.* Bacterial gasdermins reveal an ancient mechanism of cell death. *Science.* **375**, 221–225 (2022).

474. Shi, J. *et al.* Cleavage of GSDMD by inflammatory caspases determines pyroptotic cell death. *Nature* **526**, 660–665 (2015).

475. Pearson, J. S. & Murphy, J. M. Down the rabbit hole: Is necroptosis truly an innate response to infection? *Cell. Microbiol.* **19**, e12750 (2017).

476. Petrie, E. J., Czabotar, P. E. & Murphy, J. M. The structural basis of necroptotic cell death signaling. *Trends Biochem. Sci.* **44**, 53–63 (2019).

477. Ros, U. *et al.* Necroptosis execution is mediated by plasma membrane nanopores independent of calcium. *Cell Rep.* **19**, 175–187 (2017).

478. Mermigka, G., Amprazi, M., Mentzelopoulou, A., Amartolou, A. & Sarris, P. F. Plant and animal innate immunity complexes: fighting different enemies with similar weapons. *Trends Plant Sci.* **25**, 80–91 (2020).

479. Mizushima, N. & Komatsu, M. Autophagy: renovation of cells and tissues. *Cell* **147**, 728–741 (2011).

480. Bialik, S., Dasari, S. K. & Kimchi, A. Autophagy-dependent cell death - where, how and why a cell eats itself to death. *J. Cell Sci.* **131**, jcs215152 (2018).

481. Minina, E. A., Bozhkov, P. V. & Hofius, D. Autophagy as initiator or executioner of cell death. *Trends Plant Sci.* **19**, 692–697 (2014).

482. Tasset, I. & Cuervo, A. M. Role of chaperone-mediated autophagy in metabolism. *FEBS J.* **283**, 2403–2413 (2016).

483. Lescat, L. *et al.* Chaperone-mediated autophagy in the light of evolution: Insight from fish. *Mol. Biol. Evol.* **37**, 2887–2899 (2020).

484. Schuck, S. Microautophagy – distinct molecular mechanisms handle cargoes of many sizes. *J. Cell Sci.* **133**, (2020).

485. Chanoca, A. *et al.* Anthocyanin vacuolar inclusions form by a microautophagy mechanism. *Plant Cell* **27**, 2545–2559 (2015).

486. Nakamura, S., Hidema, J., Sakamoto, W., Ishida, H. & Izumi, M. Selective elimination of membrane-damaged chloroplasts via microautophagy. *Plant Physiol.* **177**, 1007–1026 (2018).

487. Nakamura, S. & Izumi, M. Chlorophagy is ATG gene-dependent microautophagy process. *Plant Signal. Behav.* **14**, 1554469 (2019).

488. Goto-Yamada, S. *et al.* Sucrose starvation induces microautophagy in plant root cells. *Front. Plant Sci.* **10**, 1–16 (2019).

489. Ding, X., Zhang, X. & Otegui, M. S. Plant autophagy: new flavors on the menu. *Curr. Opin. Plant Biol.* **46**, 113–121 (2018).

490. Hofius, D., Li, L., Hafrén, A. & Coll, N. S. Autophagy as an emerging arena for plant–pathogen interactions. *Curr. Opin. Plant Biol.* **38**, 117–123 (2017).

491. Üstün, S., Hafrén, A. & Hofius, D. Autophagy as a mediator of life and death in plants. *Curr. Opin. Plant Biol.* **40**, 122–130 (2017).

492. Marshall, R. S. & Vierstra, R. D. Autophagy: the master of bulk and selective recycling. *Annu. Rev. Plant Biol.* **69**, 173–208 (2018).

493. Escamez, S. & Tuominen, H. Programmes of cell death and autolysis in tracheary elements: When a suicidal cell arranges its own corpse removal. *J. Exp. Bot.* **65**, 1313–1321 (2014).

494. Escamez, S. & Tuominen, H. Contribution of cellular autolysis to tissular functions during plant development. *Curr. Opin. Plant Biol.* **35**, 124–130 (2017).

495. van Doorn, W. G. & Papini, A. Ultrastructure of autophagy in plant cells. *Autophagy* **9**, 1922–1936 (2013).

496. Wu, C. & Derevnina, L. The battle within: How pathogen effectors suppress NLR-mediated immunity. *Curr. Opin. Plant Biol.* **74**, 102396 (2023).

497. Ceulemans, E., Ibrahim, H. M. M., De Coninck, B. & Goossens, A. Pathogen effectors: exploiting the promiscuity of plant signaling hubs. *Trends Plant Sci.* **26**, 780–795 (2021).

498. Williams, B. & Dickman, M. Plant programmed cell death: can't live with it; can't live without it. *Mol. Plant Pathol.* **9**, 531–544 (2008).

499. Dutton, M. V. & Evans, C. S. Oxalate production by fungi: its role in pathogenicity and ecology in the soil environment. *Can. J. Microbiol.* **42**, 881–895 (1996).

500. Cessna, S. G., Sears, V. E., Dickman, M. B. & Low, P. S. Oxalic acid, a pathogenicity factor for *Sclerotinia sclerotiorum*, suppresses the oxidative burst of the host plant. *Plant Cell* **12**, 2191–2199 (2000).

501. Kabbage, M., Williams, B. & Dickman, M. B. Cell death control: the interplay of apoptosis and autophagy in the pathogenicity of *Sclerotinia sclerotiorum*. *PLoS Pathog.* **9**, (2013).

502. Li, W., Kabbage, M. & Dickman, M. B. Transgenic expression of an insect inhibitor of apoptosis gene, SfIAP, confers abiotic and biotic stress tolerance and delays tomato fruit ripening. *Physiol. Mol. Plant Pathol.* **74**, 363–375 (2010).

503. Lincoln, J. E. *et al.* Expression of the antiapoptotic baculovirus p35 gene in tomato blocks programmed cell death and provides broad-spectrum resistance to disease. *Proc. Natl. Acad. Sci. U. S. A.* **99**, 15217–15221 (2002).

504. Lai, Z., Wang, F., Zheng, Z., Fan, B. & Chen, Z. A critical role of autophagy in plant resistance to necrotrophic fungal pathogens. *Plant J.* **66**, 953–968 (2011).

505. Katsiarimpa, A. *et al.* The deubiquitinating enzyme AMSH1 and the ESCRT-III subunit VPS2.1 are required for autophagic degradation in *Arabidopsis*. *Plant Cell* **25**, 2236–2252 (2013).

506. Lenz, H. D. *et al.* Autophagy differentially controls plant basal immunity to biotrophic and necrotrophic pathogens. *Plant J.* **66**, 818–830 (2011).

507. Faris, J. D. & Friesen, T. L. Plant genes hijacked by necrotrophic fungal pathogens. *Curr. Opin. Plant Biol.* **56**, 74–80 (2020).

508. Navarre, D. A. & Wolpert, T. J. Victorin induction of an apoptotic/senescence–like response in oats. *Plant Cell* **11**, 237–249 (1999).

509. Yao, N. *et al.* Novel evidence for apoptotic cell response and differential signals in chromatin condensation and DNA cleavage in victorin-treated oats. *Plant J.* **28**, 13–26 (2001).

510. Yao, N. *et al.* Mitochondrial oxidative burst involved in apoptotic response in oats. *Plant J.* **30**, 567–579 (2002).

511. Curtis, M. J. & Wolpert, T. J. The oat mitochondrial permeability transition and its implication in victorin binding and induced cell death. *Plant J.* **29**, 295–312 (2002).

512. Mayama, S., Bordin, A. P. A., Morikawa, T., Tanpo, H. & Kato, H. Association of avenalumin accumulation with co-segregation of victorin sensitivity and crown rust resistance in oat lines carrying the Pc-2 gene. *Physiol. Mol. Plant Pathol.* **46**, 263–274 (1995).

513. Welsh, J. N., Peturson, B. & Machacek, J. E. associated inheritance of reaction to races of crown rust, *Puccinia Coronata avenae* Erikss., and to victoria blight, *Helminthosporium victoriae* M. and M., in oats . *Can. J. Bot.* **32**, 55–68 (1954).

514. Rines, H. W. & Luke, H. H. Selection and regeneration of toxin-insensitive plants from tissue cultures of oats (*Avena sativa*) susceptible to *Helminthosporium victoriae*. *Theor. Appl. Genet.* **71**, 16–21 (1985).

515. Lorang, J. M., Sweat, T. A. & Wolpert, T. J. Plant disease susceptibility conferred by a "resistance" gene. *Proc. Natl. Acad. Sci. U. S. A.* **104**, 14861–14866 (2007).

516. Sweat, T. A. & Wolpert, T. J. Thioredoxin h5 is required for victorin sensitivity mediated by a CC-NBS-LRR gene in *Arabidopsis*. *Plant Cell* **19**, 673–687 (2007).

517. Lorang, J. M., Hagerty, C. H., Lee, R., McClean, P. E. & Wolpert, T. J. Genetic analysis of victorin sensitivity and identification of a causal nucleotide-binding site leucine-rich repeat gene in *Phaseolus vulgaris*. *Mol. Plant-Microbe Interact.* **31**, 1069–1074 (2018).

518. Liu, Y. *et al.* Autophagy regulates programmed cell death during the plant innate immune response. *Cell* **121**, 567–577 (2005).

519. Yoshimoto, K. *et al.* Autophagy negatively regulates cell death by controlling NPR1-dependent salicylic acid signaling during senescence and the innate immune response in *Arabidopsis*. *Plant Cell* **21**, 2914–2927 (2009).

520. Patel, S. & Dinesh-Kumar, S. P. Arabidopsis ATG6 is required to limit the pathogen-associated cell death response. *Autophagy* **4**, 20–27 (2008).

521. Wang, Y., Nishimura, M. T., Zhao, T. & Tang, D. ATG2, an autophagy-related protein, negatively affects powdery mildew resistance and mildew-induced cell death in *Arabidopsis*. *Plant J.* **68**, 74–87 (2011).

522. Hofius, D. *et al.* Autophagic components contribute to hypersensitive cell death in *Arabidopsis*. *Cell* **137**, 773–783 (2009).

523. Wang, J. & Chai, J. Structural insights into the plant immune receptors PRRs and NLRs. *Plant Physiol.* **182**, 1566–1581 (2020).

524. Han, S. *et al.* Cytoplastic glyceraldehyde-3-phosphate dehydrogenases interact with ATG3 to negatively regulate autophagy and immunity in *Nicotiana benthamiana*. *Plant Cell* **27**, 1316–1331 (2015).

525. Farré, J. C. & Subramani, S. Mechanistic insights into selective autophagy pathways: Lessons from yeast. *Nat. Rev. Mol. Cell Biol.* **17**, 537–552 (2016).

526. Popa, C. *et al.* The effector AWR5 from the plant pathogen *Ralstonia solanacearum* is an inhibitor of the TOR signalling pathway. *Sci. Rep.* **6**, 27058 (2016).

527. Maqbool, A. *et al.* Structural basis of host Autophagy-related Protein 8 (ATG8) binding by the irish potato famine pathogen effector protein PexRD54. *J. Biol. Chem.* **291**, 20270–20282 (2016).

528. Dagdas, Y. F. *et al.* An effector of the irish potato famine pathogen antagonizes a host autophagy cargo receptor. *Elife* **5**, 1–23 (2016).

529. Adachi, H. *et al.* An N-terminal motif in NLR immune receptors is functionally conserved across distantly related plant species. *Elife* **8**, 1–31 (2019).

530. Lapin, D., Johanndrees, O., Wu, Z., Li, X. & Parker, J. E. Molecular innovations in plant TIR-based immunity signaling. *Plant Cell* **34**, 1479–1496 (2022).

531. Laflamme, B. *et al.* The pan-genome effector-triggered immunity landscape of a host-pathogen interaction. *Science.* **367**, 763–768 (2020).

532. Gassmann, W., Hinsch, M. E. & Staskawicz, B. J. The *Arabidopsis* RPS4 bacterial-resistance gene is a member of the TIR-NBS-LRR family of disease-resistance genes. *Plant J.* **20**, 265–277 (1999).

533. Gassmann, W. Natural variation in the *Arabidopsis* response to the avirulence gene hopPsyA uncouples the hypersensitive response from disease resistance. *Mol. Plant-Microbe Interact.* **18**, 1054–1060 (2005).

534. Menna, A., Nguyen, D., Guttman, D. S. & Desveaux, D. Elevated temperature differentially influences effector-triggered immunity outputs in *Arabidopsis*. *Front. Plant Sci.* **6**, 1–7 (2015).

535. Lee, D. H., Lee, H. S. & Belkhadir, Y. Coding of plant immune signals by surface receptors. *Curr. Opin. Plant Biol.* **62**, 102044 (2021).

536. Joosten, M. H. A. J. *et al.* The phytopathogenic fungus *Cladosporium fulvum* is not sensitive to the chitinase and β-1,3-glucanase defence proteins of its host, tomato. *Physiol. Mol. Plant Pathol.* **46**, 45–59 (1995).

537. Bi, G. *et al.* SOBIR1 requires the GxxxG dimerization motif in its transmembrane domain to form constitutive complexes with receptor-like proteins. *Mol. Plant Pathol.* **17**, 96–107 (2016).

538. Kroemer, G. *et al.* Classification of cell death: recommendations of the nomenclature committee on cell death 2009. *Cell Death Differ.* **16**, 3–11 (2009).

539. Dubiella, U. *et al.* Calcium-dependent protein kinase/NADPH oxidase activation circuit is required for rapid defense signal propagation. *Proc. Natl. Acad. Sci. U. S. A.* **110**, 8744–8749 (2013).

540. Bi, Y. *et al.* Production of reactive oxygen species, impairment of photosynthetic function and dynamic changes in mitochondria are early events in cadmium-induced cell death in *Arabidopsis thaliana*. *Biol. Cell* **101**, 629–643 (2009).

541. Fernández-Bautista, N., Domínguez-Núñez, J., Moreno, M. M. & Berrocal-Lobo, M. Plant tissue trypan blue staining during phytopathogen infection. *BIO-PROTOCOL* **6**, 1–7 (2016).

542. van Wees, S. Phenotypic analysis of *Arabidopsis* mutants: trypan blue stain for fungi, oomycetes, and dead plant cells. *Cold Spring Harb. Protoc.* **2008**, pdb.prot4982 (2008).

543. Hatsugai, N. & Katagiri, F. Quantification of plant cell death by electrolyte leakage assay. *BIO-PROTOCOL* **8**, 1–7 (2018).

544. Seidl, M. F. & Van den Ackerveken, G. Activity and phylogenetics of the broadly occurring family of microbial Nep1-like proteins. *Annu. Rev. Phytopathol.* **57**, 367–386 (2019).

545. Lenarčič, T. *et al.* Eudicot plant-specific sphingolipids determine host selectivity of microbial NLP cytolysins. *Science.* **358**, 1431–1434 (2017).

546. Steentjes, M. B. F. *et al.* Cytotoxic activity of Nep1-like proteins on monocots. *New Phytol.* **235**, 690–700 (2022).

547. Dong, J. & Chen, W. The Role of autophagy in chloroplast degradation and chlorophagy in immune defenses during Pst DC3000 (AvrRps4) infection. *PLoS One* **8**, 1–16 (2013).

548. Malvestiti, M. C. *et al.* Analysis of plant cell death-inducing proteins of the necrotrophic fungal pathogens *Botrytis squamosa* and *Botrytis elliptica*. *Front. Plant Sci.* **13**, 1–11 (2022).

549. Huang, W. R. H. *et al.* Receptor-like cytoplasmic kinases belonging to different subfamilies mediate immune responses downstream of the Cf-4 resistance protein in *Nicotiana benthamiana*. *bioRxiv* 2023.04.25.538242 (2023) doi:10.1101/2023.04.25.538242.

550. Jutras, P. V. *et al.* AgroLux: bioluminescent Agrobacterium to improve molecular pharming and study plant immunity. *Plant J.* **108**, 600–612 (2021).

551. Eschrig, S. *et al.* LORE homomerization is required for 3-OH-C10:0 induced immune signaling. *bioRxiv* 2021.09.27.461997 (2021) doi:10.1101/2021.09.27.461997.

552. Tintor, N., Nieuweboer, G. A. M., Bakker, I. A. W. & Takken, F. L. W. The intracellularly acting effector Foa3 suppresses defense responses when infiltrated into the apoplast. *Front. Plant Sci.* **13**, (2022).

553. Newman, T. E. *et al.* The broad host range pathogen Sclerotinia sclerotiorum produces multiple effector proteins that induce host cell death intracellularly. *Mol. Plant Pathol.* 1–16 (2023) doi:10.1111/mpp.13333.

554. Hoyos, L. M. *et al.* Untargeted metabolomics reveals PTI-associated metabolites in tomato. *bioRxiv* 2023.06.15.544816 (2023) doi:10.1101/2023.06.15.544816.

555. Wang, W. *et al. Phytophthora capsici* sterol reductase PcDHCR7 has a role in mycelium development and pathogenicity. *Open Biol.* **12**, (2022).

556. Jalilian, A. *et al.* The RLCK subfamily VII-4 controls pattern-triggered immunity and basal resistance to bacterial and fungal pathogens in rice. *Plant J.* 1–12 (2023) doi:10.1111/tpj.16323.

557. Tian, W. *et al.* A calmodulin-gated calcium channel links pathogen patterns to plant immunity. *Nature* **572**, 131–135 (2019).

558. Zhu, X., Caplan, J., Mamillapalli, P., Czymmek, K. & Dinesh-Kumar, S. P. Function of endoplasmic reticulum calcium ATPase in innate immunity-mediated programmed cell death. *EMBO J.* **29**, 1007–1018 (2010).

559. Littlejohn, G. R., Breen, S., Smirnoff, N. & Grant, M. Chloroplast immunity illuminated. *New Phytol.* **229**, 3088–3107 (2021).

560. Romeis, T. *et al.* Rapid Avr9- and Cf-9-dependent activation of MAP kinases in tobacco cell cultures and leaves: Convergence of resistance gene, elicitor, wound, and salicylate responses. *Plant Cell* **11**, 273–287 (1999).

SUMMARY

Plants possess an innate immune system that enables them to defend themselves against pathogenic microorganisms. This immune system is organised into two interconnected tiers, with immune receptors localised at the plasma membrane (PM) and present in the cytoplasm of the cells. At the PM, cell-surface receptors act as a first line of defence, recognising immunogenic patterns (IPs) that can be microbe-associated molecular patterns (MAMPs), damage associated molecular patterns (DAMPs), or secreted virulence factors that are referred to effectors.

Cell-surface receptors can be classified into two main types; receptor-like kinases (RLKs) and receptor-like proteins (RLPs). RLKs are transmembrane proteins with both an extracellular domain to recognise IPs and an intracellular kinase domain for the initiation of downstream signalling. In contrast, RLPs lack an intracellular signalling domain and form complexes with adaptor RLKs such as the SUPPRESSOR OF BIR1-1 (SOBIR1), to initiate downstream signalling. The tomato resistance protein Cf-4 is an example of an RLP. This cell-surface receptor confers resistance of tomato to strains of the hemi-biotrophic fungal pathogen *Cladosporium fulvum* (syn. *Fulvia fulva*), secreting the effector protein Avr4.

When Avr4 is perceived by Cf-4, this event triggers the recruitment of the RLK BRI1-ASSOCIATED KINASE 1 (BAK1) to the Cf-4/SOBIR1 complex. BAK1 association leads to a series of phosphorylation events between the cytoplasmic kinase domains of SOBIR1 and BAK1, thereby activating downstream immune signalling. The resulting immune responses include a swift production of reactive oxygen species (ROS) and the activation of a hypersensitive response (HR), which is a form of programmed cell death (PCD). The work described in this thesis focuses on the study of the early signalling mechanisms underlying the Cf-4-triggered immune responses in the model solanaceous plant *N. benthamiana*.

Chapter 1 of this thesis provides an overview of the plant immune system, focusing on the activation and signalling mechanisms of plant immune receptors. It explores the diverse repertoire of plant immune receptors that are present at the plasma membrane (PM) and in the cytoplasm of cells, describing how they are activated upon recognition of their corresponding IPs. The chapter further explores the downstream signalling events that are initiated by cell-surface receptors, highlighting the

role of receptor-like cytoplasmic kinases (RLCKs) in connecting these receptors with intracellular signalling cascades. The chapter concludes by emphasising the interconnected nature of the signalling pathways that are activated by cell-surface receptors and by cytoplasmic immune receptors, underscoring their collaborative roles in orchestrating the activation of plant defence responses.

In order to assess the role of regulatory components in modulating the intensity of the Avr4-triggered HR, **Chapter 2** of this thesis introduces a novel method for visualising and quantifying PCD in green plant tissues. This method relies on detecting red light signals emitted by cells undergoing cell death. Through various experiments involving IP infiltration and pathogen inoculations, the capability of this method to quantify PCD intensity in a standardised and reproducible manner and track its progression over time, is demonstrated. This innovative approach offers a safer and more efficient alternative to traditional staining techniques, allowing for high-throughput analysis of many samples in a shorter time.

Chapter 3 of this thesis explores the early signalling mechanisms of the Cf-4-triggered immune responses in the solanaceous model plant *N. benthamiana*. In this chapter, relevant biological information from the well-studied model plant *Arabidopsis thaliana* (*Arabidopsis*) is transferred to the solanaceous research model plant, *Nicotiana benthamiana*. Through an analysis of publicly available *Arabidopsis* microarray data, a transcriptional cluster enriched in genes related to immune responses that include known components of the SOBIR1 complex was identified. The role of various genes within this cluster in *Cf-4*-transgenic *N. benthamiana* plants was evaluated through a combination of gene silencing experiments, phenotypic analysis, and protein-protein interaction analysis. This study revealed that a biphasic ROS burst is produced by the PM-associated RESPIRATORY BURST OXIDASE HOMOLOGUE B (RBOHB) enzyme, which is dispensable for the initiation of the HR. Furthermore, the signalling cascades that are activated downstream of SOBIR1 were explored, revealing non-conserved mechanisms between *N. benthamiana* and *Arabidopsis*. While the lipase-like proteins ENHANCED DISEASE SUSCEPTIBILITY 1 (EDS1) and PHYTOALEXIN-DEFICIENT 4 (PAD4) form a heterodimer required downstream of cell-surface receptors in *Arabidopsis*, their contribution was not observed in *N. benthamiana*, indicating differences in the immune signalling between the two model species. In this chapter, the role of heterotrimeric G-proteins in the Cf-4-triggered immune signalling was also investigated and opposing roles of the different extra-large G-pro-

teins (XLGs) in regulating the activity of the SOBIR1 complex were discovered. Finally, a genetic interaction between the *N. benthamiana* homologs of the copine protein BONZAI 1 (BON1) and components of the SOBIR1-complex was revealed, suggesting its role as a negative regulator of a guarding mechanism of the Cf-4/SOBIR1 complex, based on yet unidentified cytoplasmic immune receptors.

The identification of downstream signalling components linked to the Cf-4/SOBIR1 complex has been hindered by technical limitations in detecting transient and weak protein-protein interactions involving membrane-associated proteins. For that reason, **Chapter 4** of this thesis focuses on the implementation of proximity-dependent labelling (PL) to study the proximal proteome of the Cf-4/SOBIR1 complex. This chapter describes the generation and validation of various fusion proteins containing a promiscuous biotin ligase named TurboID, to enable selective biotinylation of proteins that are present in close proximity to the receptor complex. In this way, the biotinylated proteins can then be purified using streptavidin-coated beads. It is shown that the fusion proteins NbSOBIR1-YFP-TbID and Cf-4-YFP-TbID retained their signalling competence, as indicated by their ability to mediate HR and apoplastic ROS burst production upon perception of the effector Avr4. This chapter also explores the application of PL in the apoplastic space of plant leaves. For this, a YFP-TurboID-tagged version of the effector Avr4 is shown to be capable of selective biotinylation of the immune receptor Cf-4. This result suggests that it is possible to use TurboID-tagged effector proteins to identify unknown cell-surface receptors that recognise a tagged effector in resistant plants.

The **Chapter 5** of this thesis describes the application of PL, followed by mass spectrometry (PL-MS) analysis, to identify the proteins that are located in the vicinity of the Cf-4/SOBIR1 complex in *N. benthamiana*. This study revealed that SOBIR1 actually functionally connects the Cf-4 receptor with the cytoplasmic immune signalling machinery, as none of the expected signalling components that play a role downstream of the Cf-4/SOBIR1 complex was found to be biotinylated by the TurboID-tagged Cf-4 fusion protein. The use of TurboID-tagged SOBIR1 instead, resulted in the identification of a set of proteins that was consistently detected to be in close-proximity to this bait fusion protein across multiple experiments. Among these proteins there are known interactors of the Cf-4/SOBIR1 complex, including chaperones involved in proper folding of cell-surface receptors, as well as key signalling components such as RLCKs and mitogen-activated protein kinases (MAPKs).

This study also provided insight into the potential organisation of RLP/SOBIR1-containing receptor complexes in nanodomains present at the plasma membrane, as the detected proximal proteome of SOBIR1 includes proteins associated with nanodomains, such as remorins and hypersensitive-induced responses proteins (HIRs).

Finally, **Chapter 6** of this thesis provides an overview of the major PCD pathways described in eukaryotes, focusing on their significance in plant-microbial pathogen interactions. Within this context, the chapter presents the key findings of this thesis in relation to the main signalling events triggered by the recognition of Avr4 by the Cf-4/SOBIR1 complex.

ACKNOWLEDGMENTS

Finally, the time has come that my PhD thesis is finished. Looking back, I can say this was a bigger challenge than I anticipated. Besides this, somehow, I enjoyed most of the process. To reach this point is, literally, my childhood dream. Here, I acknowledge those who accompanied me on this journey and have contributed to its success.

Matthieu, thank you for the opportunity to do my PhD in your group. I contacted you inquiring about the possibility of following a *capita selecta* course with you, and I ended up staying for two MSc theses and a PhD. Since then, I have learned a lot while working in your group. I really appreciate your guidance, the trust and freedom you gave me, as well as the positive and kind attitude you always show towards your students.

Jan, you are a particularly good teacher. I got to know you while studying genomics, and you were one of the reasons why I registered for the course Plant-Microbe Interactions. That course sparked my interest in plant molecular biology, and because of that I contacted Matthieu, who was the contact person, to follow a *capita selecta* course on the topic. So, as far as I consider this, it is because of you that I ended up being a plant molecular biologist. Thank you.

Francine, I have warm memories about the time we shared at Phyto. I appreciate the interest you always showed in our process as PhD-students, and your inquisitive attitude when attending our presentations.

Gert, thank you so much for the support you gave me during the last stretch of my PhD-studies.

Michael, thank you for your guidance during my initial approach to bioinformatic analysis and for your feedback on Chapter 3.

Johannes, thank you for your critical and constructive feedback on Chapter 3.

Sjef, you helped me a lot with the proteomic analyses. I appreciate the patience that you had with me.

My thanks also go to the **Unifarm personnel**, especially to **Bert.** Your good care of the plants has been crucial for generating most of the data in this thesis.

Einar, **Ilemi**, and **Gabriel**, my housemates, thank you for tolerating me at our home. I keep a lot of nice memories about the time we shared.

I would like to extend my thanks to all the current and former members of the **SOL-team**. **Laurens** and **Ciska**, you were the persons to go to for advice regarding technical issues during my time at Phyto. I really appreciate your kindness and positive attitude. **Aranka** and **Jinbin,** I met you as an MSc student when you were doing your PhD-studies in the SOL-team. I learned a lot from both of you, particularly from you, **Aranka**, as you were the supervisor of my major MSc thesis. **Wen**, we started our PhD-studies working together. You managed to finish earlier and soon you will go to a top-notch institute to do a postdoc. I wish you all the best. **Chris**, **Esranur**, **Nicat**, **Huan**, and **Wenyu**, you are the "new" PhD-students of the SOL-team. As I will be staying a bit longer as a postdoc at Phyto, I will be working together with you on some projects. I'm looking forward to seeing how much we can do together. Good luck with your PhDs.

I also want to thank all the MSc students that were involved in my PhD project. **Nick**, you were my first MSc student. I'm happy to know that you have just started your own PhD studies. **Maikel**, your MSc project was particularly fun. I wish you lots of luck with your PhD project at plant breeding. **Jose Juan**, you did your major thesis and a research practice under my supervision. We spent almost a year working together. We were lucky to be the students working at the time during which the tools for proximity-dependent labelling arrived at Phyto. **Sam**, you did a short internship with me. I really liked your mature and independent working attitude. **Xizheng**, you arrived during the last stretch of my PhD, and we spent a significant amount of time working together as you also did your major thesis and research practice with me. We have been sharing the struggles of the writing process. I hope to soon celebrate the finalisation of your MSc with you. In general, I've been very lucky with the MSc students that worked with me. Having such a good quality MSc students to work with is one of the perks of doing a PhD in a place like Wageningen University.

To all the fellow students and scientists, I shared time with in the department: **Nick, Edgar, Laura, Javier, Nelia, Si, Martin, Hui, Harold, Like, Desalegn, Edouard, Jelmer,**

Michiel, Carolina, Yaohua, Maikel, David, Michele, Lorena, Lisanne, Suraj, Rahim, and **Sen**. Thank you for the time we spent and the talks we shared over the last five years.

I also want to thank the staff members that helped with the work at the department: **Ali, Grardy, Giuliana, Henriek, Xiaoqian, Hanneke, Anneke, Petra, Arwen, Tijmen, Lotje** and **Sande**r.

This PhD thesis is the result of a very long journey. It is not only about the years it took me to complete this work, but also the years of preparation needed to build the profile that made me eligible for the governmental fellowships that made this journey possible. I earned my bachelor's degree in Biology from the National Agrarian University La Molina (UNALM) in Lima, Peru almost for free, paying a nearly symbolic tuition fee. Following that, my MSc in cellular and molecular biotechnology from Wageningen University was made possible by a full scholarship provided by the National Scholarship and Academic Loans Program (PRONABEC) of the Peruvian government. Afterward, my PhD project was fully funded by a generous grant from the National Council of Science, Technology, and Technological Innovation (CONCYTEC) of the Peruvian government. I am grateful that my country gave me the opportunity to access the best education possible. I hope to have the opportunity to return and repay all the support I received by contributing to my country's development.

Quiero también agradecer a mi familia sin quienes no hubiera podido llegar hasta aquí. A mis padres, **Malena** y **Alfonso**, y a mi hermano, **Guillermo**, los quiero muchísimo. Tío **Rafo**, sin tu apoyo esta aventura no hubiera sido posible.

Mara, me hace tremendamente feliz el llegar a este punto contigo a mi lado.

ABOUT THE AUTHOR

Sergio Landeo Villanueva was born in Lima, Peru, on June 4th, 1982. He studied for his bachelor's degree in biology at the National Agrarian University La Molina (UNALM), in Lima, Peru, and graduated in 2007. He then worked for a couple of years on the isolation and purification of plant secondary metabolites at the Research Institute of Biochemistry and Molecular Biology at UNALM and completed his professionalisation thesis on the study of nematophagous fungi at the same university in 2010. After this, he worked as a lecturer in molecular biology and genetics at the Scientific University of the South (UCSUR) for five years. In 2015, Sergio was awarded the Peruvian governmental scholarship "President of the Republic" by the National Scholarship and Academic Loans Program (PRONABEC) and went to study for his Master's degree in cellular and molecular biotechnology at Wageningen University. There, Sergio came into contact with the work performed on plant-microbe interactions at the Laboratory of Phytopathology and performed two MSc theses, studying the signalling mechanism of receptor-like proteins (RLPs) in *Nicotiana benthamiana* and tomato in the group of Dr. Matthieu Joosten. After graduating in February 2017, Sergio went back to his teaching duties at UCSUR. Later that year, he was awarded a governmental fellowship by the National Council of Science, Technology, and Technological Innovation (CONCYTEC) of Peru to study for obtaining his Ph.D. abroad. In February 2018, Sergio went back to the Laboratory of Phytopathology of Wageningen University to work within the SOL-team, under the supervision of Dr. Matthieu Joosten. The results of the conducted research are described in this thesis.

The research described in this thesis was financially supported by the Peruvian Council for Science, Technology and Technological Innovation (CONCYTEC) and its executive unit FONDECYT.

Financial support from Wageningen University for printing this thesis is gratefully acknowledged.

Provided by thesis specialist Ridderprint, ridderprint.nl
Printing: Ridderprint
Layout and design: Erwin Timmerman, persoonlijkproefschrift.nl